

**A Combined Synthetic, *In situ* IR Spectroscopic and
Computational Investigation of the Lithiation-Trapping
Reactions of *N*-Boc Heterocycles**

Adam Islip

PhD

University of York

Chemistry

September 2017

Abstract

This thesis describes some novel aspects of the α -lithiation-trapping of *N*-Boc heterocycles, including computational DFT modelling of the lithiation and kinetic studies of both the lithiation and trapping reactions of *N*-Boc heterocycles.

Chapter 2 details the use of *in situ* IR spectroscopy to monitor the progress of the α -lithiation reactions of a wide variety of *N*-Boc heterocycle substrates with vastly different reactivities. Different *s*-BuLi/ligand combinations were also found to have a dramatic effect on the rate of lithiation. Kinetic analysis of the *in situ* IR spectroscopic data enabled the rates of lithiation to be quantified which allowed the construction of a reactivity order for *N*-Boc heterocycles that were investigated.

In Chapter 3, the α -lithiation reactions of the *N*-Boc heterocycles studied in Chapter 2 were modelled with DFT. Many of the reactivity differences of the *N*-Boc heterocycles that were uncovered by the experimental investigation were accounted for by the DFT modelling. Correlation of the experimental and computational results allowed the reactivities of unknown *N*-Boc heterocycles to be predicted using only DFT modelling.

Chapter 4 describes the investigation of the rates of trapping of lithiated *N*-Boc heterocycles using *in situ* IR spectroscopy. Kinetic analysis of the *in situ* IR spectroscopic data revealed some remarkable differences in the rates of trapping for a small selection of different *N*-Boc heterocycles and electrophiles.

Chapter 5 reports the use of synthesis, *in situ* IR spectroscopic analysis and DFT modelling to investigate how the electrophile and ligand employed can affect the diastereoselectivity of the lithiation-trapping of a 3,4-disubstituted *N*-Boc pyrrolidine.

List of Contents

Abstract	ii
List of Contents	iii
List of Tables	vi
List of Figures	viii
List of Accompanying Material	xii
Acknowledgements	xiii
Author's Declaration	xiv
Chapter 1: Introduction	1
1.1 Directed α -Lithiation – The Complex Induced Proximity Effect	2
1.2 Lithiation-Trapping Reactions of <i>N</i> -Boc Heterocycles	4
1.2.1 <i>N</i> -Boc pyrrolidine and <i>N</i> -Boc piperidine	4
1.2.2 4-Substituted <i>N</i> -Boc piperidines	11
1.2.3 <i>N</i> -Boc piperazines	15
1.2.4 <i>N</i> -Boc morpholines	18
1.2.5 Bicyclic <i>N</i> -Boc pyrrolidines	19
1.3 <i>In situ</i> IR Spectroscopic Studies of Lithiation-Trapping Reactions	27
1.3.1 <i>In situ</i> IR spectroscopic studies of lithiation reactions	27
1.3.2 <i>In situ</i> IR spectroscopic studies of the trapping reactions of lithiated intermediates	33
1.4 Computational Studies of the α -Lithiation Reactions of <i>N</i> -Boc Heterocycles	38
1.5 Project Outline	42
Chapter 2: <i>In situ</i> IR Spectroscopic Monitoring of the α-Lithiation Reactions of <i>N</i>-Boc Heterocycles	44
2.1 Reactivity Series of the <i>s</i> -BuLi/TMEDA Lithiation of <i>N</i> -Boc Heterocycles	45
2.2 Reactivity Series for the Lithiation of <i>N</i> -Boc Heterocycles with Different Diamine Ligands	58

2.2.1	Synthesis of achiral diamine ligands and construction of a diamine reactivity series	58
2.2.2	Investigating the <i>N</i> -Boc heterocycle reactivity series obtained with <i>s</i> -BuLi/DPE 177 and comparison with <i>s</i> -BuLi/(–)-sparteine and <i>s</i> -BuLi/TMEDA reactivity series	64
2.3	Quantitative Kinetic Analysis of the <i>s</i> -BuLi/TMEDA Reactivity Series	70
2.4	Conclusions and Future Work	87
Chapter 3: Computational DFT Modelling of the α-Lithiation of <i>N</i>-Boc Heterocycles		90
3.1	Computational DFT Modelling of the α -Lithiation Reactions of <i>N</i> -Boc Pyrrolidine and <i>N</i> -Boc Piperidine	91
3.2	Use of DFT to Explore the α -Lithiation for a Range of <i>N</i> -Boc Heterocycles	101
3.2.1	Modelling the α -lithiation of <i>N</i> -Boc heterocycles to probe reactivity	101
3.2.2	Using DFT modelling to predict reactivities of unknown <i>N</i> -Boc heterocycles	112
3.2.3	Modelling the <i>i</i> -PrLi/TMEDA lithiation of <i>N</i> -Boc heterocycles	114
3.2.4	Application of solvent corrections to the modelling of the lithiation of <i>N</i> -Boc heterocycles	115
3.3	Modelling the Effect of the Ligand on the Rate of the α -Lithiation of <i>N</i> -Boc Pyrrolidine	119
3.4	Conclusions and Future Work	123
Chapter 4: Investigation of the Rate of Trapping of Lithiated <i>N</i>-Boc Heterocycles with Different Electrophiles		126
4.1	Use of <i>in situ</i> IR Spectroscopy to Study the Rates of Trapping of Lithiated <i>N</i> -Boc Heterocycles	127
4.2	Investigation of the Gelation of the Reaction Mixture When Using MeI as the Electrophile	142
4.3	Conclusions and Future Work	145

Chapter 5: Diastereoselective Lithiation-Trapping of a 3,4-Disubstituted Bicyclic <i>N</i>-Boc Pyrrolidine	147
5.1 Effect of the Electrophile on the Diastereoselectivity of the Lithiation-Trapping of a Bicyclic <i>N</i> -Boc Pyrrolidine	148
5.2 Effect of the Diamine Ligand on the Diastereoselectivity of the Lithiation-Trapping of a Bicyclic <i>N</i> -Boc Pyrrolidine	163
5.3 Computational DFT Modelling of the Diastereoselective Lithiation	173
5.4 Conclusions and Future Work	178
Chapter 6: Experimental	180
6.1 General	180
6.2 Kinetic Analysis Procedure	181
6.3 General Procedures	183
6.4 Experimental Procedures for Chapter 2	185
6.5 Experimental Procedures for Chapter 3	237
6.6 Experimental Procedures for Chapter 4	239
6.7 Experimental Procedures for Chapter 5	263
Abbreviations	296
References	299

List of Tables

Table 2.1	Reactivity series for the <i>s</i> -BuLi/TMEDA lithiation at -78 °C of <i>N</i> -Boc heterocycles	53
Table 2.2	ReactIR TM obtained lithiation times (t_{lith}) for <i>s</i> -BuLi/ligand lithiation of <i>N</i> -Boc pyrrolidine 9	61
Table 2.3	<i>s</i> -BuLi/diamine reactivity series for rapidly lithiating <i>N</i> -Boc heterocycles	65
Table 2.4	Half-lives for the <i>s</i> -BuLi/TMEDA lithiations of a selection of 10 <i>N</i> -Boc heterocycle substrates	80
Table 2.5	Half-lives determined by consumption of <i>N</i> -Boc heterocycle and prelithiation complex consumption for the <i>s</i> -BuLi/TMEDA lithiations of a selection of 10 <i>N</i> -Boc heterocycle substrates	83
Table 2.6	Half-lives for the <i>s</i> -BuLi/DPE 177 lithiations of <i>N</i> '-Me <i>N</i> -Boc piperazine 58 and <i>N</i> -Boc pyrrolidine 9	85
Table 3.1	Activation free energies (ΔG^\ddagger) calculated for the lithiation of <i>N</i> -Boc pyrrolidine 9	95
Table 3.2	Activation free energies (ΔG^\ddagger) calculated for the <i>i</i> -PrLi/di-methyl bispidine 195 lithiation of <i>N</i> -Boc piperidine 10	97
Table 3.3	Lowest energy <i>i</i> -PrLi orientation for the α -lithiation of 6-membered <i>N</i> -Boc heterocycles with B3LYP and M06 DFT functionals	105
Table 3.4	<i>N</i> -Boc heterocycle experimentally obtained reactivities ($t_{1/2}$) and B3LYP/M06 calculated activation free energies	106
Table 3.5	B3LYP calculated ΔG^\ddagger and predicted $t_{1/2}$ (at -78 °C) for <i>N</i> -Boc heterocycles <i>anti</i> - 97 , 198 and 192 with unknown reactivities	113
Table 3.6	Solvent corrected ΔG^\ddagger values for the <i>i</i> -PrLi/di-methyl bispidine 195 lithiations of selected <i>N</i> -Boc heterocycles and experimentally obtained $t_{1/2}$ for the lithiation	117
Table 3.7	Calculated <i>i</i> -PrLi/ligand lithiation activation free energies (ΔG^\ddagger) and experimental ReactIR TM determined <i>s</i> -BuLi/ligand lithiation times for <i>N</i> -Boc pyrrolidine 9	120

Table 4.1	Measured $t_{1/2}$ s and isolated yields for the Me ₃ SiCl, Me ₂ SO ₄ , MeI and PhCHO trapping reactions of lithiated intermediates 164 , <i>cis</i> - 201 and 199	135
Table 4.2	Measured initial rates (rate _{init}) for the Me ₃ SiCl, Me ₂ SO ₄ and MeI trapping reactions of lithiated intermediates 164 , <i>cis</i> - 201 and 199	136
Table 4.3	Comparison of the $t_{1/2}$ s of Me ₃ SiCl trapping and <i>s</i> -BuLi/TMEDA lithiation for lithiated <i>N</i> -Boc heterocycles 164 , <i>cis</i> - 201 and 199	138
Table 5.1	<i>s</i> -BuLi/TMEDA lithiation of <i>N</i> -Boc pyrrolidine 96 and subsequent trapping with a range of electrophiles	149
Table 5.2	<i>s</i> -BuLi/diamine and PhCHO lithiation-trapping procedure for <i>N</i> -Boc pyrrolidine 96 to determine the diastereoselectivity of the diamine ligand used	167
Table 5.3	<i>s</i> -BuLi/di- <i>i</i> -Pr bispidine 30 lithiation of <i>N</i> -Boc pyrrolidine 96 and trapping with Me ₃ SiCl, Me ₂ SO ₄ and CO ₂ electrophiles	170
Table 5.4	<i>s</i> -BuLi/di- <i>n</i> -Pr bispidine 105 lithiation of <i>N</i> -Boc pyrrolidine 96 and trapping with Me ₃ SiCl, Me ₂ SO ₄ and CO ₂ electrophiles	171
Table 5.5	Prelithiation complex and activation free-energies for the <i>anti</i> and <i>syn</i> <i>i</i> -PrLi/TMEDA lithiation of <i>N</i> -Boc pyrrolidine 96 calculated with B3LYP/6-31G* and M06/6-31G*	174
Table 5.6	Predicted <i>anti:syn</i> drs for the <i>i</i> -PrLi/TMEDA lithiation of <i>N</i> -Boc pyrrolidine 96	175
Table 5.7	Calculated diastereoselectivity of the <i>i</i> -PrLi/ligand lithiation of <i>N</i> -Boc pyrrolidine 96 with B3LYP/6-31G*	176
Table 5.8	Calculated diastereoselectivity of the <i>i</i> -PrLi/ligand lithiation of <i>N</i> -Boc pyrrolidine 96 with M06/6-31G*	177

List of Figures

Figure 1.1	Boceprevir and Telaprevir protease inhibitors	1
Figure 1.2	Directing groups used to direct α -lithiation of amines	3
Figure 1.3	Proposed pre-lithiation complexes for the RLi/(-)-sparteine lithiation of <i>N</i> -Boc pyrrolidine 9	7
Figure 1.4	Substrates whose α -lithiation reactions were monitored with ReactIR TM	32
Figure 2.1	14 <i>N</i> -Boc heterocycles used for the reactivity study	51
Figure 2.2	Steric environment of the α -proton in bicyclic pyrrolidine 84 and 2-methyl pyrrolidine 14	55
Figure 2.3	Proposed orbital overlap for <i>N</i> -Boc piperazines and <i>N</i> -Boc morpholine 169 increasing the α -proton acidity	56
Figure 2.4	Proposed orbital overlap for the 4-substituted <i>N</i> -Boc piperidines	56
Figure 2.5	Diamine ligands used for the reactivity study	59
Figure 2.6	Interconversion of rotamers for a 4-substituted <i>N</i> -Boc piperidine	66
Figure 2.7	<i>N</i> -Inversion and ring flipping of <i>N</i> -Boc piperazines	69
Figure 2.8	An attempt to mathematically find the end-point for the lithiation reaction of 4-amino <i>N</i> -Boc piperidine 168	72
Figure 2.9	Figure 2.9. ReactIR TM data for the consumption of <i>N</i> -Boc pyrrolidine 9 and the resulting first-order kinetic plot for the lithiation of <i>N</i> -Boc pyrrolidine 9	75
Figure 2.10	ReactIR TM data for the consumption of <i>N</i> -Boc pyrrolidine 9 using a different end-point and the resulting first-order kinetic plot for the lithiation of <i>N</i> -Boc pyrrolidine 9	76
Figure 2.11	Non-linear curve fitting for the <i>s</i> -BuLi/TMEDA lithiation of <i>N</i> -Boc pyrrolidine 9 to obtain k_{obs}	77
Figure 2.12	Non-linear curve fitting for the <i>s</i> -BuLi/TMEDA lithiation of 4-amino <i>N</i> -Boc piperidine 168 to obtain k_{obs}	78
Figure 2.13	Non-linear regression to obtain k_{obs} for the <i>s</i> -BuLi/TMEDA lithiation of <i>N</i> -Boc piperidine 10 with extrapolated curve of best fit to determine lithiation end-point	82

Figure 2.14	Non-linear regression to obtain k_{obs} for the <i>s</i> -BuLi/DPE 177 lithiations of <i>N</i> '-Me <i>N</i> -Boc piperazine 58 and <i>N</i> -Boc pyrrolidine 9	85
Figure 2.15	Final reactivity series of the 14 <i>N</i> -Boc heterocycle substrates studied in this thesis using <i>s</i> -BuLi/TMEDA and <i>s</i> -BuLi/DPE 177 lithiating conditions	87
Figure 2.16	<i>N</i> -Boc azepane 192	89
Figure 3.1	Partial reaction coordinate diagram for the RLi/diamine α -lithiation reaction of <i>N</i> -Boc heterocycles	90
Figure 3.2	B3LYP/6-31G(d) geometries for the prelithiation complex and transition state of the <i>N</i> -Boc pyrrolidine 9 deprotonation	93
Figure 3.3	B3LYP/6-31G(d) calculated reaction coordinate for the <i>i</i> -PrLi/dimethyl bispidine 195 lithiation of <i>N</i> -Boc pyrrolidine 9 and an output geometry from the forward path showing formation of the lithiated intermediate 196 and <i>i</i> -propane	94
Figure 3.4	Prelithiation complexes for the 'top' deprotonation and 'side-on' deprotonation of <i>N</i> -Boc piperidine 10	95
Figure 3.5	B3LYP/6-31G(d) optimised geometries for the prelithiation complex and transition state for the 'side-on' deprotonation of <i>N</i> -Boc piperidine 10	96
Figure 3.6	B3LYP/6-31G(d) optimised geometries for the prelithiation complex and transition state for the 'top' deprotonation of <i>N</i> -Boc piperidine 10	97
Figure 3.7	Non-bonding distances between <i>i</i> -PrLi and <i>N</i> -Boc heterocycle for the 'side-on' lithiation of <i>N</i> -Boc piperidine 10 , 'top' lithiation of <i>N</i> -Boc piperidine 10 and lithiation of <i>N</i> -Boc pyrrolidine 9	99
Figure 3.8	<i>N</i> -Boc heterocycles included in the DFT reactivity study	101
Figure 3.9	α -Lithiation transition state geometries for the 12 additional <i>N</i> -Boc heterocycles (excluding <i>N</i> -Boc pyrrolidine 9 and <i>N</i> -Boc piperidine 10) in Figure 3.8	102
Figure 3.10	Eyring linear regressions for experimentally obtained k_{obs} and calculated ΔG^\ddagger values for the lithiation of the 14 <i>N</i> -Boc heterocycle substrates in Table 3.4	109

Figure 3.11	Eyring linear regressions for experimentally obtained k_{obs} and calculated ΔG^\ddagger for the lithiation for the 10 <i>N</i> -Boc heterocycle substrates above	110
Figure 3.12	Eyring regression analysis for the <i>i</i> -PrLi/di-methyl bispidine 195 and <i>i</i> -PrLi/TMEDA modelled lithiation reactions of six <i>N</i> -Boc heterocycles	115
Figure 3.13	Eyring regression analysis for the solvent corrected and gas phase DFT modelled <i>i</i> -PrLi/di-methyl bispidine 195 lithiation of six <i>N</i> -Boc heterocycles	118
Figure 3.14	Ligands used to model the <i>i</i> -PrLi/ligand lithiation of <i>N</i> -Boc pyrrolidine 9	119
Figure 4.1	Semilogarithmic plots for the first 20% conversion and up to 90% conversion for the Me ₃ SiCl trapping of 2-lithio <i>N</i> -Boc pyrrolidine 164	129
Figure 4.2	Semilogarithmic plots for the first 20% conversion and up to 90% conversion for the MeI trapping of 2-lithio <i>N'</i> -Bn <i>N</i> -Boc piperazine 199	131
Figure 4.3	12 Combinations of lithiated <i>N</i> -Boc heterocycles and electrophiles	132
Figure 4.4	Initial rate analysis for the Me ₃ SiCl trapping of lithiated <i>N</i> -Boc pyrrolidine 164	136
Figure 4.5	Lithiated <i>N</i> -Boc heterocycles trapped using PhCHO	140
Figure 4.6	Rapid trapping carbonyl electrophiles	141
Figure 4.7	Reactivity series determined for the <i>N</i> -Boc heterocycle lithiated intermediates 164 , <i>cis</i> - 201 , 199 and Me ₃ SiCl, Me ₂ SO ₄ , MeI and PhCHO electrophiles used in this investigation	145
Figure 5.1	Stereogenic centres present on PhCHO trapped <i>N</i> -Boc pyrrolidine 214	151
Figure 5.2	Diastereomeric alcohol products from the <i>s</i> -BuLi/TMEDA lithiation and PhCHO trapping of <i>N</i> -Boc pyrrolidine 96	152
Figure 5.3	Diastereomeric alcohols <i>anti</i> - 31 and <i>syn</i> - 31	153
Figure 5.4	X-ray crystal structure of <i>syn</i> - 213 confirming relative stereochemistry	154

Figure 5.5	Rationale for the <i>anti</i> selectivity of the lithiation-trapping of <i>N</i> -Boc pyrrolidine 96	155
Figure 5.6	Diamine ligands used for the lithiation of bicyclic pyrrolidine 96	163
Figure 5.7	¹ H NMR spectra showing 4.5-0.0 ppm region for di- <i>i</i> -Pr bispidone 225 in CDCl ₃ and DMSO-d ₆	164
Figure 5.8	¹ H NMR spectra showing 4.0-0.0 ppm region for di- <i>n</i> -Pr bispidine 105 in CDCl ₃ and DMSO-d ₆	165
Figure 5.9	Disfavoured H _{syn} deprotonation of <i>N</i> -Boc pyrrolidine 96 with a bulky diamine ligand	166
Figure 5.10	M06/6-31G* optimised transition state geometries for the <i>syn</i> and <i>anti</i> lithiation of <i>N</i> -Boc pyrrolidine 96	174

List of Accompanying Material

Computationally optimised geometry coordinates (as .xyz files)	Disc 1
X-ray crystallography data for <i>syn-213</i>	Disc 1

Disc 1 is attached to the inside back cover of this thesis

Acknowledgements

I would like to thank my supervisors Professor Peter O'Brien and Dr Peter Karadakov for their support and advice over the five years that I have worked on this project. Without their help, this research would not have been possible. I also extend my thanks to Professor Ian Fairlamb for his help with the analysis of kinetic data and for his assistance and guidance as my independent panel member.

Next, I would like to thank the current and previous members of the O'Brien and Karadakov groups who have made these five years enjoyable. These include, in no particular order: "Donald", Mary, Joe, Nah, Sarah, Josh, Alice, Kate, Mickey, Will, Paul, Tom, Masakazu, Ike, Hannah, Sophie, Nico and Kevin. Thanks also go to all the members of the Fairlamb group for their hospitality when I have been in their lab using the ReactIR™ equipment.

I would also like to thank all of the York technical staff for the considerable support they have provided. This includes Steve and Mike in stores, Heather for running the NMR service, Karl for mass spectrometry and Charlotte for assistance with and maintenance of the ReactIR™ equipment.

My thanks also go to my family for their love and support throughout my eight years in York. Finally, I would like to thank my fiancé Rose for her love and encouragement over the course of my PhD.

Author's Declaration

The research presented in this thesis is, to the best of my knowledge, original except where due reference has been made to other authors and/or co-workers. This work has not previously been presented for an award at this, or any other, University.

Adam Islip

Chapter 1: Introduction

Nitrogen heterocycles, including pyrrolidines, piperidines and piperazines are important structural motifs in both nature and pharmaceutical compounds. For example, 44 of the “Top 200 selling pharmaceuticals in US retail sales of 2015” contain either a pyrrolidine, piperidine, morpholine or piperazine subunit.¹ The racemic and asymmetric synthesis of 2-substituted *N*-Boc heterocycles has become widespread using the *N*-Boc α -lithiation protocol pioneered by Beak.^{2,3}

Since Beak’s first publication in 1989, much research has been carried out investigating different *N*-Boc heterocycle substrates, various ligands and a variety of electrophiles to trap the lithiated intermediates. This has enabled the synthesis of a large variety of different substituted *N*-Boc heterocycles. In this thesis, synthetic, *in situ* IR spectroscopy and computational DFT modelling techniques have been used to investigate, find optimal conditions and better understand the α -lithiation reactions of *N*-Boc heterocycles.

Recently, interest in the 2,3,4-trisubstituted pyrrolidine motif has developed and such a motif can be accessed enantioselectively and diastereoselectively using α -lithiation chemistry.⁴ Subsequent trapping with an appropriate electrophile would give a functionalised heterocycle fragment which could then be further reacted to form the desired compound. This 2,3,4-trisubstituted pyrrolidine motif is present in drug compounds such as Boceprevir⁵ developed by Schering-Plough (now Merck) and Telaprevir⁶ developed by Vertex Pharmaceuticals, both of which are protease inhibitors used to treat hepatitis C (Figure 1.1).

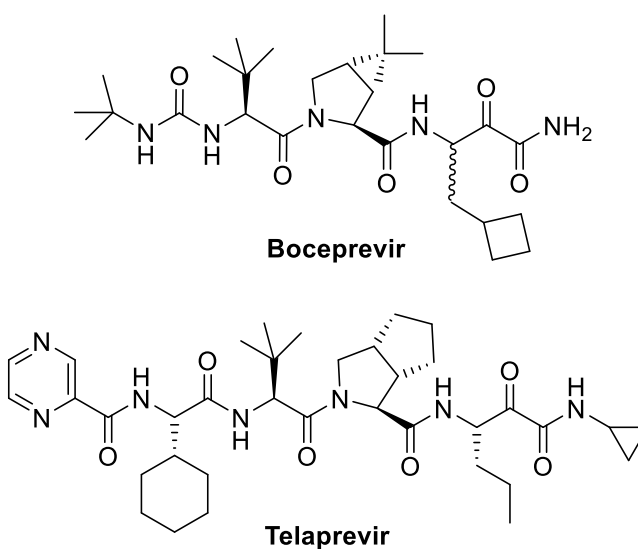
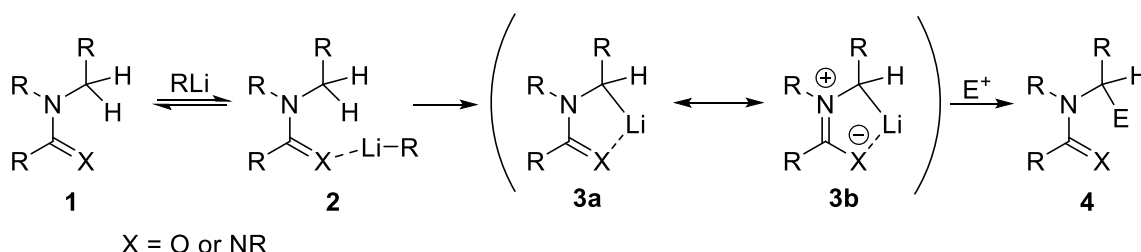


Figure 1.1. Boceprevir and Telaprevir protease inhibitors

1.1 Directed α -Lithiation - The Complex Induced Proximity Effect

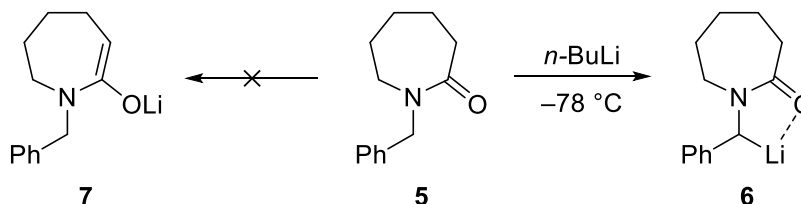
The α -deprotonation of *N*-Boc heterocycles occurs for one key reason – the directing effect afforded by the carbamate that is attached to the *N*-heterocycle. This type of directing effect has been used in synthetic organolithium chemistry for several decades and was coined the ‘Complex Induced Proximity Effect’ (CIPE) by Beak and Meyers in 1986.⁷ Beak and Meyers proposed a general mechanism for the CIPE whereby the Lewis basic directing group attached to the heteroatom (in this case nitrogen) of substrate **1** can reversibly coordinate to the organolithium reagent to form prelithiation complex **2** (Scheme 1.1). This prelithiation complex places the organolithium in close proximity to the α -protons which facilitates the α -deprotonation of **2**, forming α -lithiated intermediate **3**. Lithiated intermediate **3** is dipole-stabilised, as the positive charge in resonance form **3b** can stabilise the adjacent carbanion.⁸ Upon addition of an electrophile (E^+), lithiated intermediate **3** undergoes trapping to form trapped product **4**.

Scheme 1.1. General mechanism for the CIPE directed α -lithiation to a heteroatom



The directing effect offered by the CIPE can also strongly influence the regioselectivity of the lithiation of a substrate. For example, lithiation of benzyl lactam **5** with *n*-BuLi at -78°C resulted in exclusive formation of α -lithiated lactam **6**, rather than the thermodynamically favoured enolate **7** (Scheme 1.2).⁷

Scheme 1.2. Regioselective α -lithiation of lactam 5



Many different types of directing groups have been employed to enable the α -lithiation of amines. These directing groups need to be Lewis basic to allow coordination of the organolithium species involved and resistant to nucleophilic attack from the alkyllithium

reagents used. Some of the directing groups that have been utilised are amides (used by Beak,⁸⁻¹⁵), formamidines (reported by Meyers¹⁶⁻¹⁹), nitrosoamines (reported by Seebach^{20,21}) and ureas (used by Metallinos)^{22,23} (Figure 1.2).

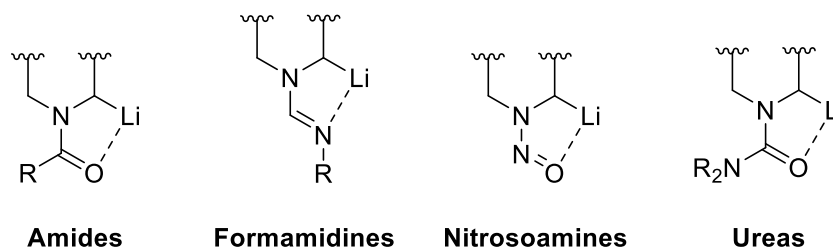
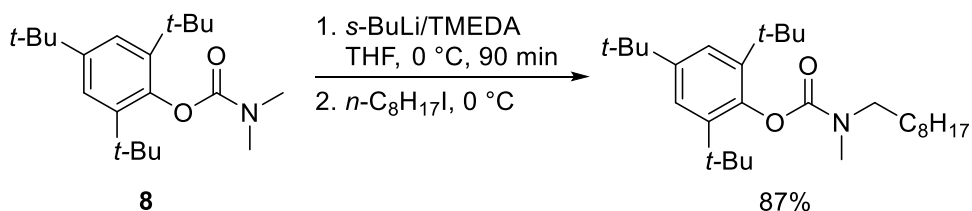


Figure 1.2. Directing groups used to direct α -lithiation of amines

Carbamates can also be used to direct lithiation α to an amine and the first α -lithiation of a carbamate was reported by Seebach in 1978.²⁴ Treatment of hindered aryl carbamate **8** with *s*-BuLi/TMEDA resulted in lithiation α to nitrogen and subsequent trapping with *n*-C₈H₁₇I provided the respective alkylated carbamate in 87% yield (Scheme 1.3). Both the lithiation and trapping reactions of **8** were conducted at 0 °C. In general, low temperatures (usually between 0 °C and –100 °C) are required for the lithiation and trapping steps to prevent side reactions and decomposition of the lithiated intermediate.

Scheme 1.3. Directed α -lithiation of carbamate **8**



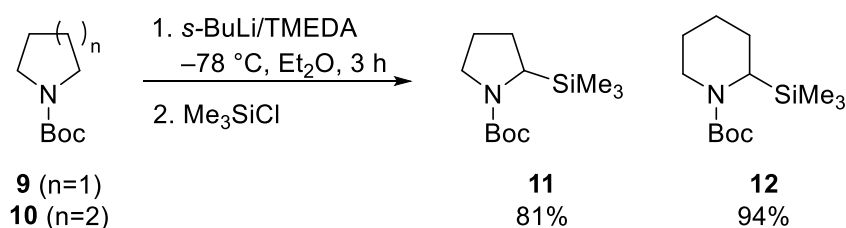
Some years later, Beak reported the directed α -lithiation of cyclic amines using a *tert*-butoxycarbonyl (Boc) carbamate to direct the lithiation in his seminal 1989 publication.² This methodology has two key advantages. First, the Boc group is a common amine protecting group, so installation of the Boc group is well known and reagents are commercially available. Second, the Boc group is easy to remove with acids such as TFA or HCl, so further functionalisation of the amine can be carried out after α -functionalisation. The use of the Boc group as a director for the α -lithiation reactions of *N*-Boc heterocycles relevant to the work described in this thesis will be discussed in the next section of this overview.

1.2 Lithiation-Trapping Reactions of *N*-Boc Heterocycles

1.2.1 *N*-Boc pyrrolidine and *N*-Boc piperidine

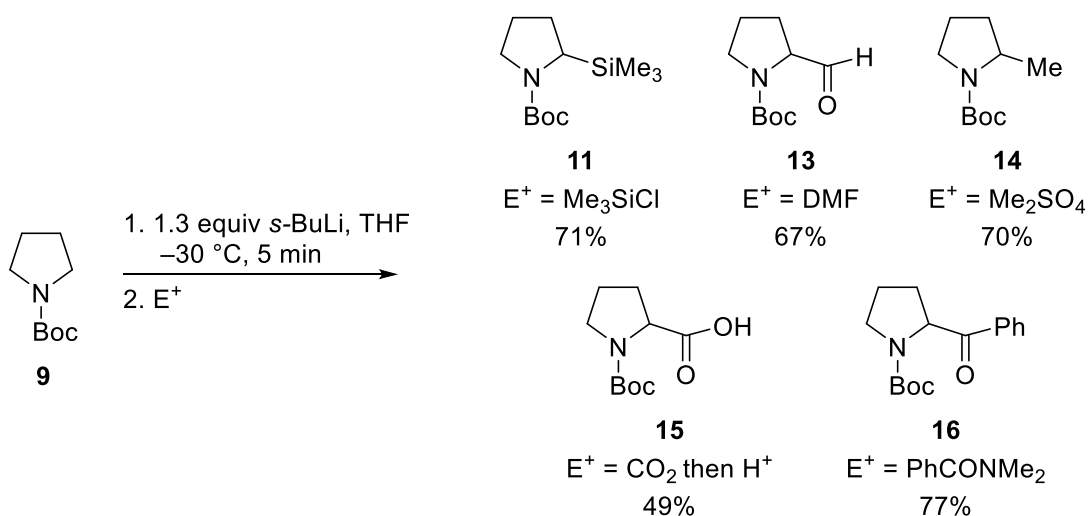
The first α -lithiation-trapping reactions of *N*-Boc pyrrolidine **9** and *N*-Boc piperidine **10** were reported by Beak in 1989.² Both heterocycles were treated with *s*-BuLi/TMEDA at $-78\text{ }^\circ\text{C}$ in Et₂O for 3 h and then Me₃SiCl was added to trap the lithiated intermediates. This afforded 2-silyl *N*-Boc pyrrolidine **11** and 2-silyl *N*-Boc piperidine **12** in 81% and 94% isolated yields respectively (Scheme 1.4).

Scheme 1.4. Racemic α -lithiation-trapping reactions of *N*-Boc pyrrolidine **9** and *N*-Boc piperidine **10**



Later, the O'Brien group developed a 'diamine-free' lithiation for the α -lithiation of *N*-Boc heterocycles.²⁵ Lithiation of *N*-Boc pyrrolidine **9** with *s*-BuLi/THF at $-30\text{ }^\circ\text{C}$ and subsequent trapping with Me₃SiCl furnished 2-silyl *N*-Boc pyrrolidine **11** in 71% yield (Scheme 1.5). With this methodology, a variety of 2-substituted *N*-Boc pyrrolidines **11**, **13-16** were synthesised in moderate to good yield ranging from 49-77%.

Scheme 1.5. 'Diamine-free' *s*-BuLi/THF lithiation-trapping of *N*-Boc pyrrolidine **9**

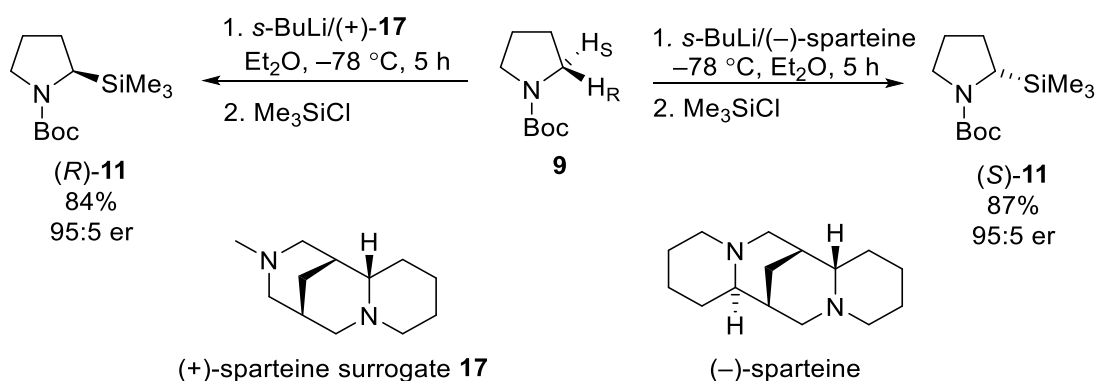


When the *s*-BuLi/THF lithiation-trapping of *N*-Boc piperidine **10** was attempted, no trapped adducts were detected. It has been proven that alkylolithiums are less stable in THF than

Et₂O²⁶ and recent unpublished work in the O'Brien group had observed the *s*-BuLi mediated decomposition of THF at higher temperatures (> -30 °C).²⁷ As *N*-Boc piperidine **10** is significantly less reactive than *N*-Boc pyrrolidine **9**, the decomposition of the THF solvent is likely the kinetically favoured reaction, meaning that no trapped adduct was observed.

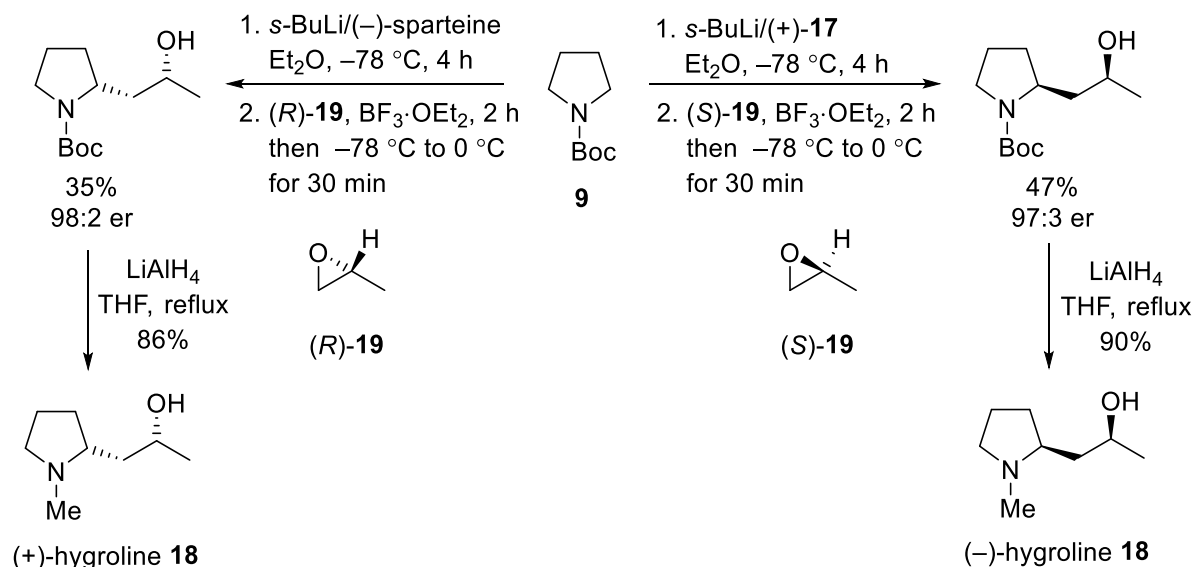
The enantioselective *s*-BuLi/(-)-sparteine-mediated lithiation-trapping of *N*-Boc pyrrolidine **9** was communicated by Beak and Kerrick in 1991³ and reported in full in 1994.²⁸ Lithiation using *s*-BuLi and the chiral diamine (-)-sparteine, followed by trapping with Me₃SiCl gave (*S*)-**11** in 87% yield and excellent 95:5 er (Scheme 1.6). The O'Brien group subsequently reported the synthesis of 2-silyl *N*-Boc pyrrolidine (*R*)-**11** in 84% yield and 95:5 er using their chiral diamine, the (+)-sparteine surrogate **17**, which behaves in an enantiocomplementary manner to (-)-sparteine (Scheme 1.6).²⁹ Throughout this thesis the degree of enantioselectivity exhibited in an asymmetric reaction will be quantified using enantiomeric ratios (er). This measure of enantioselectivity has been selected as it is mathematically more simple than enantiomeric excess (ee), making it easier for the reader to comprehend of the degree of enantioselectivity exhibited in a reaction.

Scheme 1.6. Asymmetric lithiation-trapping of *N*-Boc pyrrolidine **9 with (-)-sparteine and (+)-**17** chiral diamine ligands**



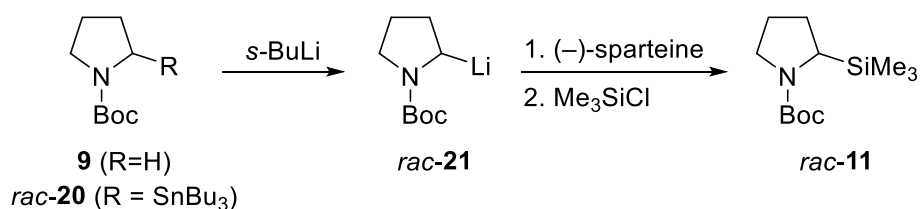
Altmann *et al.* has performed lithiations with both *s*-BuLi/(-)-sparteine and *s*-BuLi/(+)-**17** to synthesise the natural products (+)- and (-)-hygroline **18**.³⁰ The synthesis involved the asymmetric lithiation of *N*-Boc pyrrolidine **9** with either *s*-BuLi/(-)-sparteine or *s*-BuLi/(+)-**17** and then subsequent trapping with chiral epoxides (*R*)- or (*S*)-**19**, followed by reduction with LiAlH₄ to give (+)- or (-)-hygroline **18** (Scheme 1.7).

Scheme 1.7. Synthesis of (+)- and (-)- hygroline via asymmetric lithiation trapping of *N*-Boc pyrrolidine **9**



The α -lithiation reactions of *N*-Boc pyrrolidine **9** with *s*-BuLi/(-)-sparteine or *i*-PrLi/(-)-sparteine have both been subjected to mechanistic investigation. In 1991, Beak conducted several lithiation-trapping reactions of *N*-Boc pyrrolidine **9** to determine whether the enantioselectivity observed with *s*-BuLi/(-)-sparteine arises from an enantioselective deprotonation or whether the enantioselectivity is afforded post-deprotonation.³ Racemic 2-lithio *N*-Boc pyrrolidine *rac*-**21** was generated by both *s*-BuLi deprotonation of *N*-Boc pyrrolidine **9** and tin-lithium exchange of 2-stannyl pyrrolidine **20**. (-)-Sparteine was then added to the lithiated intermediate *rac*-**21** followed by Me₃SiCl. The Me₃SiCl trapped adduct **11** from both reactions was obtained as a racemate (Scheme 1.8).

Scheme 1.8. Determination of the source of enantioselectivity of the *s*-BuLi/(-)-sparteine lithiation of *N*-Boc pyrrolidine **9**

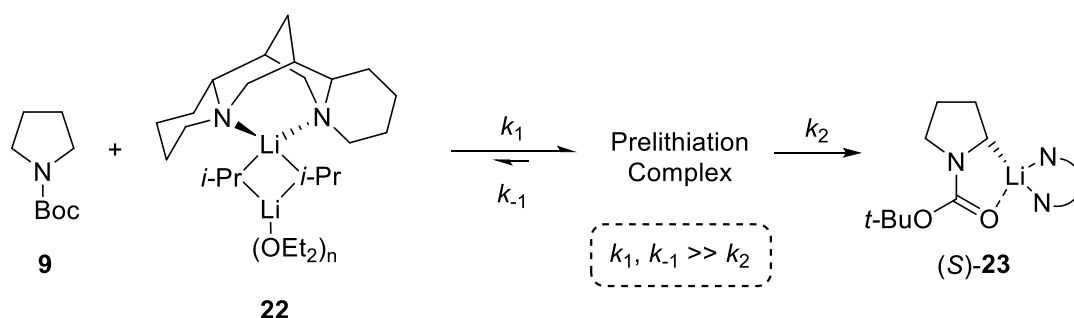


Beak therefore concluded that the enantioselectivity afforded by (-)-sparteine must arise from an enantioselective deprotonation and does not occur post-deprotonation. O'Brien *et al.* have also shown that the enantioselectivity afforded with *N*-Boc piperidine **10** and *s*-

BuLi/(+)-**17** occurs by an enantioselective deprotonation using experiments similar to those used by Beak.³¹

In 1995, Beak and Gallagher conducted a mechanistic investigation of the *i*-PrLi/(–)-sparteine lithiation of *N*-Boc pyrrolidine **9** using kinetic experiments.³² They noted that the lithiation had a zero-order dependence on the concentration of the *i*-PrLi/(–)-sparteine complex **22**, the structure of which had been determined previously.³³ This led them to propose that the rapid formation of a prelithiation complex occurs before the rate determining α -deprotonation, which accounted for the zero-order dependence of the alkyllithium (Scheme 1.9). Kinetic isotope experiments were also carried out and they confirmed that the second step of the α -lithiation where deprotonation occurs (k_2) and (*S*)-**23** is formed was rate determining.

Scheme 1.9. Proposed mechanism for the *i*-PrLi/(–)-sparteine α -lithiation of *N*-Boc pyrrolidine **9**



Three possible structures for the prelithiation complex were suggested: **24**, **25** and **26** (Figure 1.3). Beak and Gallagher suggested that the prelithiation complex was unlikely to be **24** as the (–)-sparteine was far removed from *N*-Boc pyrrolidine **9** and would not likely be able to offer any enantiocontrol over α -lithiation from this distance.

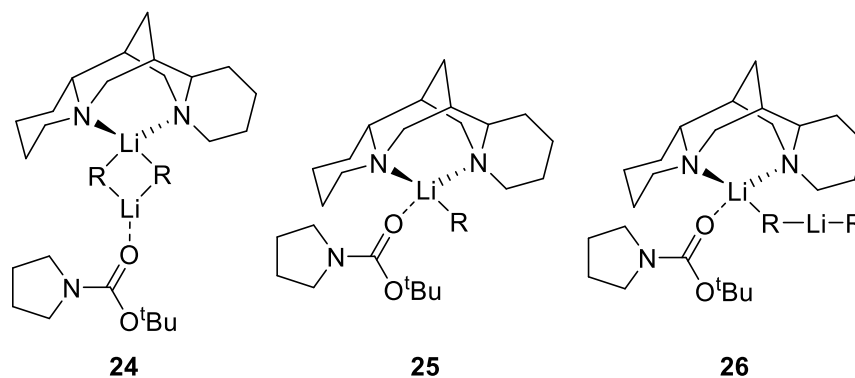
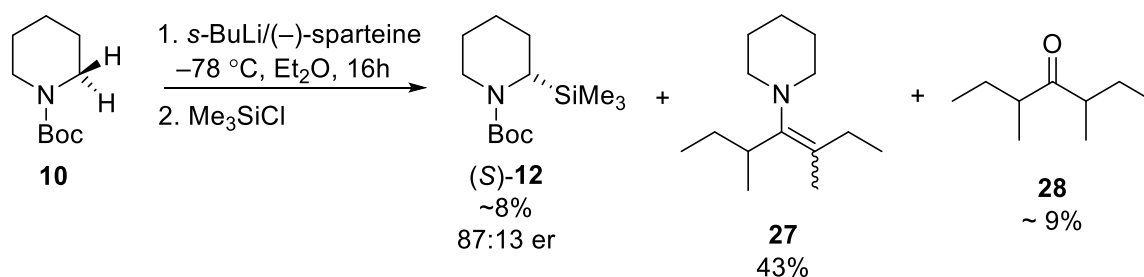


Figure 1.3. Proposed pre-lithiation complexes for the RLi/(–)-sparteine lithiation of *N*-Boc pyrrolidine **9**

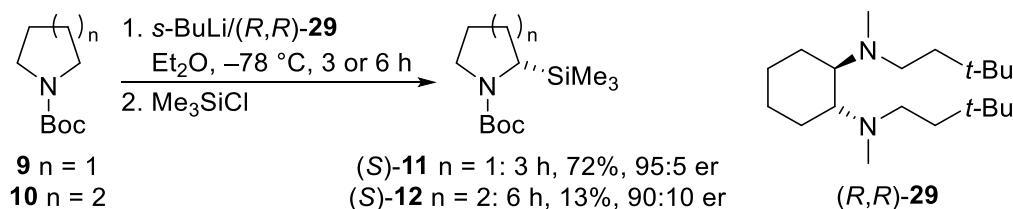
Beak and Kerrick first reported the *s*-BuLi/(-)-sparteine lithiation-trapping of *N*-Boc piperidine **10** in 2002.³⁴ Lithiation for 16 h and trapping with Me₃SiCl gave the desired 2-silyl *N*-Boc piperidine (*S*)-**12** in a low ~8% yield and moderate 87:13 er, with side-products **27** and **28** also isolated (Scheme 1.10). The slow rate of reaction between *s*-BuLi/(-)-sparteine and *N*-Boc piperidine **10** allows side reactions to occur. In particular, *s*-BuLi can perform a nucleophilic attack into the Boc carbonyl generating by-products **27** and **28**.

Scheme 1.10. Attempted *s*-BuLi/(-)-sparteine lithiation of *N*-Boc piperidine **10**



Coldham and O'Brien also attempted the asymmetric lithiation of *N*-Boc piperidine **10** using cyclohexyl diamine ligand (*R,R*)-**29** which had displayed high enantioselectivity for the lithiation of *N*-Boc pyrrolidine **9** (Scheme 1.11).^{35,36} Lithiation of *N*-Boc piperidine **10** with *s*-BuLi/(*R,R*)-**29** and trapping with Me₃SiCl provided 2-silyl adduct (*S*)-**12** in only 13% yield in 90:10 er. Comparison of this result with the 8% yield of (*S*)-**12** obtained by Beak and Kerrick with *s*-BuLi/(-)-sparteine (see Scheme 1.10), shows that the *s*-BuLi/(*R,R*)-**29** complex was more reactive and provided marginally higher enantioselectivity. However, the lithiation of *N*-Boc piperidine **10** with *s*-BuLi/(*R,R*)-**29** still did not provide a synthetically useful method of preparing enantioenriched 2-substituted piperidines.

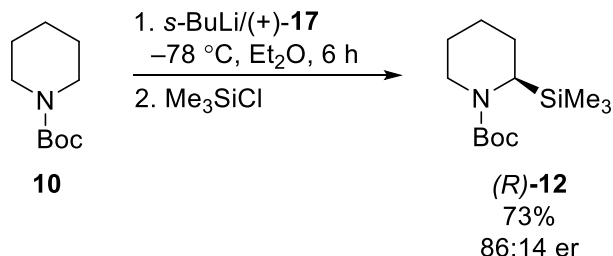
Scheme 1.11. Asymmetric lithiation-trapping of *N*-Boc piperidine and *N*-Boc pyrrolidine **10 with *s*-BuLi/(*R,R*)-**29****



Later, O'Brien reattempted the asymmetric lithiation of *N*-Boc piperidine **10** using *s*-BuLi/(+)-sparteine surrogate **17**. This afforded 2-silyl piperidine (*R*)-**12** in good 73% yield with moderate 86:14 er (Scheme 1.12).³¹ In contrast to the *s*-BuLi/(-)-sparteine lithiation of

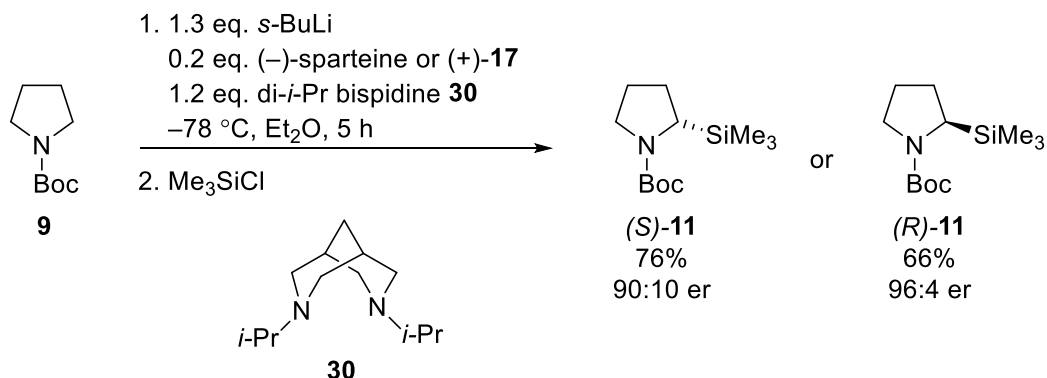
N-Boc piperidine **10**, the *s*-BuLi/(+)-sparteine surrogate lithiation gives a greatly improved yield which can be attributed to the more reactive *s*-BuLi/(+)-**17** lithiating complex.

Scheme 1.12. *s*-BuLi/(+)-sparteine surrogate **17** lithiation of *N*-Boc piperidine **10**



The O'Brien group have also presented a catalytic two-ligand enantioselective lithiation of *N*-Boc pyrrolidine **9**, using the combination of a sub-stoichiometric amount of chiral ligand (–)-sparteine or (+)-**17** and stoichiometric quantities of achiral diamine di-*i*-Pr bispidine **30**.³⁷ The presence of the achiral diamine allows the (–)-sparteine or (+)-**17**-complexed lithiated intermediate to exchange ligands with di-*i*-Pr bispidine **30**, freeing the chiral ligand to carry out further lithiation cycles. Importantly, *s*-BuLi/di-*i*-Pr bispidine **30** has a slower rate of lithiation than *s*-BuLi/(–)-sparteine or *s*-BuLi/(+)-**17**, meaning that the chiral ligand lithiates the majority of the starting material, which gives the product in high er. Use of *s*-BuLi with 0.2 eq. of either (–)-sparteine or (+)-**17** and 1.2 eq. of di-*i*-Pr bispidine **30** to lithiate *N*-Boc pyrrolidine **9** and trapping with Me₃SiCl gave 2-silyl pyrrolidines (*S*)- and (*R*)-**11** in 76% and 66% yields respectively with er varying between 90:10 and 96:4 (Scheme 1.13).

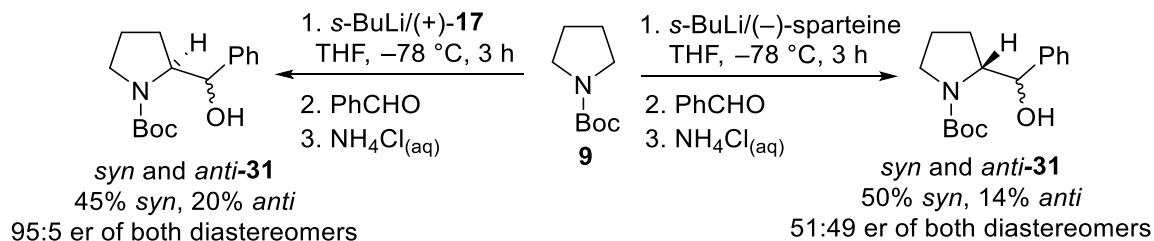
Scheme 1.13. Catalytic two-ligand *s*-BuLi/(–)-sparteine/di-*i*-Pr bispidine **30** and *s*-BuLi/(+)-**17**/di-*i*-Pr bispidine **30** lithiation of *N*-Boc pyrrolidine **9**



The lithiation of *N*-Boc pyrrolidine **9** using the chiral ligands (–)-sparteine and (+)-**17** has also been carried out in THF solvent.³¹ Earlier work by O'Brien indicated that the THF can act as ligand allowing racemic lithiation of *N*-Boc pyrrolidine **9** (see Scheme 1.5) and therefore it was uncertain whether enantioenrichment would be observed with the chiral

diamines. When the lithiation of *N*-Boc pyrrolidine **9** was conducted with *s*-BuLi/(–)-sparteine in THF, trapped products *syn*- and *anti*-**31** were obtained as near-racemates (Scheme 1.14). When the same reaction was conducted using *s*-BuLi/(+)-**17**, the trapped adducts *syn* and *anti*-**31** were obtained in 95:5 er.

Scheme 1.14. *s*-BuLi/(–)-sparteine and *s*-BuLi/(+)-17** lithiation of *N*-Boc pyrrolidine **9** in THF solvent**

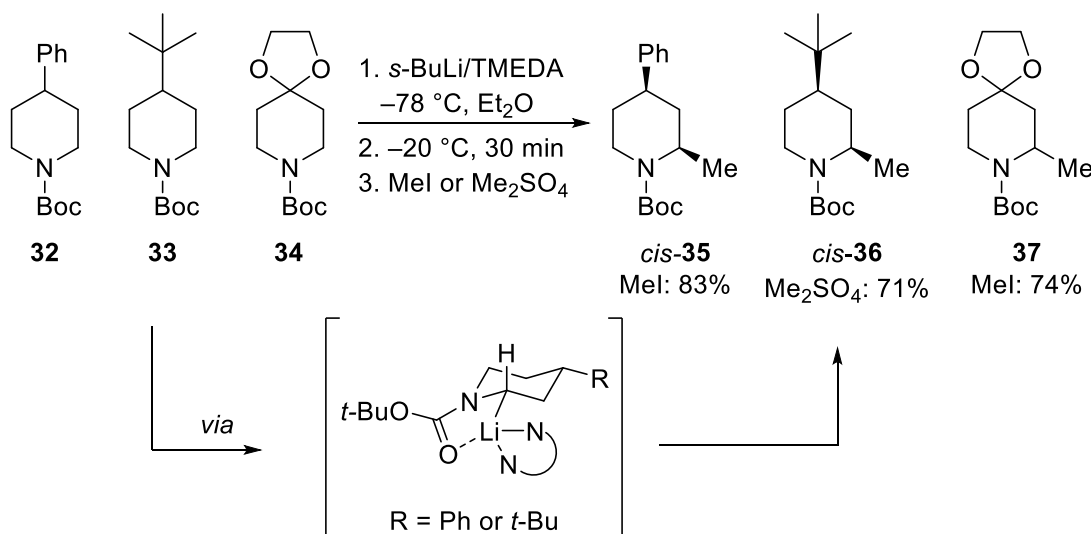


By using ^{13}C and ^6Li NMR spectroscopy, O'Brien noted that over 3.0 eq. of (–)-sparteine were required for the (–)-sparteine to displace the THF coordinated to the alkyllithium. This is likely the reason that *s*-BuLi/(–)-sparteine lithiation in THF provides only racemic product as the alkyllithium is preferentially coordinated to THF. On the other hand, addition of 1.0 eq. of (+)-**17** resulted in formation of a complex where the alkyllithium is coordinated to both (+)-**17** and a molecule of THF. This means that enantioselective lithiation will occur with 1.0 eq. of (+)-**17** and is why an asymmetric *s*-BuLi/(+)-**17** lithiation can be carried out in THF.

1.2.2. 4-Substituted *N*-Boc piperidines

Several examples of the synthesis of 2,4-disubstituted *N*-Boc piperidines using α -lithiation-trapping chemistry have also been described.^{25,38-40} Beak and Lee reported the α -lithiation-trapping reactions of 4-phenyl, 4-*t*-Bu and 4-ketal substituted *N*-Boc piperidines **32**, **33** and **34**.³⁸ Lithiation of substituted piperidines **32**, **33** and **34** with *s*-BuLi/TMEDA followed by trapping with MeI or Me₂SO₄ afforded methylated piperidines *cis*-**35**, *cis*-**36** and **37** in good (71-83%) yield (Scheme 1.15). It was noted that the products of the lithiation-trapping reactions of 4-phenyl and 4-*t*-Bu piperidines **32** and **33** were both obtained as *cis* diastereoisomers. This diastereoselectivity arises from the preference for equatorial α -lithiation which allows the CIPE to occur. In these 4-substituted piperidines, the equatorial α -proton will be *cis* to the C4-substituent as this places the substituent in an energetically favoured equatorial position. Trapping then occurs with retention of the stereochemistry so only the *cis* diastereomer was obtained.

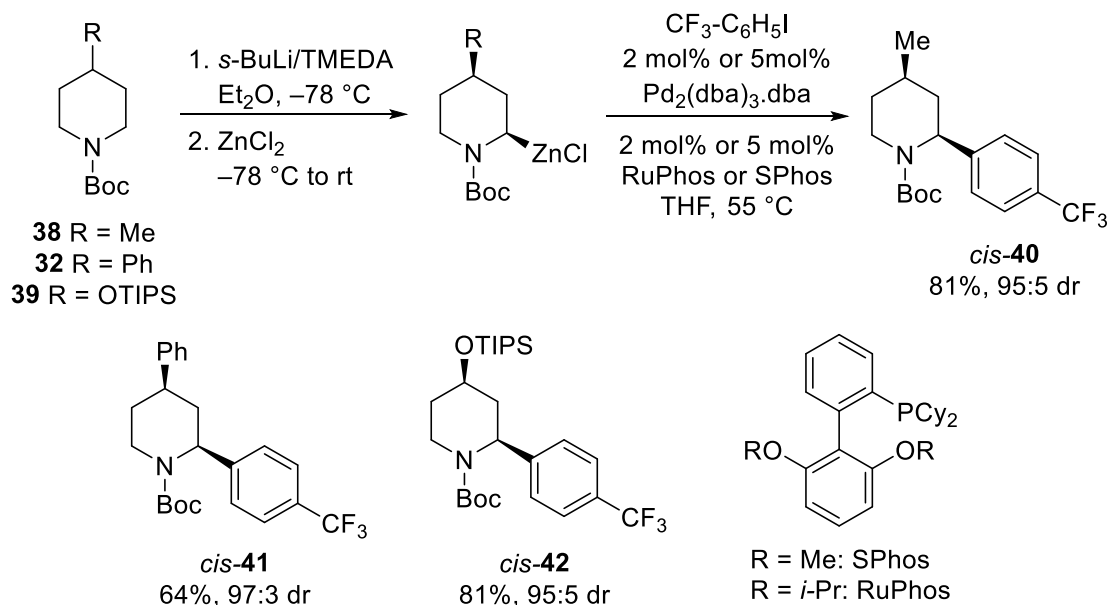
Scheme 1.15. Lithiation-trapping of 4-substituted *N*-Boc piperidines with rationale for the *cis* selectivity observed



Knochel *et al.* have also prepared a range of different 2,4-disubstituted piperidines using a diastereoselective cross-coupling reaction between aryl iodides and substituted piperidinyl-zinc reagents, prepared by α -lithiation-transmetalation.³⁹ The α -arylation of *N*-Boc pyrrolidines using α -lithiation-transmetalation and cross-coupling was reported earlier by Campos.⁴¹ Using this methodology, Knochel *et al.* prepared a variety of 2-arylated piperidines using a selection of 4-substituted piperidines including 4-methyl, 4-phenyl and 4-OTIPS *N*-Boc piperidines **38**, **32** and **39**. Zincation of these *N*-Boc piperidines with *s*-BuLi/TMEDA then ZnCl₂ and subsequent Negishi coupling with RuPhos or SPhos with 4-

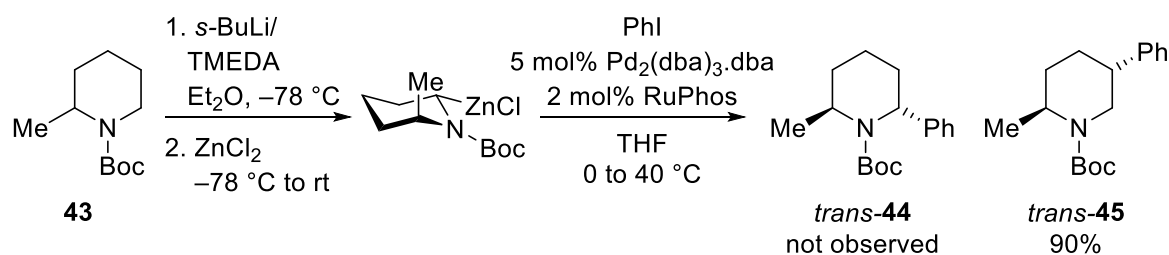
CF₃ substituted aryl iodide provided 2,4-disubstituted piperidines *cis*-**40-42** in good to moderate yield (81-64%) and very good 97:3-95:5 drs (Scheme 1.16).

Scheme 1.16. Diastereoselective cross-coupling of 4-substituted piperidines **38, **32** and **39****



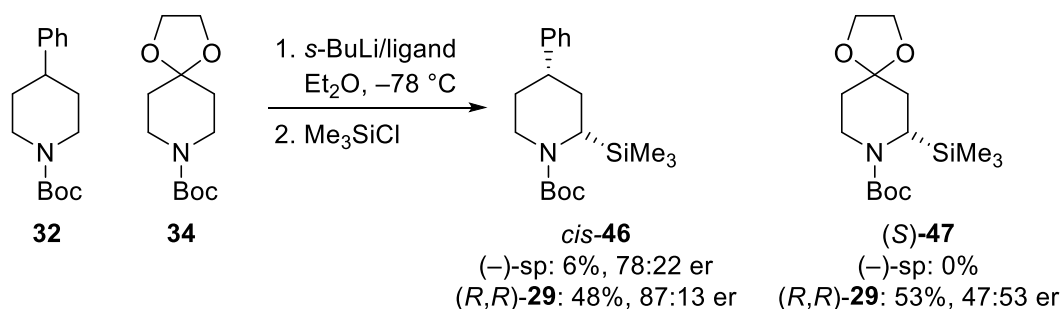
Knochel suggested that the *cis* diastereoselectivity observed in the 2-aryl piperidines *cis*-**40-42** was likely introduced during the lithiation of the piperidine substrates, as observed with Beak's work (see Scheme 1.15). In the same communication, the synthesis of *trans*-2,6-disubstituted piperidine **44** by zincation and cross-coupling of 2-methyl *N*-Boc piperidine **43** was also attempted. However, none of the expected product *trans*-**44** was obtained. Instead, 2,5-disubstituted piperidine *trans*-**45** was isolated in 90% yield (Scheme 1.17). It was rationalised that β -hydride elimination of the organopalladium intermediate occurs. The PhPdL_2H complex that is formed, remains bound to the same side of the tetrahydropyridinyl ring and *syn* addition occurs which places the Pd at the less sterically hindered C-5 position. Reductive elimination would then afford the observed 2,5-disubstituted piperidine *trans*-**45**.

Scheme 1.17. 1,2-Migration of Pd in the cross-coupling of 2-methyl *N*-Boc piperidine **43**



The asymmetric lithiation-trapping reactions of 4-phenyl and 4-ketal piperidines have been reported but both offered trapped products in only moderate yield and er.³⁶ The lithiation of the 4-substituted piperidines was conducted with *s*-BuLi/(–)-sparteine and *s*-BuLi/(*R,R*)-**29**, which Coldham and O’Brien had found provided the best enantioselectivity for the lithiation of *N*-Boc piperidine **10** (see Scheme 1.11). Lithiation of 4-phenyl *N*-Boc piperidine **32** and subsequent Me₃SiCl trapping provided only a 6% yield of the 2-silyl 4-phenyl piperidine *cis*-**46** in a moderate 78:22 er. The same lithiation-trapping of 4-ketal *N*-Boc piperidine **34** provided none of the trapped silyl adduct **47** (Scheme 1.18). When the reactions were repeated with the more reactive *s*-BuLi/(*R,R*)-**27** complex, 2-silyl piperidines **46** and **47** were obtained in improved 48% and 53% yields. The er of trapped products was variable, with 2-silyl 4-phenyl piperidine *cis*-**46** obtained in 87:13 er and 2-silyl 4-ketal piperidine **47** obtained almost as a racemate (47:53 er).

Scheme 1.18. Asymmetric lithiation-trapping reactions of 4-phenyl and 4-ketal *N*-Boc piperidines **32 and **34****

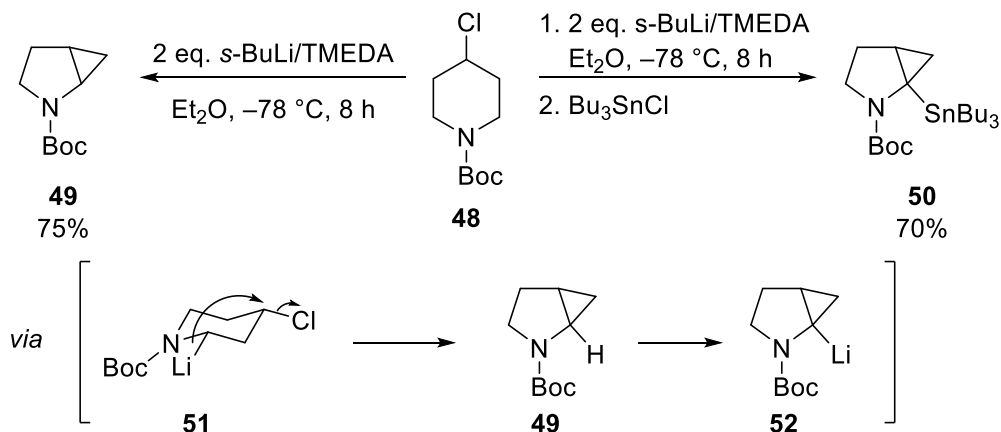


Trapped adducts *cis*-**46** and **47** were obtained in significantly higher yield than 2-silyl piperidine **12**, obtained by the lithiation-trapping of *N*-Boc piperidine **10** using the same conditions (13% yield, see Scheme 1.10). This suggested that these two 4-substituted piperidines have a higher reactivity than that of *N*-Boc piperidine **10**. Competition experiments with 4-phenyl piperidine **32** and *N*-Boc piperidine **10** have also indicated that the lithiation of 4-phenyl piperidine **32** is more facile.⁴⁰

The α -lithiation-trapping of 4-chloro *N*-Boc piperidine **48** was first reported by Beak in 1994 to synthesise bicyclic heterocycles.⁴² Lithiation of 4-chloro *N*-Boc piperidine **48** with 2 eq. *s*-BuLi/TMEDA for 8 h and subsequent quenching of the reaction provided [3.1.0] azabicyclic **49** in 75% yield (Scheme 1.19). When an electrophile was added after the lithiation, a 2-substituted bicyclic pyrrolidine was obtained. For example, the addition of Bu₃SnCl after lithiation afforded 2-stannyl bicycle **50** in 70% yield. The mechanism for the bicycle formation likely involves intramolecular cyclisation of the lithiated intermediate **51**,

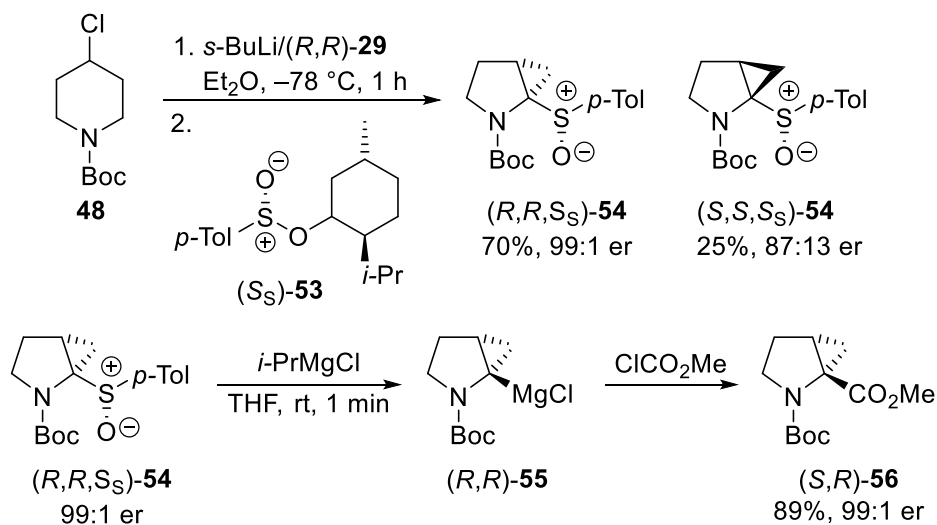
which undergoes further lithiation to provide lithiated bicyclic **52**. If the lithiation is then quenched, bicyclic pyrrolidine **49** is generated, whereas if an electrophile such as Bu_3SnCl is added, a 2-trapped adduct such as **50** is formed. Similar syntheses of bicyclic heterocycles have been reported *via* lithiation of 4-*O*-nosyl and 4-*O*-tosyl *N*-Boc piperidines.^{34,43}

Scheme 1.19. Bicycle formation *via* lithiation-trapping of 4-chloro *N*-Boc piperidine **48**



Rayner *et al.* used the α -lithiation-trapping of 4-chloro *N*-Boc piperidine **48** to prepare enantiopure chiral sulfoxides which could then be converted into enantiopure Grignard reagents.⁴⁴ The *s*-BuLi/*(R,R)*-**29** lithiation of 4-chloro piperidine **48** and trapping with enantiopure sulfinate (*S_S*)-**53** afforded (*R,R,S_S*)-**54** in 51% yield and 99:1 er and (*S,S,S_S*)-**54** in 25% yield and 87:13 er (Scheme 1.20). Sulfoxide/Mg exchange of (*R,R,S_S*)-**54** formed Grignard (*R,R*)-**55** which when trapped with ClCO_2Me provided ester (*S,R*)-**56** in 89% yield and 99:1 er.

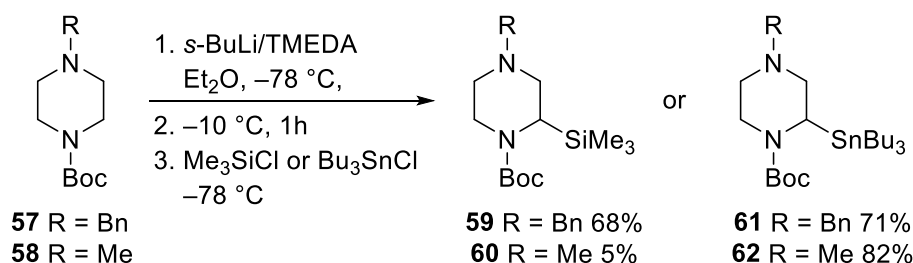
Scheme 1.20. Chiral Grignard preparation *via* synthesis of chiral sulfoxides



1.2.3. *N*-Boc piperazines

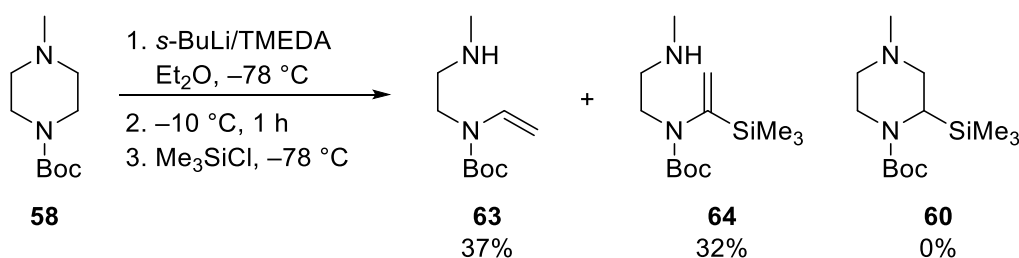
There are many examples of racemic α -lithiation-trapping reactions of *N*-Boc piperazines in the literature.^{25,45–50} The first of these was reported by Van den Hoogenband and Van Maarseveen in 2005, where *N*⁷-Bn and *N*⁷-Me *N*-Boc piperazines **57** and **58** were lithiated with *s*-BuLi/TMEDA and then trapped with Me₃SiCl and Bu₃SnCl.⁵¹ Trapping after lithiation with Bu₃SnCl provided both the *N*⁷-Bn and *N*⁷-Me stannanes **61** and **62** in good 71% and 82% yields respectively. The trapping of lithiated *N*⁷-Bn piperazine **57** with Me₃SiCl also provided the desired 2-silyl piperidine **59** in a good 68% yield. However, when *N*⁷-Me piperazine **58** was subjected to lithiation and trapping with Me₃SiCl, the desired 2-silyl piperazine **60** was obtained in only 5% yield (Scheme 1.21).

Scheme 1.21. Lithiation-trapping of *N*⁷-Bn piperazine **57 and *N*⁷-Me piperazine **58****



No explanation was offered as to why the 2-silyl piperazine **60** was obtained in such low yield. However, in a recent paper, O'Brien *et al.* repeated the *s*-BuLi/TMEDA lithiation and Me₃SiCl trapping of *N*⁷-Me piperazine **58**.⁵⁰ In their hands, none of the desired 2-silyl piperazine product **60** was obtained. Instead, a mixture of fragmentation products **63** and **64** were obtained (Scheme 1.22).

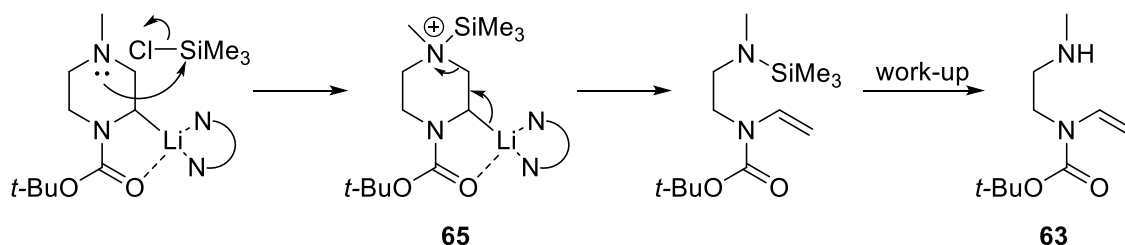
Scheme 1.22. Repeated lithiation-trapping of *N*⁷-Me piperazine **58 by O'Brien *et al.***



O'Brien encountered this piperazine fragmentation in earlier work and proposed that the fragmentation occurs as the distal nitrogen reacts with the electrophile, generating an ammonium intermediate **65** (Scheme 1.23).⁵² Subsequent β -elimination and cleavage of the weak N-Si bond during work-up would provide a vinylic carbamate as observed for the repeated lithiation-trapping of *N*⁷-Me piperazine **63** in Scheme 1.22. A subsequent vinylic

lithiation and Me₃SiCl trapping of intermediate **63** would also account for the additional fragmentation product **64** observed.

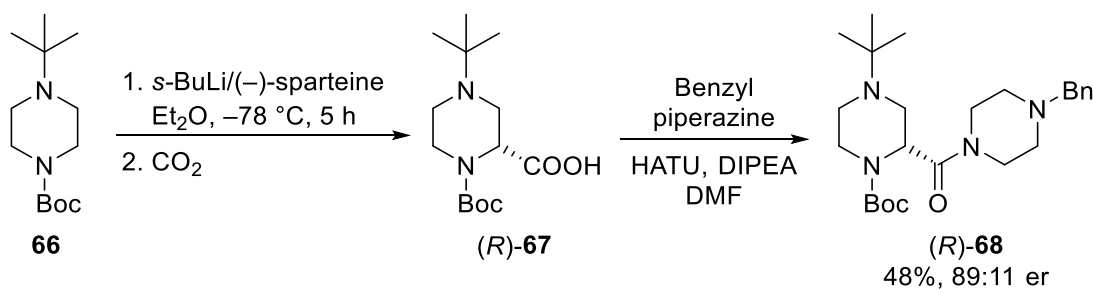
Scheme 1.23. Proposed mechanism of N'-Me piperazine 58 fragmentation



This mechanism may also explain why the same fragmentation is not observed for the lithiation and Me₃SiCl trapping of N'-Bn piperazine **57**. The greater steric bulk on the distal nitrogen afforded by the Bn group could perturb the attack of the distal nitrogen onto the bulky Me₃SiCl electrophile, meaning that fragmentation can not occur. The high yield obtained for the Bu₃SnCl trapped N'-Me piperazine **59** in Scheme 1.21 may arise from the relative rates of Bu₃SnCl and Me₃SiCl trapping. Unpublished work by the O'Brien group has found that trapping with Bu₃SnCl is rapid⁵³ whereas trapping reactions with chlorosilanes are known to be slow and work in this thesis has also confirmed this.⁵⁴⁻⁵⁶ Therefore, it is possible that with Bu₃SnCl the trapping process is faster than fragmentation so the desired 2-substituted piperazine is obtained. With the slow Me₃SiCl trapping, the fragmentation may be faster than trapping so only products of the fragmentation are obtained.

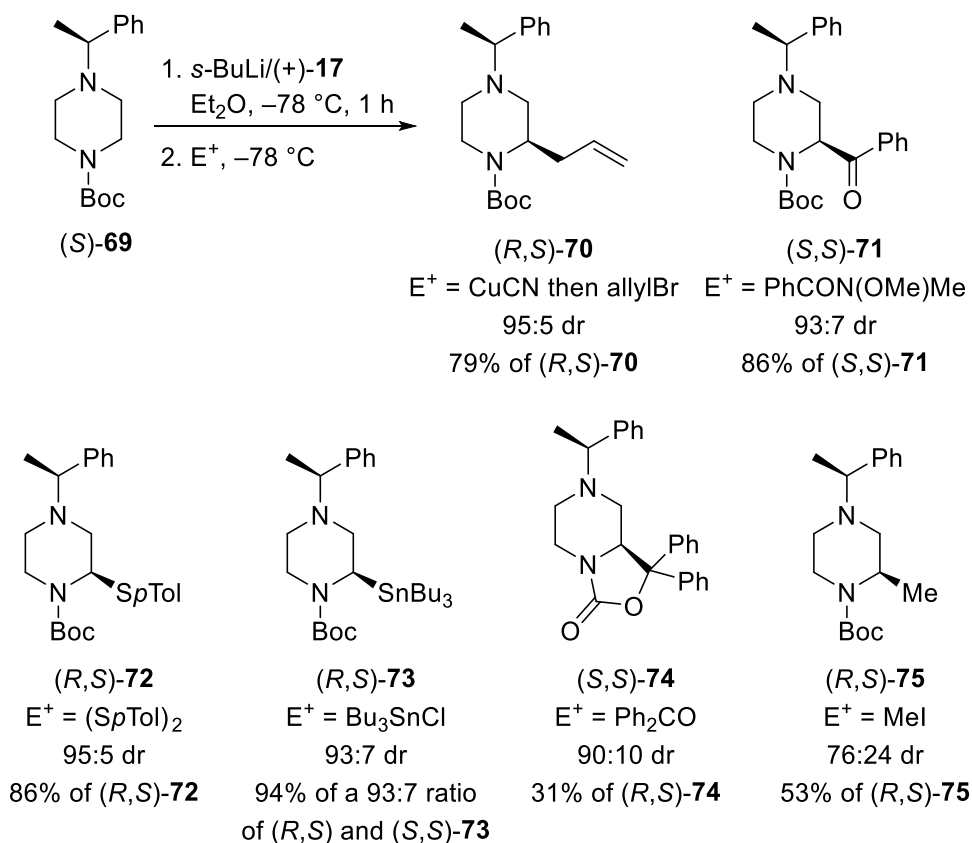
To date, there have only been two reports of the asymmetric lithiation-trapping reactions of an N-Boc piperazines. McDermott at AstraZeneca reported the lithiation of N'-t-Bu N-Boc piperazine **66** with *s*-BuLi/(-)-sparteine followed by trapping with CO₂ which afforded enantioenriched carboxylic acid (*R*)-**67**.⁵⁷ The crude acid was subsequently coupled with benzyl piperazine which provided amide (*R*)-**68** in 48% yield and 89:11 er (Scheme 1.24).

Scheme 1.24. Asymmetric lithiation-trapping of N'-t-Bu N-Boc piperazine 66



More recently, O'Brien *et al.* have reported the asymmetric lithiation-trapping of piperazines with a wide range of different substituents on the distal nitrogen.⁵² They initially performed lithiation-trapping reactions of *N'*-Bn *N*-Boc piperazine **57** with *s*-BuLi/(–)-sparteine and *s*-BuLi/(+)-sparteine surrogate **17**. However, for each of the lithiation-trapping reactions significant amounts of piperazine fragmentation occurred, as described in Scheme 1.22. As discussed earlier, they suggested that a bulkier substituent on the distal nitrogen would prevent this fragmentation by preventing the attack of the distal nitrogen onto the electrophile (see Scheme 1.23). Therefore, O'Brien *et al.* used a bulkier and enantiopure *N'*- α -methyl benzyl piperazine (*S*)-**69** which both prevented the fragmentation and introduced an additional stereocentre to the substrate. This additional stereocentre meant after the asymmetric lithiation-trapping the products were formed as diastereomers that can be more easily separated. The α -methyl benzyl substituent can also be removed readily with α -chloroethyl chloroformate allowing further functionalisation of the distal nitrogen after the lithiation-trapping.⁵⁸ Lithiation of *N'*- α -methyl benzyl piperazine (*S*)-**69** with *s*-BuLi/(+)-**17** and trapping with a range of electrophiles provided 2-substituted piperazines **70-75** in moderate to good 31%-94% yield and excellent to moderate dr (Scheme 1.25).

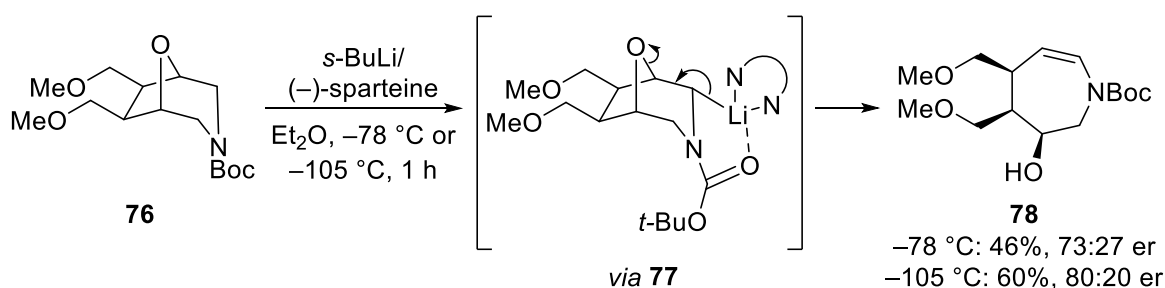
Scheme 1.25. Lithiation-trapping of *N'*- α -methyl benzyl piperazine (*S*)-69****



1.2.4. *N*-Boc morpholines

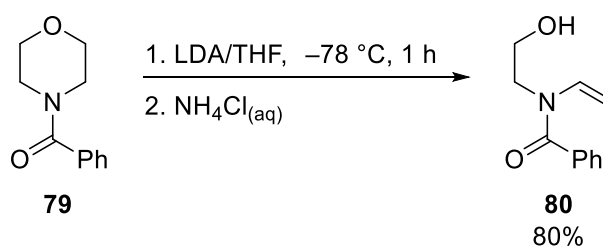
To date, the α -lithiation of only one *N*-Boc morpholine has been reported in the literature.⁵⁹ Bicyclic *N*-Boc morpholine **76** was subjected by Lautens to an enantioselective desymmetrisation using *s*-BuLi/(-)-sparteine, providing chiral trisubstituted azepane **78** (Scheme 1.26). At a reaction temperature of $-78\text{ }^{\circ}\text{C}$, azepane **78** was obtained in 46% yield and a moderate 73:27 er; at lower temperature ($-105\text{ }^{\circ}\text{C}$), azepane **78** was obtained in improved yield and er (60%, 80:20 er). Lautens suggests that the mechanism of this reaction occurs *via* formation of a 2-lithio azepane intermediate **77** which then eliminates to form ring opened azepane **78**.

Scheme 1.26. Enantioselective desymmetrization of *N*-Boc morpholine **76**



The only other α -lithiation of a morpholine that has been reported is the lithiation of *N*-benzoyl morpholine **79** with LDA.⁶⁰ After lithiation, the reaction was quenched with NH₄Cl_(aq) which provided ring opened alcohol **80** in 80% yield (Scheme 1.27). The mechanism for the ring opening is likely to be the same as that for the bicyclic morpholine in Scheme 1.26, where the α -lithiation is followed by an elimination that forms ring-opened alcohol **80**. Typically, strong alkyl lithium bases such as *s*-BuLi are required to remove the α -proton but in this case, the weaker LDA base is sufficient.

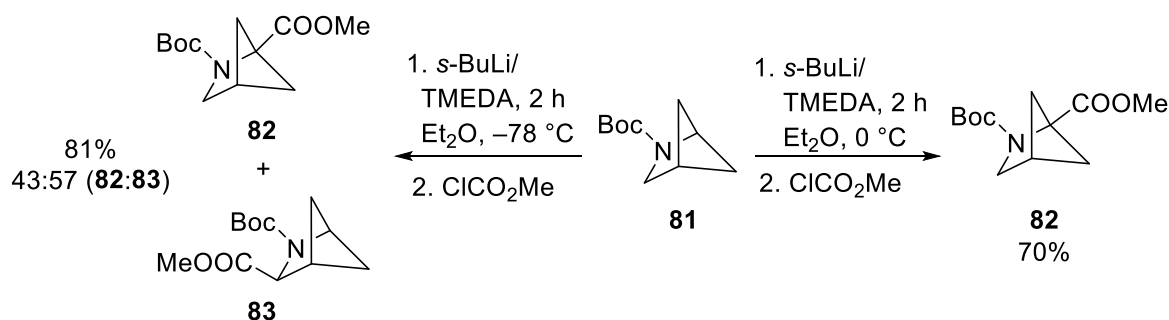
Scheme 1.27. LDA/THF lithiation of *N*-benzoyl morpholine **79**



1.2.5. Bicyclic *N*-Boc pyrrolidines

The α -lithiation-trapping reactions of bicyclic pyrrolidines has become more common, with many examples now available in the literature. One of the first α -lithiation-trapping reactions of a bicyclic *N*-Boc heterocycle was reported by Krow in 2002 in order to synthesise compounds to allow the study of conformational effects on collagen stability.⁶¹ [2.1.1]-Aza bicycle **81** was subjected to lithiation with *s*-BuLi/TMEDA followed by trapping with ClCO₂Me (Scheme 1.28). Lithiation of bicycle **81** can lead to the formation of two regioisomers, as it is possible to deprotonate either the methylene or bridgehead α -proton. When lithiation-trapping of **81** was conducted at -78 °C, a 43:57 mixture of regioisomers **82** and **83** was obtained in an 81% combined yield. However, lithiation-trapping at 0 °C provided exclusive formation of regioisomer **82** in 70% yield.

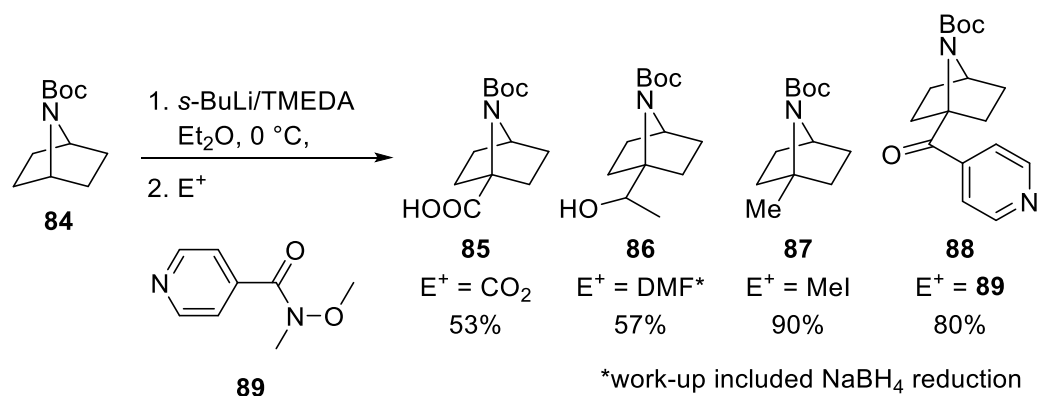
Scheme 1.28. Lithiation-trapping of bicyclic pyrrolidine 81



Krow revisited the regioselectivity of the α -lithiation of bicyclic pyrrolidine **81** in a subsequent computational investigation of the regioselectivity.⁶² The computational modelling suggested that the energy barrier for rotamer interconversion is low at 0 °C, so rapid rotamer conversion occurs. This means exclusive deprotonation of the more acidic and kinetically preferred α -proton at the bridgehead occurs. On the other hand, at -78 °C, the rotamer interconversion is slow thus the regioselectivity observed reflects the ratio of the rotamers. The α -lithiation of each rotamer occurs more readily than the interconversion of rotamers. Hence, a 43:57 mixture of regioisomers **82** and **83** is observed.

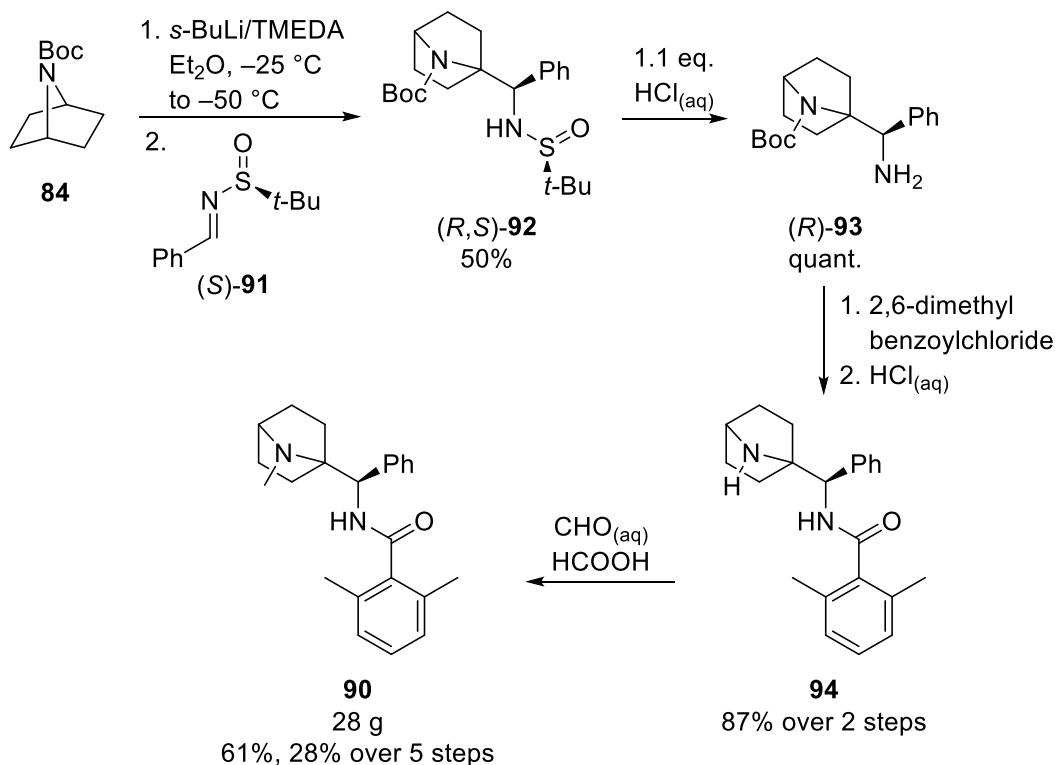
Researchers at AstraZeneca have also presented the α -lithiation-trapping of a similar but symmetrical bicyclic *N*-Boc pyrrolidine, in the development of a synthesis towards a potent glyT1 uptake inhibitor.⁶³ The α -lithiation-trapping of bicyclic pyrrolidine **84** was conducted with *s*-BuLi/TMEDA followed by trapping with a range of electrophiles including CO₂, DMF, MeI and Weinreb amide **89**. The trapped adducts **85-88** were obtained in 53-90% yield (Scheme 1.29).

Scheme 1.29. Lithiation-trapping of bicyclic pyrrolidine **84**



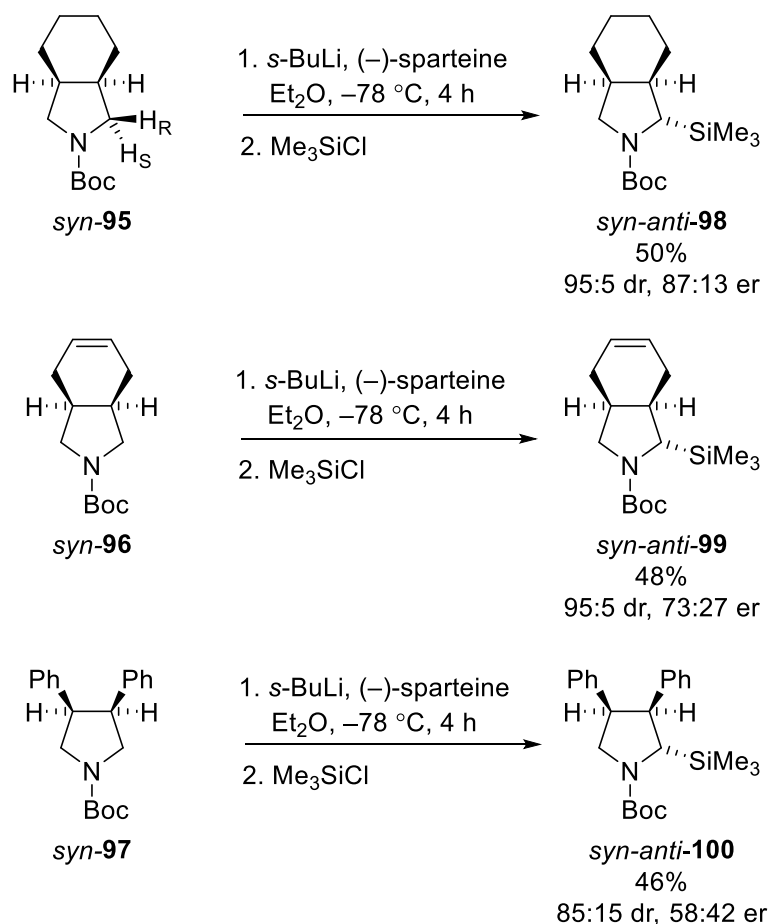
Using this α -lithiation methodology, 28 g of glyT1 uptake inhibitor **90** was synthesised in 28% overall yield from bicyclic *N*-Boc pyrrolidine **84** via a five-step synthesis (Scheme 1.30). *s*-BuLi/TMEDA lithiation of bicyclic pyrrolidine **84** and trapping with imine **91** provided intermediate (*R,R*)-**92** in 50% yield and was conducted on a ~200 g scale. Subsequent hydrolysis of the sulfinamide **92** provided primary amine **93** in quantitative yield. Amide formation with 2,6-dimethylbenzoyl chloride and Boc group cleavage with HCl provided secondary amine **94**, which was then subjected to Eschweiler-Clarke methylation to provide the desired inhibitor **90**.

Scheme 1.30. Five-step synthesis of glyT1 uptake inhibitor **90**



The α -lithiation-trapping of bicyclic 3,4-disubstituted *N*-Boc pyrrolidines was first reported by Johnson and Beak in 2002.⁴ The asymmetric *s*-BuLi/(–)-sparteine lithiations of three 3,4-disubstituted *N*-Boc pyrrolidines *syn*-**95**, *syn*-**96** and *syn*-**97** were investigated. For each of the disubstituted pyrrolidines, Me₃SiCl was used to trap the lithiated intermediate. These lithiation-trapping reactions afforded 2,3,4-trisubstituted pyrrolidines *syn*-*anti*-**98-100** in moderate 46-50% yield in good dr and variable er (Scheme 1.31).

Scheme 1.31. *s*-BuLi/(–)-sparteine lithiation-trapping of 3,4-disubstituted *N*-Boc pyrrolidines *syn*-**95**, *syn*-**96** and *syn*-**97**

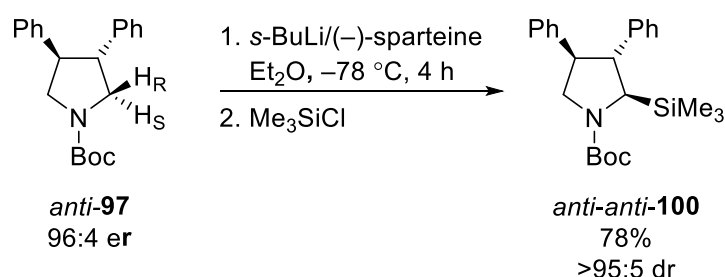


For the *s*-BuLi/(–)-sparteine-mediated asymmetric deprotonation of pyrrolidines *syn*-**95-97**, the pro-*S* proton is removed as expected when using *s*-BuLi/(–)-sparteine, as discussed in Section 1.2.1. Interestingly, the er varies significantly between the three substrates, with the trapped adduct *syn*-*anti*-**98** having the highest 87:13 er. By the addition of only a double bond on the cyclohexane ring, this er is eroded to 73:27. Diphenyl pyrrolidine *syn*-*anti*-**100** was formed in only 58:42 er. The ers observed indicate that the substrate has significant control over the enantioselectivity of the lithiation reaction. High drs were observed for all

three of the 2,3,4-trisubstituted pyrrolidine products **98-100**; this is reasonable as it will be favourable to have the *s*-BuLi/(–)-sparteine lithiating complex attacking the proton *anti* to the cyclohexyl ring to minimise steric interactions.

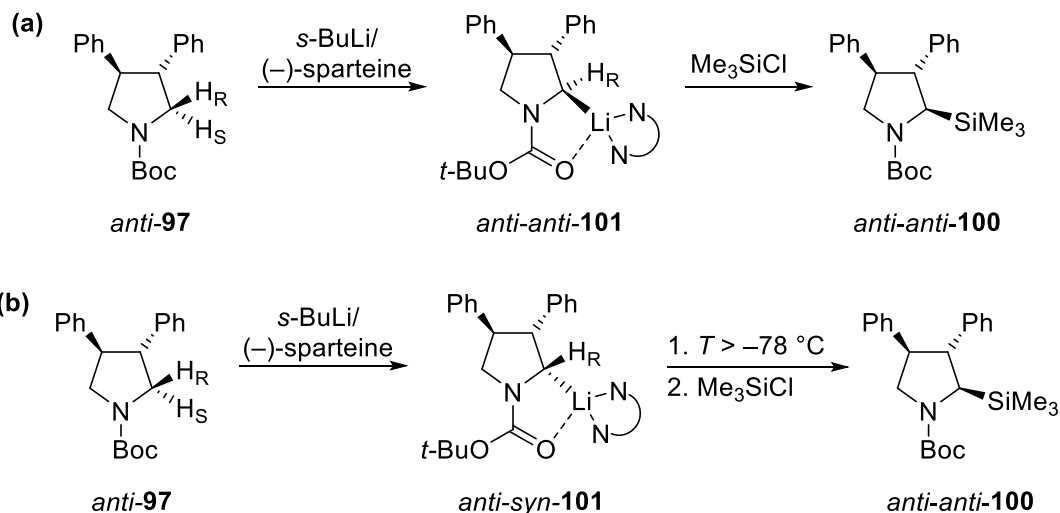
Beak and Johnson also carried out the *s*-BuLi/(–)-sparteine lithiation and Me₃SiCl trapping of C₂-symmetric *N*-Boc pyrrolidine *anti*-**97**. This lithiation-trapping reaction afforded 2,3,4-trisubstituted *N*-Boc pyrrolidine *anti-anti*-**100** in >95:5 dr and high 78% yield (Scheme 1.32).

Scheme 1.32. *s*-BuLi/(–)-sparteine lithiation-trapping of 3,4-disubstituted *N*-Boc pyrrolidine *anti*-97****



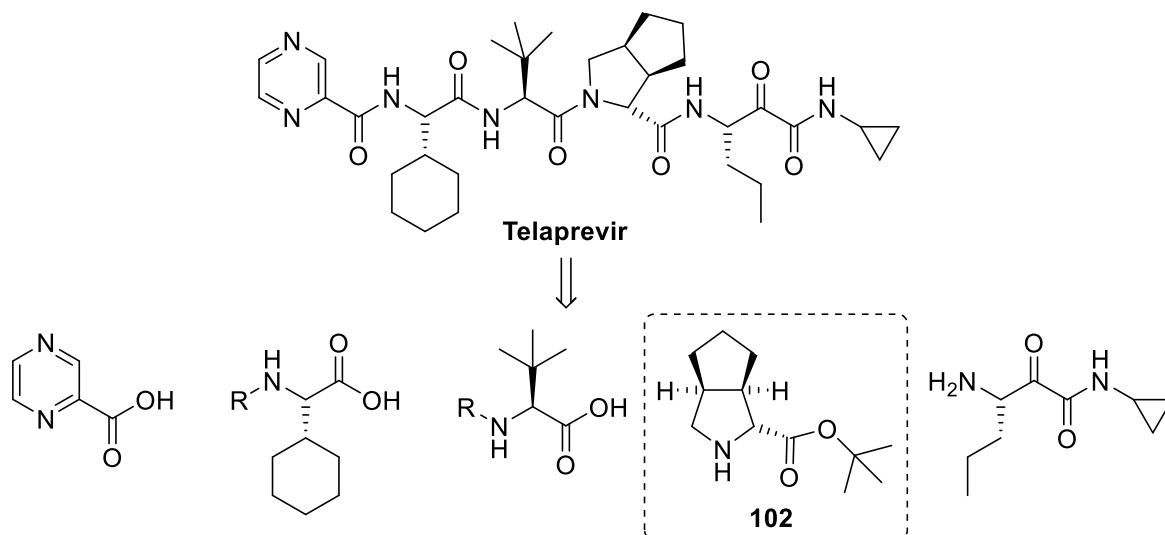
For the lithiation-trapping of *anti*-**97**, the α -nitrogen selectivity is reversed and pro-*R* deprotonation, which is usually a higher energy process for *s*-BuLi/(–)-sparteine, occurred giving product *anti-anti*-**100**. For a pro-*S* deprotonation of *anti*-**97**, the phenyl substituent and *s*-BuLi/(–)-sparteine complex would need to be on the same face; these steric interactions may be significant enough to stop this occurring (Scheme 1.33.a). Alternatively, and more likely in our opinion, the selectivity observed in this reaction may arise from the trapping reaction with Me₃SiCl, where pro-*S* deprotonation of *anti*-**97** does occur, giving the lithiated intermediate *anti-syn*-**101** that would be expected with *s*-BuLi/(–)-sparteine. If Me₃SiCl trapping is slow or non-occurring, warming the reaction after adding the electrophile could lead to the lithiated intermediate becoming configurationally unstable before it is trapped. This would allow a dynamic kinetic resolution to be established where only the lithiated intermediate *anti-anti*-**101** is trapped, giving trapped the product *anti-anti*-**100** in the high dr observed (Scheme 1.33.b).

Scheme 1.33. Possible routes for the reversed selectivity observed for the *s*-BuLi/(-)-sparteine lithiation of *anti*-97



The racemic and asymmetric α -lithiation-trapping of another 3,4-disubstituted *N*-Boc pyrrolidine, was investigated by a process development group at Vertex Pharmaceuticals.⁶⁴ They proposed a series of disconnections for the blockbuster drug Telaprevir. By cleaving amide bonds, the target molecule can be simplified to five small molecular fragments (Scheme 1.34).

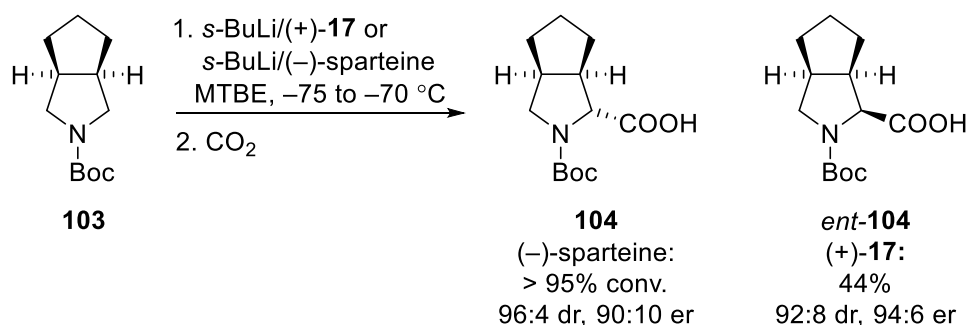
Scheme 1.34. Proposed RSA for Telaprevir



They noted that the 2,3,4-trisubstituted pyrrolidine fragment **102** could be synthesised using α -lithiation chemistry from bicyclic pyrrolidine **103**. First, lithiation of bicyclic pyrrolidine **103** was carried out asymmetrically with both *s*-BuLi/(-)-sparteine and *s*-BuLi/(+)-sparteine surrogate **17**, followed by trapping with CO₂. Use of *s*-BuLi/(-)-sparteine gave 2,3,4-trisubstituted pyrrolidine **104** in >95% conversion with 96:4 dr and 90:10 er; *s*-BuLi/(+)-

sparteine surrogate provided *ent*-**104** in 44% isolated yield with 92:8 dr and 94:6 er (Scheme 1.35).

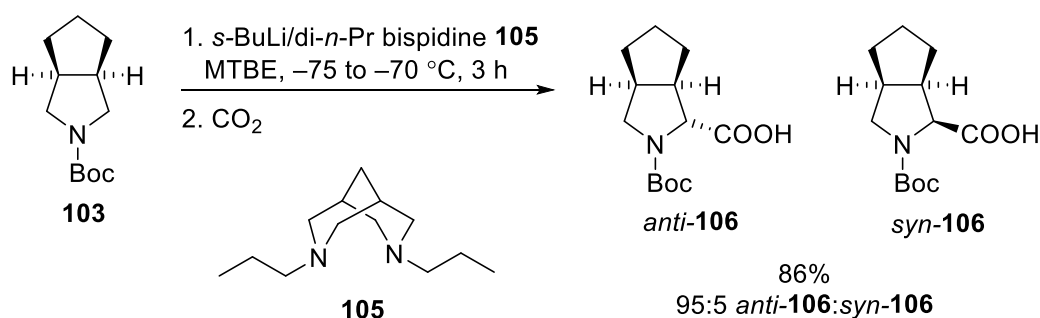
Scheme 1.35. Asymmetric lithiation-trapping of 3,4 disubstituted *N*-Boc pyrrolidine **103**



The group noted that the use of *s*-BuLi/(+)-sparteine surrogate **17** did provide promising results but decided to opt for a diastereoselective racemic lithiation followed by resolution. A racemic synthesis was decided upon due to the uncertainty of the availability of (+)-sparteine surrogate **17** which is synthesised using a plant-derived starting material (-)-cytisine. (-)-Cytisine has an uncertain supply which was deemed too high a risk for the production of the (+)-sparteine surrogate in industrial quantities.

The racemic lithiation-trapping of bicyclic pyrrolidine **103** with *s*-BuLi/*di-n*-Pr bispidine **105** and CO₂ offered a 95:5 diastereomeric mixture of carboxylic acids *anti*-**106** and *syn*-**106** which were isolated in 86% yield (Scheme 1.36). Bispidine **105** was employed as the ligand as optimisation studies showed that this sterically bulkier ligand offered better diastereoselectivity and formed fewer side-products in the trapping reaction than less bulky ligands such as TMEDA. The lithiation forms product *anti*-**106** preferentially as the less sterically hindered proton *anti* to the pentane ring on the 3- and 4-positions of the pyrrolidine ring is presumably easier to lithiate by the bulky *s*-BuLi/**105** complex.

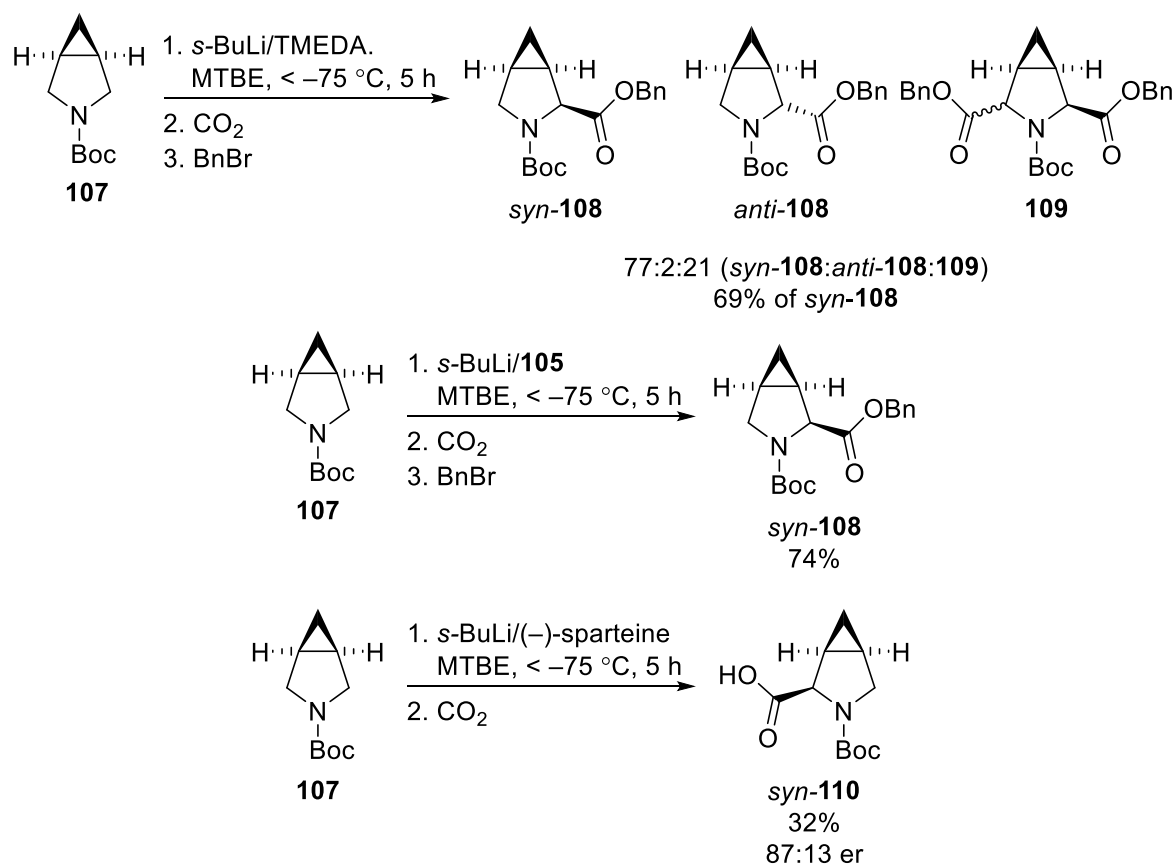
Scheme 1.36. *s*-BuLi/bispidine **105 lithiation-trapping of *N*-Boc pyrrolidine **103****



Subsequent resolution of the mixture of *anti*- and *syn*-**106** using a chiral amine furnished the desired *anti*-**106** salt in 99:1 er and 100:0 dr in 31% overall yield. After Boc cleavage and conversion of the carboxylate to a *tert*-butyl ester, key Telaprevir fragment **102** was formed in 27% overall yield from pyrrolidine **103** in >99.5:0.5 er and dr. This process has been used to manufacture 200 kg of this key intermediate.

The lithiation-trapping of a similar bicyclic *N*-Boc pyrrolidine **107** with a fused cyclopropane ring has also been reported.⁶⁵ Lithiation of bicyclic pyrrolidine **107** was attempted using *s*-BuLi and diamine ligands TMEDA, di-*n*-Pr bispidine **105** and (–)-sparteine (Scheme 1.37). Use of TMEDA gave a crude product which contained a 77:2:21 mixture of *syn*-**108**, *anti*-**108** and the 2,5-disubstituted adduct **109**; the major product *syn*-**108** was isolated in 69% yield. The use of diamine di-*n*-Pr bispidine **105** gave only pure *syn*-**108** which was isolated in 74% yield. The *s*-BuLi/(–)-sparteine lithiation of *N*-Boc pyrrolidine **107** followed by trapping with CO₂ gave carboxylic acid *syn*-**110** in 32% yield and 87:13 er.

Scheme 1.37. Lithiation-trapping reactions of bicyclic pyrrolidine 107



The *syn* diastereoselectivity of the lithiation was unexpected as the *s*-BuLi/diamine must have attacked the α -proton on the same face on which the cyclopropyl ring is located. However, the conformational differences due to the cyclopropane substituent presumably accounts for this. Computational modelling was used to model the lithiated intermediate of *N*-Boc pyrrolidine **107** with the lithium and di-*n*-Pr bispidine **105**. The energies calculated indicated that the *syn* complex was 3.90 kcal mol⁻¹ lower in energy than the respective *anti* complex. However, only the lithiated intermediates have been modelled and the kinetic energy barriers for *syn* and *anti* lithiation have not been considered. Therefore, these calculations will only give an indication of the diastereoselectivity of lithiation if the transition state is product-like or if the lithiation is under thermodynamic control, which is not likely to be the case at -78 °C.⁶⁶ For a more rigorous computational study, modelling of the deprotonation by optimisation of ground states and transitions states for the α -deprotonation reaction needs to be considered.

The examples presented in this overview of α -lithiation chemistry show the diversity of *N*-Boc heterocycles that can be subjected to α -functionalisation using Beak's α -lithiation-trapping protocol. This overview has also shown that desired products can be obtained enantioselectively or diastereoselectively by simply changing the diamine employed in the lithiation. Many of the *N*-Boc heterocycles included in this review are included in the reactivity study detailed in Chapter 2 of this thesis. In many of the examples presented, the lithiating conditions are not optimised, and therefore long > 3 h reaction times have been used. Previous unpublished work in our group has shown that many of these substrates require < 1 h for complete lithiation rather than the several hours used. Knowledge of substrate reactivity would be particularly beneficial for large-scale reactions, where the maintenance of low temperatures for extended periods of time is not cost-effective.

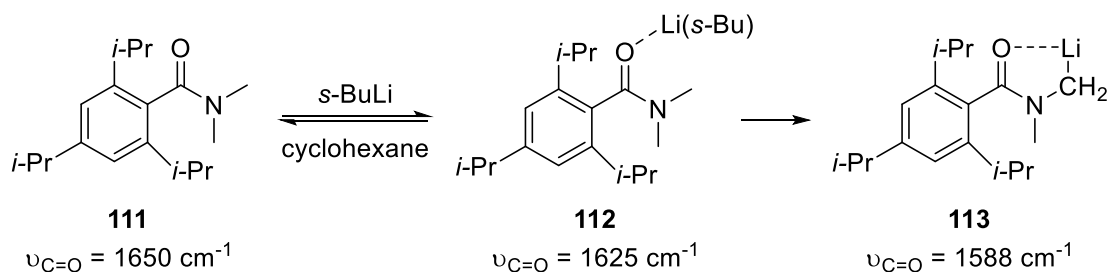
1.3 *In situ* IR Spectroscopic Studies of Lithiation-Trapping Reactions

This section explores previous work where *in situ* IR spectroscopy has been used to monitor lithiation and trapping reactions. This has not only allowed determination of the end-point of the lithiation and trapping reactions but has been used to elucidate reaction mechanism and identify reaction intermediates.

1.3.1. *In situ* IR spectroscopic studies of lithiation reactions

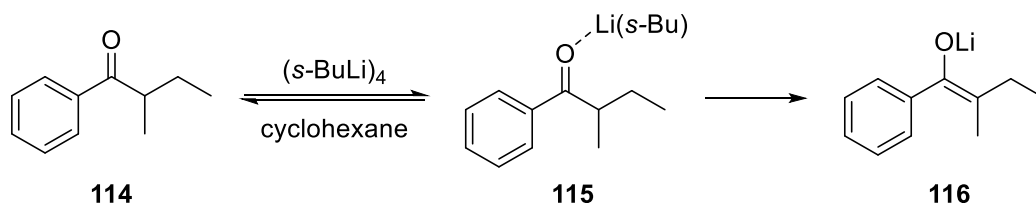
One of the earliest examples of using *in situ* IR spectroscopy to monitor lithiation α to a heteroatom was reported by Beak and Smith in 1983.¹¹ Amide **111** and *s*-BuLi were mixed in IR stopped flow apparatus and upon mixing, two IR absorptions were detected: the starting material amide **111** ($\nu_{\text{C=O}} = 1650 \text{ cm}^{-1}$) and the prelithiation complex **112** ($\nu_{\text{C=O}} = 1625 \text{ cm}^{-1}$) which forms reversibly at the start of the reaction. After mixing, these two absorptions disappeared and a new band appeared due to the formation of lithiated intermediate **113** ($\nu_{\text{C=O}} = 1588 \text{ cm}^{-1}$) (Scheme 1.38).

Scheme 1.38. *In situ* IR stopped flow monitoring of the *s*-BuLi lithiation of amide **111** ($\nu_{\text{C=O}}$ measured in cyclohexane solvent)



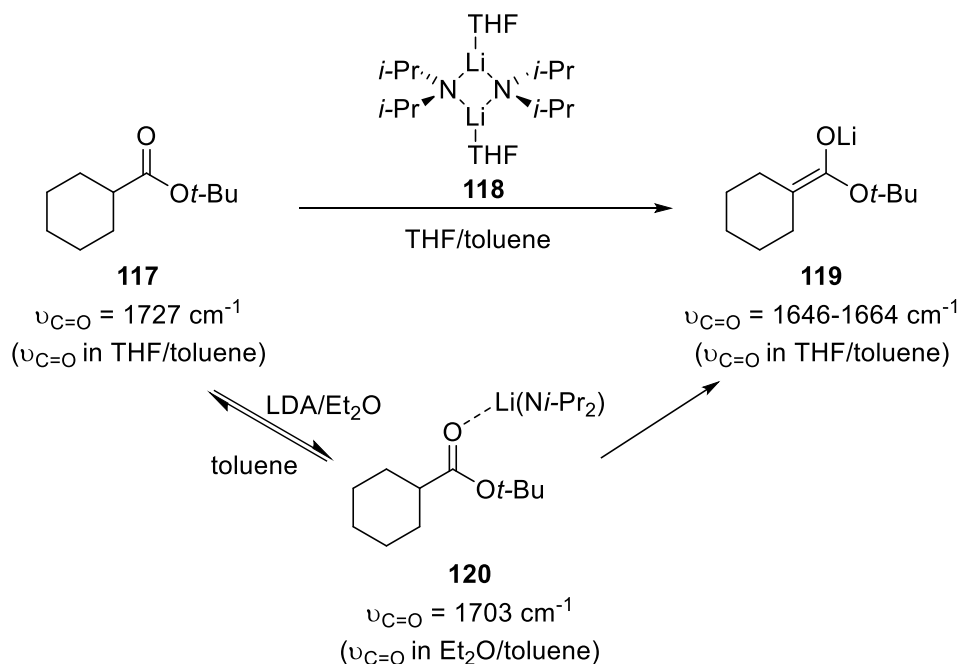
Subsequently in 1984, Smith monitored the lithiation of ketones, including phenyl ketone **114**, with the same IR stopped flow apparatus.⁶⁷ These lithiations were carried out using *s*-BuLi or *n*-BuLi in non-coordinating hydrocarbon solvents, where most of the alkyllithium will exist as aggregates (tetramer for *s*-BuLi and hexamer for *n*-BuLi). Immediately after mixing phenyl ketone **114** and *s*-BuLi in cyclohexane solvent, a new band was observed due to the reversible formation of prelithiation complex **115**, which reacts irreversibly to form enolate **116** (Scheme 1.39). Kinetic analysis indicated that in these hydrocarbon solvent conditions, both the aggregated and monomeric alkyllithium species are involved in the lithiation reaction and the relative importance of each depended on the ketone substrate used in the reaction.

Scheme 1.39. *In situ* IR stopped flow monitoring of the *s*-BuLi lithiation of ketone **114**



In 1997, Collum *et al.* used *in situ* IR spectroscopy (ReactIR™) to investigate the LDA-mediated deprotonation of ester **117** to elucidate how the coordination of LDA changes during the enolisation reaction.⁶⁸ Previous work had shown that LDA exists as a dimeric species **118** over a range of LDA and THF concentrations.^{69,70} Upon addition of ester **117** to a solution of LDA/THF in toluene, the ester **117** ($\nu_{\text{C=O}} = 1727 \text{ cm}^{-1}$) absorbance disappeared and an absorbance corresponding to the enolate **119** ($\nu_{\text{C=O}} = 1646\text{-}1664 \text{ cm}^{-1}$) formed over the period of the reaction. No prelithiation complex was observed by the ReactIR™ apparatus during the course of the LDA/THF-mediated lithiation. However, when LDA/Et₂O lithiating conditions were used, an absorption due to prelithiation complex **120** ($\nu_{\text{C=O}} = 1703 \text{ cm}^{-1}$) was observed (Scheme 1.40).⁶⁸ Further kinetic analysis indicated that solvated LDA monomers (*i*-Pr₂NLi(THF)₂·**117**) were the reactive lithiating species for the LDA/THF-mediated lithiation of esters such as **117**.⁷¹

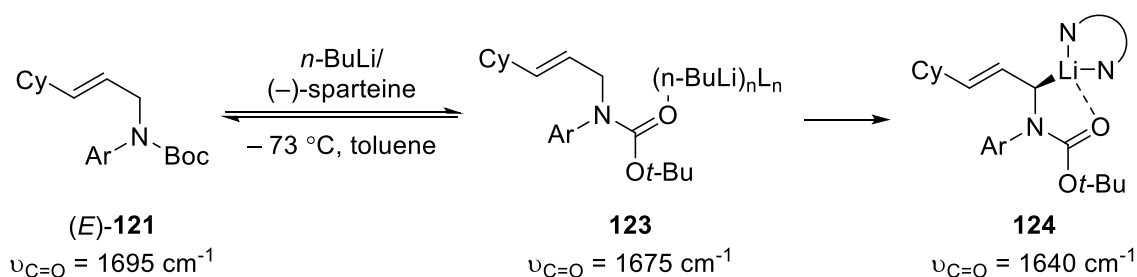
Scheme 1.40. ReactIR™ monitored LDA/THF enolisation of ester **117**



The first ReactIR™ monitored α -lithiation reaction of an *N*-Boc substrate was reported by Beak in 2001.⁷² The *n*-BuLi/(–)-sparteine-mediated lithiation of *N*-Boc allylamine (*E*)-**121**

in toluene at $-73\text{ }^{\circ}\text{C}$ was monitored using ReactIRTM equipment to investigate the kinetics and mechanism of the reaction. Upon addition of *n*-BuLi to a premixed solution of (*E*)-**121** and (–)-sparteine in toluene, an absorbance assigned to (*E*)-**121** ($\nu_{\text{C=O}} = 1695\text{ cm}^{-1}$) rapidly decreased as the starting material (*E*)-**121** was consumed. Meanwhile, an absorption for the lithiated intermediate **124** ($\nu_{\text{C=O}} = 1640\text{ cm}^{-1}$) grew in at a slower rate. A third absorbance peak was also observed during the reaction at 1675 cm^{-1} , which increased in absorbance on the addition of *n*-BuLi and decreased in intensity for the duration of the reaction and this was assigned to the $\nu_{\text{C=O}}$ of the prelithiation complex **123** (Scheme 1.41). The presence of a prelithiation complex for the alkyllithium/diamine lithiation of *N*-Boc pyrrolidine **9** was previously identified by mechanistic work carried out by Beak and Gallagher (see Scheme 1.9).³²

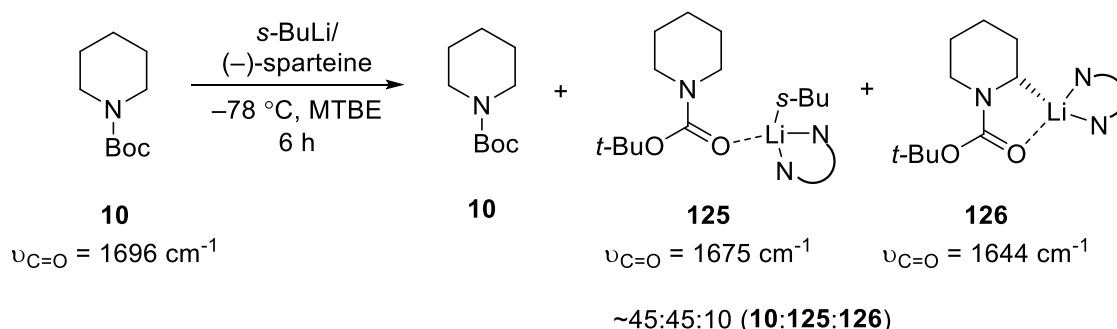
Scheme 1.41. ReactIRTM monitored *n*-BuLi/(–)-sparteine lithiation of allylamine (*E*)-121** ($\nu_{\text{C=O}}$ measured in toluene solvent)**



Ar = *p*-methoxyphenyl

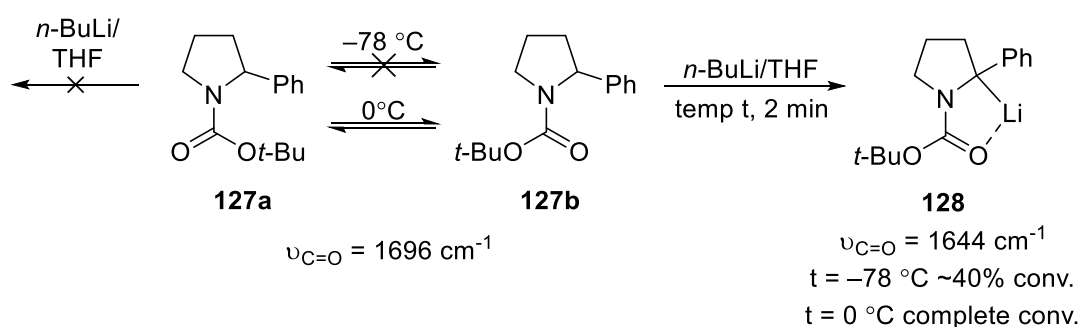
More recently, the O'Brien group has monitored the asymmetric lithiation of *N*-Boc piperidine **10** using *s*-BuLi/(–)-sparteine and *s*-BuLi/(+)-sparteine surrogate **17** by ReactIRTM.³¹ *N*-Boc piperidine **10** and (–)-sparteine were combined in MTBE at $-70\text{ }^{\circ}\text{C}$ and a peak at 1696 cm^{-1} was observed and assigned to *N*-Boc piperidine **10**. Upon addition of *s*-BuLi, two more peaks were observed at 1675 cm^{-1} and 1644 cm^{-1} and assigned to prelithiation complex **125** and lithiated intermediate **126** respectively. After a 6 h lithiation, a ~45:45:10 mixture of starting reagent **10**, prelithiation complex **125** and lithiated intermediate **126** was obtained (Scheme 1.42). This mirrored the ~8% yield of trapped product (*S*)-**12** previously reported by Beak *et al.* (see Scheme 1.10).³⁴ On the other hand, the ReactIRTM monitored *s*-BuLi/(+)-sparteine surrogate **17** lithiation of *N*-Boc piperidine **10** provided a much faster lithiation ($< 6\text{ h}$) which was consistent with the high yields of trapped adducts obtained (see Scheme 1.12).

Scheme 1.42. ReactIRTM monitored *s*-BuLi/(-)-sparteine lithiation of *N*-Boc piperidine **10 ($\nu_{\text{C=O}}$ measured in MTBE solvent)**



Coldham and O'Brien have also used ReactIRTM monitoring to find optimal reaction conditions for the lithiations of 2-substituted *N*-Boc heterocycles such as 2-phenyl pyrrolidine **127** and 2-phenyl piperidine **129**.⁷³ For 2-phenyl pyrrolidine **127**, the lithiation was initially attempted with *n*-BuLi/THF at $-78 \text{ }^\circ\text{C}$. ReactIRTM analysis showed that the initial lithiation was fast with the pyrrolidine **127** ($\nu_{\text{C=O}} = 1696 \text{ cm}^{-1}$) absorbance decreasing concurrently with a new absorbance arising due to the formation of quaternary lithiated intermediate **128** ($\nu_{\text{C=O}} = 1644 \text{ cm}^{-1}$). However, after two minutes the reaction stalled at ~40% lithiation. No further lithiation takes place due to the extremely slow interconversion of rotamers **127a** and **127b** at $-78 \text{ }^\circ\text{C}$ and the fact that *n*-BuLi/THF is not reactive enough to lithiate rotamer **127a**. When the lithiation was repeated at $0 \text{ }^\circ\text{C}$, interconversion of the rotamers **127a** and **127b** did occur and complete lithiation was achieved in 2 minutes (Scheme 1.43).

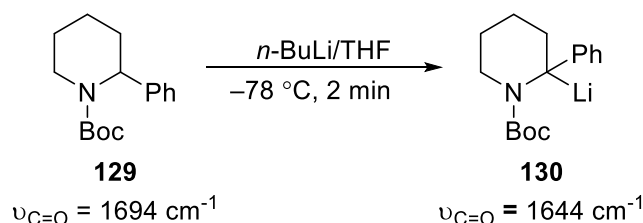
Scheme 1.43. ReactIRTM monitored *n*-BuLi/THF lithiation of 2-phenyl *N*-Boc pyrrolidine **127 ($\nu_{\text{C=O}}$ measured in THF solvent)**



Similarly, the *n*-BuLi/THF lithiation of 2-phenyl *N*-Boc piperidine **129** was also monitored at $-78 \text{ }^\circ\text{C}$. In this case, complete formation of lithiated intermediate **130** was achieved within 2 minutes (Scheme 1.44). Evidently, the rotamer interconversion for 2-phenyl piperidine **129**

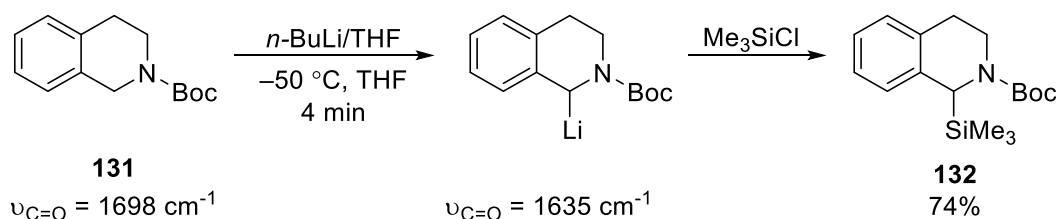
was much faster at $-78\text{ }^{\circ}\text{C}$ than that of 2-phenyl pyrrolidine **127**. VT-NMR spectroscopic studies confirmed this finding, indicating a substantial difference in the energy barriers for rotamer interconversion of 2-phenyl pyrrolidine **127** and piperidine **129** (~ 64.5 and ~ 50.0 kJ mol^{-1} respectively).

Scheme 1.44. ReactIRTM monitored *n*-BuLi/THF lithiation of 2-phenyl *N*-Boc piperidine **129 ($\nu_{\text{C=O}}$ measured in THF solvent)**



Coldham has also used ReactIRTM to find optimal reaction conditions for the lithiation of *N*-Boc tetrahydroisoquinoline **131**.⁷⁴ A range of solvents was investigated including Et_2O , THF and toluene and two different alkylolithiums were trialled (*n*-BuLi and *s*-BuLi). The reactions were also attempted with or without TMEDA. It was found that the lithiation temperature was key. At $-78\text{ }^{\circ}\text{C}$, incomplete lithiation was observed due to the slow interconversion of rotamers. However, at $-50\text{ }^{\circ}\text{C}$, rotamer interconversion was fast enough for complete lithiation of **131** to occur. Coldham found that the optimal lithiating conditions required *n*-BuLi/THF at $-50\text{ }^{\circ}\text{C}$ for < 5 min. The choice of alkylolithium is also important as the use of *n*-BuLi ensured the regioselectivity α to nitrogen and the phenyl ring. Using these optimal conditions and trapping with Me_3SiCl , the desired 2-substituted tetrahydroisoquinoline **132** was obtained in 74% yield (Scheme 1.45).

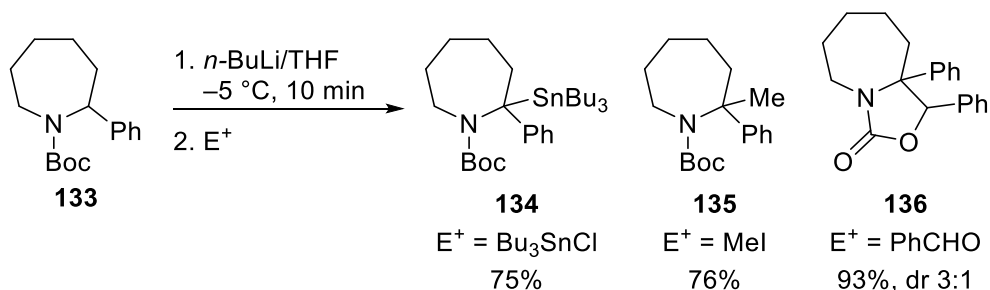
Scheme 1.45. Lithiation-trapping of tetrahydroisoquinoline **131 using optimised conditions ($\nu_{\text{C=O}}$ measured in THF solvent)**



More recently, Coldham has reported the lithiation-trapping of 2-phenyl azepane **133** and used ReactIRTM monitoring to find optimal conditions for the α -lithiation reaction.⁷⁵ As observed with other 2-phenyl *N*-Boc heterocycles, the rotamer interconversion resulted in incomplete lithiation at low temperature ($-78\text{ }^{\circ}\text{C}$) (see Schemes 1.43 and 1.45). When the

lithiation was conducted at $-5\text{ }^{\circ}\text{C}$, complete lithiation was observed within 3 min. These optimised conditions allowed the efficient synthesis of 2,2-disubstituted azepanes, such as **134-136** in good yield (Scheme 1.46).

Scheme 1.46. Lithiation-trapping of 2-phenyl *N*-Boc azepane **133**



The examples presented show that ReactIRTM is a powerful tool that can provide mechanistic information and can allow determination of optimised reaction conditions for lithiation reactions. Additionally, ReactIRTM can help to diagnose problematic lithiations where little or no lithiation is observed, for example where slow rotamer conversion prohibits lithiation. ReactIRTM is a particularly valuable method for monitoring organolithium reactions as the *in situ* nature of the technique means that the water sensitivity of the organolithium reagents and the low temperatures ($-78\text{ }^{\circ}\text{C}$) that are typically required do not pose a problem. For these reasons, the ReactIRTM monitoring of α -lithiation reactions of substrates has now become widespread. Some other substrates whose α -lithiations reactions have been monitored by ReactIRTM include *N*-Boc piperazines **137**,^{50,52} *N*-Boc dimethylamine **138**,⁷⁶ ester **139**⁷⁷ and urea **140**⁷⁸ (Figure 1.4).

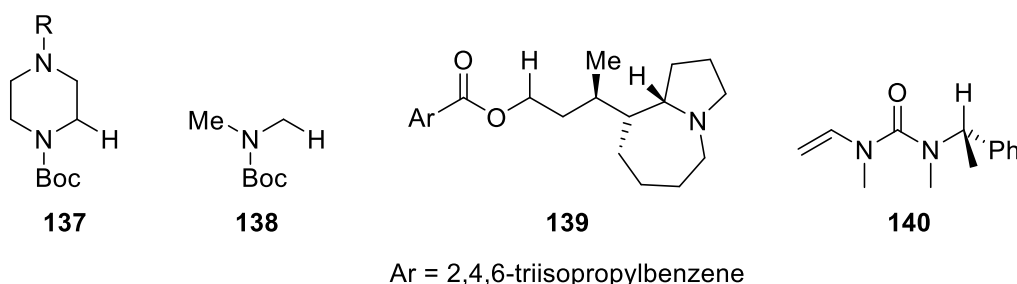
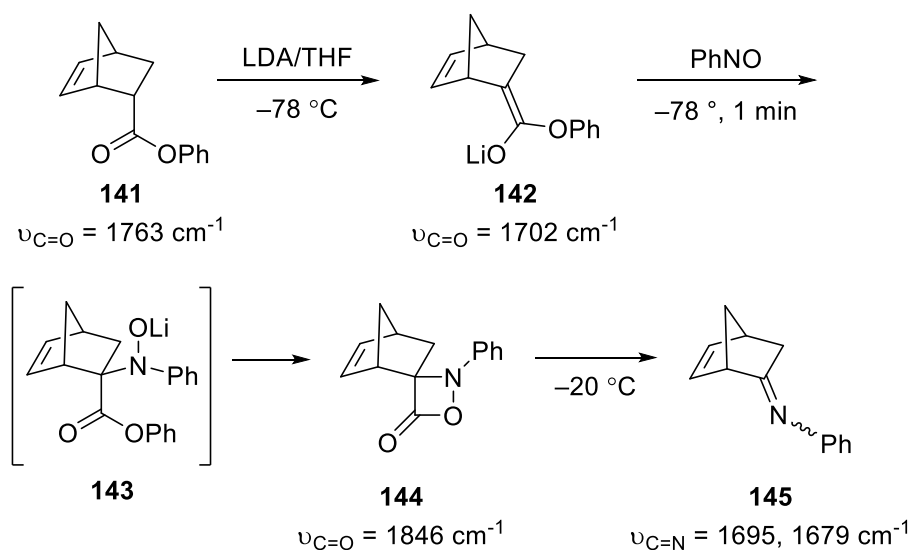


Figure 1.4. Substrates whose α -lithiation reactions were monitored with ReactIRTM

1.3.2. *In situ* ReactIR™ spectroscopic studies of the trapping reactions of lithiated intermediates

Currently, there have only been a handful of examples where the trapping reaction of a lithiated intermediate has been monitored using *in situ* ReactIR™. The first of these was reported by Yamamoto in 2008, where ReactIR™ was used to elucidate the mechanism of the oxidative decarboxylation of bicyclic carboxylates.⁷⁹ Phenyl ester **141** ($\nu_{\text{C=O}} = 1763 \text{ cm}^{-1}$) was treated with LDA at $-78 \text{ }^\circ\text{C}$ which rapidly formed the lithium enolate **142** ($\nu_{\text{C=O}} = 1702 \text{ cm}^{-1}$). Upon the addition of PhNO, the rapid trapping ($< 1 \text{ min}$) of enolate **142** was observed and a new absorption corresponding to the spirocyclic intermediate **144** ($\nu_{\text{C=O}} = 1763 \text{ cm}^{-1}$) was detected (which occurs *via* **143**). When the reaction was warmed to $-20 \text{ }^\circ\text{C}$, absorbance for intermediate **144** decayed as the fragmentation of **144** occurred. Two additional absorptions appeared and increased in intensity as this fragmentation occurred. These two new absorptions were assigned to the phenyl imine isomers **145** ($\nu_{\text{C=N}} = 1695, 1679 \text{ cm}^{-1}$) that are formed during the fragmentation (Scheme 1.47).

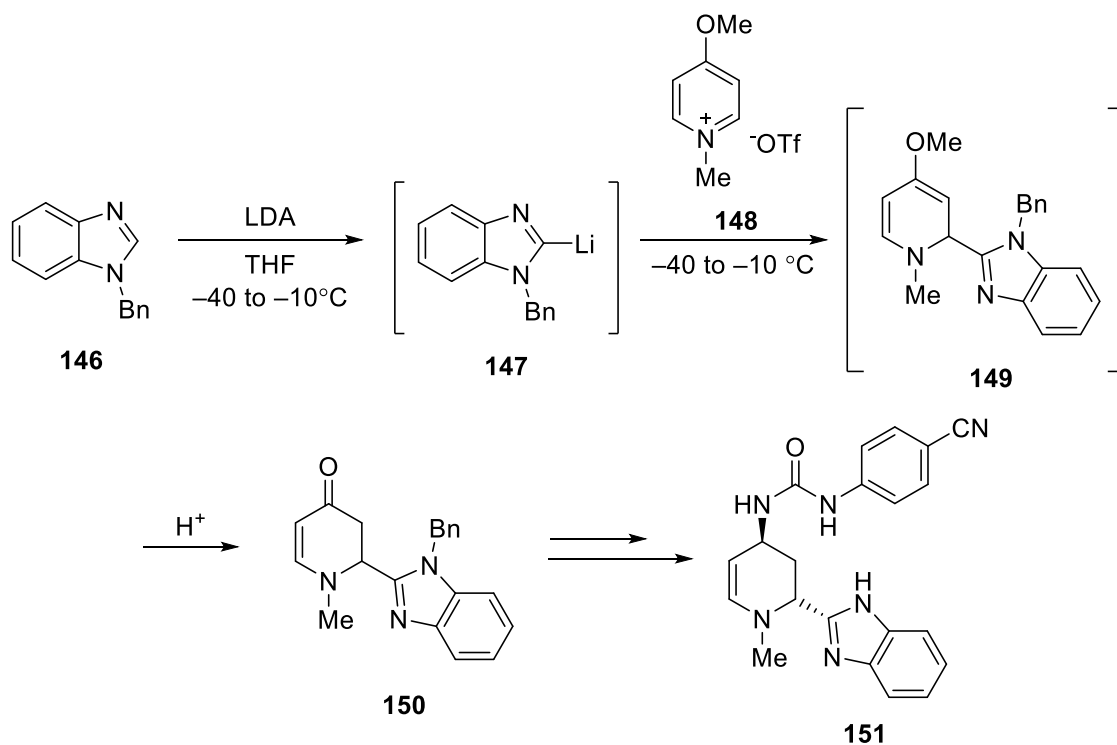
Scheme 1.47. ReactIR™ monitored lithiation-trapping of phenyl ester **141 and *in situ* rearrangement to form imine **145** ($\nu_{\text{C=O}}$ measured in THF solvent)**



A combined *in situ* IR and online NMR spectroscopic study of the lithiation and trapping reaction of benzimidazole **146** has been reported by a process development group at Pfizer.⁸⁰ The reaction involved the LDA/THF-mediated lithiation of benzimidazole **146** followed by nucleophilic addition of the generated organolithium into pyridinium triflate salt **148**. The product, dihydropyridone **150**, is of interest as it is a precursor to an active pharmaceutical ingredient (API) **151**, reported previously by Pfizer.⁸¹ Unfortunately, the desired product

dihydropyridone **150** was only isolated in 50-60% yield with 30-40% of starting material **146** recovered (Scheme 1.48). Therefore, it was decided to monitor the reaction progress using ReactIRTM and NMR spectroscopy to attempt to find the cause of the disappointing yields.

Scheme 1.48. ReactIRTM and NMR monitored LDA/THF lithiation of benzimidazole **146 and nucleophilic addition into pyridinium triflate **148****

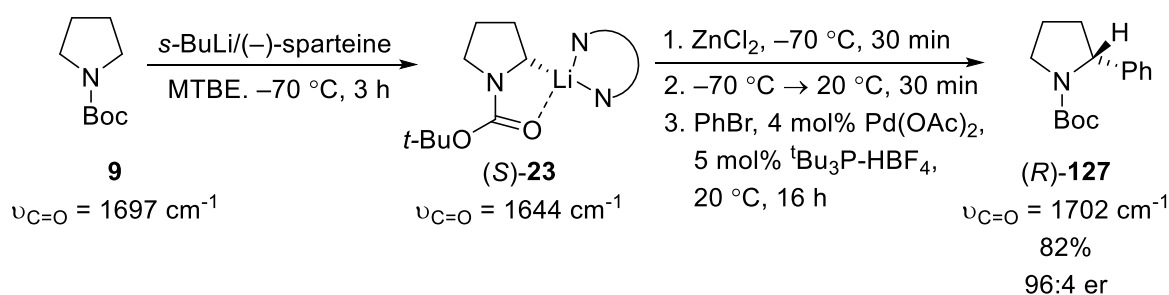


The ReactIRTM monitoring of the lithiation of benzimidazole **146** indicated that complete lithiation had occurred. This lithiation was performed at a range of temperatures between -40 to -10 °C and complete conversion occurred at each temperature. This indicated that lithiation of **146** was not the reason for the poor yield of **150**. Next, the stability of lithiated intermediate **147** was investigated. Lithiated intermediate **147** was incubated at temperatures between -40 and -10 °C for 5.5 h and only small amounts of degradation were observed, indicating that intermediate **147** was stable at these temperatures. Finally, the nucleophilic addition of **147** into pyridinium triflate **148** was monitored by ReactIRTM and online NMR spectroscopy. After addition of triflate **148**, an absorption for the desired enol ether product **149** appeared along with the reappearance of starting material **146**. This indicated that triflate **148** could act as a proton source allowing the quenching of intermediate **147**, thus giving a mixture of the desired product **150** and starting material **146**. Further kinetic studies indicated similar reaction rates for formation of trapped product **149** and quenching of

intermediate **147**. It was concluded that these similar rates of reaction would make it difficult for higher yields of the desired product **150** to be achieved.

The O'Brien group used *in situ* IR spectroscopy to monitor a one-pot lithiation, transmetallation and Negishi coupling of *N*-Boc pyrrolidine **9**, allowing the generation of α -arylated products such as (*R*)-**127**.⁸² To synthesise α -arylated pyrrolidine (*R*)-**127**, *N*-Boc pyrrolidine **9** was lithiated with *s*-BuLi/(–)-sparteine, underwent transmetallation with ZnCl₂ and then was subjected to Negishi coupling with bromobenzene. This afforded α -arylated product (*R*)-**127** in a good 82% yield with excellent 96:4 er (Scheme 1.49).

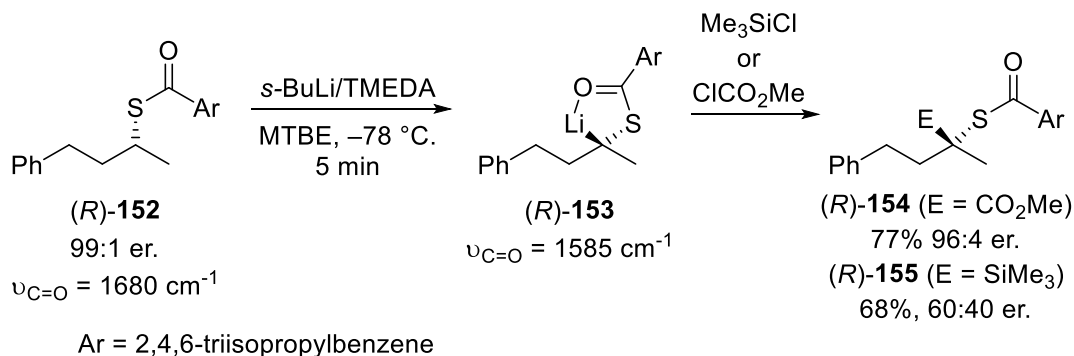
Scheme 1.49. ReactIRTM monitored *s*-BuLi/(–)-sparteine lithiation, transmetallation and Negishi coupling of *N*-Boc pyrrolidine **9 ($\nu_{\text{C=O}}$ measured in MTBE solvent)**



The ReactIRTM monitoring indicated that the *s*-BuLi/(–)-sparteine lithiation of *N*-Boc pyrrolidine **9** required 1 h for complete lithiation at $-78 \text{ }^\circ\text{C}$. During the lithiation, absorptions were observed for *N*-Boc pyrrolidine **9** ($\nu_{\text{C=O}} = 1697 \text{ cm}^{-1}$), the prelithiation, complex ($\nu_{\text{C=O}} = 1675 \text{ cm}^{-1}$) and lithiated intermediate (*S*)-**23** ($\nu_{\text{C=O}} = 1644 \text{ cm}^{-1}$). After lithiation was complete, the addition of ZnCl₂ led to little change in the IR spectra but when the reaction was warmed to $-20 \text{ }^\circ\text{C}$ a new peak ($\nu_{\text{C=O}} = 1653 \text{ cm}^{-1}$) was observed and assigned to an organozinc species (RZnCl, R₂Zn or R₃ZnLi). When the Negishi coupling reagents were added, another new signal was observed and assigned to arylated pyrrolidine (*R*)-**127** ($\nu_{\text{C=O}} = 1702 \text{ cm}^{-1}$).

Aggarwal *et al.* have used ReactIRTM to monitor the enantioselective lithiation-trapping reactions of enantioenriched benzoate (*R*)-**152**.⁸³ Lithiation of benzoate (*R*)-**152** with *s*-BuLi/TMEDA formed configurationally stable lithiated intermediate (*R*)-**153**. When intermediate (*R*)-**153** was trapped with ClCO₂Me, trapped adduct (*R*)-**154** was obtained with good stereoretention (96:4 er). However, when the lithiation-trapping was repeated with Me₃SiCl, stereoretention was poor with (*R*)-**155** obtained in only 60:40 er (Scheme 1.50).

Scheme 1.50. Enantioselective α -lithiation-trapping of benzoate (*R*-152** ($\nu_{C=O}$ measured in MTBE solvent))**

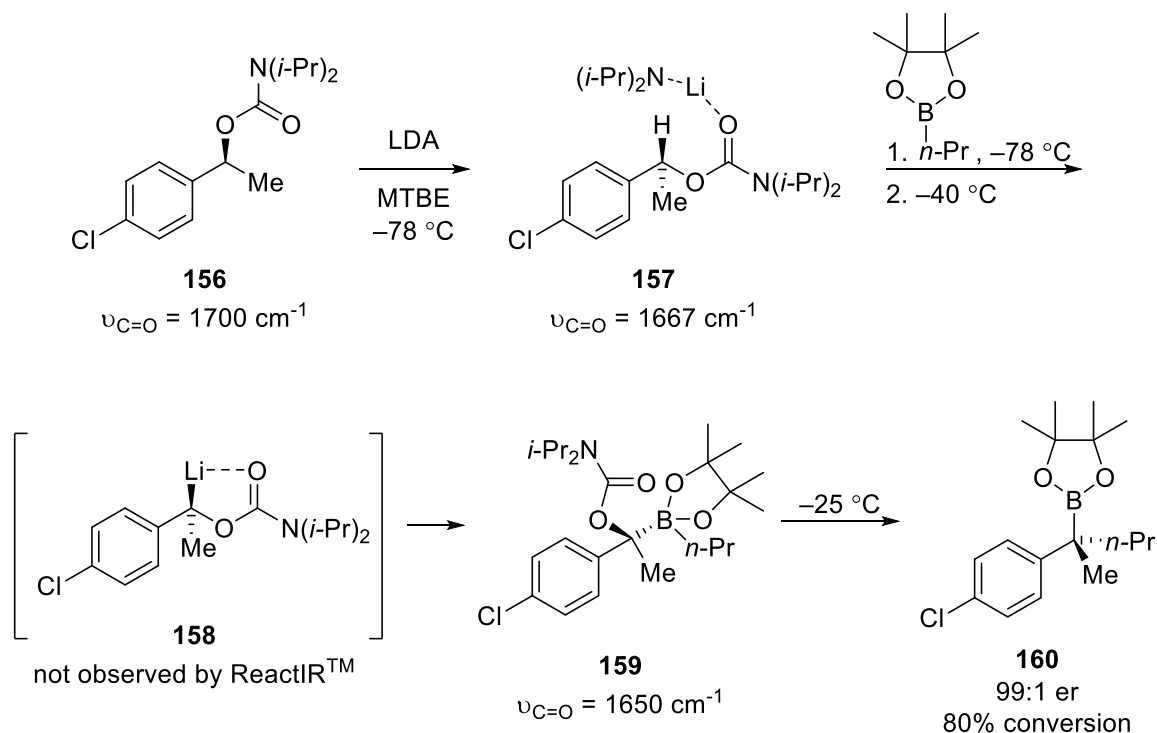


It was suggested the poor stereoretention observed for Me_3SiCl -trapped adduct (*R*-**155**) may result from a slow trapping reaction which allowed time for the erosion of stereochemistry of lithiated intermediate (*R*-**153**) to occur *via* configurational instability. To validate this hypothesis, the lithiation of (*R*-**152**) and trapping reactions with Me_3SiCl and ClCO_2Me were monitored by ReactIRTM. The ReactIRTM indicated that *s*-BuLi/TMEDA lithiation of (*R*-**152**) ($\nu_{C=O} = 1680 \text{ cm}^{-1}$) was rapid with complete formation of lithiated intermediate (*R*-**153**) ($\nu_{C=O} = 1585 \text{ cm}^{-1}$) requiring only 5 min. Upon addition of ClCO_2Me to lithiated intermediate (*R*-**153**), a fast trapping reaction was observed and complete trapping occurred within 5 min. However, when the reaction was repeated and Me_3SiCl was added to intermediate (*R*-**153**), a slow trapping reaction was observed and after 1 h, only 50% of (*R*-**153**) had been trapped. This evidence suggests that the slow rate of trapping with Me_3SiCl may indeed be responsible for the poor stereoretention observed for (*R*-**155**).

Fandrick *et al.* have also used ReactIRTM to monitor the enantioselective α -lithiation and boronate trapping of carbamate **156**. The subsequent rearrangement of boronate **159** was also observed by ReactIRTM.⁸⁴ When LDA was added to carbamate **156** ($\nu_{C=O} = 1700 \text{ cm}^{-1}$) at $-78 \text{ }^\circ\text{C}$, a new peak appeared due to the formation of the LDA-carbamate prelithiation complex **157** ($\nu_{C=O} = 1667 \text{ cm}^{-1}$). No lithiated intermediate **158** was observed and this was desired as the lithiated intermediate **158** was known to be configurationally unstable and would result in poor stereorentention. It was planned that the boronate electrophile could be added to the prelithiation complex **157** and then on warming up lithiation and trapping would occur in rapid succession, not allowing time for the er of lithiated intermediate **158** to erode. When the boronic ester was added, no change was observed by ReactIRTM. The reaction was then warmed to $-40 \text{ }^\circ\text{C}$, where rapid formation of boronate complex **159** ($\nu_{C=O} = 1650 \text{ cm}^{-1}$)

occurred and no signal for the lithiated intermediate was observed. After further warming to $-25\text{ }^{\circ}\text{C}$, the boronate complex **159** peak decreased and rearrangement product **160** was observed by HPLC in 99:1 er and 80% conversion (Scheme 1.51).

Scheme 1.51. ReactIR™ monitored cryogenic lithiation and boronate rearrangement of carbamate **156 ($\nu_{\text{C=O}}$ measured in MTBE solvent)**

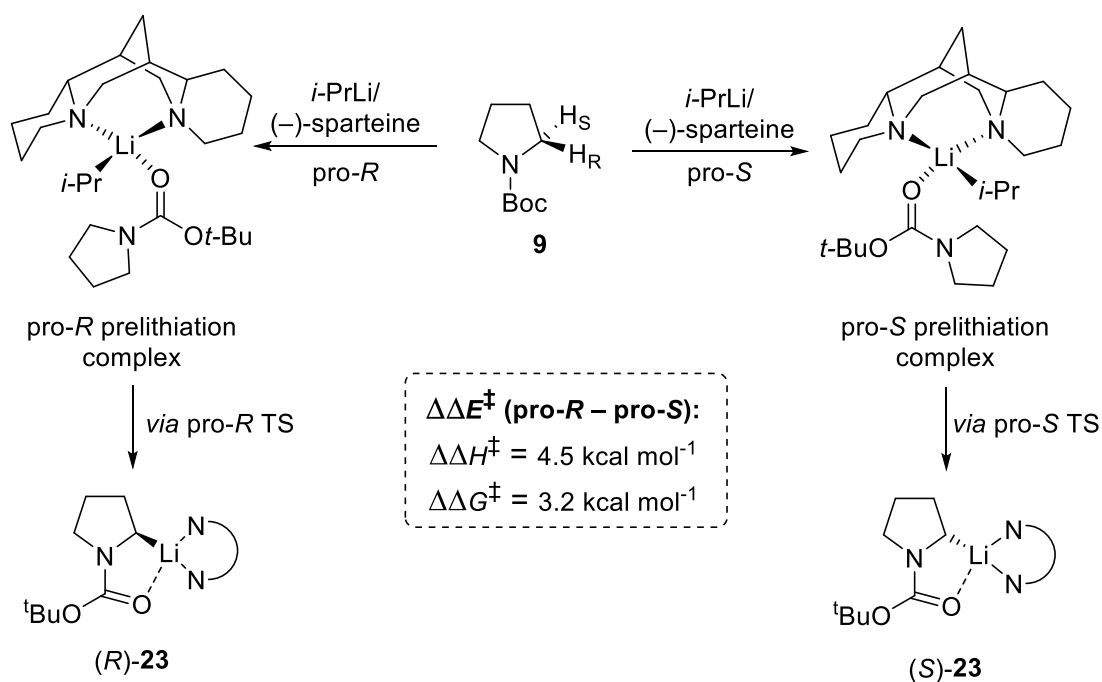


Using ReactIR™ to monitor the trapping reactions of α -lithiated intermediates does not only provide information on the time required for trapping to occur. The examples presented, show that mechanistic features of the trapping reactions and subsequent rearrangements can also be probed. In addition, the monitoring of the trapping can diagnose unexpected results such as poor enantioselectivity or quenching of the lithiated intermediate and provide evidence to suggest how they occur.

1.4 Computational Studies of the α -Lithiation Reactions of *N*-Boc Heterocycles

The asymmetric α -lithiation reaction of *N*-Boc pyrrolidine **9** has been subjected to several computational investigations to investigate the source of the enantioselectivity. Wiberg and Bailey investigated the enantioselectivity of the *i*-PrLi/(-)-sparteine α -deprotonation of *N*-Boc pyrrolidine **9** with DFT modelling.^{85,86} Experimental work by Beak and Kerrick found that the lithiation of *N*-Boc pyrrolidine **9** with *i*-PrLi/(-)-sparteine provided high levels of enantioselectivity by favourable deprotonation of the pro-*S* α -proton (96:4 er).²⁸ Prelithiation complexes and transition states were optimised for both the pro-*R* and pro-*S* *i*-PrLi/(-)-sparteine α -deprotonation of *N*-Boc pyrrolidine **9** using the B3P86 DFT functional within a 6-31G(d) basis set. The difference in enthalpy and free energy between the lower energy pro-*S* and higher energy pro-*R* transition states were 4.5 kcal mol⁻¹ ($\Delta\Delta H^\ddagger$) and 3.2 kcal mol⁻¹ ($\Delta\Delta G^\ddagger$) respectively. The significant energy differences between the transition states indicated that pro-*S* deprotonation is significantly favoured, which was consistent with the high er obtained by experiment (Scheme 1.52).³

Scheme 1.52. pro-*S* and pro-*R* pathways for the *s*-BuLi/(-)-sparteine lithiation of *N*-Boc pyrrolidine **9**

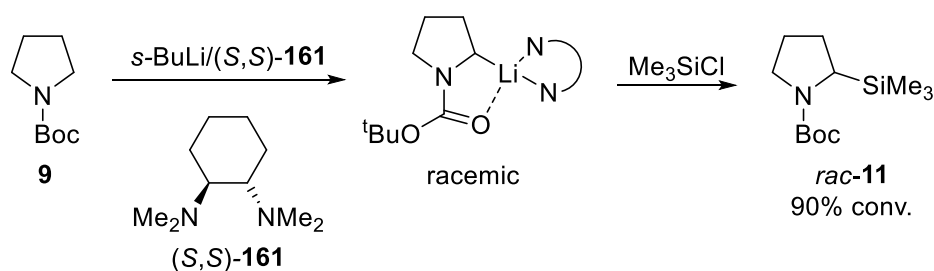


Wiberg and Bailey concluded that steric effects were responsible for the significant energy differences between the pro-*R* and pro-*S* α -deprotonation pathways. This conclusion was

reached by examination of the distances between atoms of the *i*-PrLi/(–)-sparteine and *N*-Boc pyrrolidine **9** moieties in the prelithiation complexes and transition states for the formation of both enantiomers. In the prelithiation complexes and transition states for pro-*R* α -deprotonation, the distances between these moieties were smaller than those for pro-*S*, resulting in a higher energy system for pro-*R* α -deprotonation.

Computational modelling has also been used to model the enantioselectivity of the α -lithiation of *N*-Boc pyrrolidine **9** with other chiral diamines. For example, the α -lithiation of *N*-Boc pyrrolidine **9** using chiral diamine (*S,S*)-**161**, which offers no enantioselectivity has also been modelled computationally.^{86,87} When *N*-Boc pyrrolidine **9** was subjected to lithiation with *s*-BuLi/(*S,S*)-**161** and trapping with Me₃SiCl, racemic 2-silyl *N*-Boc pyrrolidine *rac*-**11** was formed in 90% conversion (by GC) (Scheme 1.53).⁸⁸

Scheme 1.53. Lithiation-trapping of pyrrolidine **9 using chiral diamine (*S,S*)-**161****

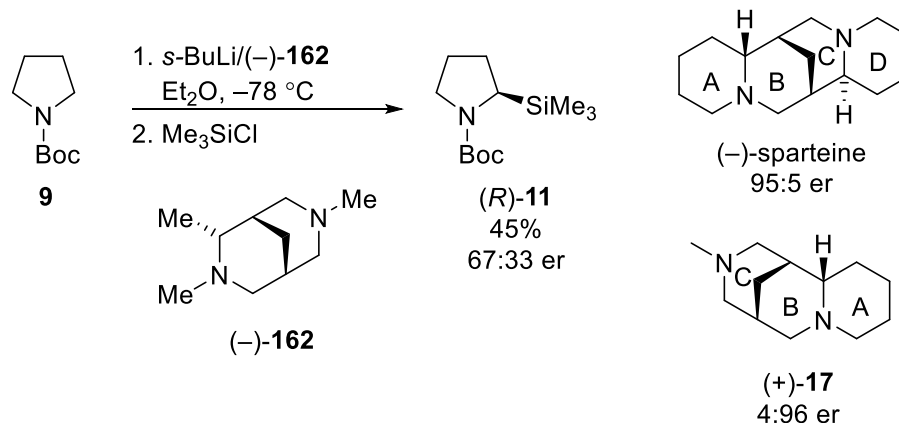


Computational modelling was conducted to investigate whether the modelling could reproduce the lack of enantioselectivity that was observed experimentally. Prelithiation complexes and transition states for the *i*-PrLi/(*S,S*)-**161**-mediated pro-*S* and pro-*R* deprotonations of *N*-Boc pyrrolidine **9** were modelled and energies were calculated for each. The difference in enthalpy and free-energy between pro-*S* and pro-*R* transition states was also less significant ($\Delta\Delta H^\ddagger = 1.1 \text{ kcal mol}^{-1}$ and $\Delta\Delta G^\ddagger = 1.2 \text{ kcal mol}^{-1}$) compared to the $\sim 3 \text{ kcal mol}^{-1}$ difference with (–)-sparteine (see Scheme 1.52). These energy differences indicated a much smaller preference for pro-*S* lithiation, which was reflected in the experimental result where *rac*-**11** was obtained.

Kozłowski *et al.* used a combined experimental and computational approach to investigate the selectivity of the most simple chiral portion of (–)-sparteine, fragment (–)-**162**. Diamine ligand (–)-**162** was synthesised and employed in the *s*-BuLi/(–)-**162** lithiation of *N*-Boc pyrrolidine **9**. After trapping with Me₃SiCl, 2-silyl *N*-Boc pyrrolidine (*R*)-**11** was formed in 45% yield and 67:33 er (Scheme 1.54). Surprisingly, the removal of the ‘A’ ring from (–)-sparteine reversed the enantioselectivity of the deprotonation forming (*R*)-**11**. This result

indicated that the 'A' ring is essential for enantioselectivity whereas the 'D' ring has little effect, as discovered by the O'Brien group with (+)-sparteine surrogate (+)-**17**.

Scheme 1.54. *s*-BuLi/(-)-**162** lithiation and Me₃SiCl trapping of *N*-Boc pyrrolidine **9**



When the *i*-PrLi/(-)-**162** lithiation of *N*-Boc pyrrolidine **9** was modelled using DFT, the modelling was able to account for the lower selectivity observed with diamine (-)-**162**. However, the modelling was not able to rationalise the reversal in the enantioselectivity that was observed experimentally.

Another combined computational and experimental study was carried out by O'Brien, Wiberg and Bailey to probe the enantioselectivity afforded by (+)-sparteine surrogate **17**.⁸⁹ DFT calculations which modelled the *i*-PrLi/(+)-**17** lithiation of *N*-Boc pyrrolidine **9** were able to emulate the enantioselectivity observed experimentally. The energies calculated provided significant energy differences between and pro-*S* and pro-*R* α -deprotonation with $\Delta\Delta H^\ddagger = 3.5$ and $\Delta\Delta G^\ddagger = 2.8$ kcal mol⁻¹. These energies indicated a clear preference for pro-*R* deprotonation which provided good agreement with the 94:6 er that was obtained experimentally with *i*-PrLi/(+)-**17** lithiation of pyrrolidine **9**.

Wiberg and Bailey have also used DFT modelling to investigate the enantioselectivity afforded by the *i*-PrLi/(-)-sparteine lithiation of *N*-Boc piperidine **10**.³⁴ The study found that the lowest energy pro-*S* and pro-*R* deprotonation pathways were similar in energy with only small differences in energy of the transition states ($\Delta\Delta H^\ddagger = 0.41$ and $\Delta\Delta G^\ddagger = 0.08$ kcal mol⁻¹). Wiberg and Bailey claimed that the small energy differences between the pro-*S* and pro-*R* deprotonation pathways explained the reduced 87:13 er observed experimentally. However, with the energy differences being this small, in the margins of calculation error, it would be expected that very little or no enantioselectivity would be observed at all. The activation energies calculated for the *i*-PrLi/(-)-sparteine lithiation of *N*-Boc piperidine **10**

were significantly higher than those calculated for the *i*-PrLi/(–)-sparteine lithiation of *N*-Boc pyrrolidine **9**. This reflected the slower rate of lithiation of *N*-Boc piperidine **10** versus *N*-Boc pyrrolidine **9** observed experimentally.

Wiberg and Deng later reattempted the modelling of the *i*-PrLi/(–)-sparteine lithiations of both *N*-Boc pyrrolidine **9** and *N*-Boc piperidine **10** using QM/QM modelling.⁹⁰ QM/QM modelling was carried out using the ONIOM method developed by Morokuma *et al.*,⁹¹ which allows the system to be separated into parts which can be treated with different levels of theory. This methodology can be particularly useful for large systems where only a small portion of the total system is chemically active. This chemically important part of the system can be calculated using a more accurate, computationally expensive method and the rest can be calculated using a less expensive method, without adversely affecting the quality of the results. This method is particularly useful for modelling enzymes and proteins where the active site can be modelled at a high level theory and the surrounding systems can be modelled with lower levels of theory or molecular mechanics.⁹² Wiberg and Deng attempted many different partitions for the lithiation of both *N*-Boc pyrrolidine **9** and *N*-Boc piperidine **10**. These included treating the entire (–)-sparteine ring with a lower level of theory and treating other half of the pyrrolidine and piperidine rings at lower levels of theory. Unfortunately, each of the QM/QM partitioning schemes that were attempted were unable to sufficiently describe the system and provided calculated energies that significantly differed to those calculated when the entire system was modelled using a high level of theory. They did, however, find that treatment of the other half of the piperidine or pyrrolidine ring at a lower level of theory did not adversely affect the results, suggesting that the totality of the heterocycle ring was not crucial for QM/QM calculations.

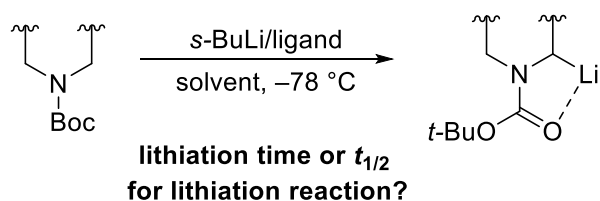
In summary, the enantioselectivity of the lithiation of *N*-Boc pyrrolidine **9** and *N*-Boc piperidine **10** can, to some extent, be rationalised with computational DFT modelling. In many cases, the calculated differences in energy between the transition states of enantiomeric α -deprotonation provides a good description of the enantioselectivity that was observed experimentally. These results suggest that DFT modelling may provide a sufficient description of the system to allow reactivity differences that arise with different *N*-Boc heterocycles and ligands to be modelled.

1.5 Project Outline

This project aims to study two of the key factors in the α -lithiation-trapping reactions of *N*-Boc heterocycles: the rate/kinetics and, where relevant, the diastereoselectivity. Both topics will be investigated using a combination of experimental (synthesis and *in-situ* IR spectroscopy) and computational DFT modelling. Combining experimental and computational techniques could potentially allow rates of reaction and the diastereoselectivity (if applicable) for unknown lithiation reactions to be modelled and predicted computationally. The combination of these techniques may also help to rationalise and/or quantify the chemical behaviour that is observed experimentally.

Chapter 2 of this thesis uses *in situ* IR spectroscopy to study the rates of lithiation when different *N*-Boc heterocycle substrates and different ligands are employed in the lithiation reaction (Scheme 1.55). We have found that both the structure of the *N*-Boc heterocycle and ligand employed in the lithiation can have a dramatic effect on the reactivity observed. This collated reactivity data can then help to identify reactivity trends which can be used to rationalise why the rate of lithiation is fast or slow for particular substrates or ligands.

Scheme 1.55. Quantification of the rate of lithiation using *in situ* IR spectroscopy

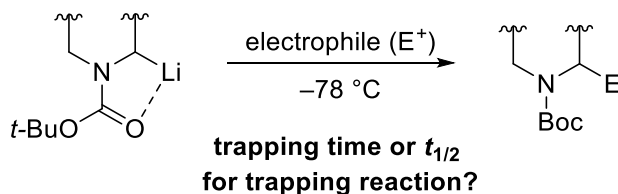


In Chapter 3, the α -lithiation reactions that were conducted in Chapter 2 are modelled computationally using DFT. This was conducted to determine whether a theoretical treatment of the α -lithiation reaction can account for the reactivity differences that were observed by experiment. If the DFT modelling can reproduce these reactivity differences then there is a potential that the computational modelling could be used to predict the reactivity of unknown *N*-Boc heterocycles or ligands.

The rates of the trapping reactions between the α -lithiated intermediates and electrophiles are studied using *in situ* IR spectroscopy in Chapter 4 (Scheme 1.56). This investigation explores the trapping reactions of a variety of different lithiated intermediates with a range of different electrophiles. Our results show that the rate of trapping can differ by several magnitudes when different combinations of lithiated intermediate and electrophile are used.

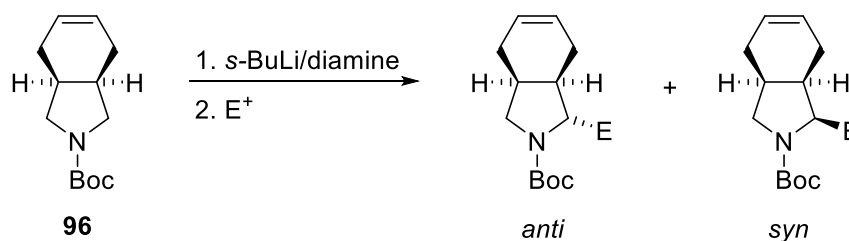
A knowledge of the rate of trapping of organolithiums is important for synthetic chemists so that products can be obtained in high yield and er/dr.

Scheme 1.56. Quantification of the rate of trapping using *in situ* IR spectroscopy



Finally, in Chapter 5, all the techniques utilised in the previous chapters are applied to investigate the diastereoselective lithiation-trapping of 3,4-disubstituted *N*-Boc pyrrolidine **96** (Scheme 1.57). The diastereoselectivity of the lithiation of **96** can be altered by the ligand employed in the lithiation and the identity of the electrophile used in the subsequent trapping reaction. The effect of the ligand on diastereoselectivity is investigated using synthetic experiments and DFT modelling. The effect that the electrophile has on diastereoselectivity has been determined with synthetic experiments and *in situ* IR spectroscopic analysis has elucidated how the choice of electrophile affects the dr of the products observed.

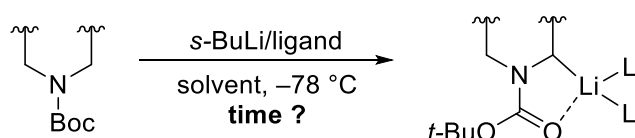
Scheme 1.57. General lithiation-trapping reaction for *N*-Boc pyrrolidine **96**



Chapter 2: *In situ* IR Spectroscopic Monitoring of the α -Lithiation Reaction of *N*-Boc Heterocycles

The *in situ* IR spectroscopic monitoring of the α -lithiation reaction provides useful information to synthetic chemists on how long such reactions require to reach completion (Scheme 2.1). If the electrophile was added too early, only partial lithiation would have occurred which would result in a decreased yield of the desired product and makes separation of the product and starting material necessary. Addition of the electrophile when large amounts of unreacted alkyllithium remain can pose a problem by forming by-products that further complicate the separation. α -Lithiation reactions are routinely conducted at $-78\text{ }^{\circ}\text{C}$ and it is important that the reaction is not allowed to warm before the electrophile is added as the lithiated intermediates could become unstable at higher temperature.

Scheme 2.1. General scheme for the α -lithiation of a *N*-Boc heterocycle



In situ IR spectroscopic monitoring of the reaction should enable optimised lithiation conditions to be obtained quickly without having to carry out many repeat reactions using a process of trial and error. It is also advantageous to have the probe in the reaction flask due to the low reaction temperatures required and the water sensitivity of both the reagents and intermediates. Many alternative methods to monitor reaction progress require aliquots of the reaction mixture to be taken from the reaction and then analysed. This method could be problematic as it is possible to quench the reaction/aliquot by exposure to air/water, the temperature of the aliquot needs to be maintained so that erroneous results are not obtained and concentration effects may occur due to the removal of portions of the reaction mixture.

On a large or industrial scale, maintaining low reaction temperatures, such as $-78\text{ }^{\circ}\text{C}$, may not pose a problem. However, it is important that the reaction is only conducted for the length of time required for complete conversion to occur, to ensure that the process is efficient. Maintaining these low temperatures for longer than is required will significantly decrease both the energy and cost efficiency of a reaction.

Previous work in the O'Brien group, both published and unpublished, has focussed on using *in situ* IR spectroscopy (ReactIRTM) to determine the reaction time for the *s*-BuLi/diamine

lithiation of a range of structurally different *N*-Boc heterocycles.^{31,50,52,53,73,93,94} This has included using several diamines, including TMEDA, (–)-sparteine and the (+)-sparteine surrogate **17**. Traditionally, these lithiation reactions have been allowed between 3-6 h for completion at –78 °C but there is little synthetic evidence that these lengthy reaction times are needed for the majority of the heterocycle substrates.

This chapter presents work that builds on this previous in-group research. This work expands the range of *N*-Boc heterocycles whose lithiation reactions have been studied by ReactIR™. There is a deeper focus on constructing a reactivity series for the different substrates and attempts to rationalise the differences in reactivity of the substrates are provided. Research in this chapter also applies kinetic modelling to the lithiation reaction. This allowed k_{obs} values to be extracted from the ReactIR™ data to enable more accurate comparisons of reactivity for the different substrates.

2.1 Reactivity Series for the *s*-BuLi/TMEDA Lithiation of *N*-Boc Heterocycles

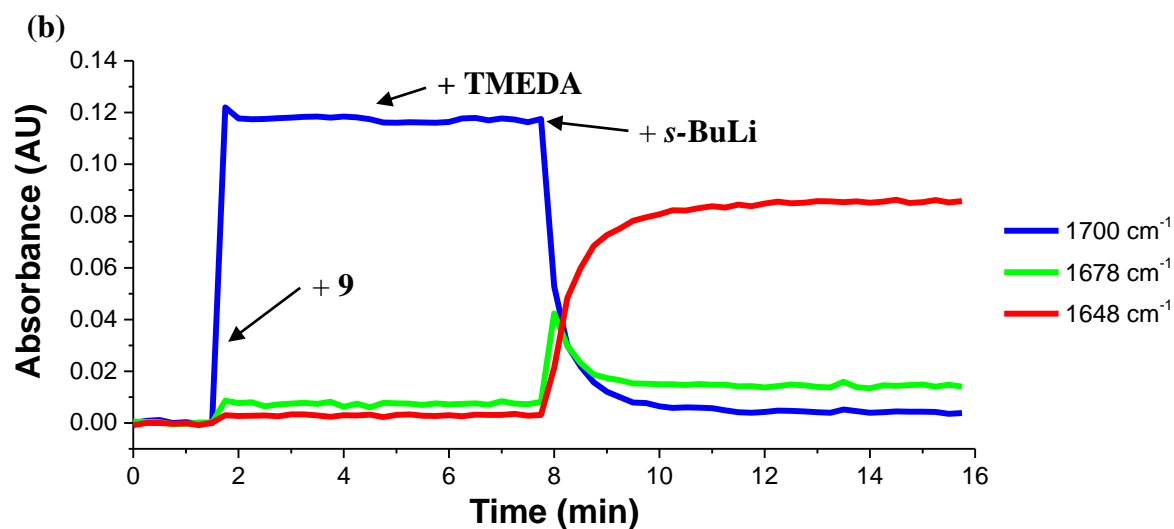
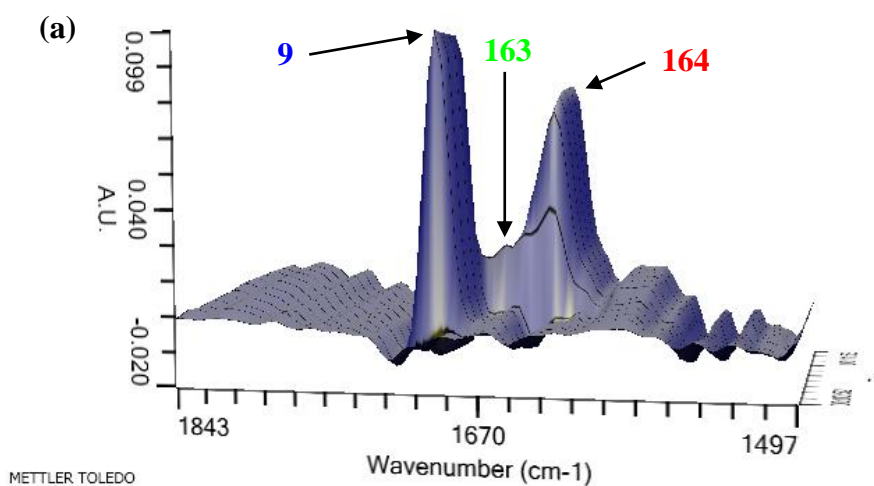
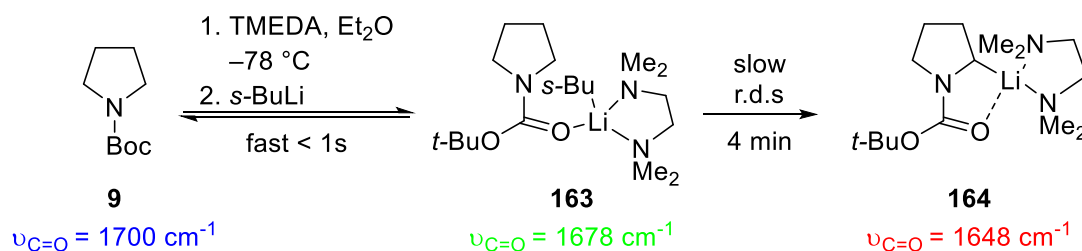
The ReactIR™ monitoring of the *s*-BuLi/TMEDA lithiation reactions of a host of different *N*-Boc heterocycles has already been carried out in the O'Brien group.^{53,94} Many of these lithiations were repeated in this investigation for two reasons. First, for the lithiation reactions which took > 1 h, the monitoring was ended prematurely in previous work due to worries that the lithiated intermediate may not be stable over longer reaction times using the ReactIR™ set-up. During this new investigation of reactivity, it was found that most lithiated intermediates were stable using the ReactIR™ apparatus for many hours. Second, some of the previous lithiations were carried out by adding the *s*-BuLi and *N*-Boc heterocycle first, forming a presumably solvent-ligated prelithiation complex to which the diamine ligand was then added to initiate lithiation. However, this order of addition can provide unreliable kinetic information, as work in this study indicated that the lithiation can still occur with just *s*-BuLi/Et₂O, albeit at a slower rate. The addition of *s*-BuLi to a mixture of the substrate and diamine provides more accurate and reliable data, as the reaction begins directly after the addition of the *s*-BuLi. The reliability and accuracy of the kinetic data is particularly important as we are attempting to compare reactivities of substrates.

The first substrate monitored using ReactIR™ in this reactivity study was *N*-Boc pyrrolidine **9**, one of the first *N*-Boc heterocycles whose lithiation was reported by Beak in 1989.² The *s*-BuLi/TMEDA lithiation of *N*-Boc pyrrolidine **9** using Beak's conditions: -78 °C in Et₂O, was monitored using *in situ* IR spectroscopy (Scheme 2.2). Our standard conditions for lithiation used 1.3 eq. of *s*-BuLi/TMEDA in 14 mL of Et₂O solvent. The only modification to Beak's conditions was that the concentration of the reaction mixture was halved, as there was concern that higher concentrations of the *s*-BuLi reagent could damage the ReactIR™ probe.

For *N*-Boc pyrrolidine **9**, the carbonyl stretching frequency ($\nu_{\text{C=O}}$) of the Boc group can be used as a spectroscopic handle.⁷² Carbonyl groups provide a particularly useful spectroscopic handle due to their strong IR absorbance signals which allow easy identification and monitoring of the carbonyl species in the reaction. In addition, there were no other absorbances in the 1800-1600 cm⁻¹ region of the IR spectrum for this chemistry which made tracking changes to these signals easier. Monitoring of the lithiation using C-H stretching and bending frequencies was not possible for two reasons. First, the ReactIR™ apparatus used can only monitor IR frequencies in the ranges of 2500-2250 cm⁻¹ and 2000-650 cm⁻¹, this meant that most C-H stretching frequencies were out of this observable window. Second, the diamine ligand and *s*-BuLi (which is in cyclohexane solvent) were added after the solvent background was recorded, this meant that many C-H stretching/bending frequencies were observed upon addition at the reaction setup. These overlapping frequencies meant that finding a correlation between reaction progress and any changes in $\nu_{\text{C-H}}$ absorbance intensity was not possible.

During the lithiation of *N*-Boc pyrrolidine **9**, three different IR signals are observed for the Boc carbonyl: the uncomplexed starting material *N*-Boc pyrrolidine **9** ($\nu_{\text{C=O}} = 1701 \text{ cm}^{-1}$), the prelithiation complex **163** ($\nu_{\text{C=O}} = 1678 \text{ cm}^{-1}$) and the lithiated intermediate **164** ($\nu_{\text{C=O}} = 1647 \text{ cm}^{-1}$) (Scheme 2.2.a). These three signals appear at different wavenumbers as the Boc carbonyl has a different coordinating environment in each of these species. The $\nu_{\text{C=O}}$ for the carbamate decreases in the three species **9**, **163** and **164**. This can be attributed to the increasing coordination of the electropositive Li centre to the carbonyl bond during the reaction which weakens the bond and therefore shifts the $\nu_{\text{C=O}}$ to lower wavenumbers.

Scheme 2.2. The ReactIR™ monitored *s*-BuLi/TMEDA lithiation of *N*-Boc pyrrolidine **9 with 3D and 2D ReactIR™ traces**



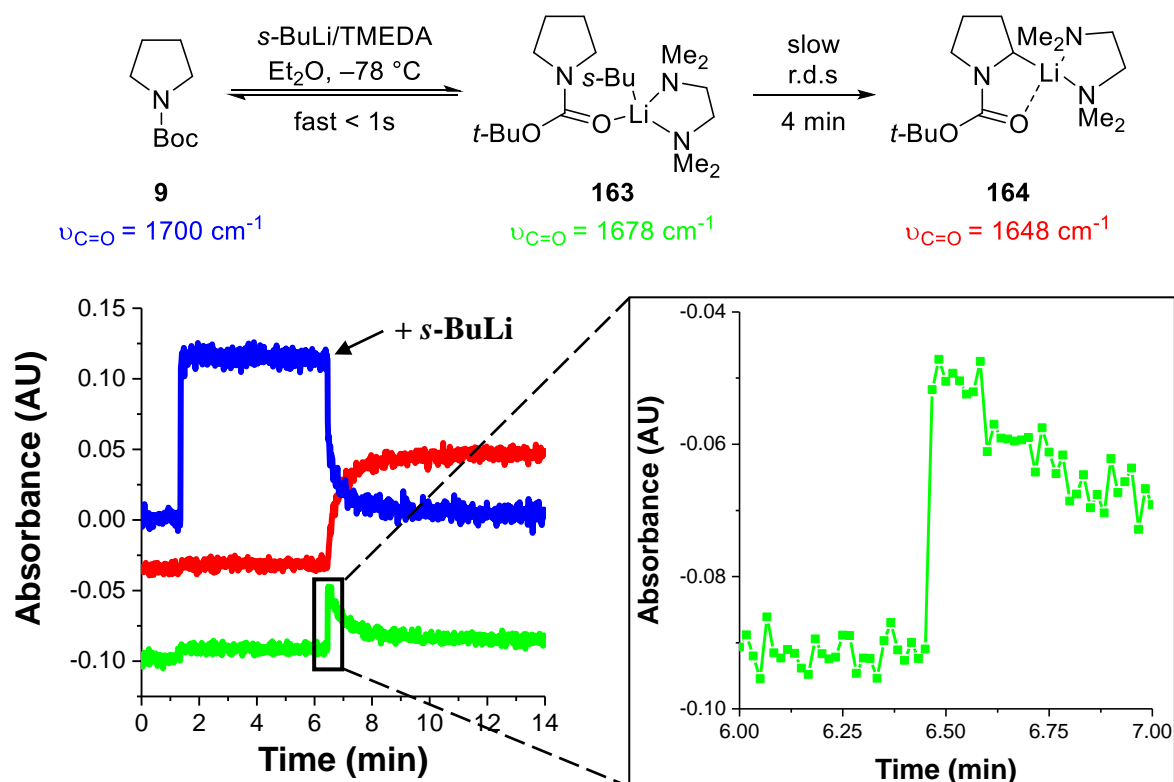
Recording the absorption of the three $\nu_{\text{C=O}}$ signals during the reaction allows the changes in concentration of the three species to be observed over the course of the lithiation (Scheme 2.2.b). Importantly, the $\nu_{\text{C=O}}$ signal for *N*-Boc pyrrolidine **9** shows consumption of the starting material and the $\nu_{\text{C=O}}$ signal of lithiated intermediate **164** tracks the formation of the product.

The $\nu_{C=O}$ absorbance of prelithiation complex **163**, a reaction intermediate, indicates that a pre-equilibria process occurs during the reaction, where the prelithiation complex **163** is formed rapidly at the start of the reaction. The rapid formation of **163** arises from the fast equilibrium reaction between the *N*-Boc pyrrolidine **9** starting material and prelithiation complex **163**. This fast equilibrium is evident in the ReactIRTM monitored lithiation reaction, as consumption of prelithiation complex **163** and the starting material **9** mirror each other during the reaction once the equilibrium has been established. This is because as prelithiation complex **163** is consumed by the slow rate determining deprotonation step, the rapidly occurring equilibrium reaction restores the original ratio of species **9** and **163**. Previous mechanistic work conducted by Beak provided evidence for this fast equilibrium between the substrate and alkyllithium/diamine, followed by a slow rate determining deprotonation for the *i*-PrLi/(–)-sparteine lithiation of *N*-Boc pyrrolidine **9** (see Scheme 1.9).³²

By visual inspection of Scheme 2.2.b, the *s*-BuLi/TMEDA lithiation *N*-Boc pyrrolidine **9** requires 4 min for complete lithiation, at which point concentrations of starting material **9** and lithiated intermediate **164** no longer change. This 4 min reaction time is a stark contrast to the 3.5 h lithiation time initially used by Beak and highlights how useful ReactIRTM can be for the optimisation of reaction conditions.²

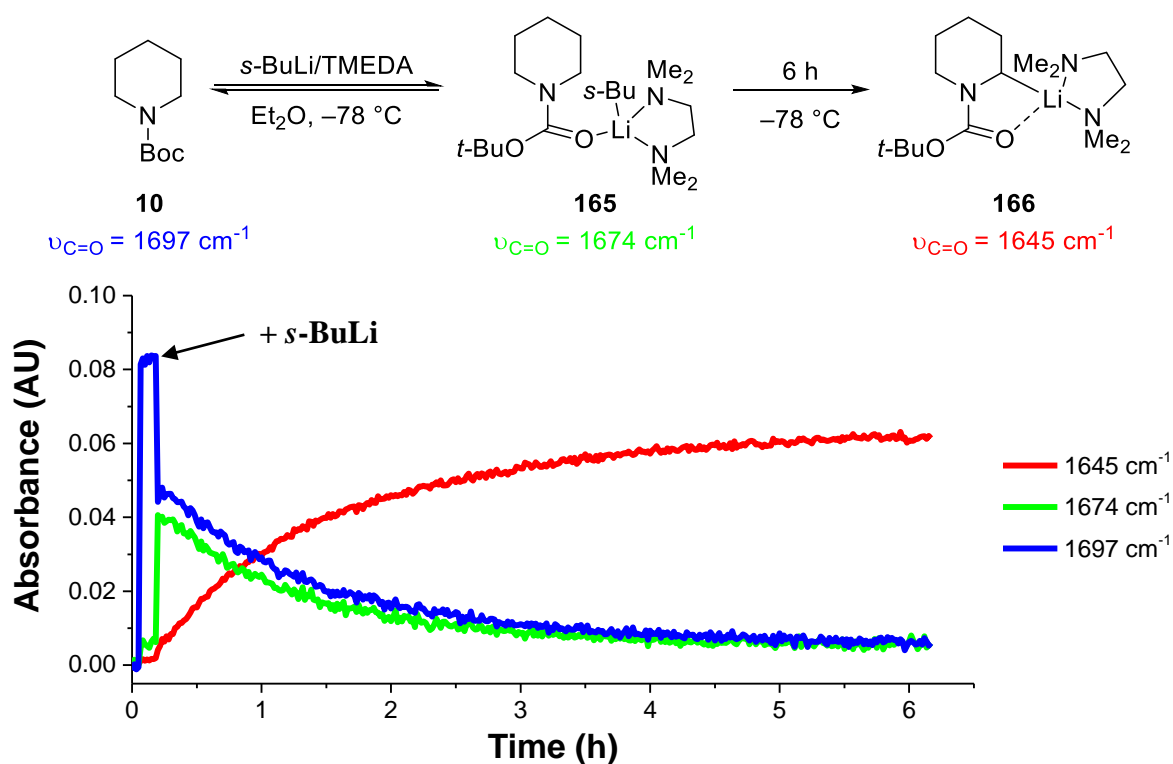
To further probe the rate of the initial equilibrium reaction between the *N*-Boc pyrrolidine **9** starting material and prelithiation complex **163**, the lithiation reaction was repeated using the rapid-collect mode on the ReactIRTM apparatus (Scheme 2.3). This allowed the collection of IR absorbance data for each second rather than at the 15, 30 or 60 second intervals used for normal ReactIRTM experiments. This method did have two constraints. First, fewer scans at each interval resulted in a low signal/noise ratio which provided a reaction trace with a significant amount of noise. Second, due to the processing power required to process the volume of data per second, the results were not given in real time and the trace was only viewable after the experiment. This was not an issue for the lithiation of *N*-Boc pyrrolidine **9** as it was a repeat reaction and timings for the addition of reagents were known. The rapid-collect ReactIRTM trace indicated that prelithiation complex formation was extremely rapid, occurring in < 1s. This offered further evidence that a rapid equilibrium reaction exists between the starting material **9** and prelithiation complex **163** and that the rate determining step is the deprotonation/lithiation of the prelithiation complex **163**.

Scheme 2.3. Rapid-collect ReactIRTM monitored *s*-BuLi/TMEDA lithiation of *N*-Boc pyrrolidine **9**



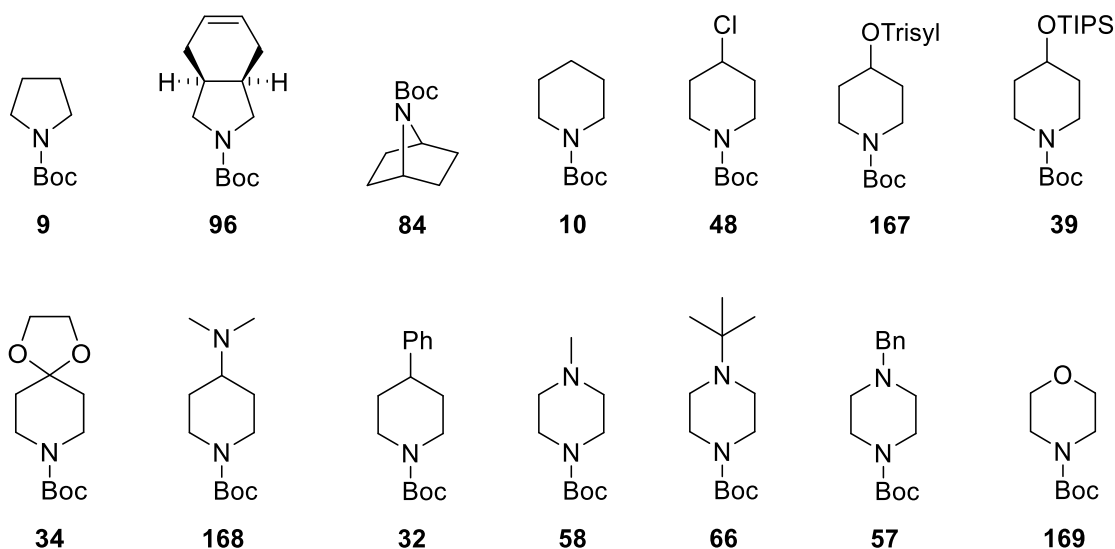
The ReactIRTM monitored lithiation of *N*-Boc piperidine **10**, another substrate whose lithiation was reported in Beak's 1989 publication,² indicated that a significantly longer time was required for complete lithiation to occur. Using *s*-BuLi/TMEDA in Et₂O at -78 °C the lithiation of *N*-Boc piperidine **10** required 6 h to reach completion (Scheme 2.4). This dramatic difference in reactivity highlights the significant effect that the structure of the *N*-Boc heterocycle has on the lithiation reaction. These large reactivity differences between substrates are a key reason why monitoring the lithiation of substrates is so important and explains why the monitoring of α -lithiation reactions by ReactIRTM is becoming more popular.

Scheme 2.4. ReactIRTM monitored *s*-BuLi/TMEDA lithiation of *N*-Boc piperidine **10**



Analogous to the lithiation of *N*-Boc pyrrolidine **9**, the carbamate $\nu_{\text{C=O}}$ of the *N*-Boc heterocycle shifts to lower wavenumbers during the lithiation reaction as the degree of coordination to the Li atom is increased in species **10**, **165** and **166**. A pre-lithiation complex intermediate was also observed for *N*-Boc piperidine, **165** ($\nu_{\text{C=O}} = 1674 \text{ cm}^{-1}$) and it displayed the same pre-equilibrium kinetics which were more easily identified over the longer reaction time.

The same ReactIRTM monitoring procedure carried out for the lithiations of *N*-Boc pyrrolidine **9** and *N*-Boc piperidine **10** was then employed to investigate the reactivity of 12 additional *N*-Boc heterocycle substrates (Figure 2.1). These substrates were selected as they provided a diverse selection of heterocycles with differing ring sizes, heteroatoms in the ring and substituents. It was envisaged that a wide spectrum of reactivity would be observed when lithiating with *s*-BuLi/TMEDA. Additionally, it was anticipated that the differing structural aspects of the *N*-Boc heterocycles may provide some trends between certain features of a substrate and the lithiation reactivity.



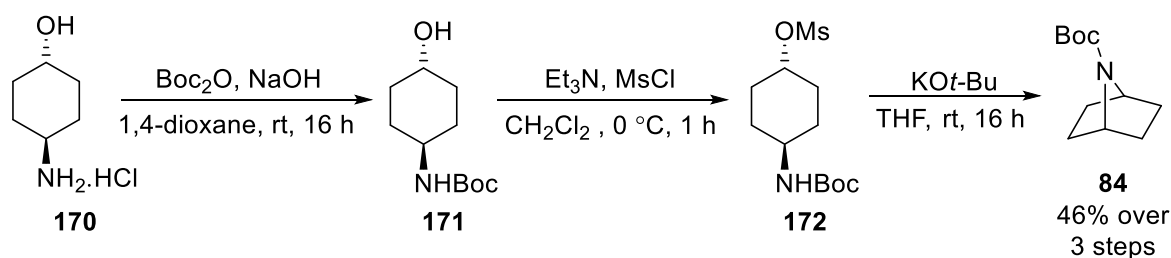
Trisyl = 2,4,6-tri-*i*-propylbenzenesulfonyl

Figure 2.1. 14 *N*-Boc heterocycles used for the reactivity study

Many substrates were selected as there was already precedent for their lithiation either in the literature (**9**, **10**, **32**, **34**, **39**, **47**, **48**, **57**, **58**, **66**, **84**, **96** – see section 1.2) or in-group (**167**, **169**)^{50,53,94}. All of the heterocycles except bicyclic pyrrolidine **84** and 4-amino *N*-Boc piperidine **168** were prepared using simple one- or two-step procedures available either in-group^{53,94–96} or from the literature.^{39,63,97,98}

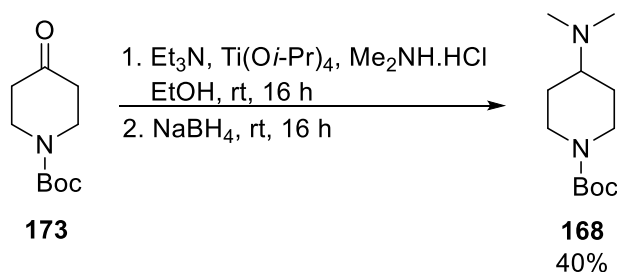
The synthesis and *s*-BuLi/TMEDA α -lithiation of bicyclic pyrrolidine **84** was previously reported by researchers at AstraZeneca as part of a synthetic route for the synthesis of a GlyT1 inhibitor for the treatment of schizophrenia (see Scheme 1.30).⁶³ Unfortunately, no kinetic data or reaction times for the lithiation were reported so it was decided to explore the lithiation with ReactIRTM monitoring. Synthesis of bicyclic pyrrolidine **84** was achieved using the literature synthetic route involving the Boc protection of amino-cyclohexanol **170** followed by mesylation of the resulting *N*-Boc alcohol **171** and subsequent cyclisation of mesylate **172** with KO*t*-Bu.⁹⁹ Bicyclic pyrrolidine **84** was afforded in multi-gram quantities and a moderate 46% yield over three steps (Scheme 2.5).

Scheme 2.5. Three-step synthesis of bicyclic *N*-Boc pyrrolidine **84**



4-Amino *N*-Boc piperidine **168** was selected to probe how the reactivity of a 4-substituted *N*-Boc piperidine would be affected with a heteroatom in the 4-position that was not oxygen. There was no precedent for the α -lithiation of **168**, although the synthesis of 4-amino *N*-Boc piperidine **168** was reported in the literature.¹⁰⁰ This synthetic route involved the reductive amination of *N*-Boc 4-piperidone **173** with dimethylamine using H_2 and Pd/C at elevated temperature and pressure. However, a synthetic procedure more amenable to a research laboratory which had been used to prepare similar amine compounds¹⁰¹ was employed to synthesise 4-amino *N*-Boc piperidine **168**. Reductive amination of *N*-Boc 4-piperidone **173** with dimethylamine hydrochloride and NaBH_4 in the presence of $\text{Ti}(\text{O}i\text{-Pr})_4$ provided the desired 4-amino *N*-Boc piperidine **168** in moderate 40% yield (Scheme 2.6).

Scheme 2.6. Synthesis of 4-amino *N*-Boc piperidine **168**



For the *s*-BuLi/TMEDA α -lithiations of all *N*-Boc heterocycles, identical reaction conditions were used and all lithiations were conducted at $-78\text{ }^\circ\text{C}$ to ensure trends in reactivity could be drawn from the results. A wide range of reactivities were displayed by the 14 substrates studied (Table 2.1). Many substrates, such as *N*-Boc morpholine **169**, 4-*O*-trisyl *N*-Boc piperidine **167** and *N*'-Me and *N*'-Bn piperazines **58** and **57** exhibited fast lithiation reactions with < 4 min lithiation times. Conversely, others such as 4-amino piperidine **168** and *N*-Boc piperidine **10** required several hours to reach completion.

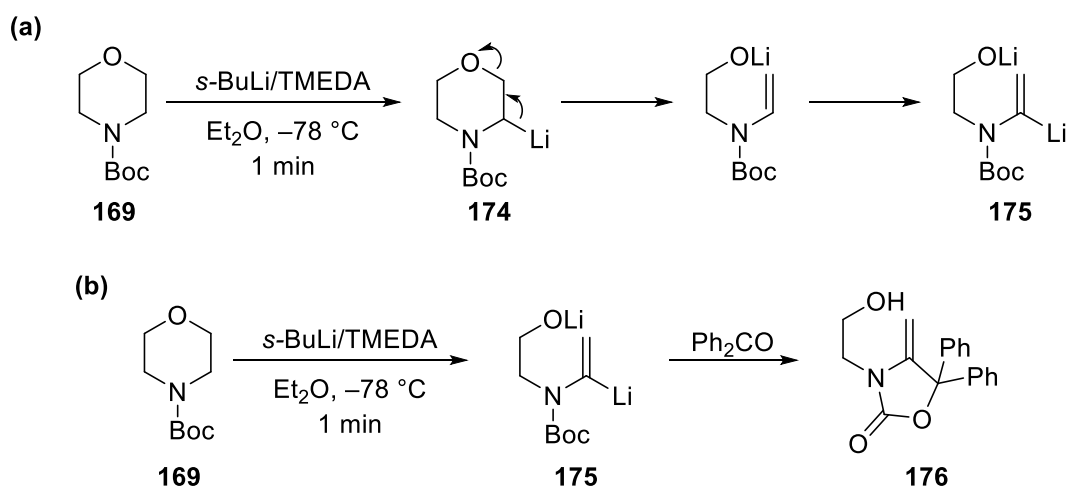
Table 2.1. Reactivity series for the *s*-BuLi/TMEDA lithiation at $-78\text{ }^{\circ}\text{C}$ of *N*-Boc heterocycles

	169	48	167	58	9	96
<i>t</i>_{lith} / min	< 1 ^a	2 ^{a, b}	2 ^{a, b, c}	4	4	4
<hr/>						
	57	84	66	39	32	34
<i>t</i>_{lith} / min	4	15	22	45	90	100
<hr/>						
	168	10				
<i>t</i>_{lith} / min	120	360				

^a 2.6 eq. of *s*-BuLi and diamine were used. ^b results from previous in-group work.⁵³ ^c Trisyl = 2,4,6-tri-*i*-propylbenzenesulfonyl

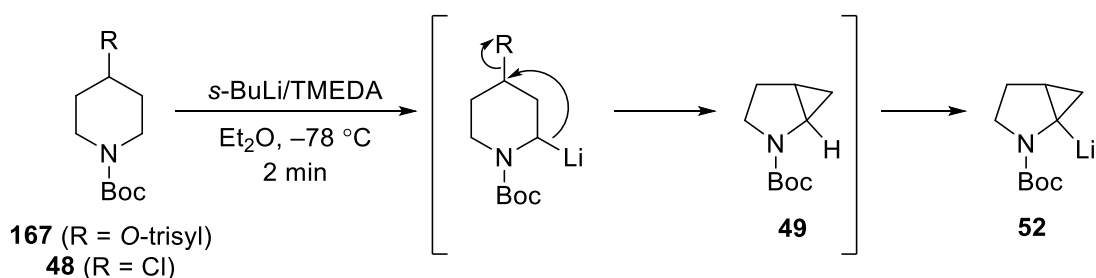
N-Boc morpholine **169** was the fastest heterocycle to lithiate and underwent rapid lithiation with *s*-BuLi/TMEDA with complete lithiation requiring < 1 min. 2.6 eq. of both the alkyl lithium and diamine were used as the initial lithiation forms lithiated intermediate **174** which subsequently ring opens and is followed by vinylic lithiation to form di-lithiated intermediate **175** (Scheme 2.7.a). This mechanism is proposed as previous unpublished work within the group described the successful trapping of di-lithiated species **175** (formed by *s*-BuLi/(–)-sparteine lithiation of **169**) with benzophenone to give trapped adduct **176** in 40% yield (Scheme 2.7.b).⁵³ The lithiation and similar ring opening of a bicyclic *N*-Boc morpholine was also reported by Lautens (see Scheme 1.26).⁵⁹

Scheme 2.7. α -Lithiation and ring opening of *N*-Boc morpholine **169**



The ReactIRTM monitoring of the lithiation reactions of both 4-chloro *N*-Boc piperidine **48** and 4-*O*-trisyl piperidine **167** indicated that lithiation was rapid, reaching completion within 2 min. Both lithiation reactions were carried out with 2.6 eq. of *s*-BuLi/TMEDA, due to the formation of a bicyclic intermediate **49** which then undergoes a second lithiation (believed to be rapid due to the acidifying effect of the cyclopropyl group) forming lithiated bicycle **52** (Scheme 2.8). It is presumed that it is lithiated bicycle **52** which is observed by ReactIRTM. Previous work has successfully trapped bicyclic intermediate **52**, generated by the lithiation of 4-chloro *N*-Boc piperidine **48** (see Scheme 1.19).^{42,44}

Scheme 2.8. Lithiation of 4-chloro and 4-*O*-trisyl piperidines **48** and **167**



Lithiation times of 4 min were observed for *N*-Boc pyrrolidines **9** and **96** which was a surprising result for two quite different pyrrolidine substrates. It was expected that the additional steric bulk from the cyclohexyl ring fused to the pyrrolidine would hinder and retard the rate of lithiation of pyrrolidine **96**. However, the identical reactivities of both **9** and **96** suggest that the steric bulk is too far away from the reaction centre to have a significant effect on the kinetics of the lithiation.

When the lithiation of bicyclic pyrrolidine **84** was monitored using ReactIR™ it was initially expected that the lithiation of **84** would be extremely slow as the deprotonation occurs at a sterically complex tertiary bridgehead carbon. However, it was discovered that only 15 min were required for complete lithiation of bicyclic pyrrolidine **84** to occur. This faster than expected lithiation may result from the rigid geometry imposed by the bridgehead making the deprotonation of the tertiary α -proton more favourable than in a non-bicyclic tertiary pyrrolidine such as 2-methyl pyrrolidine **14** (Figure 2.2).

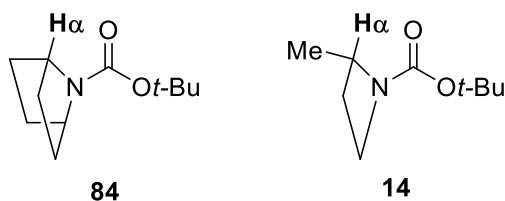


Figure 2.2. Steric environment of the α -proton in bicyclic pyrrolidine **84 and 2-methyl pyrrolidine **14****

It is also evident that the ring-size has a pronounced effect on the lithiation reactivity with a striking 6 h reaction time difference observed between the *N*-Boc pyrrolidine **9** and *N*-Boc piperidine **10** lithiations. It is possible that the difference in reactivity arises from the conformational differences of the five- and six-membered rings. However, ring-size is not the only factor that can determine reactivity. Other six-membered heterocycles including *N*-Boc morpholine **169**, piperazines **57**, **58** and **66** and 4-substituted *N*-Boc piperidines such as **39** all have significantly faster lithiation reactions than *N*-Boc piperidine **10**.

N'-Bn and *N*'-Me *N*-Boc piperazines, **57** and **58**, both exhibited short 4 min lithiation times whereas lithiation of *N*'-*t*-Bu piperazine **66** was more sluggish, requiring 22 min to reach completion. The lower reactivity of *N*'-*t*-Bu piperazine **66** compared to *N*'-Bn and *N*'-Me piperazines **57** and **58** is difficult to rationalise and, at present, we do not have an explanation for the differences in reactivity. It is unlikely that steric bulk attached to the distal nitrogen would directly hinder the lithiation as the substituent is far removed from the reaction centre.

All three of the piperazines studied have significantly faster lithiation reactions than *N*-Boc piperidine **10**. Presumably, the increased lability of the α -proton must arise from the nitrogen atom present in the heterocycle ring. We suggest that back donation can occur from the C–H σ bond of the α -proton into the lower lying C–N σ^* orbital (Figure 2.3.a). This orbital overlap would weaken the C–H bond and make the α -proton more kinetically acidic.⁵³ The

facile lithiation of *N*-Boc morpholine **169** (1 min lithiation time) may also be the result of the same orbital overlap effect (Figure 2.3.b).

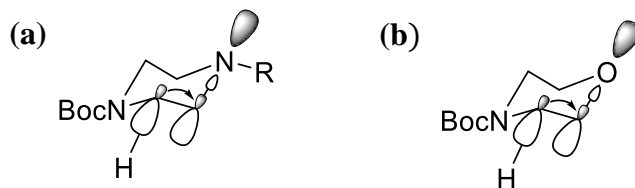


Figure 2.3. Proposed orbital overlap for *N*-Boc piperazines (a) and *N*-Boc morpholine **169 (b) increasing the α -proton acidity**

The identity of the substituent on the C-4 position of *N*-Boc piperidines also has a substantial effect on reactivity and this is evident when comparing the respective 2 min and 6 h lithiation times of 4-chloro *N*-Boc piperidine **48** and unsubstituted *N*-Boc piperidine **10**. We propose that a different type of orbital overlap could occur in the 4-substituted piperidines which would facilitate the lithiation by increasing the α -proton acidity.⁹⁶ Specifically, back donation from the C–H σ orbital of the α -proton to the C–X (where X = Cl, N, O) σ^* orbital (Figure 2.4). The conformation of the six-membered piperidine ring enables the overlap of the orbitals on the C-2 and C-4 carbons, analogous to the explanation of the 4J W-coupling that can occur between protons in ^1H NMR spectroscopy.^{102,103}

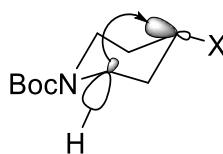


Figure 2.4. Proposed orbital overlap for the 4-substituted *N*-Boc piperidines

The various substituents (X) on the C-4 position will have differing electronic properties which may affect the extent of orbital overlap and back-donation that occurs. This would account for the wide range of reactivities observed with the different 4-substituted *N*-Boc piperidines. For example, both the 4-chloro- and 4-*O*-trisyl substituted piperidines **48** and **167** have 2 min lithiation times, presumably due to the electron-withdrawing nature of the substituents. 4-OTIPS *N*-Boc piperidine **39** has an intermediate reactivity, requiring 40 min for complete lithiation to occur. Alkoxy groups are known to have a smaller electron withdrawing ($-I$) effect than chloro groups,¹⁰⁴ this difference in inductive effect may explain why 4-OTIPS piperidine **39** exhibits a lower level of reactivity than that of 4-chloro piperidine **48**. 4-Ph piperidine **32**, ketal **34** and 4-amino *N*-Boc piperidine **168** are slower still, requiring 1.5-2 h for complete lithiation of the substrates to occur. However, all three

lithiations still only require less than a third of the time needed for the lithiation of unsubstituted piperidine **10**, indicating a significant activating effect is still present. Both 4-Ph piperidine **32** and 4-amino piperidine **168** have groups on the C-4 position of the piperidine ring with weak electron withdrawing effects, meaning that these substituents will offer a more modest activating effect for the lithiation reaction. An explanation of the lower reactivity observed with ketal **34** is more complex. This could arise due to the geometry of the ketal promoting poorer overlap between the C4 and C2 orbitals, resulting in a lesser degree of back donation between orbitals and therefore a poorer activating effect on the piperidine α -proton. Alternately, it is possible that the oxygen atoms of the ketal substituent may chelate the *s*-BuLi/TMEDA lithiating complex leading to retardation of the lithiation reaction.

In summary, a diverse selection of *N*-Boc heterocycles have exhibited a wide spectrum of reactivities for their respective *s*-BuLi/TMEDA lithiation reactions. The use of ReactIRTM can not only allow optimal conditions for each of the substrates to be determined but also allows construction of a reactivity series for the substrates. Comparisons between the experimental reactivity data and the structural differences of the substrates has allowed hypotheses to be made to rationalise the reactivity trends we observe. Furthermore, the experimentally obtained reactivity series obtained will allow comparison with the computationally predicted reactivity series for the same substrates, as described in Chapter 3 of this thesis.

2.2 Reactivity Series for the Lithiation of *N*-Boc Heterocycle Substrates with Different Diamine Ligands

Five of the 14 substrates included in the *s*-BuLi/TMEDA reactivity series had rapid lithiation reactions which were complete within 2 min. As the ReactIR™ equipment only gave absorbance readings for each signal per minute (on the older ReactIR™ iC10 apparatus used during this part of the investigation), this meant that the lithiation time was only determined to the nearest minute. This provides a significant amount of error in the lithiation times determined for rapidly reacting substrates. It was hoped that the use of a different diamine would slow the rate of the lithiation reactions so that more precise lithiation times could be obtained, thus allowing the construction of a reactivity series for the more reactive substrates.

First of all, a reactivity order was constructed using *s*-BuLi/(–)-sparteine to lithiate the *N*-Boc heterocycles that had a rapid lithiation reaction with *s*-BuLi/TMEDA. Previous in-group data was pooled for the *s*-BuLi/(–)-sparteine lithiations of seven heterocycle substrates; lithiation of *N*-Boc heterocycles with *s*-BuLi/(–)-sparteine has been studied extensively in the group previously.⁵³ It was initially expected that the reactivity order of the seven *N*-Boc heterocycles with *s*-BuLi/(–)-sparteine would be identical to that with *s*-BuLi/TMEDA but with longer lithiation times due to the more bulky (–)-sparteine ligand. All of the lithiations were slower but it was also noted that some substrates were placed in different positions in the reactivity series using *s*-BuLi/(–)-sparteine lithiating conditions. We propose that the difference in reactivity order observed for the substrates may derive from complications due to the asymmetric lithiation that occurs with *s*-BuLi/(–)-sparteine; these asymmetric effects will be discussed in detail later in this chapter.

2.2.1 Synthesis of achiral diamine ligands and construction of a diamine reactivity series

As the use of *s*-BuLi/(–)-sparteine appeared to provide outlying results for substrate reactivity, our aim was to find an achiral diamine that could be used to elucidate the differences in reactivity for the most reactive *N*-Boc heterocycles. Additionally, it was also of interest to investigate how the structure of the diamine affected the rate of lithiation. To this end, four diamine ligands were trialled: TMCDA *trans*-**161**, di-pyrrolidino ethane (DPE) **177**, tetra-isopropyl ethane **178** and TMPDA **179** (Figure 2.5). These diamines were selected for two reasons. First, they were either commercially available (TMPDA **179**) or had

relatively short synthetic sequences (*trans*-**161**, **177** and **178**). Second, we hoped that the differing levels of flexibility of the diamines and the different amounts of steric bulk around the amine groups would provide a broad range of lithiation times when used with *s*-BuLi.

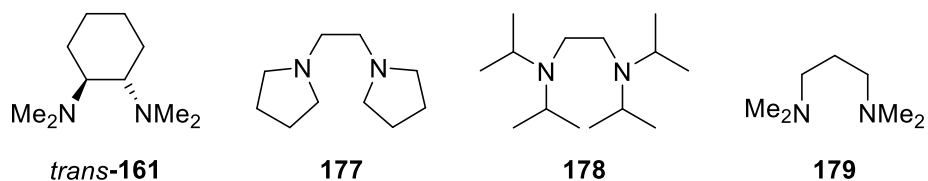
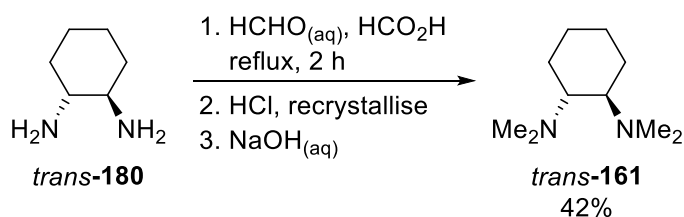


Figure 2.5. Diamine ligands used for the reactivity study

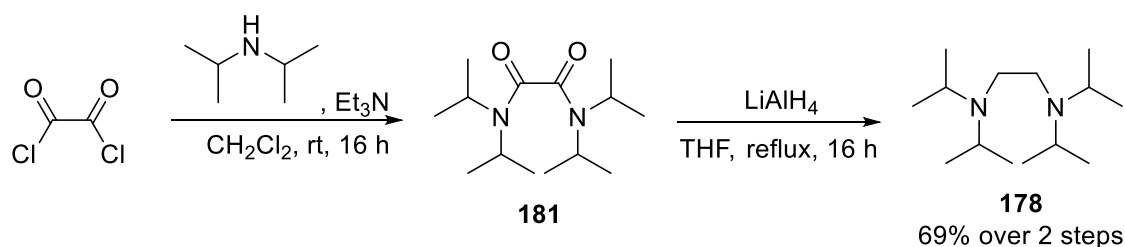
TMEDA *trans*-**161** was synthesised by Eschweiler-Clarke methylation of *trans*-cyclohexane diamine **180** by refluxing in excess formaldehyde and formic acid following a literature procedure (Scheme 2.9).¹⁰⁵ The diamine was purified by formation and subsequent recrystallisation of the bis-HCl salt. Treatment with NaOH liberated the free diamine TMEDA *trans*-**161** in 42% overall yield.

Scheme 2.9. Synthesis of the ligand TMEDA *trans*-161



The tetra-isopropyl TMEDA analogue **178** was synthesised by LiAlH₄ reduction of bis-amide **181** which was formed using oxalyl chloride and di-isopropylamine as described in the literature (Scheme 2.10).¹⁰⁶ This furnished tetra-isopropyl diamine **178** in 69% yield over both steps.

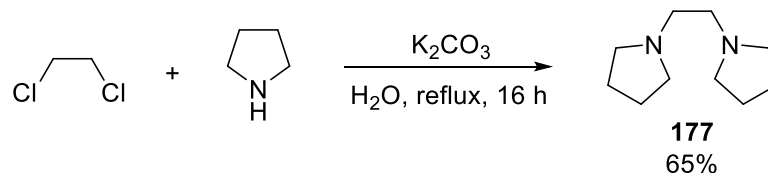
Scheme 2.10. Synthesis of *tert*-isopropyl diamine 178



TMEDA analogue di-pyrrolidino-ethane **117** (DPE) was synthesised by a double nucleophilic displacement reaction between 1,2-dichloroethane and pyrrolidine in the

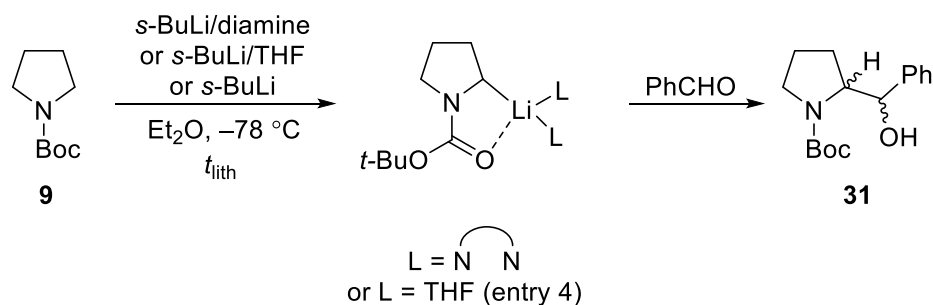
presence of K_2CO_3 (Scheme 2.11).¹⁰⁵ Subsequent fractional distillation gave the desired diamine DPE **177** in 65% yield.

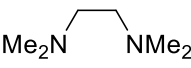
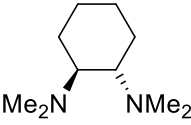
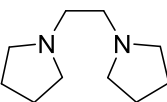
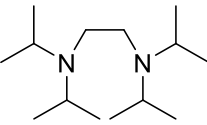
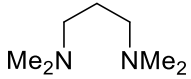
Scheme 2.11. Synthesis of TMEDA analogue DPE 177



The *s*-BuLi/diamine lithiation of *N*-Boc pyrrolidine **9** at -78 °C was selected to investigate the reactivity of the different *s*-BuLi/diamine lithiating complexes. A control lithiation reaction of *N*-Boc pyrrolidine **9** was also conducted with identical conditions but no diamine to ensure that the diamines employed were participating in the lithiation reaction. The Et_2O solvent used for the lithiation reactions is a coordinating solvent and is known to offer a mild enhancement in the reactivity of *s*-BuLi.¹⁰⁷ Therefore, slow *s*-BuLi/ Et_2O lithiation of pyrrolidine **9** is still likely to occur if the diamine does not coordinate to the *s*-BuLi. A range of different *s*-BuLi/diamine lithiating complex reactivities were observed for the lithiation of *N*-Boc pyrrolidine **9**; lithiation times ranged from minutes to several hours (Table 2.2). The lithiation time for the ‘diamine-free’ *s*-BuLi/THF lithiation of *N*-Boc pyrrolidine **9** is also included in Table 2.2 and provides insight into how a monodentate ligand affects the rate of lithiation.¹⁰⁸ For all the lithiation reactions in Table 2.2 except that with *s*-BuLi/THF, an electrophile (PhCHO) was added to trap the lithiated intermediate and the crude product was analysed by 1H NMR spectroscopy to ensure complete lithiation had occurred.

Table 2.2. ReactIR™ obtained lithiation times (t_{lith}) for *s*-BuLi/ligand lithiation of *N*-Boc pyrrolidine **9**



Entry	Diamine	t_{lith}
1	 TMEDA	4 min
2	 TMCDA <i>trans</i> - 161	4 min
3	(-)-sparteine	45 min
4	 177	46 min
5	THF	5 h ^a
6	 178	9 h
7	 179	12 h
8	No diamine	12 h

^a PhCHO trapping was not carried out for the *s*-BuLi/THF lithiation of *N*-Boc pyrrolidine **9**

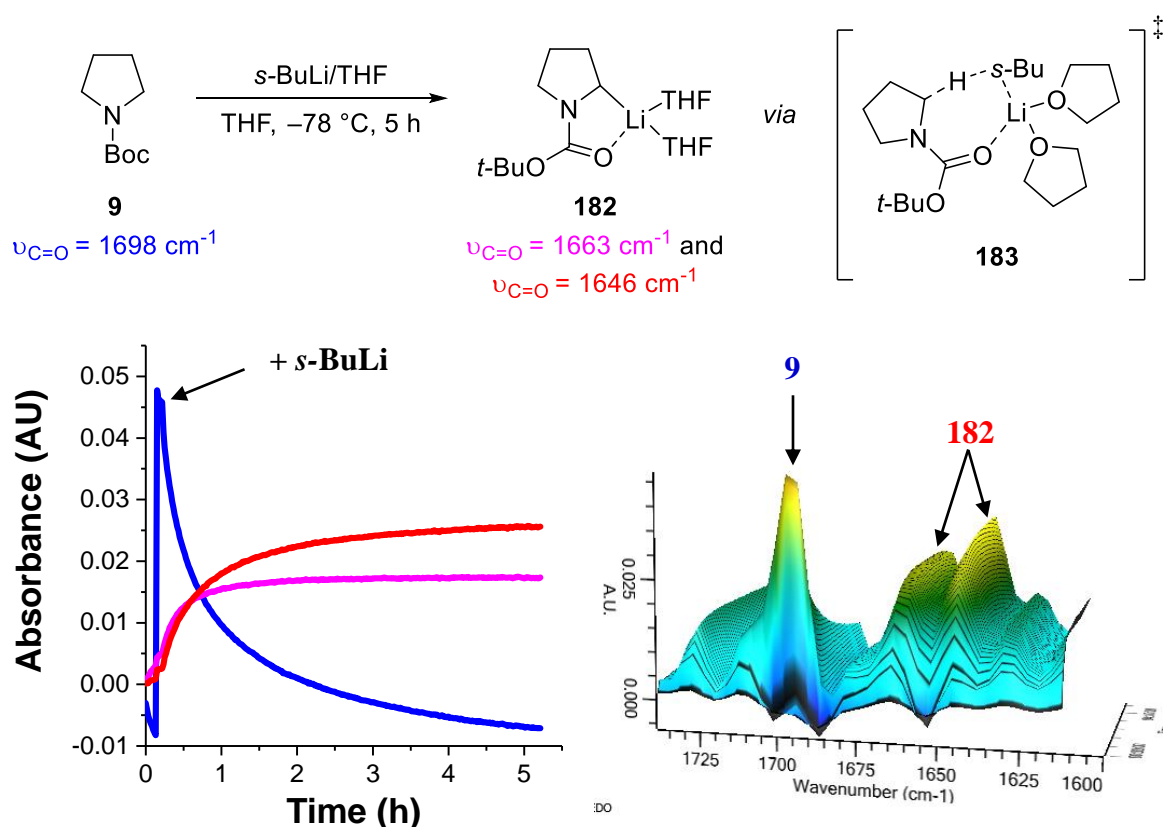
The lithiating complexes with the tetra-methyl substituted diamines *s*-BuLi/TMEDA and *s*-BuLi/TMCDA *trans*-**161** provided identical reactivities for the lithiation of *N*-Boc pyrrolidine **9** (Table 2.2, entries 1 and 2). This indicated that the additional rigidity offered by the cyclohexane ring has no effect on the reactivity of the *s*-BuLi/TMCDA *anti*-**161** lithiating complex. The steric environments of the amine groups in TMEDA and TMCDA *anti*-**161** are very similar which may explain why the reactivities of these two diamines are so similar. This result mirrors previous work carried out by the O'Brien group, where a reactivity series for the *s*-BuLi/diamine-mediated lithiation of *N*-Boc pyrrolidine **9** was

constructed using competition experiments.¹⁰⁹ The study found that *s*-BuLi/TMEDA or *s*-BuLi/TMCDA *anti*-**161** were the most reactive lithiating reagents, and were significantly more reactive than *s*-BuLi/(–)-sparteine.

The *s*-BuLi/DPE **177** lithiating complex provided a moderate reactivity with *N*-Boc pyrrolidine **9**, with lithiation requiring 46 min to complete (Table 2.2, entry 4). This result was initially a surprise, as it was expected that the 5-membered pyrrolidine rings on the ligand would constrain the steric bulk around the two amine groups resulting in a facile lithiation with a similar reactivity to that of *s*-BuLi/TMEDA. However, the slower rate of lithiation of *N*-Boc pyrrolidine **9** with *s*-BuLi/DPE **177** suggests that the pyrrolidinyl rings have an increased steric bulk which retards the lithiation. The *s*-BuLi/DPE **177** lithiating complex appears to have a similar reactivity to that of *s*-BuLi/(–)-sparteine which required 45 min for complete lithiation of *N*-Boc pyrrolidine **9** (Table 2.2, entry 3).

The *s*-BuLi/THF lithiation of *N*-Boc pyrrolidine **9** offered an even slower rate of lithiation, with the ReactIRTM monitoring indicating that complete lithiation required 5 h (Scheme 2.12.a and Table 2.2 entry 5). Unlike the *s*-BuLi/diamine lithiation reactions of *N*-Boc pyrrolidine **9**, no prelithiation complex was observed during the lithiation reaction (Scheme 2.X.b). This absence of a prelithiation complex $\nu_{C=O}$ has been observed for the ReactIRTM monitored *s*-BuLi/THF lithiation reactions of other heterocycle substrates.^{50,53,94} Another difference between the *s*-BuLi/diamine and *s*-BuLi/THF lithiations of *N*-Boc pyrrolidine **9** was that two IR signals were detected at 1663 cm⁻¹ and 1646 cm⁻¹ for the lithiated intermediate formed by *s*-BuLi/THF. It is believed that they are both due to the $\nu_{C=O}$ of the carbamate group in lithiated intermediate **182** and that the two signals may indicate that the lithiated intermediate is present in two different aggregation states.

Scheme 2.12. ReactIR™ monitored *s*-BuLi/THF lithiation of *N*-Boc pyrrolidine **9**



The slow rate of lithiation observed for the *s*-BuLi/THF lithiation of *N*-Boc pyrrolidine **9** likely results from the steric bulk of the ligand as proposed with the diamine ligands. It is conceivable that the monodentate THF ligand means that two molecules of THF ligate the alkyllithium. These two molecules of THF will have a sizeable steric bulk and an additional entropic factor of having two molecules of ligand rather than one may lead to a hindered high energy transition state **183** for the lithiation. However, this rationalisation of reactivity is uncertain as the aggregation states of the alkyllithium and intermediates is currently unknown for lithiation reactions with *s*-BuLi/THF.

Lithiation of *N*-Boc pyrrolidine **9** with *s*-BuLi/tetra-isopropyl TMEDA analogue **178** was a significantly slower reaction, with the ReactIR™ monitoring indicating that complete lithiation was only achieved after 9 h at $-78\text{ }^{\circ}\text{C}$ (Table 2.2, entry 6). The slow rate of lithiation observed is likely due to the large amount of steric bulk around the coordinating nitrogen atoms of the ligand. This could retard the lithiation due to the sterically bulky *s*-BuLi/**178** complex formed which performs the lithiation, resulting in a more sterically hindered higher energy transition state. In addition, the increased steric bulk around the two coordinating amine groups in diamine **178** afforded by the four *i*-Pr groups, could result in poor coordination between the diamine and *s*-BuLi. A lesser degree of coordination between

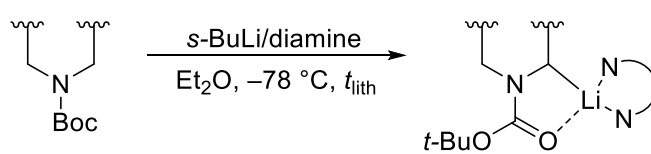
alkyllithium and diamine will likely mean that the less reactive *s*-BuLi/Et₂O species (entry 8, Table 2.2) is also present in significant quantities which may reduce the overall rate of lithiation.

The slowest lithiations of *N*-Boc pyrrolidine **9** were observed when *s*-BuLi/TMPDA **179** or *s*-BuLi/Et₂O lithiating conditions were employed, with both lithiating complexes requiring 12 h for complete lithiation of *N*-Boc pyrrolidine **9** (Table 2.2, entries 7 and 8). As both lithiating complexes required the same lithiation time for *N*-Boc pyrrolidine **9**, this suggested that either *s*-BuLi/TMPDA and *s*-BuLi/Et₂O have the same reactivities or more likely that the TMPDA ligand **179** does not coordinate to *s*-BuLi and so it is the *s*-BuLi/Et₂O reagent that conducts the lithiation. If the slow lithiation reaction is indeed caused by a lack of coordination of TMPDA **179** and *s*-BuLi, it is possible that the additional methylene group in the linker between the two amines may be responsible. The longer linker means that the coordinating amine groups are further apart, which may disrupt the coordination of TMPDA **179** to the *s*-BuLi.

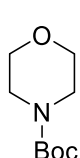
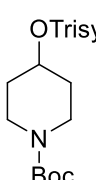
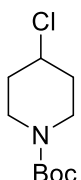
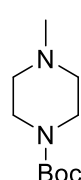
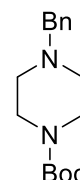
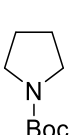
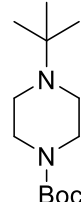
2.2.2 Investigating the *N*-Boc heterocycle reactivity series obtained with *s*-BuLi/DPE **177** and comparison with *s*-BuLi/(–)-sparteine and *s*-BuLi/TMEDA reactivity series

As the *s*-BuLi/DPE **177** lithiating complex offered a moderate reactivity with *N*-Boc pyrrolidine **9** similar to that of *s*-BuLi/(–)-sparteine, the construction of a reactivity series of the more reactive substrates with *s*-BuLi/DPE **177** lithiating conditions was attempted. Five of the most reactive substrates that were investigated using both *s*-BuLi/TMEDA and *s*-BuLi/(–)-sparteine lithiating conditions were lithiated using *s*-BuLi/DPE **177**. The lithiation times for these five substrates with *s*-BuLi/DPE **177** and the seven substrates studied using *s*-BuLi/(–)-sparteine are presented in Table 2.3, along with the corresponding *s*-BuLi/TMEDA lithiation times. The order of the substrates in the reactivity series obtained with both *s*-BuLi/DPE **177** and *s*-BuLi/TMEDA lithiating conditions were identical. However, there were significant differences in the reactivity order of the substrates obtained with *s*-BuLi/(–)-sparteine, which suggested that *N*'-Me and *N*'-Bn piperazines **58** and **57** were less reactive than *N*-Boc pyrrolidine **9**. This contradicted the reactivity series obtained with both *s*-BuLi/TMEDA and *s*-BuLi/DPE **177** lithiating conditions.

Table 2.3. *s*-BuLi/diamine reactivity series for rapidly lithiating *N*-Boc heterocycles



$s\text{-BuLi/diamine}$
 $\text{Et}_2\text{O}, -78\text{ }^\circ\text{C}, t_{\text{lith}}$

	 169	 167	 48	 58	 57	 9	 66
DPE 177 $t_{\text{lith}} / \text{min}$	0.25 ^a	1 ^a	5 ^a	30	--	46	--
(-)-sparteine $t_{\text{lith}} / \text{min}$	1 ^a	10 ^a	30 ^a	90	60	45	>300
TMEDA $t_{\text{lith}} / \text{min}$	1 ^a	2 ^a	2 ^a	4	4	4	22

^a 2.6 eq. of *s*-BuLi and diamine were used (see Scheme 2.8).

All three of the *s*-BuLi/diamine combinations indicated that *N*-Boc morpholine **169** was the most reactive substrate. Both *s*-BuLi/TMEDA and *s*-BuLi/(-)-sparteine required only 1 min for complete lithiation of morpholine **169** to occur and with *s*-BuLi/DPE **177** the newer ReactIRTM apparatus (which takes reading every 15 s) provided a lithiation time of 15 s for **169**. This provides further evidence that the presence of the oxygen atom in the six-membered ring has a significant activating effect on the α -deprotonation.

4-*O*-trisyl and 4-chloro piperidines **167** and **48** were placed in the same positions in the substrate reactivity series by each of the three *s*-BuLi/diamine combinations. The slower lithiation rates offered with *s*-BuLi/DPE **177** and *s*-BuLi/(-)-sparteine allowed the elucidation of a reactivity difference between the two substituted piperidines, which indicated that 4-*O*-trisyl piperidine **167** was more reactive than 4-chloro piperidine **48**. However, the lithiation times obtained with *s*-BuLi/(-)-sparteine and *s*-BuLi/DPE **177** for each of the substituted piperidines **167** and **48** differed significantly. This was a surprise as both the *s*-BuLi/(-)-sparteine and *s*-BuLi/DPE **177** lithiating complexes showed similar reactivity for the lithiation of *N*-Boc pyrrolidine **9**. This was particularly evident for 4-chloro *N*-Boc piperidine

48 which required only 5 min for complete lithiation with *s*-BuLi/DPE **177** but presented a significantly slower 30 min lithiation with *s*-BuLi/(-)-sparteine.

We postulate that slow rotamer interconversion may be the reason for the slow rate of lithiation observed with enantiopure ligands such as (-)-sparteine; rotamers do not pose a problem when an achiral ligand such as DPE **177** is utilised. When *s*-BuLi and a chiral diamine such as (-)-sparteine are used to lithiate a 4-substituted *N*-Boc piperidine, only one rotamer has an energetically favoured, matched situation for the asymmetric deprotonation. For rotamer **184**, the kinetically favoured *pro-S* deprotonation will dominate (Figure 2.6). However, for rotamer **185**, *pro-S* deprotonation is disfavoured as the proton H_{S2} is in an axial position on the piperidine ring. In this case, the Complex Induced Proximity Effect (CIPE) cannot occur since the α -proton is not in the same plane as the coordinating Boc carbonyl group.

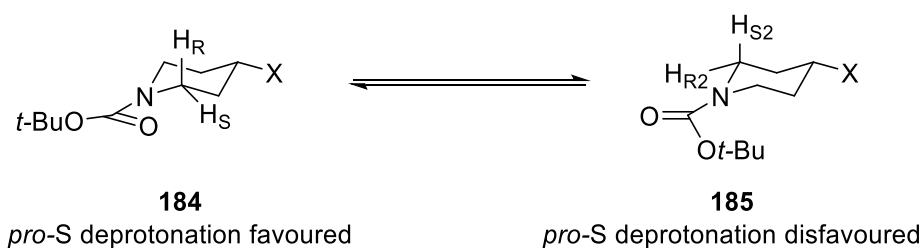
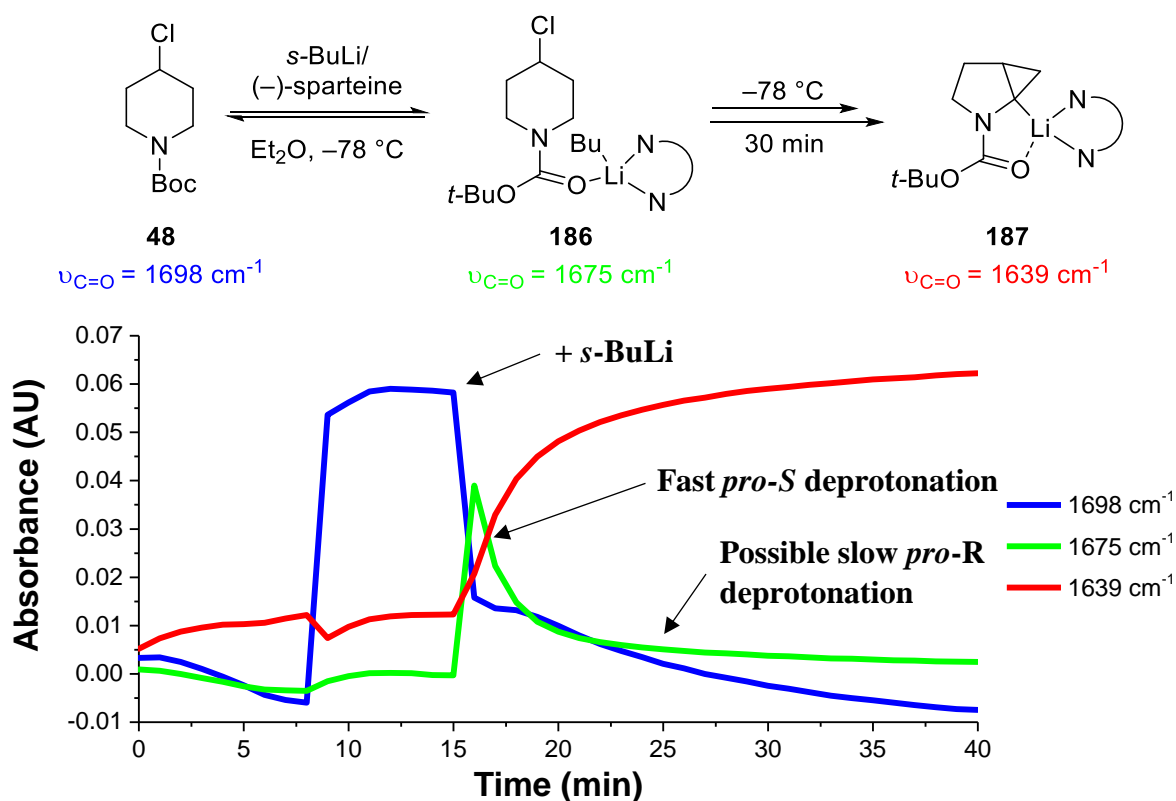


Figure 2.6. Interconversion of rotamers for a 4-substituted *N*-Boc piperidine

It is also unfavourable for the piperidine in rotamer **185** to ring-flip so that the kinetically favoured α -proton H_{S2} is in an equatorial position, as the substituent (X) at the 4-position would be placed in an energetically disfavoured axial position. If rotamer interconversion can occur at $-78\text{ }^{\circ}\text{C}$, rotamer **185** will interconvert to rotamer **184**, where *pro-S* deprotonation is the primary reaction path, providing the lithiated intermediate in an enriched *er*. Conversely, very slow or non-occurring rotamer interconversion leads to either $<50\%$ conversion as only one rotamer (**184**) would be lithiated or a $>50\%$ conversion, where both the *pro-S* and disfavoured higher energy *pro-R* (H_{R2}) deprotonation occur giving the product in an eroded *er*. In the case of $>50\%$ conversion the rate of lithiation may be slowed due to the higher energy *pro-R* (H_{R2}) deprotonation occurring and/or dependency on the rate of rotamer interconversion. This means that constructing a reactivity series using an enantioselective ligand such as (-)-sparteine will provide unreliable reactivity data as there is also a dependency on the rate of rotamer interconversion for each substrate.

When the lithiation of 4-chloro piperidine **48** with *s*-BuLi/(-)-sparteine at $-78\text{ }^{\circ}\text{C}$ was carried out previously the enantioselectivity of the reaction was found to be poor, with an almost racemic product formed in 94% yield.^{43,44} This provided strong evidence that the rotamer conversion may indeed be slow and that the disfavoured deprotonation of $\text{H}_{\text{R}2}$ does occur. Inspection of the ReactIRTM trace for the *s*-BuLi/(-)-sparteine lithiation of 4-chloro *N*-Boc piperidine **48** suggests that the reaction may have two different regions where the rates of reaction differ (Scheme 2.13). The initial fast lithiation and subsequent slow lithiation can be observed most clearly by monitoring the consumption of the prelithiation complex **186**. However, visual inspection of the ReactIRTM does not provide conclusive evidence. If the two regions of differing lithiation rates are present for the *s*-BuLi/(-)-sparteine lithiation of 4-chloro piperidine **48**, this would suggest a slow rate of rotamer interconversion for **48** at $-78\text{ }^{\circ}\text{C}$. If rotamer interconversion is slow, one rotamer would undergo a fast *pro*-*S* deprotonation as is evident at the start of the reaction and concurrently the other rotamer would undergo a slower, energetically unfavourable, *pro*-*R* deprotonation only evident later in the reaction.

Scheme 2.13. ReactIRTM monitored *s*-BuLi/(-)-sparteine lithiation of 4-chloro *N*-Boc piperidine **48**



The use of *s*-BuLi/(–)-sparteine also provided some unexpected results for the rate of lithiations of *N*'-Me and *N*'-Bn piperazines, **58** and **57**. Lithiation with *s*-BuLi/TMEDA suggests that both piperazines have similar reactivity to *N*-Boc pyrrolidine **9** with each of the three substrates requiring 4 min for complete lithiation. When the lithiation of *N*'-Me piperazine **58** was carried out with *s*-BuLi/DPE **177**, a 30 min lithiation time was observed which indicated that piperazine **58** is more reactive than *N*-Boc pyrrolidine **9**, which required 46 min for complete lithiation with *s*-BuLi/DPE **177**. In contrast, the 60 and 90 min *s*-BuLi/(–)-sparteine lithiation times of *N*'-Bn and *N*'-Me piperazines **57** and **58** suggested that both substrates had similar or lower reactivity than *N*-Boc pyrrolidine **9**.

At present, we have no conclusive evidence for why the rates of lithiation of both *N*'-Bn and *N*'-Me piperazines **57** and **58** are significantly slower with *s*-BuLi/(–)-sparteine. However, the issue of slow rotamer interconversion, discussed previously to explain the anomalous reactivities of the 4-substituted piperidines **48** and **167** with *s*-BuLi/(–)-sparteine, may provide a rationale for the slower rates of lithiation observed for piperazines **57** and **58**. This explanation differs slightly for the piperazines, as the distal nitrogen can invert and then a subsequent ring-flip would always allow the pro-*S* proton to be placed in an equatorial position allowing pro-*S* deprotonation in each rotamer (Figure 2.7). However, if the nitrogen inversion or ring-flip occurs slowly at –78 °C, this would mean that only one rotamer can undergo the energetically favoured pro-*S* deprotonation. Therefore, if >50% conversion occurs, the rate of lithiation will be retarded as higher energy pro-*R* deprotonation may occur and/or the rate of lithiation becomes dependent on rotamer interconversion or the *N*-inversion and ring flip. Low temperature (–60 °C) ¹H NMR spectroscopic studies have indicated that both conformers of *N*-*N*'-dimethyl piperazine were visible on the NMR timescale and that *N*-*N*'-dimethyl piperazine has a significantly higher ring flip-inversion energy barrier than both morpholine and *N*-methyl piperidine.^{110,111} Therefore, it is possible that for *N*-Boc piperazines such as **57** and **58**, the rate of *N*-inversion/ring-flipping may be slow at –78 °C.

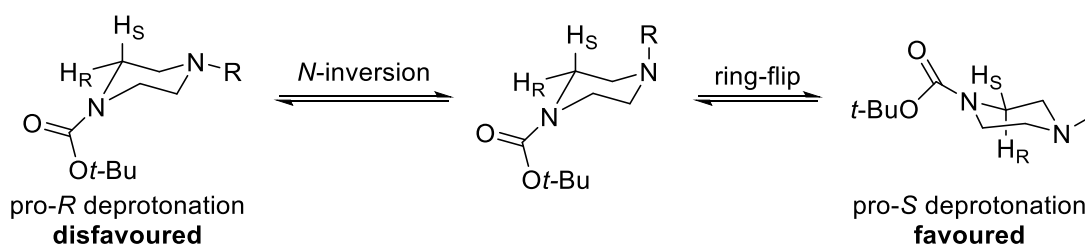


Figure 2.7. N-Inversion and ring flipping of N-Boc piperazines

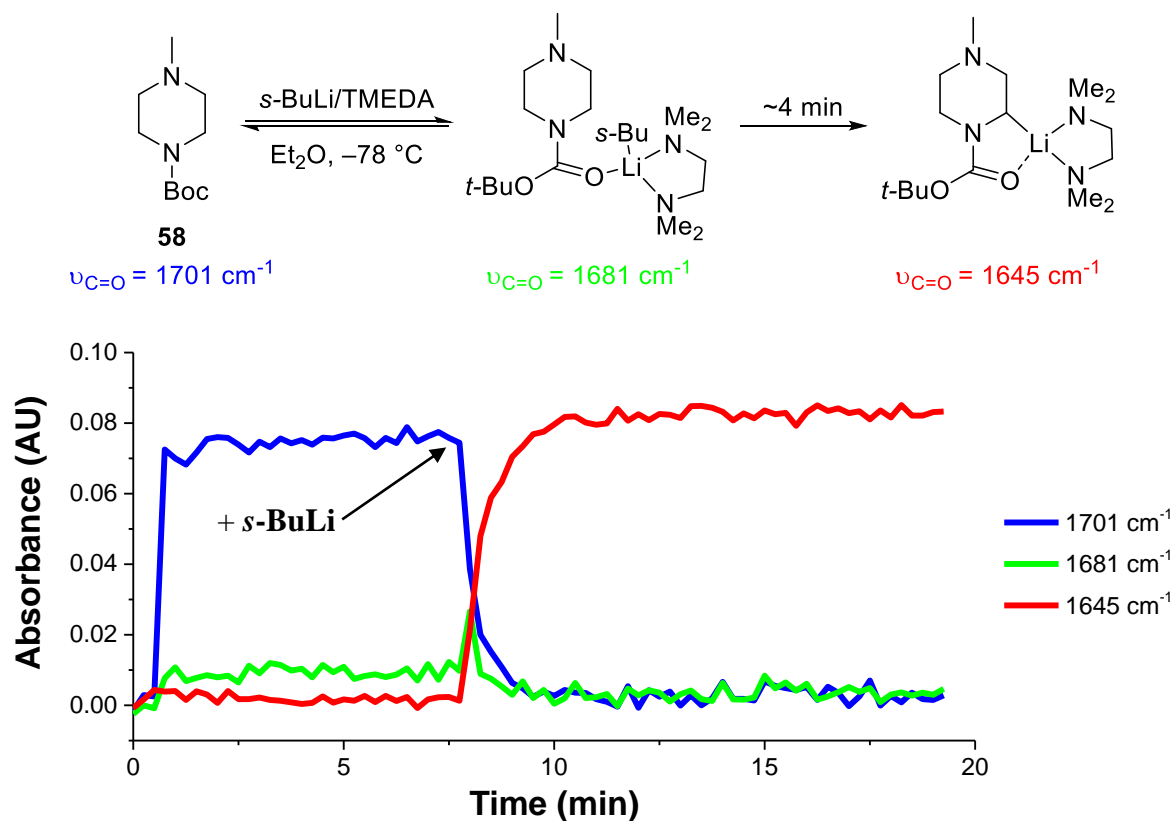
The *s*-BuLi/(–)-sparteine lithiation of *N*'-*t*-Bu piperazine **66** was the slowest of the seven substrates, with lithiation still ongoing after a 300 min reaction time. This matched the *s*-BuLi/TMEDA reactivity series, where *N*'-*t*-Bu piperazine **66** is also the least reactive of the seven substrates. However, it is difficult to ascertain whether there is any additional retardation of the *s*-BuLi/(–)-sparteine lithiation reaction of *N*'-*t*-Bu piperazine **66**, as observed with piperazines **57** and **58**, because the reaction was not allowed to go to completion.

In summary, a wide spectrum of reactivity was observed when the lithiation of *N*-Boc pyrrolidine **9** was carried out with several different *s*-BuLi/ligand lithiating complexes. This shows that the identity of the ligand can have a considerable influence on the rate of the lithiation reaction. The reactivity series constructed with the less reactive *s*-BuLi/DPE **177** lithiating complex provided a strong agreement with the reactivity series constructed with *s*-BuLi/TMEDA and allowed the subtler reactivity differences of the fast lithiating substrates to be elucidated. The reactivity series constructed using *s*-BuLi/DPE **177** will be valuable when the experimental and computationally predicted reactivities of the reactive substrates are compared in Chapter 3 of this thesis. Comparison of the *s*-BuLi/DPE **177** and *s*-BuLi/(–)-sparteine reactivity trends has indicated that *s*-BuLi/(–)-sparteine provides conflicting information about the reactivities of 4-substituted piperidines and piperazines. These anomalous results obtained with *s*-BuLi/(–)-sparteine may arise due to the retardation of the lithiation caused by slow rotamer interconversion. Therefore, lithiation times obtained using *s*-BuLi and a chiral ligand may not provide a reliable measure of the reactivity of substrates due to the possible rotamer interconversion complication.

2.3 Quantitative Kinetic Analysis of the *s*-BuLi/TMEDA Reactivity Series

Whilst conducting the substrate reactivity investigations described so far, it became apparent that determining the lithiation of time of a *N*-Boc heterocycle by visual inspection of the ReactIR™ trace can be unreliable and is not a robust method to quantify reactivity. The unreliability in the lithiation times arises as the visual inspection of ReactIR™ traces requires the user to select an end-point for the reaction. The user determines when both $\nu_{\text{C=O}}$ signals for starting material and lithiated intermediate plateau and no further change is observed which can be difficult to pinpoint with precision. This determination can be made even more difficult if the ReactIR™ data is particularly noisy, especially towards the end of a reaction where the signal/noise ratio will be small. This selection of the end-point of a lithiation reaction is a significant source of error in the determined lithiation times for both slow (> 2 h) or fast reactions (< 5 min). As an example, for a fast lithiation reaction (i.e. *N'*-Me piperazine **58** where $t_{\text{lith}} = 4$ min), an imprecise end-point provides a significant margin of error (Scheme 2.14).

Scheme 2.14. ReactIR™ monitored *s*-BuLi/TMEDA lithiation of *N'*-Me *N*-Boc piperazine **58** showing the difficulty in establishing a reaction end-point

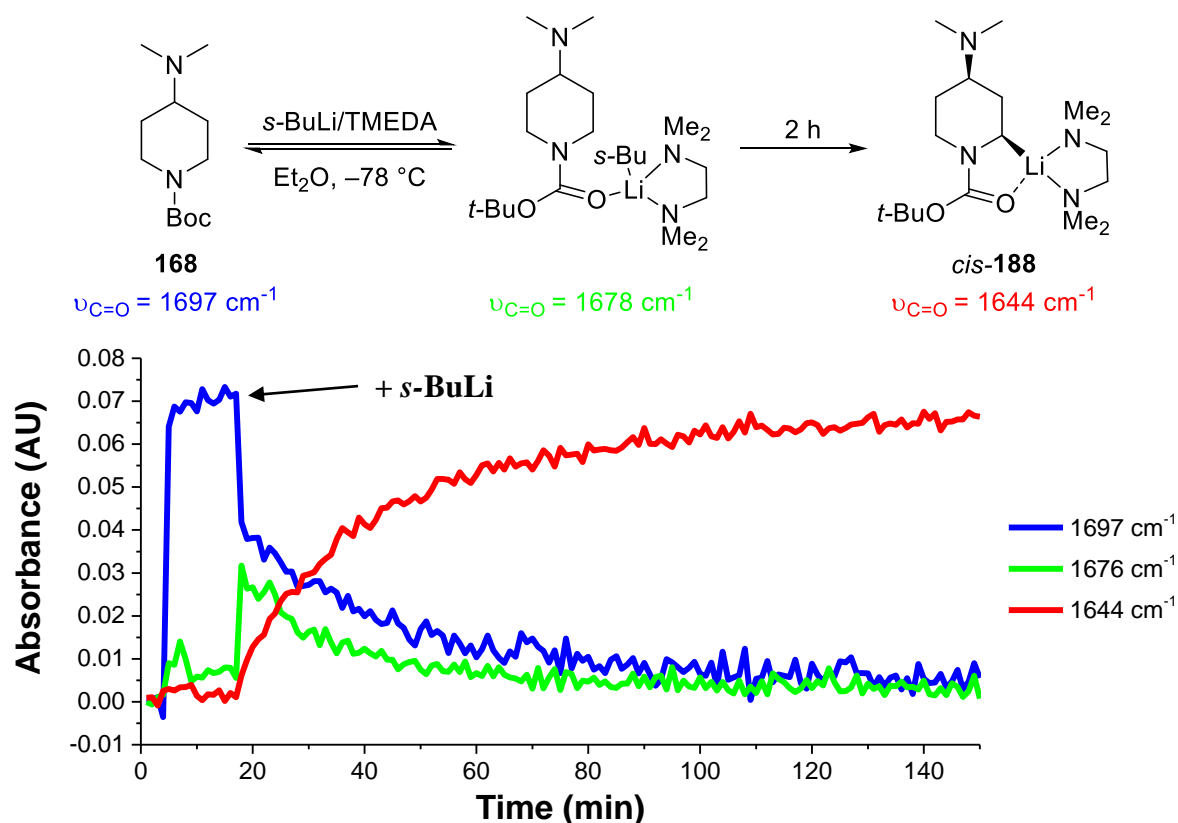


This problem is also compounded by the sampling interval, which at the fastest scanning

speed (on the newer ReactIR™ 15 apparatus) only records one data point per 15 s interval. In this case, an end-point can only be selected after each 15 s interval for the reaction which incurs a significant amount of error for a fast lithiation reaction.

For a slow lithiation reaction, determination of the reaction end-point can be problematic as it can be very difficult to locate the point in time at which both the consumption of starting material and formation of lithiated intermediate plateau. For instance, the lithiation of 4-amino *N*-Boc piperidine **168** requires 2 h to reach completion and close to the end of the reaction, the gradients of the consumption traces for both *N*-Boc piperidine **168** ($\nu_{\text{C=O}} = 1700 \text{ cm}^{-1}$) and lithiated intermediate *cis*-**188** ($\nu_{\text{C=O}} = 1644 \text{ cm}^{-1}$) become very shallow (Scheme 2.15). These shallow gradients make accurately pinpointing the end of the reaction prone to significant amounts of error.

Scheme 2.15. ReactIR™ monitored *s*-BuLi/TMEDA lithiation of 4-amino *N*-Boc piperidine **168 showing the difficulty in establishing a reaction end-point**



Initially, an attempt to mathematically locate at what point time both signals plateau was undertaken to remove the source of human error that arises from the visual inspection. The reaction end-point was located by measuring the distance between the starting material trace and the lithiated intermediate trace. At the point in time where this distance becomes

constant, the two traces will have stopped diverging and the reaction is deemed to be complete (Figure 2.8). A cut-off parameter was included so that once the change in this distance was below a certain value, an end-point would be identified. This parameter was included as the noise in the ReactIR™ readings meant that both traces would never have perfectly parallel lines.

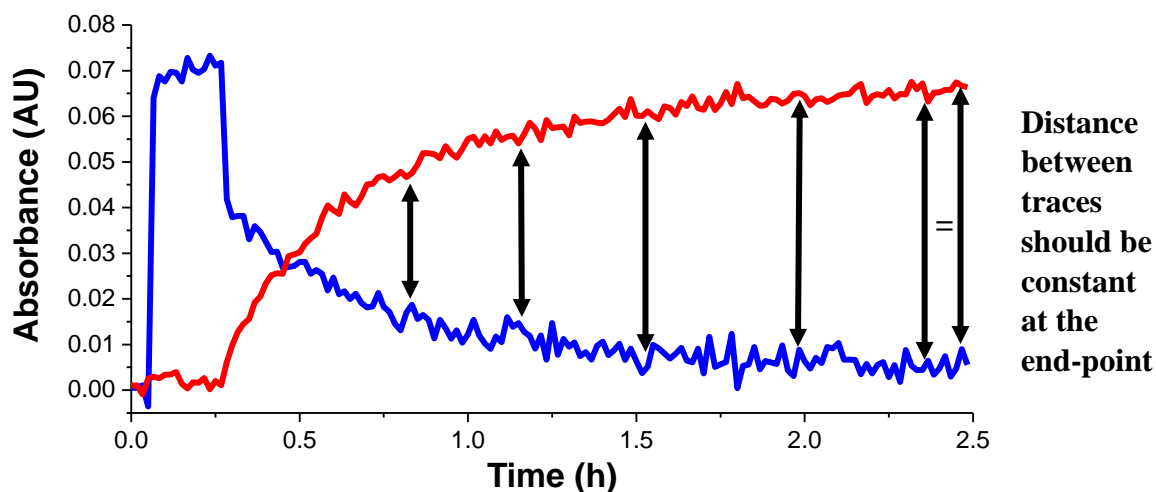
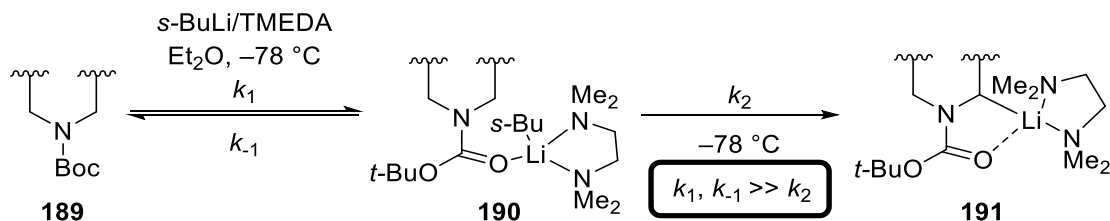


Figure 2.8. An attempt to mathematically find the end-point for the lithiation reaction of 4-amino *N*-Boc piperidine **168**

Unfortunately, this method was not able to find an end-point for lithiation reactions due to the ReactIR™ instrument noise present in the data. The noise resulted in false positives, where both lines ceased to diverge but then continued to diverge after more readings as the reaction progressed. This problem prompted us to find an alternative method to measure reaction rate without needing to accurately determine the end-point of the reaction. Hence, we turned to a kinetic investigation of the reaction which uses much more of the collected absorbance data rather just the start and end-point.

As discussed previously, the lithiation reactions for all the *N*-Boc heterocycles investigated proceeded *via* a multi-step reaction involving three different species: un-complexed substrate **189**, prelithiation complex **190** and the lithiated intermediate **191**. This involves two consecutive reactions where, initially, the un-complexed starting material **189** rapidly converts into the prelithiation complex **190** *via* an equilibrium reaction, with forward and backward rate constants, k_1 and k_{-1} . Then, pre-lithiation complex **190** undergoes the slow rate determining deprotonation, with rate constant k_2 , to form the lithiated intermediate product **191** (Scheme 2.16).

Scheme 2.16. A general reaction scheme for the *s*-BuLi/TMEDA lithiation of *N*-Boc heterocycles showing the different reaction steps occurring



As the deprotonation of the pre-lithiation complex (k_2) is unimolecular, a first order relationship is expected between the reaction rate and concentration of the pre-lithiation complex. Unfortunately, for many of the lithiation reactions studied, the equilibrium between un-complexed starting material **189** and pre-lithiation complex **190** lies toward the un-complexed reagents. This means that the IR signal for the pre-lithiation complex is small and this results in a smaller signal/noise ratio which makes kinetic analysis using the pre-lithiation complex more difficult. Additionally, for many lithiation reactions there is overlap of the $\nu_{\text{C=O}}$ signals of the pre-lithiation complex and lithiated intermediate; this also can provide erroneous and unreliable results when consumption of pre-lithiation complex is analysed. The overlap between pre-lithiation complex and lithiated intermediate $\nu_{\text{C=O}}$ signals can be observed in the 3D ReactIRTM trace for *N*-Boc pyrrolidine **9** in Scheme 2.2.a. The measurement of k_{obs} for the lithiation using consumption of pre-lithiation complex and the unreliability of these results is discussed later in this Chapter. It was therefore decided to attempt to obtain k_{obs} by measuring the consumption of *N*-Boc heterocycle and applying the pre-equilibrium approximation. As there is a rapid equilibrium reaction that forms between pre-lithiation complex **190** and the *N*-Boc heterocycle and *s*-BuLi/TMEDA, the pre-equilibrium approximation can be applied for this reaction giving a rate equation for the reaction (Equation 2.1).

$$-\frac{d[\text{N-Boc heterocycle}]}{dt} = k_2 K [\text{N-Boc heterocycle}] [\text{s-BuLi/TMEDA}] \quad \text{(Equation 2.1)}$$

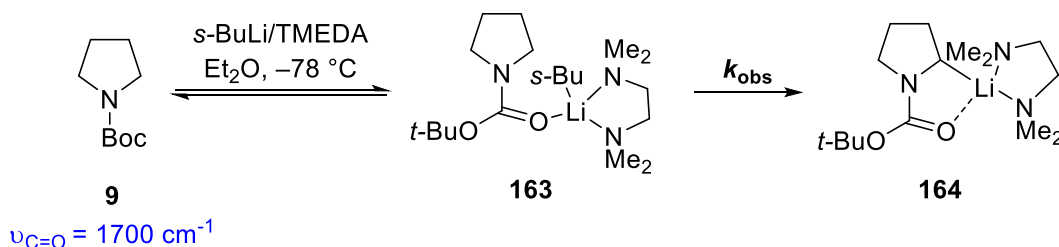
This provides a rate equation where the rate of lithiation is dependent on rate constant k_2 , the equilibrium constant between **189** and **190**, K , and the concentrations of the *N*-Boc heterocycle and *s*-BuLi/TMEDA reagents. The ReactIRTM traces collected for the *s*-BuLi/TMEDA lithiations of all *N*-Boc heterocycle substrates in this study indicated that once the equilibrium is established, both the starting material **189** and pre-lithiation complex **190** are consumed at the same rate throughout the lithiation. These identical rates of consumption

for **189** and **190** are observed since, when the prelithiation complex is consumed, the equilibrium will rapidly convert the un-complexed starting material **189** into prelithiation complex **190** to maintain the equilibrium. In addition, no dependency on $[s\text{-BuLi/TMEDA}]$ is observed at any point in the reaction, as first order kinetics are observed for all of the lithiation reactions investigated in this thesis (except for *N-t*-Bu *N*-Boc piperazine **66** which appears to display kinetics consistent with two consecutive first order reactions – see section 6.4). This suggests that either 1.3 eq. of *s*-BuLi/TMEDA is a sufficient excess to maintain pseudo-first order conditions or that the pre-equilibrium is responsible for the zero-order kinetics observed with respect to *s*-BuLi/TMEDA. Previous kinetic studies by Beak have provided evidence that the *i*-PrLi/(–)-sparteine lithiation of *N*-Boc pyrrolidine **9** has a zero order dependency on the concentration of the alkyllithium/ligand but this study was conducted using larger excesses of alkyllithium (> 10 eq.).³² Therefore, we propose that dependency on $[s\text{-BuLi/TMEDA}]$ can be removed from the pre-equilibrium rate equation for the purpose of obtaining a k_{obs} for the lithiation reaction (Equation 2.2).

$$-\frac{d[\text{N-Boc heterocycle}]}{dt} = k_{\text{obs}}[\text{N-Boc heterocycle}] \quad (\text{Equation 2.2})$$

By using the integrated form of Equation 2.2, a first order kinetic plot can be constructed that allows calculation of k_{obs} for lithiation reaction. Plotting the natural logarithm of the absorbance of the un-complexed starting material **189** vs time should provide a linear graph where the gradient is equal to $-k_{\text{obs}}$. This kinetic analysis was first applied to the lithiation of *N*-Boc pyrrolidine **9** with *s*-BuLi/TMEDA at -78 °C, for which visual inspection had indicated 4 min were required for complete lithiation to occur (Scheme 2.17).

Scheme 2.17. *s*-BuLi/TMEDA lithiation of *N*-Boc pyrrolidine **9**



The ReactIRTM absorbance data for the consumption of *N*-Boc pyrrolidine **9** (Figure 2.9.a) was used to construct a first order plot for the lithiation of *N*-Boc pyrrolidine **9** (Figure 2.9.b). The ReactIRTM reading at $t = 0$ s, where addition of *s*-BuLi occurs was not included in the analysis as the period between 0-15 s included the establishment of the equilibrium between

uncomplexed pyrrolidine **9** and prelithiation complex **163**. The pre-equilibrium approximation cannot be applied before the equilibrium is established and if these data were included, it would provide an erroneous result. The final 5% conversion for the reaction is discounted as at these low concentrations of *N*-Boc pyrrolidine **9**, the ReactIR™ signal/noise ratio becomes very small, resulting in erroneous data. All of the points excluded from the analysis are highlighted in red in Figure 2.9.a.

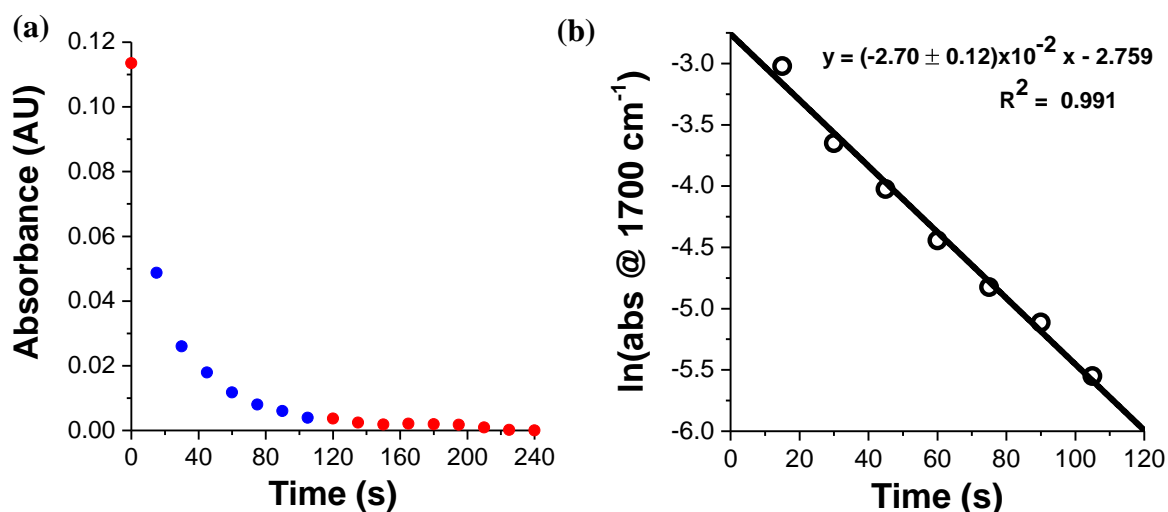


Figure 2.9. (a) ReactIR™ data for the consumption of *N*-Boc pyrrolidine **9 and (b) the resulting first-order kinetic plot for the lithiation of *N*-Boc pyrrolidine **9**. Absorbance is relative to the selected end-point ($t = 240$ s) of the reaction where absorbance has been normalised to zero)**

The first order kinetic plot provided a clear linear correlation ($R^2 = 0.991$), suggesting that the deprotonation of prelithiation complex **163** occurs *via* a first order reaction and that the pre-equilibrium approximation can be applied for the lithiation of *N*-Boc pyrrolidine **9**. An observed first order rate constant, $k_{\text{obs}} = (2.70 \pm 0.12) \times 10^{-2} \text{ s}^{-1}$ was obtained for the *s*-BuLi/TMEDA lithiation of *N*-Boc pyrrolidine **9**. A detailed procedure for the kinetic analysis and the calculation of errors for the lithiation reactions presented is detailed in section 6.2 of this thesis.

A problem that is still encountered when conducting the first order kinetic analysis arises from the fact that an end-point for the reaction is still required. This end-point is required to correct for a non-zero baseline on the ReactIR™ equipment due to the baseline shift that occurs during the lithiation. This gives a similar problem to that posed by the visual inspection method where determination of the end-point is difficult due to the low signal/noise ratio at the end of a reaction on the ReactIR™.

For the kinetic analysis of the *s*-BuLi/TMEDA lithiation of *N*-Boc pyrrolidine **9** the end-point was selected as 240 s by visual inspection of the raw data, which provided $k_{\text{obs}} = (2.70 \pm 0.12) \times 10^{-2} \text{ s}^{-1}$ for the lithiation reaction. However, by visual inspection, an end-point of 165 s could also be valid for the reaction if the decreasing absorbance of the last points are due to instrument noise. If the same kinetic analysis is conducted where the reaction is deemed to end at 165 s the value of k_{obs} is changed significantly (a 20% difference), with $k_{\text{obs}} = (3.23 \pm 0.12) \times 10^{-2} \text{ s}^{-1}$ (Figure 2.10). This indicates that inaccurate end-point determination still has a significant effect on the kinetic results for the lithiation of each of the substrates.

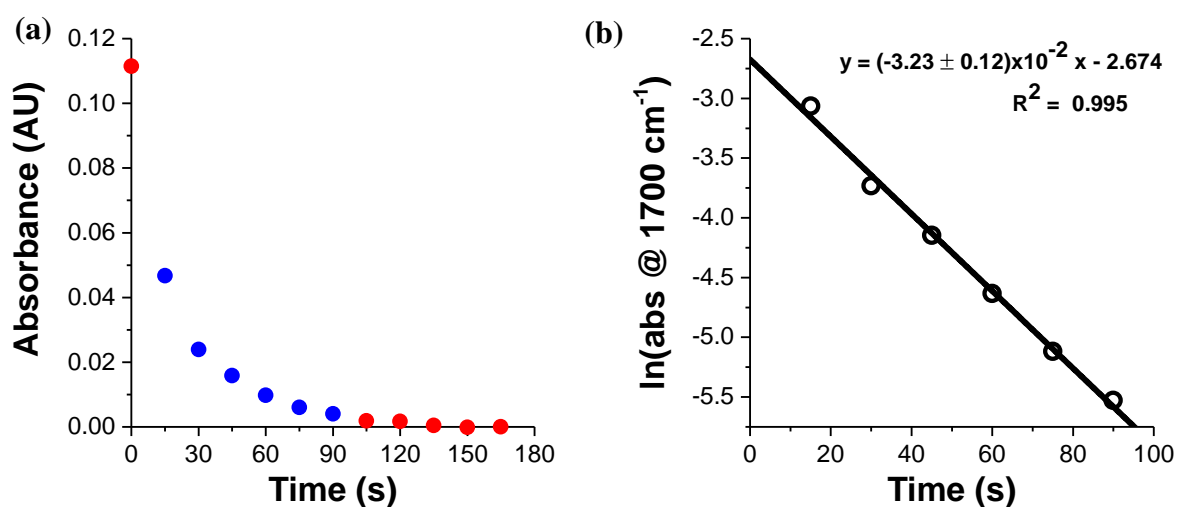


Figure 2.10. (a) ReactIR™ data for the consumption of *N*-Boc pyrrolidine **9 using a different end-point and (b) the resulting first-order kinetic plot for the lithiation of *N*-Boc pyrrolidine **9**. Absorbance relative to selected reaction endpoint ($t = 165 \text{ s}$)**

To eliminate this source of error, it was decided to improve upon this kinetic analysis by use of non-linear regression to fit the consumption curve for the *N*-Boc heterocycle substrate. By fitting a curve to the raw data, this eliminates the need to determine an end-point and so removes this source of error. This curve fitting method also has other advantages including the fact that the lithiation does not have to be complete for extraction of a rate constant so very slow reactions and/or data for incomplete reaction can still be used. Additionally, noisy ReactIR™ data poses less of a problem as the curve can be fit through all the points to average out the noise.

As the lithiation reactions of the *N*-Boc heterocycles appear to be first order with respect to the substrate, an exponential decay curve can be fitted once the equilibrium has been established after $t = 0$ (Equation 2.3). Using a curve fitting algorithm enables the k_{obs} for the

lithiation to be determined along with the curve constants A and c which are not required for this analysis.

$$\text{absorbance of substrate} = Ae^{-k_{\text{obs}}t} + c \quad \text{(Equation 2.3)}$$

For the lithiation of *N*-Boc pyrrolidine **9**, the curve fitting of the consumption of **9** provided a rate constant $k_{\text{obs}} = (3.34 \pm 0.15) \times 10^{-2} \text{ s}^{-1}$ (Figure 2.11). The k_{obs} obtained by the curve fitting matched more closely the k_{obs} from the linear plots when the end-point of the lithiation was deemed to be 165s. This suggests that the changes in the absorbance observed after 165s for the lithiation of *N*-Boc pyrrolidine **9** likely arise from the instrument rather than the reaction.

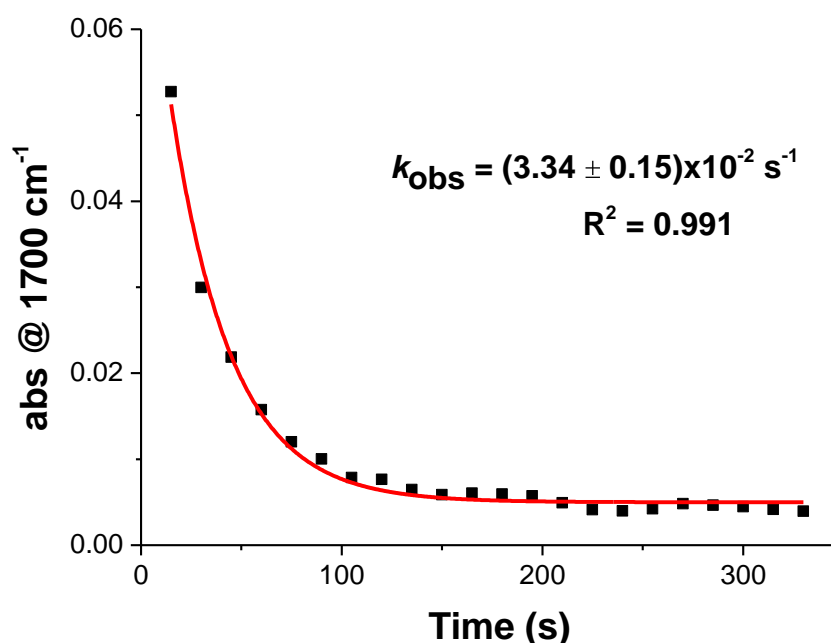


Figure 2.11. Non-linear curve fitting for the *s*-BuLi/TMEDA lithiation of *N*-Boc pyrrolidine **9 to obtain k_{obs}**

As the *s*-BuLi/TMEDA lithiation of *N*-Boc pyrrolidine **9** appears to display first order kinetics, the reaction half-life ($t_{1/2}$) can be calculated using k_{obs} and Equation 2.4. The $t_{1/2}$ for lithiation provides a more easily comprehensible measure of the rate of reaction than k_{obs} and this makes comparison between the reactivities of the different *N*-Boc heterocycles easier. For the lithiation of *N*-Boc pyrrolidine **9** with *s*-BuLi/TMEDA, $t_{1/2} = (20.7 \pm 0.9) \text{ s}$.

$$t_{1/2} = \frac{\ln 2}{k_{\text{obs}}} \quad \text{(Equation 2.4)}$$

A lithiation time can also be predicted for *N*-Boc pyrrolidine **9** using the $t_{1/2}$ value as it requires 7 half-lives for 99% conversion to occur. The $t_{1/2}$ for the *s*-BuLi/TMEDA lithiation

of *N*-Boc pyrrolidine **9** suggests that 99% conversion to lithiated intermediate **164** requires 3 min which differs to the 4 min lithiation time measured by visual inspection. For this fast lithiation reaction, the difference between 3 and 4 min is a considerable margin of error. In this case, visual inspection of the ReactIR™ trace overpredicts the lithiation time required for *N*-Boc pyrrolidine **9**. As discussed previously, when using visual inspection it is easy to overpredict lithiation time as it is hard to accurately locate where both the starting material and lithiation ReactIR™ traces have ceased diverging.

The *s*-BuLi/TMEDA lithiation of 4-amino *N*-Boc piperidine **168** at $-78\text{ }^{\circ}\text{C}$ was subjected to the same kinetic analysis (Scheme 2.18). The non-linear regression provided a first-order decay curve with a very good fit to the ReactIR™ data indicating that the lithiation of piperidine **168** obeys first order kinetics with respect to the *N*-Boc heterocycle where $k_{\text{obs}} = (6.64 \pm 0.16) \times 10^{-4} \text{ s}^{-1}$ and $t_{1/2} = (1040 \pm 20) \text{ s}$ (Figure 2.12).

Scheme 2.18. *s*-BuLi/TMEDA lithiation of 4-amino *N*-Boc piperidine **168**

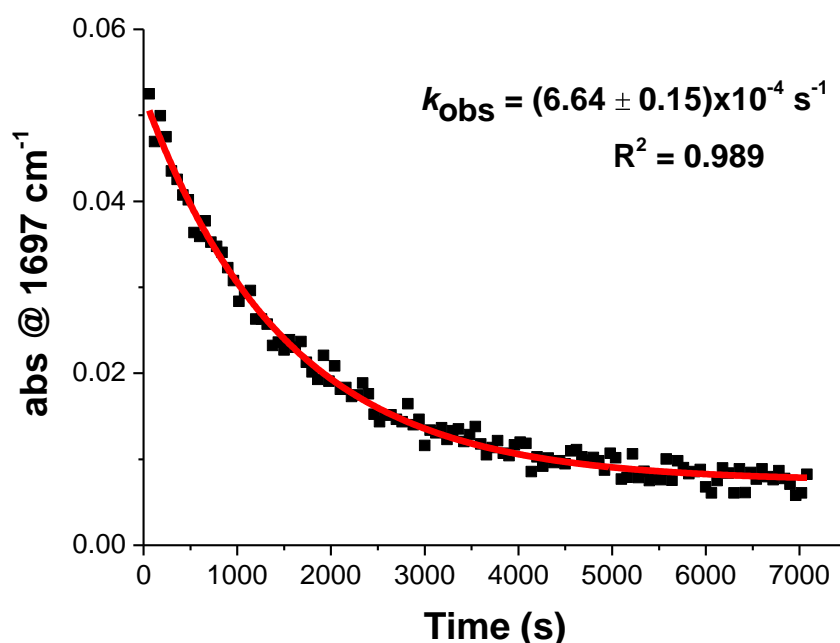
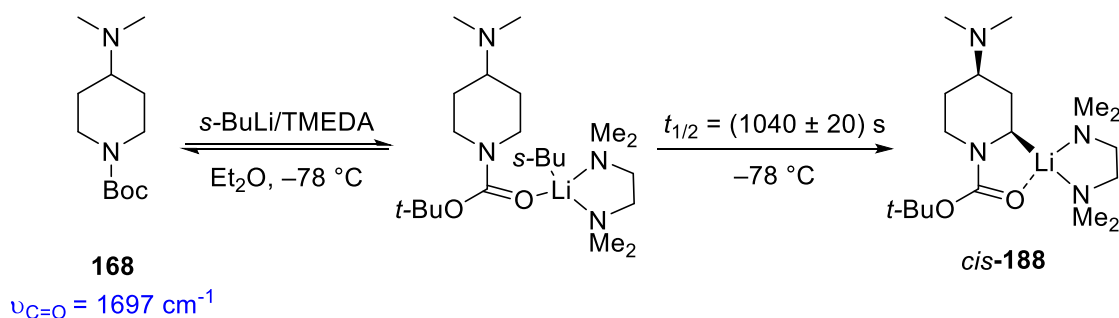
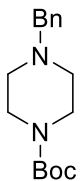
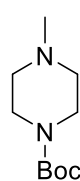
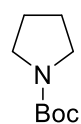
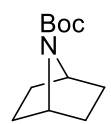
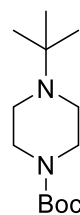
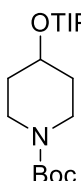
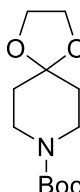
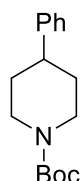
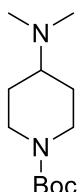
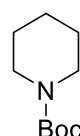


Figure 2.12. Non-linear curve fitting for the *s*-BuLi/TMEDA lithiation of 4-amino *N*-Boc piperidine **168** to obtain k_{obs}

By comparing the $t_{1/2}$ s of both *N*-Boc pyrrolidine **9** ($t_{1/2} = 20.7 \pm 0.9$ s) and 4-amino *N*-Boc piperidine **168** ($t_{1/2} = 1040 \pm 20$ s), it is evident that piperidine **168** is a much less reactive substrate. The $t_{1/2}$ s show that *N*-Boc pyrrolidine **9** is ~50 times more reactive than amino piperidine **168**. The time required for 99% conversion for 4-amino *N*-Boc piperidine **168** was also calculated using $t_{1/2}$ which provided a 121 min lithiation time, which is remarkably close to the 120 min lithiation time measured determined by visual inspection.

Finally, the *s*-BuLi/TMEDA lithiations of an additional eight *N*-Boc heterocycles whose reactivities had already quantified using visual inspection were analysed using the kinetic analysis procedure developed. The *s*-BuLi/TMEDA lithiation reactions of each of these eight substrates all displayed first order kinetics with respect to the substrate (see section 6.4 for the kinetics plots for all substrates). Substrates with fast *s*-BuLi/TMEDA lithiations (< 3 min) such as *N*-Boc morpholine **169** were not included as these fast reactions would give too few data points for regression analysis and provide results with large margins of error. The kinetically obtained k_{obs} , $t_{1/2}$, the lithiation time calculated using $t_{1/2}$ ($t_{\text{lith-half}}$) and the lithiation time obtained by visual inspection ($t_{\text{lith-visual}}$) are presented for each of the eight additional substrates plus *N*-Boc pyrrolidine **9** and piperidine **10** are presented in Table 2.4.

Table 2.4. Half-lives for the *s*-BuLi/TMEDA lithiations of a selection of 10 *N*-Boc heterocycle substrates

					
	57	58	9	84	66
$k_{\text{obs}} / \text{s}^{-1}$ ^a	3.79×10^{-2} $\pm 0.19 \times 10^{-2}$	3.72×10^{-2} $\pm 0.37 \times 10^{-2}$	3.34×10^{-2} $\pm 0.15 \times 10^{-2}$	8.16×10^{-3} $\pm 0.43 \times 10^{-3}$	6.56×10^{-3} $\pm 0.18 \times 10^{-3}$
$t_{1/2} / \text{s}$ ^b	18.3 ± 0.9	18.7 ± 1.8	20.7 ± 0.9	84.9 ± 4.4	105 ± 3
$t_{\text{lith-half}} / \text{min}$ ^c	2	2	2.5	10	12
$t_{\text{lith-visual}} / \text{min}$	4	4	4	15	22
					
	39	34	32	168	10
$k_{\text{obs}} / \text{s}^{-1}$ ^a	2.16×10^{-3} $\pm 0.05 \times 10^{-3}$	1.11×10^{-3} $\pm 0.04 \times 10^{-3}$	1.08×10^{-3} $\pm 0.01 \times 10^{-3}$	6.64×10^{-4} $\pm 0.15 \times 10^{-4}$	2.17×10^{-4} $\pm 0.02 \times 10^{-4}$
$t_{1/2} / \text{s}$ ^b	320 ± 8	624 ± 22	642 ± 5	1040 ± 20	3190 ± 30
$t_{\text{lith-half}} / \text{min}$ ^c	37	73	75	121	372
$t_{\text{lith-visual}} / \text{min}$	45	100	90	120	360 ^d

^a k_{obs} measured by non-linear regression analysis of *N*-Boc heterocycle consumption (except **66** which has been modelled as two consecutive first order processes – see experimental)

^b $t_{1/2}$ calculated using k_{obs}

^c $t_{\text{lith-half}}$ calculated using $t_{1/2} \times 7$ (as $7 t_{1/2} \text{ s} = 99\%$ conversion)

^d lithiation of *N*-Boc piperidine **10** may not be complete (see below for discussion)

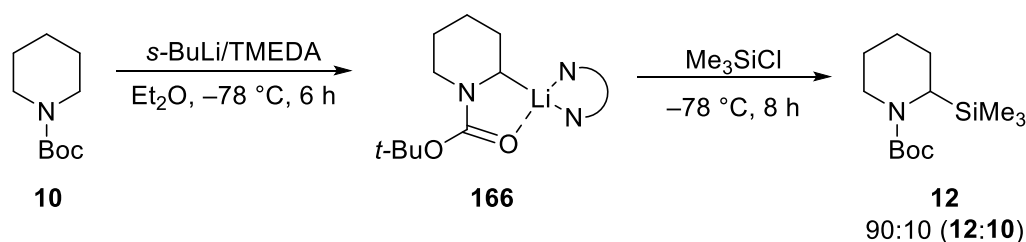
The rates of lithiation measured using the consumption of the *N*-Boc heterocycle provided an almost identical reactivity order for all of the heterocycle substrates that was obtained previously using visual inspection. The only difference in the reactivity trend was observed with ketal **34** and 4-phenyl piperidine **32**, which the kinetic analysis suggested have almost identical reactivities, whereas visual inspection indicated that ketal **34** was less reactive with a 10 min slower lithiation reaction. The kinetic analysis also allowed some of the subtle differences in reactivity between the fast lithiating heterocycles piperazines **57** and **58** and *N*-Boc pyrrolidine **9** to be elucidated. Visual inspection indicated that all three substrates

required 4 min for complete lithiation with *s*-BuLi/TMEDA so no reactivity differences for these substrates could be extracted. However, the kinetic analysis suggests that *N*'-Bn piperazine **57** is slightly more reactive than *N*-Boc pyrrolidine **9**. Unfortunately, where *N*'-Me piperazine **58** fits in this reactivity trend could not be further elucidated due to the large margin of error in the $t_{1/2}$ determined for the lithiation of **58**.

It is important to note, however, that these small differences between the lithiation $t_{1/2}$ s for substrates **9**, **57** and **58** may not be of sufficient accuracy to construct a reactivity order for these three substrates with complete certainty. This is first due to the significant amounts of standard error that are provided by the curve-fitting and secondly due to temperature variations that have not been accounted for in this kinetic treatment. These temperature variations occur at the start of the reaction due to addition of the *s*-BuLi which is kept at 5 °C (cooling the *s*-BuLi further causes the cyclohexane solvent to freeze). It is also likely that the lithiation will be exothermic which may also cause the reaction temperature to increase. When the temperature of the *s*-BuLi/TMEDA lithiation of *N*-Boc pyrrolidine **9** was monitored using a thermocouple, an 8 °C increase in reaction temperature was observed after the addition of *s*-BuLi, after 1 min the reaction temperature had returned to -78 °C.

Achieving complete conversion of *N*-Boc piperidine **10** to the trapped products proved to be problematic using *s*-BuLi/TMEDA, with starting material still present after the lithiation and trapping reactions. Me₃SiCl was used to trap lithiated piperidine **166** after the ReactIR™ monitoring and this suggested that the *s*-BuLi/TMEDA lithiation was complete after 6 h. The Me₃SiCl trapping reaction was allowed 12 h for complete trapping to occur and the ReactIR™ monitoring indicated trapping was complete within 8 h (the ReactIR™ monitoring of trapping reactions is discussed in detail in Chapter 4). The reaction was attempted twice and, after each work-up, ¹H NMR spectroscopic analysis indicated that a 90:10 ratio of the Me₃SiCl-trapped product **12** and unreacted substrate **10** was present (Scheme 2.19).

Scheme 2.19. *s*-BuLi/TMEDA lithiation and Me₃SiCl trapping of *N*-Boc piperidine **10**



The ample time allowed for the trapping reaction of lithiated intermediate **166** and the complete trapping observed by ReactIR™ indicated that the lithiation reaction of **10** was likely responsible for the incomplete conversion observed in the final products. There are two possible causes for the incomplete conversion during the lithiation. The first is that the lithiation reaction is incomplete when the electrophile is added, so unreacted piperidine **10** starting material remains. Otherwise, the recovered **10** may result from instability of lithiated intermediate **166** during the 6 h lithiation which decomposes back to the starting material; this decomposition could involve deprotonation of the Et₂O solvent by the reactive lithiated intermediate **166**. Further analysis of the non-linear regression kinetic analysis applied to the consumption of piperidine **10** indicated that the reaction may not be complete after 6 h (Figure 2.13). The kinetic analysis of the *s*-BuLi/TMEDA lithiation of *N*-Boc piperidine **10** suggested that it was not complete after 6 h and that 99% conversion required a lithiation time of 6.25 h.

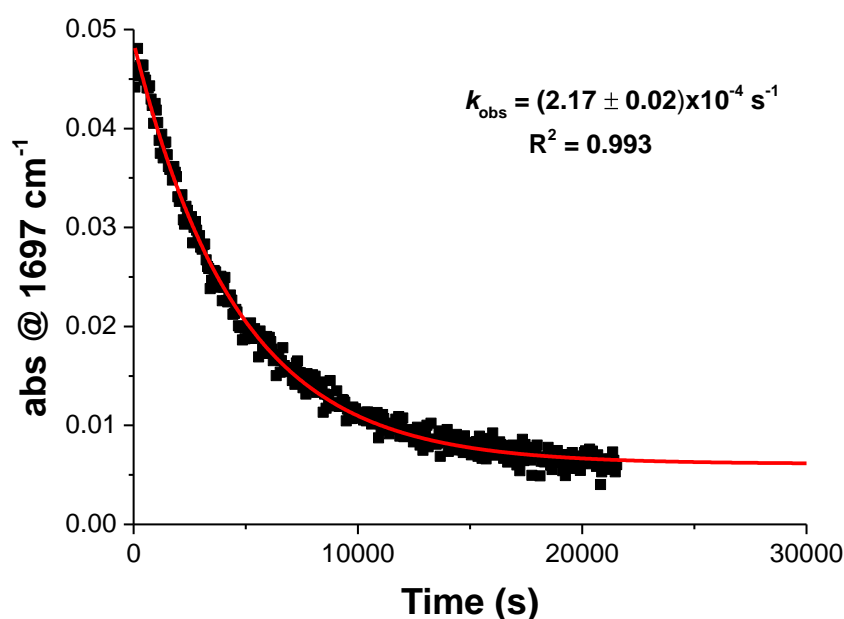
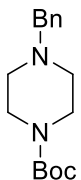
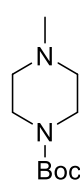
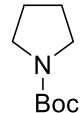
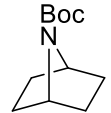
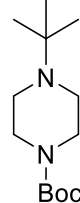
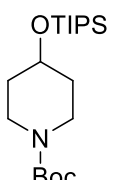
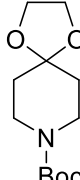
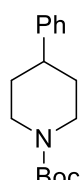
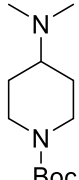
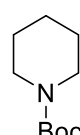


Figure 2.13. Non-linear regression to obtain k_{obs} for the *s*-BuLi/TMEDA lithiation of *N*-Boc piperidine **10 with extrapolated curve of best fit to determine lithiation end-point**

This again highlights the difficulty in determining an end-point for such a slow reaction by visual inspection of the ReactIR™ data. However, the curve of best fit for the *s*-BuLi/TMEDA lithiation of piperidine **10** indicated that 98% conversion is expected at 6 h but only 90% conversion was observed in the final crude product. This suggested that the instability of the lithiated intermediate may be a problem with the long 6 h lithiation of *N*-Boc piperidine **10**.

An attempt to measure the $t_{1/2}$ s for the lithiation of the 10 *N*-Boc heterocycles by non-linear regression analysis of the consumption of the prelithiation complex ($t_{1/2}$ -prelith) was also carried out. For comparative purposes, the $t_{1/2}$ s calculated by consumption of prelithiation complex, $t_{1/2}$ -prelith and the $t_{1/2}$ calculated by consumption of the *N*-Boc heterocycle, $t_{1/2}$ -substrate are presented in Table 2.5. The $t_{1/2}$ s obtained by non-linear regression of the consumption of the prelithiation complexes ($t_{1/2}$ -prelith) did differ somewhat from the $t_{1/2}$ s obtained by non-linear regression of the *N*-Boc heterocycle consumption ($t_{1/2}$ -substrate).

Table 2.5. Half-lives determined by consumption of *N*-Boc heterocycle and prelithiation complex consumption for the *s*-BuLi/TMEDA lithiations of a selection of 10 *N*-Boc heterocycle substrates

					
	57	58	9	84	66
$t_{1/2}$ -prelith / s ^b	15.2 ± 1.6	9.3 ± 6.6	17.8 ± 0.5	101 ± 4	65.5 ± 3.7 ^d
t_{lith} -prelith / min ^b	2	1	2	12	10 ^d
$t_{1/2}$ / s ^a	18.3 ± 0.9	18.7 ± 1.8	20.7 ± 0.9	84.9 ± 4.4	105 ± 3
t_{lith} -half / min ^a	2	2	2.5	10	15
t_{lith} -visual / min	4	4	4	15	22
					
	39	34	32	168	10
$t_{1/2}$ / s ^a	320 ± 8	624 ± 22	642 ± 5	1040 ± 20	3190 ± 30
t_{lith} -half / min ^a	37	73	75	121	372
$t_{1/2}$ -prelith / s ^b	282 ± 10	310 ± 19	502 ± 7	806 ± 24	2850 ± 30
t_{lith} -prelith / min ^b	33	36	59	94	333
t_{lith} -visual / min	45	100	90	120	360 ^c

^a $t_{1/2}$ measured by non-linear regression analysis of *N*-Boc heterocycle consumption

^b $t_{1/2}$ measured by non-linear regression analysis of prelithiation complex consumption

^c lithiation of *N*-Boc piperidine **10** may not be complete

^d lithiation of **66** modelled as two consecutive first order processes (see experimental)

For most of the substrates, an identical reactivity order was obtained using the $t_{1/2}$ s calculated by both analysis of substrate consumption and prelithiation complex consumption. However, there were a few outlying results that did not follow the trends observed by both visual inspection and kinetic analysis of the *N*-Boc heterocycle consumption. For example, the reactivity order of bicyclic pyrrolidine **84** and *N*'-*t*-Bu piperazine **66** is swapped when $t_{1/2}$ s are measured using the consumption of prelithiation complex. In addition, the $t_{1/2}$ measured for the lithiation of 4-ketal piperidine **34** using prelithiation complex consumption ($t_{1/2\text{-prelith}} = 310 \pm 19$ s) is nearly half that measured when $t_{1/2}$ is measured by the consumption of the substrate ($t_{1/2\text{-substrate}} = 624 \pm 22$ s). As mentioned previously, these unreliable results provided by the measurement of prelithiation complex consumption likely arise due to the overlap of signals for prelithiation complex and lithiated intermediate. This overlap will affect the gradient of the prelithiation complex signal during the reaction and provide unreliable data for regression analysis. Also, the smaller intensity of the $\nu_{\text{C=O}}$ signal of the prelithiation complex results in unreliable rate data as the signal/noise ratio is much smaller than that of the uncomplexed *N*-Boc heterocycle $\nu_{\text{C=O}}$ signal. For these reasons, we believe that the $t_{1/2}$ values calculated from the consumption of *N*-Boc heterocycle provide the most reliable reactivity order; hence it is these $t_{1/2}$ values that have been used when correlating the results with the DFT reactivity study described in Chapter 3.

Next, the *s*-BuLi/DPE **177** lithiation reactions of *N*-Boc heterocycles presented in Table 2.6, were also subjected to the same kinetic analysis procedure. Unfortunately, the *s*-BuLi/DPE **177** lithiations of *N*-Boc morpholine **169** and 4-chloro and 4-*O*-trisyl piperidines **48** and **167** were too rapid for sufficient ReactIRTM data to be collected for kinetic analysis. Even though the *s*-BuLi/DPE **177** lithiation of 4-chloro piperidine **48** was 5 min, ReactIR data was only collected every minute (due to the older iC10 apparatus that was used) so too few points were recorded for a reliable kinetic analysis. Therefore, non-linear regression analysis was only carried out for the *s*-BuLi/DPE **177** lithiation reactions of *N*-Boc pyrrolidine **9** and *N*'-Me *N*-Boc piperazine **58**. Close fitting, first order decay curves were obtained for the *s*-BuLi/DPE **177** lithiations of both substrates (Figure 2.14), confirming that the reaction is first order with respect to the *N*-Boc heterocycle.

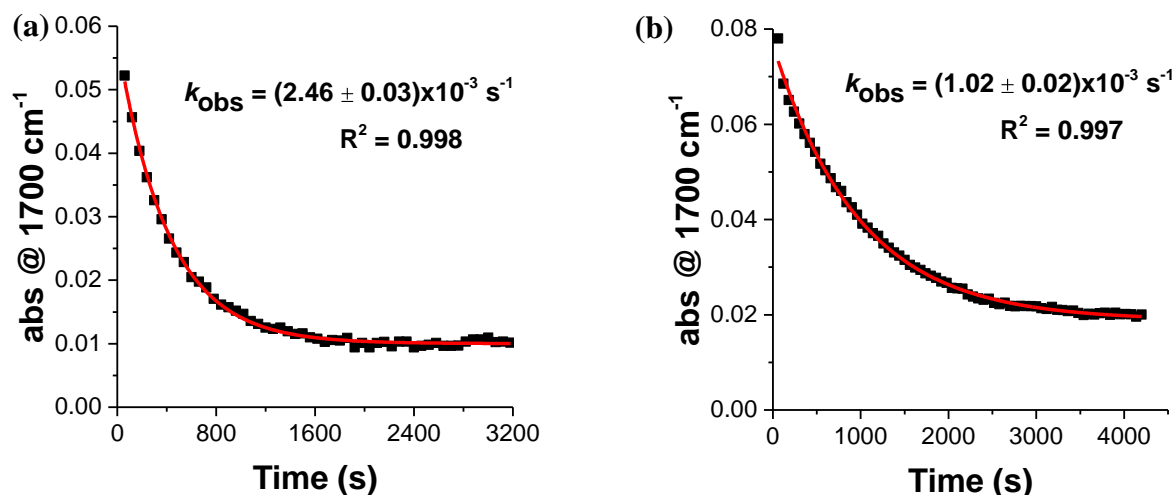
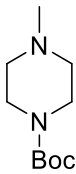
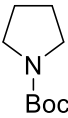


Figure 2.14. Non-linear regression to obtain k_{obs} for the *s*-BuLi/DPE **177** lithiations of *N'*-Me *N*-Boc piperazine **58** (a) and *N*-Boc pyrrolidine **9** (b)

The $t_{1/2}$ s, for each of the *s*-BuLi/DPE **177** lithiation reactions, calculated using the extracted from the kinetic analysis, are presented in Table 2.6 along with the lithiation time calculated using $t_{1/2}$ ($t_{\text{lith-half}}$) and the lithiation time obtained by visual inspection ($t_{\text{lith-visual}}$).

Table 2.6. Half-lives for the *s*-BuLi/DPE **177** lithiations of *N'*-Me *N*-Boc piperazine **58** and *N*-Boc pyrrolidine **9**

	 58	 9
$t_{1/2}$ / s	282 ± 4	680 ± 12
$t_{\text{lith-half}}$ / min	33	80
$t_{\text{lith-visual}}$ / min	30	60

The $t_{1/2}$ s obtained for the *s*-BuLi/DPE **177** lithiation of *N*-Boc pyrrolidine **9** and *N'*-Me *N*-Boc piperazine **58**, indicated that piperazine **58** is over two times faster to lithiate than *N*-Boc pyrrolidine **9** with $t_{1/2}$ s of 282 s and 680 s respectively. This two-fold increase in reactivity is not observed for these two substrates with *s*-BuLi/TMEDA, which provided very similar $t_{1/2}$ s of 18.7 and 20.7 s for heterocycles **58** and **9** respectively. It is uncertain whether the rapid reaction rates make comparisons of $t_{1/2}$ unreliable for rapid lithiations or whether subtle reactivity difference are present with the *s*-BuLi/DPE **177** and *s*-BuLi/TMEDA lithiating complexes. The 33 min lithiation time estimated using $t_{1/2}$ for the lithiation of *N'*-Me *N*-Boc piperazine **58** closely matched the 30 min lithiation time measured

by visual inspection. However, the estimated 80 min *s*-BuLi/DPE **177** lithiation time for *N*-Boc pyrrolidine **9** differed significantly to the 46 min lithiation time obtained using visual inspection. This again highlights how unreliable measuring the rate of lithiation of substrates can be using visual inspection.

In summary, the kinetic analysis provides a more reliable and precise method to determine the reactivity of the lithiation reactions of different *N*-Boc heterocycle substrates. As discussed, the lithiation reactions of the *N*-Boc heterocycle substrates can be modelled as first order reactions which allows an observed rate constant (k_{obs}) to be obtained by fitting an exponential decay curve ReactIRTM absorbance of the uncomplexed substrate. The *s*-BuLi/TMEDA reactivity series of the 10 substrates studied using the kinetic analysis was in good agreement with the reactivity series obtained by visual inspection and only measurement of the reactivity of ketal **34** provided a differing result. The kinetic analysis was particularly useful to elucidate reactivity trends for *N*-Boc heterocycle substrates with fast lithiation reactions. For example, the kinetically obtained $t_{1/2}$ s were able to identify that *N'*-Bn piperazine **57** is more reactive than *N*-Boc pyrrolidine **9** using *s*-BuLi/TMEDA lithiating conditions.

2.4 Conclusions and Future Work

In this chapter, *in situ* ReactIRTM monitoring has provided a reactivity series for 14 *N*-Boc heterocycle substrates with differing ring sizes, heteroatoms in the ring and substituents on the rings. Both *s*-BuLi/TMEDA and *s*-BuLi/DPE lithiating conditions provided the same reactivity series for the *N*-Boc heterocycles studied, with the *s*-BuLi/DPE conditions being particularly useful to elucidate the reactivity of fast reacting substrates such as *N'*-Bn piperazine **57** and *N*-Boc pyrrolidine **9**. Furthermore, a more reliable and precise method to determine the reactivity of the substrates with *s*-BuLi/TMEDA was developed which involved kinetic analysis of the lithiation reaction. This kinetic analysis has also aided in elucidating some of the reactivity trends between the fast lithiating substrates. The more precise measure of reactivity afforded by the kinetic analysis will be beneficial when the experimental reactivities and computationally predicted reactivities for substrates are compared in Chapter 3. By combining the reactivity data for the *s*-BuLi/TMEDA and *s*-BuLi/DPE **177** conditions and the kinetic analysis results, a reactivity series for the 14 *N*-Boc heterocycle substrates studied can be constructed (Figure 2.15).

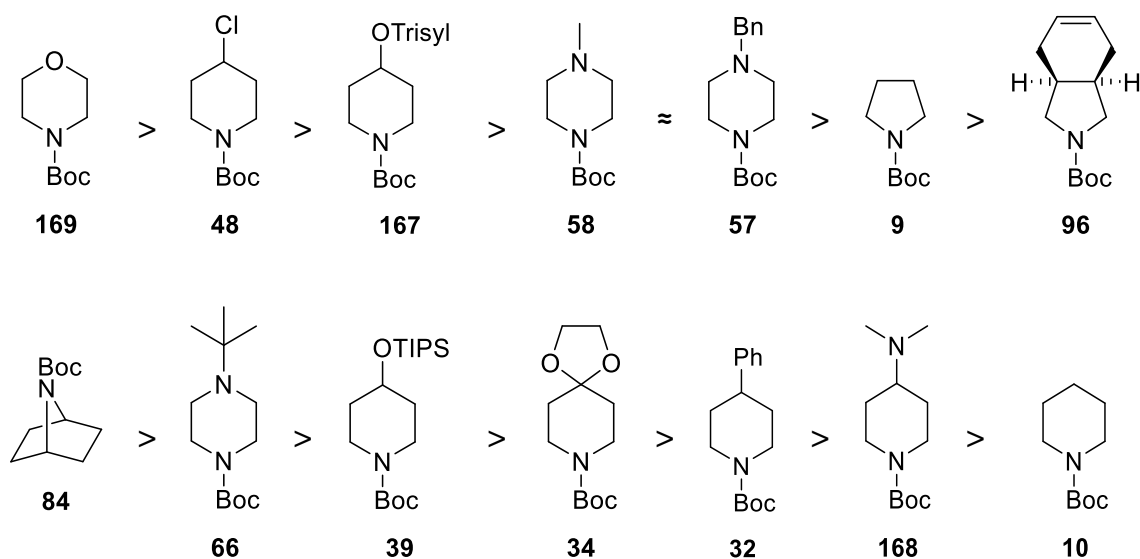


Figure 2.15. Final reactivity series of the 14 *N*-Boc heterocycle substrates studied in this thesis using *s*-BuLi/TMEDA and *s*-BuLi/DPE **177 lithiating conditions**

The use of *s*-BuLi/(–)-sparteine provided some significant differences in the reactivity series of the fast lithiating substrates compared to those obtained with both *s*-BuLi/TMEDA and *s*-BuLi/DPE. It was rationalised that the outlying reactivities displayed by 4-chloro piperidine **48** and 4-*O*-trisyl piperidine **167** with *s*-BuLi/(–)-sparteine, could be due to the combination

of the enantioselective lithiation and slow rotamer interconversion at $-78\text{ }^{\circ}\text{C}$. A combination of slow rotamer interconversion and a slow rate of *N*-inversion/ring flipping may also be the reason that *N'*-Me and *N'*-Bn piperazines **58** and **57** also displayed lower than expected reactivities with *s*-BuLi/(–)-sparteine. This effect could be probed further by investigating whether the rotamer interconversion does occur at $-78\text{ }^{\circ}\text{C}$ for the 4-substituted piperidines and piperazines using VT-NMR. However, the rates of rotamer interconversion obtained may not be applicable as the *N*-Boc heterocycle/*s*-BuLi/(–)sparteine prelithiation complex could have a different barrier for rotation of the carbamate to the uncomplexed substrate. Another possible experiment that could confirm whether the enantiopure nature of ligand is responsible for the outlying reactivity of substrates would be to conduct the lithiations with (±)-sparteine. If the *s*-BuLi/(±)-sparteine reactions were faster, giving similar results to those obtained with *s*-BuLi/DPE **177**, this would indicate the enantioselectivity of the lithiation may be responsible for the retardation of the lithiation.

The more detailed mathematical kinetic analysis of the lithiation reactions of *N*-Boc heterocycles presented in section 2.4 was developed in the latter stages of this study, this meant that further investigation and elucidation of the reaction kinetics was not possible. Our current kinetic model for the lithiation reaction assumes that the lithiation is first order with respect to the uncomplexed *N*-Boc heterocycle; the consumption of the substrate does appear to exhibit a first order decay suggesting that this is the case. However, further experiments could be conducted to conclusively confirm whether the lithiation reaction does indeed show zero order kinetics with respect to the concentration of *s*-BuLi/diamine. Repeating the lithiations of *N*-Boc heterocycles with varying concentrations of *s*-BuLi/diamine would provide clear evidence whether there is zero order response to the concentration of *s*-BuLi/diamine used. Additionally, the aggregation state of the alkyllithium and any aggregation state changes during the lithiation reaction has not been investigated. At present, it is assumed that all alkyllithium species are in a monomeric form due to the stoichiometric amounts of diamine ligand added but it possible that these alkyllithium species exist as aggregates in the reaction. A better understanding of the alkyllithium aggregates, using methods such as Li NMR, may provide a more accurate kinetic model for these lithiation reactions.

Further development of the kinetic analysis methodology used in this investigation may also be able to provide more reliable and accurate values of k_{obs} for particularly fast or slow

lithiating *N*-Boc heterocycles. For fast lithiating substrates such as *N*-Boc morpholine **169**, it may be possible to use the rapid-collect feature on the newer ReactIR™ apparatus which allows a reading to be taken every second. This was used in this project to investigate the fast equilibrium between the un-complexed heterocycle substrate and prelithiation complex (see Scheme 2.3). Due to the more significant noise present in the rapid-collect ReactIR™ trace it was not used to monitor the fast lithiation reactions as determining an end-point would be difficult by visual inspection. However, with the recently developed kinetic analysis method, a curve could be fit to these data which would be less affected by the more significant amount of noise present. Similarly, kinetic analysis using curve fitting may enable k_{obs} and $t_{1/2}$ values to be obtained for slow lithiation reactions as the curve fitting does not require the reactions to reach completion. This would be particularly useful as maintaining a temperature of $-78\text{ }^{\circ}\text{C}$ for over 10 h is problematic when monitoring slow lithiation reactions by ReactIR™. An interesting substrate to study would be the 7-membered nitrogen heterocycle, *N*-Boc azepane **192** (Figure 2.16), which in-group data suggests is even less reactive than *N*-Boc piperidine **10**. The *s*-BuLi/TMEDA lithiation of azepane **192** at $-50\text{ }^{\circ}\text{C}$ required 2 h for complete lithiation whereas piperidine **10** only required 35 min at $-50\text{ }^{\circ}\text{C}$.⁵³ This indicates that azepane **192** is significantly less reactive than piperidine **10** likely due to the conformational flexibility of the large 7-membered heterocycle.

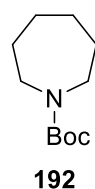


Figure 2.16. *N*-Boc azepane **192**

Chapter 3: Computational DFT Modelling of the α -Lithiation of *N*-Boc Heterocycles

The DFT modelling of the α -lithiation of *N*-Boc heterocycles has previously been reported by Wiberg and Bailey,^{34,85,89} as discussed in section 1.4. However, these previous investigations were primarily focused upon reproducing the enantioselectivity observed when a chiral diamine such as (-)-sparteine, was employed in the lithiation. The computational study reported in this Chapter focuses on exploring the differences in reactivity observed when different diamines and substrates are used in the lithiation reaction.

Previous literature precedent and the kinetic analysis of the α -lithiation reaction presented in Chapter 2 indicate that deprotonation in the prelithiation complex is the rate determining step.^{32,72} Therefore, in order to calculate the activation free energy barrier (ΔG^\ddagger) for these α -lithiation reactions, it is this step that needs to be modelled. This requires the ground state prelithiation complex **193** and transition state for the deprotonation **194** for the α -lithiation of the *N*-Boc heterocycle to be constructed and optimised (Figure 3.1).

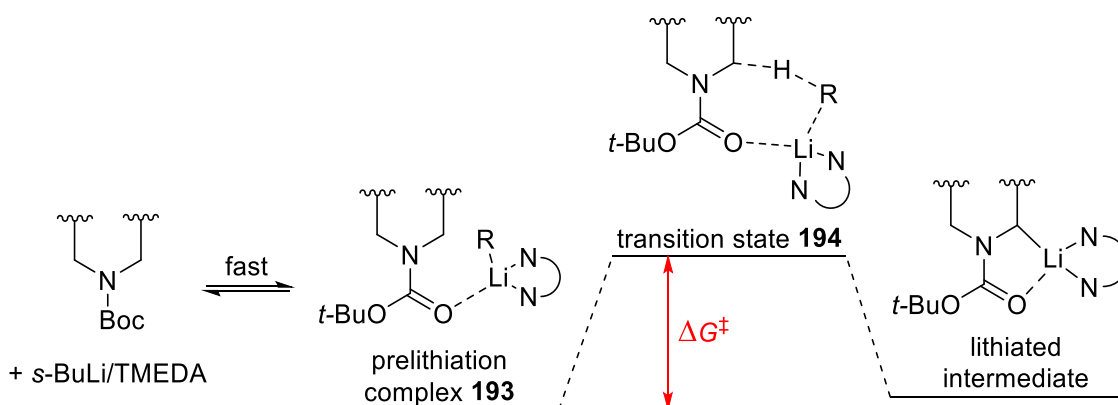


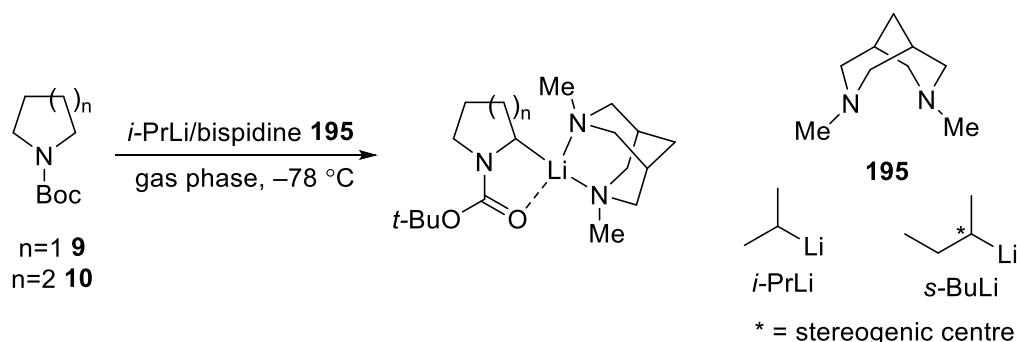
Figure 3.1. Partial reaction coordinate diagram for the RLi/diamine α -lithiation reaction of *N*-Boc heterocycles

3.1 Computational DFT Modelling of the α -Lithiation Reactions of *N*-Boc Pyrrolidine and *N*-Boc Piperidine

First, the α -lithiation reactions of both *N*-Boc pyrrolidine **9** and *N*-Boc piperidine **10** were modelled and this required the optimisation of prelithiation complexes and transition states for each of the substrates. The enantioselective α -lithiation reactions of *N*-Boc pyrrolidine **9** and *N*-Boc piperidine **10** with *i*-PrLi/(–)-sparteine have been modelled previously by Wiberg and Bailey (see section 1.4).^{34,85,86} Their computational study also optimised prelithiation complexes and deprotonation transition states for the *i*-PrLi/(–)-sparteine lithiation of **9** and **10**. Wiberg and Bailey's work provided useful information about the expected geometries of the prelithiation complex and transition states for the lithiation which assisted the construction of initial geometries for our computational study.

For the modelling of the α -lithiation reactions of *N*-Boc pyrrolidine **9** and *N*-Boc piperidine **10**, *i*-PrLi was used as the alkyllithium and di-methyl bispidine **195** as the diamine (Scheme 3.1). As with Wiberg and Bailey's method, *i*-PrLi was chosen as a model of *s*-BuLi as *i*-PrLi lacks a stereogenic centre. The absence of the stereocentre simplifies the calculations by removing the complication caused by diastereomeric prelithiation complexes and transition states. Di-methyl bispidine **195** was selected as it has a simple and rigid structure making optimisation faster and easier. It was expected that a flexible diamine such as TMEDA would provide a shallow potential energy surface making the location of minima more complex and time consuming. However, later in our computational study it was found that TMEDA could be modelled as the diamine ligand without adding significant computational expense to the optimisation process with DFT modelling. The DFT modelling of the α -lithiation of *N*-Boc heterocycles with TMEDA and other diamines will be discussed later in this chapter.

Scheme 3.1. Reaction conditions used to model the α -lithiation reactions of *N*-Boc pyrrolidine **9 and *N*-Boc piperidine **10****



All calculations were conducted in the gas phase and the enthalpies (H) and free energies (G) calculated by frequency analysis were corrected to $-78\text{ }^{\circ}\text{C}$, as this is the temperature at which the lithiation reactions were conducted experimentally. These conditions were used as the standard for all of the modelling carried out in this computational reactivity study. Solvent corrections were not applied to the calculations but are discussed briefly in section 3.2.4. DFT scaling factors were not required as the calculated energies were only used relative to one another. i.e. only the trends between the experimentally determined rate of reaction (k_{obs}) and the calculated activation energies for the lithiation of the substrates (ΔG^{\ddagger}) were compared. Scaling factors are only required when absolute activation energies comparable to experimentally determined activation energies are needed. All geometry optimisation and frequency analysis calculations were carried out using GAUSSIAN 09.¹¹²

For the α -lithiation reactions of *N*-Boc pyrrolidine **9** and *N*-Boc piperidine **10**, prelithiation complexes and transition states were optimised using two different computational methods: the *ab-initio* post-Hartree-Fock MP2 method and DFT. When the optimisations of geometries was carried out using DFT, two different hybrid functionals were used, B3LYP^{113–115} and Truhlar's M06 Minnesota functional.¹¹⁶ B3LYP is a well-established DFT functional that is commonly used for the modelling of organic systems.¹¹⁷ The M06 functional is a more recently developed DFT functional which has been shown to better describe dispersion interactions;¹¹⁸ the inaccurate description of dispersion interactions is a common pitfall when chemical systems are modelled using DFT.¹¹⁹ The DFT modelling was conducted with two functionals to allow any outliers that may have resulted from the fitting of functional to be identified. Additionally, it was envisaged that the M06 DFT functional may provide a better description of the system as it more accurately accounts for dispersion interactions.

Both the DFT and MP2 optimisation methods were used within a moderately sized Pople 6-31G(d) basis set. This size of basis set was selected to provide sufficiently flexible description of orbitals without making the computational expense of the calculations prohibitively large. The systems modelled in this study are relatively large (~80 atoms) which prohibits larger basis sets being used for optimisation as the additional basis functions on each atom would increase the complexity and time required for the calculation. For both DFT functionals, a larger than default, pruned (99,950) integral grid was used (GAUSSIAN 09 keyword Int=UltraFine).

Both the MP2 and DFT modelling with B3LYP and M06 functionals provided nearly identical optimised geometries for both the prelithiation complex and transition state for the α -lithiation of *N*-Boc pyrrolidine **9**. The geometries optimised for *N*-Boc pyrrolidine **10** using B3LYP/6-31G(d) are shown in Figure 3.2.

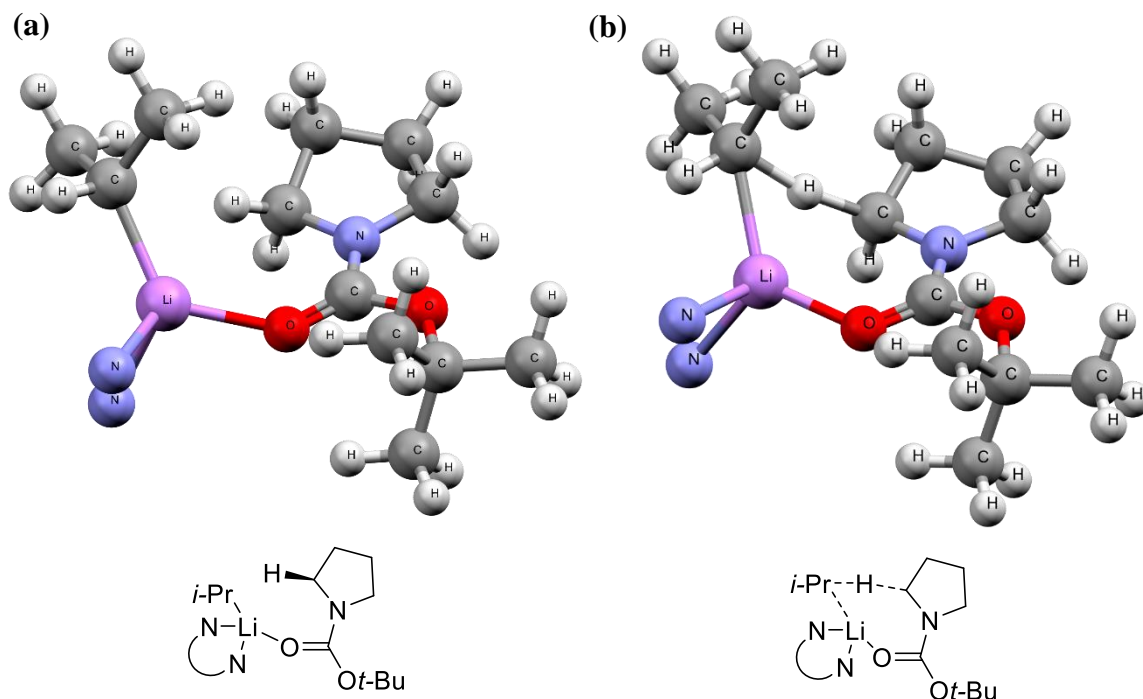


Figure 3.2. B3LYP/6-31G(d) geometries for the prelithiation complex (a) and transition state (b) of the *N*-Boc pyrrolidine **9 deprotonation (C and H atoms of the di-methyl bispidine ligand **195** are hidden for clarity)**

To confirm that the saddle point located for the α -lithiation of *N*-Boc pyrrolidine **9** was the correct transition state, corresponding to the deprotonation of the nitrogen α -proton, an Intrinsic Reaction Coordinate (IRC) calculation was also conducted. The IRC calculation followed the reaction coordinate in both a forward (towards the lithiated intermediate product **196**) and reverse (towards the prelithiation complex) direction from the transition

state. This calculation was conducted at a B3LYP/6-31G(d) level of theory using the optimised transition state geometry obtained when the lithiation of *N*-Boc pyrrolidine **9** was modelled. As expected, the reaction coordinate converged toward prelithiation complex in the reverse direction and the forward direction converged toward the lithiated intermediate **196** (Figure 3.3). This confirmed that the correct transition state for the α -lithiation of *N*-Boc pyrrolidine **9** had been located.

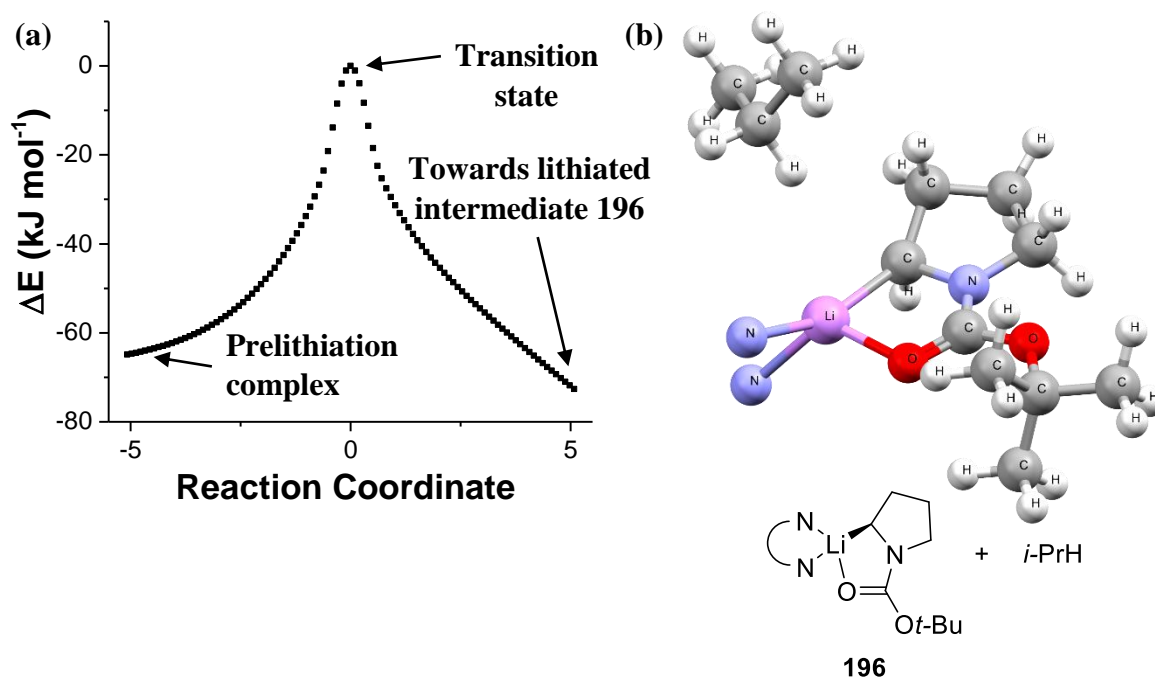


Figure 3.3. B3LYP/6-31G(d) calculated reaction coordinate for the *i*-PrLi/di-methyl bispidine **195** lithiation of *N*-Boc pyrrolidine **9** (a) and an output geometry from the forward path showing formation of the lithiated intermediate **196** and *i*-propane (b)

Once prelithiation complex and transition state geometries had been optimised for the α -lithiation reaction of *N*-Boc pyrrolidine **9**, the activation free energy for the lithiation (ΔG^\ddagger) was calculated using both the MP2 and DFT methods (Table 3.1). The calculated ΔG^\ddagger values were corrected to -78°C to replicate the temperature at which the lithiation reactions are carried out experimentally. The magnitudes of the ΔG^\ddagger values obtained were appropriate for a reaction that occurs at -78°C . The ΔG^\ddagger values obtained for the reaction from the DFT functionals and MP2 were similar, suggesting that DFT does provide a sufficient description for the interactions occurring in the reaction and a more thorough MP2 treatment may not be required for this system.

Table 3.1. Activation free energies (ΔG^\ddagger) calculated for the lithiation of *N*-Boc pyrrolidine **9**

Method	ΔG^\ddagger / kcal mol ⁻¹
B3LYP/6-31G(d)	13.77
M06/6-31G(d)	13.63
MP2/6-31G(d)	13.87

Next, the *i*-PrLi/di-methyl bispidine **195** lithiation of the corresponding 6-membered heterocycle, *N*-Boc piperidine **10**, was modelled with the same MP2 and DFT methods that were used to model the lithiation of *N*-Boc pyrrolidine **9**. Optimisation of prelithiation complexes and transition states for the lithiation of *N*-Boc piperidine **10** was more complex, as two possible reaction pathways were found. These reaction pathways differed by the location of the *i*-PrLi during the reaction. In one of the reaction pathways the *i*-PrLi straddles the piperidine ring adjacent to the α -proton that is deprotonated - this is denoted as ‘top’ deprotonation (Figure 3.4.a). The other reaction path places the *i*-PrLi reagent to the side of the piperidine ring again adjacent to the α -proton that is deprotonated - this is denoted as ‘side-on’ deprotonation’ (Figure 3.4.b).

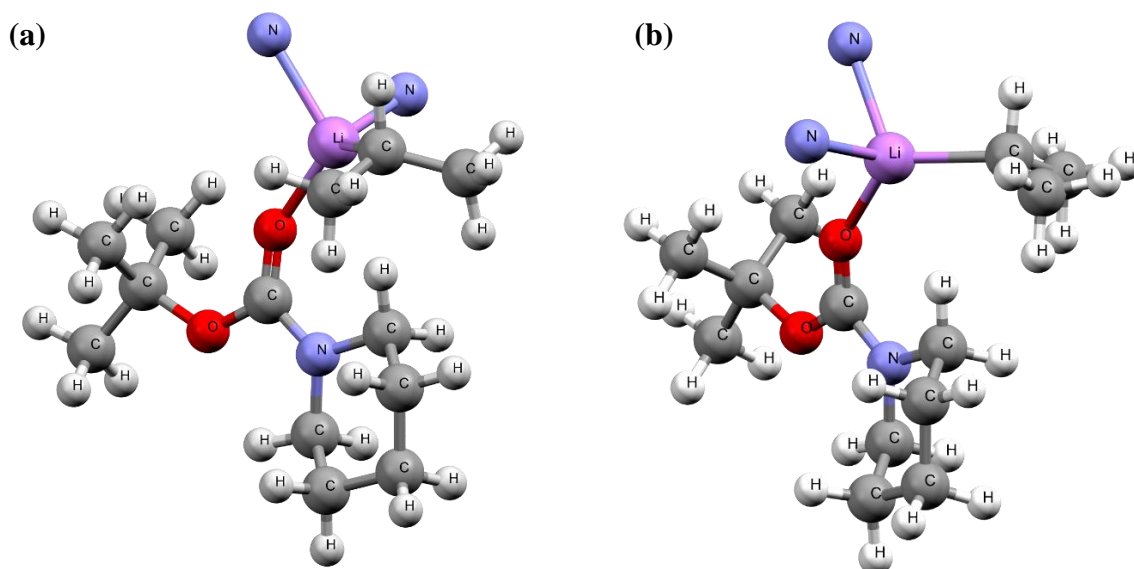


Figure 3.4. Prelithiation complexes for the ‘top’ deprotonation (a) and ‘side-on’ deprotonation (b) of *N*-Boc piperidine **10 (C and H atoms of the di-methyl bispidine ligand **195** are hidden for clarity)**

Geometries for the prelithiation complex and transition state for the ‘side-on’ and ‘top’ deprotonation of *N*-Boc piperidine **10** were optimised using MP2 and the B3LYP and M06 DFT functionals. All three methods provided very similar optimised geometries for both faces of attack from the *i*-PrLi. In all of the calculations, the experimentally observed equatorial lithiation was lowest in energy. The B3LYP/6-31G(d) optimised geometries of the prelithiation complex and transition state for the ‘side-on’ and ‘top’ deprotonation of *N*-Boc piperidine **10** are presented in Figures 3.5 and 3.6. For the transition states located for both the ‘side-on’ and ‘top’ deprotonation pathways, IRC calculations were carried out to ensure that the saddle point corresponded to the lithiation, as described previously for *N*-Boc pyrrolidine **9**. These IRC calculations confirmed that the saddle points located did indeed correspond to the transition state for the α -lithiation of *N*-Boc piperidine **10** (reaction coordinate diagrams are included in the experimental data in section 6.5).

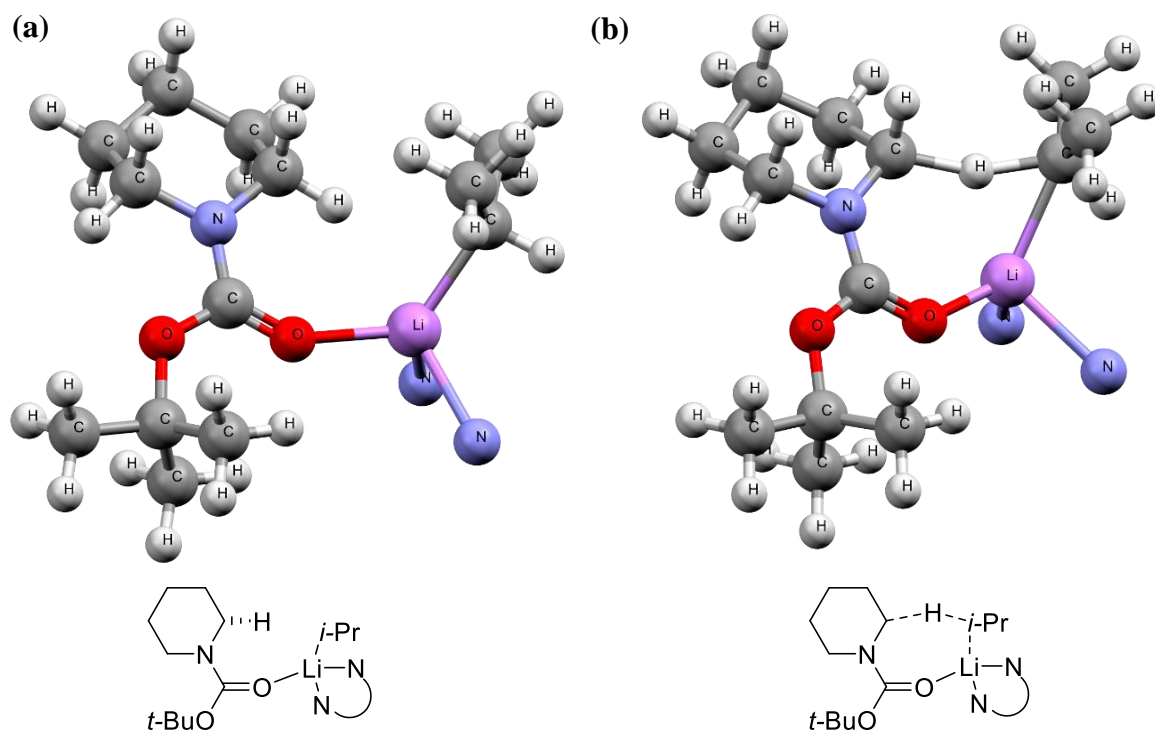


Figure 3.5. B3LYP/6-31G(d) optimised geometries for the prelithiation complex (a) and transition state (b) for the ‘side-on’ deprotonation of *N*-Boc piperidine **10** (C and H atoms of the di-methyl bispidine ligand **195** are hidden for clarity)

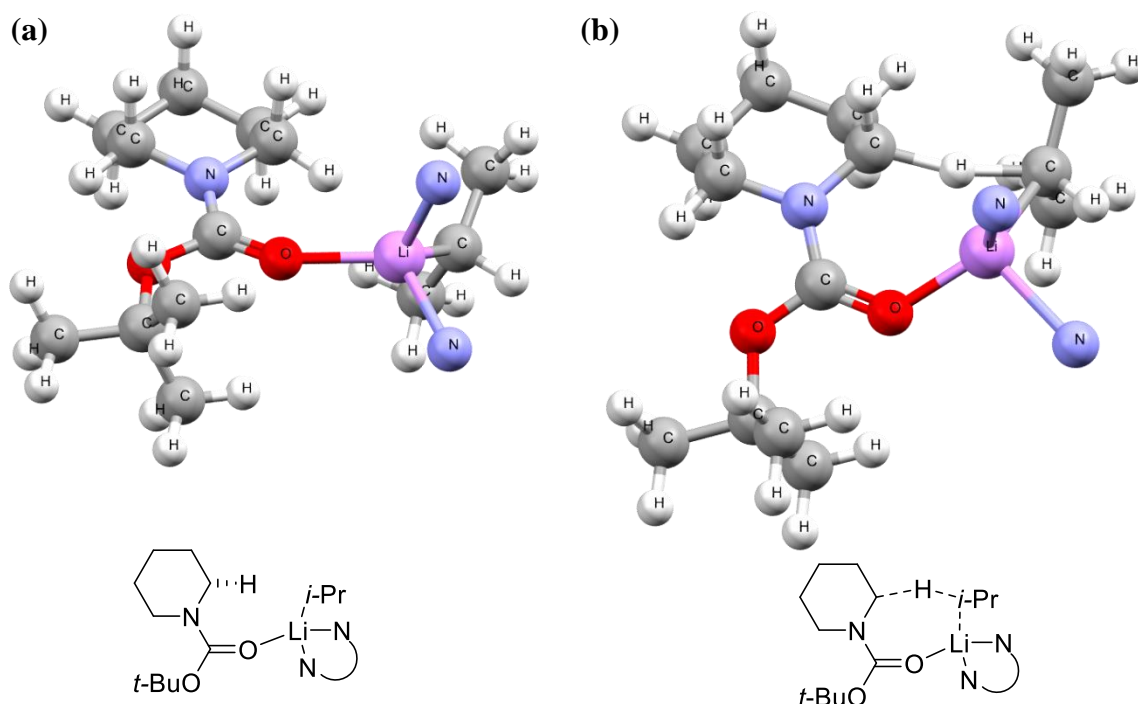


Figure 3.6. B3LYP/6-31G(d) optimised geometries for the prelithiation complex (a) and transition state (b) for the ‘top’ deprotonation of *N*-Boc piperidine **10** (C and H atoms of the di-methyl bispidine ligand **195** are hidden for clarity)

Activation free energies (ΔG^\ddagger) were also calculated for both the ‘side-on’ and ‘top’ deprotonation of *N*-Boc piperidine **10** with the three computational methods (Table 3.2). Interestingly, the calculated ΔG^\ddagger values indicated that the MP2 and the M06 DFT methods favoured the ‘top’ attack of *i*-PrLi whereas the B3LYP DFT functional favoured the ‘side-on’ attack.

Table 3.2. Activation free energies (ΔG^\ddagger) calculated for the *i*-PrLi/di-methyl bispidine **195** lithiation of *N*-Boc piperidine **10**

Method	Face of Attack	ΔG^\ddagger /kcal mol ⁻¹
B3LYP/6-31G(d)	Side-on	16.11
	Top	16.39
M06/6-31G(d)	Side-on	15.34
	Top	14.85
MP2/6-31G(d)	Side-on	15.58
	Top	15.33

Comparison of the activation energies calculated for both *N*-Boc pyrrolidine **9** and *N*-Boc piperidine **10** with all methods indicated a significant difference in the energy barriers for

the lithiation of the two substrates. For example, using B3LYP/6-31G(d) the lithiation of *N*-Boc pyrrolidine **9** showed $\Delta G^\ddagger = 13.77$ kcal mol⁻¹ whereas for *N*-Boc piperidine **10** it was found that $\Delta G^\ddagger = 16.11$ kcal mol⁻¹. This significant 2.34 kcal mol⁻¹ $\Delta\Delta G^\ddagger$ suggests that *N*-Boc pyrrolidine **9** should be substantially more reactive than *N*-Boc piperidine **10** at -78 °C. This is supported by the experimental ReactIRTM determined reactivity series, where *N*-Boc pyrrolidine **9** ($t_{1/2} = 20.7 \pm 0.9$ s) was significantly more reactive than *N*-Boc piperidine **10** ($t_{1/2} = 3190 \pm 30$ s).

We postulate that the significant difference in the free energies of activation for the lithiation of *N*-Boc pyrrolidine **9** and *N*-Boc piperidine **10** result from differences in steric interactions due to the differing conformations of the 5- and 6-membered rings. Inspection of the non-bonding distances between *i*-PrLi, di-methyl bispidine **195** and the *N*-Boc heterocycle (**9** or **10**) in the B3LYP optimised transition states did offer some differences in non-bonding distances between the protons on the *N*-Boc heterocycle and *i*-PrLi. For the ‘side-on’ lithiation of *N*-Boc piperidine **10**, there was a smaller non-bonding distance between the *i*-PrLi protons and the axial α -proton on the *N*-Boc piperidine **10** which is not deprotonated (2.438 Å) (Figure 3.7). It is possible that steric repulsion between the axial α -proton and the *i*-PrLi could raise the energy for deprotonation of *N*-Boc piperidine **10**. For the ‘top’ lithiation of *N*-Boc piperidine **10** the distance between the axial α -proton and the *i*-PrLi protons are larger (3.099 and 3.412 Å) so this steric effect is likely not to be responsible for the higher energy required for lithiation. However, there are smaller distances between the β -protons of the carbamate and the protons of *i*-PrLi in the ‘top’ lithiation transition state of *N*-Boc piperidine (2.470 and 2.346 Å) than those in the transition state for lithiation of *N*-Boc pyrrolidine **9** (2.658 and 2.349 Å). The closer proximity of the *i*-PrLi to these β -protons for the ‘top’ lithiation of *N*-Boc piperidine **10** may be responsible for the larger calculated energy barrier of the ‘top’ lithiation compared to that of *N*-Boc pyrrolidine **9**.

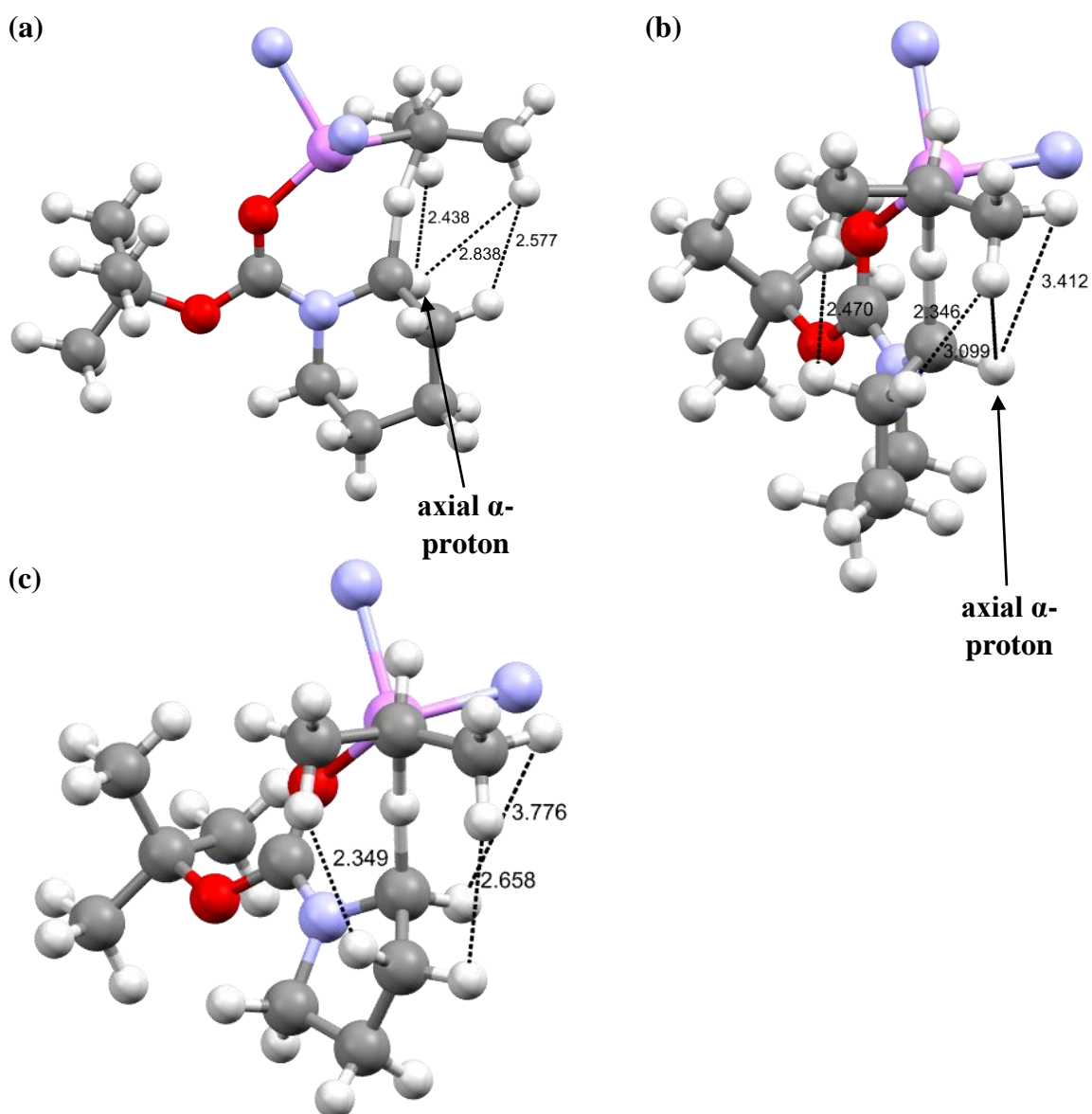


Figure 3.7. Non-bonding distances between *i*-PrLi and *N*-Boc heterocycle for the ‘side-on’ lithiation of *N*-Boc piperidine **10 (a), ‘top’ lithiation of *N*-Boc piperidine **10** (b) and lithiation of *N*-Boc pyrrolidine **9** (c) (C and H atoms of the di-methyl bispidine ligand **195** are hidden for clarity)**

The results in Table 3.2 also indicate that the modelling of the lithiation of *N*-Boc piperidine **10** with MP2 and DFT provided ΔG^\ddagger values for the lithiation with a larger variance to those calculated for *N*-Boc pyrrolidine **9**. For the α -lithiation of *N*-Boc pyrrolidine **9**, the three computational methods used provided ΔG^\ddagger values for the reaction that varied by ~ 0.1 - 0.2 kcal mol⁻¹. However, for the lithiation of *N*-Boc piperidine **10** these calculated ΔG^\ddagger varied more significantly by ~ 0.5 - 1.3 kcal mol⁻¹. The difference between the ΔG^\ddagger values calculated

by MP2 and B3LYP was 0.78 kcal mol⁻¹ and between MP2 and M06 was 0.48 kcal mol⁻¹. Clearly, the activation energies calculated with both DFT functionals deviate from the energy calculated using MP2 and this may suggest that dispersion interactions are more significant for the deprotonation of *N*-Boc piperidine **10** than *N*-Boc pyrrolidine **9**, since MP2 should describe dispersion interactions better than DFT.

However, optimisation of the prelithiation complex and transition states for the lithiation of *N*-Boc pyrrolidine **9** and *N*-Boc piperidine **10** at the MP2 level of theory proved difficult. These MP2 calculations are more computationally expensive due to inclusion of electron correlation effects by perturbation of the HF Hamiltonian. HF and DFT calculations scale to N^4 (where N is number of basis functions) whereas MP2 calculations scale to N^5 due to the addition of correlation corrections.¹²⁰ The calculations also proved difficult due to the flat potential energy surfaces of both the prelithiation complex and transition state and required analytical calculation of the second derivatives of energy (Hessian matrix) for each iteration of the geometry optimisation (using the Opt=CalcAll keyword in GAUSSIAN 09). Calculation of the second derivatives of energy during every step of the optimisation made the calculation extremely computationally expensive. The MP2 optimisation of the prelithiation complex and transition state for the α -lithiation of *N*-Boc pyrrolidine **9** required nearly one month of calculation time on an 8-core CPU. For comparison, the same optimisation using the B3LYP or M06 DFT functional required only two days using 2 CPU cores. Therefore, optimisation using the MP2 method was used only for *N*-Boc pyrrolidine **9** and *N*-Boc piperidine **10** due to the large computational expense involved and is not used in any of the modelling discussed further in this Chapter.

3.2 Use of DFT to Explore the α -Lithiation for a Range of *N*-Boc Heterocycles

3.2.1 Modelling the α -lithiation of *N*-Boc heterocycles to probe reactivity

With the modelling of the *i*-PrLi/di-methyl bispidine **195** α -lithiations of both *N*-Boc pyrrolidine **9** and *N*-Boc piperidine **10** complete, we next focussed on modelling the α -lithiation reactions of a wider range of *N*-Boc heterocycles. To this end, the *i*-PrLi/di-methyl bispidine **195** lithiation reactions of the 14 substrates included in the experimental *s*-BuLi/TMEDA reactivity study in section 2.1 were modelled with DFT. The structures of these 14 *N*-Boc heterocycles are shown in Figure 3.8.

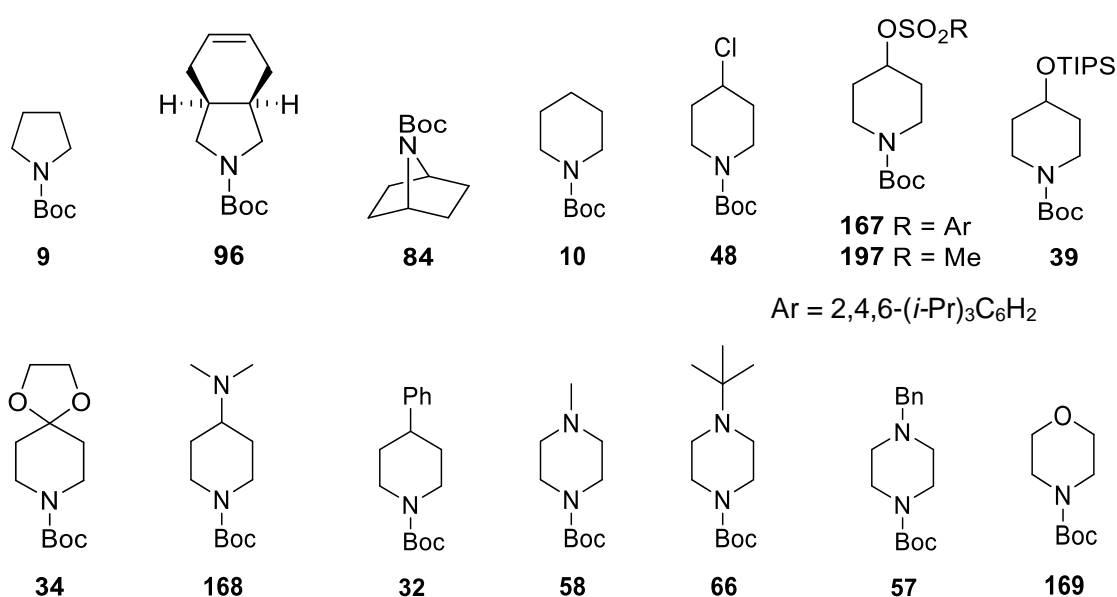


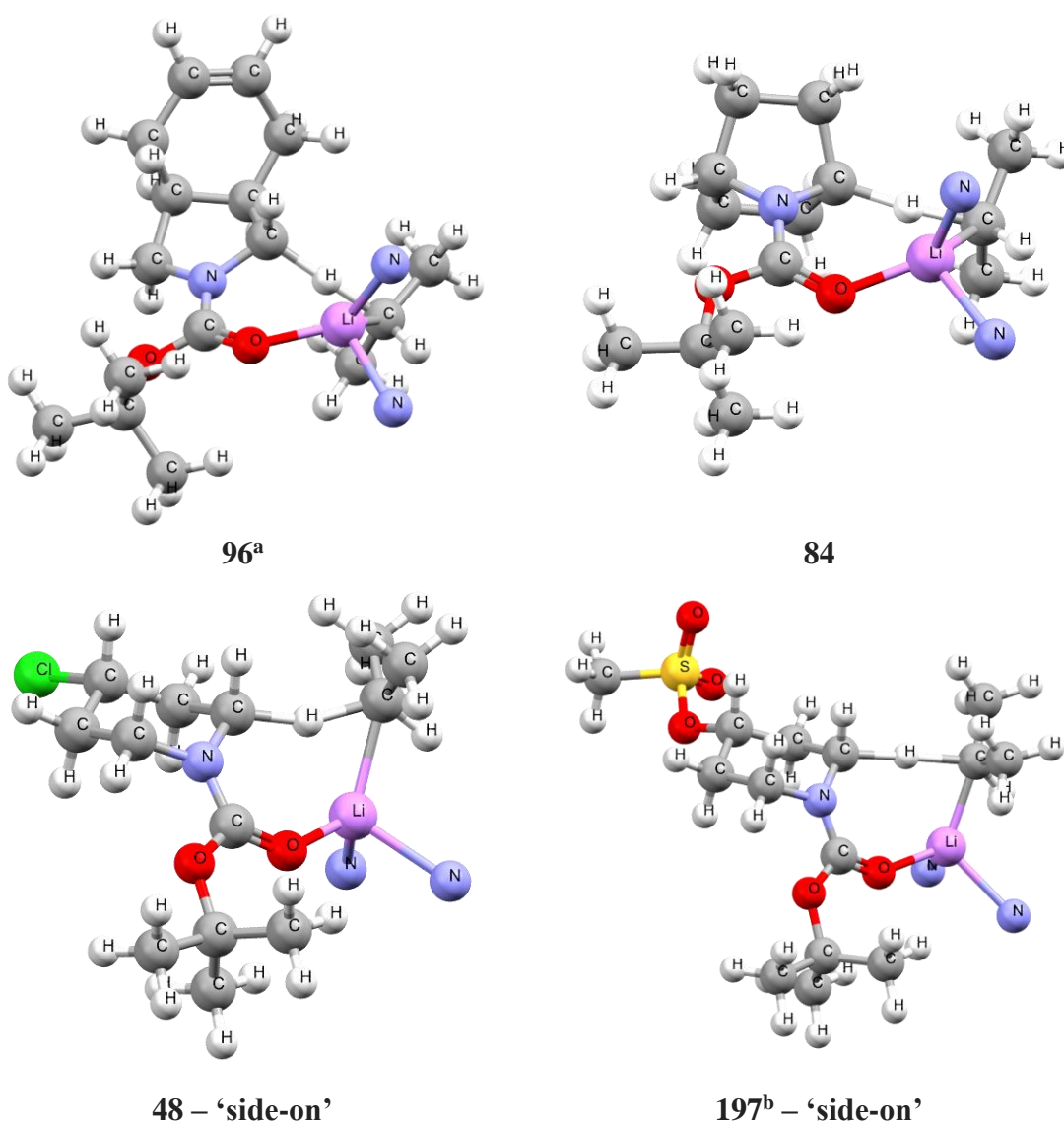
Figure 3.8. *N*-Boc heterocycles included in the DFT reactivity study

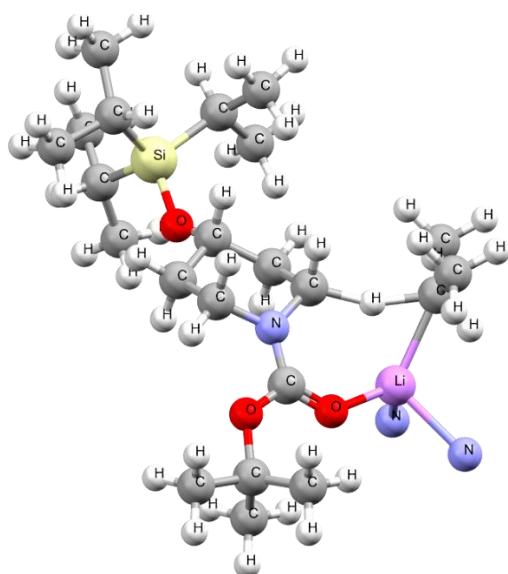
α -Lithiation reactions of each *N*-Boc heterocycle were modelled using the B3LYP and M06 DFT functionals used previously. It was envisaged that DFT modelling might be able to reproduce the reactivity differences observed experimentally with the different *N*-Boc heterocycles, as it had done for the α -lithiations of *N*-Boc pyrrolidine **9** and *N*-Boc piperidine **10**. This would provide useful information about whether the structural features of the substrates were responsible for the differences in the rates of lithiation observed.

The B3LYP optimised geometries of the transition states for the α -lithiation of the 12 additional *N*-Boc heterocycles are presented in Figure 3.9. For the lithiation of 4-*O*-trisyl *N*-Boc piperidine **167**, the lithiation of a similar *N*-Boc heterocycle 4-*O*-mesyl piperidine **197** was modelled instead, to reduce the computational complexity of the calculation. Both ‘side-

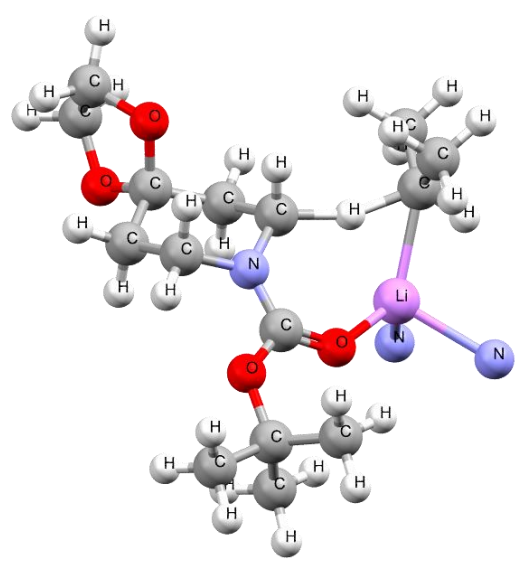
on' and 'top' faces of attack for the *i*-PrLi/di-methyl bispidine **195** were modelled for all of the six-membered heterocycles, which included *N*-Boc piperidine **10** (discussed earlier), *N*-Boc morpholine **169**, 4-substituted piperidines **32**, **34**, **39**, **48**, **168**, **197** and piperazines **57**, **58** and **66**. Only the optimised geometry for the lowest energy type of deprotonation is included in Figure 3.9.

Figure 3.9. α -Lithiation transition state geometries for the 12 additional *N*-Boc heterocycles (excluding *N*-Boc pyrrolidine **9** and *N*-Boc piperidine **10** – see Figure 3.8), the preferred type of deprotonation for 6-membered rings 'side-on' or 'top' is noted next to the compound number

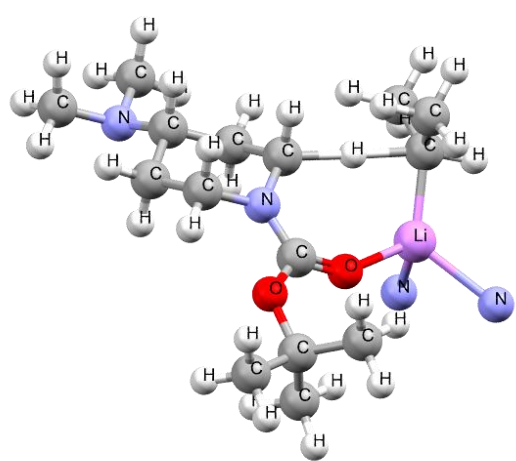




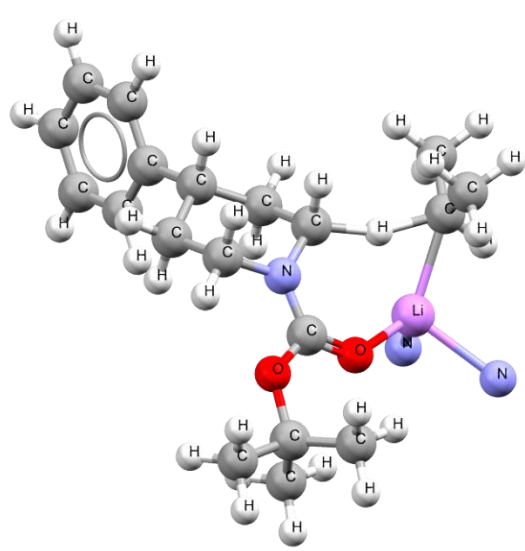
39 – ‘side-on’



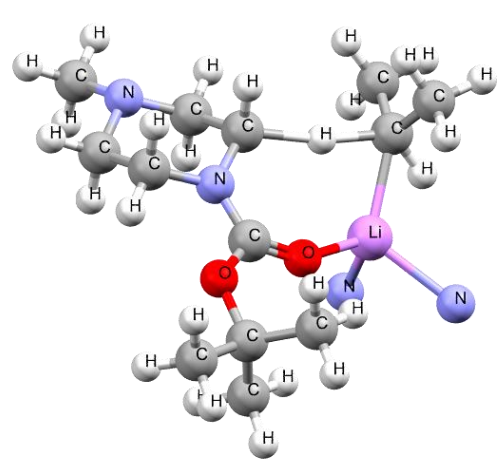
34 – ‘side on’



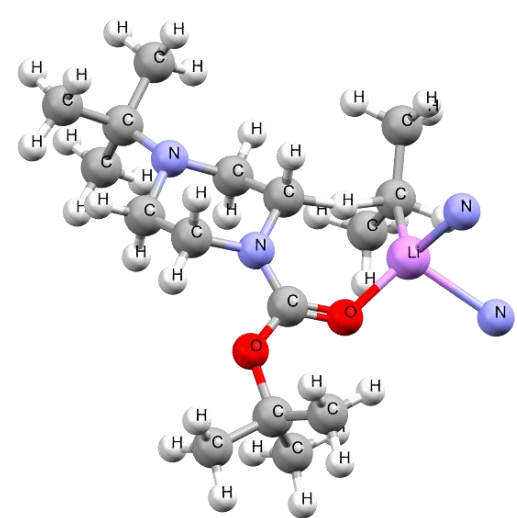
168 – ‘side-on’



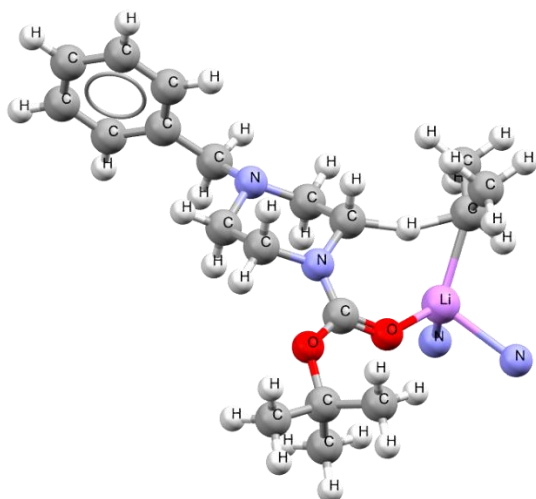
32 – ‘side-on’



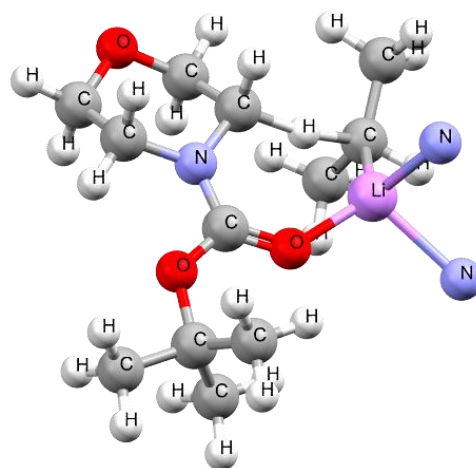
58 – ‘side-on’



66 – ‘top’



57 – ‘side-on’



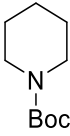
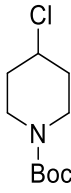
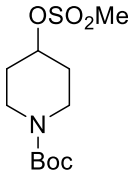
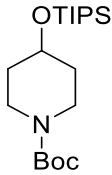
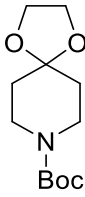
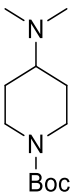
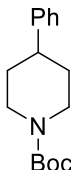
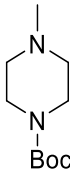
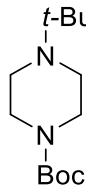
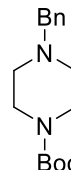
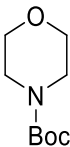
169 – ‘top’

^a α -lithiation of *N*-Boc pyrrolidine **96** can occur either *cis* or *trans* to the cyclohexyl ring, lithiation *trans* to the ring is lower energy and is used for this reactivity study (computational modelling of the *cis/trans* selectivity of *N*-Boc pyrrolidine **96** lithiation is described in Chapter 5).

^b to simplify modelling, 4-*O*-trisylyl *N*-Boc piperidine **167** was modelled as 4-*O*-mesylyl piperidine **197**.

In general, when the lithiation reactions of the 6-membered heterocycles were modelled with the B3LYP DFT functional, the ‘side-on’ deprotonation was favoured. Only for *N*’-*t*-Bu piperazine **66** and *N*-Boc morpholine **169** was the ‘top’ deprotonation lowest in energy. In contrast, when the α -lithiations of these same 6-membered heterocycles were optimised using the M06 DFT functional, there was no clear preference for either of the *i*-PrLi orientations. The lowest energy pathways for α -deprotonation of the 6-membered heterocycles with both the B3LYP and M06 DFT calculations are summarised in Table 3.3.

Table 3.3. Lowest energy *i*-PrLi orientation for the α -lithiation of 6-membered *N*-Boc heterocycles with B3LYP and M06 DFT functionals

					
	10	48	197	39	34
B3LYP	'side-on'	'side-on'	'side-on'	'side-on'	'side-on'
M06	'top'	'side-on'	'side-on'	'top'	'side-on'
					
	168	32	58	66	57
B3LYP	'side-on'	'side-on'	'side-on'	'top'	'side-on'
M06	'top'	'side-on'	'top'	'top'	'top'
					
	169				
B3LYP	'top'				
M06	'side-on'				

Free energies of activation (ΔG^\ddagger) were calculated for the α -lithiations of each of the 14 *N*-Boc heterocycles in Figure 3.8 with the B3LYP and M06 DFT functionals. These are presented in the experimentally determined order of reactivity in Table 3.4. All of the calculated ΔG^\ddagger values were corrected to a temperature of -78 °C, the temperature at which the lithiations were carried out experimentally. The experimentally determined half-lives ($t_{1/2}$) for the lithiation reactions of all 14 substrates are shown along with the computationally calculated ΔG^\ddagger , to allow comparison between the theoretical and experimentally determined reactivities for the substrates. For the substrates **169**, **48**, **167/197** and **96** for which kinetic analysis was conducted in Chapter 2, the reaction half-lives were estimated using $t_{1/2} = t_{\text{lith}}/7$ (as 7 $t_{1/2}$ s = 99% conversion). The ΔG^\ddagger values presented in Table 3.4 for each of the 6-membered heterocycles are taken from the whichever lithiation ('side-on' or 'top') has the lowest ΔG^\ddagger value (see Table 3.3).

Table 3.4. *N*-Boc heterocycle experimentally obtained reactivities ($t_{1/2}$) and B3LYP/M06 calculated activation free energies

	computational DFT study					experimental ReactIR™ study					
	169	48	167/197	58	57		9	96	84	66	39
$t_{1/2} / \text{s}$	< 9 ^b	< 17 ^b	< 17 ^b	18.7 ± 1.8	18.3 ± 0.9		20.7 ± 0.9	< 34 ^b	84.9 ± 4.4	105 ± 3	320 ± 8
ΔG^\ddagger (B3LYP) ^a	12.61	12.68	13.11 ^c	14.59	14.43		13.77	14.55	15.01	15.15	14.86
ΔG^\ddagger (M06) ^a	11.79	11.67	12.96 ^c	13.85	13.48		13.63	13.36	13.85	14.63	13.07
	34	32	168	10							
$t_{1/2} / \text{s}$	624 ± 22	642 ± 5	1040 ± 20	3190 ± 30							
ΔG^\ddagger (B3LYP) ^a	15.45	15.20	15.58	16.11							
ΔG^\ddagger (M06) ^a	13.43	14.24	14.23	14.85							

^a DFT calculated activation free energies reported in kcal mol⁻¹

^b kinetic data not available; $t_{1/2}$ estimated using lithiation time ($t_{1/2} = t_{\text{lit}}/7$)

^c DFT results for 4-*O*-trisyl piperidine **167** (R = 2,4,6-*i*-Pr)₃C₆H₂) were obtained by modelling the lithiation of 4-methanesulfonyl *N*-Boc piperidine **197** (R = Me)

By inspection of the experimental $t_{1/2S}$ and theoretical ΔG^\ddagger values in Table 3.4, a correlation between theory and experiment is observed for the lithiation of the *N*-Boc heterocycles. As expected, this general trend indicated that for most substrates the calculated energy barrier of the lithiation ΔG^\ddagger increases as the substrates become less reactive with larger experimental $t_{1/2S}$ observed.

Many of the reactivity trends observed experimentally that were attributed to key structural features of the *N*-Boc heterocycles were reproducible with the DFT modelling. For example, the DFT modelling with B3LYP and M06 functionals indicated that the 5-membered pyrrolidine substrates **9**, **96** and **84**, were more reactive than *N*-Boc piperidine **10**. Additionally, DFT modelling reproduced the activating effects that were observed for the 6-membered *N*-Boc piperidines, when either a heteroatom was included in the ring or when a C-4 substituent was present. For example, DFT modelling with B3LYP and M06 functionals indicated that morpholine **169** and piperazines **58**, **57** and **66** are more reactive than *N*-Boc piperidine **10**. For the 4-substituted piperidines, the DFT modelling could predict the magnitude of the activating effect for many of the C-4 substituents. For example, the 4-chloro and 4-*O*-trisyl piperidines **48** and **167/197** were found to be much more reactive than 4-amino piperidine **168** using the DFT modelling with B3LYP and M06 functionals.

At this present time, no further computational evidence for these activating effects or another rationale for the large differences in reactivity observed in the substrates can be suggested. The dihedral angle between the α -proton that is deprotonated and the carbonyl of the carbamate was measured in the prelithiation complexes of the 14 substrates, to establish if there was any relationship between this angle and the rate of lithiation. It could be envisaged that different dihedral angles may affect the coordination of the alkyllithium during the lithiation and affect how facile the reaction is. No trend between this dihedral angle and the rate of lithiation was observed for the *N*-Boc heterocycles studied. This same analysis was conducted by Gross and Beak for the lithiation of cyclic carbamates using competition experiments and they also noted that no correlation between the dihedral angle and rate of lithiation was observed.¹²¹

Both DFT functionals did produce outlying results for a few of the *N*-Boc heterocycles, where the reactivity order did not match that observed experimentally. For example, the B3LYP functional suggested that *N'*-Bn and *N'*-Me piperazines **57** and **58** are less reactive than observed by experiment. The calculated ΔG^\ddagger values for both of these piperazines

suggest that they were less reactive than *N*-Boc pyrrolidine **9** but the experimental $t_{1/2}$ values suggest that they are either more reactive or have similar reactivity to that of *N*-Boc pyrrolidine **9**. Also, the M06 DFT functional suggested that *N'*-*t*-Bu piperazine **66** should be one of the least reactive *N*-Boc heterocycles, with a similar reactivity to *N*-Boc piperidine **10**. However, experiment indicated the *s*-BuLi/TMEDA lithiation of *N'*-*t*-Bu piperazine **66** is ~30 times faster than that of *N*-Boc piperidine **10**.

Another outlier arose when the lithiation of 4-OTIPS piperidine **39** was modelled with DFT. Calculation of the ΔG^\ddagger for the *i*-PrLi/di-methyl bispidine lithiation **195** of 4-OTIPS piperidine **39** with M06 DFT functional suggested this substrate is extremely reactive, with a similar reactivity predicted to that of 4-*O*-trisyl piperidine **167/197**. However, the experimental study found that 4-OTIPS piperidine **39** is in fact ~20 times less reactive than 4-*O*-trisyl piperidine **167/197** with *s*-BuLi/TMEDA. Modelling with the B3LYP DFT functional also suggested that the 4-OTIPS piperidine **39** was more reactive than observed experimentally but by a much smaller margin, suggesting a reactivity between that of 3,4-disubstituted *N*-Boc pyrrolidine **9** and bicyclic pyrrolidine **84**.

The differing trends and outliers observed with each of the DFT functionals highlight an important point; different computational methods may not provide the same results. When using computational modelling to help understand chemical reactivity it is important to consider the level of theory and for DFT, the functional that is used. This is one of the primary reasons why two different DFT functionals were used for the computational modelling in this study.

With so many different *N*-Boc heterocycles and such a large quantity of reactivity data, it was difficult to judge precisely the quality of the trend between theory and experiment. Therefore, a method that allowed the linear correlation of these two sets of data was required, as this would enable the correlation between the experimental and theoretical results to be analysed quantitatively. This was achieved using the Eyring equation which relates both the rate constant k and activation energy for a reaction (ΔG^\ddagger) at a temperature T (Equation 3.1).

$$k = \frac{k_B T}{h} e^{-\frac{\Delta G^\ddagger}{RT}} \quad \text{(Equation 3.1)}$$

Using a linear form of this equation allowed linear regression of the experimentally obtained k_{obs} values for the *N*-Boc heterocycle substrates and the computationally predicted ΔG^\ddagger s (Equation 3.2). In this linear form of the Eyring equation, the experimentally obtained

$\ln(k_{\text{obs}})$ data can be plotted against the computationally obtained ΔG^\ddagger and the correlation between the two sets of data can be analysed.

$$\ln k_{\text{obs}} = -\Delta G^\ddagger \frac{1}{RT} + \ln \frac{k_B T}{h}$$

$y = mx + c$ where:

$$y = \ln k_{\text{obs}}, m = -\frac{1}{RT} \text{ and } c = \ln \frac{k_B T}{h} \quad \text{(Equation 3.2)}$$

This Eyring regression was first applied to the theoretical and experimental results for the lithiation reactions for all of the 14 *N*-Boc heterocycles included in Table 3.4. The experimentally obtained $\ln k_{\text{obs}}$ values were plotted *versus* the calculated ΔG^\ddagger values obtained with both B3LYP and M06 DFT functionals (ΔG^\ddagger values are in kJ mol^{-1} to allow analysis of the gradient) (Figure 3.10). Error bars are not included for the $\ln k_{\text{obs}}$ values as the k_{obs} standard error obtained by the kinetic analysis is too small to observe on the logarithmic scale.

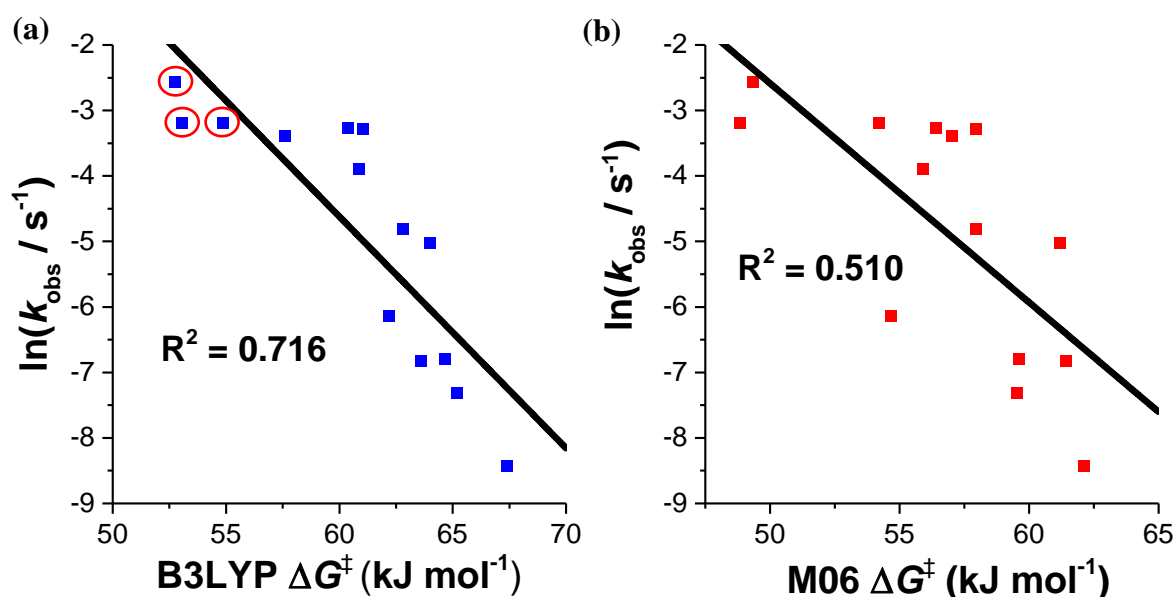


Figure 3.10. Eyring linear regressions for experimentally obtained k_{obs} and calculated ΔG^\ddagger values for the lithiation of the 14 *N*-Boc heterocycle substrates in Table 3.4

The Eyring analysis with the B3LYP calculated ΔG^\ddagger values for the *N*-Boc heterocycles in Table 3.4 provided a promising correlation ($R^2 = 0.716$) between theory and experiment. On the other hand, the ΔG^\ddagger values calculated with the M06 DFT functional provided only a moderate correlation with experiment ($R^2 = 0.510$). The Eyring analysis for each DFT

functionals indicated that the three substrates with rapid lithiation **169**, **48** and **167/197** with estimated $t_{1/2}$ s, deviated from the trend line. This was particularly evident for ΔG^\ddagger values calculated with B3LYP which are circled in Figure 3.10.a. These outliers are likely due to large amounts of error in the experimental data which are further compounded by the rapid rates of reaction. Therefore, it was decided to remove the substrates for which $t_{1/2}$ was estimated from the Eyring analysis, including **169**, **48**, **167/197** and cyclohexyl pyrrolidine **96** and re-evaluate the trend between theory and experiment for the remaining 10 *N*-Boc heterocycles (Figure 3.11).

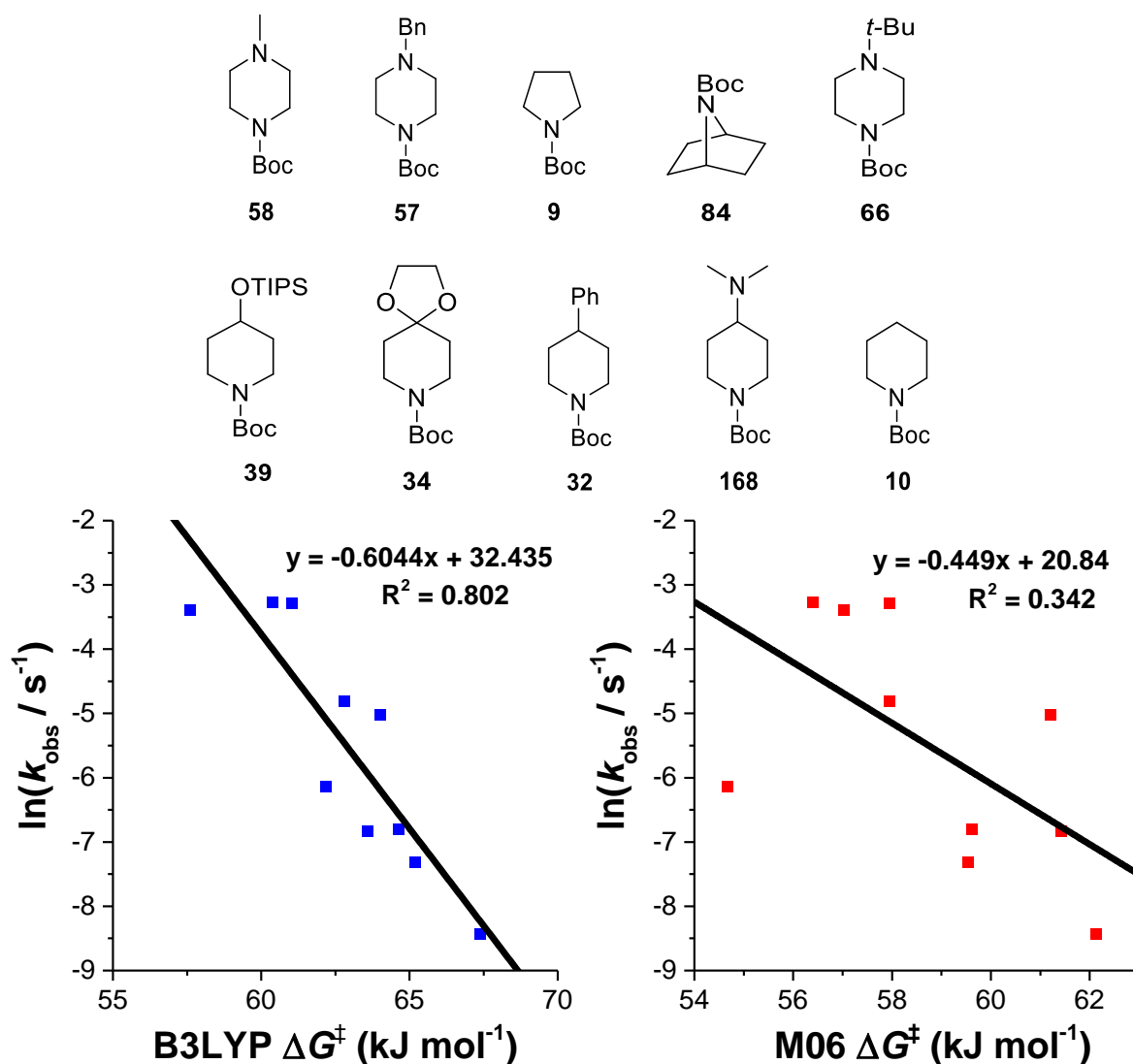


Figure 3.11. Eyring linear regressions for experimentally obtained k_{obs} and calculated ΔG^\ddagger for the lithiation for the 10 *N*-Boc heterocycle substrates above

Upon removal of the *N*-Boc heterocycles with estimated $t_{1/2}$ s, a considerable difference in the correlations between experiment and theory were observed. The ΔG^\ddagger values calculated using the B3LYP DFT functional now provided a good correlation ($R^2 = 0.802$) with the

experimental results. However, it was noted that the lithiation reactions of the three fastest substrates of the 10, pyrrolidine **9** and *N*'-Bn and *N*'-Me piperazines **57** and **58**, all had very similar experimental reactivities but the calculated ΔG^\ddagger values suggested they would have more notable differences in reactivity. This could be due to deficiencies in the modelling or the larger margins of experimental error for these fast lithiating substrates, as discussed in Chapter 2. The ΔG^\ddagger values calculated with M06 DFT functional still provided poor correlation with experiment. The quality of the fit can also be assessed by analysis of the gradient of the line of best fit plotted through the regression of the theoretical and experimental data for the 10 *N*-Boc heterocycles. For these Eyring linear analyses, the gradient is expected to equal $-1/RT$ as stated in Equation 3.2, where *R* is the universal gas constant and *T* is the temperature. In this case, *T* is equal to 195 K as the experimental reactions are conducted at -78 °C and all the free energies (ΔG) calculated have been corrected to 195 K. Therefore, the gradient of the line of best fit is expected to equal:

$$m = -\frac{1}{RT} = \frac{1}{8.314 \times 10^{-3} \times 195} = -0.617 \text{ kJ}^{-1} \text{ mol}$$

For the Eyring regression using the ΔG^\ddagger values calculated using the B3LYP DFT functional the gradient of the line of best fit was equal to $-0.604 \text{ kJ mol}^{-1}$. This is very close to the value expected and therefore provides further evidence of a good fit between experiment and theory. The line of best fit from the Eyring analysis of the M06 calculated results provided a gradient of $-0.449 \text{ kJ mol}^{-1}$ which differed significantly to what was expected. The gradient provided by the M06 results as well as the poor correlation between theory and experiment suggests that modelling with the M06 DFT functional does not provide an accurate description of this system.

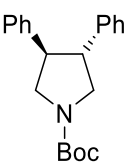
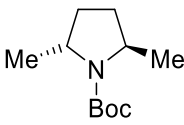
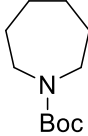
In summary, DFT modelling of the α -lithiation reactions of different *N*-Boc heterocycles does describe many of the reactivity differences that were observed experimentally. The DFT modelling does not perfectly describe the reactivity of each substrate but does account for most of the large differences in reactivity between substrates that were observed experimentally. The Eyring regression analysis indicates a good overall correlation between the B3LYP calculated ΔG^\ddagger values and experimental reactivity data. This promising correlation between theory and experiment provides an interesting avenue of further investigation which is described in the next section of this Chapter.

3.2.2 Using DFT modelling to predict reactivities of unknown *N*-Boc heterocycles

If a good correlation between the DFT modelling results and the experimentally obtained reactivities is observed, it may be possible to use DFT modelling to predict the reactivity of *N*-Boc heterocycles for which reactivity is unknown. Even if modelling could only suggest whether the lithiation would be slow (> 2 h), occur at a moderate rate (5 min to 2 h) or was fast (< 5 min), this could be of great use to a synthetic chemist. This estimated reactivity would provide information about whether the lithiation is feasible and if so, provide an idea of the reaction conditions (*e.g.* reaction temperature) that would be required. This would allow the suitability of the α -lithiation of a novel substrate to be assessed without any synthetic or kinetic work being done beforehand.

As the ΔG^\ddagger values calculated with the B3LYP DFT functional had provided a promising correlation with the experimentally obtained kinetic data, it was decided to use the Eyring regression in Figure 3.11 to attempt to predict the reactivity of *N*-Boc heterocycles for which reactivity is unknown. Hence, the *i*-PrLi/di-methyl bispidine **195** lithiation reactions of three *N*-Boc heterocycles with unknown reactivities *anti*-**97**, **198** and **192**, were modelled using the B3LYP DFT functional. The *s*-BuLi/(–)-sparteine lithiation of di-phenyl pyrrolidine *anti*-**97** had been reported previously but no reactivity data was collected (see Scheme 1.32).⁴ The lithiation of 2,5-dimethyl piperidine **198** has not been reported and it was expected that the lithiation would have a high activation energy barrier at –78 °C due to the methyl groups at each of the α -positions. The lithiation of 7-membered *N*-Boc azepane **192** has been reported using higher reaction temperatures (–40 °C) but the rate of lithiation was not studied;⁴⁰ preliminary in-group data suggests that *N*-Boc azepane **192** is less reactive than *N*-Boc piperidine **10**.⁵³ For each of the three *N*-Boc heterocycles, ΔG^\ddagger was calculated for the respective *i*-PrLi/di-methyl bispidine **195** lithiation. Using these calculated ΔG^\ddagger values, a k_{obs} for the *s*-BuLi/TMEDA lithiation of each substrate was predicted by interpolation/extrapolation of the Eyring regression obtained with the B3LYP calculated ΔG^\ddagger values in Figure 3.11. These estimated k_{obs} values have been converted to a predicted $t_{1/2}$ and predicted lithiation time for each substrate and are presented in Table 3.5.

Table 3.5. B3LYP calculated ΔG^\ddagger and predicted $t_{1/2}$ (at -78°C) for *N*-Boc heterocycles *anti*-97**, **198** and **192** with unknown reactivities**

	 <i>anti</i> - 97	 198	 192
ΔG^\ddagger / kcal mol ⁻¹	11.94	16.57	16.11
ΔG^\ddagger / kJ mol ⁻¹	49.96	69.33	67.40
Predicted $t_{1/2}$ / s	0.074	8920	2790
Predicted t_{lith} ^a	0.5 s	17 h	5.5 h

^a the predicted t_{lith} was calculated using 7 half-lives for 99% conversion ($t_{\text{lith}} = t_{1/2} \times 7$)

The DFT modelling suggests that di-phenyl pyrrolidine *anti*-**97** is very reactive, with a very small $t_{1/2} = 0.074$ s predicted for the lithiation of pyrrolidine *anti*-**97** with *s*-BuLi/TMEDA. This small predicted $t_{1/2}$ for the *s*-BuLi/TMEDA of pyrrolidine *anti*-**97** would mean only 0.5 s would be required for 99% conversion. The DFT modelling therefore suggests that the phenyl groups on the 3,4-positions of the pyrrolidine ring will have a significant activating effect on the reactivity of this pyrrolidine substrate. As theorised, the DFT modelling predicted a prohibitively high energy barrier for the *s*-BuLi/TMEDA lithiation of 2,5-dimethyl pyrrolidine **198**, with a large $t_{1/2} = 8920$ s that translates to a 17 h reaction time for 99% conversion. The DFT modelling predicted that the *s*-BuLi/TMEDA lithiation *N*-Boc azepane **192** would require 5.5 h with a similar reactivity to that of *N*-Boc piperidine **10** (azepane **192** predicted $t_{1/2} = 2790$, piperidine **10** $t_{1/2} = 3190$ s). Previous work in the O'Brien group suggests that *N*-Boc azepane **192** lithiation is slower than *N*-Boc piperidine **10** so the modelling may not provide a very accurate estimate of lithiation time for this substrate. However, the modelling still predicts that *N*-Boc azepane **192** will be on the lower end of the reactivity spectrum. For the *s*-BuLi/TMEDA lithiation of both 2,5-dimethyl pyrrolidine **198** and *N*-Boc azepane **192**, the predictive method developed indicates that higher reaction temperatures may be required for complete lithiation to occur. Furthermore, the suggested low reactivity of 2,5-dimethyl pyrrolidine **198** may suggest that the lithiation is unfeasible due to the very high energy barrier for lithiation.

3.2.3 Modelling the *i*-PrLi/TMEDA lithiation of *N*-Boc heterocycles

During this computational investigation, di-methyl bispidine **195** was selected as the diamine ligand used to model the lithiation instead of TMEDA due to its rigidity which was expected to make the location of a minima easier. It was thought that a diamine ligand such as TMEDA would complicate the modelling, as the flexibility of the ligand would provide a shallow potential energy surface, making location of a minima more difficult. However, when modelling the *i*-PrLi/TMEDA lithiation of *N*-Boc pyrrolidine **9** was conducted, the flexibility of TMEDA added little additional computational expense to the calculation.

To investigate whether the use of di-methyl bispidine **195** rather than TMEDA in the modelling affected the correlation observed between the theoretical and experimental results, the lithiation of a selection of *N*-Boc heterocycles were modelled using *i*-PrLi/TMEDA. Six of the *N*-Boc heterocycles modelled previously which spanned a wide range of reactivities were modelled using the B3LYP DFT functional and *i*-PrLi/TMEDA lithiating conditions. The geometries of the optimised prelithiation complexes and transition states of the lithiation with *i*-PrLi/TMEDA did not differ substantially when the diamine used in the model was changed. In addition, the preference for ‘side-on’ or ‘top’ deprotonation by *i*-PrLi/TMEDA for each of the five 6-membered heterocycles was the same observed when *i*-PrLi/di-methyl bispidine **195** was modelled as the lithiating complex.

When the *i*-PrLi/TMEDA calculated ΔG^\ddagger values were compared with the experimentally determined k_{obs} by Eyring linear regression analysis, a very similar correlation was observed to that obtained when the *i*-PrLi/di-methyl bispidine **195** lithiation was modelled (Figure 3.12). The Eyring regressions for the two different lithiating conditions that were modelled provided linear regressions with very similar gradients and R^2 values (0.770 and 0.799). These results suggested that the identity of the diamine used in the modelling may not have any significant effect on trends of reactivity observed for substrates. Therefore, modelling the *i*-PrLi/di-methyl bispidine **195** lithiations of the substrates and making predictions for the *s*-BuLi/TMEDA lithiation should not provide outliers due to the use of a different diamine ligand in the DFT modelling.

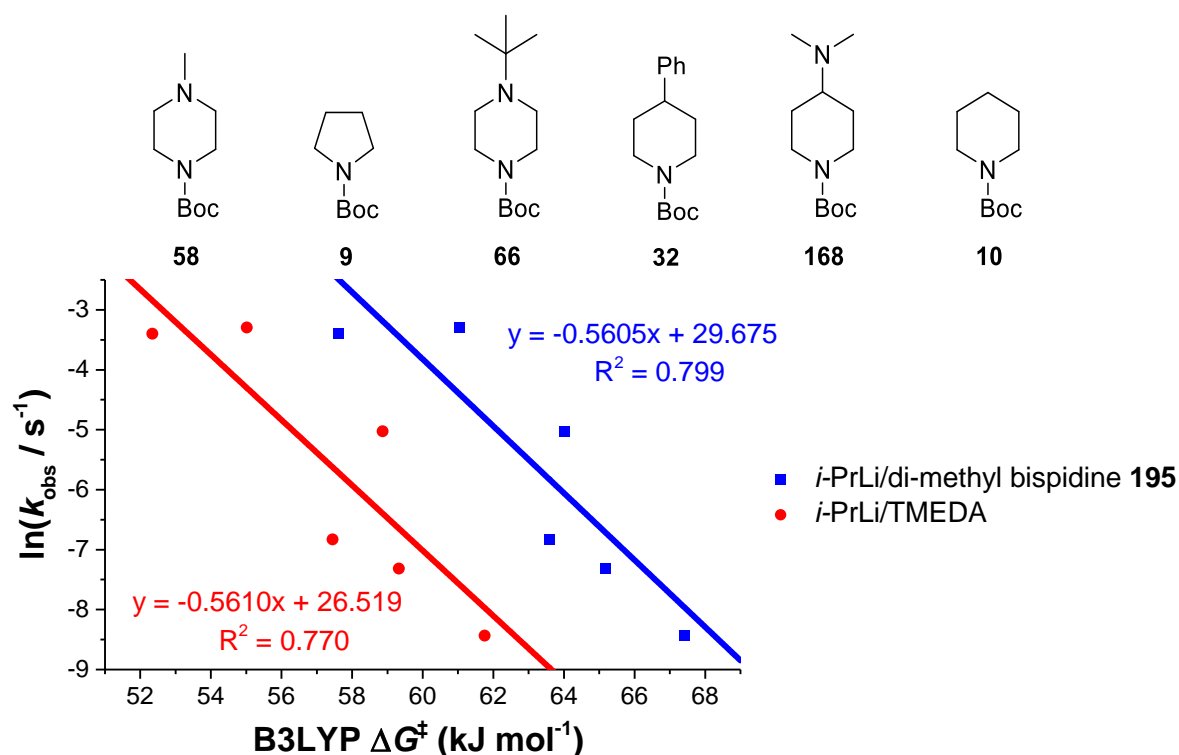


Figure 3.12. Eyring regression analysis for the *i*-PrLi/di-methyl bispidine **195 and *i*-PrLi/TMEDA modelled lithiation reactions of six *N*-Boc heterocycles**

3.2.4 Application of solvent corrections to the modelling of the lithiation of *N*-Boc heterocycles

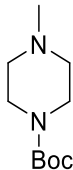
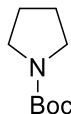
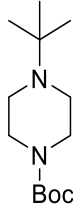
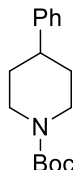
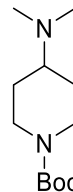
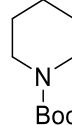
The effect that the inclusion of solvent effects has on the DFT modelling of the *i*-PrLi/di-methyl bispidine **195** lithiation was also subjected to investigation. Solvent can be modelled either explicitly, where molecules of solvent are included in the geometry that is optimised, or implicitly, where the solvent is treated as a continuum medium which is characterised by its dielectric constant and other electrostatic parameters. For the implicit modelling of solvent, the molecule to be optimised is placed into a cavity inside this medium and electrostatic properties can be calculated on points on the boundary between the cavity and the solvent field. Modelling of the solvent by implicit or explicit methods both have advantages and disadvantages.¹²² For example, explicit solvation is generally more accurate as specific solvent interactions with the molecule modelled are accounted for, whereas the treatment of solvent as an electrostatic field will not reproduce these interactions. On the other hand, the treatment of the solvent as a continuum with only a few parameters is considerably less computationally expensive than the inclusion of solvent molecules to the

geometry that is optimised. As the α -lithiation reactions modelled are relatively large systems (~80 atoms), it was opted to model the solvent implicitly so that calculations would not become prohibitively computationally expensive.

The same six *N*-Boc heterocycles used to investigate the effect of modelling with a different diamine in Section 3.2.2, were used to investigate how solvent corrections affected the modelling. The *i*-PrLi/di-methyl bispidine **195** lithiations of each of these six *N*-Boc heterocycles were modelled again using the B3LYP DFT functional with the inclusion of a solvent correction to model the Et₂O solvent used in experiment. This solvent correction was carried out using the Polarizable Continuum Method (PCM) method included in the GAUSSIAN 09 software package.¹²³

The inclusion of the solvent correction did not change the geometries of the prelithiation complexes and transition states for the six *N*-Boc heterocycles and the preference for ‘side-on’ or ‘top’ deprotonation was unchanged by the solvent corrections. However, the solvent corrected calculated ΔG^\ddagger values for the lithiation of the six substrates provided a reactivity order for the six substrates that significantly differed to the reactivity orders obtained by modelling without solvent corrections and by experiment (Table 3.6). For example, 4-phenyl piperidine **32** which displays a moderate reactivity experimentally is predicted to be the most reactive substrate to lithiate when solvent corrections were included. Additionally, *N*-Boc pyrrolidine **9** for which experiment suggests is one of the most reactive substrates, is placed between the two least reactive substrates, 4-amino piperidine **168** and *N*-Boc piperidine **10** in the reactivity series constructed with the solvent corrected DFT calculations.

Table 3.6. Solvent corrected ΔG^\ddagger values for the *i*-PrLi/di-methyl bispidine 195 lithiations of selected *N*-Boc heterocycles and experimentally obtained $t_{1/2}$ for the lithiation

						
	58	9	66	32	168	10
$t_{1/2} / \text{s}$	18.7 ± 1.8	20.7 ± 0.9	105 ± 3	642 ± 5	1040 ± 20	3190 ± 30
ΔG^\ddagger (B3LYP) / kcal mol ⁻¹	14.59	13.77	15.15	15.20	15.58	16.11
Solvent corrected ΔG^\ddagger (B3LYP) / kcal mol⁻¹	16.56	17.21	16.81	16.32	17.14	17.79

The poor correlation of the solvent corrected DFT modelling with experiment became more apparent when Eyring linear regression analysis between the experimental and theoretical results was conducted (Figure 3.13). As mentioned previously, a good correlation between experiment and theory is obtained when calculations are performed in the gas phase. However, a poor correlation ($R^2 = 0.172$) between the solvent corrected B3LYP calculated ΔG^\ddagger values and the experimentally determined k_{obs} was observed. This poor agreement between theory and experiment suggests that modelling with the B3LYP DFT functional with an implicit solvent correction does not provide an appropriate description of the lithiation reaction. It is possible that modelling solvent implicitly may not be suitable for this reaction where coordination of the solvent and alkyllithium species may need to be considered. As implicit solvation only models the solvent as a continuum, the coordination of alkyllithium and solvent is not accounted for. Therefore, for this reaction the explicit modelling of solvent may provide a better description of the solvation during the reaction and provide more accurate reactivity calculations. Unfortunately, explicit solvation is substantially more computationally expensive and hence was not feasible for this study.

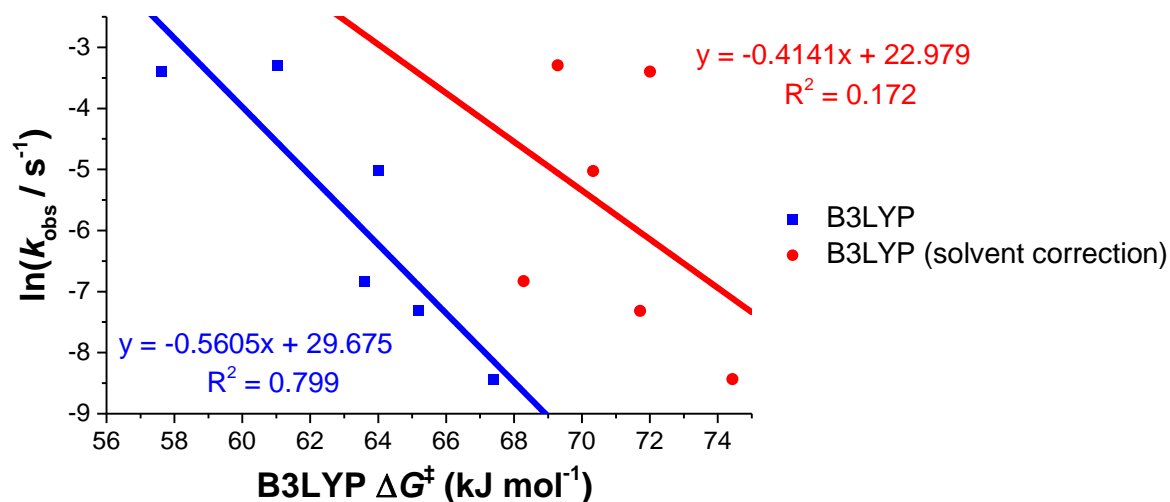


Figure 3.13. Eyring regression analysis for the solvent corrected (blue) and gas phase (red) DFT modelled *i*-PrLi/di-methyl bispidine 195 lithiation of six *N*-Boc heterocycles

In summary, the work presented in this Chapter indicates that the computational DFT modelling can reproduce many of the reactivity differences that were observed experimentally for the *N*-Boc heterocycles studied. Quantification of the correlation between the modelled ΔG^\ddagger values and the experimental k_{obs} indicated that a promising correlation between theory and experiment was observed when the B3LYP DFT functional was used. Preliminary work suggests that the identity of the ligand used in the modelling does not affect the reactivity order of substrates provided by the DFT modelling. The addition of solvent corrections to the modelling did not improve the correlation with experiment and provided some outlying predicted reactivities for substrates. We postulate that implicit modelling of solvent may not be appropriate to describe the lithiation reaction, due to the coordination of the solvent and alkyllithium species that is not specifically accounted for in this solvent model.

3.3 Modelling the Effect of the Ligand on the Rate of the α -Lithiation of *N*-Boc Pyrrolidine

With DFT modelling showing the ability to reproduce many of the reactivity differences of the *N*-Boc heterocycles observed experimentally, we next turned our attention to attempt to reproduce the differences in the rate of lithiation observed when different ligands were used. In section 2.2, we detailed how the rate of lithiation of *N*-Boc pyrrolidine **9** can be significantly altered when different ligands were employed in the lithiation reaction. In an attempt to reproduce the experimentally observed differences in reactivity, the *i*-PrLi/ligand lithiation of *N*-Boc pyrrolidine **9** was modelled using five of the achiral ligands used in the reactivity study presented in Chapter 2 (Figure 3.14). An attempt to model the lithiation of *N*-Boc pyrrolidine **9** with *i*-PrLi/tetra-isopropyl diamine **178** was made but the severe steric bulk of the ligand and overall size of the system meant that the location of minima for the prelithiation complex was not possible. The *i*-PrLi/di-methyl bispidine **195** lithiation of *N*-Boc pyrrolidine was included in this comparison, as the calculation had already been performed for the previous DFT modelling of substrate reactivity in section 3.1. This meant that a prediction for the reactivity of the *s*-BuLi/di-methyl bispidine **195** lithiation complex could be made using the experimental and DFT data collected for the other five ligands.

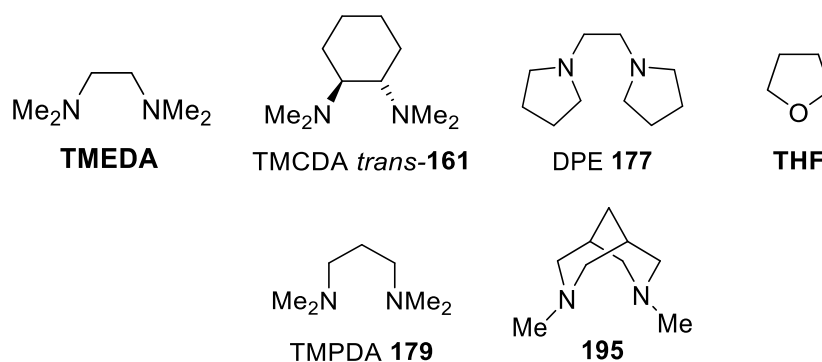
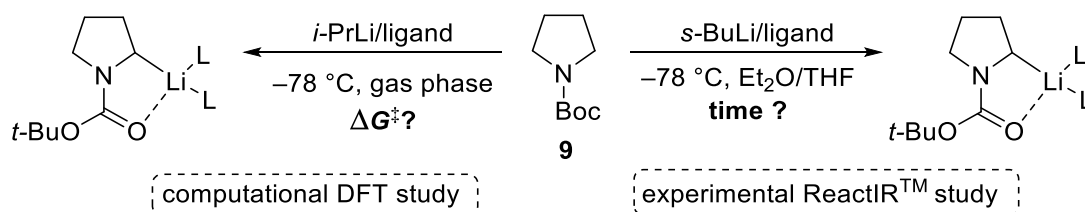


Figure 3.14. Ligands used to model the *i*-PrLi/ligand lithiation of *N*-Boc pyrrolidine **9**

Prelithiation complexes and transition states for the *i*-PrLi/ligand lithiation reactions of *N*-Boc pyrrolidine **9** were constructed for each of the six different ligands. The resulting geometries were optimised using the B3LYP and M06 DFT functionals used previously and the activation free energies (ΔG^\ddagger) for each of the different *i*-PrLi/ligand lithiation reactions were calculated and corrected to -78 °C. The DFT calculated ΔG^\ddagger values for the different *i*-PrLi/ligand lithiation of *N*-Boc pyrrolidine **9** and experimentally determined *s*-BuLi/ligand lithiation times are presented in Table 3.7.

Table 3.7. Calculated *i*-PrLi/ligand lithiation activation free energies (ΔG^\ddagger) and experimental ReactIRTM determined *s*-BuLi/ligand lithiation times for *N*-Boc pyrrolidine 9



Entry	Ligand	ReactIR TM lithiation time	ΔG^\ddagger (B3LYP) / kcal mol ⁻¹	ΔG^\ddagger (M06) / kcal mol ⁻¹
1	TMEDA	4 min	12.51	13.53
2	TMCDA <i>trans</i> -161	4 min	12.88	12.88
3	DPE 177	60 min	13.32	14.84
4	THF	5 h	13.78	14.38
5	TMPDA 179	12 h	12.76	13.18
6	195	??	13.77	13.63

By comparing the experimental and computational results in Table 3.7, it was noted that the B3LYP DFT functional was able to reproduce the experimental ligand reactivity series for each of the five diamines except TMPDA. However, modelling with the M06 DFT functional provided a substantially different reactivity trend for the lithiating complexes that did not correlate with experiment.

Both B3LYP and M06 DFT functionals predicted that the reactivity of the *i*-PrLi/TMPDA complex would be similar to that of the *i*-PrLi/TMEDA and *i*-PrLi/TMCDA *trans*-161

lithiating complexes. In fact, the experimental data indicated that *s*-BuLi/TMPDA **179** provided one of the slowest lithiation reactions of *N*-Boc pyrrolidine **9**, which required 12 h to complete. As discussed previously in Chapter 2, it was thought that the slow rate of lithiation with *s*-BuLi/TMPDA **179** may arise from a lack of coordination of the alkyllithium and that it is actually *s*-BuLi/Et₂O lithiation that occurs. The DFT modelling explicitly modelled the TMPDA **179** diamine coordinated to the alkyllithium, so will not account for preferential coordination of the alkyllithium to the solvent rather than diamine. This is the likely reason why the DFT modelling suggests that *i*-PrLi/TMPDA **179** lithiation is more facile than was observed experimentally with *s*-BuLi/TMPDA **179**.

Even though the B3LYP predicted the correct trend in reactivity for the *i*-PrLi/DPE **177** and *i*-PrLi/THF lithiations of *N*-Boc pyrrolidine **9**, the functional provided only a small 0.46 kcal mol⁻¹ difference in activation energy for each reaction. However, the experimental results showed that a significant ~5-fold difference in reactivity resulted with the two different lithiating complexes. This magnitude of reactivity difference should require a more substantial difference in the activation energies for the two different lithiations (~1.5 kcal mol⁻¹). Conversely, DFT modelling with the M06 functional suggested that *i*-PrLi/DPE **177** is less reactive than *i*-PrLi/THF for the lithiation of *N*-Boc pyrrolidine **9**, contradicting the experimental results.

Modelling with the M06 functional also suggested that the *i*-PrLi/TMEDA and *i*-PrLi/TMCDA *trans*-**161** lithiations of pyrrolidine **9** have a significant 0.65 kcal mol⁻¹ difference in activation energy. However, the experimental results indicated that *s*-BuLi/TMEDA and *s*-BuLi/TMCDA *trans*-**161** have similar reactivities with complete lithiation of *N*-Boc pyrrolidine **9** requiring 4 min for both of the *s*-BuLi/diamine complexes.

The B3LYP DFT modelling suggests that the *i*-PrLi/di-methyl bispidine **195** complex has a similar reactivity to that of *i*-PrLi/THF, with near identical calculated ΔG^\ddagger values of 13.77 kcal mol⁻¹ and 13.88 kcal mol⁻¹ respectively, for the lithiation of *N*-Boc pyrrolidine **9**. Therefore, modelling with B3LYP advocates that the *s*-BuLi/ di-methyl bispidine **195** lithiation of pyrrolidine **9** will require several hours, with similar reaction time to that of the 5 h *s*-BuLi/THF lithiation. The M06 DFT functional does not provide a clear trend with the experimental results, so prediction of the reactivity of the *s*-BuLi/di-methyl bispidine **195** lithiating complex is unreliable. However, the similar ΔG^\ddagger values calculated for the *i*-PrLi/di-methyl bispidine **195** and *i*-PrLi/TMEDA lithiations of *N*-Boc pyrrolidine **9** with the M06

DFT functional may suggest that the *s*-BuLi/di-methyl bispidine **195** lithiation of *N*-Boc pyrrolidine **9** would be fast with similar reactivity to the lithiation with *s*-BuLi/TMEDA.

These results provide evidence that computational modelling can reproduce some of the trends in reactivity observed for the different *s*-BuLi/ligand lithiating complexes. Although the B3LYP DFT functional was able to predict the correct reactivity series for four of the five lithiating complexes, the calculated ΔG^\ddagger values did not quantitatively reflect the differences in the rate of reactivity observed experimental. This suggests that at this point in the project, the DFT modelling used provides qualitative rather than quantitative information about the reactivities of the different lithiating complexes. The DFT modelling also does not account for additional factors that can affect the rate of lithiation. For example, how well the ligand binds to the alkyllithium and whether the solvent binding to the alkyllithium is more favourable, which is likely why the lithiation reactions with *s*-BuLi/TPMDA **179** were predicted to be faster than observed. As observed with the computed reactivity trends of the substrates in section 3.2, it is also clearly evident that the DFT functional used can provide very different reactivity series for the different *s*-BuLi/ligand complexes.

3.4 Conclusions and Future Work

In conclusion, this Chapter described the application of DFT modelling to attempt to reproduce and better understand the differences in the reactivities afforded when different *N*-Boc heterocycles and ligands are used in the α -lithiation reaction. Work reported in this Chapter has indicated that it is possible to reproduce many of the reactivity differences observed when different substrates are subjected to α -lithiation. This included the significant reactivity difference between unsubstituted 5- and 6-membered heterocycle rings observed with *N*-Boc pyrrolidine **9** and *N*-Boc piperidine **10**. DFT modelling was also able to reproduce the activating effects observed experimentally with the 6-membered *N*-Boc heterocycles, when substituents are added to the C-4 position or additional heteroatoms are included in the heterocycle ring. The DFT modelling has indicated that differences in the rates of lithiation of these substrates must arise due to structural differences between the substrates. Future work further could explore why these reactivity differences in the *N*-Boc heterocycles are present. We postulate that conformational and electronic orbital overlap effects may be the reason for these differences in reactivity. More in-depth computational studies may be able to probe whether these effects are the cause of various reactivities observed. For example, computational calculation of α -proton acidities may provide evidence for the electronic effects that are postulated to facilitate the lithiation reaction.

Linear correlation of the modelled activation free-energies and experimentally obtained k_{obs} values indicated that the two DFT functionals used did not provide identical amounts of agreement with experiment. This highlighted the significant impact that using differing levels of theory of DFT functionals can have on the results obtained. In this study, the correlation between theory and experiment suggested that modelling with the M06 functional may not provide an accurate description of the system. This was surprising as it is reported that M06 better describes dispersion interactions, which are likely to be significant in the α -lithiation reaction, where multiple chemical species are present. In contrast, a good correlation between the B3LYP calculated ΔG^\ddagger values and experimental results was obtained. This correlation was then used to predict the reactivities of three additional *N*-Boc heterocycles for which little or no reactivity data was available. The use of the computational modelling for a predictive purpose provides an interesting avenue for further investigation and this model could be further developed to provide reliable

predictions of reactivity for substrates. This in turn would allow optimal reaction conditions to be found *in silico* without the need to conduct the reaction in the laboratory beforehand.

The computational investigation also focussed on investigating the reactivities of alkyllithium/ligand lithiating complexes. The *i*-PrLi/ligand modelled lithiations of *N*-Boc pyrrolidine **9** with the B3LYP DFT functional provided a qualitative agreement with the experimental *s*-BuLi/ligand results, for four of the five *i*-PrLi/ligand lithiating complexes modelled. The DFT modelling suggested the alkyllithium/TMPDA **179** lithiating complex was significantly more reactive than what was observed by experiment. This is likely due to TMPDA **179** having a lower affinity for alkyllithium compared to the Et₂O solvent; the competing affinities of the ligand and solvent are not accounted for in the DFT modelling conducted. This demonstrates that other processes that occur during the reaction which are not accounted for by the modelling may significantly affect the reactivity observed in experiment.

The computational modelling used for all the studies in this chapter could be developed and investigated further. This could include the investigation of QM/QM or QM/MM modelling, where less significant parts of the molecular geometry can be treated with lower levels of theory (or molecular mechanics) to decrease the computational cost. This would also allow more crucial parts of the molecular geometry to be treated at higher levels of theory which may improve the accuracy and reliability of results without significantly increasing the computational expense. The QM/QM modelling *i*-PrLi/(–)-sparteine lithiation of *N*-Boc pyrrolidine **9** and *N*-Boc piperidine **10** have been reported by Wiberg and Deng (see section 1.4).⁹⁰

Another aspect of modelling that could be explored is the effect of basis set supposition error (BSSE) upon the results of the calculations, which has not been explored in this investigation. The BSSE results from the overlap of the basis functions on atoms that are close to each other and where this overlap does occur, that portion of the molecule has an effectively increased basis set. In the regions of the molecular geometry where this effectively increased basis set occurs, the calculations are improved as the location of electrons are better described due to the larger number of basis functions present. As only small portions of the molecular geometry that is modelled experience these increases in basis set size, this provides a source of error when energy and other properties are calculated for the entire system. BSSE can provide a significant source of error in the calculated energies

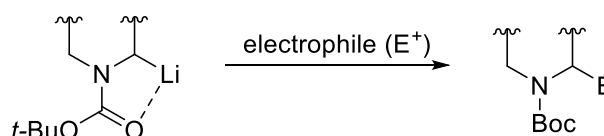
of systems especially where intermolecular reactions such as lithiation are modelled.^{124,125} There are many methods that can be used to attempt to correct for the occurrence of the BSSE such as using larger basis sets or by employing a counterpoise (CP) correction. These methods to correct for BSSE were not attempted in this study due to large computational expense of the correction calculations.

Finally, the use of alternative DFT functionals could be investigated. For example, it may be possible to screen a sub-set of the *N*-Boc heterocycles α -lithiation reactions with many different DFT functionals, to find a functional that provides the best description of the lithiation reaction. Alternatively, methods that pair DFT functionals with empirical energy corrections could also be utilised. DFT functionals with combined corrections are particularly useful as effects like dispersion can be better accounted for without the significant increases in computational expense that would result from using a higher level of theory. For example, B3LYP-D3 combines the B3LYP DFT functional with Grimme's DFT-D3 dispersion correction, allowing the inclusion of dispersion energy corrections throughout the calculation.^{126,127} As previously mentioned in this Chapter, DFT in general does not accurately describe long-range dispersion interactions¹¹⁹ and these long-range interactions are likely to play an important role in the intermolecular multi species lithiation reaction. Therefore, inclusion of a dispersion correction should mean that these lithiation reactions can be more accurately modelled using DFT. More recently, Grimme *et al.* have developed a B3LYP-gCP-D3 scheme which includes both a dispersion correction (D3) and a BSSE correction (gCP).¹²⁸ This combination of DFT functional and energy corrections may be particularly beneficial for the modelling of the lithiation chemistry presented in this thesis.

Chapter 4: Investigation of the Rates of Trapping of Lithiated *N*-Boc Heterocycles with Different Electrophiles

Ensuring a complete and efficient lithiation reaction of an *N*-Boc heterocycle is only half of the challenge when optimising the lithiation-trapping reaction of a substrate. It is also vital to ensure that complete trapping occurs with reaction conditions which ensure that the desired product is obtained with minimal side reactions (Scheme 4.1).

Scheme 4.1. General scheme for the trapping reaction of a lithiated intermediate



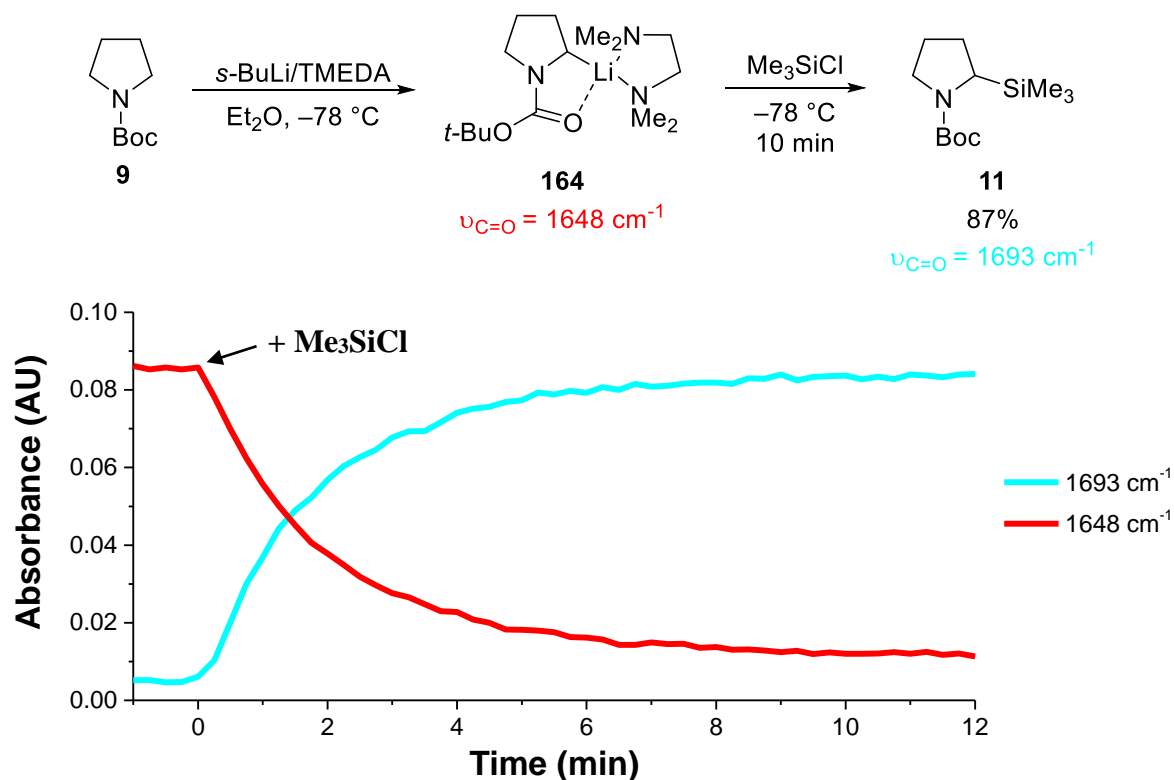
The use of *in situ* IR spectroscopy to monitor the trapping reactions of lithiated intermediates is less common than monitoring the formation of the lithiated intermediates. More recently, however, the ReactIRTM monitoring of the trapping reaction and in some cases the subsequent rearrangements of the trapped adducts is becoming popular (see section 1.3.2). Monitoring the progress of the trapping reaction can in some cases be very useful to ensure that the trapped product can be obtained in a good yield and er/dr. It is well known that lithiated intermediates can become configurationally unstable at higher temperatures and if the trapping is not complete before the reaction is warmed up then this can result in the product being formed in an eroded er.^{31,129,130} Monitoring the rate of trapping can also allow the optimisation of reaction conditions for the trapping, particularly where the trapping may be slow at low temperatures such as $-78\text{ }^{\circ}\text{C}$ which are typically used for the preceding lithiation step.

The rate of trapping between a selection of different lithiated *N*-Boc heterocycles and electrophiles at $-78\text{ }^{\circ}\text{C}$ has previously been studied qualitatively in the O'Brien group using reaction times for the trapping.⁵³ Some of these trapping reactions were very slow at $-78\text{ }^{\circ}\text{C}$ and only small amounts of incomplete trapping were observed; for these reactions, comparison of the trapping rates was not possible. Work in this chapter expands upon this previous work by measuring the rate of the trapping using a quantitative kinetic analysis, similar to that used to measure the rates of α -lithiation reactions in Chapter 2. This will allow quantitative comparisons of trapping rates for different lithiated intermediates and electrophile combinations.

4.1 Use of *in situ* IR Spectroscopy to Study the Rates of Trapping of Lithiated *N*-Boc Heterocycles

In a similar fashion to the monitoring of the α -lithiation of *N*-Boc heterocycles, the subsequent trapping reaction of the lithiated intermediate can also be followed using *in situ* IR spectroscopy with the ReactIRTM apparatus. For example, the Me₃SiCl trapping of lithiated *N*-Boc pyrrolidine **9**, whose ReactIRTM monitored *s*-BuLi/TMEDA lithiation was discussed in section 2.1, required 10 min for complete trapping to occur (Scheme 4.2). During the trapping reaction, two different species are observed: lithiated intermediate **164** ($\nu_{\text{C=O}} = 1648 \text{ cm}^{-1}$) and the trapped adduct, 2-silyl pyrrolidine **11** ($\nu_{\text{C=O}} = 1693 \text{ cm}^{-1}$). The ReactIRTM monitoring showed the consumption of the lithiated intermediate **164** and formation of the trapped product 2-silyl pyrrolidine **11** during the course of the reaction. After the trapping was complete, Me₃SiCl trapped adduct **11** was afforded in 87% isolated yield.

Scheme 4.2. ReactIRTM monitored Me₃SiCl trapping of 2-lithio *N*-Boc pyrrolidine **164**



During the trapping reaction, the $\nu_{\text{C=O}}$ of the carbamate in species **164** shifts to a higher frequency during the trapping reaction since the C=O bond becomes stronger during the trapping reaction. This occurs as the species is converted from the 2-lithio pyrrolidine **164**,

where the carbamate C=O is strongly coordinated to the lithium, into the trapped adduct **11** which will have little or no coordination between the carbamate C=O and Li.

As discussed in Chapter 2, the visually obtained reaction times from the ReactIR™ monitoring can be inaccurate and unreliable, therefore it was decided to subject the ReactIR™ data to kinetic analysis to quantify the rates of trapping. The trapping reaction of the lithiated intermediates occurs *via* an S_N2 reaction for tetrahedral electrophiles such as Me₃SiCl, Me₂SO₄ and MeI and a nucleophilic addition mechanism for sp² carbonyl electrophiles such as PhCHO. Both trapping mechanisms are bimolecular and therefore the rate of the trapping reaction is expected to be dependent on both the concentration of electrophile and lithiated intermediate (RLi) (Equation 4.1).

$$-\frac{d[RLi]}{dt} = k_{trap} [RLi][electrophile] \quad \text{(Equation 4.1)}$$

As it is a complex task to obtain a second order rate constant for a reaction, in this case k_{trap} , it was decided to apply a pseudo-first order approximation. This allows a k_{obs} to be measured which is only dependent on the concentration of the lithiated intermediate (Equation 4.2).

$$-\frac{d[RLi]}{dt} = k_{obs}[RLi] \quad \text{(Equation 4.2)}$$

The standard reaction conditions for the trapping of lithiated intermediates use 2.0 eq. of electrophile, which is only a moderate excess. However, it would be beneficial if this amount of excess electrophile could be used to obtain kinetic data for several reasons. First, all the previously collected ReactIR™ kinetic data in the group used a 2.0 eq. excess of electrophile.⁵³ Therefore, if the kinetic analysis requires a larger excess of electrophile then all of the experiments would need to be repeated. Second, the addition of large excesses of electrophile (i.e. 10.0 eq.) could result in anomalous kinetic data arising from the addition of large volumes of electrophiles that would be added to the reaction. Finally, it would be useful to obtain kinetic data from a reaction which is still conducted for a synthetic purpose allowing the trapped product to be easily isolated at the end. If a large excess of electrophile was added, then this may result in a more complex separation due to the large quantity of unreacted electrophile present.

With this in mind, we decided to use the synthetic reaction conditions and maintain a 2.0 eq. excess of the electrophiles and only use kinetic data from the first 20% of conversion of the trapping reaction, obtaining effectively an initial rate for the trapping reaction. During the

first 20% of conversion, the concentration of the electrophile should only change by a relatively small amount, effectively providing pseudo-first order kinetics with respect to the lithiated intermediate.

The Me_3SiCl trapping reaction of 2-lithio pyrrolidine **164** shown in Scheme 4.2 was the first trapping reaction that was subjected to kinetic analysis. A semilogarithmic plot was constructed using ReactIRTM kinetic data for the first 20% conversion of the trapping reaction, to obtain a pseudo-first order k_{obs} for the reaction (Figure 4.1.a). Additionally, a second semilogarithmic plot was constructed which included up to 90% conversion for the trapping reaction. This second plot (Figure 4.1.b). was constructed to identify whether pseudo-first order kinetics were observed over the entirety of the trapping reaction or not. A non-linear correlation in the 90% conversion plot would suggest first order kinetics were not exhibited throughout the reaction, thus suggesting that 2.0 eq. of the Me_3SiCl electrophile is not sufficient to provide pseudo-first order reaction conditions throughout.

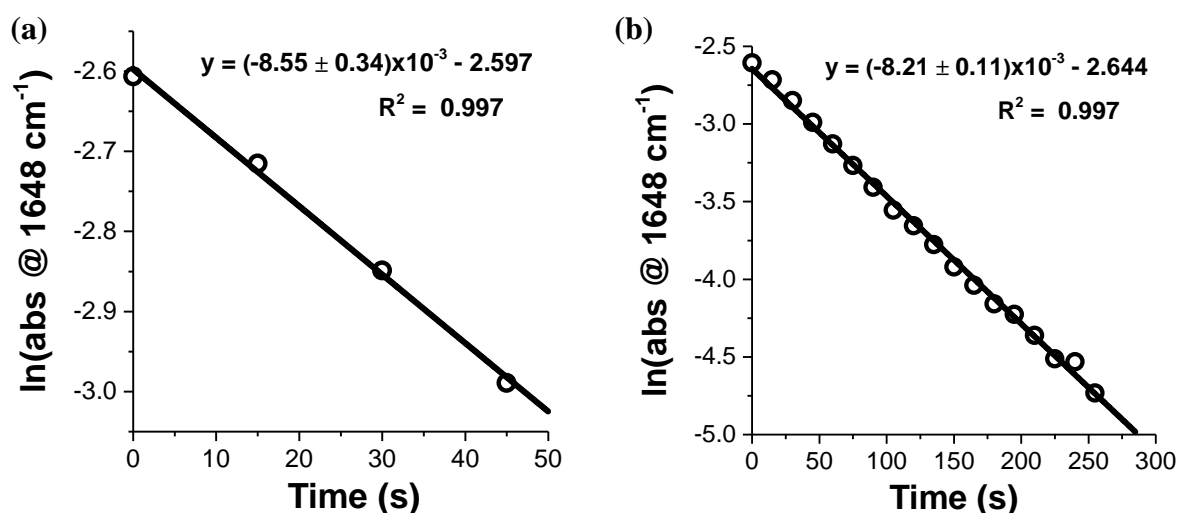


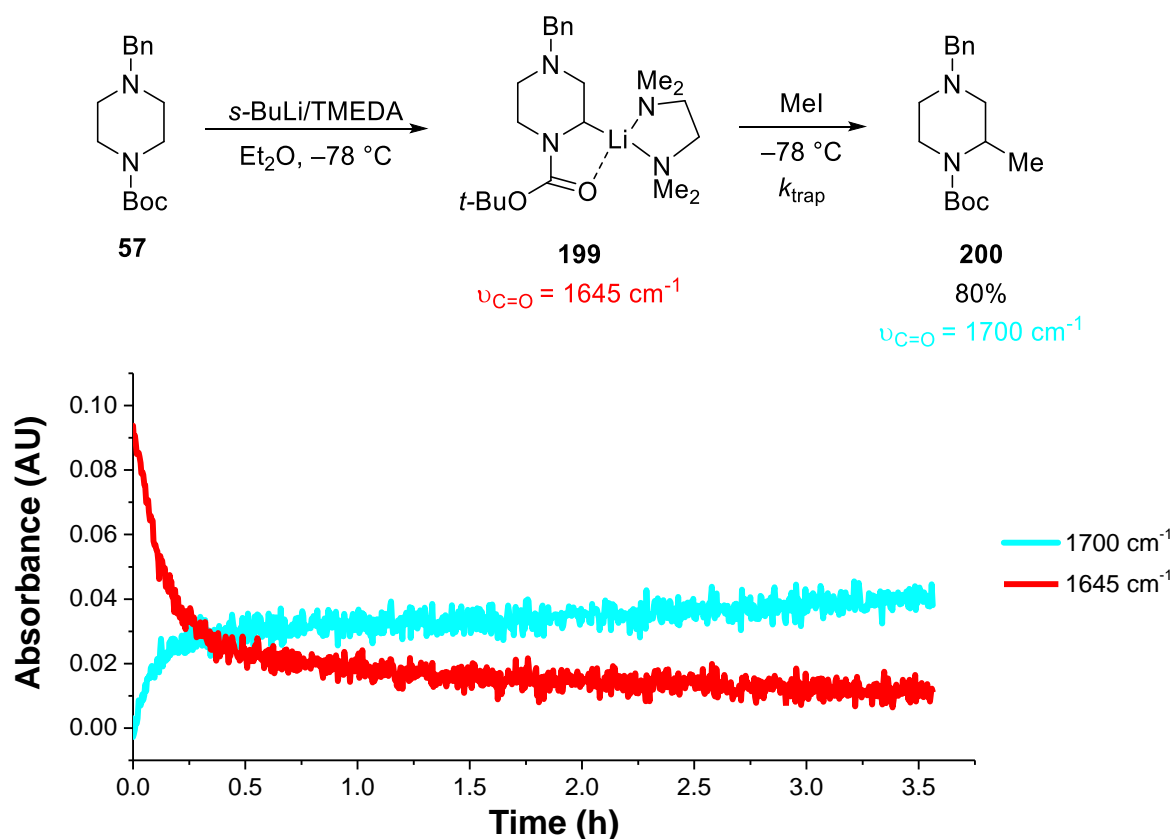
Figure 4.1. Semilogarithmic plots for (a) the first 20% conversion and (b) up to 90% conversion for the Me_3SiCl trapping of 2-lithio *N*-Boc pyrrolidine **164**

The semilogarithmic plots for both 20% and 90% conversion of 2-lithio pyrrolidine **164** provided strong linear correlations ($R^2 = 0.997$ for both plots, Figure 4.1). This indicated that a pseudo-first order reaction with respect to the lithiated intermediate **164** was observed for the whole Me_3SiCl trapping reaction of 2-lithio pyrrolidine **164**. This also suggested that 2.0 eq. of the electrophile (Me_3SiCl) is sufficient for pseudo-first order conditions to be maintained throughout this particular trapping reaction. Both semilogarithmic plots offered very similar k_{obs} values for the trapping which were within the margins error of one another. Calculation of k_{obs} using the first 20% conversion provided $k_{\text{obs}} = (8.55 \pm 0.34) \times 10^{-3} \text{ s}^{-1}$ and

for 90% conversion $k_{\text{obs}} = (8.21 \pm 0.11) \times 10^{-3} \text{ s}^{-1}$. To enable easy comparison of the rate of trapping with other substrates and electrophiles, a $t_{1/2}$ for the trapping of $(81.1 \pm 3.2) \text{ s}$ was calculated using the k_{obs} measured for 20% conversion. A detailed procedure for the kinetic analysis carried out for the trapping reactions of the lithiated *N*-Boc heterocycles presented in Chapter 4 is detailed in section 6.2 of this thesis.

When a similar kinetic analysis was carried out for the MeI trapping of 2-lithio *N'*-Bn *N*-Boc piperazine **199**, a deviation from pseudo-first order kinetics during the reaction was observed. ReactIRTM monitoring of this reaction indicated that 3.5 h were required for complete trapping to occur, after which the trapped product, 2-methyl piperazine **200** was obtained in 80% yield (Scheme 4.3). By visual inspection of the ReactIRTM trace, it is evident that the curve for the consumption of lithiated intermediate **199** appeared to match that of a multiple order reaction.

Scheme 4.3. ReactIRTM monitored MeI trapping of 2-lithio *N'*-Bn *N*-Boc piperazine **199**



Semilogarithmic plots were constructed for both 20% conversion and 90% conversion of the MeI trapping of 2-lithio *N'*-Bn piperazine **199** using ReactIRTM kinetic data, as carried out for the Me₃SiCl trapping of 2-lithio pyrrolidine **164** (Figure 4.2).

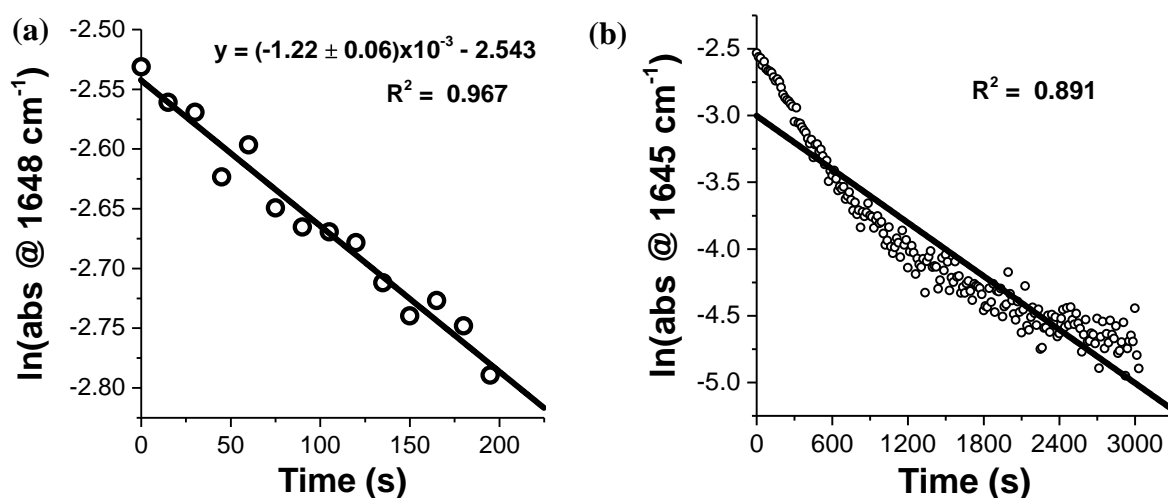


Figure 4.2. Semilogarithmic plots for (a) the first 20% conversion and (b) up to 90% conversion for the MeI trapping of 2-lithio *N'*-Bn *N*-Boc piperazine **199**

The first order plot that was constructed using the kinetic data for up to 90% conversion of 2-lithio *N'*-Bn piperazine **199** (Figure 4.2.b) did not provide a good linear correlation. It is evident that a deviation from pseudo-first order kinetics occurs roughly 600 s into the trapping reaction. This deviation from first order kinetics in the trapping reaction likely arises from the development of an insufficient excess of electrophile mid-reaction. At this point 600 s into the trapping reaction, second order kinetics are observed as the rate of trapping becomes dependant on both the concentration of lithiated intermediate and electrophile. The semilogarithmic plot of the first 20% conversion for MeI trapping of 2-lithio *N'*-Bn piperazine **199** (Figure 4.2.a) provided a good linear correlation, indicating that during this initial portion of the trapping reaction, pseudo-first order conditions with respect to the lithiated intermediate **199** were observed. This plot provided a $k_{\text{obs}} = (1.22 \pm 0.06) \times 10^{-3} \text{ s}^{-1}$ and $t_{1/2} = (569 \pm 30) \text{ s}$ for the MeI trapping of 2-lithio *N'*-Bn *N*-Boc piperazine **199**.

With a viable method to quantify the rate of the trapping reaction between a lithiated intermediate and electrophile established, our attention centred on investigating the trends in reactivity for both the different lithiated intermediates and different electrophiles. To this end, kinetic data was collected for the Me_3SiCl , Me_2SO_4 , MeI and PhCHO trapping reactions of three different lithiated *N*-Boc heterocycles: **164**, *cis*-**201** and **199** (Figure 4.3). It was envisaged that these 12 trapping reactions would provide useful information about the trends in reactivity for both the electrophile and lithiated intermediate.

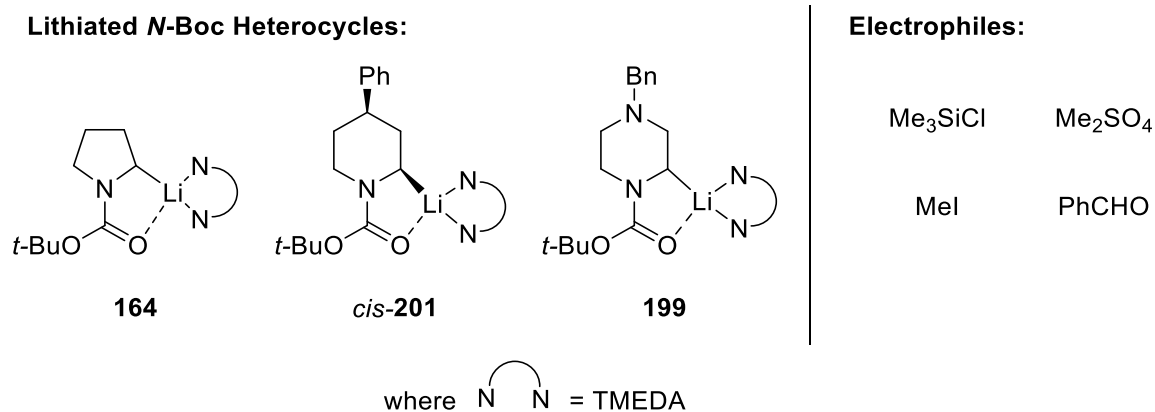
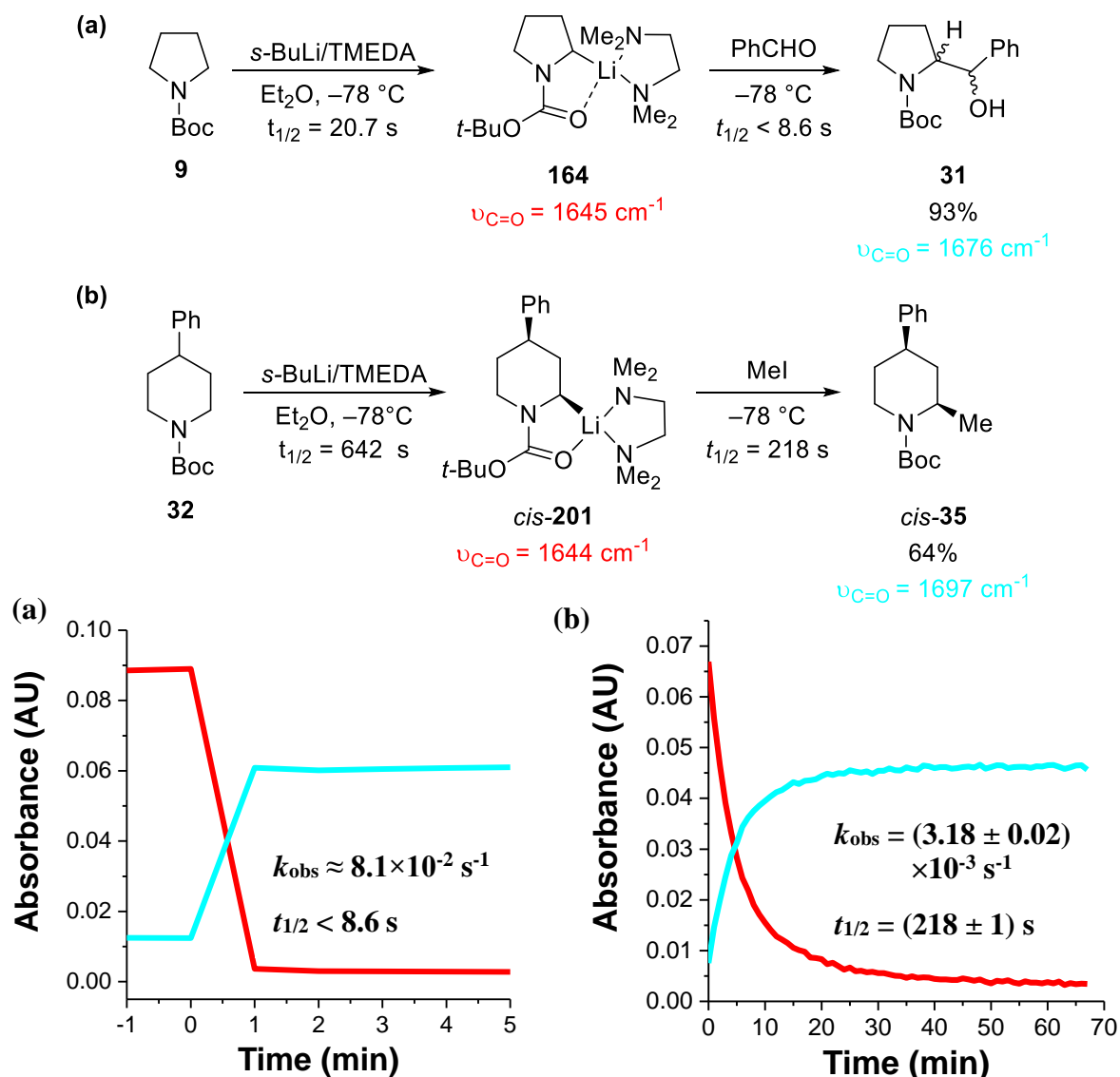


Figure 4.3. 12 Combinations of lithiated *N*-Boc heterocycles and electrophiles

A variety of different rates of trapping were observed with the different combinations of lithiated intermediate and electrophile used. Many of these combinations of lithiated intermediate and electrophile displayed fast trapping reactions. For trapping reactions where the time for complete trapping was < 3 min, k_{obs} and $t_{1/2}$ s were estimated as kinetic analysis could not be carried out as too few data points were available to measure rate constants for the trapping. For these trapping reactions, estimated $t_{1/2}$ s were approximated using $t_{1/2} \approx t_{\text{trap}}/7$ (as 7 $t_{1/2}$ s = 99% conversion), where t_{trap} was the time taken for complete trapping. For example, the PhCHO trapping of 2-lithio pyrrolidine **164** was extremely fast (complete within the 1 min time lapse between scans of the ReactIRTM) with a $t_{1/2}$ of < 8.6 s (Scheme 4.4.a).⁵³ After work-up and purification, the PhCHO trapping of 2-lithio pyrrolidine **164** provided a mixture of benzyl alcohol diastereomers **31** in 93% yield. The MeI trapping of 2-lithio phenyl piperidine *cis*-**201** also displayed a relatively fast trapping reaction, with $k_{\text{obs}} = (3.18 \pm 0.02) \times 10^{-3} \text{ s}^{-1}$ and $t_{1/2} = (218 \pm 1) \text{ s}$ calculated by kinetic analysis of the first 20% conversion of the trapping. After work-up and purification of the MeI trapping of 2-lithio phenyl piperidine *cis*-**201**, 2-methyl 4-phenyl piperidine *cis*-**35** was afforded in 64% yield (Scheme 4.4.b).

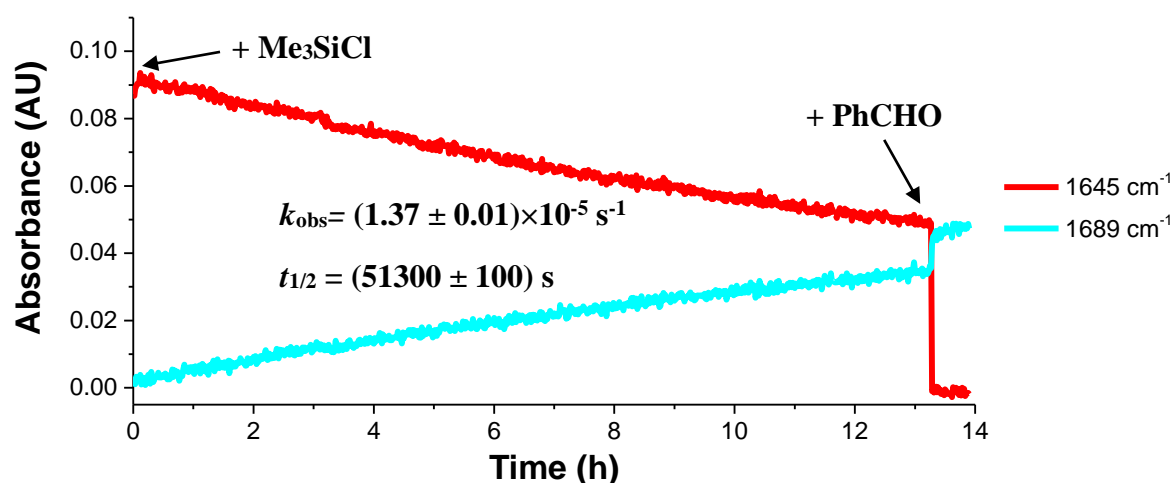
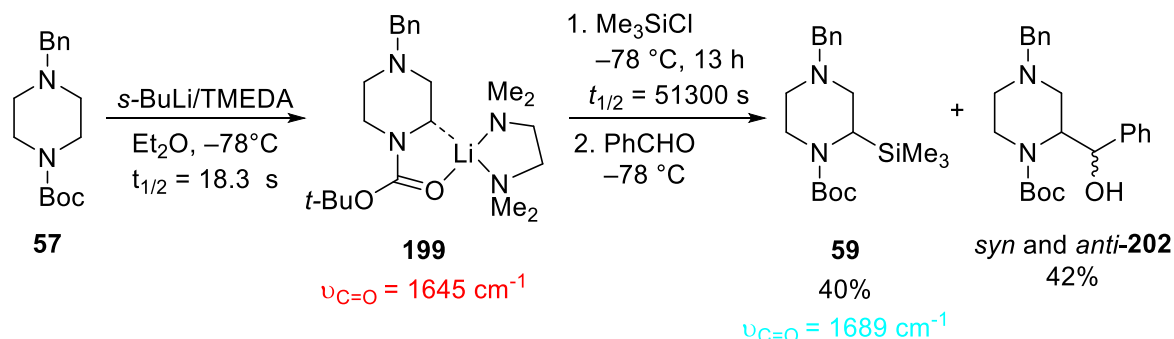
Scheme 4.4. (a) PhCHO trapping of 2-lithio *N*-Boc pyrrolidine **164 and (b) MeI trapping of 2-lithio 4-phenyl piperidine *cis*-**201****



On the other hand, there were trapping reactions of lithiated intermediates that displayed very slow rates of trapping. The Me_3SiCl trapping of 2-lithio *N'*-Bn piperazine **199** was the slowest trapping reaction observed in this investigation, with $k_{\text{obs}} = (1.37 \pm 0.01) \times 10^{-5} \text{ s}^{-1}$ and $t_{1/2} = (51300 \pm 100) \text{ s}$ measured by kinetic analysis of the first 20% conversion of the trapping. After a 13 h trapping time at $-78 \text{ }^\circ\text{C}$ only partial trapping of 2-lithio *N'*-Bn piperazine **199** was observed (Scheme 4.5). As the Me_3SiCl trapping of **199** was so slow, a second fast trapping electrophile, PhCHO, was added to trap the remaining un-trapped lithiated intermediate **199**. This second electrophile was added to ensure that the preceding lithiation was complete and to measure the baseline absorbance at 1648 cm^{-1} , which is required for the kinetic analysis. Purification after the addition of both electrophiles provided

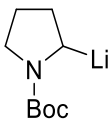
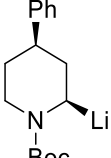
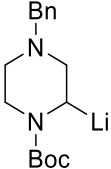
the Me₃SiCl trapped adduct **59** in 40% yield and a 60:40 mixture of PhCHO trapped benzyl alcohols *syn*- and *anti*-**202** in 42% yield.

Scheme 4.5. Me₃SiCl trapping of 2-lithio *N*'-Bn piperazine **199**



The k_{obs} and $t_{1/2}$ s for all 12 trapping reactions with isolated yields of the trapped adduct, are presented in Table 4.1. Due to their faster rates of trapping (time for complete trapping < 3 min), the results from the methylations of 2-lithio *N*-Boc pyrrolidine **164** and the PhCHO trapping reaction are estimated k_{obs} and $t_{1/2}$ values. All other k_{obs} and $t_{1/2}$ values in Table 4.1 were determined by kinetic analysis of the first 20% of trapping conversion as discussed earlier; in all of these cases the first order plots for up to 20% conversion provided good linear correlations, suggesting that during this initial portion of the trapping reaction, pseudo-first order kinetics with respect to the lithiated intermediate were observed (see section 6.5 for semilogarithmic plots). In fact, for all of the trapping reactions with Me₃SiCl, pseudo-first order kinetics with respect to the lithiated intermediate were observed over the course of the trapping reaction (up to 90% conversion for **164** and *cis*-**201**, and up to PhCHO trapping for **199**). Conversely, all of the trapping reactions with Me₂SO₄ and MeI which were subjected to kinetic analysis showed deviation from pseudo-first order kinetics at some point mid-reaction (after 20% conversion).

Table 4.1. Measured k_{obs} , $t_{1/2}$ s and isolated yields for the Me_3SiCl , Me_2SO_4 , MeI and PhCHO trapping reactions of lithiated intermediates **164, *cis*-**201** and **199****

	Me_3SiCl	Me_2SO_4	MeI	PhCHO
 164	$k_{\text{obs}} = (8.55 \pm 0.34) \times 10^{-3} \text{ s}^{-1}$ $t_{1/2} = (81.1 \pm 3.2) \text{ s}$ (81%)	$k_{\text{obs}} \approx 4.1 \times 10^{-2} \text{ s}^{-1}$ ^a $t_{1/2} < 17 \text{ s}$ (66%)	$k_{\text{obs}} \approx 2.7 \times 10^{-2} \text{ s}^{-1}$ ^{a,b} $t_{1/2} < 26 \text{ s}$ (40%)	$k_{\text{obs}} \approx 8.1 \times 10^{-2} \text{ s}^{-1}$ ^{a,c} $t_{1/2} < 8.6 \text{ s}$ (93%)
 <i>cis</i> - 201	$k_{\text{obs}} = (7.57 \pm 0.07) \times 10^{-5} \text{ s}^{-1}$ $t_{1/2} = (9160 \pm 80) \text{ s}$ (73%)	$k_{\text{obs}} = (2.74 \pm 0.05) \times 10^{-4} \text{ s}^{-1}$ $t_{1/2} = (2530 \pm 50) \text{ s}$ (63%)	$k_{\text{obs}} = (3.18 \pm 0.02) \times 10^{-3} \text{ s}^{-1}$ $t_{1/2} = (218 \pm 1) \text{ s}$ (64%)	-- ^d
 199	$k_{\text{obs}} = (1.37 \pm 0.01) \times 10^{-5} \text{ s}^{-1}$ $t_{1/2} = (51300 \pm 400) \text{ s}$ (40%)	$k_{\text{obs}} = (2.14 \pm 0.06) \times 10^{-5} \text{ s}^{-1}$ $t_{1/2} = (32400 \pm 900) \text{ s}$ (35%)	$k_{\text{obs}} = (1.22 \pm 0.06) \times 10^{-3} \text{ s}^{-1}$ $t_{1/2} = (569 \pm 30) \text{ s}$ (80%)	$k_{\text{obs}} \approx 8.1 \times 10^{-2} \text{ s}^{-1}$ ^{a,c} $t_{1/2} < 8.6 \text{ s}$ (52%)

^a k_{obs} and $t_{1/2}$ s for these trapping reactions are estimated ($t_{1/2} \approx \text{trapping time} / 7$)

^b upon addition of MeI , gelation was observed and this provided unreliable kinetics (this is discussed in more detail later)

^c previous in-group work.⁵³

^d the trapping of 2-lithio 4-phenyl piperidine *cis*-**201** has been carried out using a cyclobutanone electrophile⁵³ and estimated $k_{\text{obs}} \approx 8.1 \times 10^{-2} \text{ s}^{-1}$ and $t_{1/2}$ of $< 8.6 \text{ s}$ were calculated^a

The reactivities of the different lithiated intermediate and electrophile combinations presented in Table 4.1 were also quantified using initial rate analysis. As the initial concentrations of all reagents were kept constant for each lithiation-trapping experiment it is possible to compare the reactivities of the different lithiated intermediates and electrophiles using the initial reaction rates. Initial rates were calculated by plotting the decaying absorbance of the lithiated intermediate during the trapping reaction and then calculating a gradient of a tangent to the initial consumption where the concentrations of lithiated intermediate and electrophile are known. For example, the initial rate analysis for the Me_3SiCl trapping of lithiated *N*-Boc pyrrolidine **164** provided initial rate, $\text{rate}_{\text{init}} = (4.99 \pm 0.18) \times 10^{-4} \text{ s}^{-1}$ (Figure 4.4).

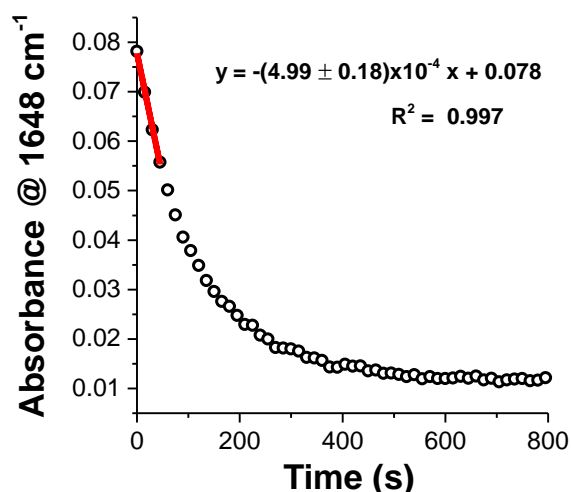
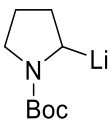
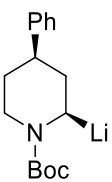
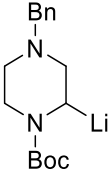


Figure 4.4. Initial rate analysis for the Me₃SiCl trapping of lithiated *N*-Boc pyrrolidine 164 (the tangent for initial rate is shown in red on the plot)

The initial rates for the trapping reactions presented in Table 4.1 are presented in Table 4.2 (initial rates for the trapping reactions with PhCHO are not included as these reactions were too rapid for kinetic analysis). The reactivity trends provided by both initial rates and the calculated k_{obs} for the lithiated intermediates and electrophiles are identical, suggesting a good agreement between both methods of trapping rate quantification.

Table 4.2. Measured initial rates ($\text{rate}_{\text{init}}$) for the Me₃SiCl, Me₂SO₄ and MeI trapping reactions of lithiated intermediates 164, *cis*-201 and 199

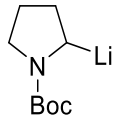
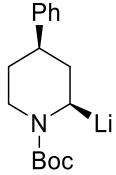
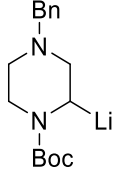
	Me ₃ SiCl	Me ₂ SO ₄	MeI
 164	$\text{rate}_{\text{init}} = (4.99 \pm 0.18) \times 10^{-4} \text{ s}^{-1}$	$\text{rate}_{\text{init}} = (8.41 \pm 0.13) \times 10^{-2} \text{ s}^{-1}$	-- ^a
 <i>cis</i> - 201	$\text{rate}_{\text{init}} = (4.76 \pm 0.12) \times 10^{-6} \text{ s}^{-1}$	$\text{rate}_{\text{init}} = (1.39 \pm 0.09) \times 10^{-5} \text{ s}^{-1}$	$\text{rate}_{\text{init}} = (1.34 \pm 0.31) \times 10^{-4} \text{ s}^{-1}$
 199	$\text{rate}_{\text{init}} = (9.70 \pm 0.70) \times 10^{-7} \text{ s}^{-1}$	$\text{rate}_{\text{init}} = (2.53 \pm 0.37) \times 10^{-6} \text{ s}^{-1}$	$\text{rate}_{\text{init}} = (8.90 \pm 0.46) \times 10^{-5} \text{ s}^{-1}$

^a this initial rate was not calculated as upon addition of MeI, gelation was observed and this provided unreliable kinetics (this is discussed in more detail later)

On inspection of the trapping reaction $t_{1/2}$ s and initial rates obtained for the three different lithiated heterocycles and four different electrophiles, trends in reactivity for both the lithiated intermediates and electrophiles are apparent. A clear trend in reactivity of the lithiated intermediates **164**, *cis*-**201** and **199** was evident with Me₃SiCl, Me₂SO₄ and MeI electrophiles, which provided trapping reactions that were slow enough for differences in reactivity of the lithiated intermediates to be observed. For each of these three electrophiles, the same lithiated intermediate reactivity series was observed where 2-lithio pyrrolidine **164** > 2-lithio 4-phenyl piperidine *cis*-**201** > 2-lithio *N'*-Bn piperazine **199**.

At first glance, the trapping reactivity of these three *N*-Boc heterocycles appears to show no relationship with the lithiation reactivity order for the same substrates (Table 4.3). For example, *N'*-Bn piperazine **57** affords the fastest lithiation reaction with *s*-BuLi/TMEDA with $t_{1/2} = 18.3$ s but the respective lithiated intermediate **199** provides the slowest trapping reactions of the three substrates. On closer inspection however, there may be a possible correlation between the lithiation and trapping reactivities of the two 6-membered heterocycles in Table 4.2, 4-phenyl *N*-Boc piperidine *cis*-**201** and *N'*-Bn *N*-Boc piperazine **199**. For these two 6-membered heterocycles we observe that a more facile lithiation means a slower rate of trapping with Me₃SiCl. At present, only kinetic data for the trapping reactions of the two 6-membered heterocycles **199** and **201** has been collected and hence this trend may be an artefact from the small amount of data rather than an actual physical effect. Kinetic analysis of the trapping reactions of other 6-membered heterocycles would need to be carried out to better determine whether there is an inverse trend between lithiation and trapping reactivities of these 6-membered heterocycles. If this trend is not an artefact, it is possible that orbital overlap effects may be responsible for this inverse correlation in lithiation and trapping reactivities. In Chapter 2 we proposed that orbital overlap in the 6-membered heterocycles could facilitate the lithiation *via* back donation from the C-H σ orbital of the α -proton making it more acidic. With the lithiated intermediates this same process could result in the stabilisation of the carbanion intermediate *via* the same back donation process. Therefore, the 6-membered heterocycle with the most facile lithiation would have the most stabilised carbanion intermediate which would offer the slowest rate of trapping. In this case, *N'*-Bn piperazine **199** would be the more stable carbanion than 4-phenyl piperidine *cis*-**201** resulting in its slower rate of trapping.

Table 4.3. Comparison of the $t_{1/2}$ s of Me₃SiCl trapping and *s*-BuLi/TMEDA lithiation for lithiated *N*-Boc heterocycles **164, *cis*-**201** and **199****

Substrate	Me ₃ SiCl trapping $t_{1/2}$	<i>s</i> -BuLi/TMEDA lithiation $t_{1/2}$
 164	(81.1 ± 3.2) s	(20.7 ± 0.9) s
 <i>cis</i> - 201	(9160 ± 80) s	(642 ± 5) s
 199	(51300 ± 400) s	(18.3 ± 0.9) s

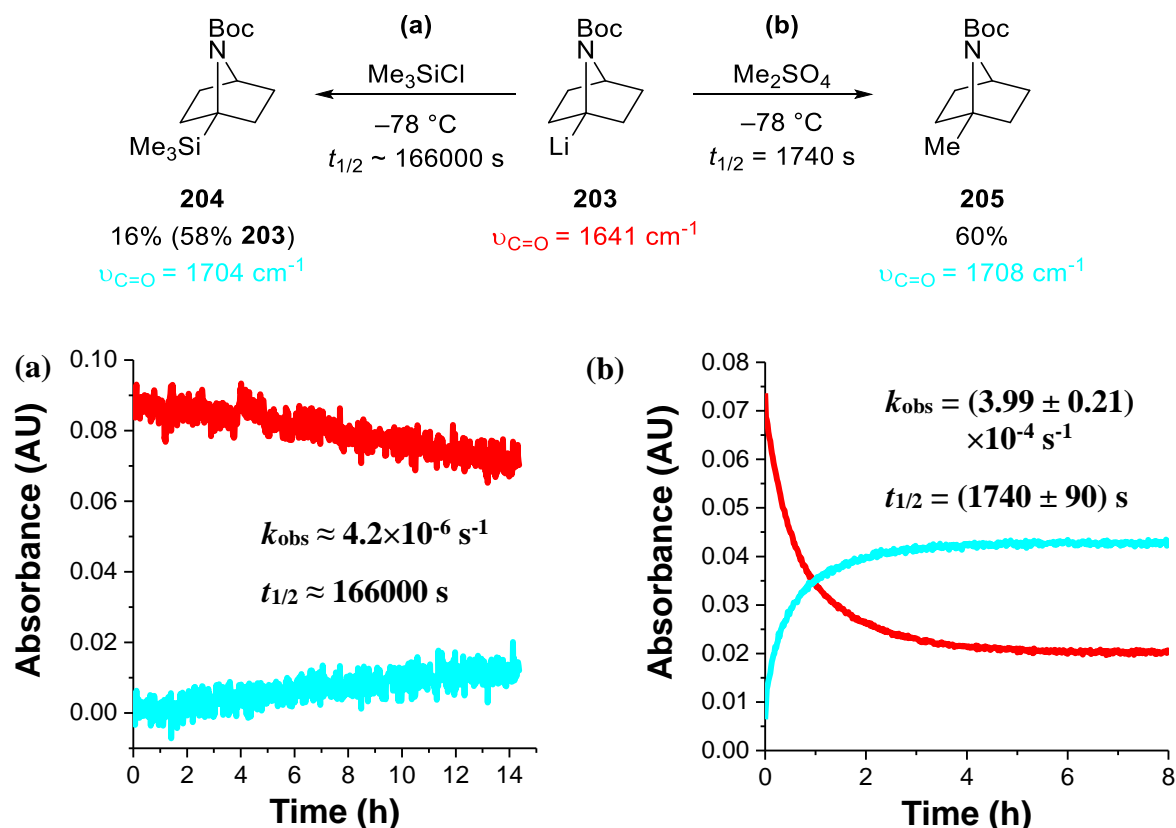
The four electrophiles used for the trapping reactions presented in Table 4.1 displayed the same reactivity trend for each of the lithiated intermediates where the rate of trapping followed the order PhCHO > MeI > Me₂SO₄ > Me₃SiCl. For the Me₂SO₄ and MeI trapping reactions of 2-lithio *N*-Boc pyrrolidine **164**, it appears that the MeI trapping is slower than that for Me₂SO₄. However, gelation of the reaction mixture was observed upon addition of the MeI electrophile which provides unreliable kinetics due to the inhomogeneity of the reaction. For the MeI trapping reactions of 2-lithio 4-phenyl piperidine *cis*-**201** and 2-lithio *N'*-Bn piperazine **199**, negligible amounts of gelation occurred. A more detailed discussion of the gelation observed with MeI is presented in section 4.2.

For both the lithiated intermediates and electrophiles presented in Tables 4.1 and 4.2, clear reactivity trends are displayed but it is difficult to provide a general rationale for why these differences in reactivity occur. Generalising the trapping reactivity for each of the lithiated intermediates is likely to be misleading, as the reactivity with different electrophiles is probably dictated by different effects that are particular to the electrophile that is used. For example, the reactivity of some electrophiles may be primarily dictated by steric interactions and others due to the electronic properties of the lithiated intermediate. This would mean

that direct comparison of certain properties of the lithiated intermediates may not provide an explanation for all the different trapping reactivities observed. This point is highlighted by the rates of reaction observed for the Me₃SiCl and Me₂SO₄ trapping reactions of 2-lithio bicyclic pyrrolidine **203**, which are presented below.

The Me₃SiCl trapping of lithiated bicyclic pyrrolidine **203** is an extremely slow reaction with $t_{1/2} \approx 166000$ s ($t_{1/2}$ is approximate as no second electrophile was added to measure baseline shift) and is much slower than the analogous trapping of 2-lithio *N*'-Bn piperazine **199** ($t_{1/2} = 51300$ s) (Scheme 4.6.a). However, the Me₂SO₄ trapping of 2-lithio bicyclic pyrrolidine **203** is relatively fast with $t_{1/2} = (1740 \pm 90)$ s and is much faster than the Me₂SO₄ trapping observed with 2-lithio *N*'-Bn piperazine **199** ($t_{1/2} = 32400$ s) (Scheme 4.6.b). This indicated that the lithiated intermediate with the slowest Me₃SiCl trapping does not necessarily mean that it will have the slowest trapping reactions with other electrophiles such as Me₂SO₄. For the case of 2-lithio bicyclic pyrrolidine **203**, it is likely that the slow Me₃SiCl trapping results from the steric interactions between the hindered tertiary organolithium and sterically bulky Me₃SiCl electrophile. It is possible that the rate of Me₂SO₄ trapping with 2-lithio bicyclic pyrrolidine **203** is dictated by electronic effects rather than steric effects and this could explain the large difference in reactivity observed between the Me₃SiCl and Me₂SO₄ trapping reactions of lithiated pyrrolidine **203**.

Scheme 4.6. Me₃SiCl (a) and Me₂SO₄ (b) trapping reactions of 2-lithio bicyclic pyrrolidine 203



Providing a complete rationale for the reactivity observed with the four electrophiles presented in Table 4.1 is also difficult. The PhCHO trapping reactions of each of the three lithiated intermediates were rapid, with complete trapping occurring between the 1 min time lapse between scans on the ReactIR™ apparatus. In fact, all trapping reactions conducted with PhCHO in this study, which involved five different lithiated intermediates, occurred rapidly with complete trapping occurring within the 1 min window between scans on the ReactIR™ apparatus (Figure 4.5).

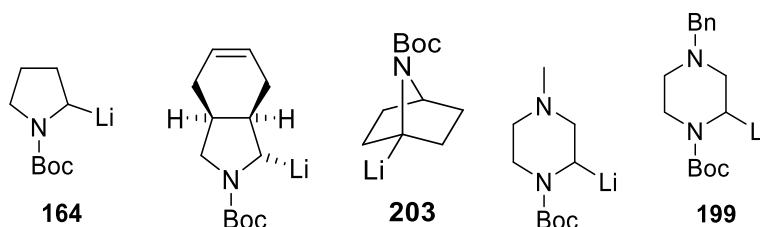


Figure 4.5. Lithiated N-Boc heterocycles trapped using PhCHO

Clearly, the carbonyl group is the key to the fast trapping reactions observed with these electrophiles. Both literature⁶⁴ and unpublished work by the O'Brien group⁵³ have also provided evidence that carbonyl electrophiles such as benzophenone **206**, cyclobutanone **207** and CO₂ also exhibit rapid, < 1 min, trapping reactions (Figure 4.6).

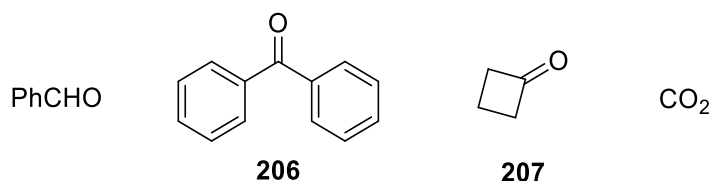


Figure 4.6. Rapid trapping carbonyl electrophiles

For each of the three lithiated intermediates whose trapping reactions were investigated (Tables 4.1 and 4.2), Me₃SiCl provided the slowest trapping reaction. It is well known that the trapping of organolithium reagents with chlorosilane electrophiles can provide slow reactions.⁵⁴⁻⁵⁶ It is likely that the slow rate of trapping observed with Me₃SiCl is due to the steric bulk of the electrophile which hinders the trapping process. There is evidence that the rate of the trapping reactions with chlorosilane electrophiles does depend on the size of the electrophile. For example, it is known the trapping reactions of organolithiums with the bulkier Ph₃SiCl electrophile are slower than those with Me₃SiCl.^{131,132}

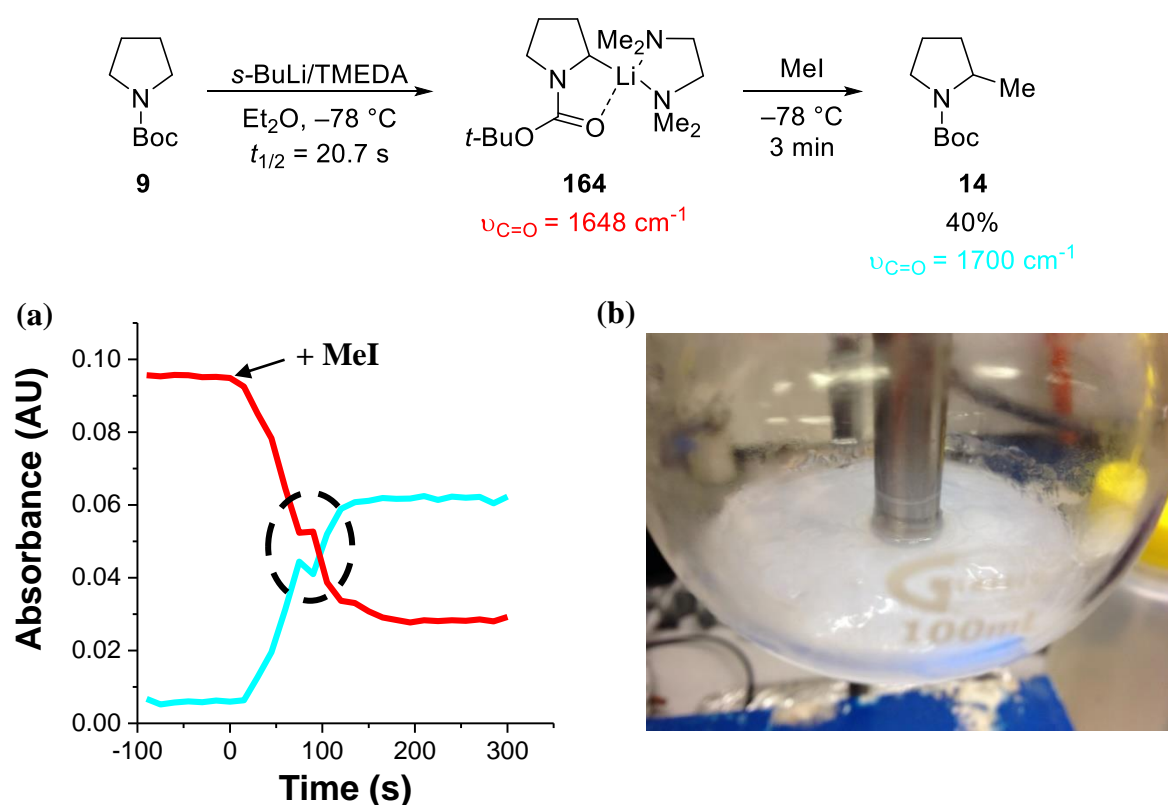
Two of our key findings from this Chapter, the fact that Me₃SiCl trapping reactions tend to be slow and that trapping with carbonyl electrophiles are fast, is mirrored by work conducted by Aggarwal (see scheme 1.50). Aggarwal noted that the slow trapping of a particular enantioenriched lithiated intermediate with Me₃SiCl was problematic, as the rates of trapping and racemisation of the intermediate were similar which resulted in the trapped products being obtained in poor er. Conversely, fast trapping electrophiles such as ClCO₂Me provided the trapped product in high er as the fast rate of trapping outcompeted the slower rate of lithiated intermediate racemisation.

Both Me₂SO₄ and MeI electrophiles provided moderate trapping reactivities between those of Me₃SiCl and PhCHO. However, the reason why Me₂SO₄ afforded slower trapping reaction than MeI is currently unclear. Based on a simple analysis, it was perhaps expected that the trapping reactions with the hard alkyl lithium and hard Me₂SO₄ electrophile would be faster than the soft MeI electrophile.

4.2 Investigation of the Gelation of the Reaction Mixture When Using MeI as the Electrophile

As mentioned in section 4.1, the MeI trapping reaction of 2-lithio *N*-Boc pyrrolidine **164** provided unreliable kinetic data and this was attributed to gelation of the reaction solution occurring upon addition of the MeI electrophile (Table 4.1 and Scheme 4.7). When MeI was added, the bulk reaction mixture solidified, stirring of the reaction ceased and the solution developed a turbid appearance. The ReactIR™ monitoring of the trapping reaction indicated that the reaction stalled mid-reaction (circled in Scheme 4.7.a) and then the trapping continued. It is likely that the lack of stirring and inhomogeneity of the solution are the reason for these anomalous kinetic data.

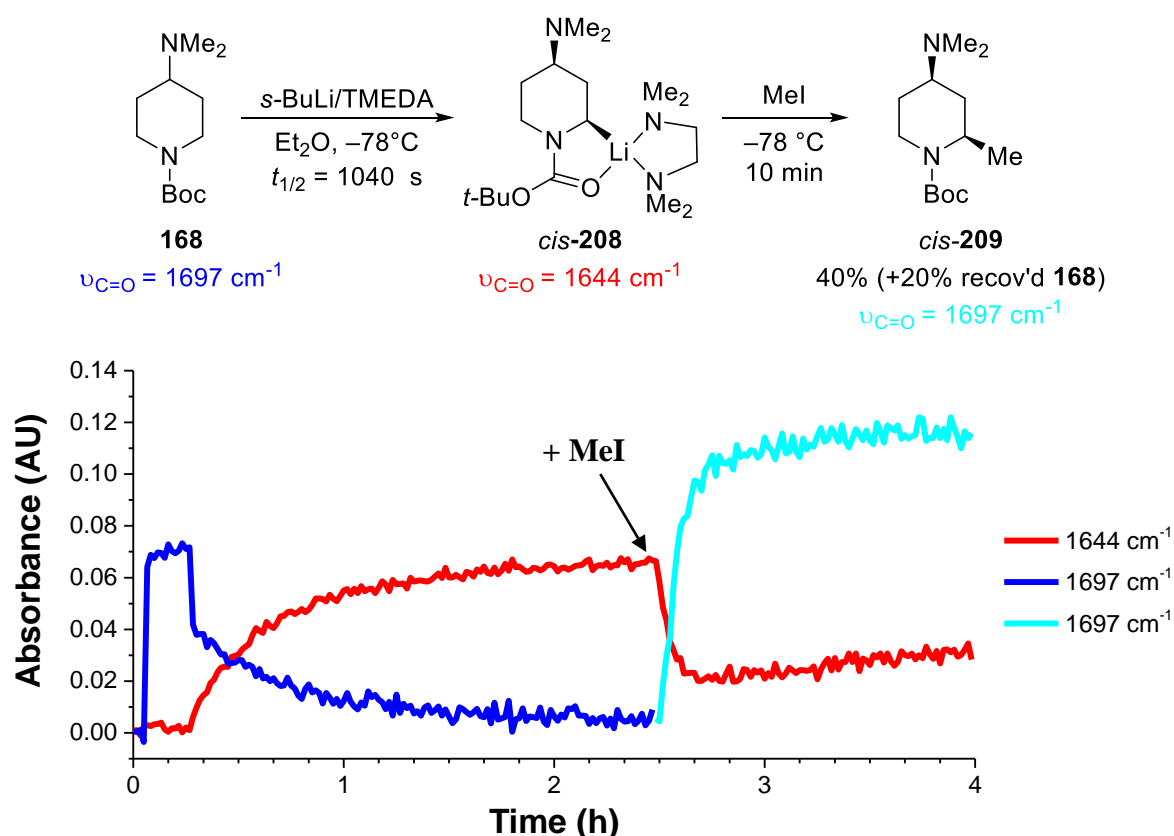
Scheme 4.7. ReactIR™ monitored MeI trapping of 2-lithio *N*-Boc pyrrolidine **164 (a) and the observed gelation in the reaction flask (b)**



For the MeI trapping reactions of 2-lithio 4-phenyl piperidine *cis*-**201** and 2-lithio *N'*-Bn piperazine **199**, only very small amounts of gelation were visually observed at the edge of the reaction flask. For each of these MeI trapping reactions, no detrimental effects on the kinetic data collected were observed due to the small amounts of gelation. It is possible that the fast rate of trapping between MeI and 2-lithio pyrrolidine **164** may result in the gelation

of the entire bulk solution, whereas slower trapping reactions of lithiated intermediates *cis*-**201** and **199** which require >1 h for complete trapping to occur, may result in only small amounts of gelation. This hypothesis is further supported by the fast MeI trapping of lithiated 4-amino *N*-Boc piperidine *cis*-**208** where the complete gelation of the bulk solution also occurred (Scheme 4.8). Upon addition of the MeI electrophile, the ReactIR™ monitoring indicated that trapping reaction had stalled after 15 min. After the work-up, ¹H NMR spectroscopy of the crude product indicated that 4-amino *N*-Boc piperidine **168** starting material was present and subsequent purification provided methylated product *cis*-**209** in 40% yield and recovered starting material **168** in 21% yield. The recovery of unreacted starting material likely arises from incomplete trapping where the gelation of the solution prevents complete trapping from occurring, as the lithiation and Me₃SiCl trapping reaction of 4-amino *N*-Boc piperidine **168** provided complete conversion to the Me₃SiCl trapped adduct (see section 6.6).

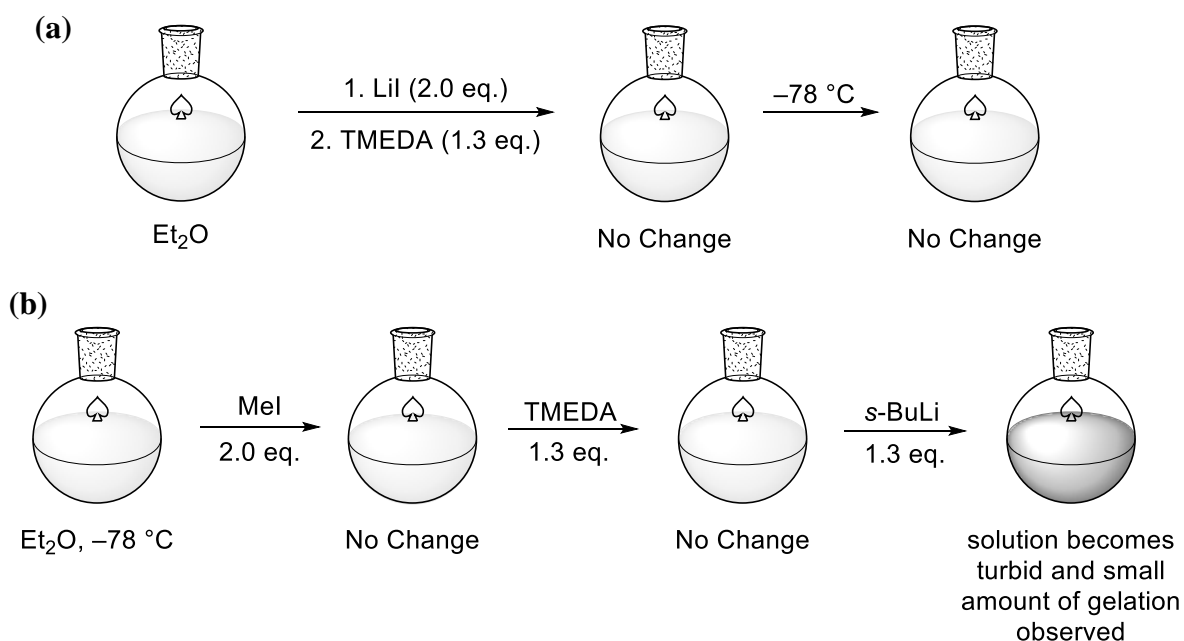
Scheme 4.8. ReactIR™ monitored MeI trapping of 2-lithio 4-amino piperidine *cis*-208****



The gelation during the trapping reactions of lithiated intermediates was not observed with any electrophiles other than MeI that were used in this investigation. Therefore, we conclude that the gelation may arise from the formation of LiI salts during the trapping reaction. To

probe whether LiI was responsible for the gelation observed, an attempt to recreate the gelation using LiI salts was explored (Scheme 4.9). LiI salt (2.0 mmol), TMEDA (1.30 mmol) and Et₂O (14 mL) were stirred at rt for 30 min and then cooled to -78 °C but no gelation was observed. A second reaction was conducted where *s*-BuLi (1.3 mmol of a 1.3 M solution in cyclohexane) was added to a stirred solution of TMEDA (1.3 mmol) and MeI (2.00 mmol) at -78 °C. Upon addition of MeI, the solution developed a turbid appearance, similar to that observed during the trapping reactions of **164**, *cis*-**201** and **199** and a small amount of gelation was observed. This experiment suggests that the liberation of LiI salts from the reaction between the alkyllithium reagents and MeI may be responsible for the gelation observed. Furthermore, we postulate that rapid trapping reactions with MeI may form the LiI salts over a short period of time which causes the gelation of the entire bulk solution, as observed with the MeI trapping reactions of 2-lithio pyrrolidine **164** and 2-lithio 4-amino piperidine *cis*-**208**.

Scheme 4.9. Attempted recreations of the gelation observed with the MeI trapping reaction using (a) LiI and TMEDA and (b) *s*-BuLi/TMEDA and MeI



4.3 Conclusions and Future Work

A comprehensive reactivity study of the trapping reactions of three different lithiated intermediates **164**, *cis*-**201** and **199** with four different electrophiles (Me₃SiCl, Me₂SO₄, MeI and PhCHO) has provided some interesting details on the reactivity observed in the trapping reactions studied. For this selection of trapping reactions, it was found that for the lithiated intermediates the reactivity was ordered as follows: 2-lithio pyrrolidine **164** > 2-lithio 4-phenyl piperidine *cis*-**201** > 2-lithio *N*'-Bn piperazine **199**. For the electrophiles, the order of reactivity observed was: PhCHO >> MeI > Me₂SO₄ > Me₃SiCl (Figure 4.7).

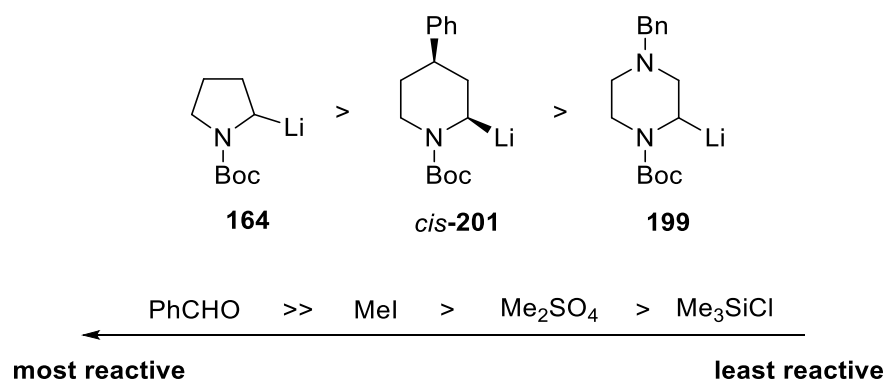


Figure 4.7. Reactivity series determined for the *N*-Boc heterocycle lithiated intermediates **164, *cis*-**201**, **199** and Me₃SiCl, Me₂SO₄, MeI and PhCHO electrophiles used in this investigation**

Providing a rationale that explained all of the trends in reactivity that were observed in this investigation was not possible. The reactivity data collected suggests that both steric and electronic factors likely influence the rate of the trapping reaction. The dominant effect that determines the rate of the trapping reaction is likely to be different for each different combination of lithiated intermediate and electrophile. Therefore, the use of a general rationale that provides information about the rate of the trapping reaction with a particular lithiated intermediate and electrophile may not be possible.

This inability to predict the reactivity of the trapping reactions of lithiated intermediate highlights how crucial ReactIRTM monitoring can be to ensure that complete trapping occurs. This is particularly important for asymmetric or diastereoselective lithiation-trapping reactions, where warming up the reaction before complete trapping has occurred can erode

the er/dr of the trapped products. The effect that the rate of the trapping reaction can have on the diastereoselectivity obtained is explored in Chapter 5.

With MeI, an additional complication arose due to the gelation of the reaction mixture that can give poor kinetic data and also results in incomplete trapping. Experiments conducted in this investigation suggest that the formation of LiI salts upon addition of MeI may be responsible for the gelation observed. This suggests that for the methylation of lithiated intermediates, Me₂SO₄ may be a more suitable electrophile. However, the lower reactivity of Me₂SO₄ also needs to be considered when evaluating the most suitable methylating electrophile.

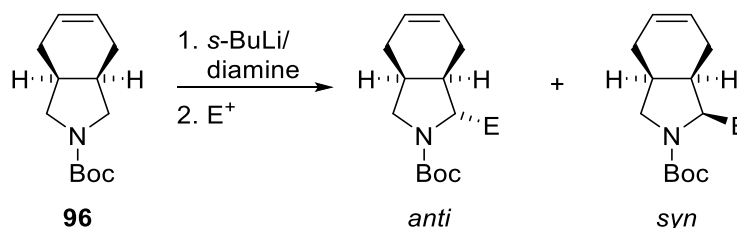
At this point in time, it is unclear whether expanding this trapping study further would provide any further useful information about the trapping reaction, as there is evidence that each combination of lithiated intermediate and electrophile may have a rate of trapping that is specific to that combination of reagents. However, the computational modelling of these trapping reactions of lithiated intermediates, similar to that conducted for the α -lithiation reaction in Chapter 2, may be able to provide an explanation for the reactivity observed. A computational model may be able to give a predicted reactivity for combinations of lithiated intermediate and electrophile and may be able to distinguish whether steric or electronic effects are primarily responsible for the reactivity observed for a specific trapping reaction. Ultimately, our overall conclusion is that real-time, *in situ* IR spectroscopic monitoring of the lithiation and trapping steps for *N*-Boc heterocycles should be widely adopted.

Chapter 5: Diastereoselective Lithiation-Trapping of a 3,4-Disubstituted Bicyclic *N*-Boc Pyrrolidine

The lithiation-trapping reactions of a significant array of *N*-Boc heterocycles have been reported since Beak's seminal publication in 1989.² However, to date, only a few of these *N*-Boc heterocycles have included a 3,4-disubstituted pyrrolidine motif as summarised in section 1.2.5.

In this Chapter, we bring together all of the methods and ideas developed in this thesis and apply them to a specific case study. The research presented in this Chapter focuses on the diastereoselective α -lithiation and trapping reactions of one particular 3,4-disubstituted *N*-Boc pyrrolidine **96** (Scheme 5.1). The effect of both the diamine ligand and the electrophile (E^+) on the diastereoselectivity of the lithiation-trapping reactions of *N*-Boc pyrrolidine **96** are investigated.

Scheme 5.1. General α -lithiation-trapping of 3,4-substituted *N*-Boc pyrrolidine **96**

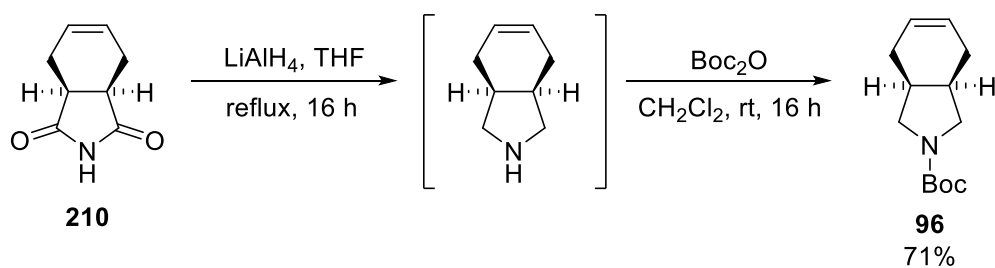


Since some interesting effects on diastereoselectivity were uncovered, additional experiments were performed and *in situ* IR spectroscopy was utilised to attempt to elucidate the results and trends that were observed. These experimental results are also complemented with computational DFT calculations in an attempt to model and rationalise the diastereoselectivity observed with the different diamine ligands employed.

5.1 Effect of the Electrophile on the Diastereoselectivity of the Lithiation-Trapping of a Bicyclic *N*-Boc Pyrrolidine

Bicyclic *N*-Boc pyrrolidine **96** was selected as a suitable substrate to investigate the diastereoselectivity of a 3,4-disubstituted pyrrolidine for two reasons. First, an asymmetric *s*-BuLi/(–)-sparteine lithiation-trapping reaction of *N*-Boc pyrrolidine **96** had previously been reported by Beak and Johnson (see Scheme 1.31).⁴ Second, *N*-Boc pyrrolidine **96** was available *via* a relatively simple two-step synthesis from imide **210**, a commercially available starting material. Reduction of imide **210** with LiAlH₄ and subsequent Boc protection of the secondary amine allowed the synthesis of 3,4-disubstituted *N*-Boc pyrrolidine **96** (71% yield) in multi-gram quantities (Scheme 5.2).

Scheme 5.2. Two-step synthesis of bicyclic *N*-Boc pyrrolidine **96**



The lithiation of *N*-Boc pyrrolidine **96** was carried out using 1.3 eq. *s*-BuLi/TMEDA in Et₂O at –78 °C with a 10 min lithiation time. This lithiation time was selected as the ReactIRTM-monitored lithiation of *N*-Boc pyrrolidine **96** conducted for the reactivity study (see Chapter 2) demonstrated that complete lithiation required just 4 min. The resulting lithiated intermediate was then trapped with a range of different electrophiles which furnished trapped products **99**, **211-214** in good yield and *anti:syn* diastereoselectivity that ranged from 87:13 \geq 95:5 (i.e. only one diastereomer detected by ¹H NMR spectroscopy) (Table 5.1).

Table 5.1. *s*-BuLi/TMEDA lithiation of *N*-Boc pyrrolidine **96** and subsequent trapping with a range of electrophiles

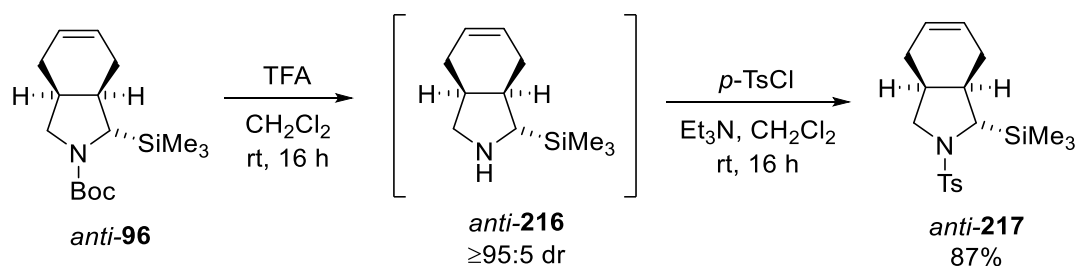
Entry	E ⁺	E	Products	Combined % yield ^a	<i>anti</i> : <i>syn</i> ^b
1	Me ₃ SiCl	SiMe ₃	<i>anti</i> - 99	75	≥95:5
2	Me ₂ SO ₄	Me	<i>anti</i> and <i>syn</i> - 211	83	90:10
3	CO ₂	COOH	<i>anti</i> and <i>syn</i> - 212	77	87:13
4	Weinreb amide 215	COPh	<i>anti</i> and <i>syn</i> - 213	73	87:13
5	PhCHO	C(OH)Ph	214 - See Figure 5.2	78	87:13

^a % yield of all diastereomers after purification by column chromatography (see text for details)

^b ratio of diastereomers determined by ¹H NMR spectroscopy (see text for details), for Me₃SiCl and Me₂SO₄ trappings the dr was determined from purified products and for CO₂, **215** and PhCHO electrophiles the dr was determined from the crude product.

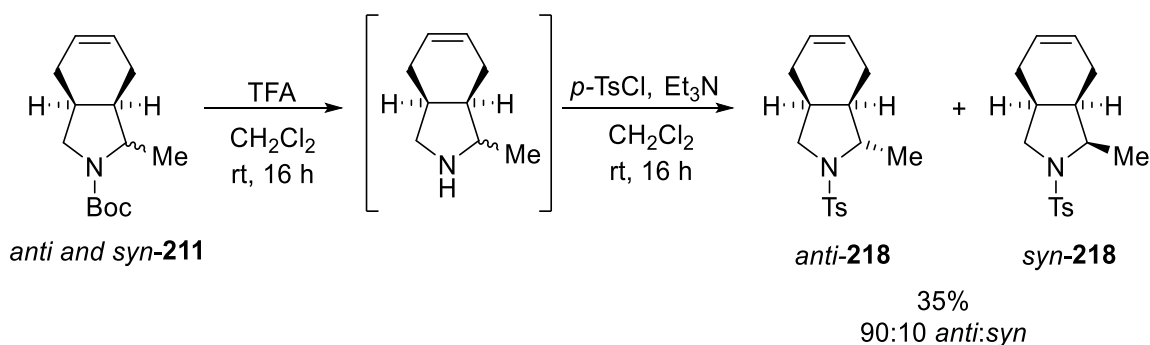
For the Me₃SiCl and Me₂SO₄ trapped adducts **99** and **211** (entries 1 and 2), it was not possible for the diastereomeric ratios to be measured directly using ¹H NMR spectroscopy. This was primarily due to rotamers (that arise due to the Boc group) which cause the signals in the ¹H NMR spectra to broaden, which can obscure the diastereomeric peaks. To remove the rotamers and this broadening effect for the Me₃SiCl-trapped product *anti*-**99**, the Boc group was removed and a sulfonamide was formed, for which rotamers do not occur. Removal of the Boc group from *anti*-**99** was accomplished using TFA and then subsequent treatment of crude amine *anti*-**216** with *p*-TsCl formed sulfonamide *anti*-**217** in 87% yield (Scheme 5.3). The ¹H NMR spectra of both crude amine *anti*-**216** and sulfonamide *anti*-**217** indicated that only one diastereomer was present and indicated that the Me₃SiCl-trapped product *anti*-**96** had been formed in ≥95:5 dr.

Scheme 5.3. Boc group cleavage and sulfonamide formation of *anti*-217



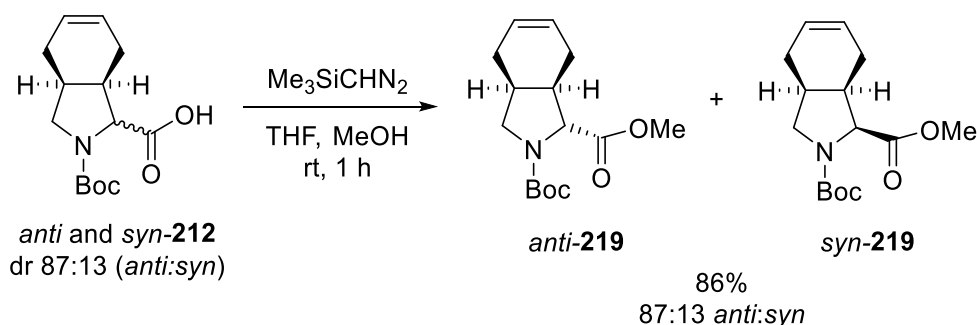
The sulfonamide formation procedure was also used to obtain the ratio of methyl-trapped adducts *anti*-211 and *syn*-211. After TFA cleavage of the Boc group and sulfonamide formation using *p*-TsCl, crude sulfonamides *anti*-218 and *syn*-218 were obtained in a 90:10 ratio. This ratio was unaffected by purification and a 90:10 mixture of sulfonamides *anti*-218 and *syn*-218 was obtained in 35% yield (Scheme 5.4).

Scheme 5.4. Boc group cleavage and sulfonamide formation of *anti*- and *syn*-218



Trapping the lithiated intermediate of *N*-Boc pyrrolidine **96** with CO_2 gave an 87:13 mixture of carboxylic acids *anti*-212 and *syn*-212 in a combined 77% yield (Table 5.1, entry 3). In this case, the dr was measured using the signals for the NCH α -proton adjacent to the carboxylic acid functional group in the ^1H NMR spectrum. This ratio was also confirmed by conversion of carboxylic acids *anti*-212 and *syn*-212 into the corresponding methyl esters, by methylation of the carboxylic acid with Me_3Si -diazomethane. This gave an 87:13 mixture of methyl esters *anti*-219 and *syn*-219 in 86% yield (Scheme 5.5).

Scheme 5.5. Esterification of carboxylic acids *anti*- and *syn*-**212**



Trapping with Weinreb amide **215** afforded an 87:13 mixture of ketones *anti*-**213** and *syn*-**213** (Table 5.1, entry 4). Ketones *anti*-**213** and *syn*-**213** were separable by column chromatography and were obtained in 67% and 6% yield respectively. PhCHO trapping gave an 87:13 *anti*:*syn* dr of trapped products (Table 5.1, entry 5) which was the same dr as those obtained by trapping CO_2 and Weinreb amide **215** electrophiles. However, the determination of the dr from the PhCHO trapping was a more complex task as it is possible to form four diastereomers of the PhCHO trapped product, due to the additional stereocentre (C4) on the benzylic alcohol (Figure 5.1).

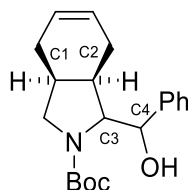


Figure 5.1. Stereogenic centres present on PhCHO trapped *N*-Boc pyrrolidine **214**

A convention to assign the relative stereochemistry was adopted for the four possible diastereomers formed by the PhCHO lithiation-trapping reaction. As the stereogenic centres C1 and C2 are fixed, it was decided to use stereogenic centres C2, C3 and C4 to define the relative stereochemistry of the product: the first label (*syn* or *anti*) defines the relative stereochemistry of the protons at C2 and C3 and the second label (*syn* or *anti*) defines the relative stereochemistry of the proton at C3 and the hydroxyl group at C4 with the phenyl group adopting the orientation depicted.

The *s*-BuLi/TMEDA lithiation and PhCHO trapping of *N*-Boc pyrrolidine **96** (Table 5.1, entry 5) gave a 4:9:29:58 mixture of diastereomeric alcohols *syn-anti*-**214**, *syn-syn*-**214**, *anti-syn*-**214** and *anti-anti*-**214** respectively (measured by ^1H NMR spectroscopy of the crude product). This gives an 87:13 *anti*:*syn* ratio for the C2-C3 relative stereochemistry (i.e. ignoring the C4 stereochemistry). After chromatography, products *syn-anti*-**214** (3%), *anti-*

syn-**214** (23%) and an 80:20 mixture of *anti*-*anti*-**214** and *syn*-*syn*-**214** (46%) were isolated by column chromatography, giving a 78% overall yield (Figure 5.2).

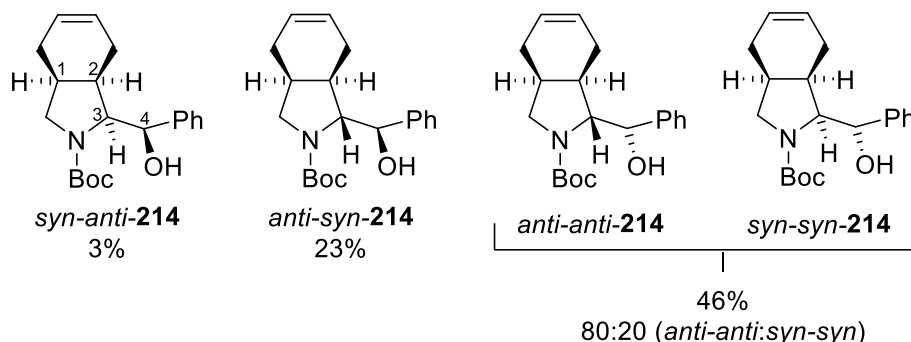
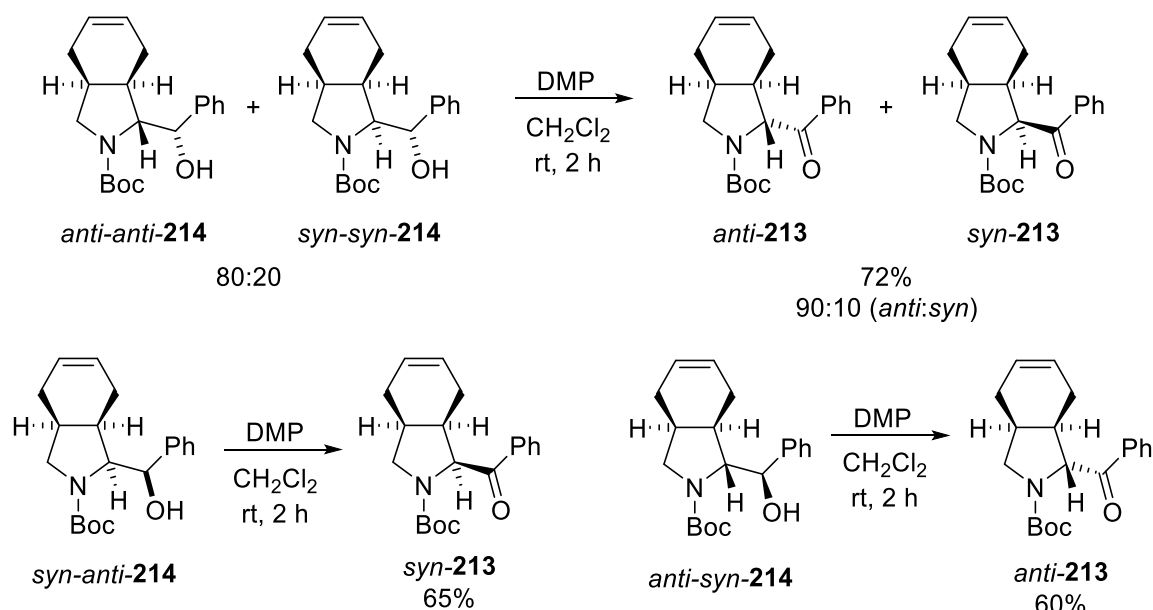


Figure 5.2. Diastereomeric alcohol products from the *s*-BuLi/TMEDA lithiation and PhCHO trapping of *N*-Boc pyrrolidine **96**

To identify the relative stereochemistry of each of the four diastereomers produced from the PhCHO trapping reaction, the alcohols were oxidised to their respective ketones using Dess-Martin periodinane (DMP). This removed the C4 benzylic stereocentre and reduced the number of diastereomers to only two. For the 80:20 mixture of *anti*-*anti*-**214** and *syn*-*syn*-**214**, DMP oxidation gave a 90:10 mixture of ketones *anti*-**213** and *syn*-**213** which were isolated in 72% yield. The presence of these two diastereomeric ketones indicated that this was a mixture of two diastereomers with different C2/C3 relative stereochemistries. For *syn*-*anti*-**214**, DMP oxidation yielded ketone *syn*-**213** (60%) and DMP oxidation of *anti*-*syn*-**214** yielded only *anti*-**213** (65%) (Scheme 5.6).

Scheme 5.6. DMP oxidation of diastereomeric alcohols **214 to identify relative stereochemistry**



The C3/C4 relative stereochemistry was determined using ^1H NMR spectroscopy. Literature precedent indicated that for similar PhCHO trapped *N*-Boc pyrrolidine **31**, *anti*-**31** had broad signals in its ^1H NMR spectrum, whereas *syn*-**31** did not show a broadening effect (Figure 5.3).¹³³ This study also included an X-ray crystal structure which confirmed the relative stereochemistry of *anti*-**31**. This same phenomenon was observed for the diastereomers of PhCHO-trapped 3,4-disubstituted pyrrolidine **214** which allowed the C3/C4 stereochemistry to be assigned.

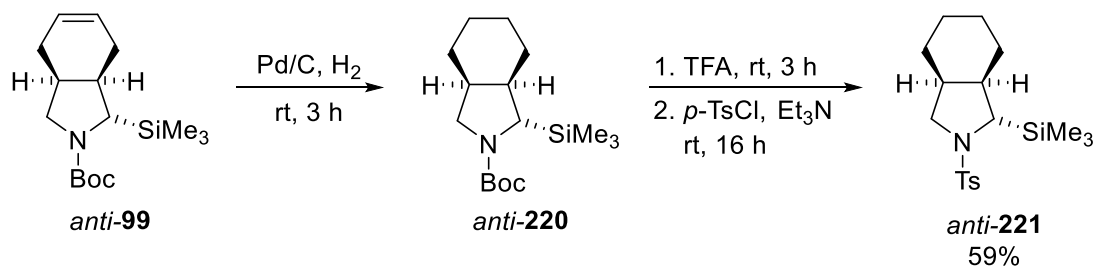


Figure 5.3. Diastereomeric alcohols *anti*-31** and *syn*-**31****

For all five lithiation-trapping reactions of *N*-Boc pyrrolidine **96** reported in Table 5.1, the *anti* diastereomer was the major diastereomer in the trapped products. The assignment of the *anti* relative stereochemistry was proved for the Me_3SiCl and the Weinreb amide **215**/PhCHO-trapped products. For methylated pyrrolidines *syn*-**211** and *anti*-**211** and carboxylic acids *syn*-**212** and *anti*-**212**, the relative stereochemistry was assigned by analogy.

For the Me_3SiCl -trapped adduct *anti*-**99**, there is literature precedent which also included an X-ray crystal structure for a similar saturated compound *anti*-**221**.⁴ To further support our assignment of this relative stereochemistry, Me_3SiCl -trapped pyrrolidine *anti*-**99** was converted into *anti*-**221**. First, *anti*-**99** was hydrogenated with Pd/C and H_2 to reduce the alkene. Then, *anti*-**220** was treated with TFA and then *p*-TsCl to cleave the Boc group and form the sulfonamide respectively. These transformations yielded sulfonamide *anti*-**221** as a single diastereomer ($\geq 95:5$ dr) in 59% yield (Scheme 5.7). The ^1H NMR spectrum of *anti*-**221** was identical to that reported in the literature, confirming the *anti* relative stereochemistry.⁴

Scheme 5.7. Hydrogenation, Boc deprotection and sulfonamide formation for Me₃SiCl-trapped product *anti*-99



The relative stereochemistry of the minor diastereomer for both the Weinreb amide **215** and PhCHO trapping reactions was proved by X-ray crystal analysis of ketone *syn*-**213**. Fortuitously, ketone *syn*-**213** was obtained as a solid after purification by column chromatography which, after recrystallisation, was subjected to X-ray analysis. X-ray analysis of *syn*-**213** confirmed the assignment of *syn* relative stereochemistry for the minor diastereomer (Figure 5.4).

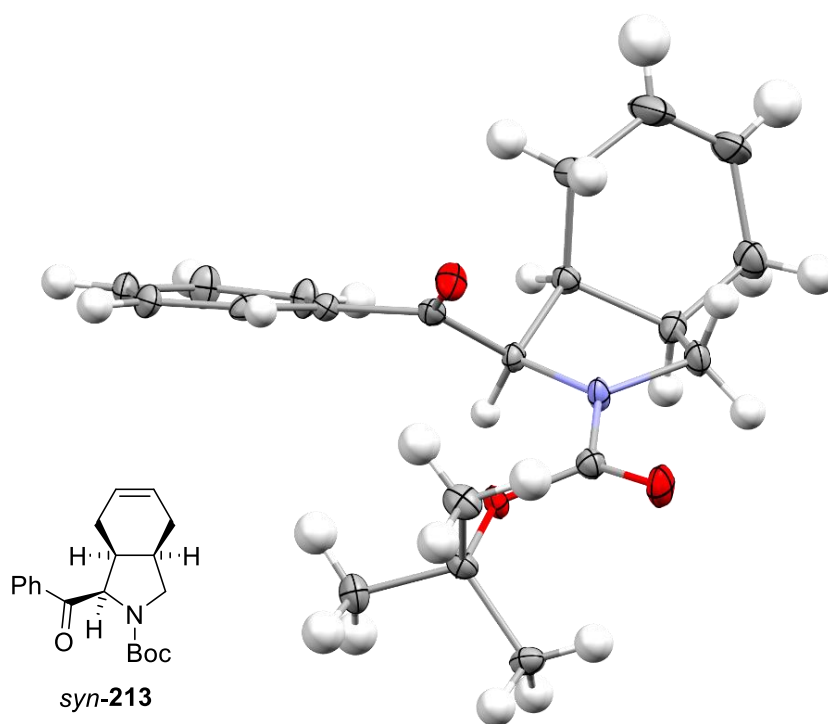


Figure 5.4. X-ray crystal structure of *syn*-213 with thermal ellipsoids set at 50%, confirming *syn* relative stereochemistry

This *anti* diastereoselectivity can be rationalised as follows. It is likely that the deprotonation of the least sterically hindered α -proton *anti* to the cyclohexene ring (H_{anti}) will be favoured,

forming lithiated intermediate *anti*-**222** as the major diastereomer (Figure 5.5). With *N*-Boc pyrrolidines, it is believed that the subsequent trapping reaction occurs with retention of stereochemistry, conserving the stereochemistries of lithiated intermediates *anti*-**222** and *syn*-**222**.

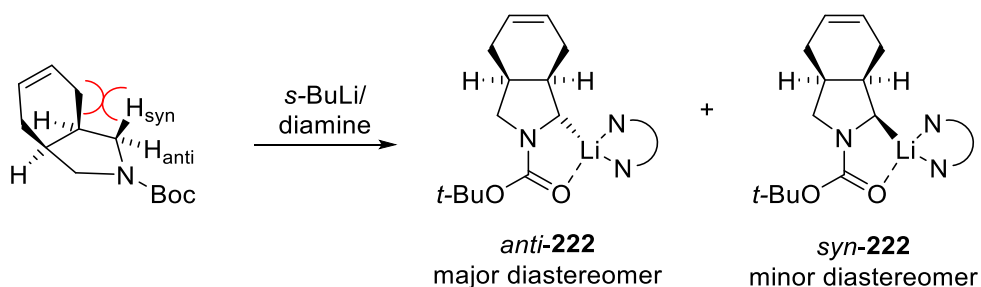


Figure 5.5. Rationale for the *anti* selectivity of the lithiation-trapping of *N*-Boc pyrrolidine **96**

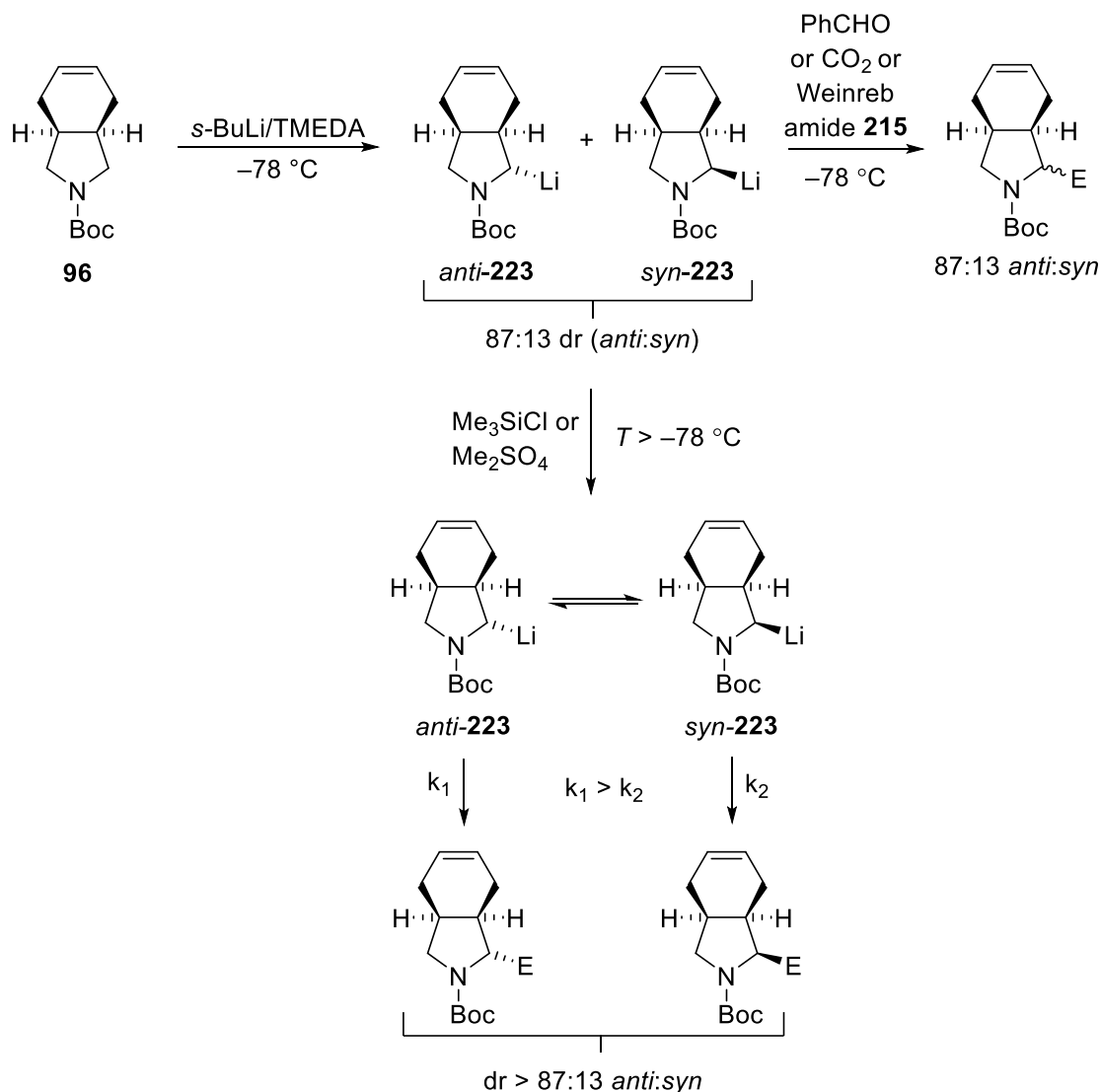
The drs obtained for the five lithiation-trapping reactions of *N*-Boc pyrrolidine **96** in Table 5.1 (87:13 to $\geq 95:5$) indicate that the reaction has good to excellent diastereoselectivity. However, the variation in the observed drs of the trapped products obtained with different electrophiles (Table 5.1) suggest that the dr of the trapped product does not simply arise from the diastereoselectivity of the lithiation reaction. If diastereoselectivity arose exclusively from the ratio of the lithiated intermediates, the drs of the products obtained by each different electrophile would be the same.

We therefore postulated that the variations in dr of the trapped products shown in Table 5.1 were caused by kinetic effects during the trapping reactions of diastereomeric lithiated intermediates *anti*-**222** and *syn*-**222**. When monitoring the trapping reactions of a similar unsubstituted lithiated *N*-Boc pyrrolidine **9** at $-78\text{ }^\circ\text{C}$, it was noted that the Me_3SiCl trapping reaction was relatively slow ($t_{1/2} = 86.9\text{ s}$) compared to other electrophiles such as PhCHO ($t_{1/2} < 8.6\text{ s}$). It is plausible that for a more hindered substrate such as 3,4-disubstituted *N*-Boc pyrrolidine **96**, this trapping reaction may be slower still. If the trapping of the lithiated intermediates *anti*-**222** and *syn*-**222** is slow, a dynamic kinetic resolution (DKR) could be established. There are many examples where establishing a DKR has been utilised to selectively generate compounds and cases where a DKR can alter the er of an asymmetric lithiation reaction.^{134–136}

It is possible that a DKR can be established if the trapping reaction is slow and the partially trapped or un-trapped lithiated intermediates are then allowed to warm to room temperature

before complete trapping has occurred (Scheme 5.8). At a temperature above $-78\text{ }^{\circ}\text{C}$ during the warming to room temperature after the trapping is believed to be complete, lithiated intermediates *anti*-**223** and *syn*-**223** will become configurationally unstable which enables them to interconvert. The configurational instability of lithiated intermediates at temperatures above $-20\text{ }^{\circ}\text{C}$ is well known.^{129,130,137} These rapidly converting lithiated intermediates can then be diastereoselectively trapped with the electrophile, as the rate of trapping for the two diastereomeric lithiated intermediates (k_1 and k_2) is likely to be different. It is logical that the trapping of lithiated intermediate *anti*-**223** will be faster than that of *syn*-**223** as there will be less steric interaction between the incoming electrophile and the cyclohexene ring. This will enrich the dr of the trapped product above that of the lithiated intermediate ($> 87:13$ for *s*-BuLi/TMEDA), thus giving a larger proportion of the *anti* diastereomer in the trapped product. Conversely, a faster trapping electrophile such as PhCHO (which was shown to trap lithiated intermediates in < 1 min in section 4.1) will trap lithiated intermediates *anti*-**223** and *syn*-**223** rapidly at $-78\text{ }^{\circ}\text{C}$, meaning that the configuration of the lithiated intermediates remains stable and the stereochemistry is retained. Therefore, the dr of the trapped products with a fast trapping electrophile should be representative of the diastereoselectivity imparted by the lithiation reaction.

Scheme 5.8. Proposed dynamic kinetic resolution for the trapping of 2-lithio *N*-Boc pyrrolidines *anti*-223 and *syn*-223

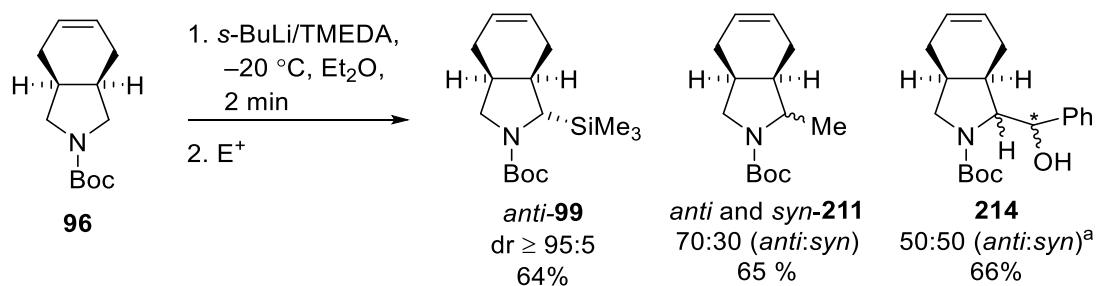


In an attempt to prove this dynamic kinetic resolution hypothesis, several ‘high temperature’ lithiation-trapping experiments were carried out using *N*-Boc pyrrolidine **96**. Lithiation of *N*-Boc pyrrolidine **96** was conducted at $-20\text{ }^\circ\text{C}$ and the resulting lithiated intermediate was trapped with Me_3SiCl , Me_2SO_4 and PhCHO electrophiles. It was expected that the lithiated intermediates formed from *N*-Boc pyrrolidine **96** would be configurationally unstable at $-20\text{ }^\circ\text{C}$, meaning that the lithiation would effectively impart no diastereoselectivity and diastereoselectivity in the products would be solely due to the trapping reaction.

The lithiation-trapping of *N*-Boc pyrrolidine **96** at $-20\text{ }^\circ\text{C}$ with PhCHO gave a 50:50 *anti:syn* mixture of diastereomeric alcohols. This result confirmed that the lithiated intermediates were not configurationally stable at $-20\text{ }^\circ\text{C}$ and that the fast PhCHO trapping reaction traps

the lithiated intermediates in the ratio that they are formed. The ‘high temperature’ lithiation-trapping of *N*-Boc pyrrolidine **96** with Me₃SiCl provided the same dr as when carried out at –78 °C, with only one diastereomer *anti*-**99** (≥95:5 dr) obtained in 64% yield. This indicated that only the trapping of diastereomeric lithiated intermediate *anti*-**222** was feasible at –20 °C, confirming that a DKR process does occur. The ‘high-temperature’ lithiation of pyrrolidine **96** and trapping with Me₂SO₄ gave a 70:30 mixture of the methylated products *anti*-**211** and *syn*-**211** (measured by ¹H NMR spectroscopy of the respective sulfonamides *anti*- and *syn*-**218** – see Scheme 5.4). This represented an eroded dr compared to the 90:10 *anti*:*syn* dr obtained at –78 °C (see Table 5.1, entry 2). This suggests there is a difference in the rate of the Me₂SO₄ trapping reactions of the lithiated intermediates *anti*-**222** and *syn*-**222** but the difference in rates was not as significant as for Me₃SiCl trapping, so both diastereomers of methylated product *anti*- and *syn*-**211** were still obtained (Scheme 5.9)

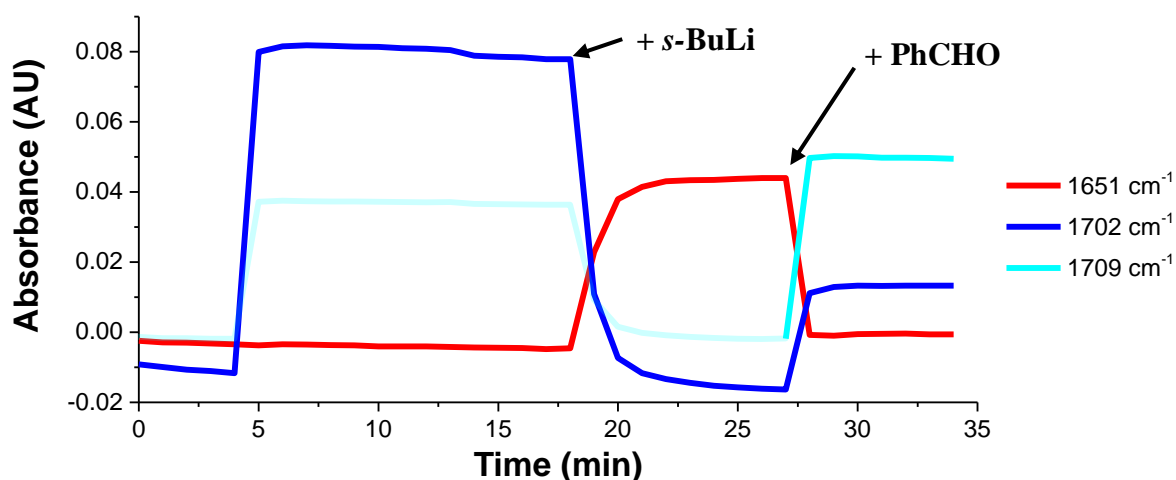
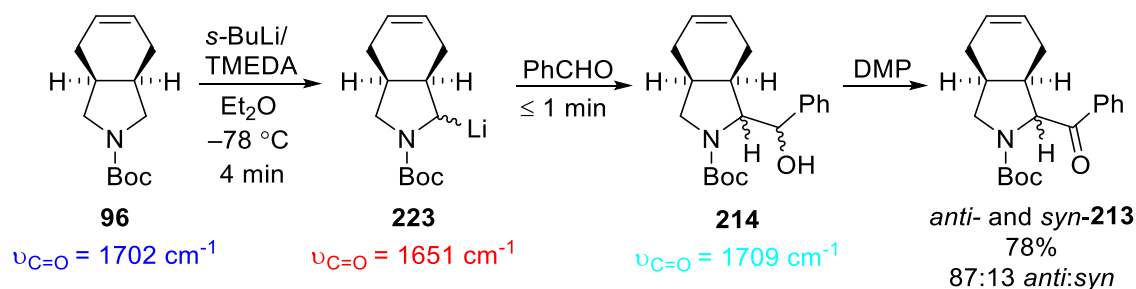
Scheme 5.9. ‘High temperature (–20 °C)’ lithiation trapping of *N*-Boc pyrrolidine **96**



^a Diastereomeric alcohols **214** were obtained in a 1:1:1:1 dr, the 50:50 dr reported ignores the highlighted stereocentre (*)

Further evidence for the occurrence of a dynamic kinetic resolution was provided by *in situ* IR spectroscopy. The ReactIRTM monitored *s*-BuLi/TMEDA lithiation and PhCHO trapping reaction of *N*-Boc pyrrolidine **96** at –78 °C confirmed our assumption that, analogous to the PhCHO trapping of unsubstituted *N*-Boc pyrrolidine **9** (see Table 4.1), PhCHO trapping occurred rapidly at –78 °C. After the lithiation of *N*-Boc pyrrolidine **96** was complete, PhCHO was added and complete trapping was observed at –78 °C within the one minute time lapse between scans (Scheme 5.10). The crude mixture of diastereomeric alcohol products **214** was oxidised with DMP to make purification and analysis easier and an 87:13 mixture of ketones *anti*-**213** and *syn*-**213** were obtained in 78% yield.

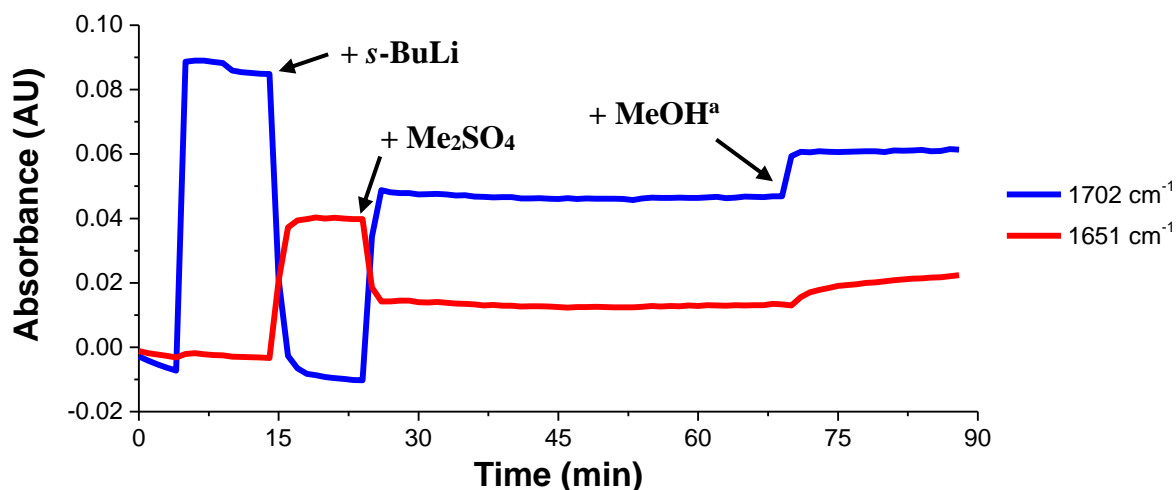
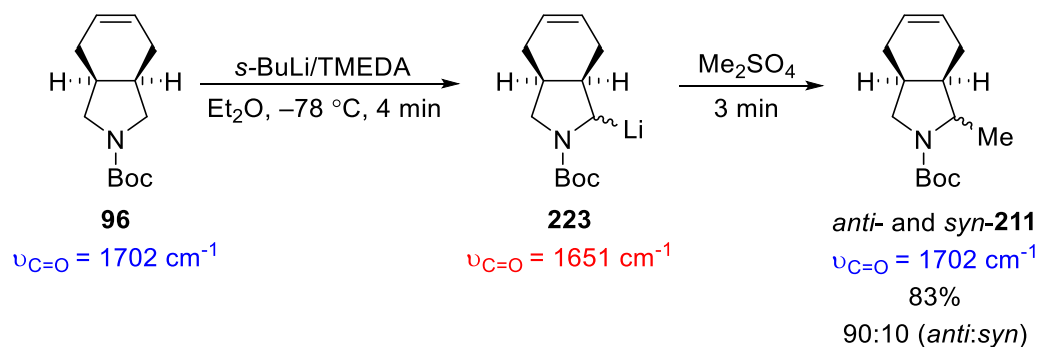
Scheme 5.10. ReactIRTM monitored lithiation-trapping of *N*-Boc pyrrolidine **96 with *s*-BuLi/TMEDA and PhCHO**



The ReactIRTM monitored lithiation-trapping of *N*-Boc pyrrolidine **96** with *s*-BuLi/TMEDA and Me₂SO₄ surprisingly gave a similar kinetic trace to that of the trapping with PhCHO. Following the lithiation of *N*-Boc pyrrolidine **96**, Me₂SO₄ was added and a relatively fast reaction (3 min trapping time) was observed (Scheme 5.11). A 3 min trapping time was also observed for the Me₂SO₄ trapping of lithiated *N*-Boc pyrrolidine **9** (see section 4.1). MeOH was added after 40 min to ensure that complete trapping had occurred at $-78 \text{ }^{\circ}\text{C}$. If any untrapped lithiated intermediate did remain it would be quenched by MeOH to reform the *N*-Boc pyrrolidine **96** starting material. No evidence of any further trapping was observed by ReactIRTM and only a small increase in both IR absorbances was observed due to a baseline shift resulting from the addition of MeOH. Additionally, ¹H NMR spectroscopic analysis of the crude product and purification indicated that no starting material was present confirming that complete trapping had occurred. As the trapping with Me₂SO₄ is fast at $-78 \text{ }^{\circ}\text{C}$, the lithiated intermediate should remain configurationally stable throughout. There is a slight difference between the 90:10 dr obtained with Me₂SO₄ and 87:13 drs obtained with CO₂, PhCHO and Weinreb amide **215** electrophiles. It is not currently known why this apparently fast trapping reaction provides a different dr to those with other fast trapping electrophiles.

It is possible this small difference in dr may arise due to measurement error in the ^1H NMR spectroscopic analysis.

Scheme 5.11. ReactIRTM monitored lithiation-trapping of *N*-Boc pyrrolidine **96 with *s*-BuLi/TMEDA and Me₂SO₄**

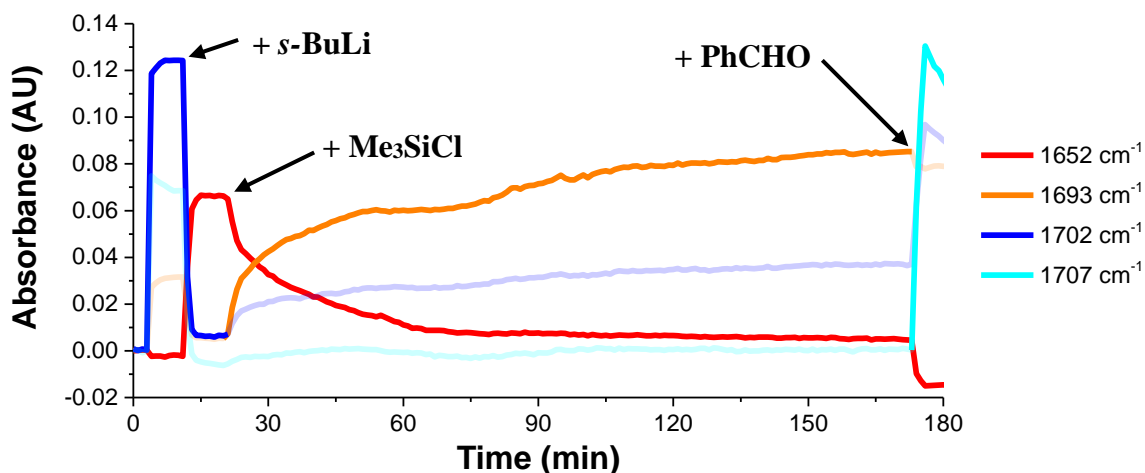
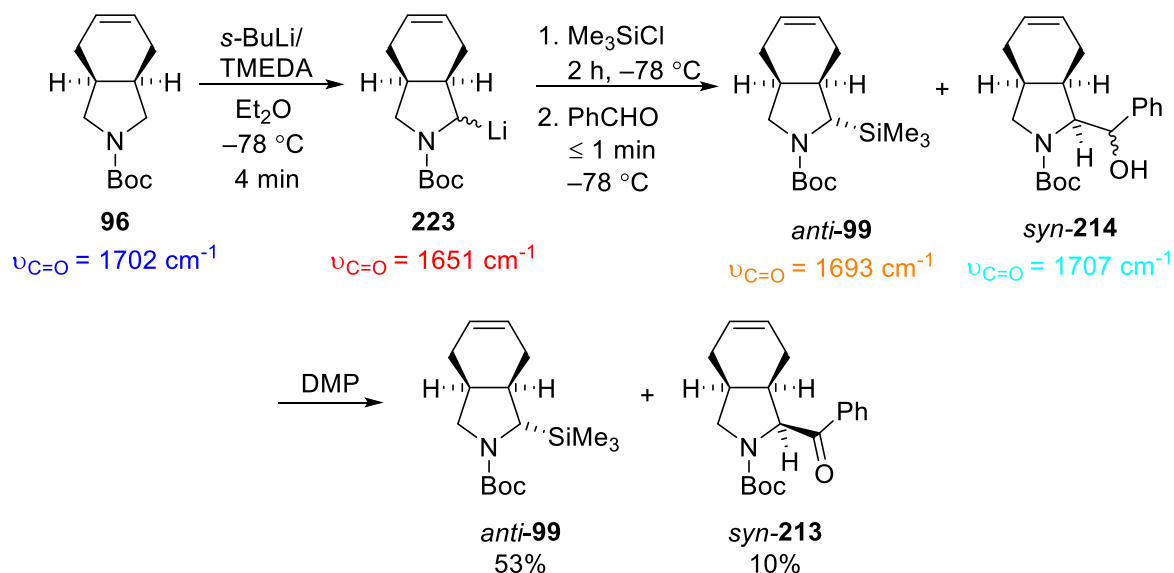


^a the increase in absorbance at 1702 cm^{-1} and 1651 cm^{-1} when MeOH was added is due to a shift in the baseline and is not due a change in the quantities of species **223** or **211**.

Finally, the *s*-BuLi/TMEDA lithiation-trapping of *N*-Boc pyrrolidine **96** was carried out using Me₃SiCl to trap the lithiated intermediates. After the 4 min lithiation at $-78 \text{ }^\circ\text{C}$, Me₃SiCl was added and, as expected, a slow trapping reaction was observed by ReactIRTM. The reaction is likely impeded by steric effects due to the sterically bulky Me₃SiCl electrophile. After 2 h at $-78 \text{ }^\circ\text{C}$, the consumption of the lithiated intermediate ceased. A second, fast-trapping electrophile, PhCHO, was added to trap any remaining un-trapped lithiated intermediate. Upon addition of PhCHO, the ReactIRTM monitoring indicated further consumption of lithiated intermediate which was complete within 1 min (Scheme 5.12). Clearly, a second trapping event with the PhCHO had occurred. The crude product was then treated with DMP to oxidise the alcohol diastereomers to simplify analysis and purification.

After oxidation, Me₃SiCl trapped *anti*-**99** and PhCHO trapped and oxidised *syn*-**213** were isolated in 53% and 10% yield respectively.

Scheme 5.12. ReactIR™ monitored lithiation-trapping of *N*-Boc pyrrolidine **96 with *s*-BuLi/TMEDA and Me₃SiCl/PhCHO**



This result indicated that the trapping of lithiated intermediate *syn*-**223** with Me₃SiCl is either extremely slow or does not occur. Thus, when Me₃SiCl was used as the electrophile only lithiated intermediate *anti*-**223** underwent trapping to form 2-silyl product *anti*-**99** at $-78 \text{ }^\circ\text{C}$. In this two-electrophile example, the un-trapped lithiated intermediate *syn*-**223** was trapped when the PhCHO electrophile was added. This explains why the two products obtained, *anti*-**99** and *syn*-**213**, are diastereomerically pure. On the other hand, if Me₃SiCl was the only electrophile added, the unreacted *syn*-**223** lithiated intermediate would lose configurational stability during the warming of the reaction and interconvert into *anti*-**223** which is then

trapped by Me₃SiCl. This accounts for why trapping with Me₃SiCl gives only one observed diastereomer ($\geq 95:5$ dr, see Table 5.1, entry 1), as the reaction was allowed to warm slowly to room temperature after addition of Me₃SiCl.

In conclusion, these lithiated intermediate trapping studies have shown that the electrophile used can have a significant effect on the diastereoselectivity observed for the lithiation-trapping of a 3,4-disubstituted *N*-Boc pyrrolidine such as **96**. A less reactive/slower trapping electrophile can allow a dynamic kinetic resolution to be established, which can then enrich dr of the trapped products beyond that established by the lithiation reaction itself.

5.2 Effect of the Diamine Ligand on the Diastereoselectivity of the Lithiation-Trapping of a Bicyclic *N*-Boc Pyrrolidine

The effect that the diamine ligand has on the diastereoselectivity of the lithiation-trapping of 3,4-disubstituted *N*-Boc pyrrolidine **96** was also studied. The study used five of the diamine ligands which had previously been employed for the reactivity study in Chapter 2: TMPDA **179**, TMEDA, TMCDA *trans*-**161**, DPE **177** and tetraisopropyl diamine **178**. In addition to these ligands, two bispidine ligands di-*n*-Pr bispidine **105** and di-*i*-Pr bispidine **30** were also used to probe how the identity of the diamine would affect the diastereoselectivity observed (Figure 5.6).

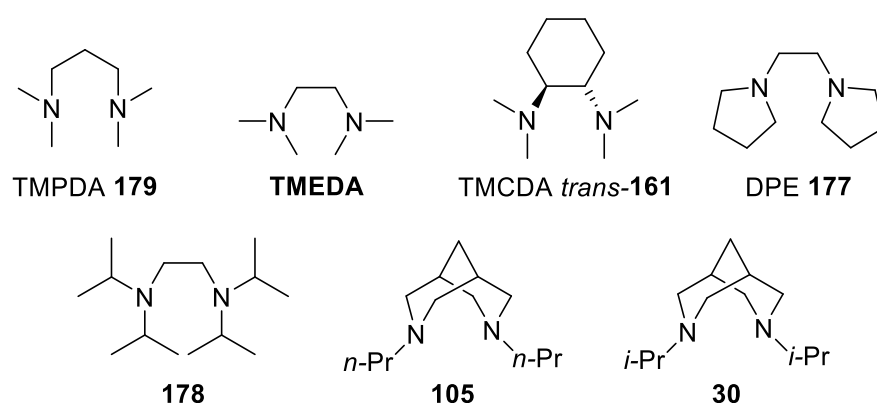
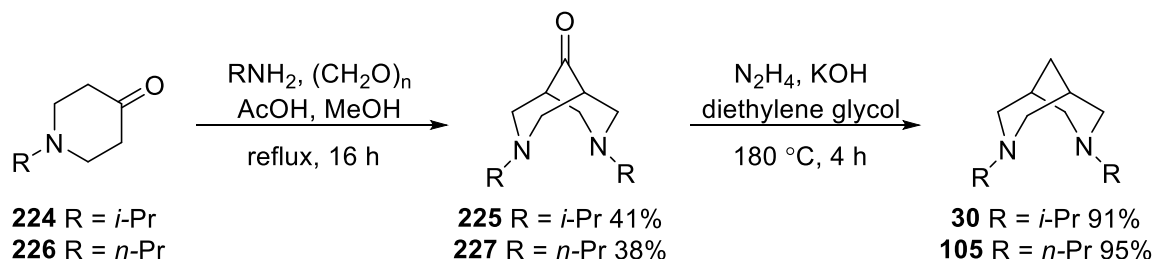


Figure 5.6. Diamine ligands used for the lithiation of bicyclic pyrrolidine **96**

Bispidine ligands **105** and **30** have both been prepared and used in previous work conducted by the O'Brien group. However, this previous work was in a different vein where they were used in conjunction with (–)-sparteine for a catalytic purpose.^{37,138} Both di-*i*-Pr bispidine **30** and di-*n*-Pr bispidine **105** were synthesised following an existing optimised procedure.¹³⁸ For di-*i*-Pr bispidine **30**, this involved the synthesis of bispidone **225** (in 41% yield) *via* a double Mannich reaction of *N*-*i*-Pr-piperid-4-one **224** with paraformaldehyde and *i*-PrNH₂. A subsequent Huang-Minlon modified Wolff-Kishner reduction of the resulting bispidone **225** gave bispidine **30** in a good 91% yield (Scheme 5.13). The same procedure was used for the synthesis of di-*n*-Pr bispidine **105**. The bispidone intermediate was synthesised using a double Mannich reaction with *N*-*n*-Pr-piperid-4-one **226** and *n*-PrNH₂ which gave bispidone **227** in 38% yield. Next, bispidone **227** was subjected to Wolf-Kishner reduction giving di-*n*-Pr bispidine in 95% yield. The double Mannich reaction provided only moderate 41% and 38% yields of bispidone intermediates **225** and **227**; it is likely that the poor yields result from the purification of the intermediates. Bispidones **225** and **227** were purified by vacuum distillation but complete separation from the messy crude product was difficult and

distillation at higher temperature resulted in decomposition of bispidones **225** and **227**. ^1H NMR spectroscopic analysis of the resulting tar-like residue indicated that significant amounts of the bispidone were still present after distillation. The problematic purification and low yielding double Mannich reaction for a different bispidone has also been reported.⁵³

Scheme 5.13. Synthesis of the di-*i*-Pr and di-*n*-Pr bispidone ligands **30 and **105****



During the synthesis of the bispidones **225** and **227** and bispidines **30** and **105**, another complexity arose when characterising the compounds using ^1H NMR spectroscopy. It appeared that these compounds were reacting with the CDCl_3 NMR solvent. The ^1H NMR spectra for the bispidones **225** and **227** showed the expected peaks but there was also a complex mixture of products that were unidentifiable (Figure 5.7). NMR samples of **225** and **227** were then prepared using a DMSO-d_6 solvent which gave the expected spectra.

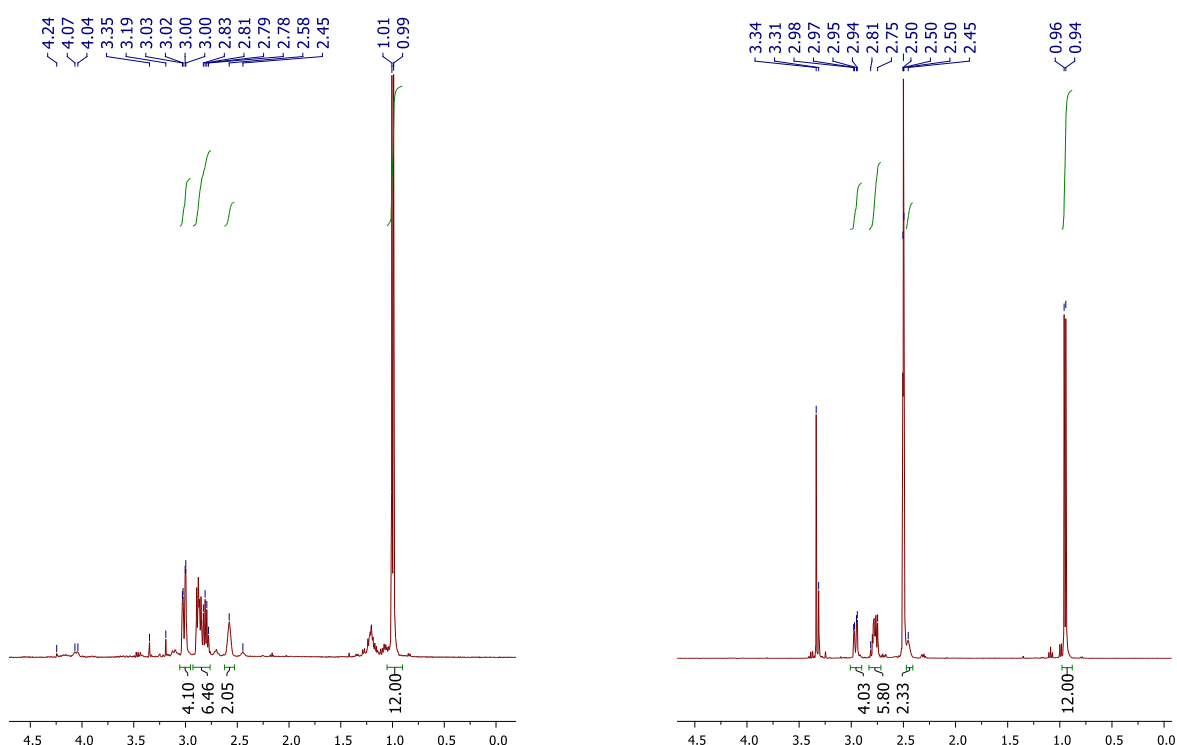


Figure 5.7. ^1H NMR spectra showing 4.5-0.0 ppm region for di-*i*-Pr bispidone **225 in CDCl_3 (left) and DMSO-d_6 (right) (peaks at 3.34, 3.31 and 2.50 due to H_2O , HOD and DMSO solvent)**

When ^1H NMR spectroscopic analysis of bispidines **30** and **105** was conducted in CDCl_3 , none of the expected signals were observed and an unidentifiable complex mixture of products was recorded instead. In contrast, when NMR samples of bispidines **30** and **105** were prepared using a DMSO-d_6 solvent, the expected well resolved spectra were obtained (Figure 5.8).

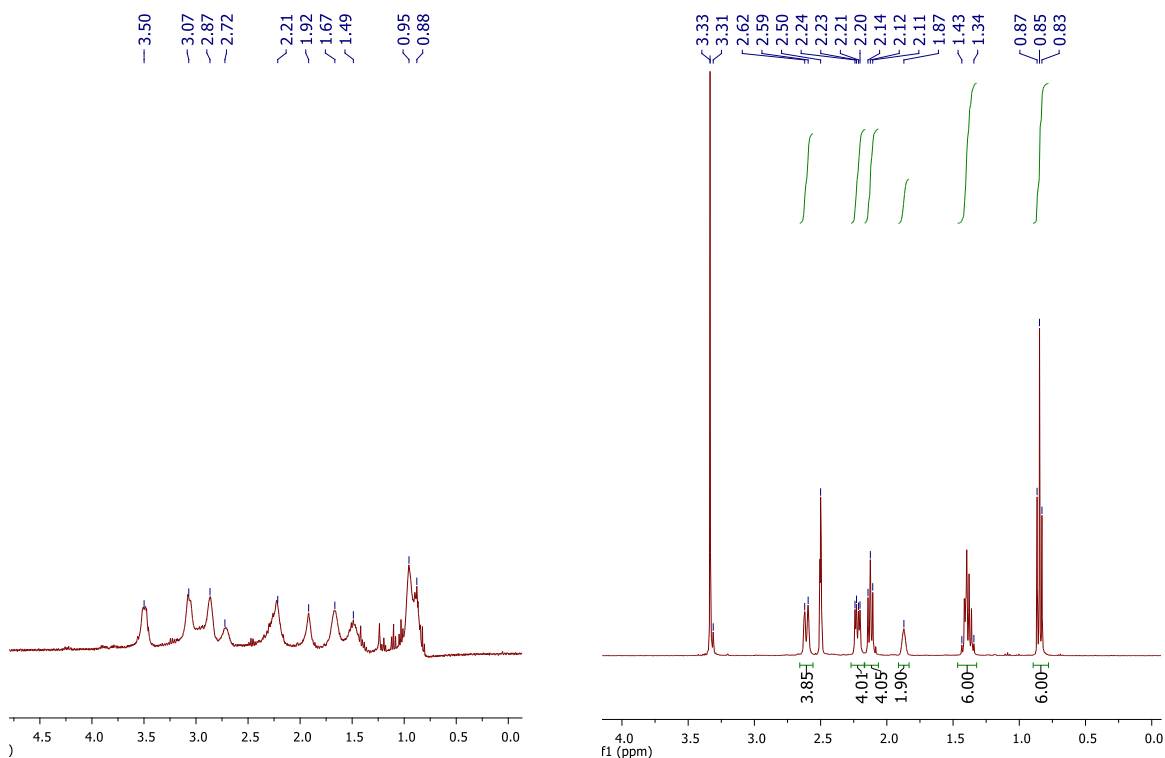
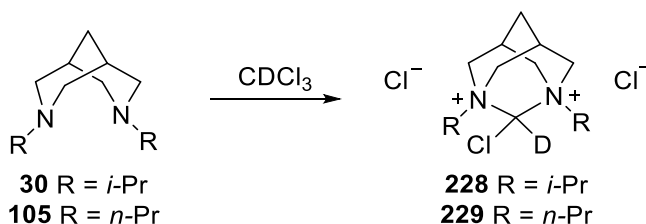


Figure 5.8. ^1H NMR spectra showing 4.0-0.0 ppm region for di-*n*-Pr bispidine **105** in CDCl_3 (left) and DMSO-d_6 (right) (peaks at 3.33, 3.31 and 2.50 due to H_2O , HOD and DMSO solvent)

As the use of the DMSO-d_6 solvent gave the expected spectra for bispidones **225** and **227** and bispidines **30** and **105**, it was likely that the CDCl_3 solvent was reacting with the diamines. This undesired reaction would account for the complex and messy ^1H NMR spectra collected in CDCl_3 . The two tertiary amines on the diamines could perform a nucleophilic attack on CDCl_3 forming a chloro-methylene bridge between the amine centres, giving salts **228** and **229** (Scheme 5.14). This type of reaction has been observed between the bispidine (–)-sparteine and CH_2Br_2 but a 12 h reflux was required to form the dibromo salt.¹³⁹ Unpublished work by a researcher at Merck also observed an analogous salt formation (characterised by X-ray crystallography) from an NMR sample of the (+)-sparteine surrogate **17** in CDCl_2 , stored at room temperature.¹⁴⁰

Scheme 5.14. Proposed reaction between bispidines **30** and **105** and CDCl_3



The selection of diamine ligands in Figure 5.6 were chosen as it was considered that the varying steric bulk on the different diamines may provide a wide range of diastereoselectivities. The use of a more sterically hindered diamine will result in a more sterically bulky *s*-BuLi/diamine lithiation complex. Therefore, this bulky lithiating complex will likely encounter more steric hindrance than *s*-BuLi/TMEDA when the *syn* proton of *N*-Boc pyrrolidine **96** (H_{syn}) is deprotonated due to the interactions between the cyclohexyl substituent and the lithiating complex (Figure 5.9). This will raise further the energy barrier of H_{syn} deprotonation whilst having a negligible effect on the H_{anti} deprotonation barrier. This increased difference between the H_{syn} and H_{anti} deprotonation energies should increase the diastereoselectivity furnishing a higher proportion of the *anti* trapped product.

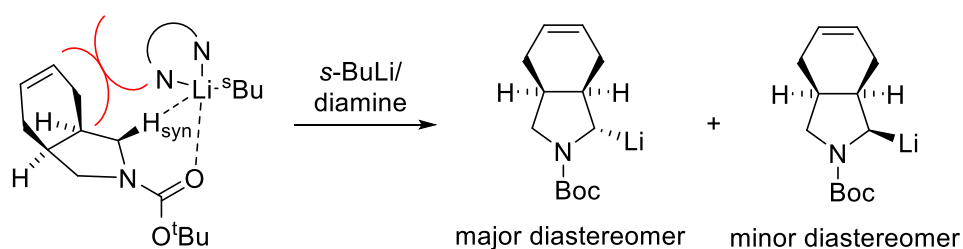
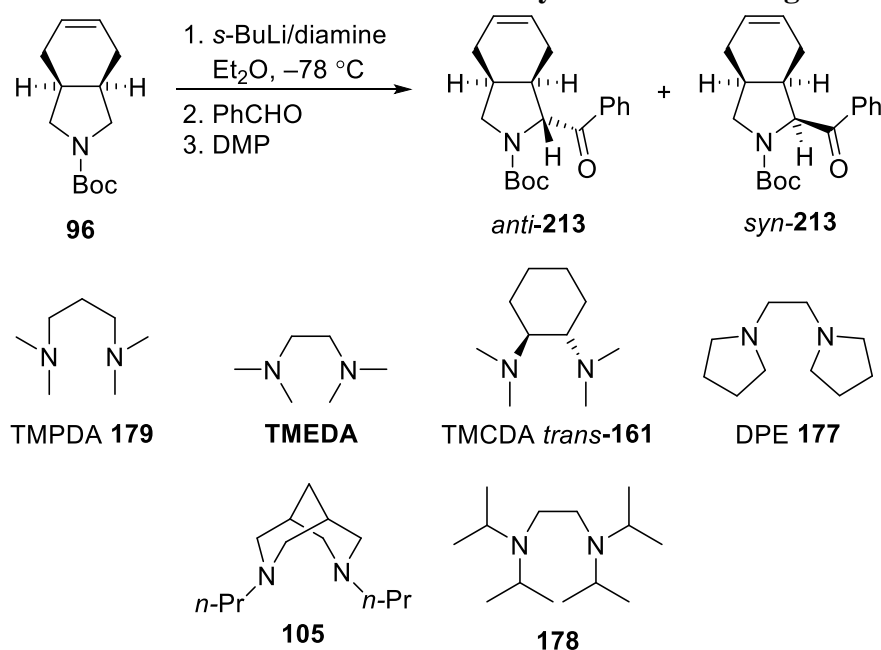


Figure 5.9. Disfavoured H_{syn} deprotonation of *N*-Boc pyrrolidine **96 with a bulky diamine ligand**

The *s*-BuLi/diamine lithiation and PhCHO trapping at $-78\text{ }^\circ\text{C}$ in Et_2O was selected as the control reaction to investigate how the choice of diamine affected the diastereoselectivity of the lithiation of *N*-Boc pyrrolidine **96**. PhCHO was selected as the trapping electrophile due to its compatibility with the ReactIRTM and the fast rate of trapping. This fast rate of trapping ensured that the dr of the trapped product should mirror the dr in which the lithiated intermediates were generated, as explained earlier in this chapter. All the lithiation-trapping reactions were monitored using ReactIRTM to ensure that reactions were given enough time for complete lithiation of *N*-Boc pyrrolidine **96** to occur. The crude product was then oxidised with DMP making analysis and purification of the diastereomeric products easier. The lithiation-trapping of *N*-Boc pyrrolidine **96** with the different *s*-BuLi/diamine complexes

provided ketones *anti*-**213** and *syn*-**213** in good yield over the two steps and in a narrow range of diastereoselectivity (80:20->95:5 dr) (Table 5.2). On the other hand, the lithiation times required for complete lithiation of *N*-Boc pyrrolidine **96** varied significantly with the different *s*-BuLi/diamine combinations. The lithiation-trapping of *N*-Boc pyrrolidine **96** with *s*-BuLi/di-*i*-Pr bispidine **30** was problematic and is not included in Table 5.2 – it is discussed later.

Table 5.2. *s*-BuLi/diamine and PhCHO lithiation-trapping procedure for *N*-Boc pyrrolidine **96** to determine the diastereoselectivity of the diamine ligand used



Entry	Ligand	dr (<i>anti</i> : <i>syn</i>) ^a	%Yield ^b	Lithiation time ^c
1	TMPDA 179	80:20	67	9 h
2	TMEDA	87:13	78	4 min
3	TMCDA <i>trans</i> - 161	87:13	76	4 min
4	DPE 177	92:8	86	50 min
5	di- <i>n</i> -Pr bispidine 105	94:6 ^d	86 ^d	40 min
6	178	>95:5	16	> 16 h ^e

^a dr measured by ¹H NMR spectroscopy of crude mixture of ketones *anti*-**213** and *syn*-**213** after DMP oxidation

^b combined isolated yield of ketones *anti*-**213** and *syn*-**213** after DMP oxidation

^c ReactIRTM measured lithiation time for the *s*-BuLi/diamine lithiation of *N*-Boc pyrrolidine **96** at -78 °C

^d trapping was conducted with CO₂, forming acids *anti*-**212** and *syn*-**212**

^e lithiation was only monitored for the first 7 h by ReactIRTM. However, after a 16 h lithiation at -78 °C, ketones *anti*-**213** and *syn*-**213** were obtained in only 16% yield and a 62% yield of unreacted **96** was recovered

Lithiation of *N*-Boc pyrrolidine **96** with *s*-BuLi/TMPDA **179** offered the lowest degree of diastereoselectivity, giving an 80:20 mixture of ketones *anti*-**213** and *syn*-**213** (entry 1). The slow 9 h lithiation time suggests that lithiation may occur with *s*-BuLi/Et₂O rather than *s*-BuLi/TMPDA **179**, due to poor coordination of the TMPDA **179** ligand to the *s*-BuLi, as suggested for lithiation of *N*-Boc pyrrolidine **9** (see Section 2.2). It is therefore possible that the *s*-BuLi/Et₂O lithiation of *N*-Boc pyrrolidine **96** is actually responsible for the 80:20 *anti:syn* dr observed.

The lithiation of *N*-Boc pyrrolidine **96** with both *s*-BuLi/TMEDA and *s*-BuLi/TMCDA *trans*-**161** gave diastereomeric ketones *anti*-**213** and *syn*-**213** in identical 87:13 dr (entries 2 and 3). This is likely due to the structural similarity of both ligands, both having similar steric arrangement around the nitrogen atoms of the amine groups. The rates of the lithiation of *N*-Boc pyrrolidine **96** with both *s*-BuLi/TMEDA and *s*-BuLi/TMCDA *trans*-**161** were similar, with both requiring 4 min for complete lithiation. The same 4 min lithiation time was observed for the *s*-BuLi/TMEDA and *s*-BuLi/TMCDA *trans*-**161** lithiations of *N*-Boc pyrrolidine **9** (see section 2.2) which suggests the substituents of the 3- and 4-positions of the pyrrolidine do not have any significant effect on the rate of lithiation with these diamine ligands.

The *s*-BuLi/DPE **177** lithiation of *N*-Boc pyrrolidine **96** provided an enhanced level of diastereoselectivity over that exhibited with *s*-BuLi/TMEDA, with ketones *anti*-**213** and *syn*-**213** obtained in a 92:8 dr (entry 4). The 50 min lithiation of *N*-Boc pyrrolidine **96** with *s*-BuLi/DPE **177** was significantly slower than the lithiation of **96** with *s*-BuLi/TMEDA. The same reduction in the rate of lithiation was observed for the *s*-BuLi/DPE **177** lithiation of unsubstituted *N*-Boc pyrrolidine **9** (60 min lithiation time – see section 2.2). In Chapter 2, it was proposed that *s*-BuLi/DPE may be significantly more sterically bulky than *s*-BuLi/TMEDA and hence the slower rate of lithiation. The increased steric bulk of *s*-BuLi/DPE **177** would also provide a reason for the enriched *anti:syn* dr measured in the trapped products.

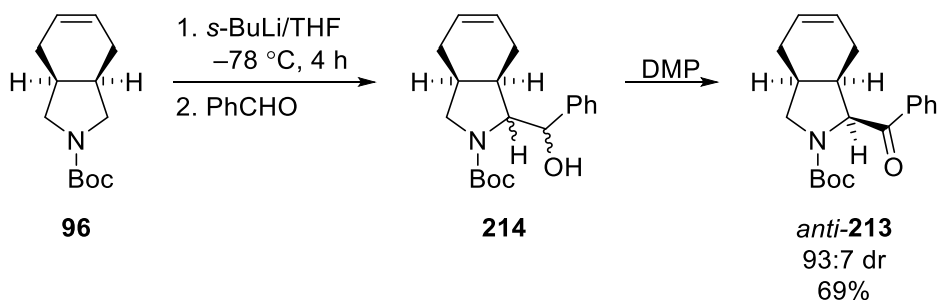
The *s*-BuLi/di-*n*-Pr bispidine **105** lithiation of *N*-Boc pyrrolidine **96** provided further enhancement to the level diastereoselectivity that was afforded, with a 94:6 mixture of acids *anti*-**212** and *syn*-**212** obtained (entry 5). This improvement in diastereoselectivity over the 87:13 dr obtained with *s*-BuLi/TMEDA (entry 2) most likely arises from the increasing bulk of diamine which further hinders the formation of the *syn* diastereomer. Lithiation of a

similar bicyclic *N*-Boc pyrrolidine with *s*-BuLi/di-*n*-Pr bispidine **105** and trapping with CO₂ afforded a 95:5 *anti:syn* ratio of trapped products (see Scheme 1.36).

A 16 h *s*-BuLi/**178** lithiation of *N*-Boc pyrrolidine **96** provided ketones *anti*-**213** and *syn*-**213** in a promising $\geq 95:5$ dr but in only 16% yield (entry 6). *N*-Boc pyrrolidine **96** starting material was recovered in 62% yield suggesting that either the lithiated intermediate is not stable with diamine **178** or that lithiation is very slow (> 16 h). A technical issue with the ReactIRTM equipment meant that only the first 7 h of the lithiation was recorded and lithiation was not complete within this 7 h window. This result hints at the fact that the bulky ligands required to achieve complete diastereoselectivity may have an adverse effect on the reactivity, slowing the lithiation reaction. Therefore, a compromise between the reactivity and the diastereoselectivity of the diamine may be required to obtain both a good yield and dr of the trapped product.

The lithiation of *N*-Boc pyrrolidine **96** was also attempted using the ‘diamine free’ *s*-BuLi/THF lithiating conditions developed by our group.²⁵ ReactIRTM monitoring of the reaction indicated that, after 4 h, the lithiation of *N*-Boc pyrrolidine **96** was complete and PhCHO was added. After DMP oxidation of the crude product, a mixture of ketones *anti*-**213** and *syn*-**213** was obtained in a good 93:7 *anti:syn* dr and 69% yield (Scheme 5.15). We postulate that the increased diastereoselectivity observed in the *s*-BuLi/THF lithiation of pyrrolidine **96** could be due to the sterically bulky *s*-BuLi/THF complex (probably with two THF molecules ligating the lithium).

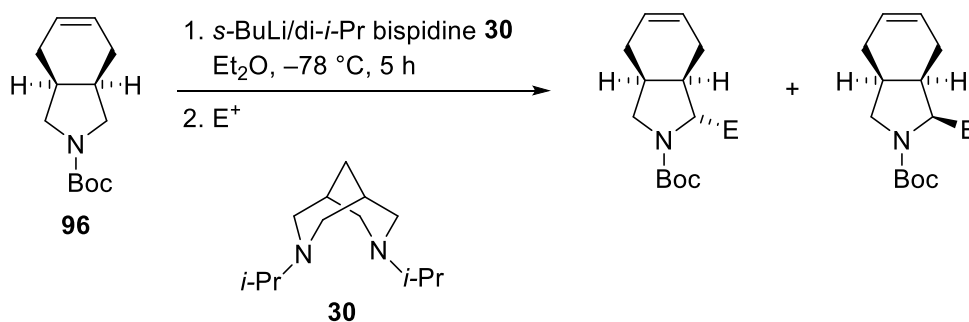
Scheme 5.15 *s*-BuLi/THF lithiation *N*-Boc pyrrolidine **96**, PhCHO trapping and oxidation with DMP



As mentioned, the lithiation-trapping of *N*-Boc pyrrolidine **96** with *s*-BuLi/di-*i*-Pr bispidine **30** proved to be problematic. ReactIRTM monitoring indicated that *s*-BuLi/di-*i*-Pr bispidine **30** lithiation of **96** was slow, with 5 h required for complete lithiation to occur. Using this lithiation time determined by ReactIRTM, the *s*-BuLi/di-*i*-Pr bispidine **30** lithiation-trapping

of *N*-Boc pyrrolidine **96** was carried out using Me₃SiCl, Me₂SO₄ and CO₂ electrophiles (Table 5.3). Trapping with Me₃SiCl provided only recovered starting material (by ¹H NMR spectroscopic analysis of the crude product) (entry 1). Trapping with Me₂SO₄ provided a 90:10 mixture of methylated pyrrolidines *anti*-**211** and *syn*-**211** in 38% yield together with 34% starting material recovery (entry 2). CO₂ trapping provided a 90:10 mixture of acids *anti*-**212** and *syn*-**212** in 51% yield and 47% recovered starting material (entry 3).

Table 5.3. *s*-BuLi/di-*i*-Pr bispidine **30** lithiation of *N*-Boc pyrrolidine **96** and trapping with Me₃SiCl, Me₂SO₄ and CO₂ electrophiles



Entry	E ⁺	E	dr (<i>anti</i> : <i>syn</i>) ^a	%Yield ^b	SM, %Yield ^c
1	Me ₃ SiCl	SiMe ₃	--	--	100 ^d
2	Me ₂ SO ₄	Me	90:10	38	34
3	CO ₂	COOH	90:10	51	47

^a drs measured by ¹H NMR spectroscopy (for Me₂SO₄ trapping, dr measured by sulfonamide formation - see Scheme 5.4)

^b combined isolated yield of *anti* and *syn* diastereoisomers

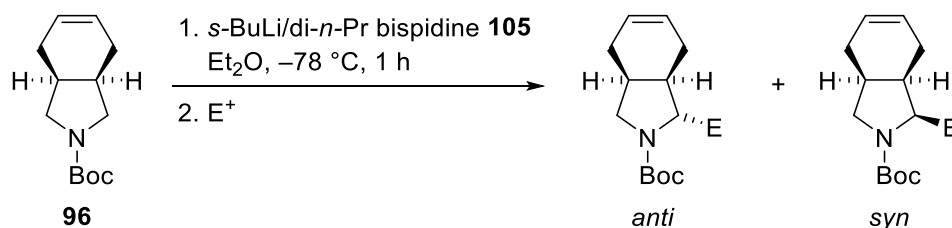
^c % yield of isolated starting material **96** after purification of trapped products

^d ¹H NMR spectroscopy of crude product indicated that only starting material was present

The lithiation-trapping reactions with all three electrophiles indicated that complete trapping had not occurred. In the case of the Me₃SiCl trapping, no trapped product was detected (entry 1) which may result from the bulky di-*i*-Pr bispidine ligand **30** hindering the trapping process with the bulky Me₃SiCl electrophile (even after warming to room temperature). Both Me₂SO₄ and CO₂ trapping reactions provided a 90:10 mixture of *anti* and *syn* products with starting material also recovered. It was anticipated that the dr observed with the di-*i*-Pr bispidine ligand **30** would be similar or greater than that of the di-*n*-Pr bispidine **105** due to the additional steric bulk of the *i*-Pr groups but the drs are potentially unreliable as complete trapping has not occurred. It is possible that the recovery of starting materials may indicate poor stability of the lithiated intermediate with bispidine ligand **30**.

For comparative purposes, the lithiation of *N*-Boc pyrrolidine **96** with *s*-BuLi/*di-n*-Pr bispidine **105** and trapping with Me₃SiCl, Me₂SO₄ and CO₂ electrophiles was also conducted. This provided tri-substituted pyrrolidines **99**, **211-214** in drs varying from 90:10-94:6 (*anti*:*syn*) and yields ranging from 64-87% (Table 5.4).

Table 5.4. *s*-BuLi/*di-n*-Pr bispidine **105** lithiation of *N*-Boc pyrrolidine **96** and trapping with Me₃SiCl, Me₂SO₄ and CO₂ electrophiles



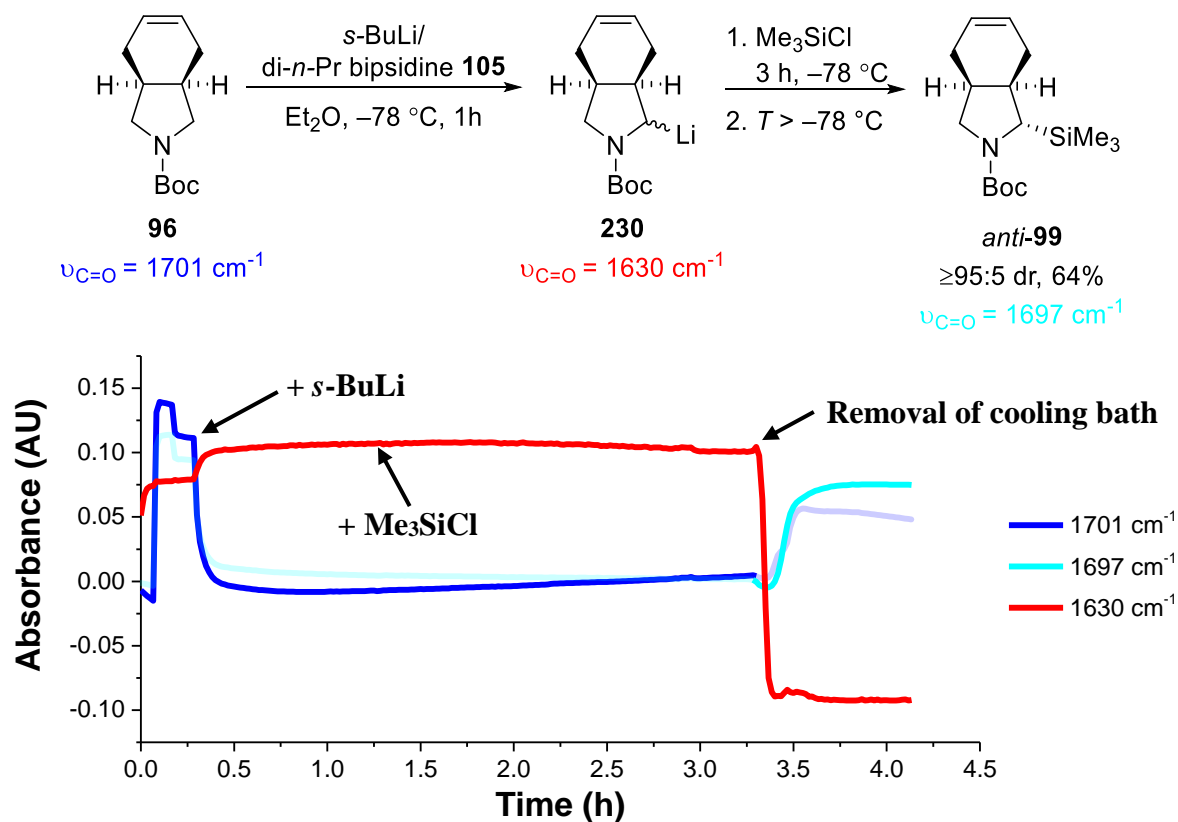
Entry	E ⁺	E	dr (<i>anti</i> : <i>syn</i>) ^a	%Yield ^b
1	Me ₃ SiCl	SiMe ₃	≥95:5	64
2	Me ₂ SO ₄	Me	90:10	77
3	CO ₂	COOH	94:6	86

^a drs measured by ¹H NMR spectroscopy (for Me₂SO₄ trapping, dr measured by sulfonamide formation - see Scheme 5.4)

^b combined isolated yield of *anti* and *syn* diastereoisomers

The *s*-BuLi/*di-n*-Pr bispidine **105** lithiation of *N*-Boc pyrrolidine **96** and subsequent trapping with CO₂ provided a 94:6 ratio of carboxylic acids of *anti*-**212** and *syn*-**212** (entry 3). Presumably, the fast trapping CO₂ electrophile will give the trapped products in the dr that the lithiated intermediates are formed in. Trapping with Me₃SiCl provided only the *anti*-**99** diastereomer and Me₂SO₄ gave a 90:10 *anti*:*syn* dr, both of these results were identical to those using the *s*-BuLi/TMEDA lithiating conditions (Table 5.1, entries 1 and 2). These trapping reactions with Me₃SiCl and Me₂SO₄ provide further evidence that a dynamic kinetic resolution likely occurs with the slower trapping electrophiles. The *s*-BuLi/*di-n*-Pr bispidine and Me₃SiCl lithiation-trapping of *N*-Boc pyrrolidine **96** was also monitored using ReactIRTM to probe the rate of trapping. After lithiation of pyrrolidine **96** was complete, Me₃SiCl was added and very little or no trapping was observed at -78 °C; it was only upon the warming of the reaction that trapping was observed (Scheme 5.16).

Scheme 5.16. ReactIR™ monitored lithiation-trapping of *N*-Boc pyrrolidine **96 with *s*-BuLi/*di-n*-Pr bispidine **105** and Me₃SiCl**



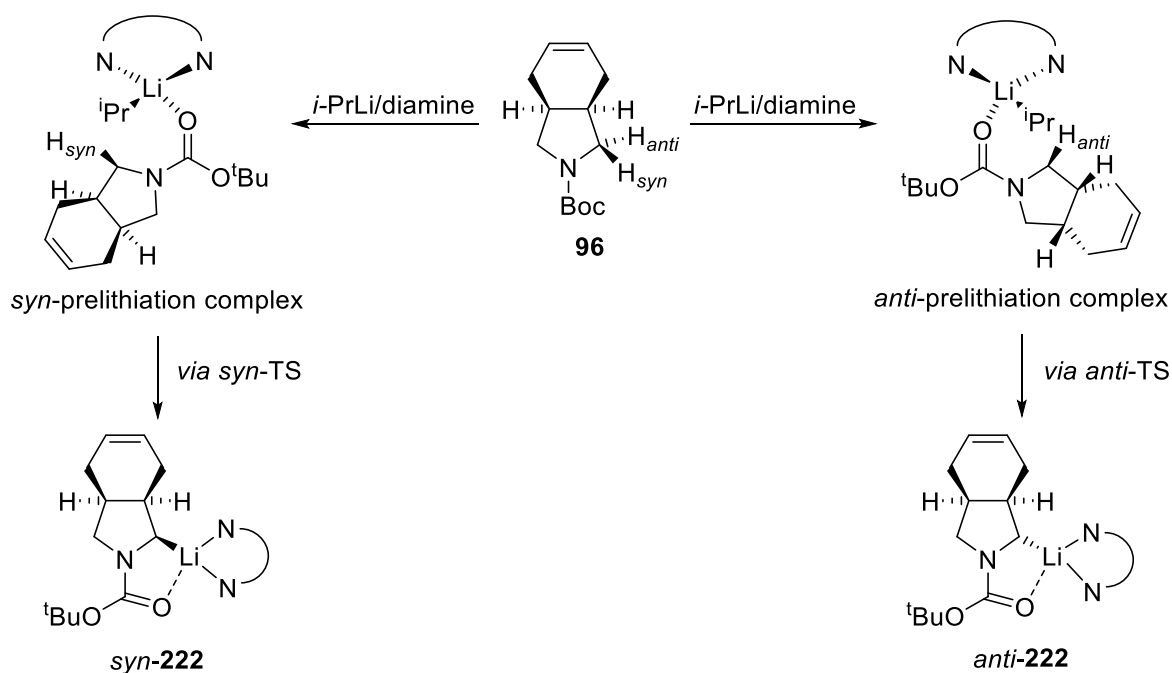
The Me₃SiCl trapping of *N*-Boc pyrrolidine **96** with *s*-BuLi/*di-n*-Pr bispidine **105** displayed slightly different kinetics to that with *s*-BuLi/TMEDA (see Scheme 5.12). No trapping occurs at all with *s*-BuLi/*di-n*-Pr bispidine **105** at -78 °C whereas with *s*-BuLi/TMEDA, trapping of the *anti*-**223** lithiated intermediate does occur at -78 °C. This difference is likely due to the increased steric bulk of the *di-n*-Pr bispidine **105** diamine ligand, making the trapping of lithiated intermediate *anti*-**230** unfeasible at such a low temperature. Conversely, trapping of *anti*-**223** which is coordinated to the less bulky TMEDA ligand is facile enough to occur at -78 °C.

To conclude, a range of diamine ligands have been employed to investigate the diastereoselective lithiation of *N*-Boc pyrrolidine **96**. A narrow range of diastereoselectivity in the lithiation reaction was observed when different *s*-BuLi/ligand combinations were employed resulting in the formation in trapped products in good to excellent dr. A trend between the steric bulk of the ligand and diastereoselectivity was discovered. It was also noted that the dynamic kinetic resolution established with slow trapping electrophiles was also observed when a different diamine ligand was employed.

5.3 Computational DFT Modelling of the Diastereoselective Lithiation

An attempt to model the diastereoselective lithiation of 3,4-disubstituted *N*-Boc pyrrolidine **96** with the different *s*-BuLi/ligand lithiating complexes was undertaken using DFT, following a similar approach to that used in Chapter 3. This involved modelling prelithiation complexes and transition states for the lithiation of *N*-Boc pyrrolidine **96** for the formation of both lithiated intermediates *anti*-**222** and *syn*-**222** (Scheme 5.17). The pro-*syn* and pro-*anti* reaction pathways were modelled using *i*-PrLi as the alkyllithium (as detailed in Chapter 3) and models were constructed for each of the different ligands investigated experimentally in Table 5.2.

Scheme 5.17. DFT modelling of the diastereoselective lithiation of *N*-Boc pyrrolidine **96**



First, the *i*-PrLi/TMEDA lithiation of *N*-Boc pyrrolidine **96** was modelled to explore whether DFT modelling could calculate an energy difference between the pathways for the formation of lithiated intermediates *anti*-**222** and *syn*-**222**. The B3LYP and M06 DFT functionals used for modelling in the reactivity study in Chapter 3, were utilised to model this diastereoselective lithiation reaction. Both DFT functionals used gave near identical optimised geometries and the M06/6-31G* optimised transition states for both the *syn* and *anti* diastereomer formation are presented in Figure 5.10.

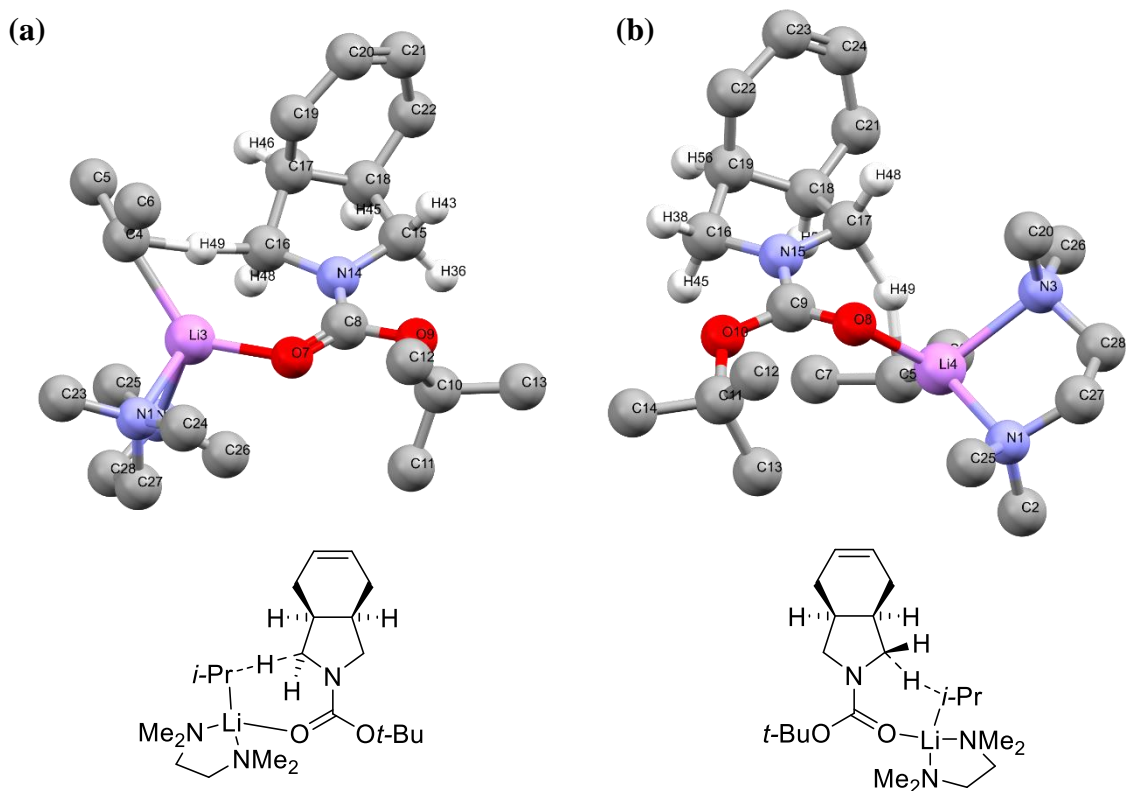


Figure 5.10. M06/6-31G* optimised transition state geometries for the *syn* (a) and *anti* (b) lithiation of *N*-Boc pyrrolidine **96** – only protons on the pyrrolidine ring shown for clarity

The energies calculated with both DFT functionals did indeed show an energy difference between the *anti* and *syn* pathways with both indicating that the *anti* pathway is favoured (Table 5.5).

Table 5.5. Prelithiation complex and activation free-energies for the *anti* and *syn* *i*-PrLi/TMEDA lithiation of *N*-Boc pyrrolidine **96** calculated with B3LYP/6-31G* and M06/6-31G*

Method	ΔG^a	<i>syn</i> ΔG^\ddagger	<i>anti</i> ΔG^\ddagger	$\Delta\Delta G^\ddagger$
	/kcal mol ⁻¹	/kcal mol ⁻¹	/kcal mol ⁻¹	/kcal mol ⁻¹
B3LYP/6-31G*	0.41	14.07	12.98	1.50
M06/6-31G*	0.00	12.54	11.52	1.02

^a difference in free energy between the *anti* and *syn* prelithiation complexes ($G_{syn} - G_{anti}$)

The B3LYP functional indicated that the *anti* prelithiation complex was lower in energy than the *syn* prelithiation complex which was 0.41 kcal mol⁻¹ higher in energy. However, the M06 functional gave no difference between the free energies of the *syn* and *anti* prelithiation

complexes. Both DFT functionals indicated that the major driving force for the diastereoselectivity is due to the significant difference in activation free energies (ΔG^\ddagger) for *anti* and *syn* lithiation. Both DFT functionals calculated that the activation energy for the formation of the *anti* lithiated intermediate was lower than that of the *syn* intermediate. As there is evidence that pre-lithiation complex formation is fast and reversible, as discussed in Chapter 2, the Curtin-Hammett principle can be used to relate these calculated energies to the ratio of diastereomers that should be observed in the reaction. The Curtin-Hammett principle states that the ratio of products (in this case diastereomers) depends on the value $\Delta\Delta G^\ddagger$, the difference in energy of the transition states for the formation of each product.

The energy difference between transition states of *anti* and *syn* lithiation of pyrrolidine **96** ($\Delta\Delta G^\ddagger$) with *i*-PrLi/TMEDA was calculated as 1.50 kcal mol⁻¹ with the B3LYP functional and $\Delta\Delta G^\ddagger = 1.02$ kcal mol⁻¹ using the M06 functional. These energy differences appear to be small but at a low temperature of -78 °C, this small energy difference can have a marked effect on the selectivity. Use of the Curtin-Hammett equation (Equation 5.1) and the calculated $\Delta\Delta G^\ddagger$ from the DFT modelling allows a predicted *anti:syn* ratio to be calculated using the theoretical data (Table 5.6).

$$\frac{anti}{syn} = e^{-\frac{\Delta\Delta G^\ddagger}{RT}} \quad \text{(Equation 5.1)}$$

where $\Delta\Delta G^\ddagger$ is the energy difference between the diastereomer transition states (in J mol⁻¹), R is the universal gas constant (8.314 J K⁻¹) and T is temperature (195 K \equiv -78 °C).

Table 5.6. Predicted *anti:syn* drs for the *i*-PrLi/TMEDA lithiation of *N*-Boc pyrrolidine **96**

Entry	DFT Functional	Calculated $\Delta\Delta G^\ddagger$ /kcal mol ⁻¹	Predicted dr (<i>anti:syn</i>)
1	B3LYP	1.50	98:2
2	M06	1.02	93:7

The B3LYP modelled lithiation of *N*-Boc pyrrolidine **96** significantly overestimates the diastereoselectivity of the reaction providing an estimated 98:2 *anti:syn* dr. DFT modelling with the M06 function also overestimates the diastereoselectivity of the lithiation, albeit to a lesser extent with a predicted 93:7 *anti:syn* dr calculated. However, this is a promising result which is somewhat closer to the experimentally measured 87:13 dr.

With these initial results for TMEDA in hand, the same modelling procedure was conducted for a selection of the ligands used in the experimental diastereoselectivity study. Both the *syn* and *anti* lithiated intermediate formation for *N*-Boc pyrrolidine **96** with TMPDA **179**, DPE **177**, di-*n*-Pr bispidine **105** and THF ligands were modelled using the B3LYP and M06 DFT functionals (Tables 5.7 and 5.8). The lithiation of pyrrolidine **96** was not modelled with *i*-PrLi/TMCDA *trans*-**161** as it provided an identical experimental result to that with TMEDA.

Table 5.7. Calculated diastereoselectivity of the *i*-PrLi/ligand lithiation of *N*-Boc pyrrolidine **96 with B3LYP/6-31G***

Entry	Ligand	Calculated $\Delta\Delta G^\ddagger$ /kcal mol ⁻¹	Predicted dr (<i>anti:syn</i>)	Experimental dr (<i>anti:syn</i>)
1	TMPDA 179	1.08	94:6	80:20
2	TMEDA	1.50	98:2	87:13
3	DPE 177	0.82	89:11	92:8
4	di- <i>n</i> -Pr bispidine 105	1.36	97:3	94:6
5	THF	1.17	95:5	93:7

The predicted diastereoselectivities obtained from the B3LYP functional presented in Table 5.7 exhibited very little correlation to the experimental drs. Ligands such as di-*n*-Pr bispidine **105** (entry 4) and THF (entry 5) which offered improved diastereoselectivity over TMEDA in the experimental study were predicted to be less diastereoselective than TMEDA by the DFT modelling. The B3LYP functional also predicted that lithiation using DPE **177** as the ligand would result in the least diastereoselective lithiation which disagrees with the experimental dr obtained (entry 3). *i*-PrLi/TMPDA was predicted to afford a good level of diastereoselectivity in the lithiation reaction (entry 1), similar to that of *i*-PrLi/di-*n*-Pr bispidine **105** and *i*-PrLi/THF (entries 4 and 5 respectively). This result conflicted with the experimentally determined drs which indicated that TMPDA imparted the least diastereoselectivity in the lithiation of *N*-Boc pyrrolidine **96**.

The M06 DFT functional provided some predicted diastereoselectivities for the lithiation of *N*-Boc pyrrolidine **96** that were in slightly better agreement with those observed experimentally (Table 5.8). However, similar to the diastereoselectivities predicted with the

B3LYP DFT functional, most of the drs predicted with the M06 DFT functional were also overestimated.

Table 5.8. Calculated diastereoselectivity of the *i*-PrLi/ligand lithiation of *N*-Boc pyrrolidine **96 with M06/6-31G***

Entry	Ligand	Calculated $\Delta\Delta G^\ddagger$ /kcal mol ⁻¹	Predicted dr (<i>anti</i> : <i>syn</i>)	Experimental dr (<i>anti</i> : <i>syn</i>)
1	TMPDA 179	1.80	99:1	80:20
2	TMEDA	1.02	97:3	87:13
3	DPE 177	0.56	81:19	92:8
4	di- <i>n</i> -Pr bispidine 105	2.26	99.5:0.5	94:6
5	THF	3.28	100:0	93:7

Modelling the diastereoselectivity of the lithiation of *N*-Boc pyrrolidine **96** with the M06 DFT functional did provide two significant outliers. First, as with the results obtained with the B3LYP functional, the M06 functional suggested that *i*-PrLi/DPE **177** (entry 3) would offer worse diastereoselectivity than *i*-PrLi/TMEDA (entry 2) which contradicted the experimental result. Second, the *i*-PrLi/TMPDA **179** lithiation of **96** was predicted to be highly diastereoselective by the DFT modelling (entry 1). This contradicted the experimental results which indicated that *s*-BuLi/TMPDA exhibited poorer diastereoselectivity than *s*-BuLi/TMEDA for the lithiation of *N*-Boc pyrrolidine **96**. The occurrence of these anomalous results when modelling the lithiation of **96** with *i*-PrLi/TMPDA with both B3LYP and M06 DFT functional could arise due to a possible lack of coordination of TMPDA to the alkyllithium; this possibility was suggested previously when the nominal reactivity of the *s*-BuLi/TMPDA complex was discussed. A lack of coordination of the alkyllithium and ligand is not accounted for in the computational model where the ligand and alkyllithium are explicitly modelled as being coordinated to each other.

In summary, the computational DFT modelling correctly predicted the *anti* diastereoselectivity observed for the lithiation of *N*-Boc pyrrolidine **96**. However, attempting to predict the dr for the different diamines using both B3LYP and M06 DFT functionals provided no clear overall correlation between the experimental and calculated drs. The narrow range of diastereoselectivity observed for the lithiation of *N*-Boc pyrrolidine **96** with the different *s*-BuLi/ligand combinations further complicated this investigation, as

the relatively small differences in diastereoselectivity require accurate computational calculations to reproduce these small differences in energy between diastereomer formation. This problem is also further exacerbated by the low reaction temperatures used ($-78\text{ }^{\circ}\text{C}$) which mean that small differences in energy between the pathways of *anti* and *syn* lithiation can have a significant effect on the dr obtained. More accurate geometry optimisations and energy calculations are difficult to obtain without significant additional computational expense and this is further compounded by the relatively large size of the model (~ 80 atoms). For this study, DFT was chosen to optimise these models as it is a good compromise between accuracy and performance but for the modelling of diastereoselectivity, the level of theory used may not provide sufficiently accurate energies.

5.4 Conclusions and Future Work

Research in this Chapter has indicated that both the electrophile and the diamine can influence the diastereoselectivity of the lithiation of 3,4-disubstituted *N*-Boc pyrrolidine **96**. The choice of electrophile affects the rate of the trapping reaction between the lithiated intermediate and electrophile, and can therefore affect the dr. Slow trapping electrophiles such as Me_3SiCl result in a dynamic kinetic resolution which enriches the dr of the trapped products whereas we presume that fast trapping electrophiles trap the lithiated intermediates in the dr they are formed. The lithiation of *N*-Boc pyrrolidine **96** with a range of *s*-BuLi/ligand complexes indicated that the diastereoselectivity of the reaction can also be modified by the ligand employed. A general trend between the diastereoselectivity of the lithiation and steric bulk of the ligand was observed, where bulky ligands enhanced the diastereoselectivity. However, for very bulky ligands such as diamine **178**, this comes at a cost with a reduced reactivity of the *s*-BuLi/diamine complex leading to poor yields of the product.

Computational DFT modelling of the lithiation of *N*-Boc pyrrolidine **96** correctly predicted that formation of the *anti* diastereomer was the lowest in energy. However, using DFT to predict the diastereoselectivity of the lithiation of *N*-Boc pyrrolidine **96** with different *s*-BuLi/ligand complexes gave disappointing results. There was no clear agreement between the computationally predicted and experimentally obtained drs for both of the DFT functionals used. Therefore, our DFT modelling does not provide useful data about the diastereoselectivity offered by the different *s*-BuLi/ligand complexes at this point in time.

Attempting to improve the computational prediction of diastereoselectivity for the lithiation of *N*-Boc pyrrolidine **96** with different *s*-BuLi/ligand complexes could be an interesting avenue for further study. Potential improvements could include modelling the systems with higher levels of theory, use of alternative DFT functionals and the inclusion of solvent effects (discussed in section 3.3). Using higher levels of theory or different DFT functionals, especially those that better describe dispersion interactions, could have a substantial impact on the accuracy of the modelling. As discussed above, accurate energies for the diastereomeric lithiations need to be calculated to provide a better prediction of the diastereoselectivity that will be observed. However, applying higher levels of theory to this system of ~80 atoms would greatly increase the computational expense of calculations. Therefore, investigating alternate DFT functionals may be more practical. DFT functionals with included dispersion corrections such as B3LYP-D3, discussed in section 3.4, may be particularly beneficial for this study. This is because the diastereoselectivity likely arises from steric interactions between the *s*-BuLi/ligand complex and *N*-Boc heterocycle; thus, a computational method which can better account for the long-range interactions between these two moieties may provide more accurate calculated energy differences for diastereomer formation. If further work did yield a more accurate computational model for diastereoselectivity then this could potentially be used to design more selective ligands for the lithiation of *N*-Boc heterocycles.

Our application of a combination of synthetic, *in situ* IR spectroscopic and computational techniques to investigate the lithiation-trapping of *N*-Boc pyrrolidine **96** provides a useful framework for obtaining a better understanding of these types of lithiation-trapping reactions. This could be expanded as a general approach to many other systems, allowing a better understanding of the processes occurring and providing suggestions about optimal reaction conditions and reagents to improve the reaction outcome.

Chapter 6: Experimental

6.1 General

All non-aqueous reactions were carried out under oxygen free Ar using flame-dried glassware. Et₂O and THF were freshly distilled from sodium and benzophenone respectively. Alkylolithiums were titrated against *N*-benzylbenzamide before use.¹⁴¹ All diamines used in lithiations were distilled over CaH₂ before use. Me₃SiCl, Me₂SO₄, MeI and PhCHO electrophiles were distilled over CaH₂ before use. Dry CO_{2(g)} was generated from solid CO₂, flushed through CaCl₂ and added into reaction *via* cannula. Petrol refers to the fraction of petroleum ether boiling in the range 40-60 °C and was purchased in Winchester quantities. Brine refers to a saturated solution. Water is distilled water.

Flash column chromatography was carried out using Fluka Chemie GmbH silica (220-440 mesh). Thin layer chromatography was carried out using commercially available Merck F₂₅₄ aluminium backed silica plates. Proton (400 MHz) and carbon (100.6 MHz) NMR spectra were recorded on a Jeol ECX-400 instrument using an internal deuterium lock. For samples recorded in CHCl₃, chemical shifts are quoted in parts per million relative to CHCl₃ (δ_{H} 7.26) and CDCl₃ (δ_{C} 77.0, central line of triplet). Carbon NMR spectra were recorded with broad band proton decoupling and assigned using DEPT experiments. Coupling constants (*J*) are quoted in Hertz. Boiling points give for compounds purified by K \ddot{u} gelrohr distillation correspond to the oven temperature during distillation. Infrared spectra were recorded on a Perkin Elmer Spectrum Two FT-IR spectrometer with UATR attachment. Electrospray high and low resonance mass spectra were recorded at room temperature on a Bruker Daltronics microOTOF spectrometer. *In situ* ReactIRTM infra-red spectroscopic monitoring was performed on either a Mettler-Toledo ReactIRTM iC10 or ReactIRTM 15 spectrometer equipped with a silicon-tipped (SiComp) or diamond-tipped (DiComp) probe.

6.2 Kinetic Analysis Procedure

Trend fitting and error calculation:

For the kinetic analysis using linear regression (in Chapters 2 and 4) lines of best fit and standard errors were calculated using the LINEST (least squares) function in Microsoft® Excel. Non-linear regression kinetic analyses (Chapter 2) were conducted with Origin 2016 and the curve fitting and standard error calculation were carried out using the Levenberg-Marquardt algorithm (non-linear least squares) included in the software package. The standard errors provided on the kinetic plots are calculated with LINEST (linear regression) and the Levenberg-Marquardt algorithm (curve fitting). The errors quoted on k_{obs} and $t_{1/2S}$ values presented in this thesis use the standard errors calculated by these fitting methods.

Kinetic analysis of the lithiation reactions of *N*-Boc heterocycles (Chapter 2):

When the lithiation reactions of *N*-Boc heterocycles were subjected to linear regression analysis, the first ReactIR™ measurement at $t = 0$ was discarded to allow the pre-equilibrium approximation to be applied. In addition, subsequent readings after 90% conversion were discarded from the linear regression analysis to minimise the effect of instrument noise on the kinetic analysis. The values of absorbance used in the linear regression plots in this thesis are relative, i.e. the absorbance has been normalised to be zero at the end of the reaction (the end-point of the reactions has been determined by visual inspection of the ReactIR™ data).

For the calculation of the lithiation k_{obs} using curve fitting, the first ReactIR™ measurement at $t = 0$ was discarded to allow the pre-equilibrium approximation to be applied but all subsequent ReactIR™ data for the duration of the reaction were used in the analysis. The absolute absorbance recorded by the ReactIR™ equipment was used in the curve fitting analysis and no normalisation was applied to the absorbance data. To compare the reactivities of the different *N*-Boc heterocycles presented in Chapter 2, the k_{obs} values for the lithiation reactions obtained by the curve fitting analysis were used (Tables 2.4 and 2.5). The kinetic data from the linear regression was not used as it is susceptible to significant variation in k_{obs} which arises due to selection of the reaction end-point which is not required for the curve fitting, this is discussed in section 2.3 of this thesis.

Percentage errors which compare the error between the lithiation k_{obs} obtained by analysis of the *N*-Boc heterocycle substrate consumption and the prelithiation complex consumption are not presented in this thesis. These % errors were not included as the measurement of k_{obs}

using the consumption of prelithiation complex is unreliable due to the low concentration and low absorbance of prelithiation complex and overlapping of signals with the uncomplexed starting material and lithiated intermediate (this is discussed in section 2.3).

Kinetic analysis of the trapping reactions of lithiated *N*-Boc heterocycles (Chapter 4):

The trapping reactions of all lithiated intermediates with PhCHO and the trapping of lithiated *N*-Boc pyrrolidine **164** with MeI and Me₂SO₄ were too rapid for kinetic analysis to be conducted. For these rapid trapping reactions, k_{obs} and $t_{1/2\text{S}}$ were estimated by using the trapping times obtained by visual inspection of the ReactIRTM traces ($t_{1/2} \approx \text{trapping time} \div 7$).

The k_{obs} and $t_{1/2\text{S}}$ for the trapping reactions of the lithiated intermediates presented in Chapter 4 with Me₃SiCl, MeI and Me₂SO₄ were obtained using linear regression analysis of first order semilogarithmic plots. These first order semilogarithmic plots use the logarithm of relative absorbance (i.e. the absorbance has been normalised to be zero at the end of the reaction). For the kinetic analysis of the trapping reactions the first ReactIRTM measurement at $t = 0$ has been discarded to ensure that the reaction mixture is well mixed and homogenous after the electrophile is added.

For the trapping reactions subjected to kinetic analysis semilogarithmic plots have been included for both 20% and 90% conversion of the lithiated intermediate. Trapping reactions of the lithiated *N*-Boc heterocycles with both Me₂SO₄ and MeI both displayed a deviation from first order kinetics mid reaction and this is evident in the semilogarithmic plots which present 90% trapping conversion. For this reason, trapping k_{obs} and $t_{1/2\text{S}}$ for all substrates have been calculated using the semilogarithmic plots with the first 20% trapping conversion. For this initial portion of the reaction pseudo-first order kinetics are observed (this is discussed in Chapter 4). For consistency, k_{obs} and $t_{1/2\text{S}}$ for the trapping reactions with Me₃SiCl have also been calculated using kinetic data for the first 20% of trapping conversion.

The trapping reactions of lithiated intermediates presented in Table 4.1 were also subjected to initial rate analysis. For this initial rate analysis, ReactIRTM absorbance data for the consumption of the lithiated intermediate from $t = 0$ (the start of the trapping reaction) to the end of the reaction has been plotted and then a tangent has been fitted to the decay observed in the initial stage of the trapping reaction. The absorbance data used for the initial rate

analyses uses the absolute absorbance recorded by the ReactIR™ equipment with no normalisation applied to the data. The standard errors quoted on the initial rates obtained ($\text{rate}_{\text{init}}$) have been calculated by the LINEST algorithm used for linear regression included in the Microsoft® Excel package.

6.3 General Procedures

General Procedure A: Lithiation-trapping of *N*-Boc pyrrolidine **96**

s-BuLi (1.3 M in hexanes, 1.3 eq.) was added dropwise to a stirred solution of *N*-Boc pyrrolidine **96** (223 mg, 1.0 mmol, 1.0 eq.) and diamine (1.3 eq.) in Et₂O (7 mL) at –78 °C under Ar. The resulting solution was stirred at –78 °C for 10 min, 1 h or 5 h. Then, the electrophile (2.0 eq.) was added and the resulting solution was stirred at –78 °C for 1 h and then allowed to slowly warm to rt over 16 h. Saturated NH₄Cl_(aq) (10 mL) was added and the two layers were separated. The aqueous layer was extracted with Et₂O (3 x 10 mL) and the combined organic layers were dried (MgSO₄), filtered and evaporated under reduced pressure to give the crude product.

General Procedure B: High Temperature (–20 °C) Lithiation-trapping of *N*-Boc pyrrolidine **96**

s-BuLi (1.3 M in hexanes, 1.3 eq.) was added dropwise to a stirred solution of *N*-Boc pyrrolidine **96** (223 mg, 1.0 mmol, 1.0 eq.) and diamine (1.3 eq.) in Et₂O (7 mL) at –20 °C under Ar. The resulting solution was stirred at –20 °C for 2 min. Then, the electrophile (2.0 eq.) was added and the resulting solution was stirred at –20 °C for 1 h and warmed to rt. Saturated NH₄Cl_(aq) (10 mL) was added and the two layers were separated. The aqueous layer was extracted with Et₂O (3 x 10 mL) and the combined organic layers were dried (MgSO₄), filtered and evaporated under reduced pressure to give the crude product.

General Procedure C: Lithiation-trapping of *N*-Boc pyrrolidine **96** with CO_{2(g)}

s-BuLi (1.3 M in hexanes, 1.3 eq.) was added dropwise to a stirred solution of *N*-Boc pyrrolidine **96** (223 mg, 1.0 mmol, 1.0 eq.) and diamine (1.3 eq.) in Et₂O (7 mL) at –78 °C under Ar. The resulting solution was stirred at –78 °C for 10 min, 1 h or 5 h. Then, dry CO₂ was bubbled through for 30 min at –78 °C and then allowed to warm to rt over 1 h. Saturated NH₄Cl_(aq) (10 mL) was added followed by 2 M HCl_(aq) (10 mL) and the two layers were separated. The aqueous layer was extracted with Et₂O (3 x 10 mL) and the combined organic

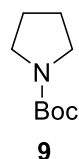
layers were dried (MgSO_4), filtered and evaporated under reduced pressure to give the crude product.

General Procedure D: DMP oxidation of alcohols

A solution of the alcohol (1.0 eq.) in CH_2Cl_2 (5 mL) was added dropwise to a stirred suspension of DMP (1.5 eq.) in CH_2Cl_2 (10 mL) at 0 °C under Ar. The resulting solution was allowed to warm to rt and then at rt stirred for 2 h. Saturated $\text{NaHCO}_{3(\text{aq})}$ (10 mL) was added and the solution stirred at rt for 16 h. The solids were removed by filtration and the two layers were separated. The aqueous layer was extracted with CH_2Cl_2 (3 x 10 mL) and the combined organic layers were dried (Na_2SO_4), filtered and evaporated under reduced pressure to give the crude ketone product.

6.4 Experimental Procedures for Chapter 2

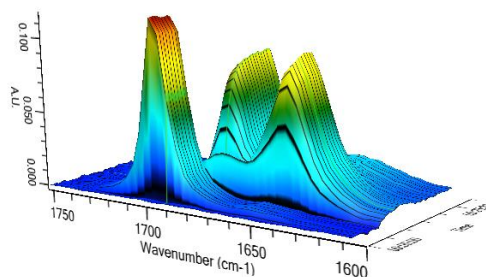
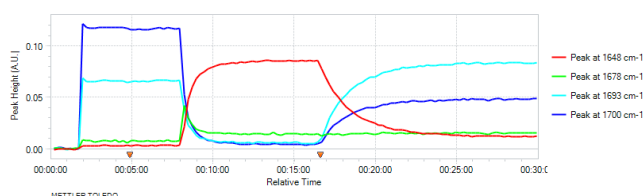
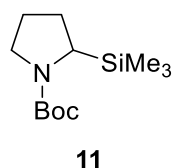
tert-Butyl pyrrolidine-1-carboxylate **9**



Pyrrolidine (4.00 g, 4.70 mL, 56.24 mmol, 1.2 eq.) was added dropwise to a stirred solution of di-*tert*-butyl dicarbonate (10.28 g, 47.12 mmol, 1.0 eq.) in CH₂Cl₂ (200 mL) at 0 °C under Ar. The resulting solution was then allowed to warm to rt and stirred for 16 h. 1 M HCl_(aq) (100 mL) was added and the two layers were separated. The aqueous layer was extracted with CH₂Cl₂ (3 x 50 mL) and the combined organic layers were dried (MgSO₄), filtered and evaporated under reduced pressure to give the crude product. Purification by Kügelrohr distillation gave *N*-Boc pyrrolidine **9** (6.48 g, 80%) as a colourless oil, bp 115-120°C/3.5 mmHg (lit.,¹⁴² bp 70-75 °C/0.05 mmHg); ¹H NMR (400 MHz, CDCl₃) δ 3.32-3.28 (m, 4H, NCH₂), 1.84-1.81 (m, 4H, CH₂), 1.45 (s, 9H, CMe₃); ¹³C NMR (100.6 MHz, CDCl₃) δ 154.8 (C=O), 79.0 (CMe₃), 45.9 (NCH₂), 28.6 (CMe₃), 25.5 (CH₂). Spectroscopic data consistent with those reported in the literature.¹⁴²

Lab Book Reference: AMI_2

tert-Butyl 2-(trimethylsilyl)pyrrolidine-1-carboxylate **11**

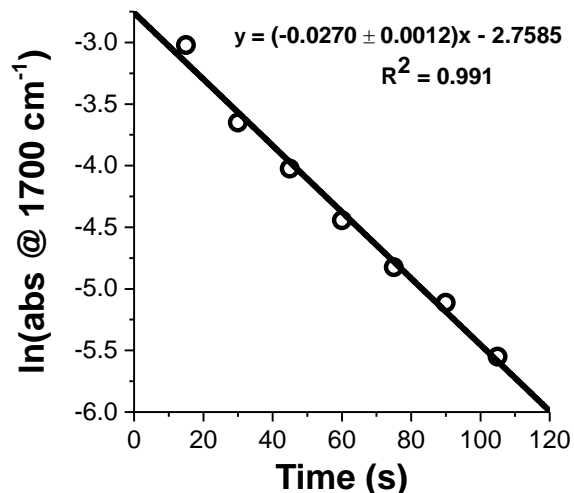
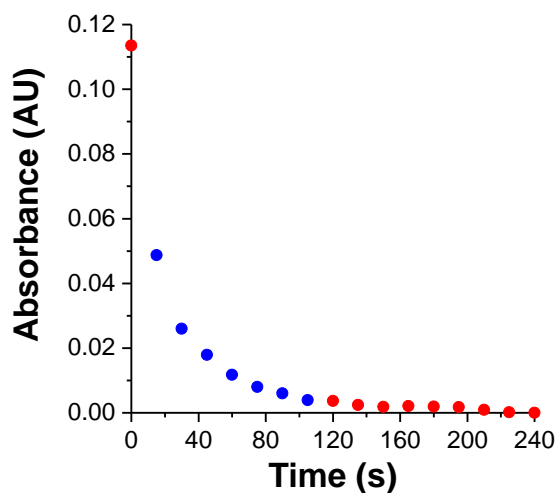


Et₂O (14 mL) was added to a flask equipped with a stirrer bar and ReactIRTM probe (ReactIRTM 15, DiComp) at rt under Ar. After cooling to -78 °C, *N*-Boc pyrrolidine **9** (171

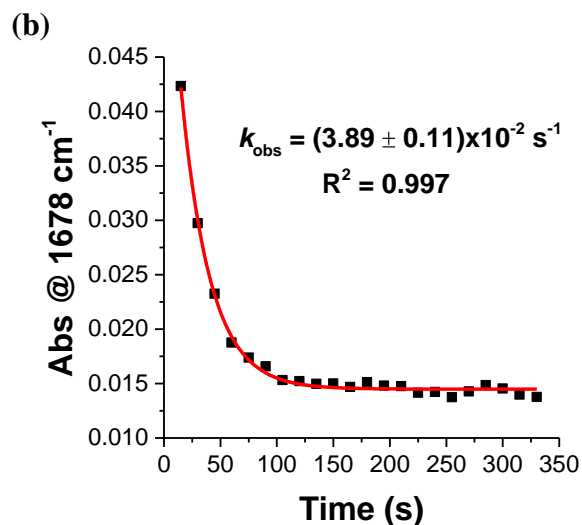
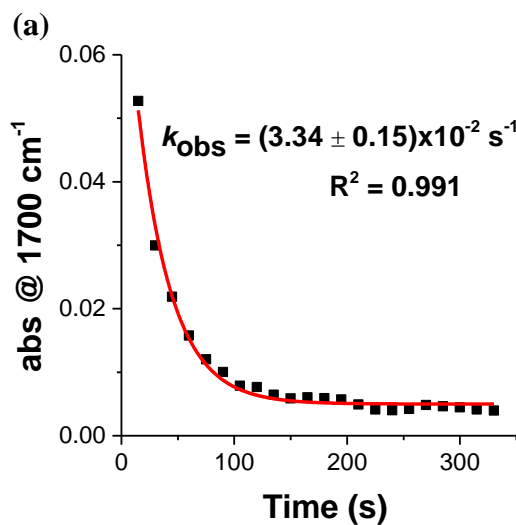
mg, 1.00 mmol, 0.18 mL, 1.0 eq.) was added followed by TMEDA (151 mg, 0.19 mL, 1.30 mmol, 1.3 eq.). The solution was stirred for 5 min (to verify the stability of readout on ReactIR™). Then *s*-BuLi (1.0 mL of a 1.3 M solution in hexanes, 1.30 mmol, 1.3 eq.) was added. The resulting solution was stirred at $-78\text{ }^{\circ}\text{C}$ for 9 min. Then, Me_3SiCl (217 mg, 0.25 mL, 2.00 mmol, 2.0 eq.) was added and the solution was stirred at $-78\text{ }^{\circ}\text{C}$ for a further 13 min. Saturated $\text{NH}_4\text{Cl}_{(\text{aq})}$ was added and the solution was then allowed to warm to rt over 30 min and the two layers were separated. The aqueous layer was extracted with Et_2O (3 x 10 mL) and the combined organics were dried (MgSO_4), filtered and evaporated under reduced pressure to give the crude product. Purification by flash column chromatography on silica using 90:10 Hexane- Et_2O as eluent gave 2-silyl *N*-Boc pyrrolidine **10** (211 mg, 87%) as a colourless oil, R_F (90:10 Hexane- Et_2O) 0.22; ^1H NMR (400 MHz, CDCl_3) δ 3.63-3.38 (m, 1H, NCH), 3.36-3.09 (m, 2H, NCH), 2.11-1.90 (m, 1H, CH), 1.90-1.64 (m, 3H, CH), 1.45 (s, 9H, CMe_3), 0.04 (s, 9H, SiMe_3); ^{13}C NMR (100.6 MHz, CDCl_3) (mixture of rotamers) δ 155.1 (C=O), 79.3 (CMe_3), 78.5 (CMe_3), 47.8 (NCH), 47.2 (NCH_2), 46.7 (NCH_2), 28.7 (CMe_3), 28.0 (CH), 26.2 (CH_2), 25.0 (CH_2), -2.0 (SiMe_3). Spectroscopic data consistent with those reported in the literature.²⁸

For *N*-Boc pyrrolidine **9**, a peak at 1700 cm^{-1} was observed and assigned to $\nu_{\text{C=O}}$. After addition of *s*-BuLi, a new peak at 1678 cm^{-1} was observed which was assigned to $\nu_{\text{C=O}}$ in the prelithiation complex. A new peak at 1648 cm^{-1} was also observed and this was assigned to the lithiated intermediate. After a lithiation time of 4 min, complete lithiation of *N*-Boc pyrrolidine **9** to give the lithiated intermediate was observed. When Me_3SiCl was added (after 9 min total lithiation time), the signal for the lithiated intermediate ($\nu_{\text{C=O}} = 1648\text{ cm}^{-1}$) disappeared after 10 min, indicating complete trapping had occurred. During the trapping process, another peak appeared at 1693 cm^{-1} which was assigned to the trapped adduct **11**.

Kinetic analysis using linear regression indicated that the lithiation of *N*-Boc pyrrolidine **9** was first order with respect to *N*-Boc pyrrolidine **9**, $k_{\text{obs}} = (2.70 \pm 0.12)\text{ s}^{-1}$ and $t_{1/2} = (25.7 \pm 1.1)\text{ s}$.

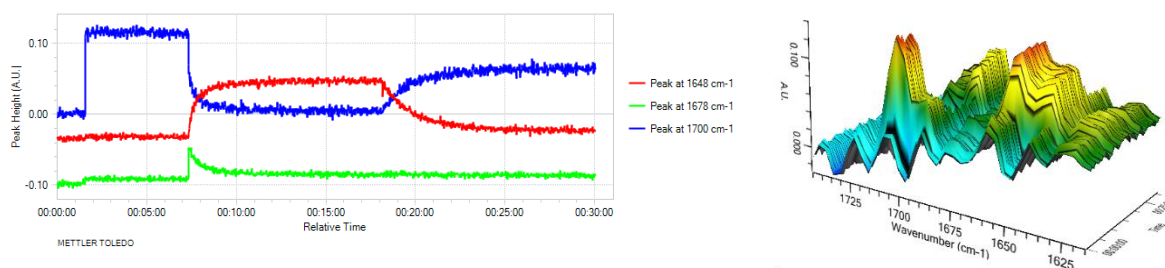


First order exponential decay curves ($y = Ae^{-k_{\text{obs}}t} + c$) were fit to the consumption of *N*-Boc pyrrolidine **9** (a) and consumption of the prelithiation complex of **9** (b) for the lithiation of *N*-Boc pyrrolidine **9**. Both provided good fit with a first order exponential decay. Curve fitting of *N*-Boc pyrrolidine **9** consumption (a) provided $k_{\text{obs}} = (3.34 \pm 0.15) \times 10^{-2} \text{ s}^{-1}$ and $t_{1/2} = (20.7 \pm 0.9) \text{ s}$. Curve fitting of prelithiation complex consumption (b) provided $k_{\text{obs}} = (3.89 \pm 0.11) \times 10^{-2} \text{ s}^{-1}$ and $t_{1/2} = (17.8 \pm 0.5) \text{ s}$.



Lab Book Reference: AMI_168

Rapid collect ReactIR™ spectroscopic monitoring of the lithiation and Me₃SiCl trapping of *N*-Boc pyrrolidine **9**

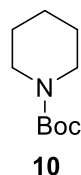


Et₂O (14 mL) was added to a flask equipped with a stirrer bar and ReactIR™ probe (ReactIR™ 15, DiComp using rapid collection mode with 1 scan collected per second) at rt under Ar. After cooling to -78 °C, *N*-Boc pyrrolidine **9** (171 mg, 1.00 mmol, 0.18 mL, 1.0 eq.) was added followed by TMEDA (151 mg, 0.19 mL, 1.30 mmol, 1.3 eq.). The solution was stirred for 5 min (to verify the stability of readout on ReactIR™). Then *s*-BuLi (1.0 mL of a 1.3 M solution in hexanes, 1.30 mmol, 1.3 eq.) was added. The resulting solution was stirred at -78 °C for 11 min. Then, Me₃SiCl (217 mg, 0.25 mL, 2.00 mmol, 2.0 eq.) was added and the solution was stirred at -78 °C for a further 12 min.

For *N*-Boc pyrrolidine **9**, a peak at 1700 cm⁻¹ was observed and assigned to $\nu_{C=O}$. After addition of *s*-BuLi, a new peak at 1678 cm⁻¹ was observed which was assigned to $\nu_{C=O}$ in the prelithiation complex. Formation of prelithiation complex and establishment of an equilibrium was complete in < 1 s. A new peak at 1648 cm⁻¹ was observed which was assigned to the lithiated intermediate. After a lithiation time of 4 min, complete lithiation of *N*-Boc pyrrolidine **9** to give the lithiated intermediate was observed. When Me₃SiCl was added (after 11 min total lithiation time), the signal for the lithiated intermediate ($\nu_{C=O} = 1648$ cm⁻¹) disappeared after 10 min, indicating complete trapping had occurred.

Lab Book Reference: AMI_169

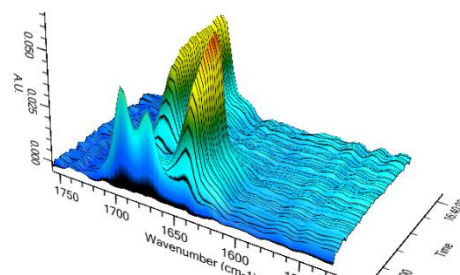
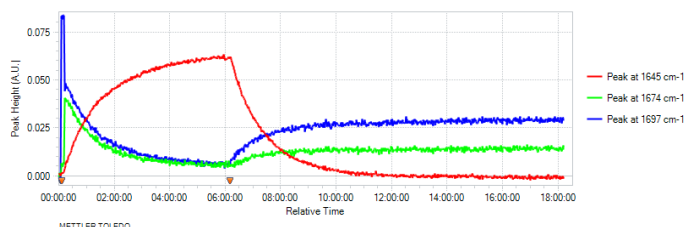
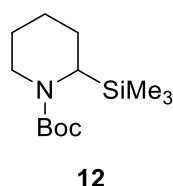
tert*-Butyl piperidine-1-carboxylate **10*



Piperidine (3.00 g, 3.48 mL, 35.23 mmol, 1.3 eq.) was added dropwise to a stirred solution of di-*tert*-butyl dicarbonate (6.14 g, 28.13 mmol, 1.0 eq.) in THF (30 mL) at 0 °C under Ar. The resulting colourless solution was allowed to warm to rt and stirred for 30 min. Then, 10% NaHCO_{3(aq)} (30 mL) was added and the two layers were separated. The aqueous layer was extracted with Et₂O (2 x 70 mL). The combined organic layers were washed with saturated brine (50 mL), dried (K₂CO₃), filtered and evaporated under reduced pressure to give the crude product. Purification by Kugelrohr distillation gave *N*-Boc piperidine **10** (5.16 g, 99%) as a colourless oil, bp 90-100 °C/0.5 mmHg (lit.,⁴⁰ bp 60-70 °C/1.0 mmHg); ¹H NMR (400 MHz, CDCl₃) δ 3.37-3.34 (m, 4H, NCH₂), 1.58-1.48 (m, 6H, CH₂), 1.45 (s, 9H, CMe₃); ¹³C NMR (100.6 MHz, CDCl₃) δ 155.1 (C=O), 79.2 (CMe₃), 44.9 (br s, NCH₂), 28.6 (CMe₃), 25.9 (CH₂), 24.6 (CH₂). Spectroscopic data consistent with those reported in the literature.⁴⁰

Lab Book Reference: AMI_22

tert*-Butyl 2-(trimethylsilyl)piperidine-1-carboxylate **12*

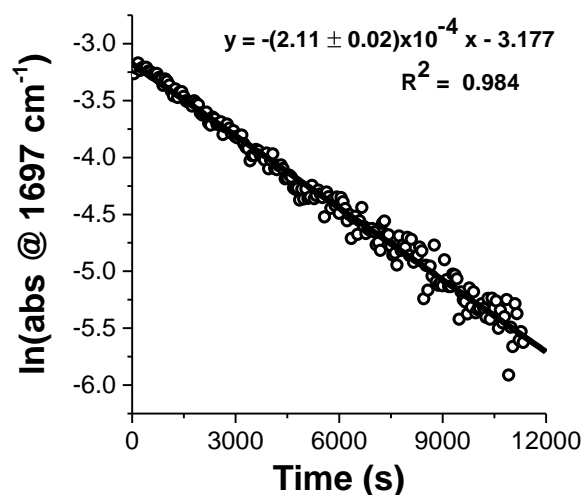
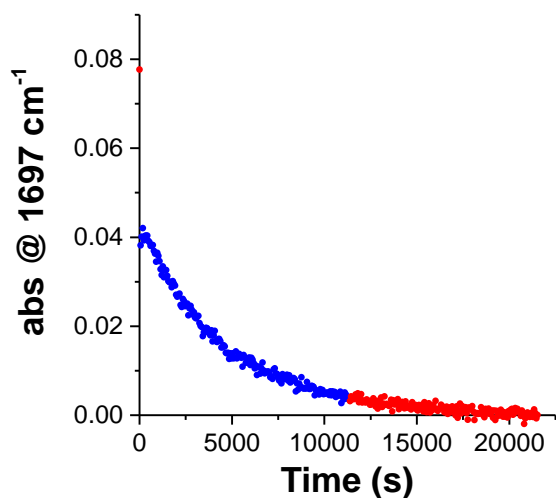


Et₂O (14 mL) was added to a flask equipped with a stirrer bar and ReactIRTM probe (ReactIRTM 15, DiComp) at rt under Ar. After cooling to -78 °C, *N*-Boc piperidine **10** (185

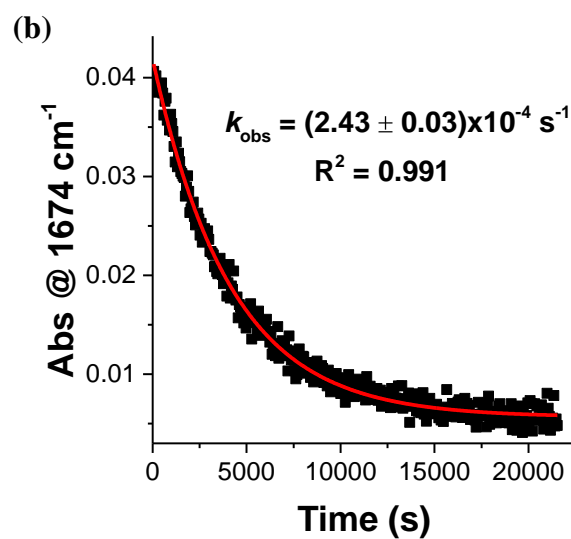
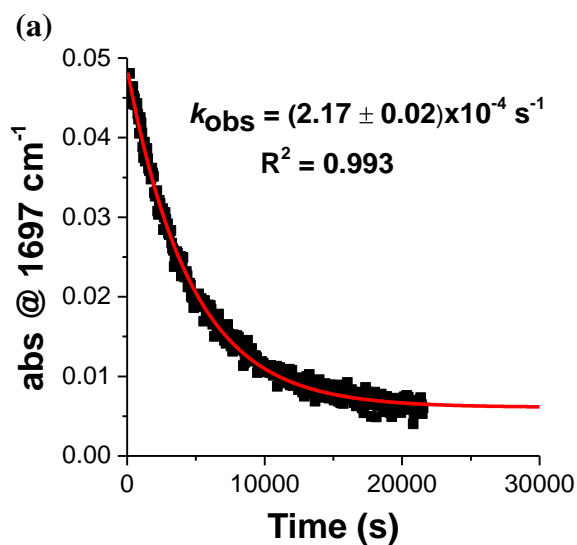
mg, 1.00 mmol, 1.0 eq.) was added followed by TMEDA (151 mg, 0.20 mL, 1.30 mmol, 1.3 eq.). The solution was stirred for 5 min (to verify the stability of readout on ReactIR™). Then *s*-BuLi (1.0 mL of a 1.3 M solution in hexanes, 1.30 mmol, 1.3 eq.) was added dropwise. The resulting solution was stirred at $-78\text{ }^{\circ}\text{C}$ for 6 h. Then, Me_3SiCl (217 mg, 0.25 mL, 2.00 mmol, 2.0 eq.) was added and the solution was stirred at $-78\text{ }^{\circ}\text{C}$ for a further 12 h. Saturated $\text{NH}_4\text{Cl}_{(\text{aq})}$ (10 mL) was added and the solution was then allowed to warm to rt over 30 min and the two layers were separated. The aqueous layer was extracted with Et_2O (3 x 10 mL) and the combined organics were dried (MgSO_4), filtered and evaporated under reduced pressure to give the crude product as a 90:10 mixture of 2-silyl *N*-Boc piperidine **12** and *N*-Boc piperidine **10** (by ^1H NMR spectroscopy). Purification by flash column chromatography on silica using 90:10 hexane- Et_2O as eluent gave 2-silyl *N*-Boc piperidine **12** (145 mg, 56%) as a colourless oil, R_F (90:10 hexane- Et_2O) 0.27; ^1H NMR (400 MHz, CDCl_3) (50:50 mixture of rotamers) δ 4.20 (br s, 0.5H, NCH), 3.86-3.52 (m, 1.5 H, NCH), 2.95 (br s, 0.5H, NCH), 2.62 (br s, 0.5H, NCH), 1.75-1.32 (m, 6H, CH), 1.45 (s, 9H, CMe_3), 0.08 (s, 9H, SiMe_3); ^{13}C NMR (100.6 MHz, CDCl_3) (rotamers) δ 155.0 ($\text{C}=\text{O}$), 79.0 (CMe_3), 45.1 (NCH), 44.4 (NCH), 42.1 (NCH_2), 41.9 (NCH_2), 28.4 (CMe_3), 26.1 (CH_2), 23.5 (CH_2), 22.7 (CH_2), -0.6 (SiMe_3) and *N*-Boc piperidine **10** (7 mg, 4%) as a colourless oil. Spectroscopic data for **12** consistent with those reported in the literature.³¹

For *N*-Boc piperidine **10**, a peak at 1697 cm^{-1} was observed and assigned to $\nu_{\text{C}=\text{O}}$. After addition of *s*-BuLi, a new peak at 1674 cm^{-1} was observed which was assigned to $\nu_{\text{C}=\text{O}}$ in the prelithiation complex. A new peak at 1645 cm^{-1} was also observed and this was assigned to the lithiated intermediate. After a lithiation time of 6 h, incomplete lithiation of *N*-Boc piperidine **10** to give the lithiated intermediate was observed. When Me_3SiCl was added (after 6 h total lithiation time), the signal for the lithiated intermediate ($\nu_{\text{C}=\text{O}} = 1645\text{ cm}^{-1}$) disappeared after 7 h suggesting that complete trapping had occurred.

Kinetic analysis indicated that the lithiation of *N*-Boc piperidine **10** was first order with respect to *N*-Boc piperidine **10**, $k_{\text{obs}} = (2.11 \pm 0.02) \times 10^{-4}\text{ s}^{-1}$ and $t_{1/2} = (3290 \pm 30)\text{ s}$.

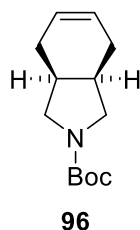


First order exponential decay curves ($y = Ae^{-k_{\text{obs}}t} + c$) were fit to the consumption of *N*-Boc piperidine **10** (a) and consumption of the prelithiation complex of **10** (b) for the lithiation of *N*-Boc piperidine **10**. Both provided good fit with a first order exponential decay. Curve fitting of *N*-Boc piperidine **10** consumption (a) provided $k_{\text{obs}} = (2.17 \pm 0.02) \times 10^{-4} \text{ s}^{-1}$ and $t_{1/2} = (3190 \pm 30) \text{ s}$. Curve fitting of prelithiation complex consumption (b) provided $k_{\text{obs}} = (2.43 \pm 0.03) \times 10^{-4} \text{ s}^{-1}$ and $t_{1/2} = (2850 \pm 30) \text{ s}$.



Lab Book Reference: AMI_252

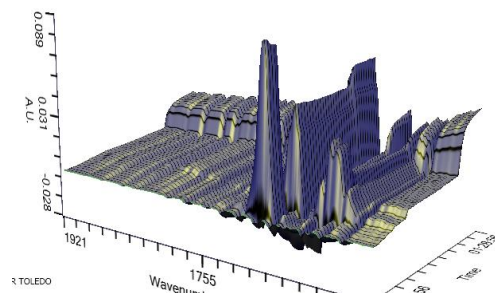
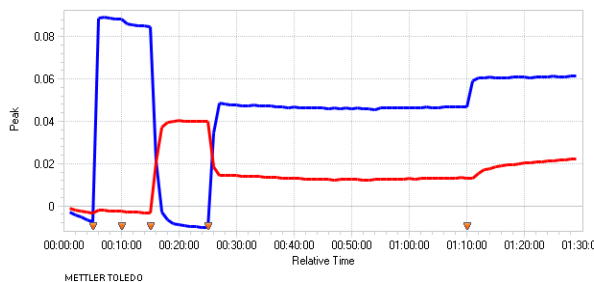
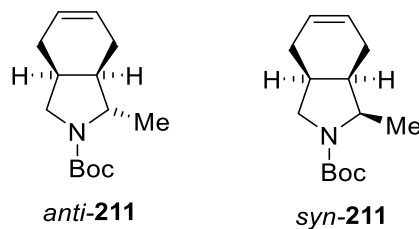
tert*-Butyl (3a*R**,7a*S**)-2,3,3a,4,7,7a-hexahydro-1H-isoindole-2-carboxylate **96*



A solution of *cis*-1,2,3,6-tetrahydrophthalimide (2.00 g, 13.23 mmol, 1.0 eq.) in THF (20 mL) was added dropwise to a stirred suspension of LiAlH₄ (3.01 g, 79.39 mmol, 6.0 eq.) in THF (90 mL) at 0 °C under Ar. The resulting solution was stirred and heated at reflux for 16 h. The solution was then cooled to 0 °C and quenched by careful dropwise addition of H₂O (3 mL), 20% NaOH_(aq) (6 mL) and H₂O (3 mL). The resulting mixture was allowed to warm to rt, stirred for 30 min and MgSO₄ was added. The solids were removed by filtration through Celite® and washed with 9:1 CH₂Cl₂/MeOH (50 mL). The solvent was evaporated under reduced pressure and the residue was dissolved in CH₂Cl₂ (15 mL). After cooling to 0 °C, a solution of di-*tert*-butyl dicarbonate in CH₂Cl₂ (10 mL) was added dropwise and the resulting solution was stirred at rt for 16 h. Saturated NaHCO_{3(aq)} (15 mL) and CH₂Cl₂ (25 mL) were added and the two layers were separated. The organic layer was dried (MgSO₄), filtered and evaporated under reduced pressure to give the crude product. Purification by flash column chromatography on silica using CH₂Cl₂ and then 96:4 CH₂Cl₂-Et₂O as eluent gave 3,4-disubstituted pyrrolidine **96** (1.87 g, 63%) as a pale orange oil, *R_F* (96:4 CH₂Cl₂-Et₂O) 0.31; IR (CHCl₃) 2934, 2894, 2838, 2798, 1657 (C=O), 1453, 1391, 1345, 1153, 1111 cm⁻¹; ¹H NMR (400 MHz, CDCl₃) δ 5.61 (s, 2H, =CH), 3.37 (dd, *J* = 10.0, 6.5 Hz, 2H, NCH), 3.09 (br dd, *J* = 10.0, 4.5 Hz, 2H, NCH), 2.34-2.12 (m, 4H, CH), 1.87 (dd, *J* = 16.0, 4.0 Hz, 2H, CH), 1.43 (s, 9H, CMe₃); ¹³C NMR (100.6 MHz, CDCl₃) δ 155.4 (C=O), 124.5 (=CH), 79.0 (CMe₃), 51.0 (NCH₂), 33.9 (br, CH), 28.6 (CMe₃), 24.8 (CH₂); HRMS (ESI) *m/z* calcd for C₁₃H₂₁NO₂ (M + Na)⁺ 246.1465, found 246.1459 (+2.3 ppm error).

Lab Book Reference: AMI_1

(1*S,3*aS**,7*aR**) and (1*R**,3*aS**,7*aR**)-*tert*-Butyl-1-methyl-2,3,3*a*,4,7,7*a*-hexahydro-1*H*-isoindole-2-carboxylate *anti*-**211** and *syn*-**211****



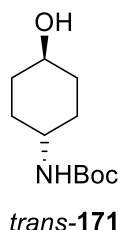
Et₂O (10 mL) was added to a flask equipped with a stirrer bar and ReactIRTM probe (iC 10, SiComp) at rt under Ar. After cooling to -78 °C, a solution of *N*-Boc pyrrolidine **96** (226 mg, 1.01 mmol, 1.0 eq.) was added followed by TMEDA (153 mg, 1.31 mmol, 1.3 eq., 0.20 mL). The solution was stirred for 5 min (to verify the stability of readout on ReactIRTM). Then, *s*-BuLi (1.0 mL of a 1.3 M solution in hexanes, 1.35 mmol, 1.3 eq.) was added dropwise. The resulting solution was stirred at -78 °C for 10 min. Then, Me₂SO₄ (255 mg, 2.02 mmol, 2.0 eq., 0.19 mL) was added and the solution was stirred for a further 45 min at -78 °C. Then, saturated NH₄Cl_(aq) (10 mL) was added and the two layers were separated. The aqueous layer was extracted with Et₂O (3 x 10 mL) and combined organic layers were dried (MgSO₄), filtered and evaporated under reduced pressure to give the crude product. Purification by flash column chromatography on silica using 85:15 hexane-EtOAc as eluent gave a 90:10 mixture (by ¹H NMR spectroscopy of sulfonamides *anti*-**218** and *syn*-**218**) of 2,3,4-trisubstituted pyrrolidines *anti*-**211** and *syn*-**211** (192 mg, 80%) as a colourless oil, *R_F* (85:15 hexane-EtOAc) 0.30; IR (ATR) 2970, 2935, 1690 (C=O), 1388, 1363, 1174, 1128, 1104, 1090, 664 cm⁻¹; ¹H NMR (400 MHz, CDCl₃) for *anti*-**211** δ 5.63 (s, 2H, =CH), 3.58-3.37 (br m, 1H, NCH), 3.40 (dd, *J* = 10.5, 7.0 Hz, 1H, NCH), 3.18 (br s, 1H, NCH), 2.39 (br s, 1H, CH), 2.24-2.18 (m, 2H, CH), 1.89-1.83 (m, 3H, CH), 1.46 (s, 9H, CMe₃), 1.22 (d, *J* = 6.0 Hz, 3H, Me); ¹³C NMR (100.6 MHz, CDCl₃) for *anti*-**211** (rotamers) δ 155.3 (C=O), 124.8 (=CH), 124.8 (=CH), 124.5 (=CH), 124.4 (=CH), 79.1 (CMe₃), 78.9 (CMe₃), 58.9 (NCH), 58.6 (NCH), 51.1 (NCH₂), 50.9 (NCH₂), 41.9 (CH), 40.8 (CH), 32.3 (CH), 31.8

(CH), 28.7 (CMe₃), 25.3 (CH₂), 24.6 (CH₂), 20.0 (Me), 19.3 (Me); HRMS (ESI) *m/z* calcd for C₁₄H₂₃NO₂ (M + Na)⁺ 260.1621, found 260.1612 (+4.3 ppm error). The stereochemistry of *anti*-**211** and *syn*-**211** has not been proven but is assumed from literature precedent.⁴

For *N*-Boc pyrrolidine **96**, a peak at 1702 cm⁻¹ was observed and assigned to ν_{C=O}. After addition of *s*-BuLi, a new peak at 1651 cm⁻¹ was observed which was assigned to ν_{C=O} in the lithiated intermediate. After a lithiation time of 4 min, complete lithiation of *N*-Boc pyrrolidine **96** to give the lithiated intermediate was observed. When Me₂SO₄ was added (after a 10 min total lithiation time), the signal for the lithiated intermediate (ν_{C=O} = 1651 cm⁻¹) disappeared after 3 min, indicating complete trapping had occurred.

Lab Book Reference: AMI_96

***tert*-Butyl *N*-[4-hydroxycyclohexyl]carbamate *trans*-171**

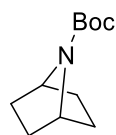


1 M NaOH_(aq) (40 mL) was added to a stirred suspension of *trans*-aminocyclohexanol hydrochloride *trans*-**170** (5.00 g, 32.98 mmol, 1.0 eq.) in 1,4-dioxane (180 mL) at 0 °C. The resulting solution was then stirred at 0 °C for 15 min. Then, a solution of di-*tert*-butyl dicarbonate (7.90 g, 36.20 mmol, 1.1 eq.) in 1,4-dioxane (60 mL) was added dropwise. The resulting solution was allowed to warm to rt and stirred at rt for 16 h. 1 M HCl_(aq) was added until pH > 7 was reached and EtOAc (100 mL) was added and the two layers were separated. The aqueous layer was extracted with EtOAc (2 x 50 mL) and the combined organics were washed with 1 M HCl_(aq) (50 mL), H₂O (50 mL) and brine (50 mL), dried (Na₂SO₄), filtered and evaporated under reduced pressure to give the crude product. Purification by flash column chromatography on silica using 70:30 EtOAc-hexane as eluent gave *N*-Boc aminocyclohexanol *trans*-**171** (6.13 g, 86%) as a white solid, mp 158-160 °C; *R*_F (70:30 EtOAc, hexane) 0.24; ¹H NMR (400 MHz, CDCl₃) δ 4.38 (br s, 1H, NH), 3.63-3.56 (m, 1H, NCH), 3.48-3.36 (m, 1H, CHOH), 2.03-1.94 (m, 4H, CH), 1.44 (CMe₃), 1.36-1.12 (m, 4H, CH); ¹³C NMR (100.6 MHz, CDCl₃) δ 155.4 (C=O), 79.4 (CMe₃), 70.0 (OCH), 49.0 (NCH),

34.1 (CH₂), 31.3 (CH₂), 28.5 (CMe₃). Spectroscopic data consistent with those reported in the literature.¹⁴³

Lab book Reference: AMI_125

tert*-Butyl 7-azabicyclo[2.2.1]heptane-7-carboxylate **84*

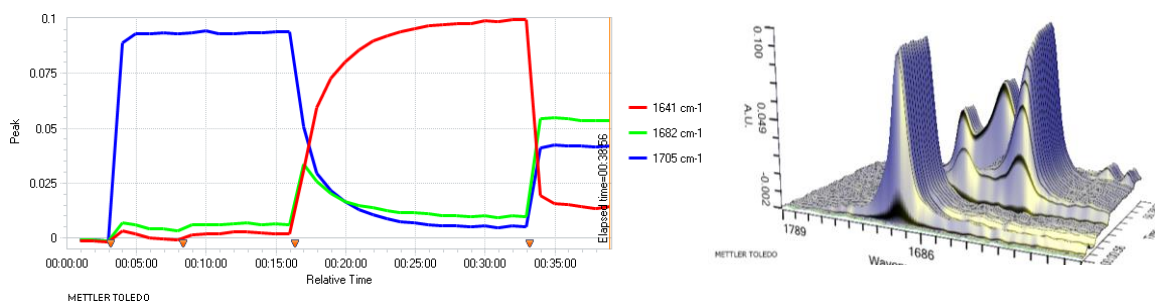
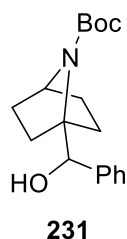


84

Methanesulfonyl chloride (2.40 g, 20.98 mmol, 1.5 eq., 1.62 mL) was added dropwise to a stirred solution of *N*-Boc aminocyclohexanol *trans*-**171** (3.01 g, 13.99 mmol, 1.0 eq.) and Et₃N (2.12 g, 20.98 mmol, 1.5 e.q., 2.93 mL) in CH₂Cl₂ (120 mL) at 0 °C under Ar. The resulting solution was stirred at 0 °C for 1 h. Then, saturated NaHCO_{3(aq)} (60 mL) was added dropwise with vigorous stirring. The two layers were separated and the organic layer was washed with H₂O (50 mL), dried (Na₂SO₄), filtered and evaporated under reduced pressure to give the intermediate mesylate as a white solid. KO*t*-Bu (785 mg, 7.00 mmol, 0.5 eq.) was added to a stirred solution of the crude mesylate in THF (120 mL) at rt under Ar. The resulting solution was stirred at rt for 2 h. KO*t*-Bu (2.355, 21.00 mmol, 1.5 eq.) was added and the resulting solution was stirred at rt for 16 h. After cooling to 0 °C, 1 M HCl_(aq) (60 mL) was added followed by Et₂O (100 mL) and the two layers were separated. The organic layer was washed with brine (50 mL), dried (Na₂SO₄), filtered and evaporated under reduced pressure to give the crude product. Purification by flash column chromatography on silica using 90:10 hexane-EtOAc as eluent gave bicyclic compound **84** (1.27 g, 46%) as a colourless oil, *R*_F (90:10 hexane-EtOAc) 0.40; ¹H NMR (400 MHz, CDCl₃) δ 4.19-4.17 (m, 2H, NCH), 1.78-1.73 (m, 4H, CH), 1.44 (s, 9H, CMe₃), 1.38 (d, *J* = 7.0 Hz, 4H, CH); ¹³C NMR (100.6 MHz, CDCl₃) δ 156.0 (C=O), 79.4 (CMe₃), 56.3 (NCH), 29.7 (CH₂), 28.4 (CMe₃). Spectroscopic data consistent with those reported in the literature.⁹⁹

Lab Book Reference: AMI_129

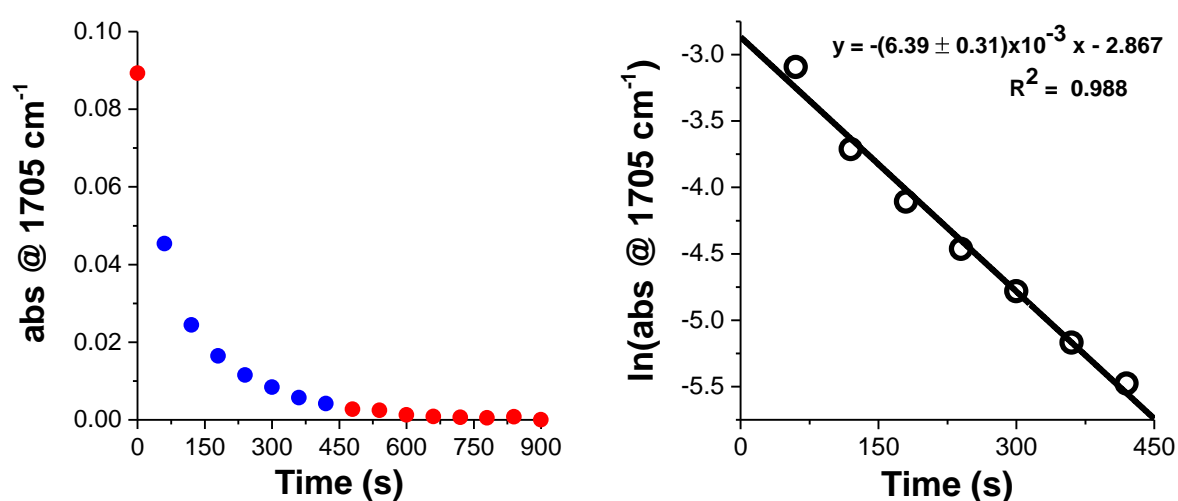
tert*-Butyl 1-[hydroxy(phenyl)methyl]-7-azabicyclo[2.2.1]heptane-7-carboxylate **231*



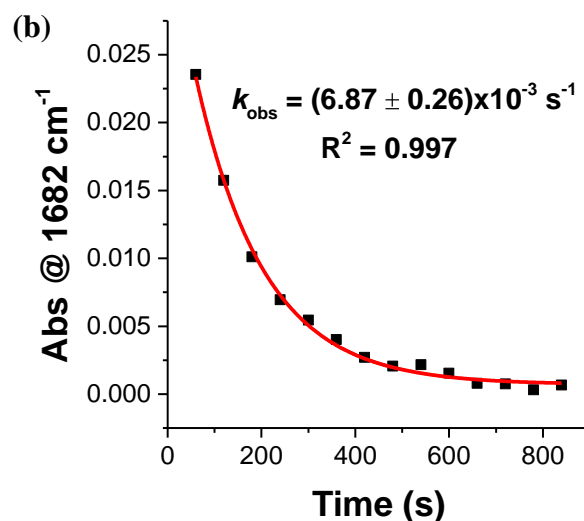
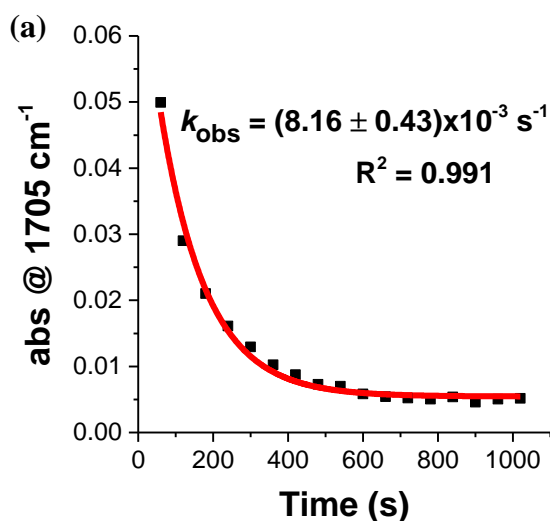
Et₂O (12 mL) was added to a flask equipped with a stirrer bar and ReactIR™ probe (iC10, DiComp) at rt under Ar. After cooling to -78 °C, a solution of bicyclic pyrrolidine **84** (196 mg, 0.99 mmol, 1.0 eq.) in Et₂O (2 mL) was added followed by TMEDA (150 mg, 0.19 mL, 1.29 mmol, 1.3 eq.). The solution was stirred for 5 min (to verify the stability of readout on ReactIR™). Then *s*-BuLi (1.0 mL of a 1.3 M solution in hexanes, 1.30 mmol, 1.3 eq.) was added dropwise. The resulting solution was stirred at -78 °C for 35 min. Then, PhCHO (211 mg, 0.20 mL, 1.99 mmol, 2.0 eq.) was added and the solution was stirred at -78 °C for a further 5 min. The solution was then allowed to warm to rt over 30 min and saturated NH₄Cl(aq) (10 mL) was added and the two layers were separated. The aqueous layer was extracted with Et₂O (3 x 10 mL) and the combined organics were dried (MgSO₄), filtered and evaporated under reduced pressure to give the crude product. Purification by flash column chromatography on silica using 99.5:0.5 CH₂Cl₂-acetone as eluent gave 2-substituted bicyclic pyrrolidine **231** (204 mg, 68%) as a white solid, mp 100-102 °C; *R*_F (99.5:0.5 CH₂Cl₂-acetone) 0.22; IR (ATR) 3269 (OH), 2979, 2873, 1663 (C=O), 1402, 1367, 1150, 1128, 1053, 713 cm⁻¹; ¹H NMR (400 MHz, CDCl₃) δ 7.40-7.37 (m, 2H, Ph), 7.31-7.21 (m, 3H, Ph), 5.61 (br s, 1H, OH), 5.32 (s, 1H, OCH), 4.28 (dd, *J* = 5.0, 5.0 Hz, 1H, NCH), 2.29 (dddd, *J* = 12.0, 12.0, 3.5, 3.5 Hz, 1H, CH), 1.81-1.67 (m, 3H, CH₂), 1.48 (s, 9H, CMe₃), 1.36-1.28 (m, 2H, CH), 1.19-1.12 (m, 1H, CH), 1.09-1.04 (m, 1H, CH); ¹³C NMR (100.6 MHz, CDCl₃) δ 154.9 (C=O), 141.0 (*ipso*-Ph), 128.0 (Ph), 127.6 (Ph), 127.5 (Ph), 80.5 (CMe₃), 73.8 (CHO), 72.8 (NC), 58.4 (NCH), 35.1 (CH₂), 29.2 (CH₂), 29.1 (CH₂), 28.6 (CMe₃), 28.1 (CH₂); HRMS (ESI) *m/z* calcd for C₁₈H₂₄NO₃ (M + Na)⁺ 326.1727, found 326.1718 (+2.1 ppm error).

For bicyclic pyrrolidine **84**, a peak at 1705 cm^{-1} was observed and assigned to $\nu_{\text{C=O}}$. After addition of *s*-BuLi, a new peak at 1682 cm^{-1} was observed which was assigned to $\nu_{\text{C=O}}$ in the prelithiation complex. A new peak at 1641 cm^{-1} was also observed and this was assigned to the lithiated intermediate. After a lithiation time of 15 min, complete lithiation of bicyclic pyrrolidine **84** to give the lithiated intermediate was observed. When PhCHO was added (after a 15 min total lithiation time), the signal for the lithiated intermediate ($\nu_{\text{C=O}} = 1641\text{ cm}^{-1}$) disappeared after 1 min, indicating complete trapping had occurred.

Kinetic analysis indicated that the lithiation of bicyclic pyrrolidine **84** was first order with respect to bicyclic pyrrolidine **84**, $k_{\text{obs}} = (6.39 \pm 0.31) \times 10^{-3}\text{ s}^{-1}$ and $t_{1/2} = (108 \pm 5)\text{ s}$.

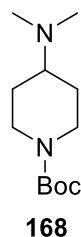


First order exponential decay curves ($y = Ae^{-k_{\text{obs}}t} + c$) were fit to the consumption of bicyclic pyrrolidine **84** (a) and consumption of the prelithiation complex of **84** (b) for the lithiation of bicyclic pyrrolidine **84**. Both provided good fit with a first order exponential decay. Curve fitting of bicyclic pyrrolidine **84** consumption (a) provided $k_{\text{obs}} = (8.16 \pm 0.43) \times 10^{-3}\text{ s}^{-1}$ and $t_{1/2} = (84.9 \pm 4.4)\text{ s}$. Curve fitting of prelithiation complex consumption (b) provided $k_{\text{obs}} = (6.87 \pm 0.26) \times 10^{-3}\text{ s}^{-1}$ and $t_{1/2} = (101 \pm 4)\text{ s}$.



Lab Book Reference: AMI_133

tert*-Butyl 4-(dimethylamino)piperidine-1-carboxylate **168*

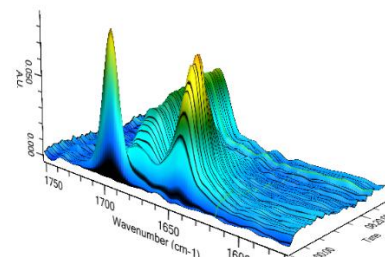
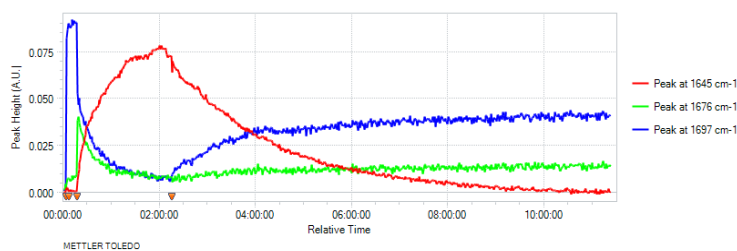
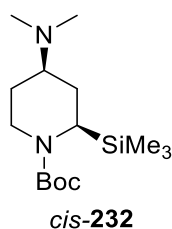


$\text{Me}_2\text{NH}\cdot\text{HCl}$ (326 mg, 4.00 mmol, 2.0 eq.) and $\text{Ti}(\text{O}i\text{-Pr})_4$ (1.137 g, 4.00 mmol, 2.0 eq., 1.18 mL) were added to a stirred solution of *N*-Boc piperidin-4-one (399 mg, 2.00 mmol, 1.0 eq.) and Et_3N (405 mg, 4.00 mmol, 2.0 eq., 0.56 mL) in EtOH (5 mL) at rt under Ar. The resulting solution was stirred at rt for 16 h. Then, NaBH_4 (113 mg, 3.0 mmol, 1.5 eq.) was added and the mixture was stirred at rt for 16 h. 2 M $\text{NH}_4\text{OH}_{(\text{aq})}$ (10 mL) was added to the solution and the solids were removed by filtration and washed with CH_2Cl_2 (20 mL). The two layers of the filtrate were separated and the aqueous layer was extracted with CH_2Cl_2 (2 x 20 mL). The combined organics were extracted with 2 M $\text{HCl}_{(\text{aq})}$ (2 x 10 mL). 10% $\text{NaOH}_{(\text{aq})}$ was added to the combined aqueous extracts until pH > 10 was reached and then this solution was extracted with CH_2Cl_2 (2 x 25 mL). These combined organics were dried (K_2CO_3), filtered and evaporated under reduced pressure to give the crude product. Purification by flash column chromatography on silica using 90:9.9:0.1 CH_2Cl_2 -MeOH- Et_3N as eluent gave dimethyl *N*-Boc piperidine **168** (180 mg, 40%) as a yellow oil, R_F (90:10 CH_2Cl_2 -MeOH) 0.16; IR (ATR) 2933, 2861, 2771, 1690 (C=O), 1419, 1364, 1239, 1155, 1057, 879 cm^{-1} ; ^1H NMR (400 MHz, CDCl_3) δ 4.14 (br s, 2H, NCH), 2.77-2.63 (m, 2H, NCH), 2.37-2.27 (m,

7H, NCH + NMe₂), 1.86-1.78 (m, 2H, CH), 1.45 (s, 9H, CMe₃), 1.44-1.32 (m, 2H, CH); ¹³C NMR (100.6 MHz, CDCl₃) δ 154.9 (C=O), 79.5 (CMe₃), 62.3 (NCH), 43.2 (NCH₂), 41.7 (NMe₂), 28.5 (CMe₃), 28.4 (CH₂); HRMS (ESI) *m/z* calcd for C₁₂H₂₄N₂O₂ (M + Na)⁺ 229.1911, found 229.1903 (+3.4 ppm error).

Lab book Reference: AMI_118

tert*-Butyl (2*R**,4*R**)-4-(dimethylamino)-2-(trimethylsilyl)piperidine-1-carboxylate *cis*-**232*

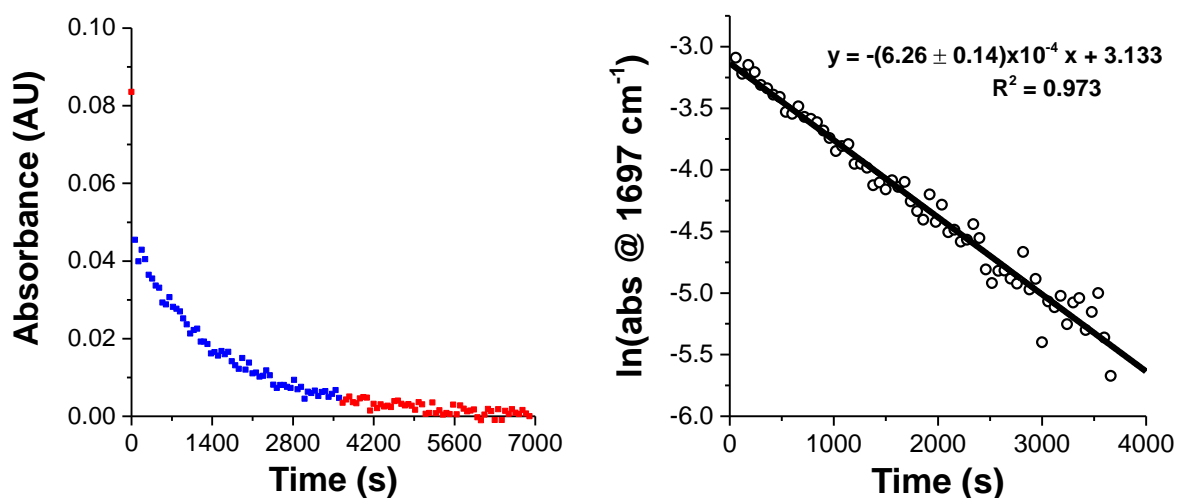


Et₂O (12 mL) was added to a flask equipped with a stirrer bar and ReactIRTM probe (ReactIRTM 15, DiComp) at rt under Ar. After cooling to -78 °C, a solution of 4-amino piperidine **168** (228 mg, 1.00 mmol, 1.0 eq.) in Et₂O (2 mL) was added followed by TMEDA (151 mg, 195 μL, 1.31 mmol, 1.3 eq.). The solution was stirred for 5 min (to verify the stability of readout on ReactIRTM). Then *s*-BuLi (1.0 mL of a 1.3 M solution in hexanes, 1.31 mmol, 1.3 eq.) was added. The resulting solution was stirred at -78 °C for 2 h. Then, Me₃SiCl (217 mg, 0.254 μL, 2.00 mmol, 2.0 eq.) was added and the solution was stirred at -78 °C for a further 9 h. Saturated NH₄Cl_(aq) (10 mL) was added and the solution was then allowed to warm to rt over 30 min and the two layers were separated. The aqueous layer was extracted with Et₂O (3 x 10 mL) and the combined organics were dried (MgSO₄), filtered and evaporated under reduced pressure to give the crude product. Purification by flash column chromatography on silica using 93:5:1 CH₂Cl₂-MeOH-NH₄OH as eluent gave 2-silyl *N*-Boc piperidine *cis*-**232** (197 mg, 66%) as a pale orange oil, *R*_F 0.14 (93:5:1 CH₂Cl₂-MeOH-NH₄OH), IR (ATR) 2941, 2820, 2769, 1687 (C=O), 1422, 1365, 1243, 1158, 1068,

837 cm^{-1} ; ^1H NMR (400 MHz, CDCl_3) δ 3.96 (br s, 1H, NCH), 2.84 (br s, 1H, NCH), 2.36-2.10 (m, 2H, NCH), 2.27 (s, 6H, NMe_2), 1.84-1.71 (m, 2H, CH), 1.42 (s, 9H, CMe_3), 1.39-1.21 (m, 2H, CH), 0.06 (s, 9H, SiMe_3); ^{13}C NMR (100.6 MHz, CDCl_3) δ 155.2 ($\text{C}=\text{O}$), 79.2 (CMe_3), 63.9 (NCH), 49.2 (NCH), 46.8 (NCH_2), 41.6 (NMe_2), 35.5 (CH_2), 29.1 (CH_2), 28.5 (CMe_3), -0.8 (SiMe_3); HRMS (ESI) m/z calcd for $\text{C}_{15}\text{H}_{32}\text{N}_2\text{O}_2\text{Si}$ ($\text{M} + \text{H}$) $^+$ 301.2306, found 301.2300 (+2.1 ppm error). The stereochemistry of *cis*-**232** has not been proven but is assumed from literature precedent.³⁸

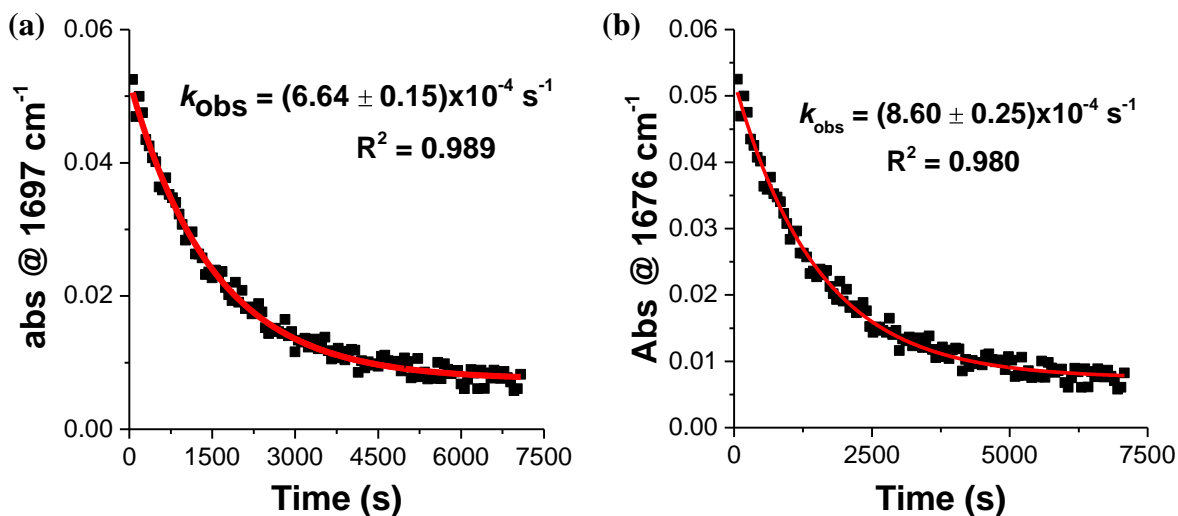
For 4-amino piperidine **168**, a peak at 1697 cm^{-1} was observed and assigned to $\nu_{\text{C}=\text{O}}$. After addition of *s*-BuLi, a new peak at 1676 cm^{-1} was observed which was assigned to $\nu_{\text{C}=\text{O}}$ in the prelithiation complex. A new peak at 1645 cm^{-1} was also observed and this was assigned to the lithiated intermediate. After a lithiation time of 2 h, complete lithiation of 4-amino piperidine **168** to give the lithiated intermediate was observed. When Me_3SiCl was added (after 2 h total lithiation time), the signal for the lithiated intermediate ($\nu_{\text{C}=\text{O}} = 1645\text{ cm}^{-1}$) disappeared after 8.5 h, indicating complete trapping had occurred.

Kinetic analysis indicated that the lithiation of 4-amino *N*-Boc piperidine **168** was first order with respect to 4-amino *N*-Boc piperidine **168**, $k_{\text{obs}} = (6.26 \pm 0.14) \times 10^{-4}\text{ s}^{-1}$ and $t_{1/2} = (1110 \pm 20)\text{ s}$.



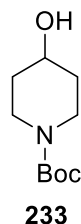
First order exponential decay curves ($y = Ae^{-k_{\text{obs}} t} + c$) were fit to the consumption of 4-amino *N*-Boc piperidine **168** (a) and consumption of the prelithiation complex of **168** (b) for the lithiation of 4-amino *N*-Boc piperidine **168**. Both provided good fit with a first order exponential decay. Curve fitting of 4-amino *N*-Boc piperidine **168** consumption (a) provided

$k_{\text{obs}} = (6.64 \pm 0.15) \times 10^{-4} \text{ s}^{-1}$ and $t_{1/2} = (1040 \pm 20) \text{ s}$. Curve fitting of pre lithiation complex consumption (b) provided $k_{\text{obs}} = (8.60 \pm 0.25) \times 10^{-4} \text{ s}^{-1}$ and $t_{1/2} = (806 \pm 24) \text{ s}$.



Lab Book Reference: AMI_266

tert-Butyl 4-hydroxypiperidine-1-carboxylate **233**

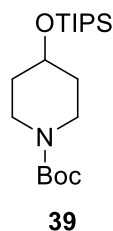


NaBH_4 (200 mg, 7.50 mmol, 1.5 eq.) was added to a stirred solution of *N*-Boc piperidin-4-one (1.00 g, 5.00 mmol, 1.0 eq.) in EtOH (5 mL) at 0 °C under Ar. The resulting solution was allowed to warm to rt and stirred at rt for 4 h. Then, the mixture was cooled to 0 °C and saturated $\text{NH}_4\text{Cl}_{(\text{aq})}$ (20 mL) was added dropwise. The solvent was evaporated under reduced pressure and EtOAc (15 mL) was added. The two layers were separated and the aqueous layer was extracted with EtOAc (2 x 15 mL). The combined organics were dried (Na_2SO_4), filtered and evaporated under reduced pressure to give the crude product. Purification by flash column chromatography on silica using 9:1 CH_2Cl_2 -acetone as eluent gave *N*-Boc-4-hydroxy piperidine **233** (913 mg, 91 %) as a white solid, mp 66-68 °C (lit.,¹⁴⁴ 64.6-66.5 °C); R_F (90:10 CH_2Cl_2 -acetone) 0.21; ^1H NMR (400 MHz, CDCl_3) δ 3.89-3.80 (m, 3H, NCH + OCH), 3.02 (ddd, $J = 13.0, 10.0, 3.0 \text{ Hz}$, 2H, NCH), 2.17 (br s, 1H, OH), 1.89-1.81 (m, 2H,

CH), 1.50-1.41 (m, 2H, CH), 1.45 (s, 9H, CMe₃). Spectroscopic data consistent with those reported in the literature.¹⁴⁴

Lab Book Reference: AMI_148

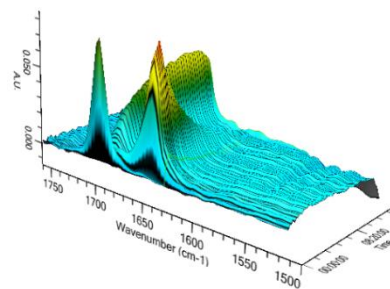
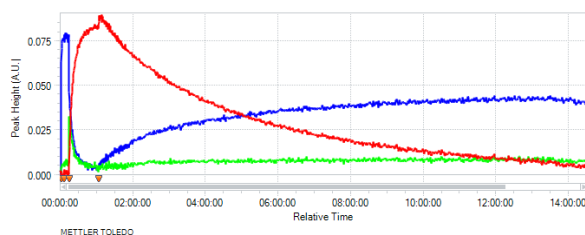
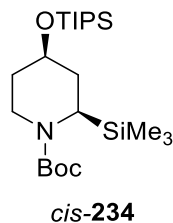
tert*-Butyl 4-[[tris(propan-2-yl)silyl]oxy]piperidine-1-carboxylate **39*



Triisopropylsilyl chloride (3.48 g, 3.87 mL, 18.07 mmol, 1.2 eq.) was added dropwise to a stirred solution of 4-hydroxy piperidine **233** (3.03 g, 15.06 mmol, 1.0 eq.) and imidazole (2.56 g, 37.65 mmol, 2.5 eq.) in DMF (40 mL) at rt under Ar. The resulting solution was stirred at rt for 6 h. Saturated NaHCO_{3(aq)} (40 mL) and Et₂O (40 mL) were added and the two resulting layers were separated. The aqueous layer was then extracted with Et₂O (4 x 30 mL) and the combined organics were washed with brine (50 mL), dried (Na₂SO₄), filtered evaporated under reduced pressure to give the crude product. Purification by flash column chromatography on silica using 93:7 hexane:EtOAc as eluent gave 4-OTIPS piperidine **39** (4.84 g, 90%) as a colourless oil, *R*_F (93:7 hexane:EtOAc) 0.28; ¹H NMR (400 MHz, CDCl₃) δ 3.99 (tt, *J* = 6.5, 3.3 Hz, 1H, OCH), 3.60 (ddd, *J* = 12.0, 8.0, 3.5 Hz, 2H, NCH), 3.28 (ddd, *J* = 12.0, 7.0, 4.0 Hz, 2H, NCH), 1.78-1.67 (m, 2H, CH), 1.58-1.49 (m, 2H, CH), 1.45 (s, 9H, CMe₃), 1.08-1.03 (m, 21H, Si(*i*-Pr)₃); ¹³C NMR (100.6 MHz, CDCl₃) δ 155.1 (C=O), 79.4 (CMe₃), 67.2 (OCH), 40.9 (NCH₂), 34.5 (CH₂), 28.6 (CMe₃), 18.2 (SiCHCH₃), 12.4 (SiCHCH₃). Spectroscopic data consistent with those reported in the literature.³⁹

Lab Book Reference: AMI_218

***tert*-Butyl (2*R**,4*R**)-2-(trimethylsilyl)-4-[[tris(propan-2-yl)silyl]oxy]piperidine-1-carboxylate *cis*-234**

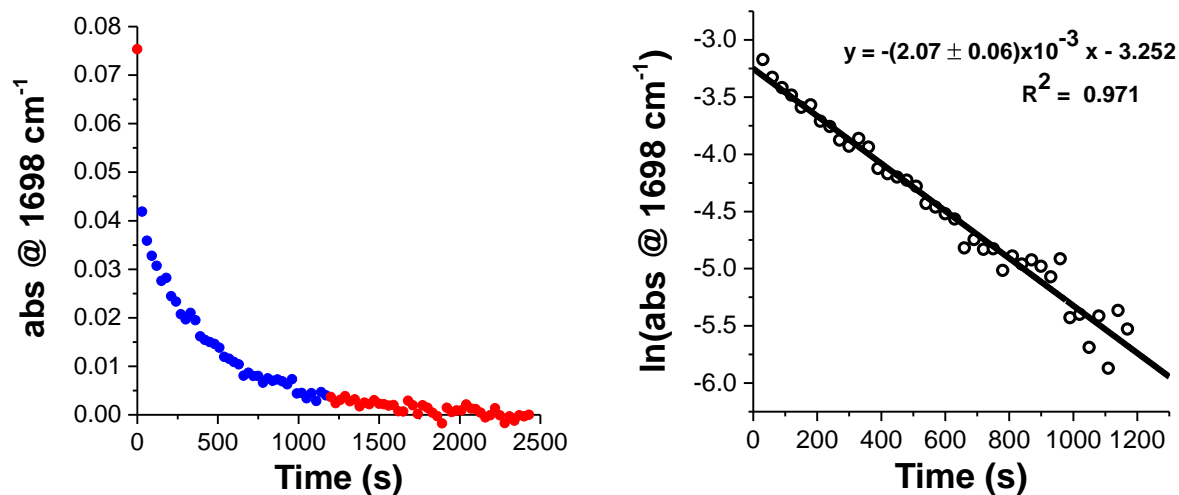


Et₂O (12 mL) was added to a flask equipped with a stirrer bar and ReactIR™ probe (ReactIR™ 15, DiComp) at rt under Ar. After cooling to −78 °C, a solution of 4-OTIPS piperidine **39** (355 mg, 0.99 mmol, 1.0 eq.) in Et₂O (2 mL) was added followed by TMEDA (151 mg, 0.19 mL, 1.30 mmol, 1.3 eq.). The solution was stirred for 5 min (to verify the stability of readout on ReactIR™). Then *s*-BuLi (1.0 mL of a 1.3 M solution in hexanes, 1.30 mmol, 1.3 eq.) was added. The resulting solution was stirred at −78 °C for 50 min. Then, Me₃SiCl (215 mg, 0.25 mL, 1.98 mmol, 2.0 eq.) was added and the solution was stirred at −78 °C for a further 14.5 h. Saturated NH₄Cl_(aq) (10 mL) was added and the solution was then allowed to warm to rt over 30 min and the two layers were separated. The aqueous layer was extracted with Et₂O (3 x 10 mL) and the combined organics were dried (MgSO₄), filtered and evaporated under reduced pressure to give the crude product. Purification by flash column chromatography on silica using 98:2-95:5 hexane:Et₂O as eluent gave 2-silyl piperidine *cis*-**234** (301 mg, 70%) as a colourless oil, *R*_F (95:5 hexane:Et₂O) 0.30; IR (ATR) 2943, 2866, 1691, 1464, 1422, 1245, 1150, 1104, 880, 826 cm^{−1}; ¹H NMR (400 MHz, CDCl₃) δ 3.92 (br s, 1H, CHO), 3.84–3.69 (m, 1H, NCH₂), 2.83 (br s, 1H, NCH₂), 2.26 (br s, 1H, NCH), 1.90–1.80 (m, 2H, CH), 1.49–1.34 (m, 2H, CH), 1.43 (s, 9H, CMe₃), 1.08–1.01 (m, 21H, Si(*i*-Pr)₃), 0.07 (s, 9H, SiMe₃); ¹³C NMR (100.6 MHz, CDCl₃) δ 155.1 (C=O), 79.2 (CMe₃), 66.0 (CHO), 36.4 (NCH₂), 30.5 (NCH), 28.5 (CMe₃), 18.2 (SiCHCH₃), 12.5 (SiCHCH₃), −0.7 (SiMe₃); HRMS (ESI) *m/z* calcd for C₂₂H₄₇NO₃Si₂ (M + Na)⁺ 452.2987,

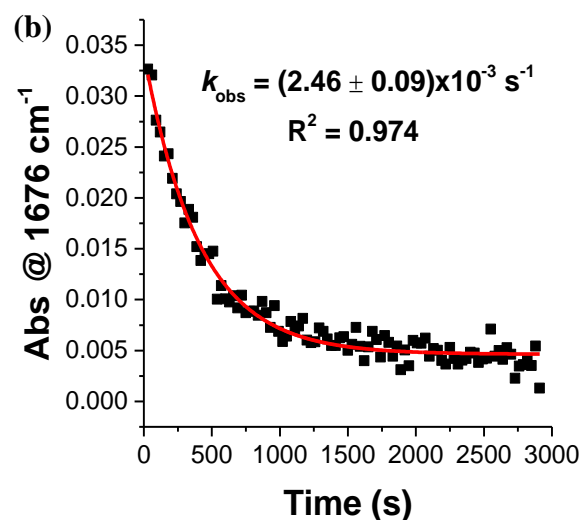
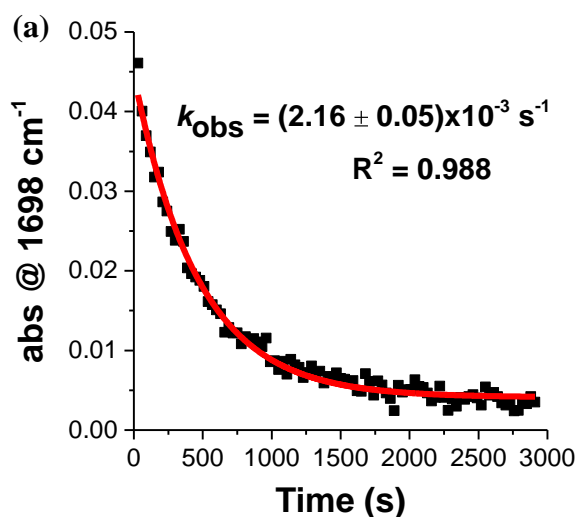
found 452.3007 (+2.8 ppm error). The stereochemistry of *cis*-**234** has not been proven but is assumed from literature precedent.³⁸

For 4-OTIPS piperidine **39**, a peak at 1698 cm⁻¹ was observed and assigned to $\nu_{C=O}$. After addition of *s*-BuLi, a new peak at 1676 cm⁻¹ was observed which was assigned to $\nu_{C=O}$ in the prelithiation complex. A new peak at 1645 cm⁻¹ was also observed and this was assigned to the lithiated intermediate. After a lithiation time of 45 min, complete lithiation of 4-OTIPS piperidine **39** to give the lithiated intermediate was observed. When Me₃SiCl was added (after 50 min total lithiation time), the signal for the lithiated intermediate ($\nu_{C=O} = 1645$ cm⁻¹) disappeared after 14.5 h, indicating complete trapping had occurred.

Kinetic analysis indicated that the lithiation of 4-OTIPS *N*-Boc piperidine **39** was first order with respect to 4-OTIPS *N*-Boc piperidine **39**, $k_{\text{obs}} = (2.07 \pm 0.06) \times 10^{-3} \text{ s}^{-1}$ and $t_{1/2} = (335 \pm 9) \text{ s}$.

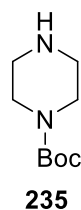


First order exponential decay curves ($y = Ae^{-k_{\text{obs}} t} + c$) were fit to the consumption of 4-OTIPS *N*-Boc piperidine **39** (a) and consumption of the prelithiation complex of **39** (b) for the lithiation of 4-OTIPS *N*-Boc piperidine **39**. Both provided good fit with a first order exponential decay. Curve fitting of 4-OTIPS *N*-Boc piperidine **39** consumption (a) provided $k_{\text{obs}} = (2.16 \pm 0.05) \times 10^{-3} \text{ s}^{-1}$ and $t_{1/2} = (321 \pm 8) \text{ s}$. Curve fitting of prelithiation complex consumption (b) provided $k_{\text{obs}} = (2.46 \pm 0.09) \times 10^{-3} \text{ s}^{-1}$ and $t_{1/2} = (281 \pm 10) \text{ s}$.



Lab Book Reference: AMI_228

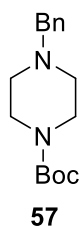
tert-Butyl piperazine-1-carboxylate **235**



A solution of Boc_2O (7.00 g, 32.07 mmol, 1.0 eq.) in CH_2Cl_2 (50 mL) was added dropwise over 1 h to a stirred solution of piperazine (5.53 g, 64.15 mmol, 2.0 eq.) in CH_2Cl_2 (180 mL) at rt. The resulting solution was stirred at rt for 16 h. The solvent was evaporated under reduced pressure to give a white solid. H_2O (100 mL) was added and the insoluble solids were removed by filtration and washed with H_2O (50 mL). The aqueous filtrate was extracted with CH_2Cl_2 (3 x 50 mL) and the combined organics were evaporated under reduced pressure to give *N*-Boc piperazine **235** (4.35 g, 73%) as a white solid, mp 43-45 °C (lit.,¹⁴⁵ 42.5-45 °C); ^1H NMR (400 MHz, CDCl_3) δ 3.38 (t, $J = 5.0$ Hz, 4H, NCH_2), 2.80 (t, $J = 5.0$ Hz, 4H, NCH_2), 1.65 (s, 1H, NH), 1.45 (s, 9H, CMe_3); ^{13}C NMR (100.6 MHz, CDCl_3) δ 154.6 (C=O), 79.4 (CMe_3), 45.6 (NCH_2), 44.6 (NCH_2), 28.4 (CMe_3). Spectroscopic data consistent with those reported in the literature.¹⁴⁵

Lab Book Reference: AMI_182

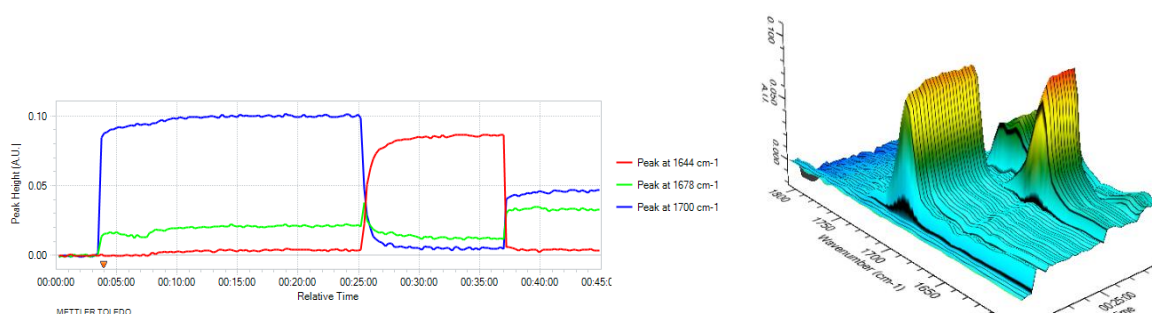
tert*-Butyl 4-benzylpiperazine-1-carboxylate **57*



N-Boc piperazine **235** (4.35 g, 23.37 mmol, 1.0 eq.) and K₂CO₃ (6.46 g, 46.74 mmol, 2.0 eq.) were added portionwise to a stirred solution of benzyl chloride (2.96 g, 2.69 mL, 23.37 mmol, 1.0 eq.) in EtOH (80 mL) at rt. The resulting white suspension was stirred and heated at reflux for 16 h. After cooling to rt, the solvent was evaporated under reduced pressure and the residue was partitioned between H₂O (50 mL) and CH₂Cl₂ (50 mL). The two layers were separated and the aqueous layer was extracted with CH₂Cl₂ (3 x 25 mL). The combined organic layers were dried (MgSO₄), filtered and evaporated under reduced pressure to give the crude product. Purification by flash column chromatography on silica using 80:20 hexane-EtOAc as eluent gave *N*-Boc *N'*-Bn piperazine **57** (5.10 g, 79%) as a pale yellow solid, mp 74-76 °C (lit.,¹⁴⁶ 72-75 °C); *R*_F (80:20 hexane-EtOAc) 0.19; ¹H NMR (400 MHz, CDCl₃) δ 7.38-7.29 (m, 4H, Ph), 7.28-7.23 (m, 1H, Ph), 3.51 (s, 2H, CH₂Ph), 3.42 (t, *J* = 5.0 Hz, 4H, NCH₂), 2.39 (t, *J* = 5.0 Hz, 4H, NCH₂), 1.45 (s, 9H, CMe₃); ¹³C NMR (100.6 MHz, CDCl₃) δ 154.9 (C=O), 138.0 (*ipso*-Ph), 129.3 (Ph), 128.4 (Ph), 127.3 (Ph), 79.7 (CMe₃), 63.2 (CH₂Ph), 53.0 (NCH₂), 44.2 (NCH₂), 28.6 (CMe₃); Spectroscopic data consistent with those reported in the literature.¹⁴⁶

Lab Book Reference: AMI_187

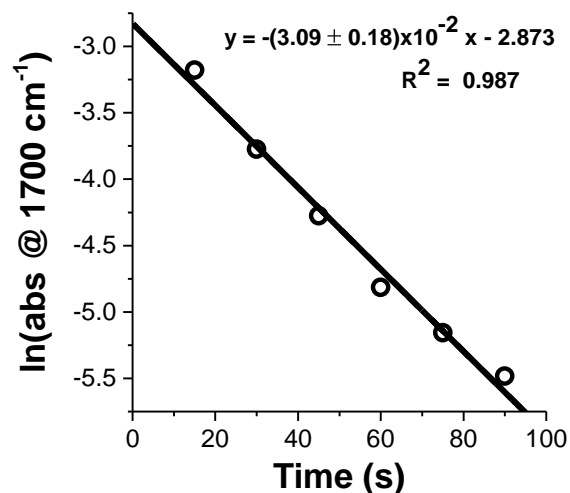
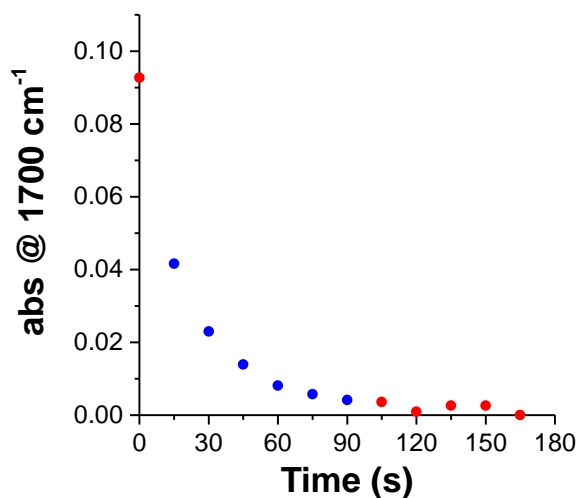
ReactIRTM spectroscopic monitoring of the *s*-BuLi/TMEDA lithiation and PhCHO trapping of *N'*-Bn *N*-Boc piperazine **57**



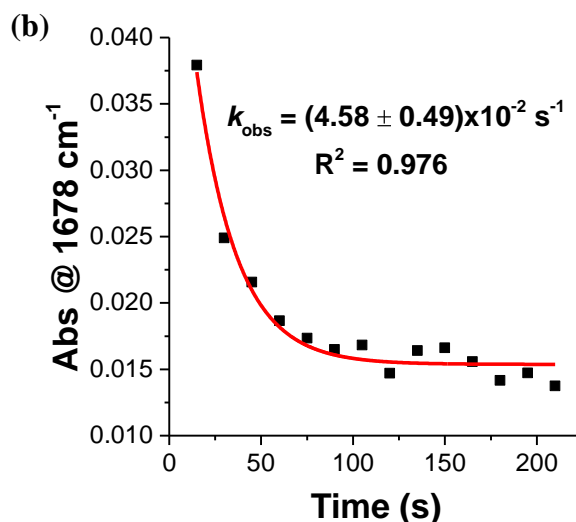
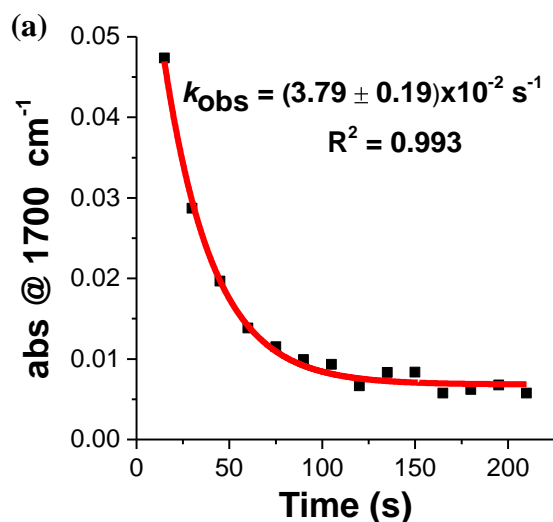
Et₂O (12 mL) was added to a flask equipped with a stirrer bar and ReactIRTM probe (ReactIRTM 15, DiComp) at rt under Ar. After cooling to -78 °C, a solution of *N'*-Bn piperazine **57** (278 mg, 1.00 mmol, 1.0 eq.) in Et₂O (2 mL) was added followed by TMEDA (151 mg, 0.20 mL, 1.30 mmol, 1.3 eq.). The solution was stirred for 5 min (to verify the stability of readout on ReactIRTM). Then *s*-BuLi (1.0 mL of a 1.3 M solution in hexanes, 1.30 mmol, 1.3 eq.) was added dropwise. The resulting solution was stirred at -78 °C for 12 min. Then, PhCHO (212 mg, 0.20 mL, 2.00 mmol, 2.0 eq.) was added and the solution was stirred at -78 °C for a further 8 min. Saturated NH₄Cl_(aq) (10 mL) was added and the solution was then allowed to warm to rt over 30 min and the two layers were separated. The aqueous layer was extracted with Et₂O (3 x 10 mL) and combined organic extracted were dried (MgSO₄), filtered and evaporated under reduced pressure to give the crude product. ¹H NMR spectroscopic analysis of the crude product indicated that no unreacted *N'*-Bn *N*-Boc piperazine **57** was present, confirming complete lithiation of *N'*-Bn *N*-Boc piperazine **57** had occurred.

For *N'*-Bn *N*-Boc piperazine **57**, a peak at 1701 cm⁻¹ was observed and assigned to $\nu_{C=O}$. After addition of *s*-BuLi, a new peak at 1678 cm⁻¹ was observed which was assigned to $\nu_{C=O}$ in the prelithiation complex. A new peak at 1644 cm⁻¹ was also observed and this was assigned to the lithiated intermediate. After a lithiation time of 4 min, complete lithiation of *N'*-Bn *N*-Boc piperazine **57** to give the lithiated intermediate was observed. When PhCHO was added (after 12 min total lithiation time), the signal for the lithiated intermediate ($\nu_{C=O} = 1644$ cm⁻¹) disappeared after 1 min, indicating complete trapping had occurred.

Kinetic analysis indicated that the lithiation of *N'*-Bn *N*-Boc piperazine **57** was first order with respect to *N'*-Bn *N*-Boc piperazine **57**, $k_{\text{obs}} = (3.09 \pm 0.18) \times 10^{-2} \text{ s}^{-1}$ and $t_{1/2} = (22.5 \pm 1.3) \text{ s}$.

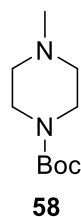


First order exponential decay curves ($y = Ae^{-k_{\text{obs}}t} + c$) were fit to the consumption of *N'*-Bn *N*-Boc piperazine **57** (a) and consumption of the prelithiation complex of **57** (b) for the lithiation of *N'*-Bn *N*-Boc piperazine **57**. Both provided good fit with a first order exponential decay. Curve fitting of *N'*-Bn *N*-Boc piperazine **57** consumption (a) provided $k_{\text{obs}} = (3.79 \pm 0.19) \times 10^{-2} \text{ s}^{-1}$ and $t_{1/2} = (18.3 \pm 0.9) \text{ s}$. Curve fitting of prelithiation complex consumption (b) provided $k_{\text{obs}} = (4.58 \pm 0.49) \times 10^{-2} \text{ s}^{-1}$ and $t_{1/2} = (15.2 \pm 1.6) \text{ s}$.



Lab Book Reference: AMI_191

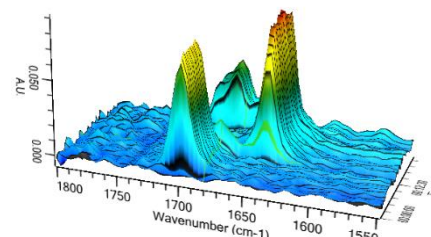
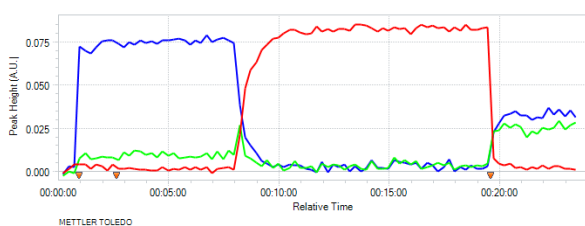
tert-Butyl 4-methylpiperazine-1-carboxylate **58**



A solution of di-*tert*-butyl dicarbonate (7.20 g, 33.00 mmol, 1.1 eq.) in CH₂Cl₂ (20 mL) was added dropwise to a stirred solution of *N*-methyl piperazine (3.00 g, 30.00 mmol, 1.0 eq., 3.3 mL) in CH₂Cl₂ at 0 °C under Ar. The resulting solution was allowed to warm to rt and stirred at rt for 16 h. Water (50 mL) and 20% NaOH_(aq) (50 mL) were added and the two layers were separated. The aqueous layer was extracted with CH₂Cl₂ (3 x 40 mL). The combined organics were dried (MgSO₄), filtered and evaporated under reduced pressure to give the crude product. Purification by Kugelrohr distillation gave *N*-Boc-*N'*-methyl piperazine **58** (5.44 g, 91%) as a colourless oil, bp 92-97°C/ 0.5 mmHg; ¹H NMR (400 MHz, CDCl₃) δ 3.42 (t, *J* = 5.0 Hz, 4H, NCH₂), 2.32 (t, *J* = 5.0 Hz, 4H, NCH₂), 2.28 (s, 3H, NMe), 1.44 (s, 9H, CMe₃); ¹³C NMR (100.6 MHz, CDCl₃) δ 154.9 (C=O), 79.7 (CMe₃), 55.0 (NCH₂), 46.3 (NMe), 43.6 (br, NCH₂), 28.5 (CMe₃). Spectroscopic data consistent with those reported in the literature.¹⁴⁶

Lab Book Reference: AMI_156

ReactIR™ spectroscopic monitoring of the *s*-BuLi/TMEDA lithiation and PhCHO trapping of *N'*-Me *N*-Boc piperazine **58**

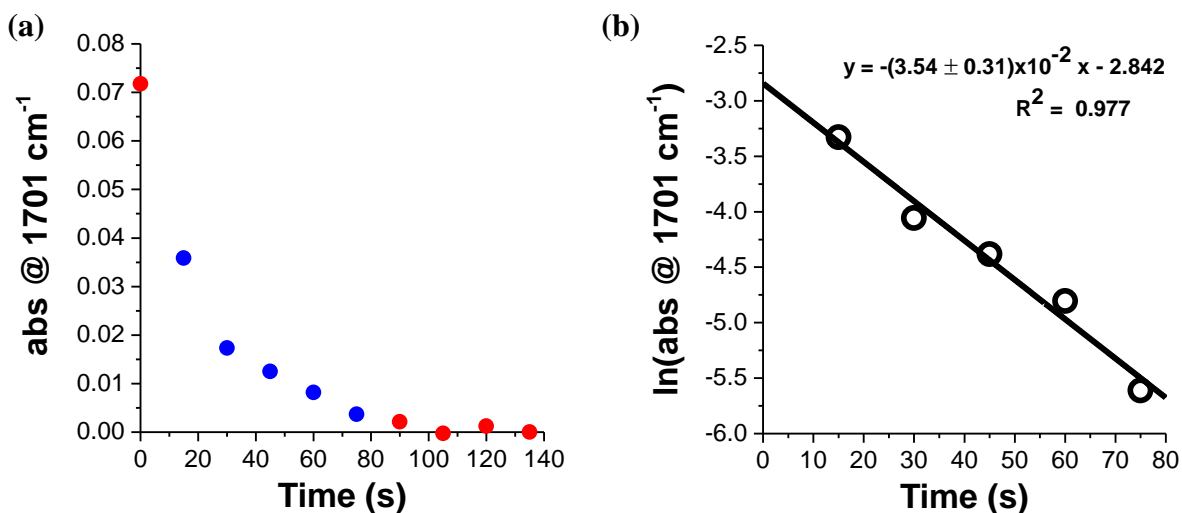


Et₂O (12 mL) was added to a flask equipped with a stirrer bar and ReactIR™ probe (ReactIR™ 15, DiComp) at rt under Ar. After cooling to -78 °C, a solution of *N'*-Me *N*-Boc piperazine **58** (199 mg, 0.99 mmol, 1.0 eq.) in Et₂O (2 mL) was added followed by TMEDA (150 mg, 0.19 mL, 1.29 mmol, 1.3 eq.). The solution was stirred for 5 min (to verify the stability of readout on ReactIR™). Then *s*-BuLi (1.0 mL of a 1.3 M solution in hexanes, 1.30 mmol, 1.3 eq.) was added dropwise. The resulting solution was stirred at -78 °C for 12

min. Then, PhCHO (210 mg, 0.20 mL, 1.99 mmol, 2.0 eq.) was added and the solution was stirred at $-78\text{ }^{\circ}\text{C}$ for a further 5 min. Saturated $\text{NH}_4\text{Cl}_{(\text{aq})}$ (10 mL) was added and the solution was then allowed to warm to rt over 30 min and the two layers were separated. The aqueous layer was extracted with Et_2O (3 x 10 mL) and the combined organics were dried (MgSO_4), filtered and evaporated under reduced pressure to give the crude product. ^1H NMR spectroscopic analysis of the crude product indicated that no unreacted *N'*-Me *N*-Boc piperazine **58** was present, confirming complete lithiation of *N'*-Me *N*-Boc piperazine **58** had occurred.

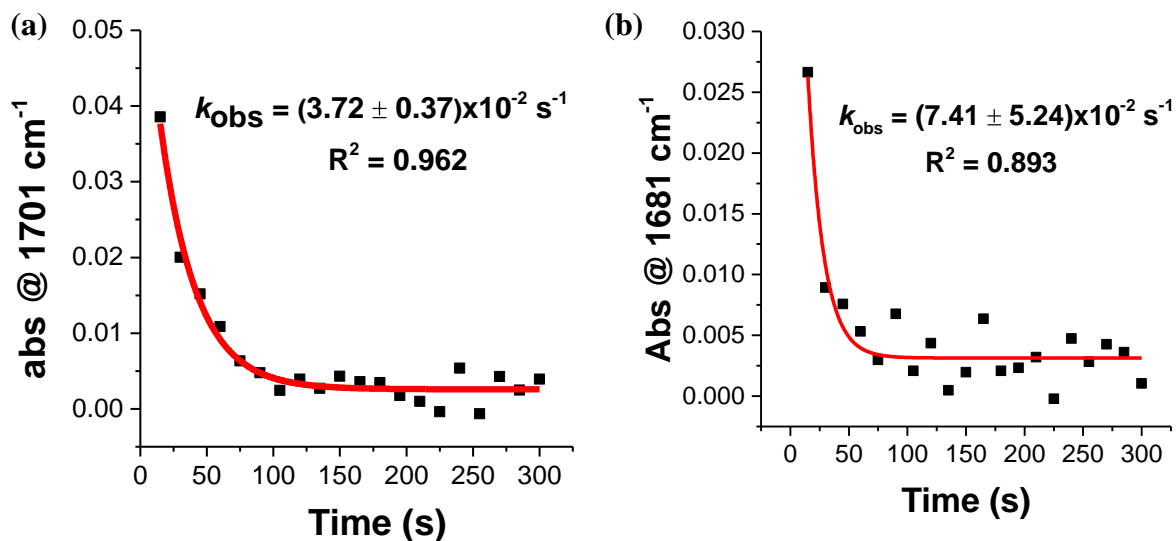
For *N'*-Me *N*-Boc piperazine **58**, a peak at 1701 cm^{-1} was observed and assigned to $\nu_{\text{C=O}}$. After addition of *s*-BuLi, a new peak at 1681 cm^{-1} was observed which was assigned to $\nu_{\text{C=O}}$ in the prelithiation complex. A new peak at 1645 cm^{-1} was also observed and this was assigned to the lithiated intermediate. After a lithiation time of 4 min, complete lithiation of *N'*-Me *N*-Boc piperazine **58** to give the lithiated intermediate was observed. When PhCHO was added (after 12 min total lithiation time), the signal for the lithiated intermediate ($\nu_{\text{C=O}} = 1645\text{ cm}^{-1}$) disappeared after 1 min, indicating complete trapping had occurred.

Kinetic analysis indicated that the lithiation of *N'*-Me *N*-Boc piperazine **58** was first order with respect to *N'*-Me *N*-Boc piperazine **58**, $k_{\text{obs}} = (3.54 \pm 0.31) \times 10^{-2}\text{ s}^{-1}$ and $t_{1/2} = (19.6 \pm 1.7)\text{ s}$.



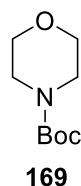
First order exponential decay curves ($y = Ae^{-k_{\text{obs}} t} + c$) were fit to the consumption of *N'*-Me *N*-Boc piperazine **58** (a) and consumption of the prelithiation complex of **58** (b) for the lithiation of *N'*-Me *N*-Boc piperazine **58**. Both provided good fit with a first order exponential decay. Curve fitting of *N'*-Me *N*-Boc piperazine **58** consumption (a) provided

$k_{\text{obs}} = (3.72 \pm 0.37) \times 10^{-2} \text{ s}^{-1}$ and $t_{1/2} = (18.7 \pm 1.8) \text{ s}$. Curve fitting of pre lithiation complex consumption (b) provided $k_{\text{obs}} = (7.41 \pm 5.24) \times 10^{-2} \text{ s}^{-1}$ and $t_{1/2} = (9.36 \pm 6.62) \text{ s}$.



Lab Book Reference: AMI_238

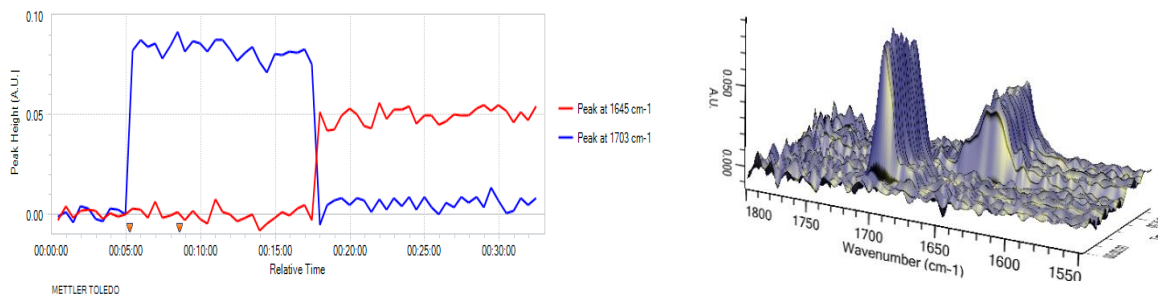
tert-Butyl morpholine-4-carboxylate **169**



Di-*tert*-butyl dicarbonate (5.51 g, 25.25 mmol, 1.1 eq.) was added to a stirred solution of morpholine (2.00 g, 22.96 mmol, 1.0 eq., 2.0 mL) in H₂O (30 mL) at rt. The resulting solution was stirred at rt for 10 min and EtOAc (30 mL) was added and the two layers were separated. The aqueous layer was extracted with EtOAc (2 x 30 mL) and the combined organics were dried (MgSO₄), filtered and evaporated under reduced pressure to give the crude product. Purification by flash column chromatography on silica using 80:20 hexane-EtOAc as eluent gave *N*-Boc morpholine **169** (2.40 g, 56%) as a white solid, mp 55-58 °C, R_F (80:20 hexane:EtOAc) 0.25; ¹H NMR (400 MHz, CDCl₃) δ 3.64 (t, $J = 4.5$ Hz, 4H, CH₂), 3.41 (t, $J = 4.5$ Hz, 4H, CH₂), 1.46 (s, 9H, CMe₃); ¹³C NMR (100.6 MHz, CDCl₃) δ 154.9 (C=O), 80.0 (CMe₃), 66.8 (CH₂), 44.0 (CH₂), 28.5 (CMe₃). Spectroscopic data consistent with those reported in the literature.¹⁴⁷

Lab Book Reference: AMI_157

ReactIR™ spectroscopic monitoring of the lithiation of *N*-Boc morpholine **169** using *s*-BuLi/TMEDA

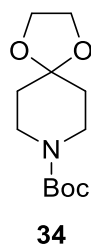


Et₂O (12 mL) was added to a flask equipped with a stirrer bar and ReactIR™ probe (ReactIR™ 15, DiComp) at rt under Ar. After cooling to $-78\text{ }^{\circ}\text{C}$, a solution of solution of *N*-Boc morpholine **169** (187 mg, 1.00 mmol, 1.0 eq.) in Et₂O (2 mL) was added followed by TMEDA (300 mg, 2.60 mmol, 2.6 eq., 0.39 mL). The solution was stirred for 5 min (to verify the stability of readout on ReactIR™). Then *s*-BuLi (2.0 mL of a 1.3 M solution in hexanes, 2.60 mmol, 2.6 eq.) was added. The resulting solution was stirred at $-78\text{ }^{\circ}\text{C}$ for 15 min.

For *N*-Boc morpholine **169**, a peak at 1703 cm^{-1} was observed and assigned to $\nu_{\text{C=O}}$. After addition of *s*-BuLi, a new peak at 1645 cm^{-1} was observed which was assigned to $\nu_{\text{C=O}}$ in the lithiated intermediate. After a lithiation time of 1 min, complete lithiation of *N*-Boc morpholine **169** to give the lithiated intermediate was observed.

Lab Book Reference: AMI_282

tert-Butyl 1,4-dioxo-8-azaspiro[4.5]decane-8-carboxylate **34**

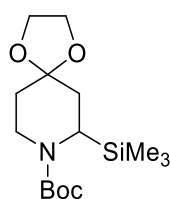


A solution of *N*-Boc-4-piperidone (3.00g, 15.06 mmol, 1 eq.), *p*-toluenesulfonic acid monohydrate (0.20g, 1.05 mmol, 0.07 eq.) and ethylene glycol (9.35 g, 150.56 mmol, 10 eq., 8.40 mL) in toluene (75 mL) was stirred and heated at reflux under Dean-Stark conditions for 72 h. After cooling to rt, the solvent was evaporated under reduced pressure and CH₂Cl₂ (30 mL) was added. The organic solution was washed with sat. NaHCO_{3(aq)} (30 mL), dried (MgSO₄), filtered and evaporated under reduced pressure to give the crude product.

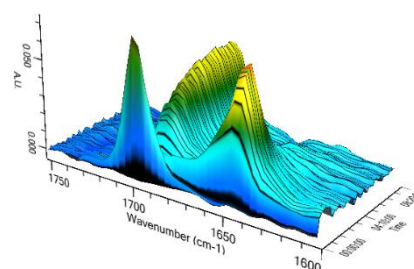
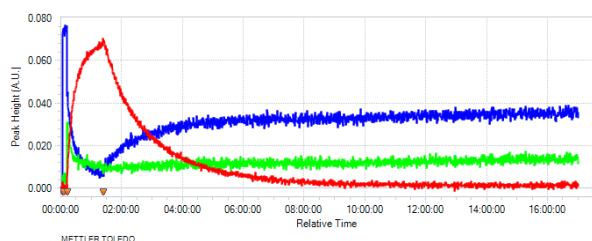
Purification by flash column chromatography on silica using 70:30 hexane-EtOAc as eluent gave 4-ketal piperidine **34** (2.91 g, 79%) as a colourless oil, R_F (70:30 hexane-EtOAc) 0.26; ^1H NMR (400 MHz, CDCl_3) δ 3.96 (s, 4H, OCH_2), 3.50 (dd, $J = 5.5, 5.5$ Hz, 4H, NCH_2), 1.65 (dd, $J = 5.5, 5.5$ Hz, 4H, CH_2), 1.45 (s, 9H, CMe_3); ^{13}C NMR (100.6 MHz, CDCl_3) 154.8 (C=O), 107.3 (OCO), 79.7 (CMe_3), 64.5 (OCH_2), 41.9 (NCH_2), 35.0 (CH_2), 28.5 (CMe_3). Spectroscopic data consistent with those reported in the literature.²⁵

Lab Book Reference: AMI_223

tert-Butyl 7-(trimethylsilyl)-1,4-dioxa-8-azaspiro[4.5]decane-8-carboxylate **47**



47

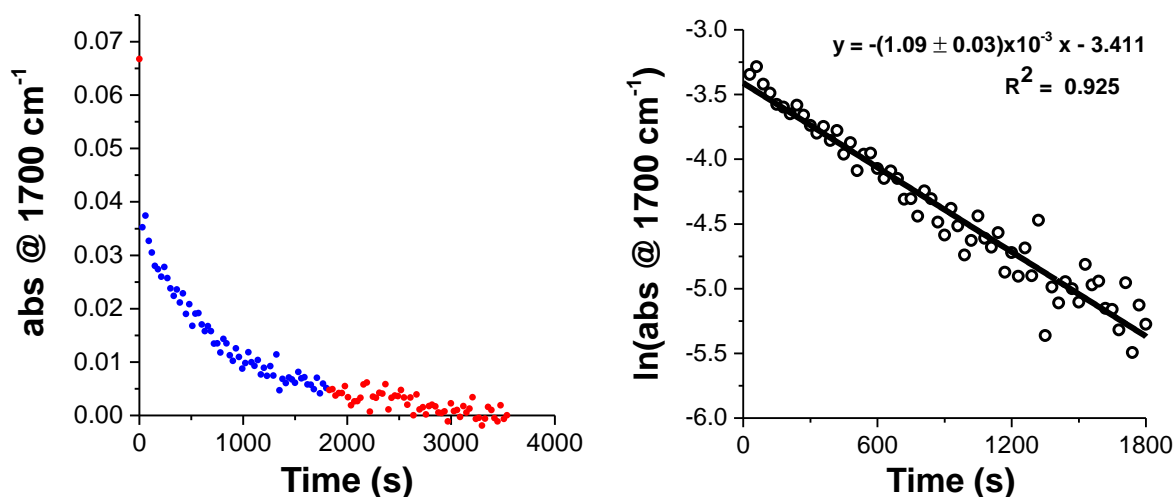


Et_2O (12 mL) was added to a flask equipped with a stirrer bar and ReactIRTM probe (ReactIRTM 15, DiComp) at rt under Ar. After cooling to -78 °C, a solution of acetal **34** (240 mg, 0.99 mmol, 1.0 eq.) in Et_2O (2 mL) was added followed by TMEDA (149 mg, 192 μL , 1.28 mmol, 1.3 eq.). The solution was stirred for 5 min (to verify the stability of readout on ReactIRTM). Then *s*-BuLi (1.0 mL of a 1.3 M solution in hexanes, 1.30 mmol, 1.3 eq.) was added. The resulting solution was stirred at -78 °C for 70 min. Then, Me_3SiCl (214 mg, 250 μL , 1.97 mmol, 2.0 eq.) was added and the solution was stirred at -78 °C for a further 14.5 h. Saturated $\text{NH}_4\text{Cl}_{(\text{aq})}$ (10 mL) was added and the solution was then allowed to warm to rt over 30 min. The two layers were separated and the aqueous layer was extracted with Et_2O (3 x 10 mL). The combined organics were dried (MgSO_4), filtered and evaporated under reduced pressure to give the crude product. Purification by flash column chromatography on silica using 85:15 hexane-EtOAc as eluent gave 2-substituted *N*-Boc piperidine **47** (220 mg, 71%) as a yellow solid, mp 62-64 °C; R_F (85:15 hexane-EtOAc) 0.3; IR (ATR) 2975, 2948,

2924, 2896, 1678 (C=O), 1361, 1234, 1166, 1100, 836, cm^{-1} ; ^1H NMR (400 MHz, CDCl_3) δ 3.95 (s, 4H, OCH_2), 3.71 (br s, 1H, NCH), 3.27 (br s, 1H, NCH_2), 2.94 (br s, 1H, NCH_2), 1.78-1.57 (m, 4H, CH), 1.44 (s, 9H, CMe_3), 0.07 (s, 9H, SiMe_3); ^{13}C NMR (100.6 MHz, CDCl_3) δ 155.1 (C=O), 107.7 (OCH_2), 79.4 (CMe_3), 64.6 (OCH_2), 64.4 (OCH_2), 44.2 (NCH_2), 35.6 (CH_2), 28.5 (CMe_3), -0.08 (SiMe_3); HRMS (ESI) m/z calcd for $\text{C}_{15}\text{H}_{29}\text{NO}_4\text{Si}$ ($\text{M} + \text{Na}$) $^+$ 338.1758, found 338.1750 (+1.5 ppm error). Spectroscopic data consistent with those reported in the literature.¹⁴⁸

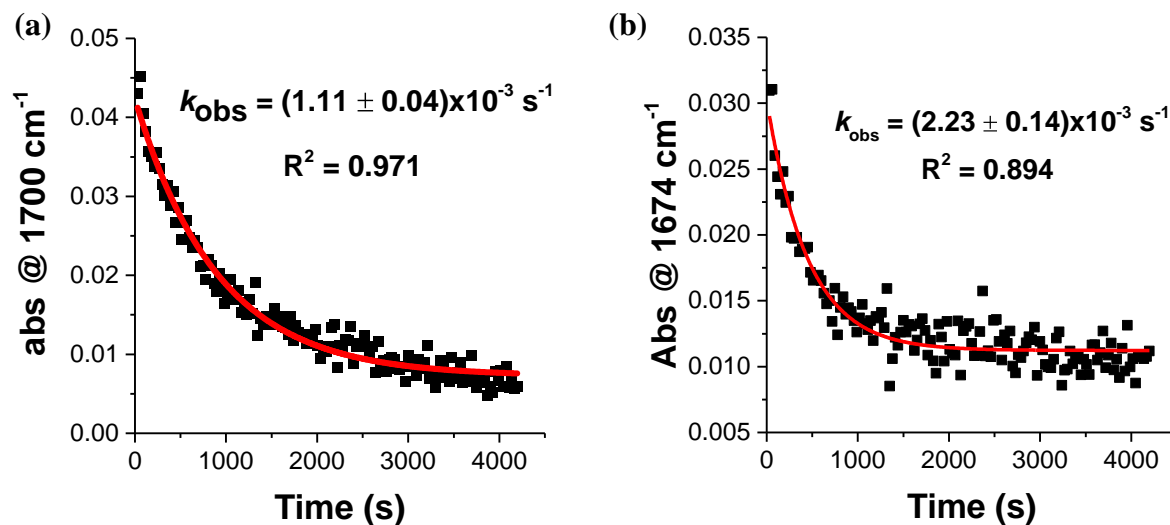
For 4-ketal *N*-Boc piperidine **34**, a peak at 1700 cm^{-1} was observed and assigned to $\nu_{\text{C=O}}$. After addition of *s*-BuLi, a new peak at 1674 cm^{-1} was observed which was assigned to $\nu_{\text{C=O}}$ in the prelithiation complex. A new peak at 1646 cm^{-1} was also observed and this was assigned to the lithiated intermediate. After a lithiation time of 70 min, complete lithiation of 4-ketal *N*-Boc piperidine **34** to give the lithiated intermediate was observed. When Me_3SiCl was added (after 70 min total lithiation time), the signal for the lithiated intermediate ($\nu_{\text{C=O}} = 1646\text{ cm}^{-1}$) disappeared after 8.5 h, indicating complete trapping had occurred.

Kinetic analysis indicated that the lithiation of 4-ketal *N*-Boc piperidine **34** was first order with respect to 4-ketal *N*-Boc piperidine **34**, $k_{\text{obs}} = (1.09 \pm 0.03) \times 10^{-3}\text{ s}^{-1}$ and $t_{1/2} = (636 \pm 18)$ s.



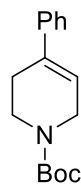
First order exponential decay curves ($y = Ae^{-k_{\text{obs}}t} + c$) were fit to the consumption of 4-ketal *N*-Boc piperidine **34** (a) and consumption of the prelithiation complex of **34** (b) for the lithiation of 4-ketal *N*-Boc piperidine **34**. Both provided good fit with a first order exponential decay. Curve fitting of 4-ketal *N*-Boc piperidine **34** consumption (a) provided

$k_{\text{obs}} = (1.11 \pm 0.04) \times 10^{-3} \text{ s}^{-1}$ and $t_{1/2} = (624 \pm 22) \text{ s}$. Curve fitting of pre lithiation complex consumption (b) provided $k_{\text{obs}} = (2.23 \pm 0.14) \times 10^{-3} \text{ s}^{-1}$ and $t_{1/2} = (311 \pm 19) \text{ s}$.



Lab Book Reference: AMI_236

tert-Butyl 4-phenyl-1,2,3,6-tetrahydropyridine-1-carboxylate 236



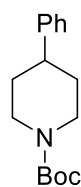
236

n-BuLi (6.48 mL of a 2.3 M solution in hexanes, 15.04 mmol, 1.0 eq.) was added dropwise to a solution of bromobenzene (2.36 g, 1.57 mL, 15.04 mmol, 1.0 eq.) in THF (80 mL) at $-78 \text{ }^\circ\text{C}$ under Ar. The resulting solution was stirred at $-78 \text{ }^\circ\text{C}$ for 30 min. A solution of *N*-Boc piperidin-4-one (3.00 g, 15.04 mmol, 1.0 eq.) in THF (20 mL) was added dropwise to the reaction mixture. The reaction mixture was stirred for a further 1 h at $-78 \text{ }^\circ\text{C}$ and then allowed to warm to rt and stirred at rt for a further 1h. The reaction was then cooled to $-78 \text{ }^\circ\text{C}$ and methanesulfonyl chloride (6.89 g, 4.66 mL, 60.16 mmol, 4.0 eq.) and Et_3N (12.18 g, 16.8 mL, 120.32 mmol, 8.0 eq.) were added dropwise. The reaction mixture was then allowed to warm to rt and stirred at rt for 15 h. Saturated $\text{NaHCO}_3(\text{aq})$ (60 mL) was then added with vigorous stirring followed by addition of EtOAc (60 mL). The two layers were separated and the aqueous layer was extracted with EtOAc (2 x 40 mL). The combined organics were washed with brine (50 mL), dried (MgSO_4), filtered and evaporated under

reduced pressure to give the crude product. Purification by flash column chromatography on silica using 90:10 hexane:EtOAc as eluent gave tetrahydropyridine **236** (2.61 g, 67%) as a colourless oil, R_F (90:10 hexane:EtOAc) 0.21; $^1\text{H NMR}$ (400 MHz, CDCl_3) δ 7.40-7.31 (m, 4H, Ph), 7.28-7.23 (m, 1H, Ph), 6.03 (br s, 1H, =CH), 4.10-4.04 (m, 2H, NCH), 3.64 (dd, $J = 5.5, 5.5$ Hz, 2H, NCH), 2.53 (br s, 2H, CH_2), 1.49 (s, 9H, CMe_3); $^{13}\text{C NMR}$ (100.6 MHz, CDCl_3) δ 154.5 (C=O), 141.4 (*ipso*-Ph), 135.1 (=C), 128.6 (Ph), 128.4 (Ph), 126.9 (Ph), 124.5 (=CH), 79.7 (CMe_3), 43.6 (NCH₂), 40.0 (NCH₂), 28.6 (CMe_3), 27.3 (CH_2). Spectroscopic data consistent with those reported in the literature.¹⁴⁹

Lab Book Reference: AMI_180

tert*-Butyl 4-phenylpiperidine-1-carboxylate **32*

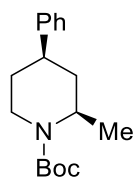


32

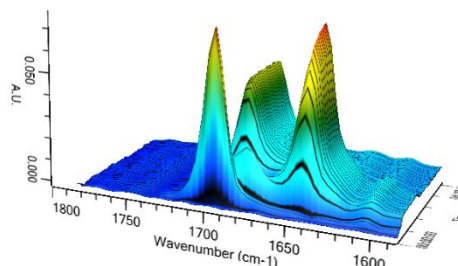
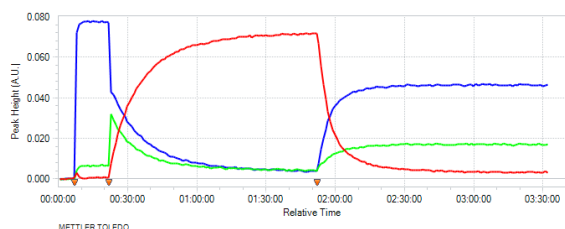
Pd/C (261 mg, 10% w/w, 0.25 mmol) was added to a solution of tetrahydropyridine **236** (2.61 g, 10.00 mmol) in MeOH (80 mL). The resulting suspension was degassed and then H₂ gas (1 atm) was supplied *via* a balloon. The suspension was stirred at rt under a H₂ atmosphere (balloon) for 16 h. The solids were removed by filtration through Celite® and washed with MeOH (10 mL). The solvent was evaporated to give the crude product as a colourless oil. Purification by flash column chromatography on silica using 90:10 hexane:EtOAc as eluent gave 4-phenyl *N*-Boc piperidine **32** (1.93 g, 74%) as a colourless oil, R_F (90:10 hexane:EtOAc) 0.22; $^1\text{H NMR}$ (400 MHz, CDCl_3) δ 7.35-7.28 (m, 2H, Ph), 7.24-7.18 (m, 3H, Ph), 4.24 (br s, 2H NCH), 2.89-2.71 (m, 2H, NCH), 2.64 (tt, $J = 12.0, 3.5$ Hz, 1H, *CHPh*), 1.87-1.77 (m, 2H, CH), 1.68-1.57 (m, 2H, CH), 1.48 (s, 9H, CMe_3); $^{13}\text{C NMR}$ (100.6 MHz, CDCl_3) δ 155.0 (C=O), 145.9 (*ipso*-Ph), 128.6 (Ph), 126.9 (Ph), 126.4 (Ph), 79.5 (CMe_3), 44.6 (NCH₂), 42.8 (*CHPh*), 33.3 (CH_2), 28.6 (CMe_3). Spectroscopic data consistent with those reported in the literature.¹⁵⁰

Lab Book Reference: AMI_186

***tert*-Butyl (2*R**, 4*R**)-2-methyl-4-phenylpiperidine-1-carboxylate *cis*-35**



***cis*-35**

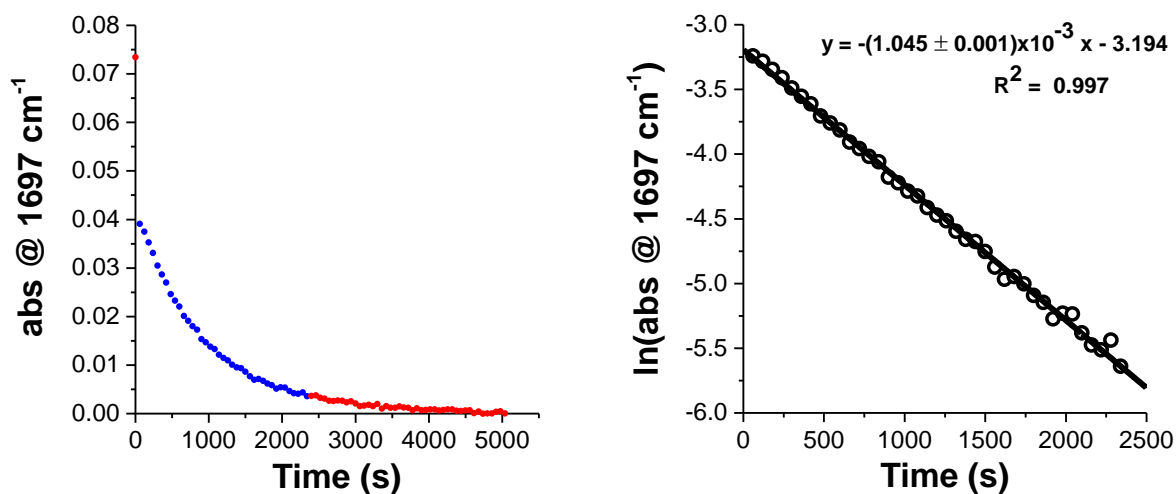


Et₂O (12 mL) was added to a flask equipped with a stirrer bar and ReactIR™ probe (ReactIR™ 15, DiComp) at rt under Ar. After cooling to -78 °C, a solution of 4-Phenyl *N*-Boc piperidine **32** (261 mg, 1.00 mmol, 1.0 eq.) in Et₂O (2 mL) was added followed by TMEDA (151 mg, 0.19 mL, 1.30 mmol, 1.3 eq.). The solution was stirred for 5 min (to verify the stability of readout on ReactIR™). Then *s*-BuLi (1.0 mL of a 1.3 M solution in hexanes, 1.30 mmol, 1.3 eq.) was added. The resulting solution was stirred at -78 °C for 2 h. Then, MeI (283 mg, 0.13 mL, 2.00 mmol, 2.0 eq.) was added and the solution was stirred at -78 °C for a further 4 h. Saturated NH₄Cl_(aq) was added and the solution was then allowed to warm to rt over 30 min and the two layers were separated. The aqueous layer was extracted with Et₂O (3 x 10 mL) and the combined organics were dried (MgSO₄), filtered and evaporated under reduced pressure to give the crude product. Purification by flash column chromatography on silica using 95:5 Hexane-EtOAc as eluent gave 2-methyl *N*-Boc piperidine *cis*-**35** (175 mg, 64%) as a colourless oil, *R*_F (95:5 Hexane-EtOAc) 0.13; ¹H NMR (400 MHz, CDCl₃) δ 7.33-7.27 (m, 2H, Ph), 7.24-7.17 (m, 3H, Ph), 4.01-3.92 (m, 1H, NCH), 3.81 (ddd, *J* = 14.0, 7.5, 3.0 Hz, 1H, NCH), 3.25 (ddd, *J* = 14.0, 10, 6.5 Hz, 1H, NCH), 2.80-2.72 (m, 1H, CHPh), 2.21-2.11 (m, 1H, CH), 1.92 (dddd, *J* = 13.5, 6.0, 3.5, 1.0 Hz, 1H, CH), 1.65-1.57 (m, 2H, CH), 1.50 (s, 9H, CMe₃), 1.21 (d, *J* = 6.5 Hz, 3H, CHMe); ¹³C NMR (100.6 MHz, CDCl₃) δ 155.5 (C=O), 146.2 (*ipso*-Ph), 128.6 (Ph), 127.0 (Ph), 126.2 (Ph), 79.3 (CMe₃), 50.2 (NCH), 38.1 (CHPh), 37.7 (NCH₂), 37.2 (CH₂), 31.4 (CH₂), 28.7 (CMe₃), 20.0 (CHMe). Spectroscopic data consistent with those reported in the literature.¹⁵¹

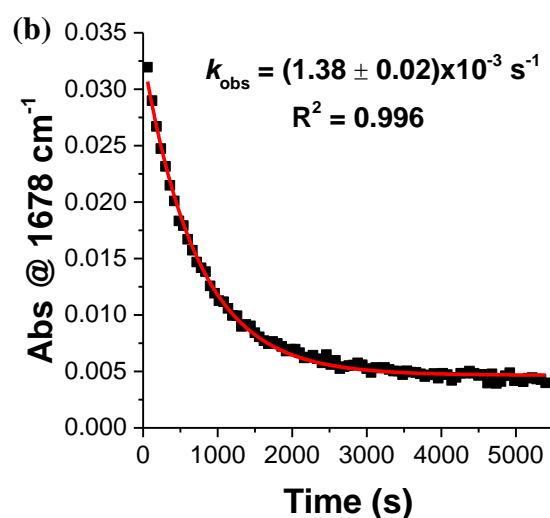
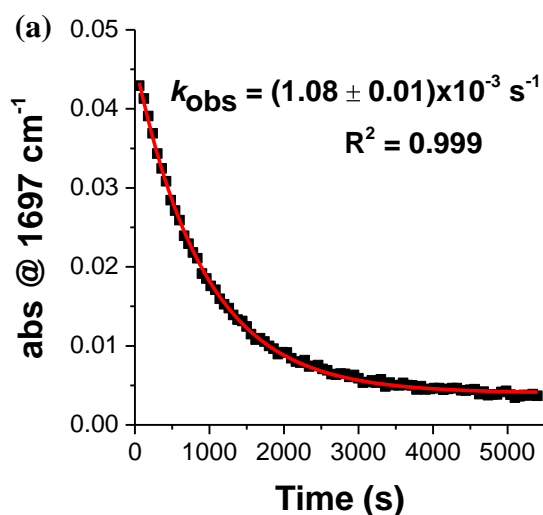
For 4-phenyl *N*-Boc piperidine **32**, a peak at 1697 cm⁻¹ was observed and assigned to ν_{C=O}. After addition of *s*-BuLi, a new peak at 1678 cm⁻¹ was observed which was assigned to ν_{C=O}.

in the prelithiation complex. A new peak at 1644 cm^{-1} was also observed and this was assigned to the lithiated intermediate. After a lithiation time of 90 min, complete lithiation of 4-phenyl *N*-Boc piperidine **32** to give the lithiated intermediate was observed. When MeI was added (after 100 min total lithiation time), the signal for the lithiated intermediate ($\nu_{\text{C=O}} = 1641\text{ cm}^{-1}$) disappeared after 90 min, indicating that complete trapping had occurred.

Kinetic analysis indicated that the lithiation of 4-phenyl *N*-Boc piperidine **32** was first order with respect to 4-phenyl *N*-Boc piperidine **32**, $k_{\text{obs}} = (1.045 \pm 0.001) \times 10^{-3}\text{ s}^{-1}$ and $t_{1/2} = (663 \pm 6)\text{ s}$.

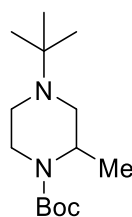


First order exponential decay curves ($y = Ae^{-k_{\text{obs}} t} + c$) were fit to the consumption of 4-phenyl *N*-Boc piperidine **32** (a) and consumption of the prelithiation complex of **32** (b) for the lithiation of 4-phenyl *N*-Boc piperidine **32**. Both provided good fit with a first order exponential decay. Curve fitting of 4-phenyl *N*-Boc piperidine **32** consumption (a) provided $k_{\text{obs}} = (1.08 \pm 0.01) \times 10^{-3}\text{ s}^{-1}$ and $t_{1/2} = (642 \pm 5)\text{ s}$. Curve fitting of prelithiation complex consumption (b) provided $k_{\text{obs}} = (1.38 \pm 0.02) \times 10^{-3}\text{ s}^{-1}$ and $t_{1/2} = (502 \pm 7)\text{ s}$.

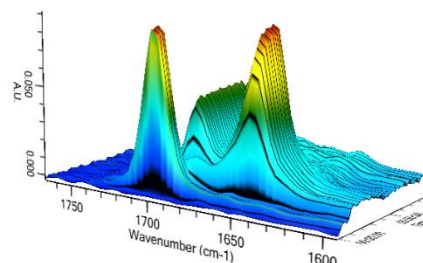
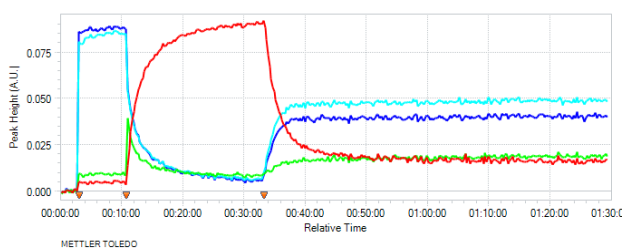


Lab Book Reference: AMI_189

***tert*-Butyl 4-*tert*-butyl-2-methylpiperazine-1-carboxylate 237**



237

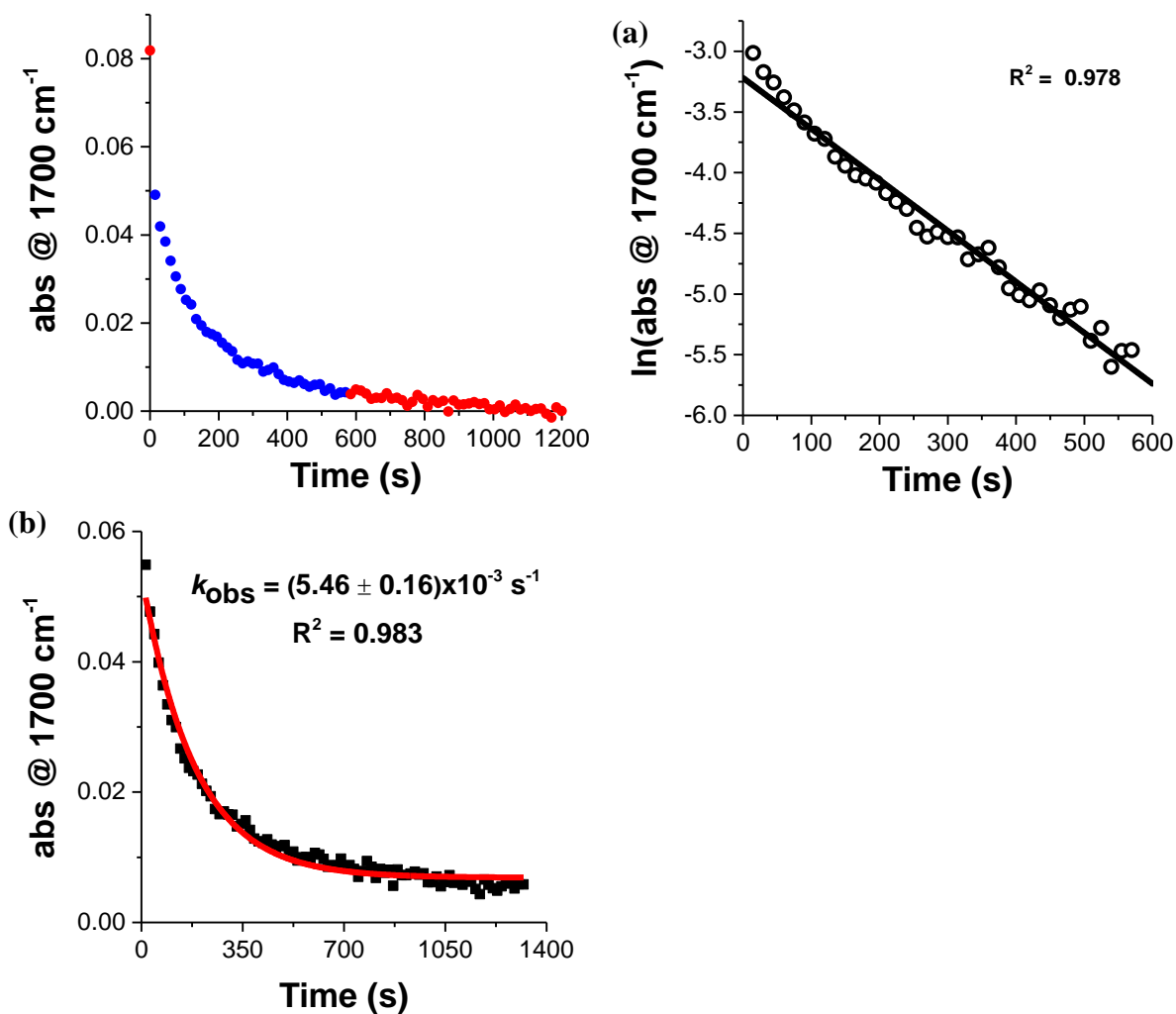


Et₂O (12 mL) was added to a flask equipped with a stirrer bar and ReactIR™ probe (ReactIR™ 15, DiComp) at rt under Ar. After cooling to -78 °C, a solution of *N*'-*t*-Bu *N*-Boc piperazine **66** (241 mg, 0.99 mmol, 1.0 eq.) in Et₂O (2 mL) was added followed by TMEDA (150 mg, 0.19 mL, 1.30 mmol, 1.3 eq.). The solution was stirred for 5 min (to verify the stability of readout on ReactIR™). Then *s*-BuLi (1.0 mL of a 1.3 M solution in hexanes, 1.30 mmol, 1.3 eq.) was added. The resulting solution was stirred at -78 °C for 22 min. Then, MeI (281 mg, 0.13 mL, 1.98 mmol, 2.0 eq.) was added and the solution was stirred at -78 °C for a further 3.5 h. Saturated NH₄Cl_(aq) (10 mL) was added and the solution was then allowed to warm to rt over 30 min and the two layers were separated. The aqueous layer was extracted with Et₂O (3 x 10 mL) and the combined organics were dried (MgSO₄), filtered

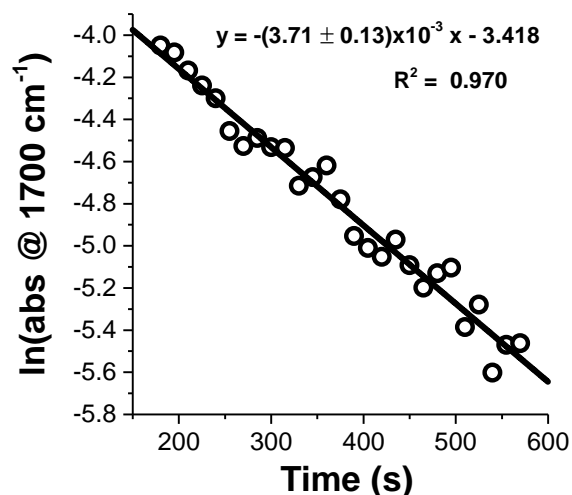
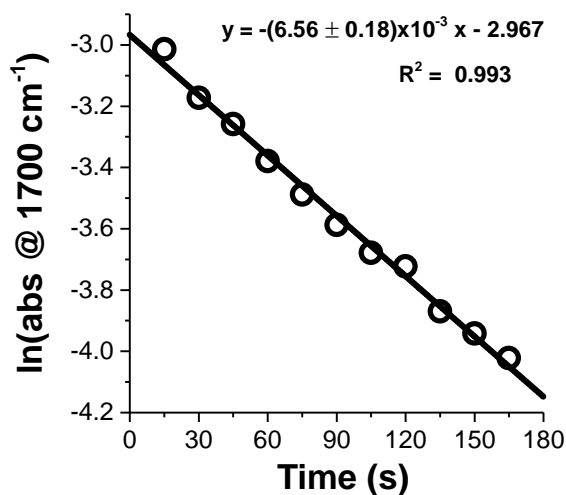
and evaporated under reduced pressure to give the crude product. Purification by flash column chromatography on silica using 95:5 CH₂Cl₂-MeOH as eluent gave 2-methyl *N*-Boc piperazine **237** (177 mg, 69%) as a white solid, mp 46-48 °C, *R_F* (95:5 CH₂Cl₂-MeOH) 0.22; IR (ATR) 2968, 2811, 1680 (C=O), 1418, 1230, 1155, 1100, 1016, 894, 767 cm⁻¹; ¹H NMR (400 MHz, CDCl₃) δ 4.20-4.10 (m, 1H, NCH), 3.77 (br d, *J* = 13.0 Hz, 1H, NCH), 2.98 (ddd, *J* = 12.5, 12.5, 3.5 Hz, 1H NCH), 2.87 (ddd, *J* = 11.0, 5.5, 2.5 Hz, 1H, NCH), 2.71 (ddd, *J* = 11.0, 2.0, 2.0 Hz, 1H, NCH), 2.24 (dd, *J* = 11.0, 3.5, Hz, 1H, NCH), 2.05 (ddd, *J* = 12.0, 11.0, 3.5 Hz, 1H, NCH), 1.44 (s, 9H, OMe₃), 1.18 (d, *J* = 6.5 Hz, 3H, CHMe), 1.00 (s, 9H, NMe₃); ¹³C NMR (100.6 MHz, CDCl₃) δ 155.0 (C=O), 79.2 (OMe₃), 53.2 (NMe₃), 50.7 (NCH₂), 47.5 (NCH), 46.1 (NCH₂), 40.2 (NCH₂), 28.6 (NMe₃), 26.1 (OMe₃), 15.8 (CHMe); HRMS (ESI) *m/z* calcd for C₁₄H₂₈N₂O₂ (M + H)⁺ 257.2224, found 257.2221 (+0.7 ppm error).

For *N'*-*t*-Bu *N*-Boc piperazine **66**, a peak at 1700 cm⁻¹ was observed and assigned to ν_{C=O}. After addition of *s*-BuLi, a new peak at 1678 cm⁻¹ was observed which was assigned to ν_{C=O} in the prelithiation complex. A new peak at 1648 cm⁻¹ was also observed and this was assigned to the lithiated intermediate. After a lithiation time of 22 min, complete lithiation of *N'*-*t*-Bu *N*-Boc piperazine **66** to give the lithiated intermediate was observed. When MeI was added (after 22 min total lithiation time), the signal for the lithiated intermediate (ν_{C=O} = 1645 cm⁻¹) disappeared after 27 min, indicating complete trapping had occurred. During the trapping process, another peak appeared at 1697 cm⁻¹ which was assigned to the trapped adduct **237**.

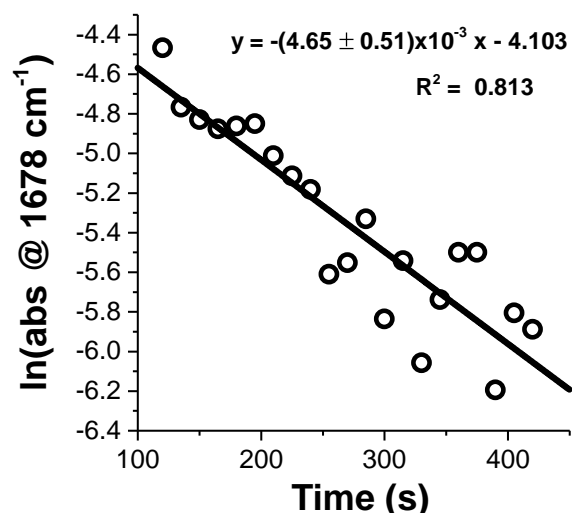
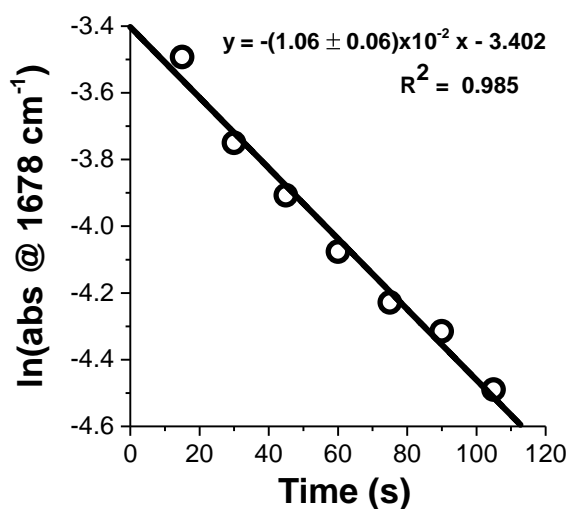
Kinetic analysis of the lithiation of *N'*-*t*-Bu *N*-Boc piperazine **66** using the consumption of *N'*-*t*-Bu *N*-Boc piperazine **66** with a semilogarithmic plot of up to 90 % lithiation conversion (a) suggested that the reaction may involve two consecutive first order processes. A first order exponential decay curve was also fitted to consumption of *N'*-*t*-Bu *N*-Boc piperazine **66** throughout the lithiation provided only a moderate fit suggesting that two consecutive first order processes may occur.



For this reason, the lithiation of *N*'-*t*-Bu *N*-Boc piperazine **66** was modelled as two consecutive first order processes. The lithiation of *N*'-*t*-Bu *N*-Boc piperazine **66** between 15 and 165 s was first order with respect to *N*'-*t*-Bu *N*-Boc piperazine **66** with $k_{\text{obs}} = (6.56 \pm 0.18) \times 10^{-3} \text{ s}^{-1}$ and $t_{1/2} = (105 \pm 3) \text{ s}$. From 180s to 90% conversion (570 s) the lithiation of *N*'-*t*-Bu *N*-Boc piperazine **66** was first order with respect to *N*'-*t*-Bu *N*-Boc piperazine **66** with $k_{\text{obs}} = (3.71 \pm 0.13) \times 10^{-3} \text{ s}^{-1}$ and $t_{1/2} = (186 \pm 7) \text{ s}$



Kinetic analysis of the lithiation of *N'*-*t*-Bu *N*-Boc piperazine **66** using the consumption of *N'*-*t*-Bu *N*-Boc piperazine **66** prelithiation complex also suggested the lithiation proceeds *via* two consecutive first order reactions. The lithiation of *N'*-*t*-Bu *N*-Boc piperazine **66** between 15 and 165 s was first order with respect to the *N'*-*t*-Bu *N*-Boc piperazine **66** prelithiation complex with $k_{\text{obs}} = (1.06 \pm 0.06) \times 10^{-3} \text{ s}^{-1}$ and $t_{1/2} = (65 \pm 4) \text{ s}$. From 180s to 90% conversion (570 s) the lithiation of *N'*-*t*-Bu *N*-Boc piperazine **66** was first order with respect to *N'*-*t*-Bu *N*-Boc piperazine **66** with $k_{\text{obs}} = (4.65 \pm 0.51) \times 10^{-3} \text{ s}^{-1}$ and $t_{1/2} = (149 \pm 16) \text{ s}$.

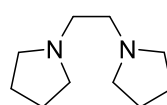


At present, the reason why the lithiation of *N'*-*t*-Bu *N*-Boc piperazine **66** appears to follow two consecutive first order reactions is not known. It is possible that the changing excess of the *s*-BuLi/TMEDA reagent or the build-up of the lithiated product during the reaction could cause the lithiation to proceed *via* a different mechanism. To compare the reactivity of *N'*-*t*-Bu *N*-Boc piperazine **66** with the other *N*-Boc heterocycles presented in this thesis the rate of the initial first order process has been used. This initial first order process has been selected for the kinetic comparison as the reagent quantities will more closely mirror those

present in the lithiation reactions of the other *N*-Boc heterocycles at the beginning of the reaction. In addition, if the lithiated product or another intermediate species formed during the reaction is changing the mechanistic pathway of the reaction, this effect will be less pronounced during the initial stages of the reaction where the concentrations of intermediates and products will be smaller.

Lab Book Reference: AMI_193

1-[2-(pyrrolidin-1-yl)ethyl]pyrrolidine **177**

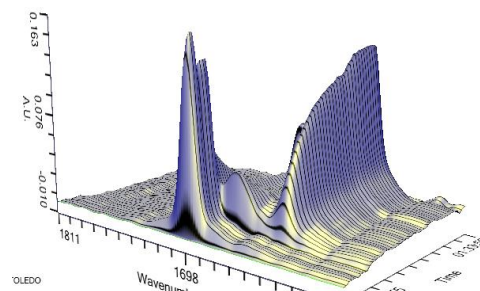
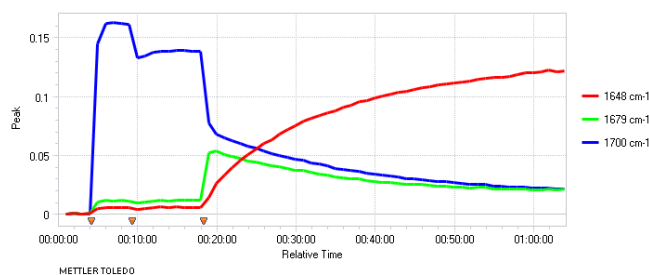


177

A mixture of 1,2-dichloroethane (4.3 mL, 55.0 mmol, 1.0 eq.), pyrrolidine (10.7 mL, 132.0 mmol, 2.4 eq.), K₂CO₃ (9.88 g, 71.5 mmol, 1.3 eq.) and H₂O (10 mL) were stirred and heated at reflux for 16 h. The resulting mixture was then allowed to cool to rt and toluene (10 mL) was added. The two layers were separated and the aqueous layer was extracted with toluene (2 x 10 mL). The combined organics were dried (KOH), filtered and evaporated under reduced pressure to give the crude product. Purification by vacuum distillation, collecting the distillate between 120-140 °C/5 mmHg gave diamine **177** (6.02g, 65%) as a colourless oil, bp 78-85°C/1 mmHg; ¹H NMR (400 MHz, CDCl₃) δ 2.63 (s, 4H, NCH₂), 2.54-2.51 (m, 8H, NCH₂), 1.79-1.75 (m, 8H, CH₂); ¹³C NMR (100.6 MHz, CDCl₃) δ 55.8 (NCH₂), 54.7 (NCH₂), 23.5 (CH₂). Spectroscopic data consistent with those reported in the literature.¹⁰⁵

Lab Book Reference: AMI_94

ReactIR™ spectroscopic monitoring of the lithiation of *N*-Boc pyrrolidine **9** using *s*-BuLi/di-pyrrolidino ethane **177**

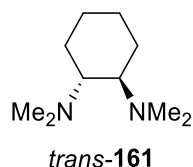


Et₂O (12 mL) was added to a flask equipped with a stirrer bar and ReactIR™ probe (iC 10, SiComp) at rt under Ar. After cooling to $-78\text{ }^{\circ}\text{C}$, *N*-Boc pyrrolidine **9** (171 mg, 1.00 mmol, 0.18 mL, 1.0 eq.) was added followed by a solution of di-pyrrolidino ethane **177** (219 mg, 1.30 mmol, 1.3 eq.) in Et₂O (2 mL). The solution was stirred for 5 min (to verify the stability of readout on ReactIR™). Then *s*-BuLi (1.0 mL of a 1.3 M solution in hexanes, 1.30 mmol, 1.3 eq.) was added. The resulting solution was stirred at $-78\text{ }^{\circ}\text{C}$ for 1 h. Then, PhCHO (211 mg, 0.20 mL, 2.00 mmol, 2.0 eq.) was added and the solution was stirred at $-78\text{ }^{\circ}\text{C}$ for a further 10 min. Saturated NH₄Cl_(aq) (10 mL) was added and the solution was then allowed to warm to rt over 30 min and the two layers were separated. The aqueous layer was extracted with Et₂O (3 x 10 mL) and the combined organics were dried (MgSO₄), filtered and evaporated under reduced pressure to give the crude product. Analysis of the crude product by ¹H NMR spectroscopy indicated no *N*-Boc pyrrolidine **9** starting material was present.

For *N*-Boc pyrrolidine **9**, a peak at 1700 cm^{-1} was observed and assigned to $\nu_{\text{C=O}}$. After addition of *s*-BuLi, a new peak at 1679 cm^{-1} was observed which was assigned to $\nu_{\text{C=O}}$ in the prelithiation complex. A new peak at 1648 cm^{-1} was also observed and this was assigned to the lithiated intermediate. After a lithiation time of 46 min, complete lithiation of *N*-Boc pyrrolidine **9** to give the lithiated intermediate was observed. The PhCHO trapping was not monitored by ReactIR™. ¹H NMR analysis of the crude indicated no *N*-Boc pyrrolidine **9** starting material was present.

Lab Book Reference: AMI_144

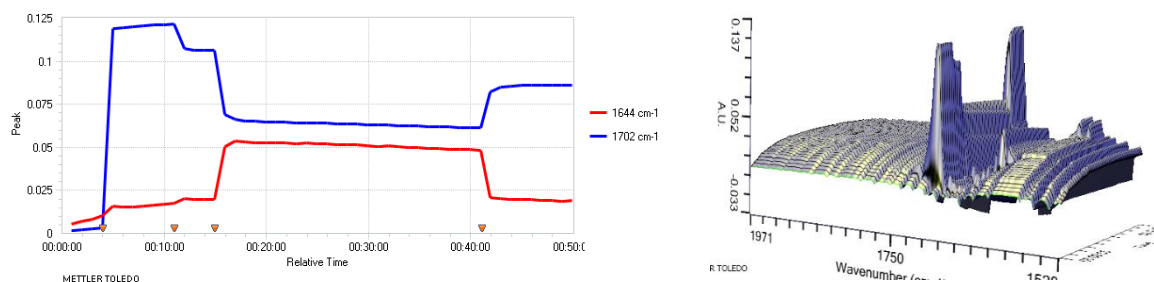
(1*R,2*R**)-*N*¹,*N*¹,*N*²,*N*²-Tetramethylcyclohexane-1,2-diamine *trans*-161**



Formaldehyde (9.1 mL of a 37% w/v solution in H₂O, 128.87 mmol, 7.0 eq.) was added dropwise to a stirred solution of *trans*-diaminocyclohexane (2.00 g, 17.51 mmol, 1.0 eq., 2.1 mL) and formic acid (7.0 mL, 185.53 mmol, 10.6 eq.) at 0 °C. The resulting solution was stirred and heated at reflux for 2 h. The solution was then cooled to 0 °C and NaOH_(s) was added until pH = 12 was reached. The mixture was extracted with Et₂O (3 x 20 mL) and the combined organic layers were dried (KOH), filtered and evaporated under reduced pressure to give the crude product. Then, acetyl chloride (5.50 g, 70.04 mmol, 4.0 eq., 5.0 mL) was added dropwise to a stirred solution of the crude product and EtOH (4.1 mL, 70.04 mmol, 4.0 eq.) in EtOAc (25 mL) at 0 °C under Ar. The resulting suspension was allowed to warm to rt over 1 h. The solids were collected by filtration through a sintered glass funnel and washed with EtOAc (2 x 10 mL). Recrystallisation from hot EtOH gave the bis-hydrochloride salt as a white solid. 20% NaOH_(aq) (20 mL) and Et₂O (20 mL) were added to the recrystallised solid and the layers separated. The aqueous layer was extracted with Et₂O (3 x 10 mL) and the combined organics were dried (MgSO₄), filtered and evaporated under reduced pressure to give the crude diamine. Purification by Kugelrohr distillation gave TMCDA *trans*-161 (1.25 g, 42%) as a colourless oil, bp 66-71 °C/2.6 mmHg (lit.,¹⁵² bp 50 °C/0.1 mmHg); ¹H NMR (400 MHz, CDCl₃) δ 2.43-2.37 (m, 2H, NCH), 2.29 (s, 12H, NMe₂), 1.87-1.84 (m, 2H, CH), 1.75-1.71 (m, 2H, CH). 1.19-1.06 (m, 4H, CH); ¹³C NMR (100.6 MHz, CDCl₃) δ 64.0 (NCH), 40.3 (NMe₂), 25.8 (CH₂), 23.0 (CH₂). Spectroscopic data consistent with those reported in the literature.¹⁰⁵

Lab Book Reference: AMI_69

ReactIR™ spectroscopic monitoring of the lithiation of *N*-Boc pyrrolidine **9** using *s*-BuLi/TMCDA *trans*-**161**

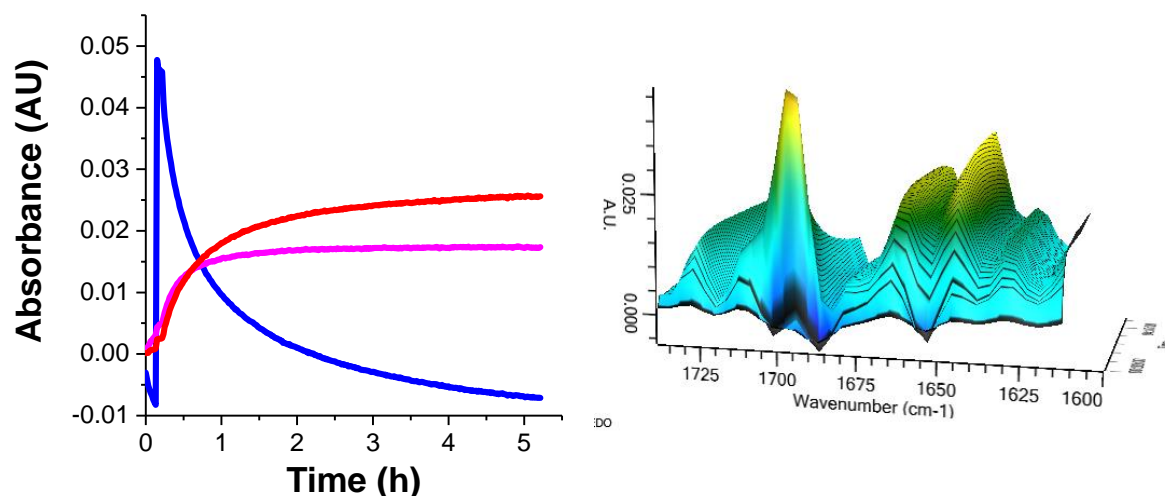


Et₂O (12 mL) was added to a flask equipped with a stirrer bar and ReactIR™ probe (iC 10, SiComp) at rt under Ar. After cooling to -78 °C, *N*-Boc pyrrolidine **9** (171 mg, 1.00 mmol, 0.18 mL, 1.0 eq.) was added followed by a solution of TMCDA *trans*-**161** (170 mg, 1.30 mmol, 1.3 eq.) in Et₂O (2 mL). The solution was stirred for 5 min (to verify the stability of readout on ReactIR™). Then *s*-BuLi (1.0 mL of a 1.3 M solution in hexanes, 1.30 mmol, 1.3 eq.) was added. The resulting solution was stirred at -78 °C for 25 min. Then, PhCHO (211 mg, 0.20 mL, 2.00 mmol, 2.0 eq.) was added and the solution was stirred at -78 °C for a further 10 min. Saturated NH₄Cl_(aq) (10 mL) was added and the solution was then allowed to warm to rt over 30 min and the two layers were separated. The aqueous layer was extracted with Et₂O (3 x 10 mL) and the combined organics were dried (MgSO₄), filtered and evaporated under reduced pressure to give the crude product. Analysis of the crude product by ¹H NMR spectroscopy indicated that no *N*-Boc pyrrolidine **9** starting material was present.

For *N*-Boc pyrrolidine **9**, a peak at 1702 cm⁻¹ was observed and assigned to $\nu_{C=O}$. After addition of *s*-BuLi, a new peak at 1644 cm⁻¹ was observed which was assigned to $\nu_{C=O}$ in the lithiated intermediate. After a lithiation time of 4 min, complete lithiation of *N*-Boc pyrrolidine **9** to give the lithiated intermediate was observed. When PhCHO was added (after a 25 min total lithiation time), the signal for the lithiated intermediate ($\nu_{C=O} = 1644$ cm⁻¹) disappeared after 1 min, indicating complete trapping had occurred.

Lab Book Reference: AMI_109

ReactIR™ spectroscopic monitoring of the lithiation of *N*-Boc pyrrolidine **9** using *s*-BuLi/THF

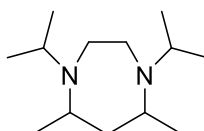


THF (14 mL) was added to a flask equipped with a stirrer bar and ReactIR™ probe (iC10, SiComp) at rt under Ar. After cooling to $-78\text{ }^{\circ}\text{C}$, *N*-Boc pyrrolidine **9** (171 mg, 0.175 mL, 1.0 mmol, 1.0 eq.) was added. The solution was stirred for 5 min (to verify the stability of readout on ReactIR®). Then *s*-BuLi (1.0 mL of a 1.3 M solution in hexanes, 1.3 mmol, 1.3 eq.) was added. The resulting solution was stirred at $-78\text{ }^{\circ}\text{C}$ for 5 h.

For *N*-Boc pyrrolidine **9**, a peak at 1696 cm^{-1} was observed and assigned to $\nu_{\text{C=O}}$. New peaks at 1663 cm^{-1} and 1648 cm^{-1} were observed and assigned to $\nu_{\text{C=O}}$ in the lithiated intermediate. After a lithiation time of 5 h, complete lithiation of *N*-Boc pyrrolidine **9** to give the lithiated intermediate was observed.

Lab Book Reference: AI_77

*N*¹,*N*¹,*N*²,*N*²-Tetraisopropylethane-1,2-diamine **178**



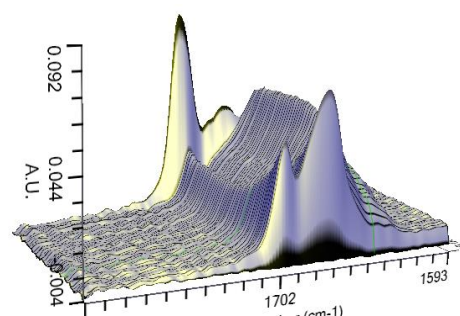
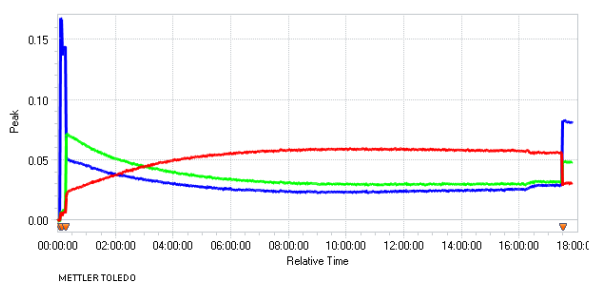
178

Oxalyl chloride (0.43 mL, 5.0 mmol, 1.0 eq.) was added dropwise to a stirred solution of diisopropylamine (1.40 mL, 10.0 mmol, 2.0 eq.) and Et₃N (1.81 mL, 13.0 mmol, 2.6 eq.) in CH₂Cl₂ (10 mL) at 0 °C under Ar. The resulting solution was stirred at rt for 16 h. CH₂Cl₂ (10 mL) and 1 M HCl_(aq) (10 mL) were added and the two layers were separated. The aqueous

layer was extracted with CH₂Cl₂ (3 x 10 mL) and the combined organics were washed with H₂O (20 mL) and brine (20 mL), dried (MgSO₄), filtered and evaporated under reduced pressure to give the crude bisamide as a pale brown solid. A solution of the crude bisamide in THF (10 mL) was added dropwise to a stirred suspension of LiAlH₄ (0.94 g, 24.65 mmol, 5.0 eq.) in THF (30 mL) at 0 °C under Ar. The resulting suspension was stirred and heated at reflux for 16 h. The suspension was then cooled to 0 °C and quenched by careful addition of H₂O (1 mL), 20% NaOH_(aq) (2 mL) and H₂O (1 mL). The resulting mixture was allowed to warm to rt, stirred for 30 min and MgSO₄ was added. The solids were removed by filtration through Celite® and washed with 9:1 CH₂Cl₂-MeOH (50 mL). The filtrate was evaporated under reduced pressure to give the crude diamine product. Purification by Kugelrohr distillation gave diamine **178** (788 mg, 69%) as a colourless oil, bp 95-100 °C/5.0 mmHg (lit.,¹⁵³ bp 110-115 °C/16 mmHg); ¹H NMR (400 MHz, CDCl₃) δ 2.98 (sept, *J* = 6.5 Hz, 4H, NCH), 2.36 (s, 4H, NCH₂), 1.01 (d, *J* = 6.5 Hz, 24H, Me); ¹³C NMR (100.6 MHz, CDCl₃) δ 21.0 (Me), 48.1 (NCH₂), 49.4 (NCH). Spectroscopic data consistent with those reported in the literature.¹⁵³

Lab Book Reference: AMI_ 92

ReactIR™ spectroscopic monitoring of the lithiation of *N*-Boc pyrrolidine **9** using *s*-BuLi/**178**



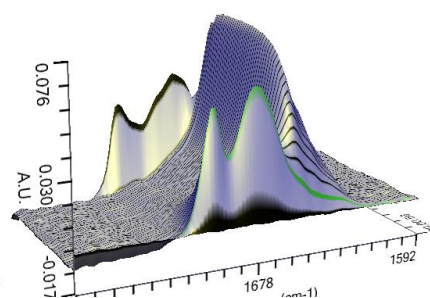
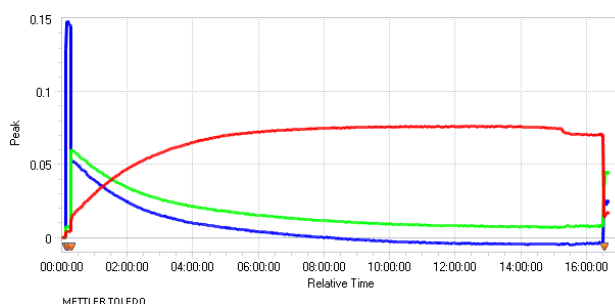
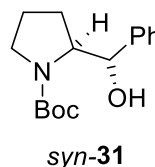
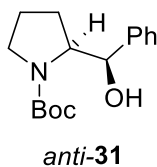
Et₂O (12 mL) was added to a flask equipped with a stirrer bar and ReactIR™ probe (iC 10, DiComp) at rt under Ar. After cooling to -78 °C, *N*-Boc pyrrolidine **9** (171 mg, 1.00 mmol, 0.18 mL, 1.0 eq.) was added followed by a solution of tetra-isopropyl ligand **178** (297 mg, 1.30 mmol, 1.3 eq.) in Et₂O (2 mL). The solution was stirred for 5 min (to verify the stability of readout on ReactIR™). Then *s*-BuLi (1.0 mL of a 1.3 M solution in hexanes, 1.30 mmol, 1.3 eq.) was added. The resulting solution was stirred at -78 °C for 17 h. Then, PhCHO (211 mg, 0.20 mL, 2.00 mmol, 2.0 eq.) was added and the solution was stirred at -78 °C for a

further 15 min. Saturated $\text{NH}_4\text{Cl}_{(\text{aq})}$ (10 mL) was added and the solution was then allowed to warm to rt over 30 min and the two layers were separated. The aqueous layer was extracted with Et_2O (3 x 10 mL) and the combined organics were dried (MgSO_4), filtered and evaporated under reduced pressure to give the crude product. Analysis of the crude product by ^1H NMR spectroscopy indicated no *N*-Boc pyrrolidine **9** starting material was present.

For *N*-Boc pyrrolidine **9**, a peak at 1701 cm^{-1} was observed and assigned to $\nu_{\text{C=O}}$. After addition of *s*-BuLi, a new peak at 1676 cm^{-1} was observed which was assigned to $\nu_{\text{C=O}}$ in the prelithiation complex. A new peak at 1657 cm^{-1} was also observed and this was assigned to the lithiated intermediate. After a lithiation time of 8 h, complete lithiation of *N*-Boc pyrrolidine **9** to give the lithiated intermediate was observed. When PhCHO was added (after a 17 h total lithiation time), the signal for the lithiated intermediate ($\nu_{\text{C=O}} = 1657\text{ cm}^{-1}$) disappeared after 1 min, indicating complete trapping had occurred.

Lab Book Reference: AMI_145

***tert*-Butyl (2*S**)-2-[(*R**) and (*S**)-hydroxy(phenyl)methyl]pyrrolidine-1-carboxylate
anti-31 and *syn*-31**



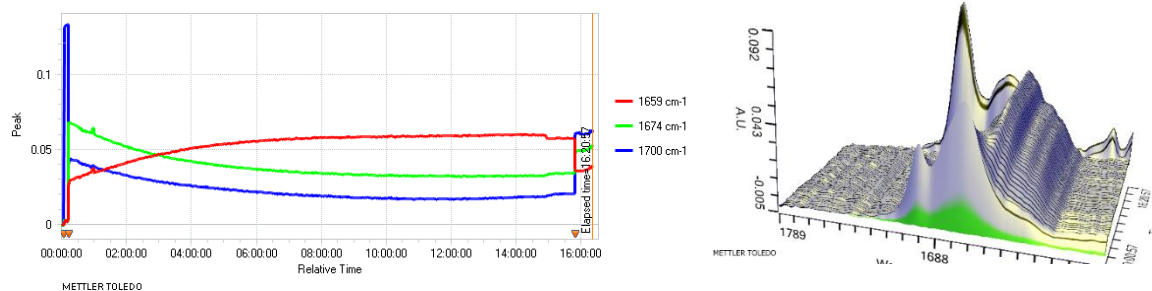
Et_2O (14 mL) was added to a flask equipped with a stirrer bar and ReactIRTM probe (iC 10, DiComp) at rt under Ar. After cooling to $-78\text{ }^\circ\text{C}$, *N*-Boc pyrrolidine **9** (171 mg, 1.00 mmol, 0.18 mL, 1.0 eq.) was added followed by TMPDA **179** (170 mg, 0.22 mL, 1.30 mmol, 1.3 eq.). The solution was stirred for 5 min (to verify the stability of readout on ReactIRTM). Then *s*-BuLi (1.0 mL of a 1.3 M solution in hexanes, 1.30 mmol, 1.3 eq.) was added. The

resulting solution was stirred at $-78\text{ }^{\circ}\text{C}$ for 16 h. Then, PhCHO (211 mg, 0.20 mL, 2.00 mmol, 2.0 eq.) was added and the solution was stirred at $-78\text{ }^{\circ}\text{C}$ for a further 10 min. Saturated $\text{NH}_4\text{Cl}_{(\text{aq})}$ (10 mL) was added and the solution was then allowed to warm to rt over 30 min and the two layers were separated. The aqueous layer was extracted with Et_2O (3 x 10 mL) and the combined organics were dried (MgSO_4), filtered and evaporated under reduced pressure to give the crude product. Purification by flash column chromatography on silica using 98:2 CH_2Cl_2 -acetone as eluent gave 2-substituted pyrrolidine *syn*-**31** (188 mg, 68%) as a colourless oil, R_F (98:2 CH_2Cl_2 -acetone) 0.30; ^1H NMR (400 MHz, CDCl_3) δ 7.38-7.27 (m, 5H, Ph), 4.70 (s, 1H, OH), 4.54 (br d, $J = 8.0$ Hz, 1H, OCH), 4.09 (ddd, $J = 8.0, 3.5$ Hz, 1H, NCH), 3.50-3.43 (m, 1H, NCH), 3.37-3.29 (m, 1H, NCH), 1.77-1.44 (m, 4H, CH), 1.52 (s, 9H, CMe_3); ^{13}C NMR (100.6 MHz, CDCl_3) (rotamers) δ 158.4 (C=O), 141.1 (*ipso*-Ph), 128.7 (Ph), 128.5 (Ph), 127.9 (Ph), 127.7 (Ph), 127.4 (Ph), 127.1 (Ph), 80.9 (CMe_3), 79.4 (CHO), 65.5 (NCH), 64.3 (NCH), 47.8 (NCH_2), 28.8 (CH_2), 28.6 (CMe_3), 23.9 (CH_2) and *anti*-**31** (81 mg, 29%) as a colourless oil, R_F (98:2 CH_2Cl_2 :acetone) 0.21; ^1H NMR (400 MHz, CDCl_3) δ 7.33-7.24 (m, 5H, Ph), 4.94 (br s, 1H, OCH), 4.23 (br s, 1H, NCH), 3.42-3.30 (m, 1H, NCH), 2.94 (br s, 1H, NCH), 1.89-1.75 (m, 2H, CH), 1.52 (s, 9H, CMe_3), 1.46-1.22 (m, 2H, CH); ^{13}C NMR (100.6 MHz, CDCl_3) δ 157.4 (C=O), 141.4 (*ipso*-Ph), 128.1 (Ph), 127.4 (Ph), 127.1 (Ph), 80.49 (CMe_3), 80.47 (CHO), 63.4 (NCH), 48.0 (NCH_2), 28.6 (CMe_3), 27.6 (CH_2), 23.6 (CH_2). Spectroscopic data consistent with those reported in the literature.¹³³

For *N*-Boc pyrrolidine **9**, a peak at 1700 cm^{-1} was observed and assigned to $\nu_{\text{C=O}}$. After addition of *s*-BuLi, a new peak at 1680 cm^{-1} was observed which was assigned to $\nu_{\text{C=O}}$ in the prelithiation complex. A new peak at 1656 cm^{-1} was also observed and this was assigned to the lithiated intermediate. After a lithiation time of 14 h, complete lithiation of *N*-Boc pyrrolidine **9** to give the lithiated intermediate was observed. When PhCHO was added (after a 16 h total lithiation time), the signal for the lithiated intermediate ($\nu_{\text{C=O}} = 1656\text{ cm}^{-1}$) disappeared after 1 min, indicating complete trapping had occurred.

Lab Book Reference: AMI_128

ReactIR™ spectroscopic monitoring of the lithiation of *N*-Boc pyrrolidine **9** using *s*-BuLi/Et₂O

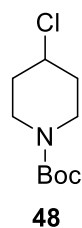


Et₂O (14 mL) was added to a flask equipped with a stirrer bar and ReactIR™ probe (iC 10, DiComp) at rt under Ar. After cooling to $-78\text{ }^{\circ}\text{C}$, *N*-Boc pyrrolidine **9** (171 mg, 1.00 mmol, 0.18 mL, 1.0 eq.) was added. The solution was stirred for 5 min (to verify the stability of readout on ReactIR™). Then *s*-BuLi (1.0 mL of a 1.3 M solution in hexanes, 1.30 mmol, 1.3 eq.) was added. The resulting solution was stirred at $-78\text{ }^{\circ}\text{C}$ for 16 h. Then, PhCHO (211 mg, 0.20 mL, 2.00 mmol, 2.0 eq.) was added and the solution was stirred at $-78\text{ }^{\circ}\text{C}$ for a further 15 min. Saturated NH₄Cl_(aq) (10 mL) was added and the solution was then allowed to warm to rt over 30 min and the two layers were separated. The aqueous layer was extracted with Et₂O (3 x 10 mL) and the combined organics were dried (MgSO₄), filtered and evaporated under reduced pressure to give the crude product. Analysis of the crude product by ¹H NMR spectroscopy indicated no *N*-Boc pyrrolidine **9** starting material was present.

For *N*-Boc pyrrolidine **9**, a peak at 1700 cm^{-1} was observed and assigned to $\nu_{\text{C=O}}$. After addition of *s*-BuLi, a new peak at 1674 cm^{-1} was observed which was assigned to $\nu_{\text{C=O}}$ in the prelithiation complex. A new peak at 1659 cm^{-1} was also observed and this was assigned to the lithiated intermediate. After a lithiation time of 11 h, complete lithiation of *N*-Boc pyrrolidine **9** to give the lithiated intermediate was observed. When PhCHO was added (after a 16.5 h total lithiation time), the signal for the lithiated intermediate ($\nu_{\text{C=O}} = 1659\text{ cm}^{-1}$) disappeared after 1 min, indicating complete trapping had occurred.

Lab Book Reference: AMI_132

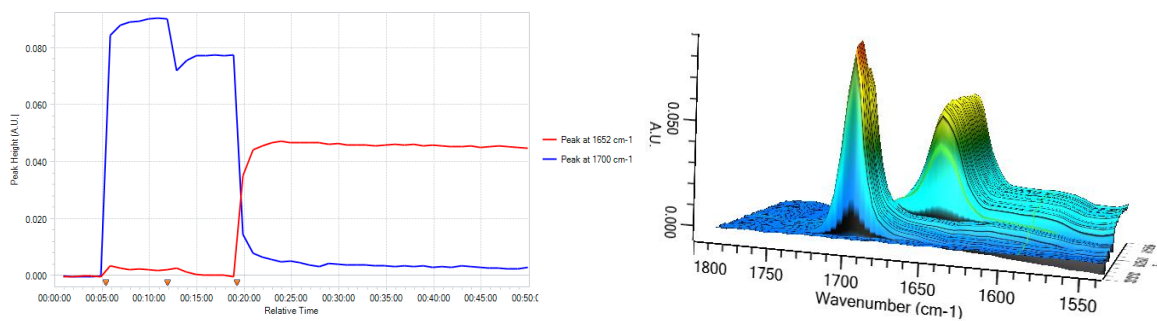
tert*-Butyl 4-chloropiperidine-1-carboxylate **48*



A solution of hexachloroethane (7.25 g, 30.62 mmol, 2.0 eq.) in CH₂Cl₂ (25 mL) was added to a stirred solution of *N*-Boc 4-hydroxy piperidine **223** (3.05 g, 15.31 mmol, 1.0 eq.) and PPh₃ (8.03 g, 30.62 mmol, 2.0 eq.) in CH₂Cl₂ (75 mL) at rt under Ar. The resulting solution was stirred at rt for 16 h. The solvent was evaporated under reduced pressure to give the crude product. Purification by flash column chromatography on silica using 80:20 hexane-Et₂O gave 4-chloro *N*-Boc piperidine **48** (1.27 g, 38%) as a colourless oil, *R*_F (80:20 hexane-Et₂O) 0.26; ¹H NMR (400 MHz, CDCl₃) δ 4.20 (tt, *J* = 7.5, 3.5 Hz, 1H, CHCl), 3.70 (ddd, *J* = 13.0, 7.0, 3.5 Hz, 2H, NCH), 3.30 (ddd, *J* = 13.0, 7.5, 3.5 Hz, 2H, NCH), 2.02 (dddd, *J* = 13.5, 7.0, 3.5, 3.5 Hz, 2H, CH), 1.79 (dddd, *J* = 13.5, 7.5, 7.5, 3.5 Hz, 2H, CH), 1.46 (s, 9H, CMe₃); ¹³C NMR (100.6 MHz, CDCl₃) δ 154.8 (C=O), 79.9 (CMe₃), 57.1 (CHCl), 41.3 (br, NCH₂), 35.0 (CH₂), 28.6 (CMe₃). Spectroscopic data consistent with those reported in the literature.⁴⁴

Lab Book Reference: AMI_152

ReactIR™ spectroscopic monitoring of the lithiation of 4-chloro *N*-Boc piperidine **48 using *s*-BuLi/di-pyrrolidino ethane **177****



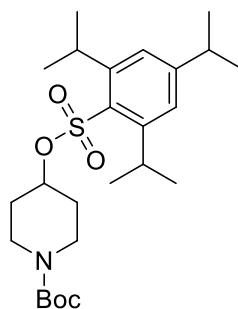
Et₂O (10 mL) was added to a flask equipped with a stirrer bar and ReactIR™ probe (ReactIR™ 15, DiComp) at rt under Ar. After cooling to -78 °C, a solution of solution of 4-chloro *N*-Boc piperidine **48** (215 mg, 0.98 mmol, 1.0 eq.) in Et₂O (2 mL) was added followed

by a solution of di-pyrrolidino ethane **177** (429 mg, 2.55 mmol, 2.6 eq.) in Et₂O (2 mL). The solution was stirred for 5 min (to verify the stability of readout on ReactIR™). Then *s*-BuLi (2.0 mL of a 1.3 M solution in hexanes, 2.55 mmol, 2.6 eq.) was added. The resulting solution was stirred at -78 °C for 30 min.

For 4-chloro *N*-Boc piperidine **48**, a peak at 1700 cm⁻¹ was observed and assigned to ν_{C=O}. After addition of *s*-BuLi, a new peak at 1652 cm⁻¹ was observed which was assigned to ν_{C=O} in the lithiated intermediate. After a lithiation time of 5 min, complete lithiation of 4-chloro *N*-Boc piperidine **48** to give the lithiated intermediate was observed.

Lab Book Reference: AMI_154

tert*-Butyl 4-{[2,4,6-tris(propan-2-yl)benzenesulfonyl]oxy}piperidine-1-carboxylate **167*



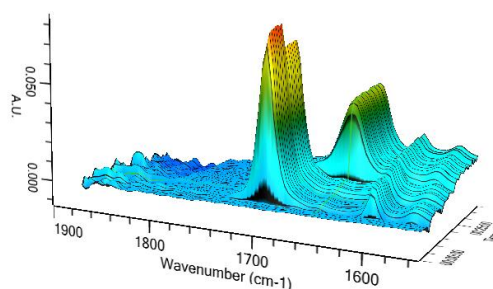
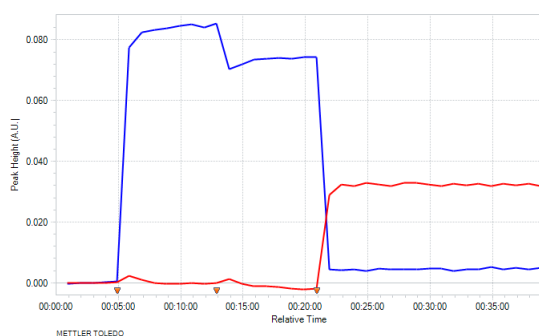
167

Trisopropylsulfonyl chloride (5.95 g, 19.66 mmol, 1.3 eq.) was added portionwise to a stirred solution of *N*-Boc 4-hydroxy piperidine **223** (3.04 g, 15.12 mmol, 1.0 eq.), Et₃N (1.68 g, 16.63 mmol, 1.1 eq., 2.32 mL) and DMAP (18 mg, 0.15 mmol, 0.01 eq.) in CH₂Cl₂ (50 mL) at 0 °C under Ar. The resulting solution was allowed to warm to rt and stirred at rt for 16 h. Then, H₂O (20 mL) was added and the two layers were separated. The organic layer was washed with 1 M HCl_(aq) (20 mL), dried (Na₂SO₄), filtered and evaporated under reduced pressure to give the crude product. Purification by flash column chromatography using 80:20 hexane-EtOAc gave 4-*O*-trisyl *N*-Boc piperidine **167** (696 mg, 10%) as a white solid, mp 70-74 °C; *R*_F (80:20 hexane-EtOAc) 0.19; IR (ATR) 2961, 2865, 1694 (C=O), 1425, 1344, 1240, 1178, 1014, 952, 830, 668, 565 cm⁻¹; ¹H NMR (400 MHz, CDCl₃) δ 7.17 (s, 2H, Ar), 4.83 (tt, *J* = 7.5, 3.5 Hz, 1H, CHOSO₂Ar), 4.15 (sept, *J* = 7.0 Hz, 2H, CHMe₂), 3.69-3.63 (m, 2H, NCH), 3.25 (ddd, *J* = 13.5, 8.0, 4.0 Hz, 2H, NCH), 2.91 (sept, *J* = 7.0 Hz, 1H, CHMe₂), 1.90-1.83 (m, 2H, NCH), 1.78-1.70 (m, 2H, CH), 1.44 (s, 9H, CMe₃), 1.26 (d, *J* = 7.0 Hz, 12H, CHMe₂), 1.26 (d, *J* = 7.0 Hz, 6H, CHMe₂); ¹³C NMR (100.6 MHz, CDCl₃) δ

154.7 (C=O), 153.8 (*ipso*-Ar), 150.5 (*ipso*-Ar), 130.8 (*ipso*-Ar), 123.9 (Ar), 80.0 (CMe₃), 77.0 (CHOSO₂Ar), 34.4 (CHMe₂), 31.7 (br, NCH₂), 29.7 (br, CH₂), 29.7 (CHMe₂), 28.5 (CMe₃), 24.8 (CHMe₂), 23.7 (CHMe₂); HRMS (ESI) *m/z* calcd for C₂₅H₄₁NO₅S (M + Na)⁺ 490.2598, found 490.2575 (+4.2 ppm error).

Lab Book Reference: AMI_151

ReactIR™ spectroscopic monitoring of the lithiation of 4-*O*-trisyl *N*-Boc piperidine **167** using *s*-BuLi/di-pyrrolidino ethane **177**

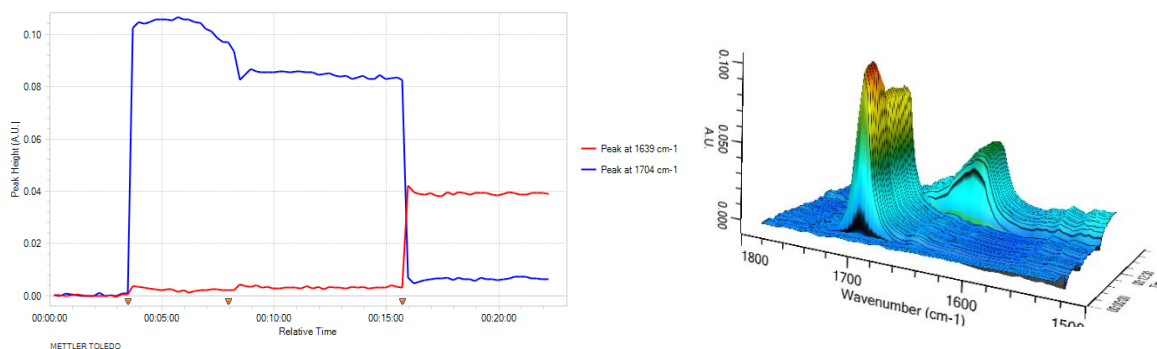


Et₂O (10 mL) was added to a flask equipped with a stirrer bar and ReactIR™ probe (ReactIR™ 15, DiComp) at rt under Ar. After cooling to -78 °C, a solution of 4-*O*-trisyl *N*-Boc piperidine **167** (489 mg, 1.04 mmol, 1.0 eq.) in Et₂O (2 mL) was added followed by a solution of di-pyrrolidino ethane **177** (457 mg, 2.72 mmol, 2.6 eq.) in Et₂O (2 mL). The solution was stirred for 5 min (to verify the stability of readout on ReactIR™). Then *s*-BuLi (2.1 mL of a 1.3 M solution in hexanes, 2.72 mmol, 2.6 eq.) was added. The resulting solution was stirred at -78 °C for 15 min.

For 4-*O*-trisyl *N*-Boc piperidine **167**, a peak at 1700 cm⁻¹ was observed and assigned to $\nu_{\text{C=O}}$. After addition of *s*-BuLi, a new peak at 1648 cm⁻¹ was observed which was assigned to $\nu_{\text{C=O}}$ in the lithiated intermediate. After a lithiation time of 2 min, complete lithiation of 4-*O*-trisyl *N*-Boc piperidine **167** to give the lithiated intermediate was observed.

Lab Book Reference: AMI_155

ReactIR™ spectroscopic monitoring of the lithiation of *N*-Boc morpholine **169** using *s*-BuLi/di-pyrrolidino ethane **177**

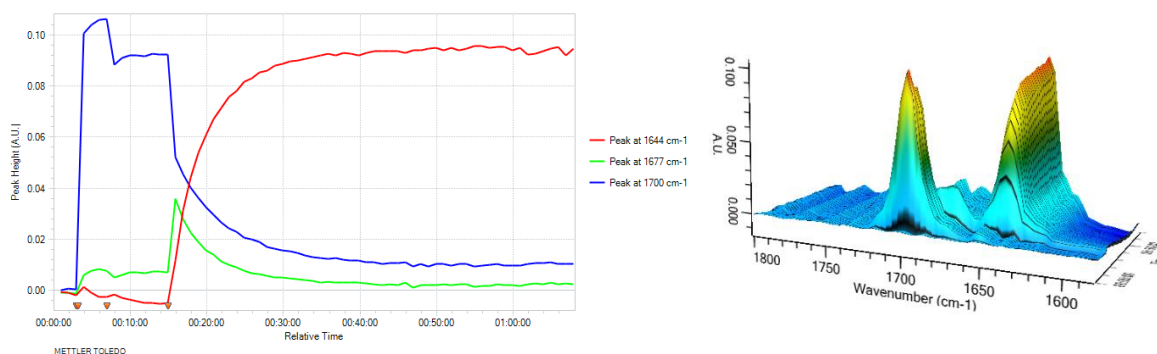


Et₂O (10 mL) was added to a flask equipped with a stirrer bar and ReactIR™ probe (ReactIR™ 15, DiComp) at rt under Ar. After cooling to -78 °C, a solution of *N*-Boc morpholine **169** (187 mg, 1.00 mmol, 1.0 eq.) in Et₂O (2 mL) was added followed by a solution of di-pyrrolidino ethane **177** (436 mg, 2.60 mmol, 2.6 eq.) in Et₂O (2 mL). The solution was stirred for 5 min (to verify the stability of readout on ReactIR™). Then *s*-BuLi (2.0 mL of a 1.3 M solution in hexanes, 2.6 mmol, 2.6 eq.) was added. The resulting solution was stirred at -78 °C for 8 min.

For *N*-Boc morpholine **169**, a peak at 1704 cm^{-1} was observed and assigned to $\nu_{\text{C=O}}$. After addition of *s*-BuLi, a new peak at 1639 cm^{-1} was observed which was assigned to $\nu_{\text{C=O}}$ in the lithiated intermediate. After a lithiation time of 15 s, complete lithiation of *N*-Boc morpholine **169** to give the lithiated intermediate was observed.

Lab Book Reference: AMI_160

ReactIR™ spectroscopic monitoring of the lithiation of *N*'-Me *N*-Boc piperazine **58** using *s*-BuLi/di-pyrrolidino ethane **177**



Et₂O (10 mL) was added to a flask equipped with a stirrer bar and ReactIR™ probe (ReactIR™ 15, DiComp) at rt under Ar. After cooling to -78 °C, a solution of *N*'-Me *N*-Boc piperazine **58** (205 mg, 1.02 mmol, 1.0 eq.) in Et₂O (2 mL) was added followed by a solution of di-pyrrolidino ethane **177** (223 mg, 1.33 mmol, 1.3 eq.) in Et₂O (2 mL). The solution was stirred for 5 min (to verify the stability of readout on ReactIR™). Then *s*-BuLi (1.0 mL of a 1.3 M solution in hexanes, 1.3 mmol, 1.3 eq.) was added. The resulting solution was stirred at -78 °C for 50 min.

For *N*'-Me *N*-Boc piperazine **58**, a peak at 1700 cm⁻¹ was observed and assigned to $\nu_{C=O}$. After addition of *s*-BuLi, a new peak at 1677 cm⁻¹ was observed which was assigned to $\nu_{C=O}$ in the prelithiation complex. A new peak at 1644 cm⁻¹ was also observed and this was assigned to the lithiated intermediate. After a lithiation time of 35 min, complete lithiation of *N*-Boc *N*'-Me *N*-Boc piperazine **58** to give the lithiated intermediate was observed.

Lab Book Reference: AMI_161

6.5 Experimental Procedures for Chapter 3

6.5.1 General Computational Procedures

All computational MP2 and DFT calculations were performed using GAUSSIAN 09.¹¹² Both MP2 calculations and DFT calculations were used with a Pople 6-31G(d) split valence basis set. MP2 calculations were performed with calculation of the Hessian matrix for each iteration of the geometry optimisation (GAUSSIAN keyword = CalcAll) due to the flat nature of the potential energy surface. All DFT calculations used a pruned (99, 950) grid for numerical integrations, GAUSSIAN keyword = Int(UltraFine). All geometry optimisations used the deprecated GDIIS algorithm which assisted in the location of minima.

All ground states were confirmed by the absence of imaginary frequencies and transition states were confirmed by the presence of one imaginary frequency. The vibrational modes of the imaginary frequencies obtained for transition states were inspected to ensure the mode corresponded to the α -lithiation of the substrate. The XYZ coordinates of all optimised geometries are included (as .xyz files) in the electronic supplementary information included with this thesis. Frequency calculations were performed after geometry optimisation at the same level of theory; enthalpies (H) and free-energies (G) were corrected to a temperature of 195 K (-78 °C), the temperature at which these reactions were conducted.

For optimisation of the prelithiation complexes the following parameters were used:

Opt(GDIIS, Tight) Temperature=195 Freq Int=UltraFine *–only for DFT*

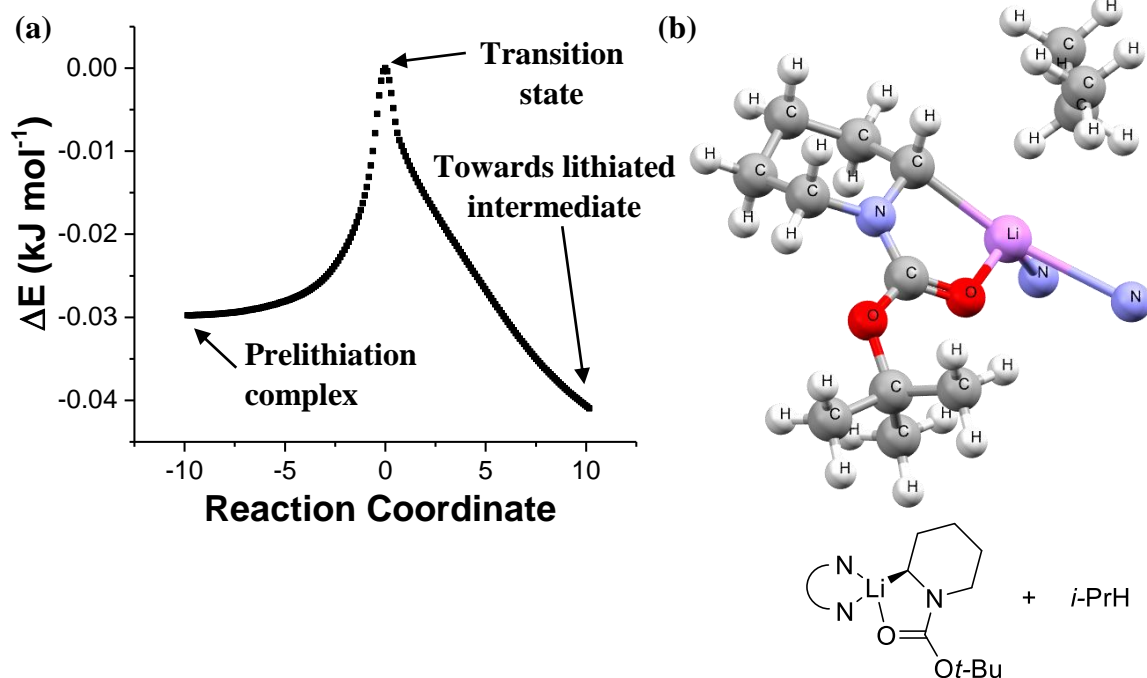
For optimisation of the transition states the following parameters were used:

Opt(TS, GDIIS, CalcFC, NoEigen, Tight) Temperature=195 Freq Int=UltraFine *– only for DFT*

6.5.2 *N*-Boc piperidine IRC calculation results:

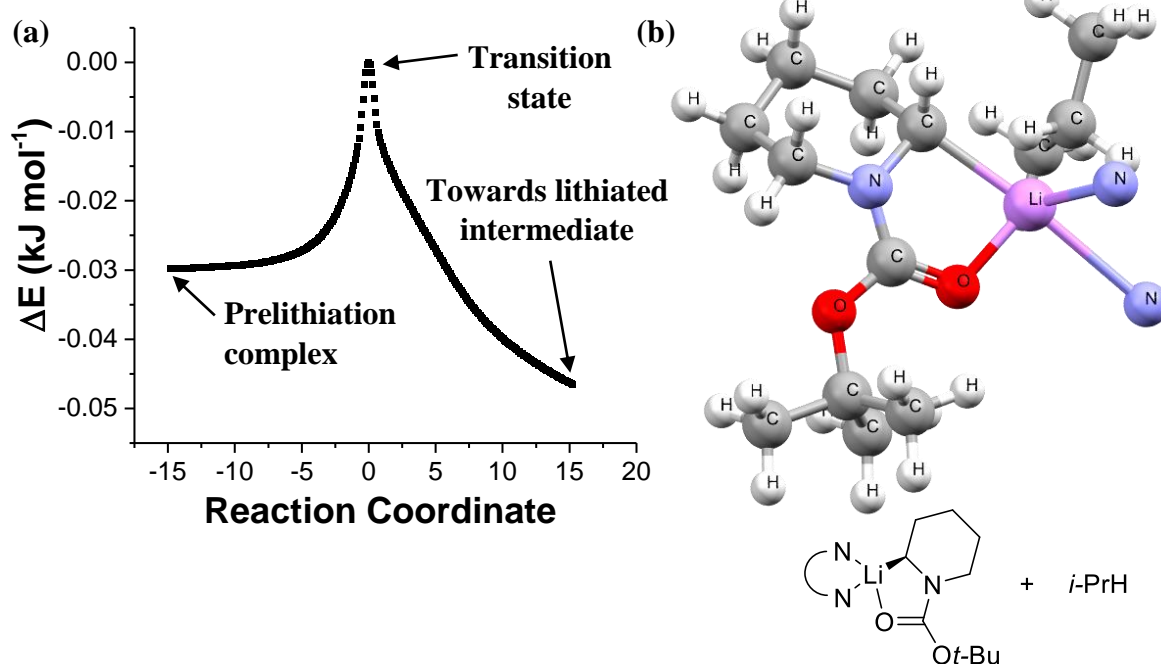
N-Boc piperidine **10** ‘side-on’ lithiation:

B3LYP/6-31G(d) calculated reaction coordinate for the *i*-PrLi/di-methyl bispidine **195** ‘side-on’ lithiation of *N*-Boc piperidine **10** (a) and an output geometry from the forward path showing formation of the lithiated intermediate and *i*-propane (b).



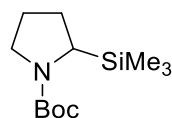
N-Boc piperidine **10** ‘top’ lithiation:

B3LYP/6-31G(d) calculated reaction coordinate for the *i*-PrLi/di-methyl bispidine **195** ‘top’ lithiation of *N*-Boc piperidine **10** (a) and an output geometry from the forward path showing formation of the lithiated intermediate and *i*-propane (b).

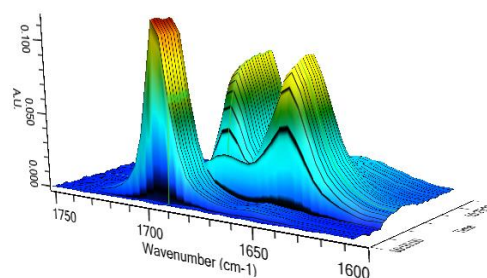
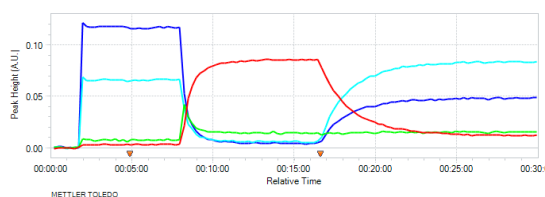


6.6 Experimental Procedures for Chapter 4

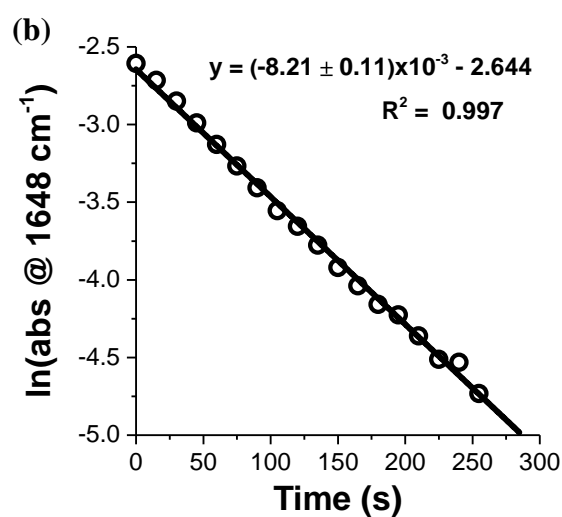
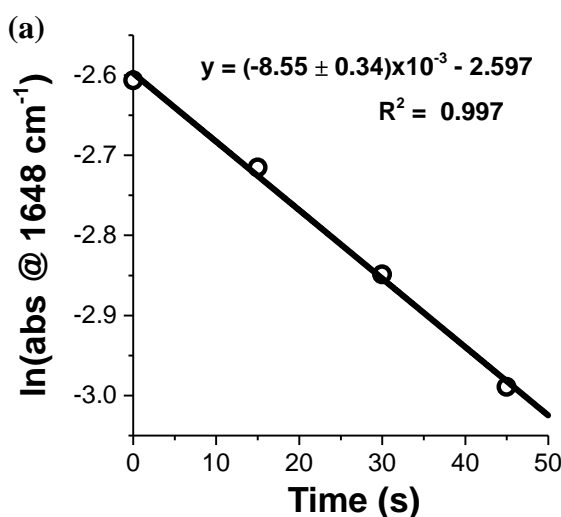
tert-Butyl 2-(trimethylsilyl)pyrrolidine-1-carboxylate **11**



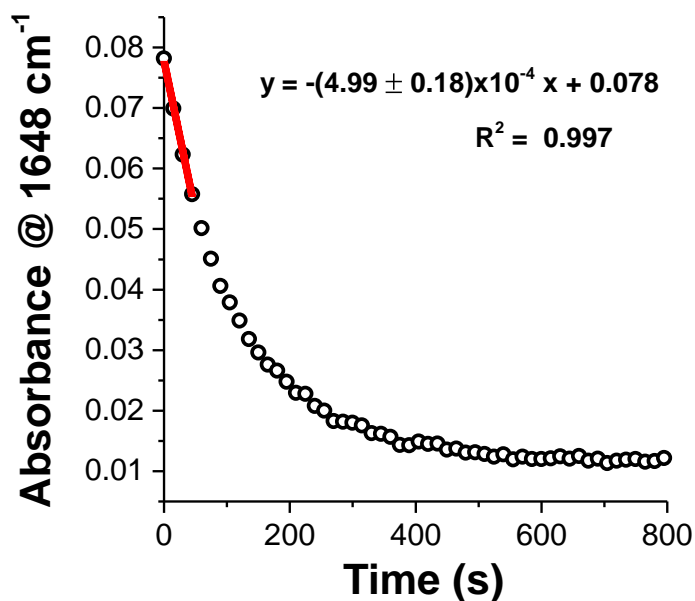
11



For experimental procedure for the lithiation-trapping of *N*-Boc pyrrolidine **9** with Me_3SiCl , see Chapter 6.3. Kinetic analysis of the Me_3SiCl trapping of 2-lithio *N*-Boc pyrrolidine **9** indicated that trapping was pseudo first order with respect to 2-lithio *N*-Boc pyrrolidine **9**. Semilogarithmic plots for both 90% conversion (a) and the first 20% of conversion (b) of the trapping reaction indicated that pseudo-first order conditions were maintained throughout the reaction. A pseudo-first order k_{obs} of $(8.55 \pm 0.34) \times 10^{-3} \text{ s}^{-1}$ and $t_{1/2} = (81.1 \pm 3.2) \text{ s}$ were measured for the trapping reaction using the semilogarithmic plot for 20% conversion.

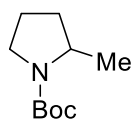


Initial rate analysis of the Me_3SiCl trapping of lithiated *N*-Boc pyrrolidine **9** provided an initial rate of trapping, $\text{rate}_{\text{init}} = (4.99 \pm 0.18) \times 10^{-4} \text{ s}^{-1}$ (initial rate tangent is displayed on the plot in red).

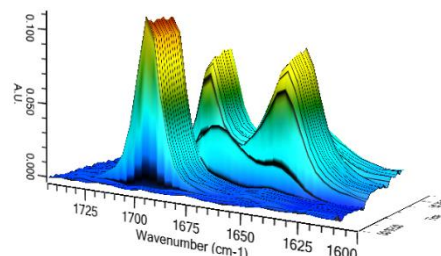
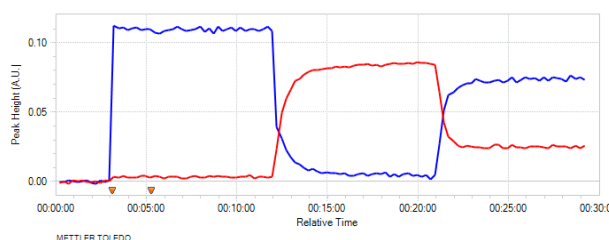


Lab Book Reference: AMI_168

tert-Butyl 2-methylpyrrolidine-1-carboxylate **14**



14

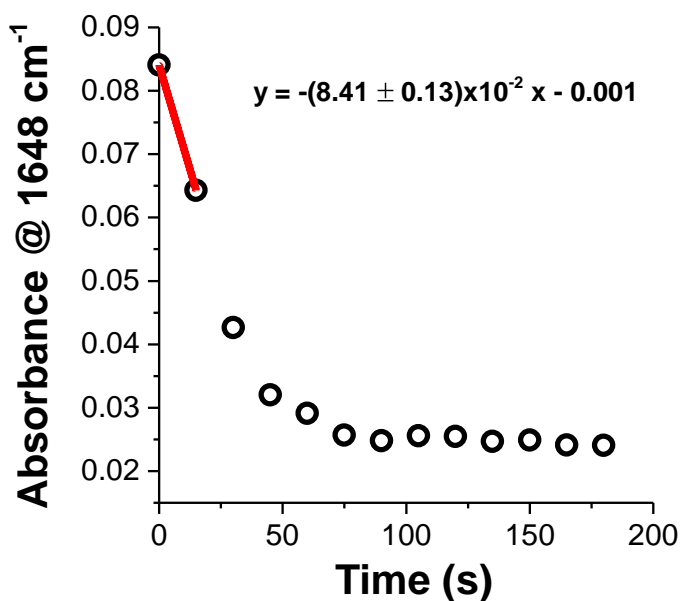


Et₂O (14 mL) was added to a flask equipped with a stirrer bar and ReactIR™ probe (ReactIR™ 15, DiComp) at rt under Ar. After cooling to -78 °C, *N*-Boc pyrrolidine **9** (171 mg, 1.00 mmol, 0.18 mL, 1.0 eq.) was added followed by TMEDA (151 mg, 0.19 mL, 1.30 mmol, 1.3 eq.). The solution was stirred for 5 min (to verify the stability of readout on ReactIR™). Then *s*-BuLi (1.0 mL of a 1.3 M solution in hexanes, 1.30 mmol, 1.3 eq.) was added. The resulting solution was stirred at -78 °C for 10 min. Then, Me₂SO₄ (252 mg, 0.19 mL, 2.00 mmol, 2.0 eq.) was added and the solution was stirred at -78 °C for a further 5 min. Saturated NH₄Cl_(aq) (10 mL) was added and the solution was then allowed to warm to rt over 30 min and the two layers were separated. The aqueous layer was extracted with Et₂O (3 x

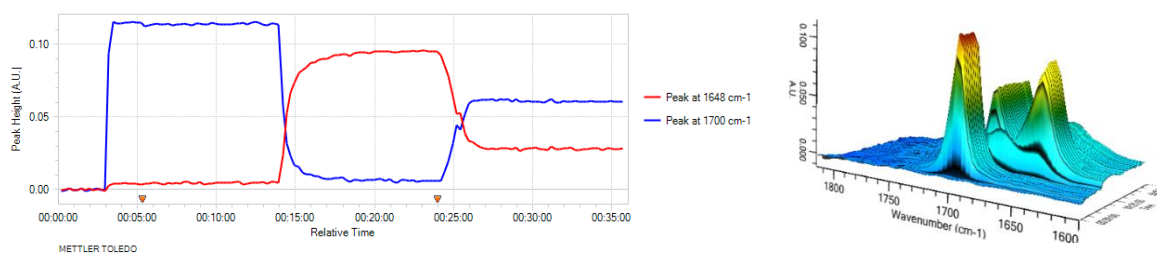
10 mL) and the combined organics were dried (MgSO_4), filtered and evaporated under reduced pressure to give the crude product. Purification by flash column chromatography on silica using 90:10 Hexane-EtOAc as eluent gave 2-methyl *N*-Boc pyrrolidine **14** (122 mg, 66%) as a colourless oil, R_F (90:10 Hexane-EtOAc) 0.23; ^1H NMR (400 MHz, CDCl_3) δ 3.98-3.78 (m, 1H, NCH), 3.44-3.22 (m, 2H, NCH), 2.05-1.92 (m, 1H, CH), 1.92-1.82 (m, 1H, CH), 1.82-1.71 (m, 1H, CH), 1.61-1.49 (m, 1H, CH), 1.46 (s, 9H, CMe_3), 1.21-1.09 (m, 3H, NCHMe); ^{13}C NMR (100.6 MHz, CDCl_3) (mixture of rotamers) δ 154.6 (C=O), 78.9 (CMe_3), 52.9 (NCH), 46.5 (NCH₂), 46.2 (NCH₂), 33.4 (CH₂), 32.7 (CH₂), 28.7 (CMe_3), 23.7 (CH₂), 23.1 (CH₂), 20.9 (NCH₂Me), 20.3 (NCH₂Me). Spectroscopic data consistent with those reported in the literature.⁴⁰

For *N*-Boc pyrrolidine **9**, a peak at 1701 cm^{-1} was observed and assigned to $\nu_{\text{C=O}}$. After addition of *s*-BuLi, a new peak at 1648 cm^{-1} was observed which was assigned to the lithiated intermediate. After a lithiation time of 4 min, complete lithiation of *N*-Boc pyrrolidine **9** to give the lithiated intermediate was observed. When Me_2SO_4 was added (after a 9 min total lithiation time), the signal for the lithiated intermediate ($\nu_{\text{C=O}} = 1641\text{ cm}^{-1}$) disappeared after 1 min, indicating complete trapping had occurred.

Initial rate analysis of the Me_2SO_4 trapping of lithiated *N*-Boc pyrrolidine **9** provided an initial rate of trapping, $\text{rate}_{\text{init}} = (8.41 \pm 0.13) \times 10^{-2}\text{ s}^{-1}$ (initial rate tangent is displayed on the plot in red).



Lab Book Reference: AMI_177

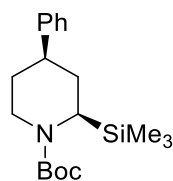


Et₂O (14 mL) was added to a flask equipped with a stirrer bar and ReactIR™ probe (ReactIR™ 15, DiComp) at rt under Ar. After cooling to $-78\text{ }^{\circ}\text{C}$, *N*-Boc pyrrolidine **9** (171 mg, 1.00 mmol, 0.18 mL, 1.0 eq.) was added followed by TMEDA (151 mg, 0.19 mL, 1.30 mmol, 1.3 eq.). The solution was stirred for 5 min (to verify the stability of readout on ReactIR™). Then *s*-BuLi (1.0 mL of a 1.3 M solution in hexanes, 1.30 mmol, 1.3 eq.) was added. The resulting solution was stirred at $-78\text{ }^{\circ}\text{C}$ for 10 min. Then, MeI (283 mg, 0.13 mL, 2.00 mmol, 2.0 eq.) was added, the solution rapidly gelled and the stirring ceased, the gel was held at $-78\text{ }^{\circ}\text{C}$ for a further 10 min. Saturated NH₄Cl_(aq) (10 mL) was added and the solution was then allowed to warm to rt over 30 min and the two layers were separated. The aqueous layer was extracted with Et₂O (3 x 10 mL) and the combined organics were dried (MgSO₄), filtered and evaporated under reduced pressure to give the crude product. Purification by flash column chromatography on silica using 90:10 Hexane-EtOAc as eluent gave 2-methyl *N*-Boc pyrrolidine **14** (75 mg, 40%) as a colourless oil.

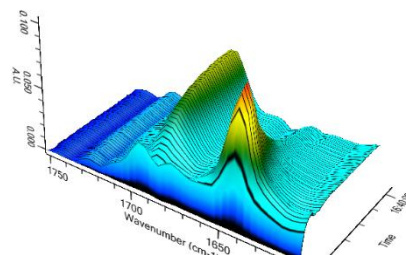
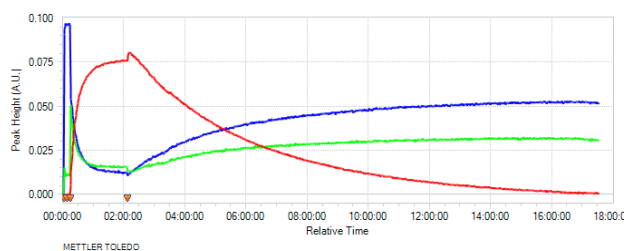
For *N*-Boc pyrrolidine **9**, a peak at 1700 cm^{-1} was observed and assigned to $\nu_{\text{C=O}}$. After addition of *s*-BuLi, a new peak at 1648 cm^{-1} was observed which was assigned to the lithiated intermediate. After a lithiation time of 4 min, complete lithiation of *N*-Boc pyrrolidine **9** to give the lithiated intermediate was observed. When Me₂SO₄ was added (after 10 min total lithiation time), the signal for the lithiated intermediate ($\nu_{\text{C=O}} = 1648\text{ cm}^{-1}$) disappeared after 3 min, indicating complete trapping had occurred.

Lab Book Reference: AMI_174

***tert*-Butyl (2*R**, 4*R**)-4-phenyl-2-(trimethylsilyl)piperidine-1-carboxylate *cis*-238**



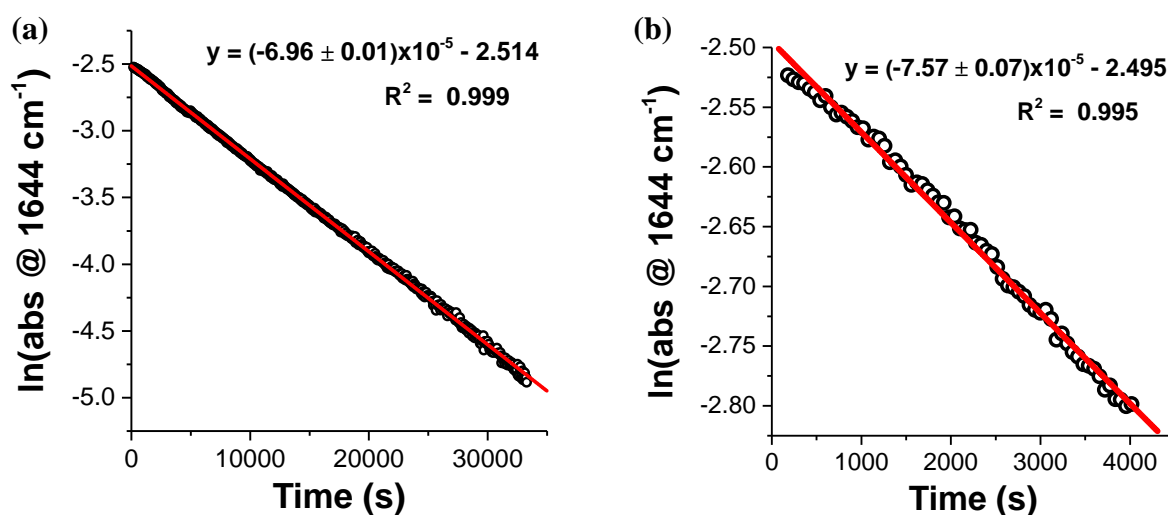
***cis*-238**



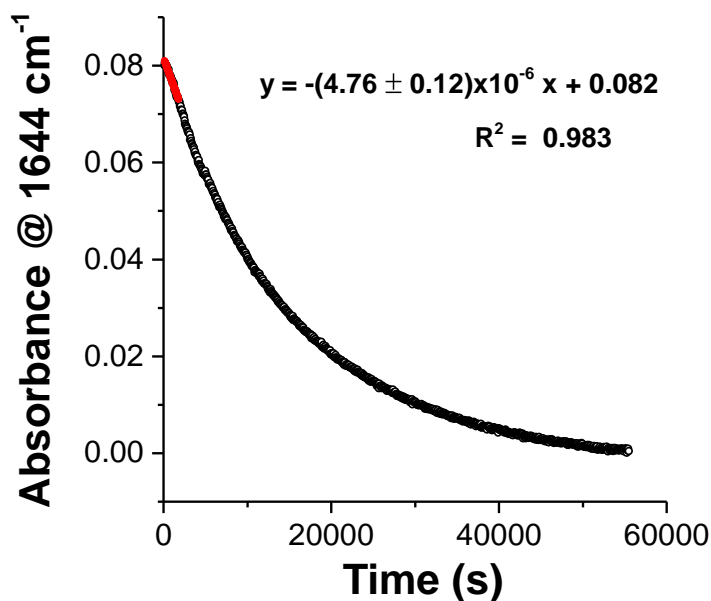
Et₂O (12 mL) was added to a flask equipped with a stirrer bar and ReactIR™ probe (ReactIR™ 15, DiComp) at rt under Ar. After cooling to -78 °C, a solution of 4-Phenyl *N*-Boc piperidine **32** (264 mg, 1.01 mmol, 0.18, 1.0 eq.) in Et₂O (2 mL) was added followed by TMEDA (153 mg, 0.20 mL, 1.31 mmol, 1.3 eq.). The solution was stirred for 5 min (to verify the stability of readout on ReactIR™). Then *s*-BuLi (1.0 mL of a 1.3 M solution in hexanes, 1.30 mmol, 1.3 eq.) was added. The resulting solution was stirred at -78 °C for 2 h. Then, Me₃SiCl (219 mg, 0.26 mL, 2.02 mmol, 2.0 eq.) was added and the solution was stirred at -78 °C for a further 16 h. Saturated NH₄Cl_(aq) was added and the solution was then allowed to warm to rt over 30 min and the two layers were separated. The aqueous layer was extracted with Et₂O (3 x 10 mL) and the combined organics were dried (MgSO₄), filtered and evaporated under reduced pressure to give the crude product. Purification by flash column chromatography on silica using 97.5:2.5 Hexane-Et₂O as eluent gave 2-silyl *N*-Boc piperidine *cis*-**238** (247 mg, 73%) as a colourless oil, *R*_F (97.5:2.5 Hexane-Et₂O) 0.25; ¹H NMR (400 MHz, CDCl₃) δ 7.36-7.29 (m, 2H, Ph), 7.25-7.19 (m, 3H, Ph), 4.12 (br d, *J* = 13.0 Hz, 1H, NCH), 2.97 (br t, *J* = 12.0 Hz, 1H, NCH), 2.76-2.68 (tt, 1H, *J* = 12.0, 4.0 Hz, 1H, CHPh), 2.43 (br d, *J* = 12.0 Hz, 1H, NCH), 1.88-1.76 (m, 2H, CH), 1.68-1.51 (m, 2H, CH), 1.48 (s, 9H, CMe₃), 0.09 (s, 9H, SiMe₃); ¹³C NMR (100.6 MHz, CDCl₃) δ 155.3 (C=O), 146.4 (*ipso*-Ph), 128.6 (Ph), 127.0 (Ph), 126.4 (Ph), 79.2 (CMe₃), 51.2 (NCH), 48.1 (NCH₂), 45.0 (CHPh), 34.4 (CH₂), 33.7 (CH₂), 28.6 (CMe₃), -0.6 (SiMe₃). Spectroscopic data consistent with those reported in the literature.³⁶

For 4-phenyl *N*-Boc piperidine **32**, a peak at 1697 cm⁻¹ was observed and assigned to $\nu_{\text{C=O}}$. After addition of *s*-BuLi, a new peak at 1644 cm⁻¹ was observed which was assigned to the lithiated intermediate. After a lithiation time of 90 min, complete lithiation of 4-phenyl *N*-Boc piperidine **32** to give the lithiated intermediate was observed. When Me₃SiCl was added (after 2 h total lithiation time), the signal for the lithiated intermediate ($\nu_{\text{C=O}} = 1644$ cm⁻¹) disappeared after 15.5 h, indicating complete trapping had occurred.

Kinetic analysis of the Me₃SiCl trapping of 2-lithio 4-phenyl *N*-Boc piperidine **32** indicated that trapping was pseudo first order with respect to 2-lithio 4-phenyl *N*-Boc piperidine **32**. Semilogarithmic plots for both 90% conversion (a) and the first 20% of conversion (b) of the trapping reaction indicated that pseudo-first order conditions were maintained throughout the reaction. A pseudo-first order k_{obs} of $(7.57 \pm 0.07) \times 10^{-5}$ s⁻¹ and $t_{1/2} = (9160 \pm 80)$ s were measured using the semilogarithmic plot for 90% conversion of the trapping reaction.

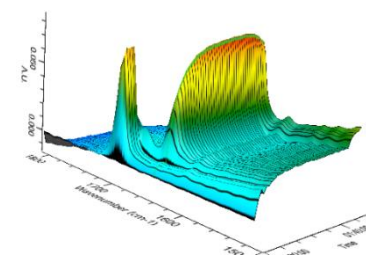
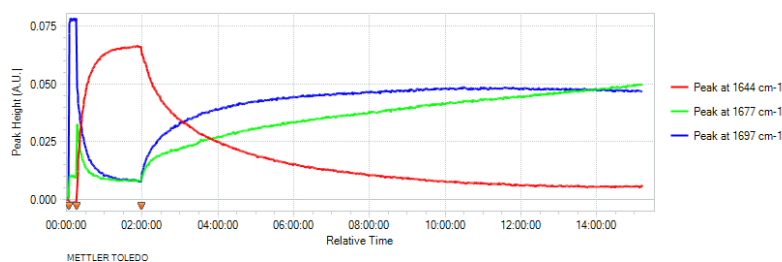
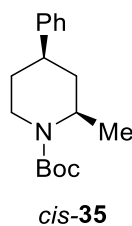


Initial rate analysis of the Me₃SiCl trapping of lithiated 4-phenyl *N*-Boc piperidine **32** provided an initial rate of trapping, $\text{rate}_{\text{init}} = (4.76 \pm 0.12) \times 10^{-6}$ s⁻¹ (initial rate tangent is displayed on the plot in red).



Lab Book Reference: AMI_192

***tert*-Butyl (2*R**, 4*R**)-2-methyl-4-phenylpiperidine-1-carboxylate *cis*-35**

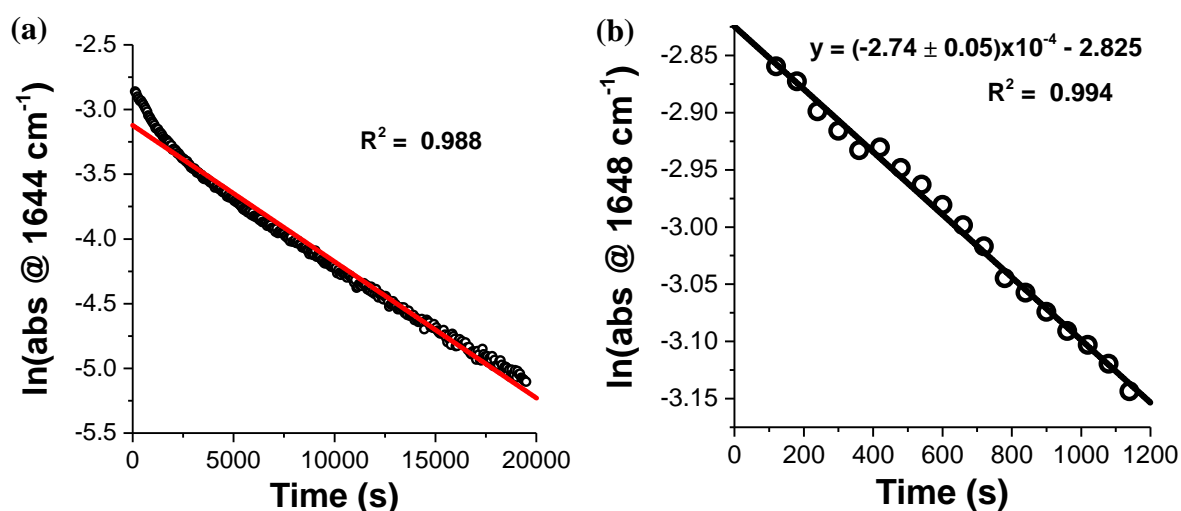


Et₂O (12 mL) was added to a flask equipped with a stirrer bar and ReactIR™ probe (ReactIR™ 15, DiComp) at rt under Ar. After cooling to −78 °C, a solution of 4-Phenyl *N*-Boc piperidine **32** (264 mg, 1.01 mmol, 1.0 eq.) in Et₂O (2 mL) was added followed by TMEDA (152 mg, 0.20 mL, 1.31 mmol, 1.3 eq.). The solution was stirred for 5 min (to verify the stability of readout on ReactIR™). Then *s*-BuLi (1.0 mL of a 1.3 M solution in hexanes, 1.30 mmol, 1.3 eq.) was added. The resulting solution was stirred at −78 °C for 2 h. Then, Me₂SO₄ (254 mg, 0.19 mL, 2.02 mmol, 2.0 eq.) was added and the solution was stirred at −78 °C for a further 16 h. Saturated NH₄Cl_(aq) was added and the solution was then allowed

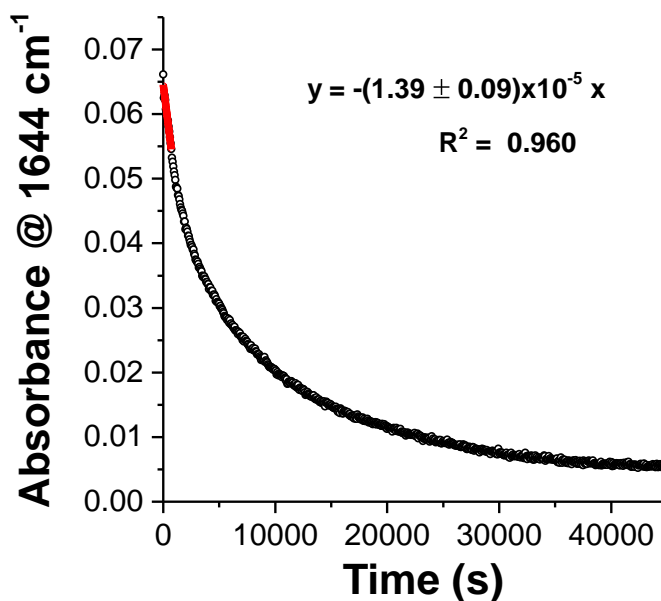
to warm to rt over 30 min and the two layers were separated. The aqueous layer was extracted with Et₂O (3 x 10 mL) and the combined organics were dried (MgSO₄), filtered and evaporated under reduced pressure to give the crude product. Purification by flash column chromatography on silica using 95:5 Hexane-EtOAc as eluent gave 2-methyl *N*-Boc piperidine *cis*-**35** (175 mg, 63%) as a colourless oil. For spectroscopic data see section 6.4.

For 4-phenyl *N*-Boc piperidine **32**, a peak at 1697 cm⁻¹ was observed and assigned to $\nu_{C=O}$. After addition of *s*-BuLi, a new peak at 1644 cm⁻¹ was observed which was assigned to the lithiated intermediate. After a lithiation time of 90 min, complete lithiation of 4-phenyl *N*-Boc piperidine **32** to give the lithiated intermediate was observed. When Me₂SO₄ was added (after 2 h total lithiation time), the signal for the lithiated intermediate ($\nu_{C=O} = 1641$ cm⁻¹) disappeared after 12 h, indicating complete trapping had occurred.

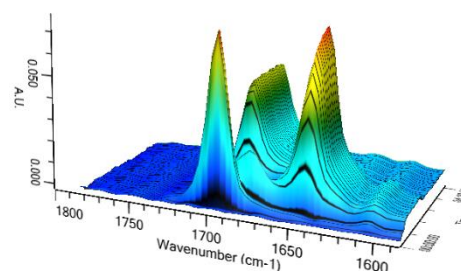
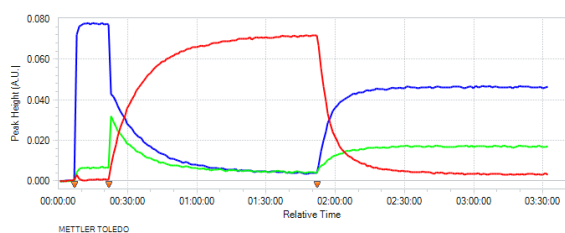
Kinetic analysis of the Me₂SO₄ trapping of 2-lithio 4-phenyl *N*-Boc piperidine **32** indicated that trapping was pseudo first order with respect to 2-lithio 4-phenyl *N*-Boc piperidine **32**. A semilogarithmic plot for 90% conversion of the trapping (a) indicated that pseudo-first order conditions were not maintained throughout the reaction, with deviation from pseudo-first order kinetics occurring at ~2500 s. However, the semilogarithmic plot for the first 20% of conversion indicated that pseudo-first order behaviour was observed in this portion of the reaction. Therefore, a pseudo-first order k_{obs} of $(2.74 \pm 0.05) \times 10^{-4}$ s⁻¹ and $t_{1/2} = (2530 \pm 50)$ s were measured using the semilogarithmic plot for 20% conversion of the trapping reaction.



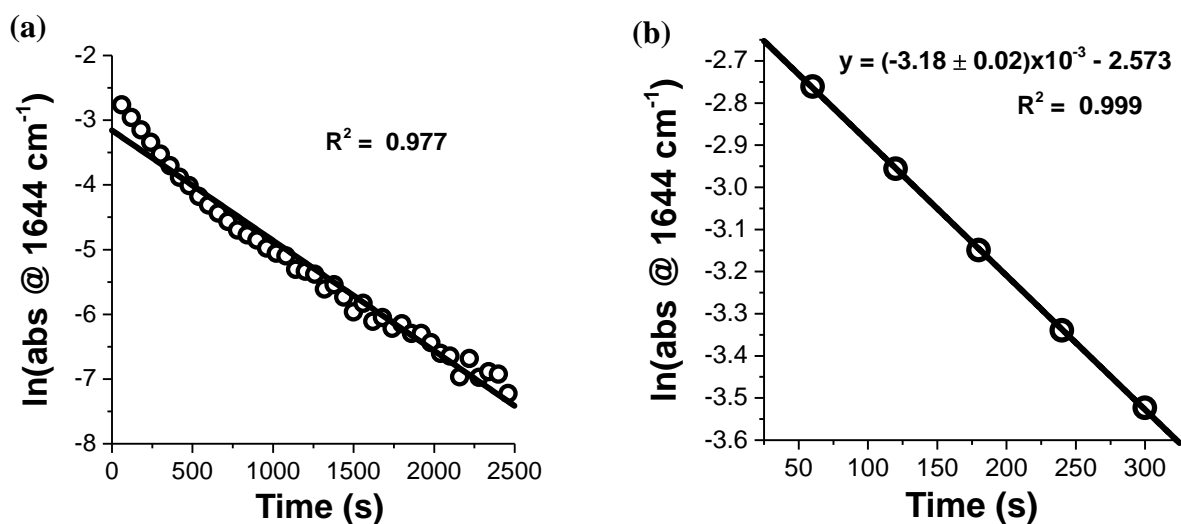
Initial rate analysis of the Me₂SO₄ trapping of lithiated 4-phenyl *N*-Boc piperidine **32** provided an initial rate of trapping, $\text{rate}_{\text{init}} = (1.39 \pm 0.09) \times 10^{-5}$ s⁻¹ (initial rate tangent is displayed on the plot in red).



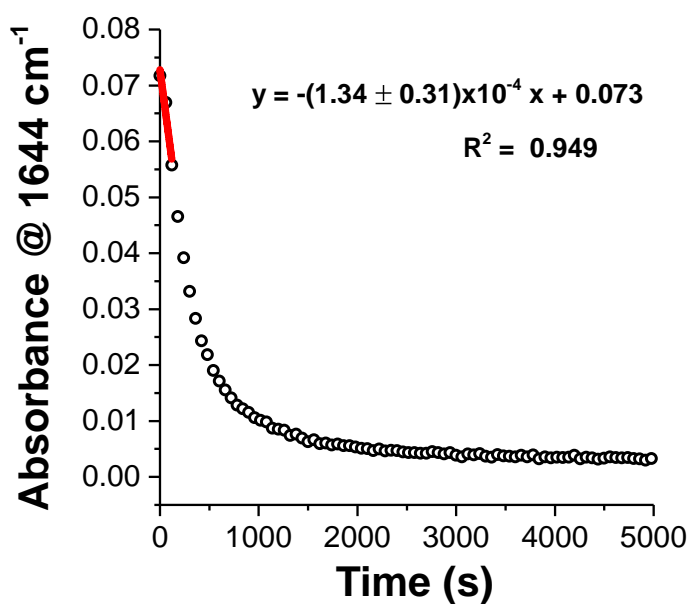
Lab Book Reference: AMI_190



For experimental procedure for the lithiation-trapping of 4-Phenyl *N*-Boc piperidine **32** with MeI, see Chapter 6.3. Kinetic analysis of the MeI trapping of 2-lithio 4-Phenyl *N*-Boc piperidine **32** indicated that trapping was pseudo first order with respect to of 2-lithio 4-Phenyl *N*-Boc piperidine **32**. A semilogarithmic plot for 90% conversion of the trapping (a) indicated that pseudo-first order conditions were not maintained throughout the reaction with deviation from pseudo-first order kinetics occurring at ~ 500 s. However, the semilogarithmic plot for the first 50% of conversion indicated that pseudo-first order behaviour was observed in this portion of the reaction. 55% trapping conversion was used rather than 20% due to the faster rate of reaction and lesser amount of data collected with ReactIRTM. A pseudo-first order k_{obs} of $(3.18 \pm 0.02) \times 10^{-3} \text{ s}^{-1}$ and $t_{1/2} = (218 \pm 1) \text{ s}$ were measured for the trapping reaction using the semilogarithmic plot for 55% conversion of the trapping reaction.

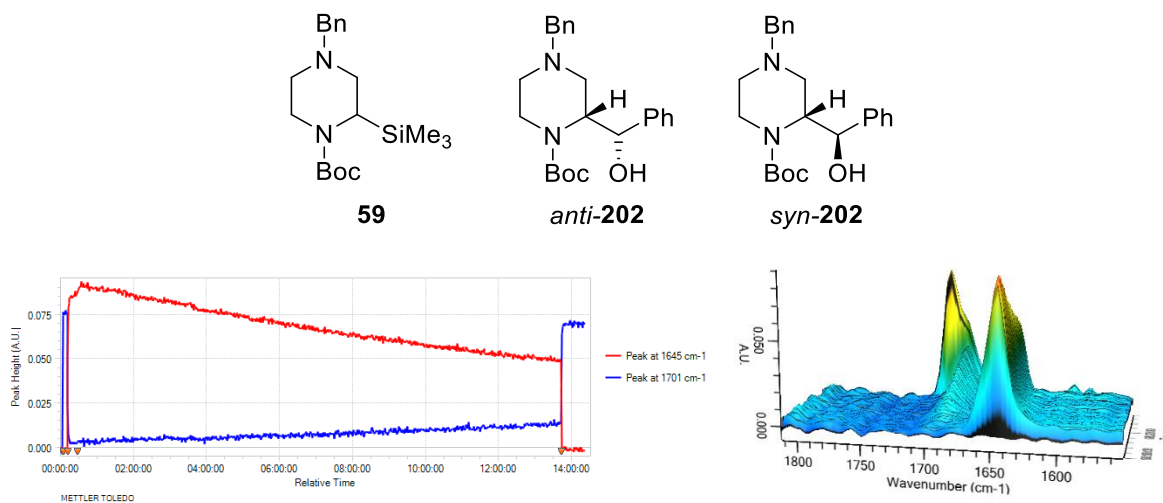


Initial rate analysis of the MeI trapping of lithiated 4-phenyl *N*-Boc piperidine **32** provided an initial rate of trapping, $\text{rate}_{\text{init}} = (1.34 \pm 0.31) \times 10^{-4} \text{ s}^{-1}$ (initial rate tangent is displayed on the plot in red).



Lab Book Reference: AMI_189

tert*-Butyl 4-benzyl-2-(trimethylsilyl)piperazine-1-carboxylate **59** and *tert*-butyl (2*R**)-4-benzyl-2-[(*S**) and (*R**)-hydroxy(phenyl)methyl]piperazine-1-carboxylate *anti*-**202** and *syn*-**202*



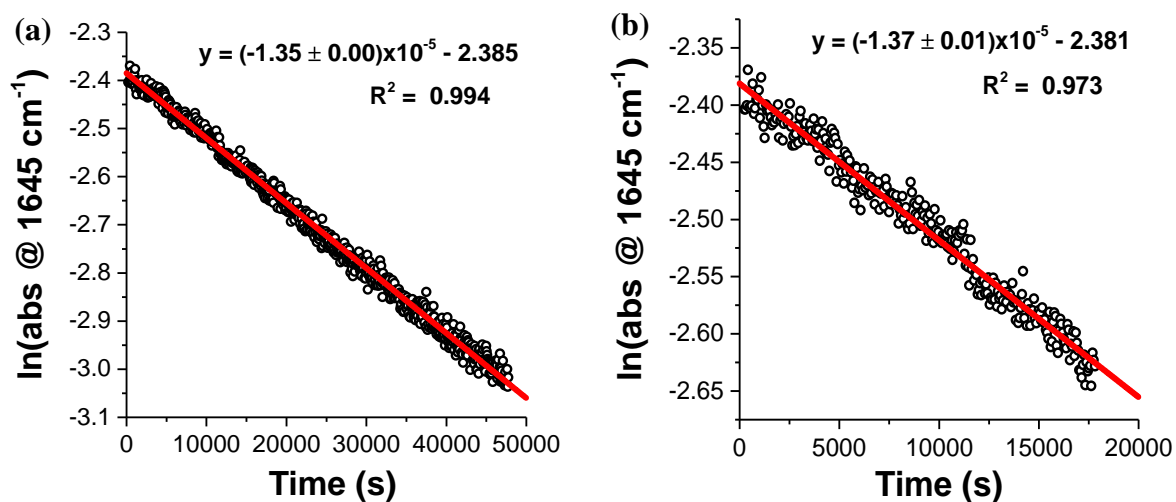
Et₂O (12 mL) was added to a flask equipped with a stirrer bar and ReactIR™ probe (ReactIR™ 15, DiComp) at rt under Ar. After cooling to -78 °C, a solution of *N*'-Bn *N*-Boc piperazine **57** (275 mg, 1.00 mmol, 1.0 eq.) in Et₂O (2 mL) was added followed by TMEDA (150 mg, 0.19 mL, 1.30 mmol, 1.3 eq.). The solution was stirred for 5 min (to verify the stability of readout on ReactIR®). Then *s*-BuLi (1.0 mL of a 1.3 M solution in hexanes, 1.30 mmol, 1.3 eq.) was added. The resulting solution was stirred at -78 °C for 15 min. Then, Me₃SiCl (216 mg, 0.25 mL, 2.00 mmol, 2.0 eq.) was added and the solution was stirred at -78 °C for a further 13 h. Then, PhCHO (211 mg, 0.20 mL, 2.00 mmol, 2.0 eq.) was added and the solution was stirred at -78 °C for an additional 30 min. Saturated NH₄Cl_(aq) (10 mL) was added and the solution was then allowed to warm to rt over 30 min and the two layers were separated. The aqueous layer was extracted with Et₂O (3 x 10 mL) and the combined organics were dried (MgSO₄), filtered and evaporated under reduced pressure to give the crude product. Purification by flash column chromatography on silica using 90:10 hexane-Et₂O as eluent gave 2-silyl *N*'-Bn *N*-Boc piperazine **59** (140 mg, 40%) as a colourless oil, *R*_F(50:50 hexane-Et₂O) 0.6, ¹H NMR (400 MHz, CDCl₃) (60:40 mixture of rotamers) δ 7.35-7.29 (m, 4H, Ph), 7.28-7.22 (m, 1H, Ph), 4.03 (br s, 0.6H, NCH), 3.79 (br s, 0.4H, NCH), 3.67-3.50 (m, 1H, NCH), 3.43 (d, *J* = 13.0 Hz, CH_AH_BPh), 3.40 (d, *J* = 13.0 Hz, CH_AH_BPh), 3.13-2.85 (m, 1H, NCH), 2.79 (d, *J* = 11.5 Hz, 1H, NCH), 2.76-2.57 (m, 1H, NCH), 2.24 (br s, 1H, NCH), 1.92 (td, *J* = 11.5, 3.2 Hz, 1H, NCH), 1.44 (s, 9H, CMe₃), 0.07 (s, 9H, SiMe₃); ¹³C NMR (100.6 MHz, CDCl₃) (rotamers) δ 154.6 (C=O), 138.4 (*ipso*-Ph), 129.2 (Ph), 128.0

(Ph), 127.2 (Ph), 79.1 (CMe₃), 63.5 (NCH₂), 54.3 (NCH₂), 53.1 (NCH₂), 45.2 (NCH), 41.5 (NCH), 28.5 (CMe₃), -0.7 (SiMe₃) and *anti*-**202** (99 mg, 26%) as a yellow solid, *R*_F (50:50 hexane-Et₂O) 0.3; mp 99-102 °C; IR (ATR) 3203 (OH), 2970, 2781, 1659 (C=O), 1428, 1387, 1346, 1301, 1196, 1150 cm⁻¹; ¹H NMR (400 MHz, CDCl₃) δ 7.43-7.36 (m, 3H, Ph), 7.28-7.21 (m, 2H, Ph), 7.21-6.97 (m, 5H, Ph), 6.33 (br s, 1H, CHOH), 5.05 (br s, 1H, CHOH), 4.13-4.01 (m, 1H, NCH), 3.98-3.86 (m, 1H, NCH), 3.62 (d, *J* = 12.0 Hz, 1H, CH_AH_BPh), 3.26 (d, *J* = 12.0 Hz, H, CH_AH_BPh), 3.10-2.94 (m, 1H, NCH), 2.96 (d, *J* = 12.0 Hz, 1H, CH_AH_BPh), 2.34-2.17 (m, 1H, NCH), 1.99 (dd, *J* = 12.0, 3.5 Hz, 1H, NCH), 1.71-1.57 (m, 1H, NCH), 1.50 (s, 9H, CMe₃); ¹³C NMR (100.6 MHz, CDCl₃) (rotamers) δ 155.1 (C=O), 143.3 (*ipso*-Ph), 136.5 (*ipso*-Ph), 129.6 (Ph), 128.7 (Ph), 128.1 (Ph), 127.7 (Ph), 126.6 (Ph), 126.4 (Ph), 125.4 (Ph), 80.4 (CMe₃), 80.2 (CMe₃), 79.1 (CHOH), 63.2 (NCH₂Ph), 55.7 (NCH), 54.5 (NCH), 52.9 (NCH₂), 50.3 (NCH₂), 42.2 (NCH₂), 41.0 (NCH₂), 28.5 (CMe₃); HRMS (ESI) *m/z* calcd for C₂₃H₃₀N₂O₃ (M + H)⁺ 383.2329, found 383.2338 (-2.6 ppm error) and *syn*-**202** (61 mg, 16%) as a white solid, *R*_F (50:50 hexane-Et₂O) 0.2; mp 120-123 °C; IR (ATR) 3155 (OH), 2965, 1654 (C=O), 1434, 1388, 1347, 1277, 1231, 1195, 1152 cm⁻¹; ¹H NMR (400 MHz, CDCl₃) (50:50 mixture of rotamers) δ 7.39-7.15 (m, 10H, Ph), 5.99 (br s, 0.5H, OH), 5.27 (br s, 0.5H, OH), 5.17-5.04 (m, 1H, CHOH), 4.34-4.27 (m, 0.5 H, NCH), 4.17-4.10 (m, 1H, NCH), 3.88 (br d, *J* = 13.0 Hz, 0.5 H, NCH), 3.67-3.41 (m, 3H, NCH + CH₂Ph), 3.12 (d, *J* = 11.5 Hz, 0.5 H, NCH), 2.97-2.80 (m, 1.5 H, NCH), 2.43 (dd, *J* = 11.5, 4.0 Hz, 0.5 H, NCH), 2.31-2.26 (m, 0.5H, NCH), 2.19-2.05 (m, 1H, NCH), 1.29 (s, 4.5 H, CMe₃), 1.08 (s, 4.5 H, CMe₃); ¹³C NMR (100.6 MHz, CDCl₃) (rotamers) δ 154.5 (C=O), 141.5 (*ipso*-Ph), 137.2 (*ipso*-Ph), 136.6 (*ipso*-Ph), 129.1 (Ph), 128.7 (Ph), 128.6 (Ph), 128.3 (Ph), 128.1 (Ph), 127.7 (Ph), 127.5 (Ph), 127.2 (Ph), 126.7 (Ph), 80.0 (CMe₃), 79.6 (CHOH), 63.2 (NCH₂Ph), 56.3 (NCH₂), 54.9 (NCH), 54.5 (NCH), 52.7 (NCH₂), 52.4 (NCH₂), 41.8 (NCH₂), 41.0 (NCH₂), 28.1 (CMe₃), 27.9 (CMe₃); HRMS (ESI) *m/z* calcd for C₂₃H₃₀N₂O₃ (M + H)⁺ 383.2329, found 383.2336 (-2.1 ppm error). Spectroscopic data for 2-silyl *N'*-Bn *N*-Boc piperazine **59** is consistent with those reported in the literature.²⁵ The relative stereochemistry of *syn*-**202** has been determined by X-ray crystallography conducted previously in-group.⁵³

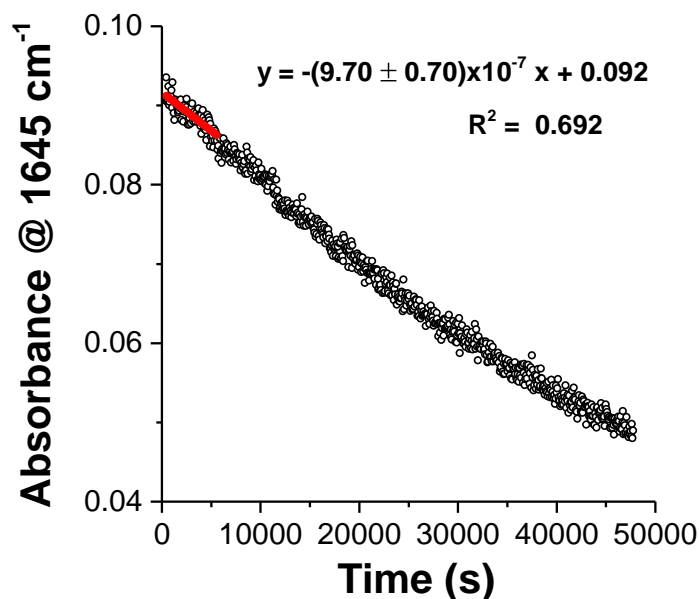
For *N'*-Bn *N*-Boc piperazine **57**, a peak at 1701 cm⁻¹ was observed and assigned to $\nu_{C=O}$. After addition of *s*-BuLi, a new peak at 1645 cm⁻¹ was observed which was assigned to the lithiated intermediate. After a lithiation time of 2 min, complete lithiation of *N'*-Bn *N*-Boc piperazine **57** to give the lithiated intermediate was observed. When Me₃SiCl was added

(after 15 min total lithiation time), the signal for the lithiated intermediate ($\nu_{C=O} = 1645 \text{ cm}^{-1}$) began to disappear and when PhCHO was added 13 h after the previous addition of Me_3SiCl the signal for the lithiated intermediate disappeared after 1 min, indicating complete trapping had occurred.

Kinetic analysis of the Me_3SiCl trapping of 2-lithio N' -Bn N -Boc piperazine **57** indicated that trapping was pseudo first order with respect to 2-lithio N' -Bn N -Boc piperazine **57**. Semilogarithmic plots for both ~46% conversion (a) and the first 20% of conversion (b) of the trapping reaction indicated that pseudo-first order conditions were maintained throughout the reaction. A pseudo-first order k_{obs} of $(1.37 \pm 0.01) \times 10^{-5} \text{ s}^{-1}$ and $t_{1/2} = (51300 \pm 400) \text{ s}$ were measured using the semilogarithmic plot for up to 20% conversion of the trapping reaction.

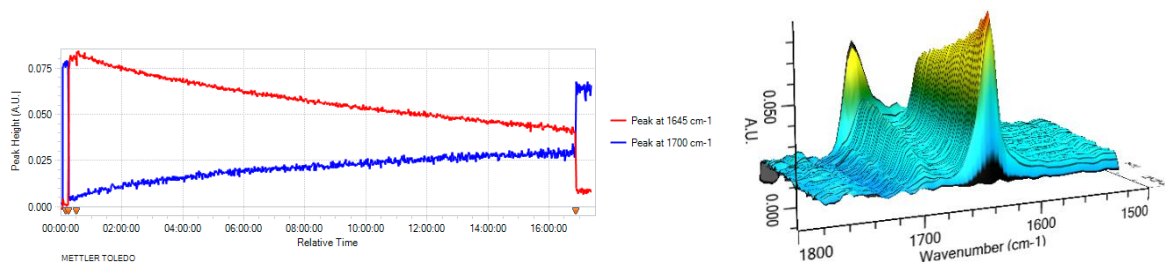
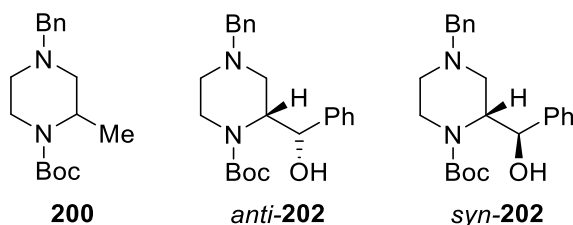


Initial rate analysis of the Me_3SiCl trapping of lithiated N' -Bn N -Boc piperazine **57** provided an initial rate of trapping, $\text{rate}_{\text{init}} = (9.70 \pm 0.70) \times 10^{-7} \text{ s}^{-1}$ (initial rate tangent is displayed on the plot in red).



Lab Book Reference: AMI_251

tert*-Butyl 4-benzyl-2-methylpiperazine-1-carboxylate **200** and *tert*-butyl (2*R**)-4-benzyl-2-[(*S**) and (*R**)-hydroxy(phenyl)methyl]piperazine-1-carboxylate *anti*-**202** and *syn*-**202*



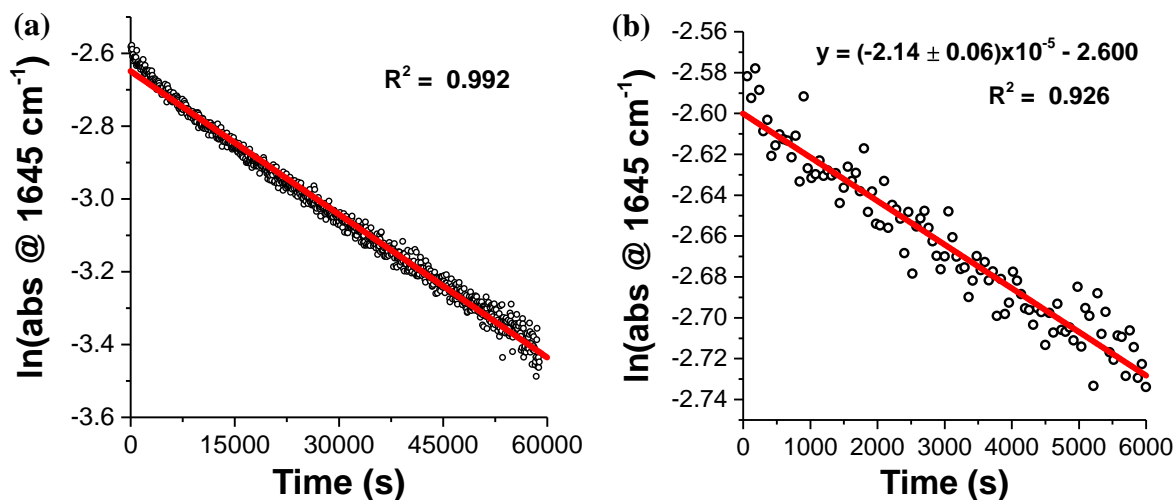
Et₂O (12 mL) was added to a flask equipped with a stirrer bar and ReactIR probe (ReactIR 15, DiComp) at rt under Ar. After cooling to -78 °C, a solution of *N*'-Bn *N*-Boc piperazine **57** (271 mg, 0.98 mmol, 1.0 eq.) in Et₂O (2 mL) was added followed by TMEDA (148 mg, 0.19 mL, 1.28 mmol, 1.3 eq.). The solution was stirred for 5 min (to verify the stability of readout on ReactIR®). Then *s*-BuLi (1.0 mL of a 1.3 M solution in hexanes, 1.28 mmol, 1.3 eq.) was added. The resulting solution was stirred at -78 °C for 15 min. Then, Me₂SO₄ (247 mg, 0.19 mL, 1.96 mmol, 2.0 eq.) was added and the

solution was stirred at $-78\text{ }^{\circ}\text{C}$ for a further 16.5 h. Then, PhCHO (208 mg, 0.20 mL, 1.96 mmol, 2.0 eq.) was added and the solution was stirred at $-78\text{ }^{\circ}\text{C}$ for an additional 30 min. Saturated $\text{NH}_4\text{Cl}_{(\text{aq})}$ (10 mL) was added and the solution was then allowed to warm to rt over 30 min and the two layers were separated. The aqueous layer was extracted with Et_2O (3 x 10 mL) and the combined organics were dried (MgSO_4), filtered and evaporated under reduced pressure to give the crude product. Purification by flash column chromatography on silica using 90:10 hexane-EtOAc as eluent gave 2-methyl *N'*-Bn piperazine **200** (100 mg, 35%) as a colourless oil, R_F (60:40 hexane:EtOAc) 0.4, ^1H NMR (400 MHz, CDCl_3) δ 7.33-7.26 (m, 4H, Ph), 7.24-7.18 (m, 1H, Ph), 4.15 (br s, 1H, NCH), 3.77 (br d, $J = 13.0$ Hz, 1H, NCH), 3.50 (d, $J = 13.5$ Hz, 1H, $\text{CH}_A\text{H}_B\text{Ph}$), 3.37 (d, $J = 13.5$ Hz, 1H, $\text{CH}_A\text{H}_B\text{Ph}$), 3.08 (td, $J = 12.5, 3.5$ Hz, 1H, NCH), 2.74-2.71 (m, 1H, NCH), 2.56 (dt, $J = 11.0, 1.5$ Hz, 1H, NCH), 2.09 (dd, $J = 11.0, 4.0$ Hz, 1H, NCH), (ddd, $J = 12.0, 11.5, 3.5$, 1H, NCH), 1.43 (s, 9H, CMe_3), 1.21 (d, $J = 7.0$ Hz, 3H, CHMe); ^{13}C NMR (100.6 MHz, CDCl_3) δ 154.9 (C=O), 138.5 (*ipso*-Ph), 128.8 (Ph), 128.3 (Ph), 127.1 (Ph), 79.4 (CMe_3), 62.9 (NCH_2), 57.5 (NCH_2), 53.3 (NCH_2), 47.2 (NCH), 39.2 (NCH_2), 28.6 (CMe_3), 16.0 (Me) and alcohol *anti*-**202** (68 mg, 18%) as a white solid and alcohol *syn*-**202** (45 mg, 12%) as white solid. Spectroscopic data for 2-methyl *N'*-Bn piperazine **200** consistent with those reported in the literature.¹⁵⁴

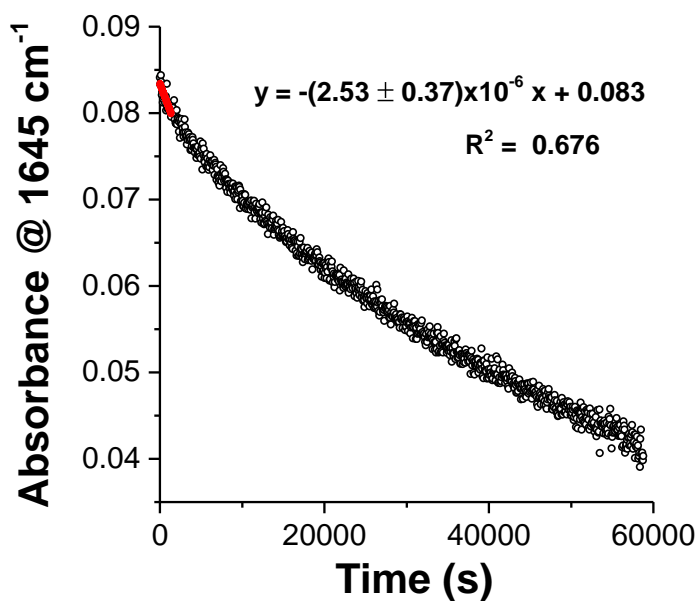
For *N'*-Bn *N*-Boc piperazine **57**, a peak at 1700 cm^{-1} was observed and assigned to $\nu_{\text{C=O}}$. After addition of *s*-BuLi, a new peak at 1645 cm^{-1} was observed which was assigned to the lithiated intermediate. After a lithiation time of 4 min, complete lithiation of *N'*-Bn *N*-Boc piperazine **57** to give the lithiated intermediate was observed. When Me_2SO_4 was added (after 15 min total lithiation time), the signal for the lithiated intermediate ($\nu_{\text{C=O}} = 1645\text{ cm}^{-1}$) began to disappear and when PhCHO was added 16.5 h after the previous addition of Me_2SO_4 the signal for the lithiated intermediate disappeared after 1 min, indicating complete trapping had occurred.

Kinetic analysis of the Me_2SO_4 trapping of 2-lithio *N'*-Bn *N*-Boc piperazine **57** indicated that trapping was pseudo first order with respect to 2-lithio *N'*-Bn *N*-Boc piperazine **57**. A semilogarithmic plot for 90% conversion of the trapping (a) indicated that pseudo-first order conditions were not maintained throughout the reaction, with deviation from pseudo-first order kinetics occurring at ~ 6000 s. However, the semilogarithmic plot for the first 20% of conversion indicated that pseudo-first order behaviour was observed in this portion of the

reaction. Therefore, a pseudo-first order k_{obs} of $(2.14 \pm 0.06) \times 10^{-5} \text{ s}^{-1}$ and $t_{1/2} = (32400 \pm 900)$ s were measured using the semilogarithmic plot for 20% conversion of the trapping reaction.

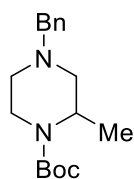


Initial rate analysis of the Me_2SO_4 trapping of lithiated N^2 -Bn N -Boc piperazine **57** provided an initial rate of trapping, $\text{rate}_{\text{init}} = (2.53 \pm 0.37) \times 10^{-6} \text{ s}^{-1}$ (initial rate tangent is displayed on the plot in red).

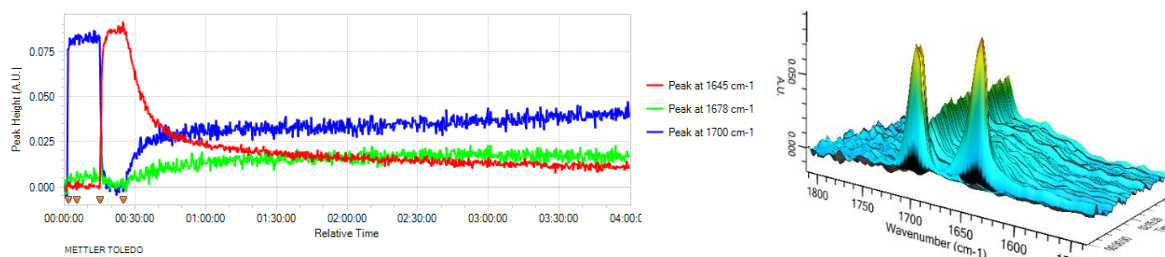


Lab Book Reference: AMI_246

tert-Butyl 4-benzyl-2-methylpiperazine-1-carboxylate **200**



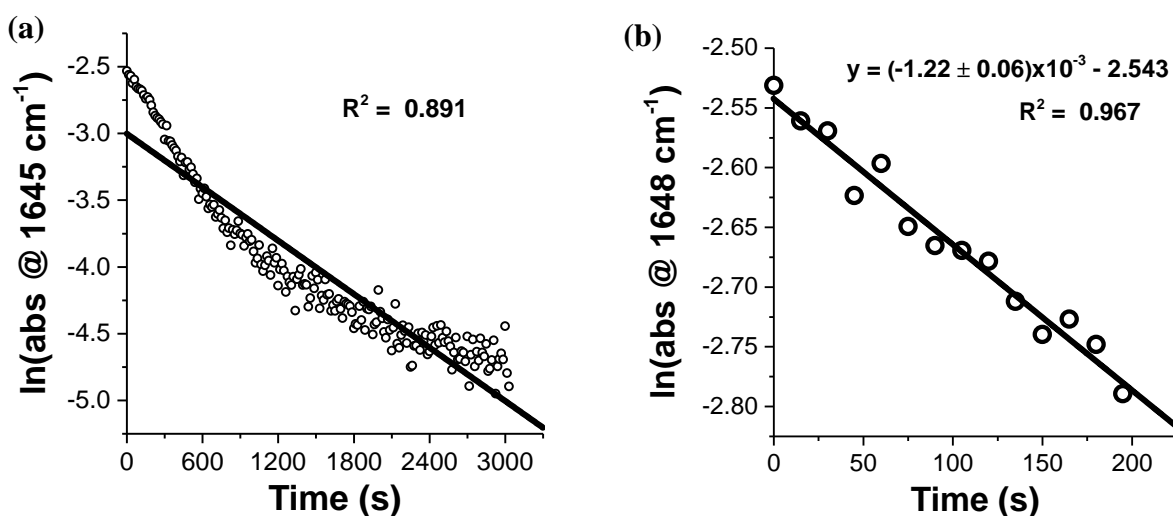
200



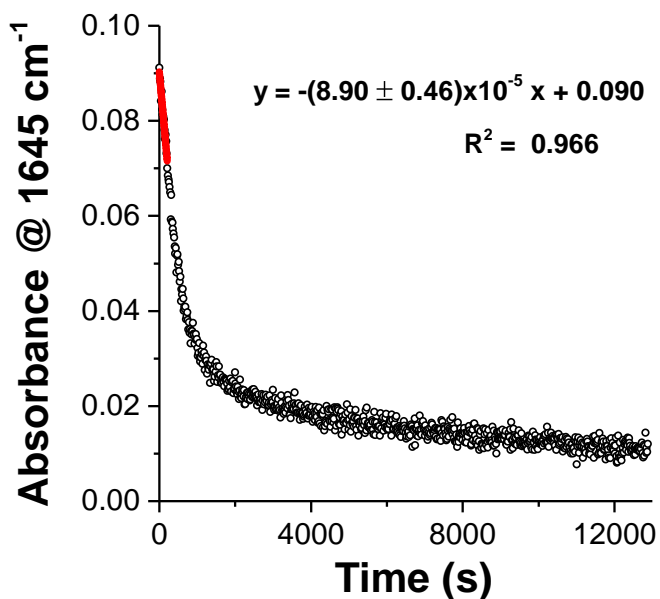
Et₂O (12 mL) was added to a flask equipped with a stirrer bar and ReactIRTM probe (ReactIRTM 15, DiComp) at rt under Ar. After cooling to -78 °C, a solution of *N'*-Bn *N*-Boc piperazine **57** (276 mg, 1.00 mmol, 1.0 eq.) in Et₂O (2 mL) was added followed by TMEDA (151 mg, 0.19 mL, 1.30 mmol, 1.3 eq.). The solution was stirred for 5 min (to verify the stability of readout on ReactIRTM). Then *s*-BuLi (1.0 mL of a 1.3 M solution in hexanes, 1.30 mmol, 1.3 eq.) was added. The resulting solution was stirred at -78 °C for 10 min. Then, MeI (284 mg, 0.13 mL, 2.00 mmol, 2.0 eq.) was added and the solution was stirred at -78 °C for a further 3.5 h. Saturated NH₄Cl_(aq) was added and the solution was then allowed to warm to rt over 30 min and the two layers were separated. The aqueous layer was extracted with Et₂O (3 x 10 mL) and the combined organics were dried (MgSO₄), filtered and evaporated under reduced pressure to give the crude product. Purification by flash column chromatography on silica using 95:5 Hexane-EtOAc as eluent gave 2-methyl *N*-Boc piperazine **200** (231 mg, 80%) as a colourless oil.

For *N'*-Bn *N*-Boc piperazine **57**, a peak at 1700 cm⁻¹ was observed and assigned to $\nu_{C=O}$. After addition of *s*-BuLi, a new peak at 1645 cm⁻¹ was observed which was assigned to the lithiated intermediate. After a lithiation time of 4 min, complete lithiation of piperazine **57** to give the lithiated intermediate was observed. When MeI was added (after 10 min total lithiation time), the signal for the lithiated intermediate ($\nu_{C=O} = 1645$ cm⁻¹) disappeared after 3.5 h, indicating complete trapping had occurred.

Kinetic analysis of the MeI trapping of 2-lithio *N'*-Bn *N*-Boc piperazine **57** indicated that trapping was pseudo first order with respect to 2-lithio *N'*-Bn *N*-Boc piperazine **57**. A semilogarithmic plot for 90% conversion of the trapping (a) indicated that pseudo-first order conditions were not maintained throughout the reaction, with deviation from pseudo-first order kinetics occurring at ~600 s. However, the semilogarithmic plot for the first 20% of conversion indicated that pseudo-first order behaviour was observed in this portion of the reaction. Therefore, a pseudo-first order k_{obs} of $(1.22 \pm 0.06) \times 10^{-3} \text{ s}^{-1}$ and $t_{1/2} = (568 \pm 30) \text{ s}$ were measured using the semilogarithmic plot for 20% conversion of the trapping reaction.

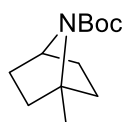


Initial rate analysis of the MeI trapping of lithiated *N'*-Bn *N*-Boc piperazine **57** provided an initial rate of trapping, $\text{rate}_{\text{init}} = (8.90 \pm 0.46) \times 10^{-5} \text{ s}^{-1}$ (initial rate tangent is displayed on the plot in red).

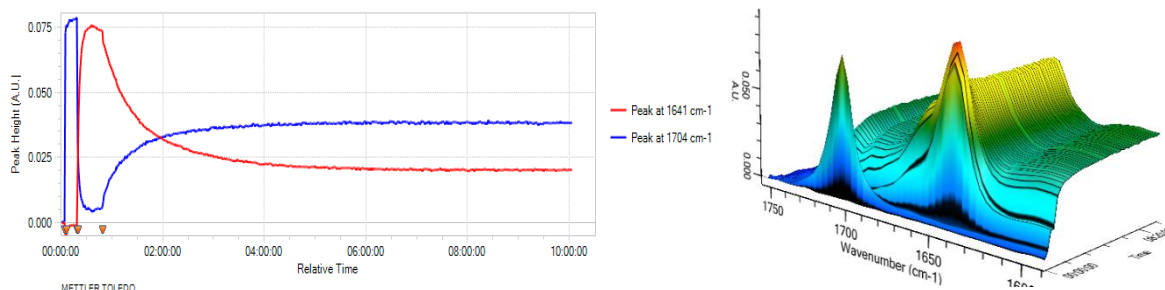


Lab Book Reference: AMI_230

tert*-Butyl-1-methyl-7-azabicyclo[2.2.1]heptane-7-carboxylate **205*



205

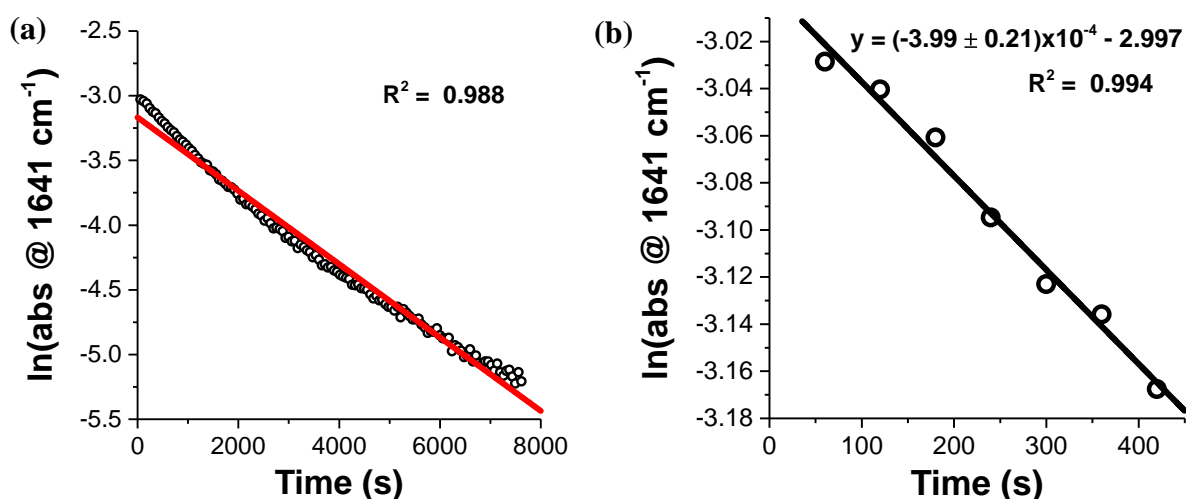


Et₂O (12 mL) was added to a flask equipped with a stirrer bar and ReactIR™ probe (ReactIR™ 15, DiComp) at rt under Ar. After cooling to -78 °C, a solution of bicyclic pyrrolidine **84** (201 mg, 1.02 mmol, 1.0 eq.) in Et₂O (2 mL) was added followed by TMEDA (154 mg, 0.19 mL, 1.32 mmol, 1.3 eq.). The solution was stirred for 5 min (to verify the stability of readout on ReactIR™). Then *s*-BuLi (1.0 mL of a 1.3 M solution in hexanes, 1.32 mmol, 1.3 eq.) was added. The resulting solution was stirred at -78 °C for 30 min. Then, Me₂SO₄ (257 mg, 0.19 mL, 2.04 mmol, 2.0 eq.) was added and the solution was stirred at -78 °C for a further 9.5 h. Saturated NH₄Cl(aq) was added and the solution was then allowed to warm to rt over 30 min and the two layers were separated. The aqueous layer was extracted with Et₂O (3 x 10 mL) and the combined organics were dried (MgSO₄), filtered and evaporated under reduced pressure to give the crude product. Purification by flash column chromatography on silica using 95:5 petrol-EtOAc as eluent gave 2-methyl bicyclic pyrrolidine **205** (130 mg, 60%) as a colourless oil, *R*_F (95:5 petrol-EtOAc) 0.15; IR (ATR) 2968, 2872, 1690 (C=O), 1455, 1364, 1341, 1163, 1129, 1025, 874 cm⁻¹; ¹H NMR (400 MHz, CDCl₃) δ 4.23 (dd, *J* = 5.0, 5.0 Hz, 1H, NCH), 1.81-1.72 (m, 2H, CH), 1.65-1.57 (m, 2H, CH), 1.60 (s, 3H, Me), 1.53-1.47 (ddd, *J* = 11.0, 9.0, 4.5 Hz, 2H, CH), 1.43 (s, 9H, CMe₃), 1.39-1.33 (ddd, *J* = 11.0, 9.0, 4.5 Hz, 2H, CH); ¹³C NMR (100.6 MHz, CDCl₃) δ 156.0 (C=O), 79.2 (CMe₃), 64.8 (NCMe), 58.6 (NCH), 37.5 (CH₂), 29.3 (CH₂), 28.5 (CMe₃), 20.6 (Me); HRMS (ESI) *m/z* calcd for C₁₂H₂₁NO₂ (M + Na)⁺ 234.1464, found 234.1462 (+1.2 ppm error).

For bicyclic pyrrolidine **84** a peak at 1704 cm⁻¹ was observed and assigned to ν_{C=O}. After addition of *s*-BuLi, a new peak at 1641 cm⁻¹ was observed which was assigned to the lithiated intermediate. After a lithiation time of 15 min, complete lithiation of bicyclic pyrrolidine **84**

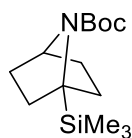
to give the lithiated intermediate was observed. When PhCHO was added (after 30 min total lithiation time), the signal for the lithiated intermediate ($\nu_{\text{C=O}} = 1641 \text{ cm}^{-1}$) disappeared after 6.5 h, indicating complete trapping had occurred.

Kinetic analysis of the Me_2SO_4 trapping of lithiated bicyclic pyrrolidine **84** indicated that trapping was pseudo first order with respect to lithiated bicyclic pyrrolidine **84**. A semilogarithmic plot for 90% conversion of the trapping (a) indicated that pseudo-first order conditions were not maintained throughout the reaction, with deviation from pseudo-first order kinetics occurring at $\sim 1200 \text{ s}$. However, the semilogarithmic plot for the first 20% of conversion indicated that pseudo-first order behaviour was observed in this portion of the reaction. Therefore, a pseudo-first order k_{obs} of $(3.99 \pm 0.21) \times 10^{-4} \text{ s}^{-1}$ and $t_{1/2} = (1740 \pm 90) \text{ s}$ were measured using the semilogarithmic plot for 20% conversion of the trapping reaction.

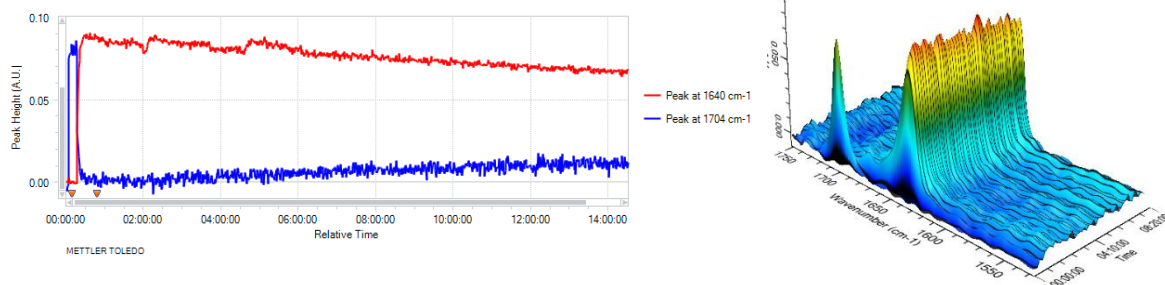


Lab Book Reference: AMI_210

tert*-Butyl-1-(trimethylsilyl)-7-azabicyclo[2.2.1]heptane-7-carboxylate **204*



204

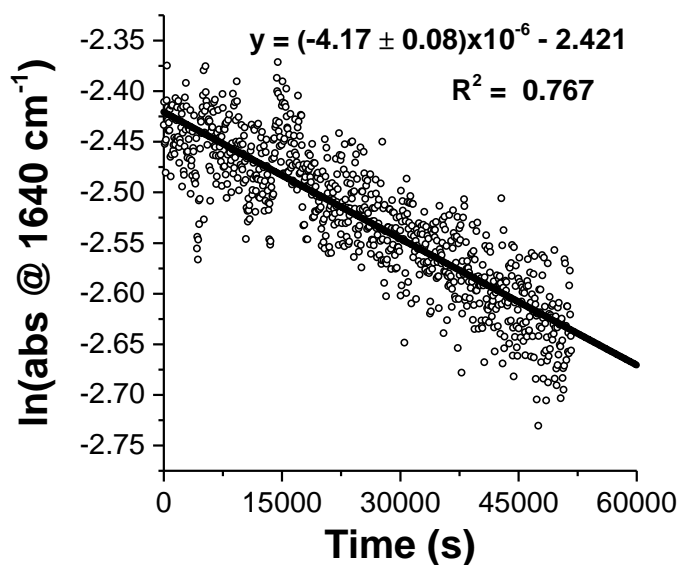


Et₂O (12 mL) was added to a flask equipped with a stirrer bar and ReactIRTM probe (ReactIRTM 15, DiComp) at rt under Ar. After cooling to -78 °C, a solution of bicyclic pyrrolidine **84** (195 mg, 0.99 mmol, 1.0 eq.) in Et₂O (2 mL) was added followed by TMEDA (149 mg, 0.19 mL, 1.28 mmol, 1.3 eq.). The solution was stirred for 5 min (to verify the stability of readout on ReactIRTM). Then *s*-BuLi (1.0 mL of a 1.3 M solution in hexanes, 1.28 mmol, 1.3 eq.) was added. The resulting solution was stirred at -78 °C for 20 min. Then, Me₃SiCl (215 mg, 0.25 mL, 1.98 mmol, 2.0 eq.) was added and the solution was stirred at -78 °C for a further 14 h. Saturated NH₄Cl_(aq) was added and the solution was then allowed to warm to rt over 30 min and the two layers were separated. The aqueous layer was extracted with Et₂O (3 x 10 mL) and the combined organics were dried (MgSO₄), filtered and evaporated under reduced pressure to give the crude product. Purification by flash column chromatography on silica using 90:10 petrol-EtOAc as eluent gave 2-silyl bicyclic pyrrolidine **204** (42 mg, 16%) as a white solid, mp 75-75 °C; *R*_F (95:5 petrol-EtOAc) 0.21; IR (ATR) 2953, 1679, 1390, 1364, 1240, 1156, 1113, 1095, 835, 765 cm⁻¹, ¹H NMR (400 MHz, CDCl₃) δ 4.28 (dd, *J* = 4.5, 4.5 Hz, 1H, NCH), 1.76-1.61 (m, 4H, CH), 1.42 (s, 9H, CMe₃), 1.41-1.28 (m, 4H, CH), 0.15 (s, 9H, SiMe₃); ¹³C NMR (100.6 MHz, CDCl₃) δ 154.9 (C=O), 79.0 (CMe₃), 59.0 (NCH), 55.4 (NCSi), 33.5 (CH₂), 30.1 (CH₂), 28.5 (CMe₃), -1.6 (SiMe₃); HRMS (ESI) *m/z* calcd for C₁₄H₂₇NO₂Si (M + Na)⁺ 292.1703, found 292.1703 (-0.2 ppm error) and bicyclic pyrrolidine **84** (114 mg, 58%) as a colourless oil.

For bicyclic pyrrolidine **84** a peak at 1704 cm⁻¹ was observed and assigned to $\nu_{C=O}$. After addition of *s*-BuLi, a new peak at 1641 cm⁻¹ was observed which was assigned to the lithiated

intermediate. After a lithiation time of 15 min, complete lithiation of bicyclic pyrrolidine **84** to give the lithiated intermediate was observed. When Me₃SiCl was added (after 20 min total lithiation time), the signal for the lithiated intermediate ($\nu_{\text{C=O}} = 1641 \text{ cm}^{-1}$) only partly decreased after 14.5 h, indicating that in-complete trapping had occurred.

Kinetic analysis of the Me₃SiCl trapping of lithiated bicyclic pyrrolidine **84** indicated that trapping was pseudo first order with respect to lithiated bicyclic pyrrolidine **84**. As no baseline absorbance for the signal at 1641 cm^{-1} was collected at the end of reaction only an approximate k_{obs} for the trapping could be measured. An approximate pseudo-first order k_{obs} of $(4.17 \pm 0.08) \times 10^{-6} \text{ s}^{-1}$ and $t_{1/2} = (166000 \pm 3000) \text{ s}$ were measured using the semilogarithmic plot for the partial trapping (~ 20% conversion).



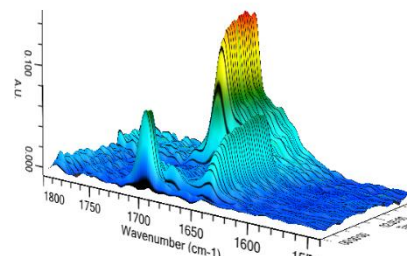
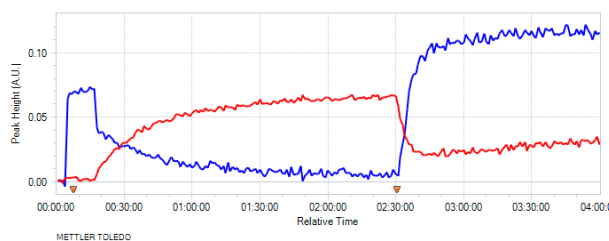
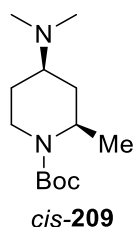
Lab Book Reference: AMI_277

s-BuLi (1.0 mL of a 1.3M solution in hexanes, 1.34 mmol, 1.3 eq.) was added dropwise to a stirred solution of bicyclic pyrrolidine **84** (204 mg, 1.03 mmol, 1.0 eq.) and TMEDA (156 mg, 1.34 mmol, 0.20 mL, 1.3 eq.) in Et₂O (7 mL) under Ar. The resulting solution was stirred at -78 °C for 40 min and then Me₃SiCl (224 mg, 2.06 mmol, 0.26 mL, 2.0 eq.) was added. The reaction mixture was allowed to warm to rt over 16 h and then saturated NH₄Cl_(aq) (10 mL) was added and the two layers were separated. The aqueous layer was extracted with Et₂O (3 x 10 mL) and the combined organics were dried (MgSO₄), filtered and evaporated under reduced pressure to give the crude product. Purification by flash column

chromatography on silica using 95:5 hexane-Et₂O as eluent gave silyl pyrrolidine **204** (224 mg, 81%) as a white solid.

Lab Book Reference: AMI_278

***tert*-Butyl (2*R**,4*R**)-4-(dimethylamino)-2-methylpiperidine-1-carboxylate *cis*-209**



Et₂O (12 mL) was added to a flask equipped with a stirrer bar and ReactIRTM probe (ReactIRTM 15, DiComp) at rt under Ar. After cooling to -78 °C, a solution of 4-amino piperidine **168** (225 mg, 0.99 mmol, 1.0 eq.) in Et₂O (2 mL) was added followed by TMEDA (149 mg, 192 μL, 1.28 mmol, 1.3 eq.). The solution was stirred for 5 min (to verify the stability of readout on ReactIRTM). Then *s*-BuLi (1.0 mL of a 1.3 M solution in hexanes, 1.28 mmol, 1.3 eq.) was added. The resulting solution was stirred at -78 °C for 130 min. Then, MeI (280 mg, 122 μL, 1.97 mmol, 2.0 eq.) was added, the solution rapidly gelled and the stirring ceased, the gel was held at -78 °C for a further 1.5 h. Saturated NH₄Cl_(aq) (10 mL) was added and the solution was then allowed to warm to rt over 30 min and the two layers were separated. The aqueous layer was extracted with Et₂O (3 x 10 mL) and the combined organics were dried (MgSO₄), filtered and evaporated under reduced pressure to give the crude product. Purification by flash column chromatography on silica using 93:6:1 CH₂Cl₂-MeOH-NH₄OH as eluent gave 2-methyl piperidine *cis*-**209** (96 mg, 40%) as a colourless oil, *R*_F (93:6:1 CH₂Cl₂-MeOH-NH₄OH) 0.13; IR (ATR) 2972, 2870, 2813, 2771, 1681 (C=O), 1410, 1362, 1152, 1074, 768 cm⁻¹; ¹H NMR (400 MHz, CDCl₃) δ 3.93-3.83 (m, 1H, NCH), 3.74 (ddd, *J* = 13.5, 7.0, 2.5 Hz, 1H, NCH), 3.06 (ddd, *J* = 13.5, 11.0, 5.5 Hz, 1H, NCH), 2.33-2.25 (m, 1H, NCH), 2.22 (s, 6H, NMe₂), 1.90-1.77 (m, 2H, CH), 1.60-1.49 (m, 1H, CH), 1.47-1.38 (m, 1H, CH), 1.44 (s, 9H, CMe₃), 1.21 (d, *J* = 6.5 Hz, 3H,

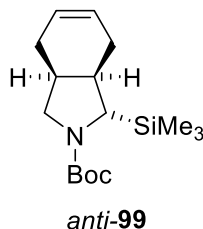
NCHMe); ^{13}C NMR (100.6 MHz, CDCl_3) δ 155.2 (C=O), 79.2 (CMe_3), 58.9 (NCH), 48.6 (NCH), 42.5 (NMe_2), 36.4 (NCH_2), 32.3 (CH_2), 28.6 (CMe_3), 27.0 (CH_2), 19.9 (NCHMe); HRMS (ESI) m/z calcd for $\text{C}_{13}\text{H}_{26}\text{N}_2\text{O}_2$ ($\text{M} + \text{H}$) $^+$ 243.2067, found 243.2064 (+2.8 ppm error) and 4-amino piperidine **168** (47 mg, 21%) as a colourless oil. The stereochemistry of *cis*-**209** has not been proven but is assumed from literature precedent.³⁸

For 4-amino piperidine **168**, a peak at 1697 cm^{-1} was observed and assigned to $\nu_{\text{C=O}}$. After addition of *s*-BuLi, a new peak at 1644 cm^{-1} was observed which was assigned to the lithiated intermediate. After a lithiation time of 2 h, complete lithiation of 4-amino piperidine **168** to give the lithiated intermediate was observed. When MeI was added (after 2 h total lithiation time), the signal for the lithiated intermediate ($\nu_{\text{C=O}} = 1645\text{ cm}^{-1}$) plateaued after 15 min. ^1H NMR spectroscopy of the crude product indicated starting material **168** was present so complete trapping had not occurred.

Lab Book Reference: AMI_279

6.7 Experimental Procedures for Chapter 5

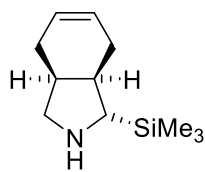
tert-Butyl (1*S**, 3*aS**, 7*aR**)-1-(trimethylsilyl)-2,3,3*a*,4,7,7*a*-hexahydro-1*H*-isoindole-2-carboxylate *anti*-**99**



Using general procedure A, *s*-BuLi (1.0 mL of a 1.3 M solution in hexanes, 1.3 mmol, 1.3 eq.), *N*-Boc pyrrolidine **96** (223 mg, 1.0 mmol, 1.0 eq.) and TMEDA (151 mg, 0.19 mL, 1.3 mmol, 1.3 eq.) in Et₂O (7 mL) for 10 min and then Me₃SiCl (217 mg, 0.25 mL, 2.0 mmol, 2.0 eq.) gave the crude product. Purification by flash column chromatography on silica using 90:10 hexane-EtOAc as eluent gave a single diastereomer (by ¹H NMR spectroscopy of amine *anti*-**99**) of 2,3,4-trisubstituted pyrrolidine *anti*-**99** (222 mg, 75%) as a colourless oil, *R*_F(90:10 hexane-EtOAc) 0.18; IR (ATR) 2929, 1686 (C=O), 1389, 1364, 1246, 1168, 1113, 1073, 835, 766 cm⁻¹; ¹H NMR (400 MHz, CDCl₃) (50:50 mixture of rotamers) δ 5.62 (s, 2H, =CH), 3.30-3.27 (m, 1.5 H, NCH), 3.18-3.14 (m, 0.5H, NCH), 3.04 (d, *J* = 3.5 Hz 0.5H, NCH), 2.98 (d, *J* = 3.5 Hz 0.5H, NCH), 2.29-2.17 (m, 4H, CH), 1.90-1.79 (m, 2H, CH), 1.47 (s, 4.5H, CMe₃), 1.44 (s, 4.5H, CMe₃), 0.07 (s, 4.5H, SiMe₃), 0.06 (s, 4.5H, SiMe₃); ¹³C NMR (100.6 MHz, CDCl₃) (rotamers) δ 155.4 (C=O), 125.0 (=CH), 124.7 (=CH), 124.4 (=CH), 124.3 (=CH), 79.4 (CMe₃), 78.6 (CMe₃), 55.7 (NCH), 54.7 (NCH), 51.2 (NCH₂), 50.8 (NCH₂), 36.7 (CH), 36.1 (CH), 34.7 (CH), 33.9 (CH), 28.8 (CMe₃), 28.7 (CMe₃), 27.4 (CH₂), 27.2 (CH₂), 24.7 (CH₂), 24.6 (CH₂), -1.6 (SiMe₃); HRMS (ESI) *m/z* calcd for C₁₆H₂₉NO₂Si (M + Na)⁺ 318.1860, found 318.1852 (+2.0 ppm error). Spectroscopic data consistent with those reported in the literature.⁴ The stereochemistry of *anti*-**99** has not been proven but is assumed from literature precedent.⁴

Lab Book Reference: AMI_5

(1*S,3*aS**,7*aR**)-1-(Trimethylsilyl)-2,3,3*a*,4,7,7*a*-hexahydro-1*H*-isoindole *anti*-216**

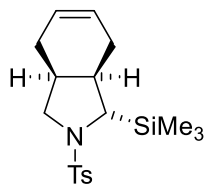


anti-216

TFA (240 mg, 0.13 mL, 1.69 mmol, 10.0 eq.) was added dropwise to a stirred solution of 2-silyl *N*-Boc pyrrolidine *anti*-99 (50 mg, 0.169 mmol, 1.0 eq.) in CH₂Cl₂ (2 mL) at rt under Ar. The resulting solution was stirred at rt for 3 h. Then, saturated NaHCO_{3(aq)} (20 mL) was added with vigorous stirring until gas evolution ceased. The two layers were separated and the aqueous layer was extracted with CH₂Cl₂ (3 x 10 mL). The combined organics were dried (Na₂SO₄), filtered and evaporated under reduced pressure to give crude amine *anti*-216 (17 mg, 52%) as a brown oil. The ¹H NMR spectrum indicated the presence of only one diastereomer. Diagnostic signals for *anti*-216: ¹H NMR (400 MHz, CDCl₃) δ 5.79-5.71 (m, 2H, =CH), 3.08 (dd, *J* = 10.5, 5.5 Hz, 1H), 2.62 (dd, *J* = 10.5, 5.0 Hz, 1H).

Lab Book Reference: AMI_11

(1*S,3*aS**,7*aR**)-2-(4-Methylbenzenesulfonyl)-1-(trimethylsilyl)-2,3,3*a*,4,7,7*a*-hexahydro-1*H*-isoindole *anti*-217**



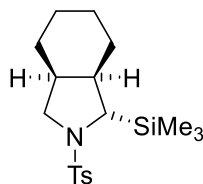
anti-217

TFA (1.94 g, 1.30 mL, 17.01 mmol, 36.0 eq.) was added dropwise to a stirred solution of 2-silyl *N*-Boc pyrrolidine *anti*-99 (140 mg, 0.47 mmol, 1.0 eq.) in CH₂Cl₂ (13 mL) at rt under Ar. The resulting solution was stirred at rt for 1 h. Then, saturated NaHCO_{3(aq)} (20 mL) was added with vigorous stirring until gas evolution ceased. The two layers were separated and the aqueous layer was extracted with CH₂Cl₂ (3 x 10 mL). The combined organics were dried (Na₂SO₄), filtered and evaporated under reduced pressure. The residue was dissolved in CH₂Cl₂ (5 mL) and Et₃N (119 mg, 0.17 mL, 1.18 mmol, 2.5 eq.) and *p*-TsCl (108 mg, 0.57 mmol, 1.2 eq.) were added. The resulting solution was stirred at rt for 1 h. Then, CH₂Cl₂ (10 mL) and 0.1 M HCl_(aq) (10 mL) were added and the two layers were separated. The aqueous layer was extracted with CH₂Cl₂ (3 x 10 mL) and the combined organics were dried

(MgSO₄), filtered and evaporated under reduced pressure to give the crude product. Purification by flash column chromatography on silica using 85:15 hexane-Et₂O as eluent gave sulfonamide *anti*-**217** (164 mg, 87%) as a white solid, mp 94-96 °C; *R_F* (80:20 hexane-Et₂O) 0.18; IR (ATR) 2930, 2895, 1345, 1248, 1166, 1100, 870, 837, 817, 657 cm⁻¹; ¹H NMR (400 MHz, CDCl₃) δ 7.72-7.67 (m, 2H, Ar), 7.30 (d, *J* = 8.0 Hz, 2H, Ar), 5.46-5.39 (m, 1H, =CH), 5.33-5.23 (m, 1H, =CH), 3.42 (dd, *J* = 9.0, 7.5 Hz, 1H, NCH), 2.87 (dd, *J* = 10.5, 9.0 Hz, 1H, NCH), 2.80 (d, *J* = 2.0 Hz, 1H, NCH), 2.44-2.33 (m, 1H, CH) 2.43 (s, 3H, Ar-Me), 2.20-2.01 (m, 2H, CH), 1.79-1.66 (m, 2H, CH), 0.74-0.62 (m, 1H, CH), 0.15 (s, 9H, SiMe₃); ¹³C NMR (100.6 MHz, CDCl₃) δ 143.2 (*ipso*-Ar), 134.0 (Ar), 129.6 (Ar), 127.9 (Ar), 124.2 (=CH), 123.7 (=CH), 59.1 (NCH), 52.0 (NCH₂), 36.5 (CH), 34.9 (CH), 26.8 (CH₂), 23.8 (CH₂), 21.7 (Ar-Me), -1.7 (SiMe₃); HRMS (ESI) *m/z*. calcd for C₁₈H₂₇NO₂SSi (M + H)⁺ 350.1605, found 350.1599 (+0.5 ppm error).

Lab Book Reference: AMI_271

(1*S,3*aS**,7*aR**)-2-(4-Methylbenzenesulfonyl)-1-(trimethylsilyl)-octahydro-1H-isoindole *anti*-**221****



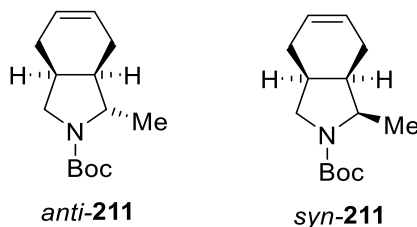
anti-**221**

Pd/C (25 mg, 25% w/w, 0.025 mmol) was added to a stirred solution of 2,3,4-trisubstituted pyrrolidine *anti*-**99** (101 mg, 0.340 mmol, 1.0 eq.) in EtOAc (5 mL) at rt. The resulting suspension was degassed and then H₂ gas (1 atm) was supplied *via* a balloon. The suspension was stirred at rt under a H₂ atmosphere (balloon) for 3 h. The solids were removed by filtration through Celite[®] and washed with EtOAc (10 mL). The filtrate was evaporated under reduced pressure and the residue was dissolved in CH₂Cl₂ (5 mL) and TFA (0.26 mL, 3.40 mmol, 10.0 eq.) was added at rt under Ar. The resulting solution was stirred at rt for 3 h. Then, saturated NaHCO_{3(aq)} (20 mL) was added with vigorous stirring until gas evolution ceased. The mixture was extracted with CH₂Cl₂ (3 x 10 mL) and the combined organics were dried (Na₂SO₄), filtered and evaporated under reduced pressure. The residue was dissolved in CH₂Cl₂ (2 mL) and Et₃N (0.06 mL, 0.408 mmol, 1.2 eq.) and *p*-TsCl (78 mg, 0.408 mmol,

1.2 eq.) were added. The resulting solution was stirred at rt for 16 h. Then, CH₂Cl₂ (10 mL) and 0.1 M HCl_(aq) (10 mL) were added and the two layers were separated. The aqueous layer was extracted with CH₂Cl₂ (3 x 10 mL) and the combined organics were dried (MgSO₄), filtered and evaporated under reduced pressure to give the crude product. Purification by flash column chromatography on silica using 50:50 hexane-Et₂O as eluent gave sulfonamide *anti*-**221** (71 mg, 59%) as a grey solid, mp 130-135 °C (lit.,⁴ bp 120-121 °C), *R*_F (50:50 hexane-Et₂O) 0.29; ¹H NMR (400 MHz, CDCl₃) δ 7.73 (d, *J* = 8.0 Hz, 2H, Ar), 7.31 (d, *J* = 8.0 Hz, 2H, Ar), 3.27 (dd, *J* = 9.5, 8.0 Hz, 1H, NCH), 3.13-3.03 (m, 1H, NCH), 2.80 (d, *J* = 2.0 Hz, 1H, NCH), 2.43 (s, 3H, Ar-Me), 2.30 (m, 1H, CH), 1.89 (dddd, *J* = 7.5, 5.5, 5.5, 2.0 Hz, 1H, CH), 1.63-0.93 (m, 8H, CH), 0.12 (s, 9H, SiMe₃); ¹³C NMR (100.6 MHz, CDCl₃) δ 143.2 (*ipso*-Ar), 134.2 (Ar), 129.5 (Ar), 128.0 (Ar), 58.7 (NCH), 50.3 (NCH₂), 40.5 (CH), 37.1 (CH), 28.7 (CH₂), 24.8 (CH₂), 24.5 (CH₂), 21.7 (Ar-Me), 21.1 (CH₂), -1.9 (SiMe₃). Spectroscopic data consistent with those reported in the literature.⁴

Lab Book Reference: AMI_21

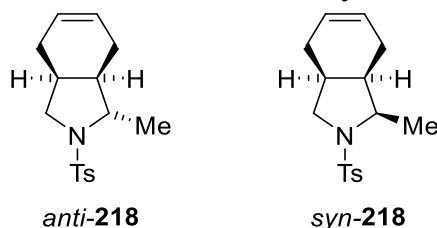
(1*S**,3*aS**,7*aR**) and (1*R**,3*aS**,7*aR**)-*tert*-Butyl-1-methyl-2,3,3*a*,4,7,7*a*-hexahydro-1*H*-isoindole-2-carboxylate *anti*-**211** and *syn*-**211**



Using general procedure A, *s*-BuLi (1.26 mL of a 1.3 M solution in hexanes, 1.64 mmol, 1.3 eq.), *N*-Boc pyrrolidine **96** (282 mg, 1.26 mmol, 1.0 eq.) and TMEDA (190 mg, 0.25 mL, 1.64 mmol, 1.3 eq.) in Et₂O (7 mL) for 10 min and then Me₂SO₄ (318 mg, 0.24 mL, 2.52 mmol, 2.0 eq.) gave the crude product. Purification by flash column chromatography on silica using 85:15 hexane-EtOAc as eluent gave a 90:10 mixture (by ¹H NMR spectroscopy of sulfonamides *anti*-**218** and *syn*-**218**) of 2,3,4-trisubstituted pyrrolidines *anti*-**211** and *syn*-**211** (249 mg, 83%) as a colourless oil. For spectroscopic data see section 6.4.

Lab Book Reference: AMI_6

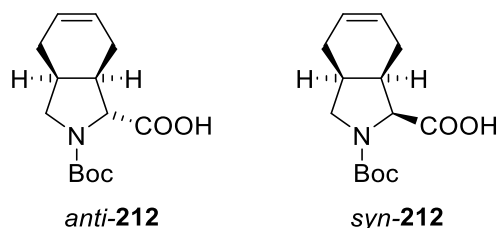
(1*S**,3*aS**,7*aR**) and (1*R**,3*aS**,7*aR**)-1-Methyl-2-(4-methylbenzenesulfonyl)-2,3,3*a*,4,7,7*a*-hexahydro-1*H*-isoindole *anti*-**218** and *syn*-**218**



TFA (259 mg, 0.17 mL, 2.30 mmol, 10 eq.) was added to a stirred solution of 2,3,4-trisubstituted pyrrolidine **211** (54 mg, 0.23 mmol, 1.0 eq.) in CH₂Cl₂ (7 mL) at rt under Ar. The resulting solution was stirred at rt for 16 h. Then, saturated NaHCO_{3(aq)} (20 mL) was added with vigorous stirring until gas evolution ceased. The mixture was extracted with CH₂Cl₂ (3 x 10 mL) and the combined organics were dried (Na₂SO₄), filtered and evaporated under reduced pressure. The residue was dissolved in CH₂Cl₂ (4 mL) and Et₃N (28 mg, 0.04 mL, 0.28 mmol, 1.2 eq.) and *p*-TsCl (28 mg, 0.28 mmol, 1.2 eq.) were added. The resulting solution was stirred at rt for 16 h. Then, CH₂Cl₂ (10 mL) and 0.1 M HCl_(aq) (10 mL) were added and the two layers were separated. The aqueous layer was extracted with CH₂Cl₂ (3 x 10 mL) and the combined organics were dried (MgSO₄), filtered and evaporated under reduced pressure to give the crude product, which contained a 90:10 mixture (by ¹H NMR spectroscopy) of *anti*-**218** and *syn*-**218**. Purification by flash column chromatography on silica using 85:15 hexane-EtOAc as eluent gave a 90:10 mixture of sulfonamides *anti*-**218** and *syn*-**218** (33 mg, 48%) as a white solid, mp 92-97 °C, *R_F* (50:50 Hexane-Et₂O) 0.29; IR (CHCl₃) 1337 (S=O), 1162, 1098, 816, 664, 593, 548 cm⁻¹; ¹H NMR (400 MHz, CDCl₃) δ 7.74-7.70 (m, 2H, Ar), 7.33-7.29 (m, 2H, Ar), 5.70-5.57 (m, 0.2H, =CH), 5.47-5.35 (m, 1.8H, =CH), 3.59-3.53 (m, 0.1H, NCH), 3.48 (dd, *J* = 9.0, 6.5 Hz, 0.9H, NCH), 3.40-3.30 (m, 1H, NCH), 3.23 (dd, *J* = 10.5, 8.0 Hz, 0.1H, NCH), 2.95-2.91 (m, 0.9H, NCH), 2.49-2.44 (br, m, 1H, CH), 2.42 (s, 3H, Ar-*Me*), 2.19-1.80 (m, 4H, CH), 1.60 (br s, 1H, CH), 1.36 (d, *J* = 6.5 Hz, 2.1H, NCH*Me*), 1.35 (d, *J* = 6.5 Hz, 0.9H, NCH*Me*); ¹³C NMR (100.6 MHz, CDCl₃) δ 143.3 (Ar_{anti}), 141.9 (Ar_{syn}), 135.1 (Ar_{anti}), 134.7 (Ar_{syn}), 129.7 (Ar_{syn}), 129.6 (Ar_{anti}), 127.7 (Ar_{syn}), 127.5 (Ar_{anti}), 125.0 (=CH_{syn}), 124.7 (=CH_{syn}), 124.2 (=CH_{anti}), 123.9 (=CH_{anti}), 61.9 (NCH_{anti}), 60.4 (NCH_{syn}), 53.4 (NCH_{2syn}), 52.5 (NCH_{2anti}), 41.5 (CH_{anti}), 38.5 (CH_{syn}), 33.9 (CH_{syn}), 32.5 (CH_{anti}), 25.0 (CH_{2syn}), 24.4 (CH_{2anti}), 23.9 (CH_{2syn}), 23.8 (CH_{2anti}), 22.1 (NCH*Me*_{anti}), 21.73(Ar-*Me*_{syn}), 21.68 (Ar-*Me*_{anti}), 17.7 (NCH*Me*_{syn}); HRMS (ESI) *m/z* calcd for C₁₆H₂₁NO₂S (M + Na)⁺ 314.1185, found 314.1171 (+3.4 ppm error).

Lab Book Reference: AMI_7

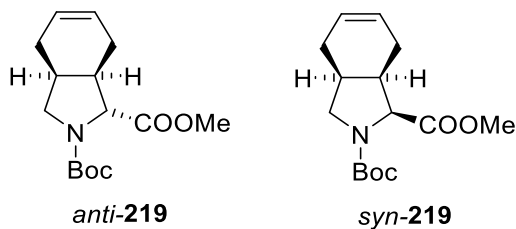
(1*R**,3*aS**,7*aR**) and (1*S**,3*aS**,7*aR**)-2-[(*tert*-Butoxy)carbonyl]-2,3,3*a*,4,7,7*a*-hexahydro-1*H*-isoindole-1-carboxylic acid *anti*-**212** and *syn*-**212**



Using general procedure C, *s*-BuLi (1.1 mL of a 1.3 M solution in hexanes, 1.38 mmol, 1.3 eq.), *N*-Boc pyrrolidine **96** (237 mg, 1.06 mmol, 1.0 eq.) and TMEDA (160 mg, 0.21 mL, 1.38 mmol, 1.3 eq.) in Et₂O (7 mL) for 10 min and then dry CO₂ was bubbled through for 30 min to give the crude product, which contained an 87:13 mixture (by ¹H NMR spectroscopy) of carboxylic acids *anti*-**212** and *syn*-**212**. Purification by flash column chromatography on silica using 50:49.5:0.5 EtOAc-hexane-AcOH as eluent gave an 87:13 mixture of carboxylic acids *anti*-**212** and *syn*-**212** (218 mg, 77%) as a white solid, mp 110-112 °C, *R_F* (50:49.5:0.5 EtOAc-hexane-AcOH) 0.16; IR 2973, 2928, 1727 (C=O, CO₂H), 1632 (C=O, Boc), 1431, 1235, 1139, 913 859, 672 cm⁻¹; ¹H NMR (400 MHz, CDCl₃) (50:50 mixture of rotamers for each of *anti*-**212** and *syn*-**212**) δ 5.65 (s, 2H, =CH), 4.37 (m, 0.065H, NCH), 4.30 (d, *J* = 7.5 Hz, 0.065H, NCH), 4.04 (d, *J* = 4.0 Hz, 0.435H, NCH), 3.92 (d, *J* = 6.5 Hz, 0.435H, NCH), 3.59 (dd, *J* = 10.0, 7.0 Hz, 0.5H, NCH), 3.49 (dd, *J* = 10.0, 6.0 Hz, 0.5H, NCH), 3.31 (dd, *J* = 10.0, 5.0 Hz, 0.5H, NCH), 3.21 (dd, *J* = 10.0, 8.0 Hz, NCH), 2.67-1.82 (m, 6H, CH), 1.48 (s, 4.5H, CMe₃), 1.41 (s, 4.5H, CMe₃); ¹³C NMR (100.6 MHz, CDCl₃) for *anti*-**212** (rotamers) δ 178.8 (C=O, CO₂H), 175.3 (C=O, CO₂H), 156.9 (C=O, Boc), 154.5 (C=O, Boc), 124.8 (=CH), 124.4 (=CH), 124.0 (=CH), 123.7 (=CH), 81.4 (CMe₃), 80.6 (CMe₃), 64.7 (NCH), 63.7 (NCH), 51.5 (NCH₂), 51.3 (NCH₂), 40.4 (CH), 37.6 (CH), 33.3 (CH), 32.7 (CH), 28.5 (CMe₃), 28.4 (CMe₃), 24.8 (CH₂), 24.7 (CH₂), 24.6 (CH₂), 24.2 (CH₂); HRMS (ESI) *m/z* calcd for C₁₄H₂₁NO₄ (M + Na)⁺ 290.1363, found 290.1348 (+4.6 ppm error). The stereochemistry of *anti*-**212** and *syn*-**212** has not been proven but is assumed from literature precedent.⁴

Lab Book Reference: AMI_12

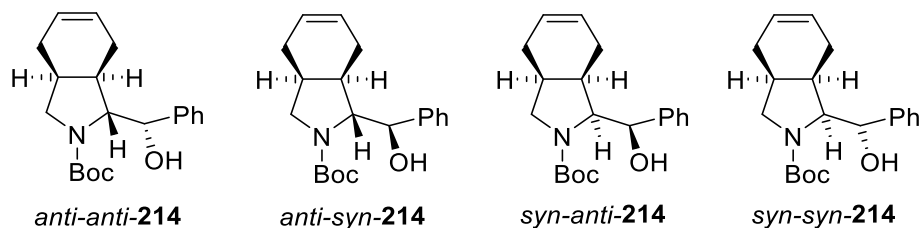
(1*S,3*aS**,7*aR**) and (1*R**,3*aS**,7*aR**)-2-*tert*-Butyl 1-methyl-2,3,3*a*,4,7,7*a*-hexahydro-1*H*-isoindole-1,2-dicarboxylate *anti*-**219** and *syn*-**219****



Me₃Si-diazomethane (0.40 mL of a 2 M solution in hexanes, 2.0 eq.) was added to a stirred solution of an 87:13 mixture of carboxylic acids *anti*-**212** and *syn*-**212** (71 mg, 0.264 mmol, 1.0 eq.) in toluene (1.8 mL) and MeOH (1.2 mL) at 0 °C under Ar. The resulting solution was stirred at 0 °C for 30 min and then warmed to rt over 30 min. AcOH (16 mg, 0.02 mL, 1.0 eq.) was added and then the solvent was evaporated under reduced pressure. The residue was partitioned between H₂O and Et₂O and the two layers were separated. The aqueous layer was extracted with Et₂O (3 x 10 mL) and the combined organics were dried (MgSO₄), filtered and evaporated under reduced pressure to give the crude product which contained an 87:13 mixture (by ¹H NMR spectroscopy) of methyl esters *anti*-**219** and *syn*-**219**. Purification by flash column chromatography on silica using 80:20 hexane-EtOAc as eluent gave an 87:13 mixture of methyl esters *anti*-**219** and *syn*-**219** (64 mg, 86%) as a colourless oil, *R_F* (80:20 hexane-EtOAc) 0.18; IR 2979, 2927, 1750 (C=O), 1697 (C=O), 1391, 1365, 1252, 1162, 1126, 731, 665 cm⁻¹; ¹H NMR (400 MHz, CDCl₃) (60:40 mixture of rotamers for each of *anti*-**219** and *syn*-**219**) δ 5.64 (s, 2H, =CH), 4.33 (d, *J* = 7.0 Hz, 0.05H, NCH), 4.27 (d, *J* = 7.0 Hz, 0.08H, NCH), 4.02 (d, *J* = 4.5 Hz, 0.35H, NCH), 3.90 (d, *J* = 6.0 Hz, 0.52H, NCH), 3.74 (s, 1.04H, OMe), 3.73 (s, 1.57H, OMe), 3.70 (s, 0.23H, OMe), 3.68 (s, 0.16H, OMe), 3.62-3.56 (m, 1H, NCH), 3.29 (dd, *J* = 10.0, 4.5 Hz, 0.6H, NCH), 3.18 (dd, *J* = 10.0, 7.0 Hz, 0.4H, NCH), 2.49-2.14 (m, 4H, CH), 1.98-1.91 (m, 1H, CH), 1.91-1.84 (m, 1H, CH), 1.45 (s, 3.6H, CMe₃), 1.40 (s, 5.4H, CMe₃); ¹³C NMR (100.6 MHz, CDCl₃) for *anti*-**219** (rotamers) δ 173.5 (C=O, COOMe), 173.1 (C=O, COOMe), 150.1 (C=O, Boc), 154.4 (C=O, Boc), 124.8 (=CH), 124.5 (=CH), 124.0 (=CH), 123.7 (=CH), 80.1 (CMe₃), 80.0 (CMe₃), 64.1 (NCH), 63.9 (NCH), 52.3 (OMe), 52.1 (OMe), 51.5 (NCH₂), 51.3 (NCH₂), 40.3 (CH), 39.0 (CH), 33.2 (CH), 32.6 (CH), 28.5 (CMe₃), 28.4 (CMe₃), 25.0 (CH₂), 24.7 (CH₂), 24.6 (CH₂), 24.4 (CH₂); HRMS (ESI) *m/z* calcd for C₁₅H₂₃NO₄ (M + Na)⁺ 304.1519, found 304.1515 (+0.8 ppm error).

Lab Book Reference AMI_20

(1*R,3*aS**,7*aR**) and (1*S**,3*aS**,7*aR**)-tert-Butyl-1-[(*S*) and (*R*)-hydroxy(phenyl)methyl]-2,3,3*a*,4,7,7*a*-hexahydro-1*H*-isoindole-2-carboxylate *anti-anti*-**214**, *anti-syn*-**214**, *syn-anti*-**214** and *syn-syn*-**214****

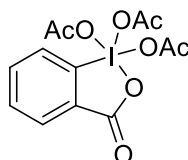


Using general procedure A, *s*-BuLi (1.1 mL of a 1.3 M solution in hexanes, 1.40 mmol, 1.3 eq.), *N*-Boc pyrrolidine **96** (241 mg, 1.08 mmol, 1.0 eq.) and TMEDA (163 mg, 0.21 mL, 1.40 mmol, 1.3 eq.) in Et₂O (7 mL) and then PhCHO (229 mg, 0.22 mL, 2.16 mmol, 2.0 eq.) gave the crude product, which contained a 58:29:9:4 mixture (by ¹H NMR spectroscopy) of *anti-anti*-**214**, *anti-syn*-**214**, *syn-anti*-**214**, *syn-syn*-**214**. Purification by flash column chromatography on silica using 99:1 CH₂Cl₂-acetone as eluent gave an 80:20 mixture of pyrrolidines *anti-anti*-**214** and *syn-syn*-**214** (164 mg, 46%) as a colourless oil, *R_F* (98:2 CH₂Cl₂-acetone) 0.16; IR (ATR) 3386 (OH), 2970, 2890, 1663 (C=O), 1404, 1367, 1159, 1126, 1051, 701 cm⁻¹; ¹H NMR (400 MHz, CDCl₃) δ 7.42-7.30 (m, 5H, Ph), 5.74 (d, *J* = 3.0 Hz, 0.8 H, OH), 5.56-5.49 (m, 2H, =CH), 4.70 (d, *J* = 5.0 Hz, 0.2H, PhCHO), 4.61 (dd, *J* = 9.0, 3.0 Hz, 0.8H, PhCHO), 4.11 (dd, *J* = 5.0, 4.0 Hz, 0.2H, NCH), 3.78 (d, *J* = 9.0 Hz, 0.8H, NCH), 3.64 (br s, 0.2H, NCH), 3.49 (dd, *J* = 10.5, 8.0 Hz, 0.8H, NCH), 3.21 (dd, *J* = 10.5, 10.5 Hz, 0.8H, NCH), 3.12 (dd, *J* = 10.5, 10.5 Hz, 0.2H, NCH), 2.54-1.64 (m, 6H, CH), 1.50 (s, 9H, CMe₃); ¹³C NMR (100.6 MHz, CDCl₃) δ 168.4 (C=O_{*syn-syn*}), 159.2 (C=O_{*anti-anti*}), 142.7 (*ipso*-Ph_{*anti-anti*}), 142.0 (*ipso*-Ph_{*syn-syn*}), 128.7 (Ph_{*syn-syn*}), 128.6 (Ph_{*anti-anti*}), 128.1 (Ph_{*anti-anti*}), 128.0 (Ph_{*syn-syn*}), 127.3 (Ph_{*anti-anti*}), 127.1 (Ph_{*syn-syn*}), 127.1 (=CH_{*syn-syn*}), 126.9 (=CH_{*syn-syn*}), 124.6 (=CH_{*anti-anti*}), 124.2 (=CH_{*anti-anti*}), 81.0 (CMe₃_{*anti-anti*}), 80.2 (CMe₃_{*syn-syn*}), 79.1 (PhCHO_{*anti-anti*}), 75.7 (PhCHO_{*syn-syn*}), 72.0 (NCH_{*syn-syn*}), 71.5 (NCH_{*anti-anti*}), 52.0 (NCH₂_{*syn-syn*}), 50.9 (NCH₂_{*anti-anti*}), 36.0 (CH_{*anti-anti*}), 33.8 (CH_{*syn-syn*}), 32.7 (CH_{*anti-anti*}), 29.8 (CH_{*syn-syn*}), 28.61 (CMe₃_{*syn-syn*}), 28.59 (CMe₃_{*anti-anti*}), 25.6 (CH₂_{*anti-anti*}), 24.0 (CH₂_{*anti-anti*}), 23.4 (CH₂_{*syn-syn*}), 21.67 (CH₂_{*syn-syn*}); HRMS (ESI) *m/z* calcd for C₂₀H₂₇NO₃ (M + Na)⁺ 352.1883, found 352.1880 (+0.9 ppm error), pyrrolidine *anti-syn*-**214** (82 mg, 23%) as a colourless oil, *R_F* (98:2 CH₂Cl₂-acetone) 0.13; IR (ATR) 3407 (OH), 2974, 2927, 1666 (C=O), 1392, 1365, 1160, 1127, 702, 662 cm⁻¹; ¹H NMR (400 MHz, CDCl₃) δ 7.33-7.28 (m, 5H, Ph), 6.07 (d, *J*

= 7.5 Hz, 1H, OH), 5.61 (m, 2H, =CH), 4.83 (d, $J = 7.5$ Hz, 1H, PhCHO), 3.97 (d, $J = 7.0$ Hz, 1H, NCH), 3.13 (dd, $J = 10.5, 5.0$ Hz, 1H, NCH), 2.75 (dd, $J = 10.5, 6.0$ Hz, NCH), 2.45-1.94 (m, 5H, CH), 1.80-1.75 (m, 1H, CH), 1.51 (s, 9H, CMe₃); ¹³C NMR (100.6 MHz, CDCl₃) δ 158.2 (C=O), 141.3 (*ipso*-Ph), 128.1 (Ph), 127.5 (Ph), 127.1 (Ph), 124.9 (=CH), 124.1 (=CH), 80.7 (CMe₃), 76.3 (PCHO), 68.3 (NCH), 53.0 (NCH₂), 36.6 (CH), 31.9 (CH), 28.6 (CMe₃), 25.2 (CH₂), 24.7 (CH₂); HRMS (ESI) m/z calcd for C₂₀H₂₇NO₃ (M + Na)⁺ 352.1883, found 352.1888 (-1.8 ppm error) and pyrrolidine *syn-anti*-**214** (11 mg, 3%) as a pale yellow solid, mp 124-126 °C, R_F (98:2 CH₂Cl₂-acetone) 0.19; IR (ATR) 3295 (OH), 2933, 2876, 1668 (C=O), 1409, 1228, 1151, 1122, 762, 704, 681 cm⁻¹; ¹H NMR (400 MHz, CDCl₃) δ 7.43-7.69 (m, 5H, Ph), 5.56-5.46 (m, 2H, =CH), 4.69 (dd, $J = 8.5, 2.0$ Hz, 1H, PhCH₂), 4.19 (dd, $J = 8.5, 4.0$, 1H, NCH), 3.61 (dd, $J = 10.5, 8.0$ Hz, 1H, NCH), 3.23 (dd, $J = 10.5, 10.5$ Hz, NCH), 2.28-1.80 (m, 6H, CH), 1.50 (s, 9H, CMe₃); ¹³C NMR (100.6 MHz, CDCl₃) δ 158.6 (C=O), 142.7 (*ipso*-Ph), 128.5 (Ph), 127.95 (Ph), 127.93 (Ph), 124.8 (=CH), 123.6 (=CH), 81.0 (CMe₃), 75.7 (PCHO), 74.9 (NCH), 52.5 (NCH₂), 37.2 (CH), 33.7 (CH), 28.6 (CMe₃), 24.1 (CH₂), 20.7 (CH₂); HRMS (ESI) m/z calcd for C₂₀H₂₇NO₃ (M + Na)⁺ 352.1883, found 352.1881 (+0.4 ppm error).

Lab Book Reference: AMI_51

1,1,1-Triacetoxy-1,1-dihydro-1,2-benziodoxol-3(1H)-one **239**



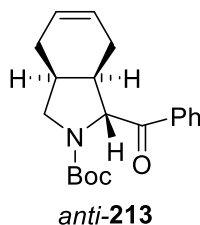
239

2-Iodobenzoic acid (10.00 g, 40.32 mmol, 1.0 eq.) was added in one portion to a solution of Oxone (37.18 g, 129.96 mmol, 3.0 eq.) in deionised water (200 mL). The resulting mixture was warmed to 70 °C over 20 min and mechanically stirred at this temperature for 3 h. The resulting suspension was cooled to 0 °C and maintained at this temperature for 1.5 h with slow stirring. The mixture was filtered through a sintered glass funnel and the collected solids were washed with water (6 x 40 mL) and acetone (2 x 40 mL) and then dried by suction to give intermediate IBX (9.12 g, 80%) as a white solid.

Acetic acid (10.49 g, 174.69 mmol, 8.7 eq., 10 mL) and acetic anhydride (20.56 g, 201.37 mmol, 10.0 eq., 19 mL) were added to IBX (3.49 g, 20.16 mmol, 1.0 eq.). The resulting suspension was stirred under Ar and heated at 85 °C for 30 min until all of the solids had dissolved. Heating and stirring were discontinued and the solution was allowed to cool to rt over 24 h. The solution of excess reagents was removed from the solid precipitate by cannula transfer under Ar. Et₂O (20 mL) was then added and the solids were washed by swirling followed by removal of the solvent by cannula transfer under Ar. This process was repeated with Et₂O (3 x 20 mL). The resulting solid was dried *in vacuo* to give Dess-Martin periodinane **239** (3.62 g, 70%) as a white solid, ¹H NMR (400 MHz, CDCl₃) δ 8.30 (dd, *J* = 7.5, 1.5 Hz, 1H, Ar), 8.28 (d, *J* = 7.5 Hz, 1H, Ar), 8.07 (ddd, *J* = 7.5, 7.5, 1.5 Hz, 1H, Ar), 7.90 (dd, *J* = 7.5, 7.5 Hz, 1H, Ar), 2.32 (s, 1H, COCH₃), 1.99 (s, 6H, COCH₃); ¹³C NMR (100.6 MHz, CDCl₃) δ 175.9 (C=O, COCH₃), 174.2 (C=O, COCH₃), 166.3 (C=O, ArCO), 142.4 (Ar), 135.9 (Ar), 133.9 (Ar), 131.9 (Ar), 126.6 (Ar), 129.1 (Ar), 20.5 (COCH₃), 20.4 (COCH₃). Spectroscopic data consistent with those reported in the literature.¹⁵⁵

Lab Book Reference: AMI_104

tert*-Butyl-(1*R**,3*aS**,7*aR**)-1-benzoyl-2,3,3*a*,4,7,7*a*-hexahydro-1*H*-isoindole-2-carboxylate *anti*-**213*

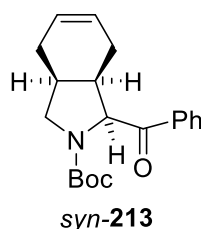


Using general procedure D, 2,3,4-trisubstituted *N*-Boc pyrrolidine *anti-syn*-**214** (82 mg, 0.248 mmol, 1.0 eq.) and DMP (116 mg, 0.272 mmol, 1.1 eq.) gave the crude product. Purification by flash column chromatography on silica using 90:10 hexane-EtOAc as eluent gave ketone *anti*-**213** (63 mg, 77%) as a colourless oil, *R_F* (98:2 CH₂Cl₂-acetone) 0.19; IR (ATR) 2975, 2930, 1686 (C=O), 1391, 1365, 1220, 1165, 1125, 1003, 696, 660 cm⁻¹; ¹H NMR (400 MHz, CDCl₃) (60:40 mixture of rotamers) δ 7.97-7.93 (m, 2H, Ph), 7.58-7.43 (m, 3H, Ph), 5.67 (m, 2H, =CH), 5.07 (d, *J* = 2.5 Hz, 0.4H, NCH), 4.89 (d, *J* = 5.0 Hz, 0.6H, NCH), 3.79 (dd, *J* = 10.5, 6.5 Hz, 0.6H, NCH), 3.74 (dd, *J* = 10.5, 7.5 Hz, 0.4H, NCH), 3.33 (dd, *J* = 10.5, 6.5 Hz, 0.6H, NCH), 3.22 (dd, *J* = 10.5, 6.5, 0.4H, NCH), 2.53-1.95 (m, 6H, CH), 1.46 (s, 3.6H, CMe₃), 1.22 (s, 5.4H, CMe₃); ¹³C NMR (100.6 MHz, CDCl₃) (rotamers)

δ 198.9 (PhC=O), 197.9 (PhC=O), 155.1 (C=O, Boc), 154.4 (C=O, Boc), 135.9 (*ipso*-Ph), 135.6 (*ipso*-Ph), 133.38 (Ph), 133.35 (Ph), 128.9 (Ph), 128.8 (Ph), 128.5 (Ph), 128.3 (Ph), 125.2 (=CH), 124.8 (=CH), 124.0 (=CH), 123.6 (=CH), 80.1 (CMe₃), 79.9 (CMe₃), 67.5 (NCH), 66.8 (NCH), 51.1 (NCH₂), 50.7 (NCH₂), 40.0 (CH), 38.5 (CH), 32.7 (CH), 32.3 (CH), 28.6 (CMe₃), 28.3 (CMe₃), 25.5 (CH₂), 25.1 (CH₂), 24.6 (CH₂), 24.2 (CH₂); HRMS (ESI) m/z calcd for C₂₀H₂₅NO₃ (M + Na)⁺ 350.1727, found 350.1735 (-2.7 ppm error).

Lab Book Reference: AMI_55

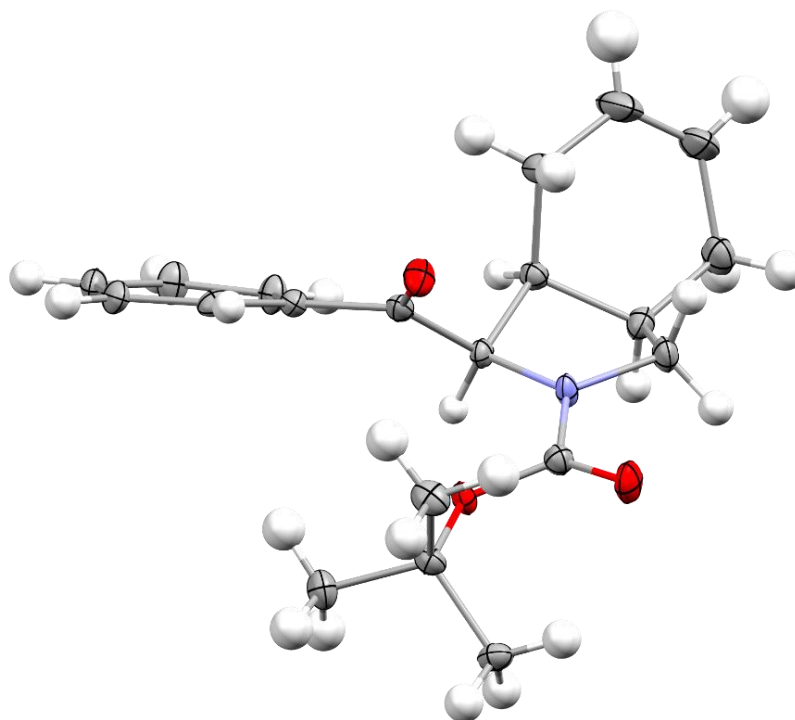
tert*-Butyl-(1*S**,3*aS**,7*aR**)-1-benzoyl-2,3,3*a*,4,7,7*a*-hexahydro-1*H*-isoindole-2-carboxylate *syn*-**213*



Using general procedure D, 2,3,4-trisubstituted *N*-Boc pyrrolidine *syn-anti*-**214** (32 mg, 0.096 mmol, 1.0 eq.) and DMP (45 mg, 0.106 mmol, 1.1 eq.) gave the crude product. Purification by flash column chromatography on silica using 90:10 hexane-EtOAc as eluent gave ketone *syn*-**213** (19 mg, 60%) as a colourless oil, R_F (98:2 CH₂Cl₂-acetone) 0.19; IR (CHCl₃) 2991, 2931, 1697 (C=O), 1406, 1366, 1216, 1168, 1123, 921 cm⁻¹; ¹H NMR (400 MHz, CDCl₃) (60:40 mixture of rotamers) δ 8.00 (d, J = 7.0 Hz, 0.8H, Ph), 7.95 (d, J = 7.5 Hz, 1.2H, Ph), 7.57-7.41 (m, 3H, Ph), 5.60-5.47 (m, 2H, =CH), 5.39 (d, J = 6.5 Hz, 0.4H, NCH), 5.32 (d, J = 6.5 Hz, 0.6H, NCH), 3.76 (dd, J = 10.5, 7.5 Hz, 0.6H, NCH), 3.69 (dd, J = 10.5, 7.5 Hz, 0.4H, NCH), 3.32-3.24 (m, 1H, NCH), 2.70-1.93 (m, 6H, CH), 1.46 (s, 3.6H, CMe₃), 1.22 (s, 5.4H, CMe₃); ¹³C NMR (100.6 MHz, CDCl₃) (rotamers) δ 196.3 (PhC=O), 171.4 (C=O, Boc), 136.9 (*ipso*-Ph), 133.2 (Ph), 128.8 (Ph), 128.7 (Ph), 128.3 (Ph), 127.9 (Ph), 124.6 (=CH), 124.3 (=CH), 124.1 (=CH), 123.9 (=CH), 80.1 (CMe₃), 79.9 (CMe₃), 66.4 (NCH), 66.2 (NCH), 50.7 (NCH₂), 50.2 (NCH₂), 38.0 (CH), 37.20 (CH), 35.6 (CH), 35.0 (CH), 28.6 (CMe₃), 28.3 (CMe₃), 24.22 (CH₂), 24.20 (CH₂), 21.5 (CH₂), 21.4 (CH₂); HRMS (ESI) m/z calcd for C₂₀H₂₅NO₃ (M + Na)⁺ 350.1727, found 350.1723 (+0.9 ppm error).

Lab Book Reference: AMI_53

***tert*-Butyl-(1*S**,3*aS**,7*aR**)-1-benzoyl-2,3,3*a*,4,7,7*a*-hexahydro-1*H*-isoindole-2-carboxylate *syn*-213**

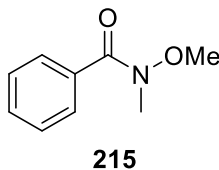


Crystal data and structure refinement for *syn*-213

Identification code	paob1607
Empirical formula	C ₂₀ H ₂₅ NO ₃
Formula weight	327.41
Temperature/K	110.05(10)
Crystal system	orthorhombic
Space group	Pca2 ₁
<i>a</i> /Å	20.5730(4)
<i>b</i> /Å	5.66784(12)
<i>c</i> /Å	29.8066(6)
α /°	90.0
β /°	90.0
γ /°	90.0
Volume/Å ³	3475.58(12)
<i>Z</i>	8
ρ_{calc} /cm ³	1.251
μ /mm ⁻¹	0.667
<i>F</i> (000)	1408.0
Crystal size/mm ³	0.294 × 0.181 × 0.129
Radiation	CuK α (λ = 1.54184)
2 θ range for data collection/°	8.596 to 142.212
Index ranges	-24 ≤ <i>h</i> ≤ 25, -6 ≤ <i>k</i> ≤ 6, -34 ≤ <i>l</i> ≤ 36
Reflections collected	7620
Independent reflections	4991 [<i>R</i> _{int} = 0.0208, <i>R</i> _{sigma} = 0.0310]

Data/restraints/parameters	4991/1/439
Goodness-of-fit on F^2	1.035
Final R indexes [$I \geq 2\sigma(I)$]	$R_1 = 0.0366$, $wR_2 = 0.0867$
Final R indexes [all data]	$R_1 = 0.0431$, $wR_2 = 0.0920$
Largest diff. peak/hole / $e \text{ \AA}^{-3}$	0.23/-0.22
Flack parameter	0.68(19)

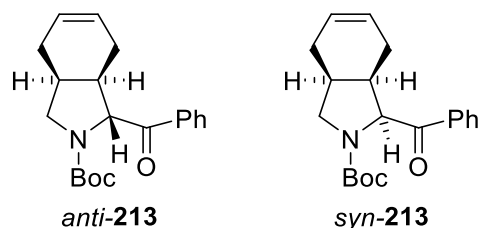
N*-Methoxy-*N*-methylbenzamide **215*



Benzoyl chloride (5.0 g, 35.6 mmol, 4.13 mL, 1.0 eq.) was added to a stirred solution of *N,O*-dimethylhydroxylamine hydrochloride (3.47 g, 35.6 mmol, 1.0 eq.) and Et_3N (10.81 g, 107 mmol, 14.9 mL, 3.0 eq.) in CH_2Cl_2 (150 mL) at rt under Ar. The resulting solution was stirred at rt for 2 h. Then, saturated $\text{NH}_4\text{Cl}_{(\text{aq})}$ (20 mL) and saturated $\text{NaHCO}_{3(\text{aq})}$ (20 mL) were added. The two layers were separated and the aqueous layer was extracted with CH_2Cl_2 (2 x 50 mL). The combined organic layers were dried (MgSO_4), filtered and evaporated under reduced pressure to give the crude product. Purification by flash column chromatography on silica with 4:1 hexane-EtOAc as eluent gave Weinreb amide **215** (5.79 g, 99%) as a colourless oil, R_F (4:1 hexane-EtOAc) 0.08; ^1H NMR (400 MHz, CDCl_3) δ 7.69-7.66 (m, 2H, Ph), 7.48-7.37 (m, 3H, Ph), 3.56 (s, 3H, OMe), 3.36 (s, 3H, NMe); ^{13}C NMR (100.6 MHz, CDCl_3) δ 169.8 (C=O), 134.0 (*ipso*-Ph), 130.4 (Ph), 128.0 (Ph), 127.9 (Ph), 60.9 (OMe), 33.7 (NMe). Spectroscopic data consistent with those reported in the literature.¹⁵⁶

Lab Book Reference: AMI_268

(1*S,3*aS**,7*aR**) and (1*R**,3*aS**,7*aR**)-tert-Butyl-1-benzoyl-2,3,3*a*,4,7,7*a*-hexahydro-1*H*-isoindole-2-carboxylate *anti*-**213** and *syn*-**213****

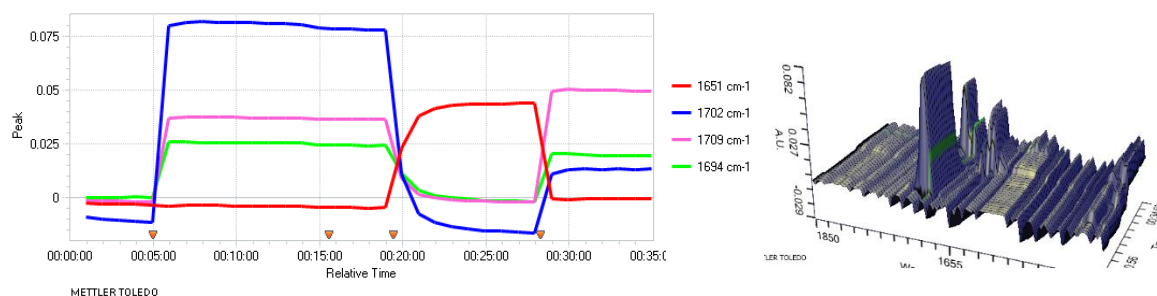


Using general procedure D, an 80:20 mixture of 2,3,4-trisubstituted *N*-Boc pyrrolidines *anti*-**214** and *syn*-**214** (164 mg, 0.498 mmol, 1.0 eq.) and DMP (232 mg, 0.548 mmol, 1.1 eq.) gave the crude product, which contained a 90:10 mixture of *anti*-**213** and *syn*-**213** (by ¹H NMR spectroscopy of *anti*-**213** and *syn*-**213**). Purification by flash column chromatography on silica using 90:10 hexane-EtOAc as eluent gave a 90:10 mixture of ketones *anti*-**213** and *syn*-**213** (117 mg, 72%) as a colourless oil.

Lab Book Reference: AMI_54

Using general procedure A, *s*-BuLi (0.90 mL of a 1.3 M solution in hexanes, 1.17 mmol, 1.3 eq.), *N*-Boc pyrrolidine **96** (201 mg, 0.90 mmol, 1.0 eq.) and TMEDA (136 mg, 1.17 mmol, 0.18 mL, 1.3 eq.) in Et₂O (7mL) for 10 min and then Weinreb amide **215** (297 mg, 1.80 mmol, 274 μL, 2.0 eq.) gave the crude product, which contained an 87:13 mixture (by ¹H NMR spectroscopy) of ketones *anti*-**213** and *syn*-**213**. Purification by flash column chromatography on silica using 85:15 hexane-EtOAc as eluent gave ketone *anti*-**213** (197 mg, 67%) as a colourless oil and ketone *syn*-**213** (19 mg, 6%) as a pale yellow solid.

Lab Book Reference: AMI_270

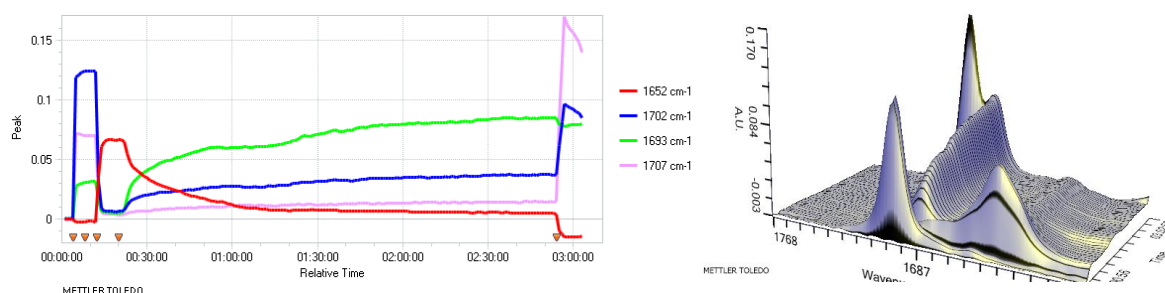
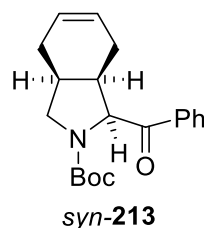
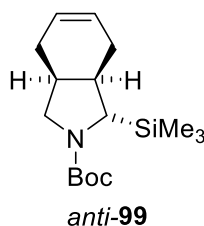


Et₂O (12 mL) was added to a flask equipped with a stirrer bar and ReactIRTM probe (iC 10, DiComp) at rt under Ar. After cooling to -78 °C, *N*-Boc pyrrolidine **96** (224 mg, 1.00 mmol, 1.0 eq.) was added followed by TMEDA (150 mg, 1.30 mmol, 1.3 eq., 0.20 mL). The solution was stirred for 5 min (to verify the stability of readout on ReactIRTM). Then, *s*-BuLi (1.0 mL of a 1.3 M solution in hexanes, 1.30 mmol, 1.3 eq.) was added. The resulting solution was stirred at -78 °C for 10 min. Then, PhCHO (211 mg, 0.20 mL, 2.00 mmol, 2.0 eq.) was added and the solution was stirred at -78 °C for a further 15 min. Saturated NH₄Cl(aq) (10 mL) was added and the solution was then allowed to warm to rt over 30 min and the two layers were separated. The aqueous layer was extracted with Et₂O (3 x 10 mL) and the combined organics were dried (MgSO₄), filtered and evaporated under reduced pressure to give the crude product. Using general procedure D, the crude product and DMP (840 mg, 1.98 mmol, 2.0 eq.) in CH₂Cl₂ (10 mL) gave the crude product, which contained an 87:13 mixture (by ¹H NMR spectroscopy) of ketones *anti*-**213** and *syn*-**213**. Purification by flash column chromatography on silica using 98:2 CH₂Cl₂:acetone as eluent gave an 87:13 mixture (by ¹H NMR spectroscopy) of ketones *anti*-**213** and *syn*-**213** (254 mg, 78%) as a colourless oil.

For *N*-Boc pyrrolidine **96**, a peak at 1702 cm⁻¹ was observed and assigned to $\nu_{C=O}$. After addition of *s*-BuLi, a new peak at 1651 cm⁻¹ was observed which was assigned to $\nu_{C=O}$ in the lithiated intermediate. After a lithiation time of 4 min, complete lithiation of *N*-Boc pyrrolidine **96** to give the lithiated intermediate was observed and complete trapping was observed after 1 min. When PhCHO was added (after a 10 min total lithiation time), the signal for the lithiated intermediate ($\nu_{C=O} = 1651$ cm⁻¹) disappeared after 1 min, indicating complete trapping had occurred. During the trapping process, another peak appeared at 1709 cm⁻¹ which was assigned to the trapped adduct **214**.

Lab Book Reference: AMI_95

(1*S,3*aS**,7*aR**)-tert-Butyl 1-(trimethylsilyl)-3*a*,4,7,7*a*-tetrahydro-1*H*-isoindole-2(3*H*)-carboxylate *anti*-**99** and (1*S**,3*aS**,7*aR**)-tert-Butyl 1-benzoyl-3*a*,4,7,7*a*-tetrahydro-1*H*-isoindole-2(3*H*)-carboxylate *syn*-**213****



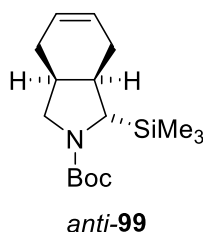
Et₂O (12 mL) was added to a flask equipped with a stirrer bar and ReactIRTM probe (iC 10, DiComp) at rt under Ar. After cooling to -78 °C, a solution of *N*-Boc pyrrolidine **96** (231 mg, 1.04 mmol, 1.0 eq.) in Et₂O (2 mL) was added followed by TMEDA (156 mg, 1.35 mmol, 1.3 eq., 0.20 mL). The solution was stirred for 5 min (to verify the stability of readout on ReactIR[®]). Then *s*-BuLi (1.0 mL of a 1.3 M solution in hexanes, 1.35 mmol, 1.3 eq.) was added dropwise. The resulting solution was stirred at -78 °C for 10 min. Then, Me₃SiCl (225 mg, 2.07 mmol, 2.0 eq., 0.26 mL) was added and the solution was stirred at -78 °C for 2.5 h. PhCHO (220 mg, 2.07 mmol, 2.0 eq., 0.21 mL) was also added and the solution was stirred for a further 10 min at -78 °C. Then, saturated NH₄Cl_(aq) (10 mL) was added and the two layers were separated. The aqueous layers was extracted with Et₂O (3 x 10 mL) and the combined organics were dried (MgSO₄), filtered and evaporated under reduced pressure to give the crude product. Using general procedure D, the crude product and DMP (484 mg, 1.08 mmol, 1.0 eq.) gave the crude product, which contained an 86:14 mixture (by ¹H NMR spectroscopy) of *anti*-**99** and *syn*-**213**. Purification by flash column chromatography on silica using 90:10 hexane-EtOAc as eluent gave 2-silyl pyrrolidine *anti*-**99** (164 mg, 53%) as a colourless oil and ketone *syn*-**213** as a pale yellow solid (35 mg, 10%).

For *N*-Boc pyrrolidine **96**, a peak at 1702 cm⁻¹ was observed and assigned to ν_{C=O}. After addition of *s*-BuLi, a new peak at 1652 cm⁻¹ was observed which was assigned to ν_{C=O} in the

lithiated intermediate. After a lithiation time of 4 min, complete lithiation of *N*-Boc pyrrolidine **96** to give the lithiated intermediate was observed. When Me₃SiCl was added (after a 10 min total lithiation time), the signal for the lithiated intermediate ($\nu_{\text{C=O}} = 1652 \text{ cm}^{-1}$) decreased slowly and then plateaued after 2.5 h. During this time, a signal for the Me₃SiCl-trapped adduct *anti*-**99** ($\nu_{\text{C=O}} = 1693 \text{ cm}^{-1}$) appeared and increased in intensity over the 2.5 h then plateaued. When PhCHO was added (after the 2.5 h Me₃SiCl trapping), the signal for the lithiated intermediate ($\nu_{\text{C=O}} = 1652 \text{ cm}^{-1}$) disappeared after 1 min and a new peak for the PhCHO-trapped product *anti*-**214** ($\nu_{\text{C=O}} = 1707 \text{ cm}^{-1}$) was observed, indicating that complete trapping had occurred.

Lab Book Reference: AMI_114

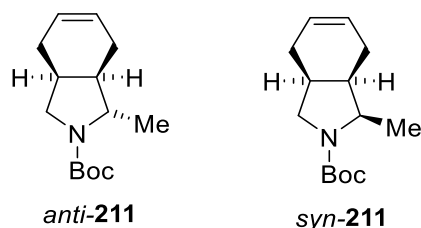
tert*-Butyl (1*S**, 3*aS**, 7*aR**)-1-(trimethylsilyl)-2,3,3*a*,4,7,7*a*-hexahydro-1*H*-isoindole-2-carboxylate *anti*-**99*



Using general procedure B, *s*-BuLi (1.1 mL of a 1.3 M solution in hexanes, 1.43 mmol, 1.3 eq.), *N*-Boc pyrrolidine **96** (246 mg, 1.10 mmol, 1.0 eq.) and TMEDA (166 mg, 1.43 mmol, 1.3 eq.) in Et₂O (7 mL) for 2 min and then Me₃SiCl (239 mg, 0.28 mL, 2.20 mmol, 2.0 eq.) gave the crude product. Purification by flash column chromatography on silica using 90:10 hexane-EtOAc as eluent gave a single diastereomer of 2,3,4-trisubstituted pyrrolidine *anti*-**99** (210 mg, 64%) as a colourless oil.

Lab Book Reference: AMI_59

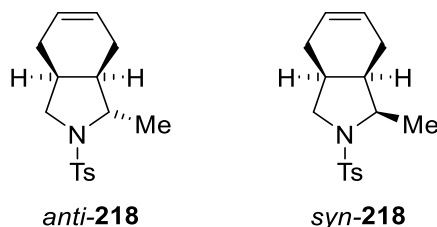
(1*S,3*aS**,7*aR**) and (1*R**,3*aS**,7*aR**)-tert-Butyl-1-methyl-2,3,3*a*,4,7,7*a*-hexahydro-1*H*-isoindole-2-carboxylate *anti*-**211** and *syn*-**211****



Using general procedure B, *s*-BuLi (1.0 mL of a 1.3 M solution in hexanes, 1.35 mmol, 1.3 eq.), *N*-Boc pyrrolidine **96** (232 mg, 1.04 mmol, 1.0 eq.) and TMEDA (157 mg, 1.35 mmol, 1.3 eq.) in Et₂O (7 mL) for 2 min and then Me₂SO₄ (261 mg, 0.20 mL, 2.07 mmol, 2.0 eq.) gave the crude product. Purification by flash column chromatography on silica using 85:15 hexane-EtOAc as eluent gave a 70:30 mixture (by ¹H NMR spectroscopy of sulfonamides *anti*-**218** and *syn*-**218**) of 2,3,4-trisubstituted pyrrolidines *anti*-**211** and *syn*-**211** (161 mg, 65%) as a colourless oil.

Lab Book Reference: AMI_61

(1*S,3*aS**,7*aR**) and (1*R**,3*aS**,7*aR**)-1-Methyl-2-(4-methylbenzenesulfonyl)-2,3,3*a*,4,7,7*a*-hexahydro-1*H*-isoindole *anti*-**218** and *syn*-**218****

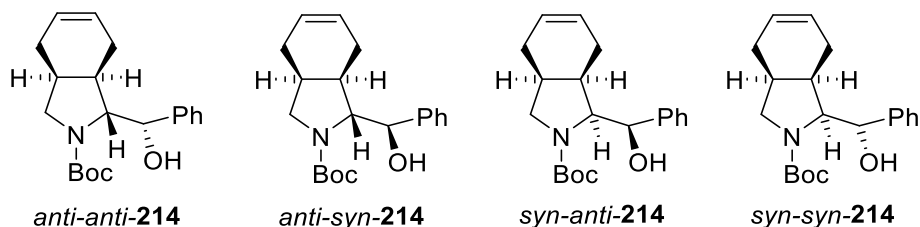


TFA (469 mg, 0.32 mL, 4.12 mmol, 10 eq.) was added to a stirred solution of 2,3,4-trisubstituted pyrrolidine **211** (98 mg, 0.412 mmol, 1.0 eq.) in CH₂Cl₂ (7 mL) at rt under Ar. The resulting solution was stirred at rt for 16 h. Then, saturated NaHCO_{3(aq)} (20 mL) was added with vigorous stirring until gas evolution ceased. The mixture was extracted with CH₂Cl₂ (3 x 10 mL) and the combined organics were dried (Na₂SO₄), filtered and evaporated under reduced pressure. The residue was dissolved in CH₂Cl₂ (4 mL) and Et₃N (51 mg, 0.07 mL, 0.494 mmol, 1.2 eq.) and *p*-TsCl (108 mg, 0.57 mmol, 1.2 eq.) were added. The resulting solution was stirred at rt for 16 h. Then, CH₂Cl₂ (10 mL) and 0.1 M HCl_(aq) (10 mL) were added and the two layers were separated. The aqueous layer was extracted with CH₂Cl₂ (3 x

10 mL) and the combined organics were dried (MgSO₄), filtered and evaporated under reduced pressure to give the crude product, which contained a 70:30 mixture (by ¹H NMR spectroscopy) of *anti*-**218** and *syn*-**218**. Purification by flash column chromatography on silica using 85:15 hexane-EtOAc as eluent gave a 70:30 mixture of sulfonamides *anti*-**218** and *syn*-**218** (44 mg, 37%) as a white solid.

Lab Book Reference: AMI_62

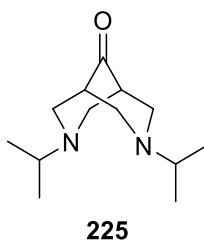
(1*R,3*aS**,7*aR**)** and **(1*S**,3*aS**,7*aR**)**-*tert*-Butyl-1-[(*S*) and (*R*)-hydroxy(phenyl)methyl]-2,3,3*a*,4,7,7*a*-hexahydro-1*H*-isoindole-2-carboxylate *anti*-*anti*-**214**, *anti*-*syn*-**214**, *syn*-*anti*-**214** and *syn*-*syn*-**214**



Using general procedure B, *s*-BuLi (1.0 mL of a 1.3 M solution in hexanes, 1.3 mmol, 1.3 eq.), *N*-Boc pyrrolidine **96** (222 mg, 0.993 mmol, 1.0 eq.), TMEDA (150 mg, 0.19 mL, 1.29 mmol, 1.3 eq.) in Et₂O (7 mL) and then PhCHO (210 mg, 0.20 mL, 2.0 mmol, 2.0 eq.) gave the crude product, which contained a 25:25:25:25 mixture (by ¹H NMR spectroscopy) of *anti*-*anti*-**214**, *anti*-*syn*-**214**, *syn*-*anti*-**214**, *syn*-*syn*-**214**. Purification by flash column chromatography on silica using 99:1 CH₂Cl₂-Acetone as eluent gave a 50:50 mixture of pyrrolidines *anti*-*anti*-**214** and *syn*-*syn*-**214** (88 mg, 27%) as a colourless oil, pyrrolidine *anti*-*syn*-**214** (54 mg, 17%) as a colourless oil and pyrrolidine *syn*-*anti*-**214** (74 mg, 23%) as a pale yellow solid.

Lab Book Reference: AMI_60

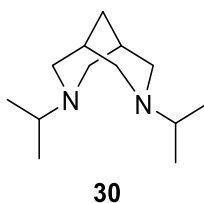
3,7-Bis(propan-2-yl)-3,7-diazabicyclo[3.3.1]nonan-9-one **225**



i-PrNH₂ (6.1 mL, 71.0 mmol, 1.0 eq.) was added dropwise to a stirred solution of *N*-*i*-Pr-4-piperidone (10.6 mL, 71.0 mmol, 1.0 eq.), paraformaldehyde (6.40 g, 213 mmol 3.0 eq.) and AcOH (4.23 mL, 75.3 mmol, 1.05 eq.) in MeOH (100 mL) at rt under Ar. The resulting solution was stirred and heated at reflux for 16 h. The solvent was evaporated under reduced pressure. Then, 50% KOH_(aq) (250 mL) and Et₂O (250 mL) were added to the residue and the layers were separated. The aqueous layer was extracted with Et₂O (2 x 250 mL) and the combined organic layers were dried (Na₂SO₄), filtered and evaporated under reduced pressure to give the crude product. Purification by fractional distillation gave bispidone **225** (6.52 g, 41%) as a colourless oil, bp 116-130 °C/2.5 mmHg (lit.,¹⁵⁷ bp 110-120 °C/10⁻⁵ mmHg); ¹H NMR (400 MHz, DMSO-*d*₆) δ 2.96 (dd, *J* = 10.5, 3.0 Hz, 4H, NCH), 2.81-2.73 (m, 6H, NCH), 2.48-2.41 (m, 2H, COCH), 0.95 (d, *J* = 6.5 Hz, 12H, NCHMe₂). Spectroscopic data consistent with those reported in the literature.¹⁵⁷

Lab Book Reference: AMI_26

3,7-Bis(propan-2-yl)-3,7-diazabicyclo[3.3.1]nonane **30**

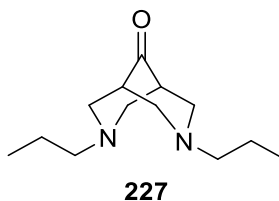


Hydrazine monohydrate (2.65 mL, 54.5 mmol, 5.6 eq.) was added dropwise to a stirred mixture of bispidone **225** (2.18 g, 9.74 mmol) and KOH (6.39 g, 113.4 mmol, 11.7 eq.) in diethylene glycol (60 mL) at rt under Ar. The resulting mixture was stirred and heated at 180 °C for 16 h. After cooling to 60 °C, the mixture was transferred to a separating funnel and H₂O (80 mL) was added. Then Et₂O (50 mL) was added and the layers were separated. The aqueous layer was extracted with Et₂O (6 x 50 mL) and the combined organic layers were washed with NaOH_(aq) (6 x 50 mL), dried (Na₂SO₄), filtered and evaporated under reduced

pressure to give the crude product. Purification by distillation gave di-*i*-Pr bispidine **30** (1.87 g, 91%) as a colourless oil, bp 120-130 °C/3.5 mmHg; ¹H NMR (400 MHz, DMSO-*d*₆) δ 2.62-2.54 (m, 2H, NCH), 2.49-2.41 (m, 8H, NCH), 1.94-1.86 (m, 2H, NCH₂CH), 1.41-1.35 (m, 2H, bridge CH₂), 0.93 (d, *J* = 6.5 Hz, 12H, NCHMe₂). Spectroscopic data consistent with those reported in the literature.¹⁵⁸

Lab Book Reference: AMI_32

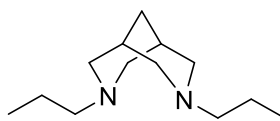
3,7-Dipropyl-3,7-diazabicyclo[3.3.1]nonan-9-one **227**



n-PrNH₂ (5.83 mL, 70.81 mmol, 1.0 eq.) was added dropwise to a stirred solution of *N-n*-Pr-4-piperidone (10.7 mL, 35.5 mmol), paraformaldehyde (6.38 g, 212.4 mmol, 3.0 eq.) and AcOH (4.2 mL, 73.8 mmol, 1.04 eq.) in MeOH (100 mL) at rt under Ar. The resulting solution was stirred and heated at reflux for 16 h. The solvent was evaporated under reduced pressure. Then, 50% KOH_(aq) solution (250 mL) and Et₂O (250 mL) were added to the residue and the layers were separated. The aqueous layer was extracted with Et₂O (2 x 250 mL) and the combined organic layers were dried (Na₂SO₄), filtered and evaporated under reduced pressure to give the crude product. Purification by fractional distillation gave bispidone **227** (6.04 g, 38%) as a colourless oil, bp 115-120 °C/1.0 mmHg; ¹H NMR (400 MHz, DMSO-*d*₆) δ 2.89 (dd, *J* = 11.0, 3.0 Hz, 4H, NCH), 2.67 (dd, *J* = 11.0, 6.0 Hz, 4H, NCH), 2.42 (br s, 2H, COCH), 2.24 (t, *J* = 7.0 Hz, 4H, NCH₂CH₂), 1.41-1.32 (m, 4H, NCH₂CH₂), 0.82 (t, *J* = 7.5 Hz, 6H, Me). Spectroscopic data consistent with those reported in the literature.¹³⁸

Lab Book Reference: AMI_33

3,7-Dipropyl-3,7-diazabicyclo[3.3.1]nonane **105**

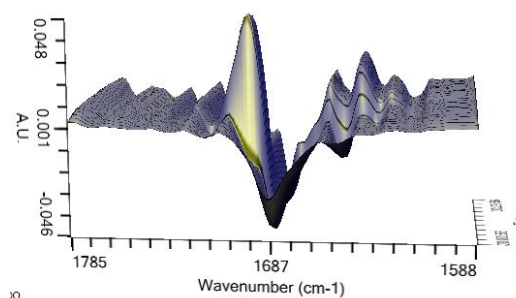
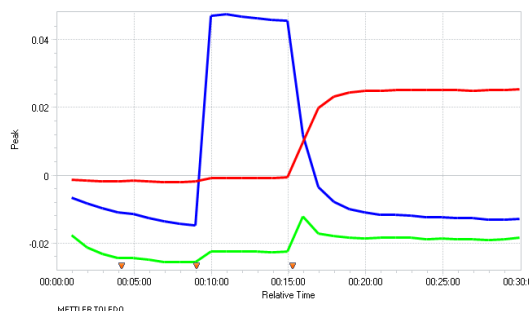
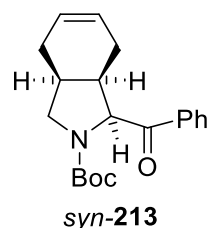
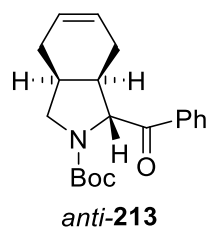


105

Hydrazine monohydrate (4.2 mL, 86.15 mmol, 5.5 eq.) was added dropwise to a stirred mixture of bispidone **227** (3.51 g, 15.66 mmol) and KOH (10.11 g, 180.13 mmol, 11.5 eq.) in diethylene glycol (90 mL) at rt under Ar. The resulting mixture was stirred and heated at 180 °C for 16 h. After cooling to 60 °C, the mixture was transferred to a separating funnel and H₂O (80 mL) was added. Then Et₂O (80 mL) was added and the layers were separated. The aqueous layer was extracted with Et₂O (6 x 60 mL) and the combined organic layers were washed with 20% NaOH_(aq) (6 x 90 mL), dried (Na₂SO₄), filtered and evaporated under reduced pressure to give the crude product. Purification by distillation gave di-*n*-Pr bispidine **105** (3.51 g, 95%) as a colourless oil, bp 105-115 °C/1.0 mmHg, ¹H NMR (400 MHz, DMSO-*d*₆) δ 2.57 (br d, *J* = 10.5 Hz, 4H, NCH), 2.19 (dd, *J* = 10.5, 4.5 Hz, 4H, NCH), 2.09 (t, *J* = 7.0 Hz, 4H, NCH₂CH₂), 1.84 (br s, 2H, NCH₂CH), 1.40-1.29 (m, 6H, NCH₂CH₂ + bridge CH₂), 0.81 (t, *J* = 7.5 Hz, 6H, Me). Spectroscopic data consistent with those reported in the literature.¹³⁸

Lab Book Reference: AMI_37

(1*R,3*aS**,7*aR**) and (1*S**,3*aS**,7*aR**) *tert*-Butyl -1-benzoyl-2,3,3*a*,4,7,7*a*-hexahydro-1*H*-isoindole-2-carboxylate *anti*-213 and *syn*-213**

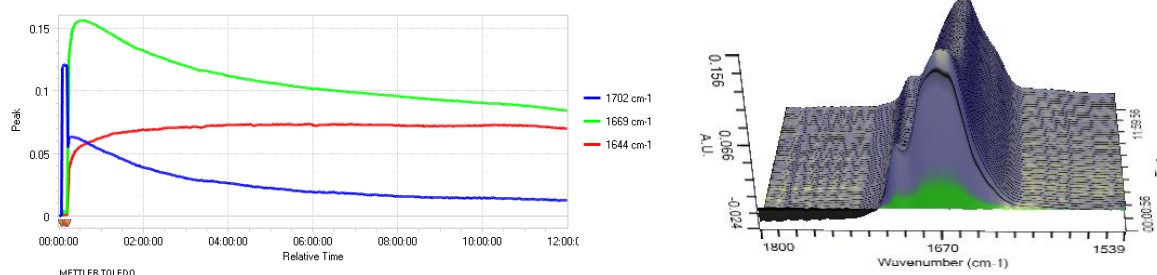


Et₂O (10 mL) was added to a flask equipped with a stirrer bar and ReactIR™ probe (iC 10, SiComp) at rt under Ar. After cooling to -78 °C, a solution of *N*-Boc pyrrolidine **96** (222 mg, 1.00 mmol, 1.0 eq.) in Et₂O (2 mL) was added followed by a solution of TMCDA *trans*-**161** (186 mg, 1.29 mmol, 1.3 eq.) in Et₂O (2 mL). The solution was stirred for 5 min (to verify the stability of readout on ReactIR™). Then, *s*-BuLi (1.0 mL of a 1.3 M solution in hexanes, 1.30 mmol, 1.3 eq.) was added. The resulting solution was stirred at -78 °C for 15 min. Then, PhCHO (211 mg, 0.20 mL, 2.00 mmol, 2.0 eq.) was added and the solution was stirred at -78 °C for a further 15 min. Saturated NH₄Cl_(aq) (10 mL) was added and the solution was then allowed to warm to rt over 30 min and the two layers were separated. The aqueous layer was extracted with Et₂O (3 x 10 mL) and the combined organics were dried (MgSO₄), filtered and evaporated under reduced pressure to give the crude product. Using general procedure D, the crude product and DMP (632 mg, 1.49 mmol, 1.5 eq.) in CH₂Cl₂ (10 mL) gave the crude product, which contained an 87:13 mixture (by ¹H NMR spectroscopy) of ketones *anti*-213 and *syn*-213. Purification by flash column chromatography on silica using 98:2 CH₂Cl₂-acetone as eluent gave an 87:13 mixture (by ¹H NMR spectroscopy) of ketones *anti*-213 and *syn*-213 (246 mg, 76%) as a colourless oil.

For *N*-Boc pyrrolidine **96**, a peak at 1701 cm⁻¹ was observed and assigned to ν_{C=O}. After addition of *s*-BuLi, a new peak at 1678 cm⁻¹ was observed which was assigned to ν_{C=O} in the prelithiation complex. A new peak at 1645 cm⁻¹ was also observed and this was assigned to

the lithiated intermediate. After a lithiation time of 4 min, complete lithiation of *N*-Boc pyrrolidine **96** to give the lithiated intermediate was observed. The PhCHO trapping was not monitored by ReactIR™.

Lab Book Reference: AMI_73 + AMI_75

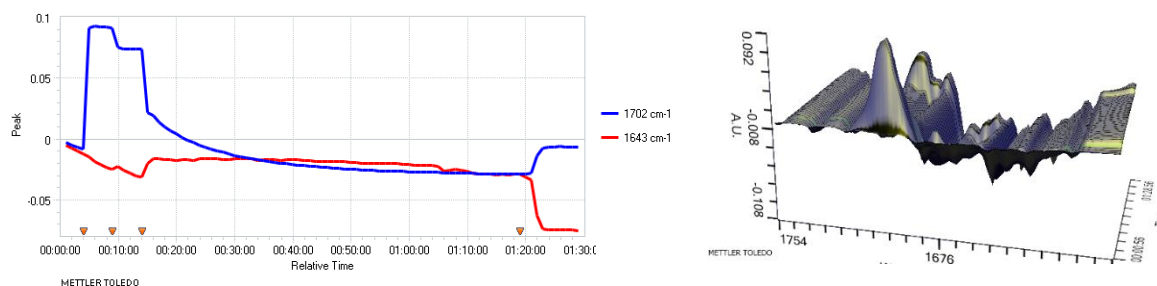


Et₂O (12 mL) was added to a flask equipped with a stirrer bar and ReactIR™ probe (iC 10, DiComp) at rt under Ar. After cooling to -78 °C, *N*-Boc pyrrolidine **96** (224 mg, 1.00 mmol, 1.0 eq.) was added followed by TMPDA **179** (170 mg, 0.22 mL, 1.30 mmol, 1.3 eq.). The solution was stirred for 5 min (to verify the stability of readout on ReactIR™). Then, *s*-BuLi (1.0 mL of a 1.3 M solution in hexanes, 1.30 mmol, 1.3 eq.) was added. The resulting solution was stirred at -78 °C for 12 h. Then, PhCHO (211 mg, 0.20 mL, 2.00 mmol, 2.0 eq.) was added and the solution was stirred at -78 °C for a further 15 min. Saturated NH₄Cl_(aq) (10 mL) was added and the solution was then allowed to warm to rt over 30 min and the two layers were separated. The aqueous layer was extracted with Et₂O (3 x 10 mL) and the combined organics were dried (MgSO₄), filtered and evaporated under reduced pressure to give the crude product. Using general procedure D, the crude product and DMP (848 mg, 2.0 mmol, 2.0 eq.) in CH₂Cl₂ (10 mL) gave the crude product, which contained an 80:20 mixture (by ¹H NMR spectroscopy) of ketones *anti*-**213** and *syn*-**213**. Purification by flash column chromatography on silica using 98:2 CH₂Cl₂-acetone as eluent gave an 80:20 mixture (by ¹H NMR spectroscopy) of ketones *anti*-**213** and *syn*-**213** (221 mg, 67%) as a colourless oil.

For *N*-Boc pyrrolidine **96**, a peak at 1702 cm⁻¹ was observed and assigned to ν_{C=O}. After addition of *s*-BuLi, a new peak at 1644 cm⁻¹ was observed which was assigned to ν_{C=O} in the lithiated intermediate. After a lithiation time of 9 h, complete lithiation of *N*-Boc pyrrolidine

96 to give the lithiated intermediate was observed. The PhCHO trapping was not monitored by ReactIR™.

Lab Book Reference: AMI_97 + AMI_99

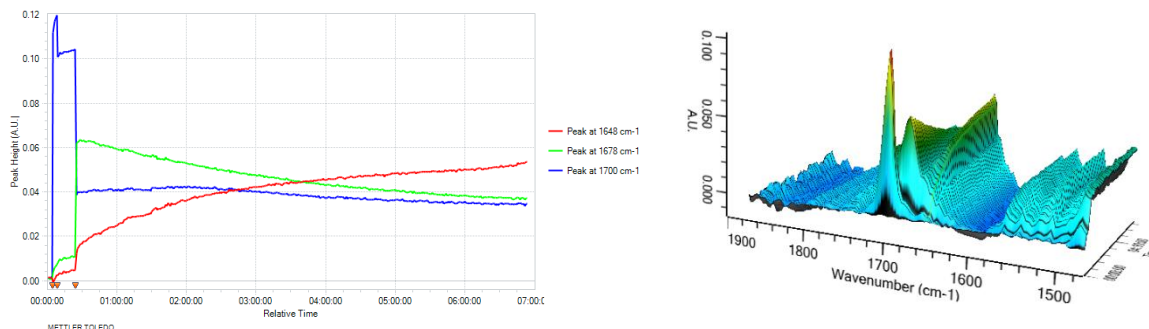


Et₂O (10 mL) was added to a flask equipped with a stirrer bar and ReactIR™ probe (iC 10, DiComp) at rt under Ar. After cooling to -78 °C, a solution of *N*-Boc pyrrolidine **96** (225 mg, 1.01 mmol, 1.0 eq.) in Et₂O (2 mL) was added followed by a solution DPE **177** (221 mg, 1.31 mmol, 1.3 eq.). The solution was stirred for 5 min (to verify the stability of readout on ReactIR™). Then, *s*-BuLi (1.0 mL of a 1.3 M solution in hexanes, 1.30 mmol, 1.3 eq.) was added. The resulting solution was stirred at -78 °C for 1 h. Then, PhCHO (211 mg, 0.20 mL, 2.00 mmol, 2.0 eq.) was added and the solution was stirred at -78 °C for a further 10 min. Saturated NH₄Cl_(aq) (10 mL) was added and the solution was then allowed to warm to rt over 30 min and the two layers were separated. The aqueous layer was extracted with Et₂O (3 x 10 mL) and the combined organics were dried (MgSO₄), filtered and evaporated under reduced pressure to give the crude product. Using general procedure D, the crude product and DMP (857 mg, 2.02 mmol, 2.0 eq.) in CH₂Cl₂ (10 mL) gave the crude product, which contained a 92:8 mixture (by ¹H NMR spectroscopy) of ketones *anti*-**213** and *syn*-**213**. Purification by flash column chromatography on silica using 98:2 CH₂Cl₂-acetone as eluent gave a 92:8 mixture (by ¹H NMR spectroscopy) of ketones *anti*-**213** and *syn*-**213** (286 mg, 86%) as a colourless oil.

For *N*-Boc pyrrolidine **96**, a peak at 1702 cm⁻¹ was observed and assigned to ν_{C=O}. After addition of *s*-BuLi, a new peak at 1643 cm⁻¹ was observed which was assigned to ν_{C=O} in the lithiated intermediate. After a lithiation time of 50 min, complete lithiation of *N*-Boc pyrrolidine **96** to give the lithiated intermediate was observed. When PhCHO was added

(after a 65 min total lithiation time), the signal for the lithiated intermediate ($\nu_{\text{C=O}} = 1643 \text{ cm}^{-1}$) disappeared after 1 min, indicating complete trapping had occurred.

Lab Book Reference: AMI_101 + AMI_102



Et₂O (10 mL) was added to a flask equipped with a stirrer bar and ReactIRTM probe (ReactIRTM 15, DiComp) at rt under Ar. After cooling to $-78 \text{ }^{\circ}\text{C}$, a solution of *N*-Boc pyrrolidine **96** (234 mg, 1.05 mmol, 1.0 eq.) in Et₂O (2 mL) was added followed by a solution tetra-isopropyl diamine **178** (311 mg, 1.36 mmol, 1.3 eq.). The solution was stirred for 5 min (to verify the stability of readout on ReactIRTM). Then, *s*-BuLi (1.1 mL of a 1.3 M solution in hexanes, 1.36 mmol, 1.3 eq.) was added. The resulting solution was stirred at $-78 \text{ }^{\circ}\text{C}$ for 16 h. Then, PhCHO (211 mg, 0.20 mL, 2.00 mmol, 2.0 eq.) was added and the solution was stirred at $-78 \text{ }^{\circ}\text{C}$ for a further 15 min. Saturated NH₄Cl_(aq) (10 mL) was added and the solution was then allowed to warm to rt over 30 min and the two layers were separated. The aqueous layer was extracted with Et₂O (3 x 10 mL) and the combined organics were dried (MgSO₄), filtered and evaporated under reduced pressure to give the crude product. Using general procedure D, the crude product and DMP (891 mg, 2.10 mmol, 2.0 eq.) in CH₂Cl₂ (10 mL) gave the crude product, which contained a >95:5 mixture (by ¹H NMR spectroscopy) of ketones *anti*-**213** and *syn*-**213**. Purification by flash column chromatography on silica using 98:2 CH₂Cl₂-acetone as eluent gave a >95:5 mixture (by ¹H NMR spectroscopy) of ketones *anti*-**213** and *syn*-**213** (54 mg, 16%) as a colourless oil and recovered starting material **96** (146 mg, 62%).

For *N*-Boc pyrrolidine **96**, a peak at 1702 cm^{-1} was observed and assigned to $\nu_{\text{C=O}}$. After addition of *s*-BuLi, a new peak at 1648 cm^{-1} was observed which was assigned to $\nu_{\text{C=O}}$ in the lithiated intermediate. After a lithiation time of 6.5 h, the ReactIRTM apparatus encountered

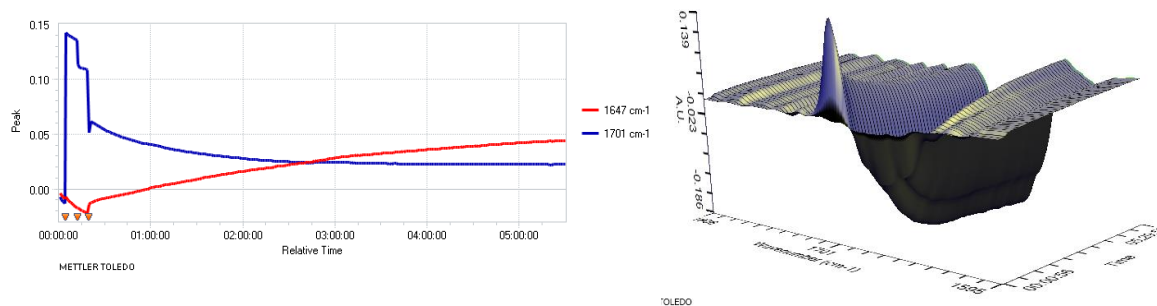
an error and data collection was stopped so a lithiation time could not be determined. The PhCHO trapping was not monitored by ReactIR™.

Lab Book Reference: AMI_164 + AMI_165

s-BuLi (1.0 mL of a 1.3 M solution in hexanes, 1.3 eq.) was added dropwise to a stirred solution of *N*-Boc pyrrolidine **96** (237 mg, 1.06 mmol, 1.0 eq.) in THF (7 mL) at $-78\text{ }^{\circ}\text{C}$ under Ar. The resulting solution was stirred at $-78\text{ }^{\circ}\text{C}$ for 4.5 h. Then, PhCHO (225 mg, 2.12 mmol, 2.0 eq., 0.22 mL) was added and the resulting solution was stirred at $-78\text{ }^{\circ}\text{C}$ for 10 min and then allowed to warm to rt. Saturated $\text{NH}_4\text{Cl}_{(\text{aq})}$ (10 mL) was added and the two layers were separated. The aqueous layer was extracted with Et_2O (3 x 10 mL) and the combined organics were dried (MgSO_4), filtered and evaporated under reduced pressure to give the crude product. Using general procedure D, the crude product and DMP (898 mg, 2.12 mmol, 2.0 eq.) in CH_2Cl_2 (10 mL) gave the crude product, which contained a 93:7 mixture (by ^1H NMR spectroscopy) of ketones *anti*-**213** and *syn*-**213**. Purification by flash column chromatography on silica using 98:2 CH_2Cl_2 -acetone as eluent gave a 93:7 mixture (by ^1H NMR spectroscopy) of ketones *anti*-**213** and *syn*-**213** (239 mg, 69%) as a colourless oil.

Lab Book Reference: AMI_74 + AMI_76

ReactIR™ spectroscopic monitoring of the lithiation of *N*-Boc pyrrolidine **96** using *s*-BuLi/*di*-*i*-Pr bispidine **30**

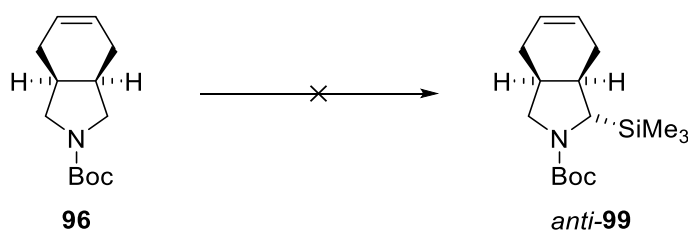


Et_2O (10 mL) was added to a flask equipped with a stirrer bar and ReactIR™ probe (iC 10, SiComp) at rt under Ar. After cooling to $-78\text{ }^{\circ}\text{C}$, a solution of *di*-*i*-Pr bispidine **30** (302 mg, 1.4 mmol, 1.3 eq.) in Et_2O (2 mL) was added followed by a solution of *N*-Boc pyrrolidine

96 (245 mg, 1.1 mmol, 1.0 eq.) in Et₂O (2 mL). The solution was stirred for 5 min (to verify the stability of readout on ReactIRTM). Then, *s*-BuLi (1.1 mL of a 1.3 M solution in hexanes, 1.4 mmol, 1.3 eq.) was added dropwise. The resulting solution was stirred at -78 °C for 5.5 h.

For *N*-Boc pyrrolidine **96**, a peak at 1701 cm⁻¹ was observed and assigned to ν_{C=O}. After addition of *s*-BuLi, a new peak at 1647 cm⁻¹ was observed which was assigned to ν_{C=O} in the lithiated intermediate. After a lithiation time of 5 h, complete lithiation of *N*-Boc pyrrolidine **96** to give the lithiated intermediate was observed.

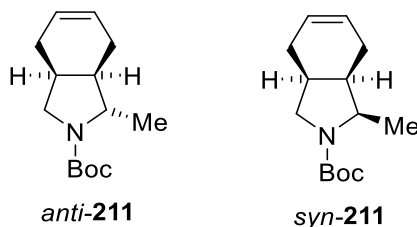
Lab Book Reference: AMI_34



Using general procedure A, *s*-BuLi (1.1 mL of a 1.3 M solution in hexanes, 1.39 mmol, 1.3 eq.), *N*-Boc pyrrolidine **96** (239 mg, 1.07 mmol, 1.0 eq.) and di-*i*-Pr bispidine **30** (292 mg, 1.39 mmol, 1.3 eq.) in Et₂O (7 mL) for 5 h and then Me₃SiCl (232 mg, 0.27 mL, 2.14 mmol, 2.0 eq.) gave the crude product, which contained only starting material **96** (by ¹H NMR spectroscopy).

Lab Book Reference: AMI_35

(1*S,3*aS**,7*aR**) and (1*R**,3*aS**,7*aR**)-tert-Butyl-1-methyl-2,3,3*a*,4,7,7*a*-hexahydro-1*H*-isoindole-2-carboxylate *anti*-211 and *syn*-211**

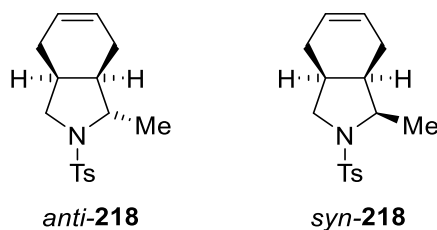


Using general procedure A, *s*-BuLi (1.00 mL of a 1.3 M solution in hexanes, 1.30 mmol, 1.3 eq.), *N*-Boc pyrrolidine **96** (223 mg, 1.00 mmol, 1.0 eq.) and di-*i*-Pr bispidine **30** (273 mg,

1.3 mmol, 1.3 eq.) in Et₂O (7 mL) for 5 h and then Me₂SO₄ (252 mg, 0.19 mL, 2.00 mmol, 2.0 eq.) gave the crude product. Purification by flash column chromatography on silica using 85:15 hexane-EtOAc as eluent gave starting material pyrrolidine **96** (75 mg, 34%) as a colourless oil and a 90:10 mixture (by ¹H NMR spectroscopy of sulfonamides *anti*-**218** and *syn*-**218**) of 2,3,4-trisubstituted pyrrolidines *anti*-**211** and *syn*-**211** (89 mg, 38%) as a colourless oil.

Lab Book Reference: AMI_36

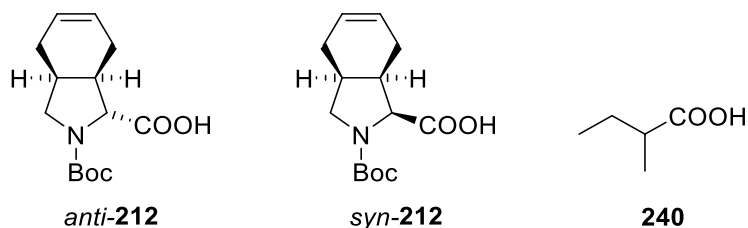
(1*S**,3*aS**,7*aR**) and (1*R**,3*aS**,7*aR**)-1-Methyl-2-(4-methylbenzenesulfonyl)-2,3,3*a*,4,7,7*a*-hexahydro-1*H*-isoindole *anti*-**218** and *syn*-**218**



TFA (427 mg, 0.29 mL, 3.75 mmol, 10 eq.) was added to a stirred solution of 2,3,4-trisubstituted pyrrolidine **211** (89 mg, 0.375 mmol, 1.0 eq.) in CH₂Cl₂ (7 mL) at rt under Ar. The resulting solution was stirred at rt for 16 h. Then, saturated NaHCO_{3(aq)} (20 mL) was added with vigorous stirring until gas evolution ceased. The mixture was extracted with CH₂Cl₂ (3 x 10 mL) and the combined organics were dried (Na₂SO₄), filtered and evaporated under reduced pressure. The residue was dissolved in CH₂Cl₂ (4 mL) and Et₃N (46 mg, 0.06 mL, 0.45 mmol, 1.2 eq.) and *p*-TsCl (86 mg, 0.45 mmol, 1.2 eq.) were added. The resulting solution was stirred at rt for 16 h. Then, CH₂Cl₂ (10 mL) and 0.1 M HCl_(aq) (10 mL) were added and the two layers were separated. The aqueous layer was extracted with CH₂Cl₂ (3 x 10 mL) and the combined organics were dried (MgSO₄), filtered and evaporated under reduced pressure to give the crude product, which contained a 90:10 mixture (by ¹H NMR spectroscopy) of sulfonamides *anti*-**218** and *syn*-**218**.

Lab Book Reference: AMI_42

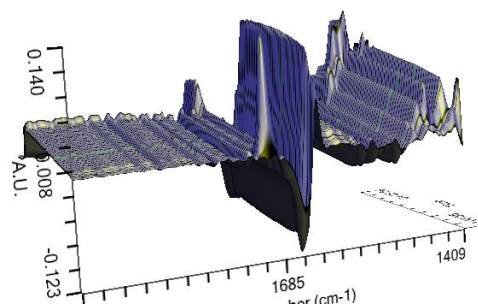
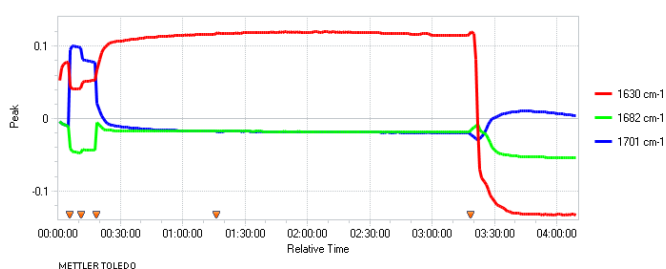
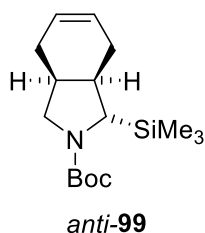
(1*R**,3*aS**,7*aR**) and (1*S**,3*aS**,7*aR**)-2-[(*tert*-Butoxy)carbonyl]-2,3,3*a*,4,7,7*a*-hexahydro-1*H*-isoindole-1-carboxylic acid *anti*-212 and *syn*-212 and 2-methylbutanoic acid **240**



Using general procedure C, *s*-BuLi (1.0 mL of a 1.3 M solution in hexanes, 1.04 mmol, 1.3 eq.), *N*-Boc pyrrolidine **96** (232 mg, 1.04 mmol, 1.0 eq.) and di-*i*-Pr bispidine **30** (284 mg, 1.35 mmol, 1.3 eq.) in Et₂O (7 mL) for 5 h and then dry CO₂ was bubbled through for 30 min to give the crude product. Purification by flash column chromatography on silica using 50:49.5:0.5 EtOAc-hexane-AcOH as eluent gave a 90:10 mixture of carboxylic acids *anti*-212 and *syn*-212 (141 mg, 51%) as a white solid and an inseparable 60:40 mixture (by ¹H NMR spectroscopy) of carboxylic acid **240** and recovered starting material **96** (171 mg, i.e. 109 mg (47%) of starting material **96**). Diagnostic signals for acid **240**: ¹H NMR (400 MHz, CDCl₃) δ 1.16 (d, *J* = 7.0 Hz, 3H, CH*Me*), 0.93 (t, *J* = 7.5 Hz, 3H, CH₂*Me*).

Lab Book Reference: AMI_48

tert-Butyl (1*S**, 3*aS**, 7*aR**)-1-(trimethylsilyl)-2,3,3*a*,4,7,7*a*-hexahydro-1*H*-isoindole-2-carboxylate *anti*-99



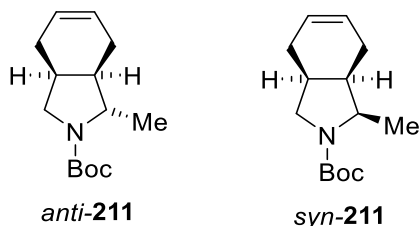
Et₂O (10 mL) was added to a flask equipped with a stirrer bar and ReactIR™ probe (iC 10, SiComp) at rt under Ar. After cooling to -78 °C, a solution of di-*n*-Pr bispidine **105** (302

mg, 1.4 mmol, 1.3 eq.) in Et₂O (2 mL) was added followed by a solution of *N*-Boc pyrrolidine **96** (245 mg, 1.1 mmol, 1.0 eq.) in Et₂O (2 mL). The solution was stirred for 5 min (to verify the stability of readout on ReactIR™). Then, *s*-BuLi (1.1 mL of a 1.3 M solution in hexanes, 1.4 mmol, 1.3 eq.) was added dropwise and the resulting solution was stirred at -78 °C for 1 h. Then, Me₃SiCl (0.27 mL, 2.16 mmol, 2.0 eq.) was added and the solution was stirred at -78 °C for 2 h. ReactIR™ monitoring indicated trapping was incomplete so the solution was warmed to rt over 30 min allowing complete trapping to occur. Saturated NH₄Cl_(aq) (10 mL) was added and the two layers were separated. The aqueous layer was extracted with Et₂O (3 x 10 mL) and the combined organic layers were dried (MgSO₄), filtered and evaporated under reduced pressure to give the crude product. Purification by flash column chromatography on silica using 90:10 hexane-EtOAc as eluent gave a single diastereomer of 2,3,4-trisubstituted pyrrolidine *anti*-**99** (207 mg, 64%) as a colourless oil.

For *N*-Boc pyrrolidine **96**, a peak at 1701 cm⁻¹ was observed and assigned to $\nu_{C=O}$. After addition of *s*-BuLi, a new peak at 1682 cm⁻¹ was observed which was assigned to $\nu_{C=O}$ in the prelithiation complex. A new peak at 1630 cm⁻¹ was also observed and this was assigned to the lithiated intermediate. After a lithiation time of 40 min, complete lithiation of *N*-Boc pyrrolidine **96** to give the lithiated intermediate was observed. When Me₃SiCl was added (after 1 h total lithiation time), the signal for the lithiated intermediate ($\nu_{C=O} = 1630$ cm⁻¹) decreased extremely slowly during the 2 h incubation at -78 °C. Whilst the reaction was warming from -78 °C to rt the signal for the lithiated intermediate disappeared, indicating complete trapping of *N*-Boc pyrrolidine **96** had occurred.

Lab Book Reference: AMI_39

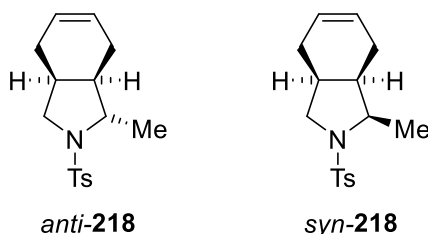
(1*S,3*aS**,7*aR**) and (1*R**,3*aS**,7*aR**)-tert-Butyl-1-methyl-2,3,3*a*,4,7,7*a*-hexahydro-1*H*-isoindole-2-carboxylate *anti*-**211** and *syn*-**211****



Using general procedure A, *s*-BuLi (1.1 mL of a 1.3 M solution in hexanes, 1.42 mmol, 1.3 eq.), *N*-Boc pyrrolidine **96** (244 mg, 1.09 mmol, 1.0 eq.) and di-*n*-Pr bispidine **105** (298 mg, 1.42 mmol, 1.3 eq.) in Et₂O (7 mL) for 1 h and then Me₂SO₄ (275 mg, 0.21 mL, 2.18 mmol, 2.0 eq.) gave the crude product. Purification by flash column chromatography on silica using 85:15 hexane-EtOAc as eluent gave a 90:10 mixture (by ¹H NMR spectroscopy of sulfonamides *anti*-**218** and *syn*-**218**) of 2,3,4-trisubstituted pyrrolidines *anti*-**211** and *syn*-**211** (200 mg, 77%) as a colourless oil.

Lab Book Reference: AMI_40

(1*S,3*aS**,7*aR**) and (1*R**,3*aS**,7*aR**)-1-Methyl-2-(4-methylbenzenesulfonyl)-2,3,3*a*,4,7,7*a*-hexahydro-1*H*-isoindole *anti*-**218** and *syn*-**218****

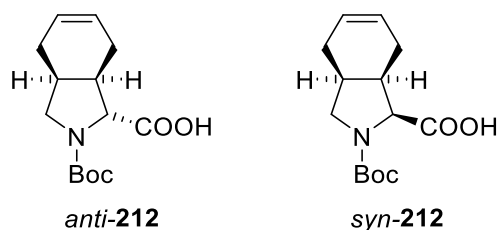


TFA (442 mg, 0.30 mL, 3.88 mmol, 10 eq.) was added to a stirred solution of 2,3,4-trisubstituted pyrrolidine **211** (92 mg, 0.388 mmol, 1.0 eq.) in CH₂Cl₂ (7 mL) at rt under Ar. The resulting solution was stirred at rt for 16 h. Then, saturated NaHCO_{3(aq)} (20 mL) was added with vigorous stirring until gas evolution ceased. The mixture was extracted with CH₂Cl₂ (3 x 10 mL) and the combined organics were dried (Na₂SO₄), filtered and evaporated under reduced pressure. The residue was dissolved in CH₂Cl₂ (4 mL) and Et₃N (47 mg, 0.06 mL, 0.466 mmol, 1.2 eq.) and *p*-TsCl (89 mg, 0.466 mmol, 1.2 eq.) were added. The resulting solution was stirred at rt for 16 h. Then, CH₂Cl₂ (10 mL) and 0.1 M HCl_(aq) (10 mL) were added and the two layers were separated. The aqueous layer was extracted with CH₂Cl₂ (3 x

10 mL) and the combined organics were dried (MgSO₄), filtered and evaporated under reduced pressure to give the crude product, which contained a 90:10 mixture (by ¹H NMR spectroscopy) of sulfonamides *anti*-**218** and *syn*-**218**.

Lab Book Reference: AMI_45

(**1R*,3aS*,7aR***) and (**1S*,3aS*,7aR***)-2-[(*tert*-Butoxy)carbonyl]-2,3,3a,4,7,7a-hexahydro-1H-isoindole-1-carboxylic acid *anti*-**212** and *syn*-**212**



Using general procedure C, *s*-BuLi (1.1 mL of a 1.3 M solution in hexanes, 1.41 mmol, 1.3 eq.), *N*-Boc pyrrolidine **96** (242 mg, 1.08 mmol, 1.0 eq.) and di-*n*-Pr bispidine **105** (296 mg, 1.41 mmol, 1.3 eq.) in Et₂O (7 mL) for 1 h and then dry CO₂ was bubbled through for 30 min to give the crude product. Purification by flash column chromatography on silica using 50:49.5:0.5 EtOAc-hexane-AcOH as eluent gave a 94:6 mixture of carboxylic acids *anti*-**212** and *syn*-**212** (253 mg, 87%) as a white solid.

Lab Book Reference: AMI_41

Abbreviations

AcOH	Acetic Acid
aq.	Aqueous
Ar	Aryl
Bn	Benzyl
Boc	<i>tert</i> -Butoxycarbonyl
bp	Boiling Point
br	Broad
Bu	Butyl
cm ⁻¹	Wavenumber
Cy	Cyclohexyl
d	Doublet
dba	Dibenzylideneacetone
DEPT	Distortionless Enhancement by Polarisation Transfer
DFT	Density Functional Theory
DIPEA	<i>N,N</i> -diisopropylamine
DKR	Dynamic kinetic resolution
DMF	Dimethylformamide
DMP	Dess-Martin Periodinane
DMSO	Dimethylsulfoxide
dr	Diastereomeric Ratio
E ⁺	Electrophile
eq.	Equivalent(s)
er	Enantiomeric Ratio
ESI	Electrospray Ionisation
Et ₂ O	Diethyl Ether
EtOAc	Ethyl Acetate
FT	Fourier Transform
g	Gram(s)
<i>G</i>	Gibbs Free Energy
ΔG^\ddagger	Gibbs Free Energy of activation
<i>H</i>	Enthalpy
ΔH^\ddagger	Enthalpy of activation
h	Hour(s)

HATU	<i>O</i> -(7-azabenzotriazol-1-yl)- <i>N,N,N',N'</i> -tetramethyluronium hexafluorophosphate
HRMS	High resolution mass spectrometry
Hz	Hertz
<i>i</i> -Pr	Isopropyl
<i>i</i> -PrLi	Isopropyllithium
IR	Infra-red
J	Coupling constant in Hz
<i>k</i>	Rate constant
<i>k</i> _{obs}	Observed rate constant
K	Kelvin
LDA	Lithium diisopropylamide
m	Multiplet
M	Molar
<i>m/z</i>	Mass to charge ratio
M ⁺	Molecular Ion
Me	Methyl
min	Minute(s)
mg	Milligram(s)
mL	Millilitre(s)
mmol	Millimole
mp	Melting point
MP2	Møller–Plesset perturbation theory (second order)
MS	Mass Spectrometry
Ms	Mesyl
MTBE	Methyl <i>tert</i> -butyl ether
<i>n</i> -BuLi	<i>n</i> -Butyllithium
NMR	Nuclear Magnetic Resonance
<i>p</i> -Tol	<i>p</i> -Tolyl
<i>p</i> -TsCl	<i>p</i> -Toluenesulfonyl chloride
Petrol	Petroleum Ether (Fraction which boils at 40-60 °C)
Ph	Phenyl
Pr	Propyl
rac	Racemic

rate _{init}	Initial Rate
RHF	Restricted Hartree Fock
R _F	Retention Factor
rt	Room Temperature
s	Singlet
<i>s</i> -BuLi	<i>sec</i> -Butyllithium
t	Triplet
THF	Tetrahydrofuran
TFA	Trifluoroacetic acid
TLC	Thin Layer Chromatography
TMEDA	<i>N,N,N',N'</i> -Tetramethylethylenediamine
Trisyl	2,4,6-triisopropylbenzenesulfonyl
Ts	<i>p</i> -Toluenesulfonyl
TS	Transition State
UV	Ultraviolet
δ	Chemical Shift
ν _{C=O}	Carbonyl IR stretching frequency

References

- (1) McGrath, N. A.; Brichacek, M.; Njardarson, J. T. *J. Chem. Educ.* **2010**, 87, 1348.
- (2) Beak, P.; Lee, W.-K. *Tetrahedron Lett.* **1989**, 30, 1197.
- (3) Kerrick, S. T.; Beak, P. *J. Am. Chem. Soc.* **1991**, 113, 9708.
- (4) Johnson, T. A.; Jang, D. O.; Slafer, B. W.; Curtis, M. D.; Beak, P. *J. Am. Chem. Soc.* **2002**, 124, 11689.
- (5) (a) F. G. Njoroge, K. X. Chen, N.-Y. Shih and J. J. Piwinski, *Acc. Chem. Res.* **2008**, 41, 50.
(b) G. Wu, F. X. Chen, P. Rashatasakhon, J. M. Eckert, G. S. Wong, H. C. Lee, N. C. Erickson, J. A. Vance, P. C. Nirchio, J. Weber, J.-S. D. Tsai and Z. Nanfei (Schering Corporation), *WO2007075790*, **2007**.
- (6) (a) P. Revill, N. Serradell, J. Bolós and E. Rosa, *Drugs Future* **2007**, 32, 788.
(b) G. J. Tanoury, M. Chen, J. E. Cochran (Vertex Pharmaceuticals Inc.), *WO2007022459*, **2007**.
- (7) Beak, P.; Meyers, A. I. *Acc. Chem. Res.* **1986**, 19, 356.
- (8) Beak, P.; Reitz, D. B. *Chem. Rev.* **1978**, 78, 275.
- (9) Beak, P.; McKinnie, B. G.; Reitz, D. B. *Tetrahedron Lett.* **1977**, 18, 1839.
- (10) Reitz, D. B.; Beak, P.; Tse, A. *J. Org. Chem.* **1981**, 46, 4316.
- (11) Al-Aseer, M.; Beak, P.; Hay, D.; Kempf, D. J.; Mills, S.; Smith, S. G. *J. Am. Chem. Soc.* **1983**, 105, 2080.
- (12) Beak, P.; Zajdel, W. J. *J. Am. Chem. Soc.* **1984**, 106, 1010.
- (13) Hay, D. R.; Song, Z.; Smith, S. G.; Beak, P. *J. Am. Chem. Soc.* **1988**, 110, 8145.
- (14) Pippel, D. J.; Curtis, M. D.; Du, H.; Beak, P. *J. Org. Chem.* **1998**, 63, 2.
- (15) Rondan, N. G.; Houk, K. N.; Beak, P.; Zajdel, W. J.; Chanrasekhar, J.; Schleyer, P. V. R. *J. Org. Chem.* **1981**, 46, 4108.
- (16) Meyers, A. I.; Hellring, S. *J. Org. Chem.* **1982**, 47, 2229.
- (17) Meyers, A. I.; Edwards, P. D.; Rieker, W. F.; Bailey, T. R. *J. Am. Chem. Soc.* **1984**, 106, 3270.
- (18) Meyers, A. I.; Dickman, D. A. *J. Am. Chem. Soc.* **1987**, 109, 1263.
- (19) Meyers, A. I.; Milot, G. *J. Org. Chem.* **1993**, 58, 6538.
- (20) Seebach, D.; Enders, D. *Angew. Chem. Int. Ed.* **1975**, 14, 15.
- (21) Seebach, D.; Isabelle, M. P. H.; Max, A. S. *Helv. Chim. Acta* **1987**, 70, 1357.
- (22) Metallinos, C.; Dudding, T.; Zaifman, J.; Chaytor, J. L.; Taylor, N. J. *J. Org. Chem.* **2007**, 72, 957.
- (23) Metallinos, C.; Xu, S. *Org. Lett.* **2010**, 12, 76.

- (24) Hassel, T.; Seebach, D. *Helv. Chim. Acta* **1978**, 61, 2237.
- (25) Barker, G.; O'Brien, P.; Campos, K. R. *Org. Lett.* **2010**, 12, 4176.
- (26) Gilman, H.; Gaj, B. J. *J. Org. Chem.* **1957**, 22, 1165.
- (27) Kwong, W. S. A. *PhD Thesis, University of York*, **2016**.
- (28) Beak, P.; Kerrick, S. T.; Wu, S.; Chu, J. *J. Am. Chem. Soc.* **1994**, 116, 3231.
- (29) Dearden, M. J.; Firkin, C. R.; Hermet, J.-P. R.; O'Brien, P. *J. Am. Chem. Soc.* **2002**, 124, 11870.
- (30) Liniger, M.; Estermann, K.; Altmann, K.-H. *J. Org. Chem.* **2013**, 78, 11066.
- (31) Stead, D.; Carbone, G.; O'Brien, P.; Campos, K. R.; Coldham, I.; Sanderson, A. *J. Am. Chem. Soc.* **2010**, 132, 7260.
- (32) Gallagher, D. J.; Beak, P. *J. Org. Chem.* **1995**, 60, 7092.
- (33) Gallagher, D. J.; Kerrick, S. T.; Beak, P. *J. Am. Chem. Soc.* **1992**, 114, 5872.
- (34) Bailey, W. F.; Beak, P.; Kerrick, S. T.; Ma, S.; Wiberg, K. B. *J. Am. Chem. Soc.* **2002**, 124, 1889.
- (35) Stead, D.; O'Brien, P.; Sanderson, A. *Org. Lett.* **2008**, 10, 1409.
- (36) Coldham, I.; O'Brien, P.; Patel, J. J.; Raimbault, S.; Sanderson, A. J.; Stead, D.; Whittaker, D. T. E. *Tetrahedron: Asymmetry* **2007**, 18, 2113.
- (37) McGrath, M. J.; O'Brien, P. *J. Am. Chem. Soc.* **2005**, 127, 16378.
- (38) Beak, P.; Lee, W. K. *J. Org. Chem.* **1990**, 55, 2578.
- (39) Seel, S.; Thaler, T.; Takatsu, K.; Zhang, C.; Zipse, H.; Straub, B. F.; Mayer, P.; Knochel, P. *J. Am. Chem. Soc.* **2011**, 133, 4774.
- (40) Beak, P.; Lee, W. K. *J. Org. Chem.* **1993**, 58, 1109.
- (41) Campos, K. R.; Klapars, A.; Waldman, J. H.; Dormer, P. G.; Chen, C. *J. Am. Chem. Soc.* **2006**, 128, 3538.
- (42) Beak, P.; Wu, S.; Yum, E. K.; Jun, Y. M. *J. Org. Chem.* **1994**, 59, 276.
- (43) Park, Y. S.; Beak, P. *Tetrahedron* **1996**, 52, 12333.
- (44) Rayner, P. J.; O'Brien, P.; Horan, R. A. *J. Am. Chem. Soc.* **2013**, 135, 8071.
- (45) Miller, K. A.; Shanahan, C. S.; Martin, S. F. *Tetrahedron* **2008**, 64, 6884.
- (46) Fukatsu, K.; Nakayama, Y.; Tarui, N.; Mori, M.; Matsumoto, H.; Kurasawa, O. *Eur. Appl., to Tak. Pharm. Co. Limited, EP 1661898A1*, **2006**.
- (47) Okamura, N.; Habay, S. A.; Zeng, J.; Chamberlin, A. R.; Reinscheid, R. K. *J. Pharmacol. Exp. Ther.* **2008**, 325, 893.
- (48) Garvey, D., S.; Larosa, G., J.; Greenwood, J., Robert; Brewer, M., L.; Quach, T.; Cote, J., B. . B. *J. Int. Appl., to Bikam Pharm. Inc., WO 2010/147653A1*, **2010**.

- (49) Robinson, S. P.; Sheikh, N. S.; Baxter, C. A.; Coldham, I. *Tetrahedron Lett.* **2010**, 51, 3642.
- (50) Firth, J. D.; O'Brien, P.; Ferris, L. *J. Org. Chem.* **2017**, 82, 7023.
- (51) Berkheij, M.; van der Sluis, L.; Sewing, C.; den Boer, D. J.; Terpstra, J. W.; Hiemstra, H.; Iwema Bakker, W. I.; van den Hoogenband, A.; van Maarseveen, J. H. *Tetrahedron Lett.* **2005**, 46, 2369.
- (52) Firth, J. D.; O'Brien, P.; Ferris, L. *J. Am. Chem. Soc.* **2016**, 138, 651.
- (53) Firth, J. D. *PhD Thesis, University of York* **2014**.
- (54) Bey, A. E.; Weyenberg, D. R. *J. Org. Chem.* **1966**, 31, 2036.
- (55) Seyferth, D.; Weinstein, R. M. *J. Am. Chem. Soc.* **1982**, 104, 5534.
- (56) Ahmed, A.; Clayden, J.; Rowley, M. *Tetrahedron Lett.* **1998**, 39, 6103.
- (57) McDermott, B. P.; Campbell, A. D.; Ertan, A. *Synlett* **2008**, 2008, 875.
- (58) Olofson, R. A.; Martz, J. T.; Senet, J. P.; Piteau, M.; Malfroot, T. *J. Org. Chem.* **1984**, 49, 2081.
- (59) Lautens, M.; Fillion, E.; Sampat, M. *J. Org. Chem.* **1997**, 62, 7080.
- (60) Babudri, F.; Florio, S.; Reho, A.; Trapani, G. *J. Chem. Soc. Perkin Trans. 1* **1984**, 1949.
- (61) Krow, G. R.; Herzon, S. B.; Lin, G.; Qiu, F.; Sonnet, P. E. *Org. Lett.* **2002**, 4, 3151.
- (62) Krow, G. R.; Sonnet, P. E. *Tetrahedron* **2008**, 64, 7131.
- (63) Xiong, H.; Fietze, W.; Andisik, D. W.; Ernst, G. E.; Palmer, W. E.; Hinkley, L.; Varnes, J. G.; Albert, J. S.; Veale, C. A. *Tetrahedron Lett.* **2010**, 51, 6741.
- (64) Tanoury, G. J.; Chen, M.; Dong, Y.; Forslund, R.; Jurkuskas, V.; Jones, A. D.; Belmont, D. *Org. Process Res. Dev.* **2014**, 18, 1234.
- (65) Bakonyi, B.; Furegati, M.; Kramer, C.; La Vecchia, L.; Ossola, F. *J. Org. Chem.* **2013**, 78, 9328.
- (66) Beak, P.; Basu, A.; Gallagher, D. J.; Park, Y. S.; Thayumanavan, S. *Acc. Chem. Res.* **1996**, 29, 552.
- (67) Al-Aseer, M. A.; Smith, S. G. *J. Org. Chem.* **1984**, 49, 2608.
- (68) Sun, X.; Kenkre, S. L.; Remenar, J. F.; Gilchrist, J. H.; Collum, D. B. *J. Am. Chem. Soc.* **1997**, 119, 4765.
- (69) Galiano-Roth, A. S.; Collum, D. B. *J. Am. Chem. Soc.* **1989**, 111, 6772.
- (70) Bernstein, M. P.; Collum, D. B. *J. Am. Chem. Soc.* **1993**, 115, 8008.
- (71) Sun, X.; Collum, D. B. *J. Am. Chem. Soc.* **2000**, 122, 2452.
- (72) Pippel, D. J.; Weisenburger, G. A.; Faibish, N. C.; Beak, P. *J. Am. Chem. Soc.* **2001**, 123, 4919.

- (73) Sheikh, N. S.; Leonori, D.; Barker, G.; Firth, J. D.; Campos, K. R.; Meijer, A. J. H. M.; O'Brien, P.; Coldham, I. *J. Am. Chem. Soc.* **2012**, 134, 5300.
- (74) Li, X.; Leonori, D.; Sheikh, N. S.; Coldham, I. *Chemistry* **2013**, 19, 7724.
- (75) Aeyad, T.; Williams, J. D.; Meijer, A. J. H. M.; Coldham, I. *Synlett* **2017**, 28.
- (76) Millet, A.; Dailier, D.; Larini, P.; Baudoin, O. *Angew. Chem. Int. Ed.* **2014**, 53, 2678.
- (77) Varela, A.; Garve, L. K. B.; Leonori, D.; Aggarwal, V. K. *Angew. Chem. Int. Ed.* **2017**, 56, 2127.
- (78) Lefranc, J.; Fournier, A. M.; Mingat, G.; Herbert, S.; Marcelli, T.; Clayden, J. *J. Am. Chem. Soc.* **2012**, 134, 7286.
- (79) Payette, J. N.; Yamamoto, H. *J. Am. Chem. Soc.* **2008**, 130, 12276.
- (80) Drexler, M. T.; Foley, D. A.; Ward, H. W.; Clarke, H. J. *Org. Process Res. Dev.* **2015**, 19, 1119.
- (81) Munchhof, M. J.; Li, Q.; Shavnya, A.; Borzillo, G. V.; Boyden, T. L.; Jones, C. S.; LaGreca, S. D.; Martinez-Alsina, L.; Patel, N.; Pelletier, K.; Reiter, L. A.; Robbins, M. D.; Tkalcevic, G. T. *ACS Med. Chem. Lett.* **2012**, 3, 106.
- (82) Barker, G.; McGrath, J. L.; Klapars, A.; Stead, D.; Zhou, G.; Campos, K. R.; O'Brien, P. *J. Org. Chem.* **2011**, 76, 5936.
- (83) Pulis, A. P.; Varela, A.; Citti, C.; Songara, P.; Leonori, D.; Aggarwal, V. K. *Angew. Chem. Int. Ed.* **2017**, 56, 10835.
- (84) Fandrick, K. R.; Patel, N. D.; Mulder, J. A.; Gao, J.; Konrad, M.; Archer, E.; Buono, F. G.; Duran, A.; Schmid, R.; Daeubler, J.; Fandrick, D. R.; Ma, S.; Grinberg, N.; Lee, H.; Busacca, C. A.; Song, J. J.; Yee, N. K.; Senanayake, C. H. *Org. Lett.* **2014**, 16, 4360.
- (85) Wiberg, K.; Bailey, W. *Angew. Chem. Int. Ed.* **2000**, 39, 2127.
- (86) Wiberg, K. B.; Bailey, W. F. *J. Am. Chem. Soc.* **2001**, 123, 8231.
- (87) Wiberg, K. B.; Bailey, W. F. *Tetrahedron Lett.* **2000**, 41, 9365.
- (88) Gallagher, D. J.; Wu, S.; Nikolic, N. A.; Beak, P. *J. Org. Chem.* **1995**, 60, 8148.
- (89) O'Brien, P.; Wiberg, K. B.; Bailey, W. F.; Hermet, J.-P. R.; McGrath, M. J. *J. Am. Chem. Soc.* **2004**, 126, 15480.
- (90) Deng, W.; Vreven, T.; Frisch, M. J.; Wiberg, K. B. *J. Mol. Struct. THEOCHEM* **2006**, 775, 93.
- (91) Dapprich, S.; Komáromi, I.; Byun, K. S.; Morokuma, K.; Frisch, M. J. *J. Mol. Struct. THEOCHEM* **1999**, 461.
- (92) Senn, H. M.; Thiel, W. *Curr. Opin. Chem. Biol.* **2007**, 11, 182.
- (93) Klapars, A.; Campos, K. R.; Waldman, J. H.; Zewge, D.; Dormer, P. G.; Chen, C. *J. Org. Chem.* **2008**, 73, 4986.
- (94) Barker, G. *PhD Thesis, University of York*, **2011**.

- (95) Gelardi, G. *PhD Thesis, University of York*, **2014**.
- (96) Rayner, P. J. *PhD Thesis, University of York*, **2013**.
- (97) Chankeshwara, S. V.; Chakraborti, A. K. *Org. Lett.* **2006**, 8, 3259.
- (98) Lee, J.-H.; Seo, S. H.; Lim, E. J.; Cho, N. C.; Nam, G.; Kang, S. B.; Pae, A. N.; Jeong, N.; Keum, G. *Eur. J. Med. Chem.* **2014**, 74, 246.
- (99) Davis, C. R.; Johnson, R. A.; Cialdella, J. I.; Liggett, W. F.; Mizesak, S. A.; Marshall, V. P. *J. Org. Chem.* **1997**, 62, 2244.
- (100) Diwan, S. S.; Dalvi, S. W.; Mulla, H. R. *Synth. Commun.* **2008**, 39, 273.
- (101) Bhattacharyya, S. *J. Org. Chem.* **1995**, 60, 4928.
- (102) Meinwald, J.; Lewis, A. *J. Am. Chem. Soc.* **1961**, 83, 2769.
- (103) Padwa, A.; Shefter, E.; Alexander, E. *J. Am. Chem. Soc.* **1968**, 90, 3717.
- (104) Marriott, S.; Topsom, R. D. *J. Am. Chem. Soc.* **1984**, 106, 7.
- (105) Remenar, J. F.; Lucht, B. L.; Collum, D. B. *J. Am. Chem. Soc.* **1997**, 119, 5567.
- (106) Bilke, J. L.; O'Brien, P. *J. Org. Chem.* **2008**, 73, 6452.
- (107) Clayden, J. *Organolithiums: Selectivity for Synthesis*; Pergamon: Oxford, **2002**.
- (108) Islip, A. *MChem Dissertation, University of York*, **2013**.
- (109) McGrath, M. J.; Bilke, J. L.; O'Brien, P. *Chem. Commun.* **2006**, 2607.
- (110) Harris, R. K.; Spragg, R. A. *Chem. Commun.* **1966**, 314.
- (111) Reeves, L. W.; Strømme, K. O. *J. Chem. Phys.* **1961**, 34, 1711.
- (112) Frisch, M. J.; Trucks, G. W.; Schlegel, H. B.; Scuseria, G. E.; Robb, M. A.; Cheeseman, J. R.; Scalmani, G.; Barone, V.; Mennucci, B.; Petersson, G. A.; Nakatsuji, H.; Caricato, M.; Li, X.; Hratchian, H. P.; Izmaylov, A. F.; Bloino, J.; Zheng, G.; Sonnenberg, J. L.; Hada, M.; Ehara, M.; Toyota, K.; Fukuda, R.; Hasegawa, J.; Ishida, M.; Nakajima, T.; Honda, Y.; Kitao, O.; Nakai, H.; Vreven, T.; Montgomery Jr., J. A.; Peralta, J. E.; Ogliaro, F.; Bearpark, M.; Heyd, J. J.; Brothers, E.; Kudin, K. N.; Staroverov, V. N.; Kobayashi, R.; Normand, J.; Raghavachari, K.; Rendell, A.; Burant, J. C.; Iyengar, S. S.; Tomasi, J.; Cossi, M.; Rega, N.; Millam, J. M.; Klene, M.; Knox, J. E.; Cross, J. B.; Bakken, V.; Adamo, C.; Jaramillo, J.; Gomperts, R.; Stratmann, R. E.; Yazyev, O.; Austin, A. J.; Cammi, R.; Pomelli, C.; Ochterski, J. W.; Martin, R. L.; Morokuma, K.; Zakrzewski, V. G.; Voth, G. A.; Salvador, P.; Dannenberg, J. J.; Dapprich, S.; Daniels, A. D.; Farkas, Ö.; Foresman, J. B.; Ortiz, J. V.; Cioslowski, J.; Fox, D. J. *Gaussian 09 Revision D.01*. Gaussian Inc. Wallingford CT 2009.
- (113) Becke, A. D. *Phys. Rev. A* **1988**, 38, 3098.
- (114) Lee, C.; Yang, W.; Parr, R. G. *Phys. Rev. B* **1988**, 37, 785.
- (115) Stephens, P. J.; Devlin, F. J.; Chabalowski, C. F.; Frisch, M. J. *J. Phys. Chem.* **1994**, 98, 11623.

- (116) Wodrich, M. D.; Corminboeuf, C.; Schreiner, P. R.; Fokin, A. A.; von Ragué Schleyer, P. *Org. Lett.* **2007**, 9, 1851.
- (117) Peverati, R.; Truhlar, D. G. *J. Chem. Phys.* **2011**, 135, 191102.
- (118) Walker, M.; Harvey, A. J. A.; Sen, A.; Dessent, C. E. H. *J. Phys. Chem. A* **2013**, 117, 12590.
- (119) Vondrášek, J.; Bendová, L.; Klusák, V.; Hobza, P. *J. Am. Chem. Soc.* **2005**, 127, 2615.
- (120) Friesner, R. A. *Proc. Natl. Acad. Sci. United States Am.* **2005**, 102, 6648.
- (121) Gross, K. M. B.; Beck, P. *J. Am. Chem. Soc.* **2001**, 123, 315.
- (122) Zhang, J.; Zhang, H.; Wu, T.; Wang, Q.; van der Spoel, D. *J. Chem. Theory Comput.* **2017**, 13, 1034.
- (123) Scalmani, G.; Frisch, M. J. *J. Chem. Phys.* **2010**, 132, 114110.
- (124) Balabin, R. M. *J. Chem. Phys.* **2008**, 129, 164101.
- (125) Kobko, N.; Dannenberg, J. J. *J. Phys. Chem. A* **2001**, 105, 1944.
- (126) Grimme, S.; Antony, J.; Ehrlich, S.; Krieg, H. *J. Chem. Phys.* **2010**, 132, 154104.
- (127) Grimme, S.; Ehrlich, S.; Goerigk, L. *J. Comput. Chem.* **2011**, 32, 1456.
- (128) Kruse, H.; Goerigk, L.; Grimme, S. *J. Org. Chem.* **2012**, 77, 10824.
- (129) Basu, A.; Thayumanavan, S. *Angew. Chem. Int. Ed.* **2002**, 41, 716.
- (130) Coldham, I.; Leonori, D.; Beng, T. K.; Gawley, R. E. *Chem. Commun.* **2009**, 5239.
- (131) Husmann, R.; Jörres, M.; Raabe, G.; Bolm, C. *Chem. Eur. J.* **2010**, 16, 12549.
- (132) Bauer, J. O.; Stiller, J.; Marqués-López, E.; Strohfeltdt, K.; Christmann, M.; Strohmam, C. *Chem. Eur. J.* **2010**, 16, 12553.
- (133) Bilke, J. L.; Moore, S. P.; O'Brien, P.; Gilday, J. *Org. Lett.* **2009**, 11, 1935.
- (134) Coldham, I.; Raimbault, S.; Whittaker, D. T. E.; Chovatia, P. T.; Leonori, D.; Patel, J. J.; Sheikh, N. S. *Chemistry* **2010**, 16, 4082.
- (135) Coldham, I.; Patel, J. J.; Sanchez-Jimenez, G. *Chem. Commun.* **2005**, 3083.
- (136) Coldham, I.; Patel, J. J.; Raimbault, S.; Whittaker, D. T. E. *Chem. Commun.* **2007**, 4534.
- (137) Gelardi, G.; Barker, G.; O'Brien, P.; Blakemore, D. C. *Org. Lett.* **2013**, 15, 5424.
- (138) Barker, G.; Brien, O.; Campos, K. R. *ARKIVOC* **2011**, 217.
- (139) Bellucci, G.; Berti, G.; Bianchini, R.; Orsini, L. *Gazz. Chim. Ital.* **1986**, 116, 77.
- (140) Campos, K. R. *Personal Communication*.
- (141) Burchat, A. F.; Chong, J. M.; Nielsen, N. *J. Organomet. Chem.* **1997**, 542, 281.
- (142) Dieter, R. K.; Li, S. *J. Org. Chem.* **1997**, 62, 7726.

- (143) Harty, M.; Nagar, M.; Atkinson, L.; Legay, C. M.; Derksen, D. J.; Bearne, S. L. *Bioorg. Med. Chem. Lett.* **2014**, 24, 390.
- (144) Chang, D.; Feiten, H.-J.; Engesser, K.-H.; van Beilen, J. B.; Witholt, B.; Li, Z. *Org. Lett.* **2002**, 4, 1859.
- (145) Carpino, L. A.; Mansour, E. M. E.; Cheng, C. H.; Williams, J. R.; MacDonald, R.; Knapczyk, J.; Carman, M.; Lopusinski, A. *J. Org. Chem.* **1983**, 48, 661.
- (146) Varala, R.; Nuvula, S.; Adapa, S. R. *J. Org. Chem.* **2006**, 71, 8283.
- (147) Jahani, F.; Tajbakhsh, M.; Golchoubian, H.; Khaksar, S. *Tetrahedron Lett.* **2011**, 52, 1260.
- (148) Laha, J. K. *Chem. Nat. Compd.* **2010**, 46, 254.
- (149) Scheiper, B.; Bonnekesel, M.; Krause, H.; Fürstner, A. *J. Org. Chem.* **2004**, 69, 3943.
- (150) Vechorkin, O.; Proust, V.; Hu, X. *J. Am. Chem. Soc.* **2009**, 131, 9756.
- (151) Amat, M.; Pérez, M.; Minaglia, A. T.; Bosch, J. *J. Org. Chem.* **2008**, 73, 6920.
- (152) Cabello, N.; Kizirian, J. C.; Gille, S.; Alexakis, A.; Bernardinelli, G.; Pinchard, L.; Caille, J. C. *Eur. J. Org. Chem.* **2005**, 4835.
- (153) Marshall, W. J.; Grushin, V. V. *Can. J. Chem.* **2005**, 83, 640.
- (154) Mickelson, J. W.; Belonga, K. L.; Jacobsen, E. J. *J. Org. Chem.* **1995**, 60, 4177.
- (155) Dess, D. B.; Martin, J. C. *J. Am. Chem. Soc.* **1991**, 113, 7277.
- (156) Banwell, M.; Smith, J. *Synth. Commun.* **2001**, 31, 2011.
- (157) Garrison, G. L.; Berlin, K. D.; Scherlag, B. J.; Lazzara, R.; Patterson, E.; Fazekas, T.; Sangiah, S.; Chen, C. L.; Schubot, F. D.; van der Helm, D. *J. Med. Chem.* **1996**, 39, 2559.
- (158) McGrath, M.; O'Brien, P. *Synthesis* **2006**, 2233.